

Photoredox C–C Cross-Coupling Reactions using Boronic Acid Derivatives



A dissertation presented by

Fabio Lima

This dissertation is submitted for the degree of

Doctor of Philosophy

at the

University of Cambridge

Fitzwilliam College

January 2018

Declaration

This dissertation is submitted in fulfilment of the requirements for the degree of Doctor of Philosophy in Chemistry. It describes the work carried out in the Department of Chemistry between October 2014 and December 2017. Unless specifically indicated in the text, the research described is my own and not the product of a collaboration.

Fabio Lima

January 2018

Statement of Length

This thesis does not exceed the word limit of 60,000 as set by the Degree Committee for the Faculty of Physics and Chemistry.

Fabio Lima

January 2018

Acknowledgements

I would like to begin by thanking Professor Steven Ley for accepting me in his group as well as supervising and supporting my work throughout these past three and half years. You have been truly inspiring for me and made my time in Cambridge both challenging and stimulating at the same time. I am glad to now be part of the Ley Group family.

Of course, none of this work would have been possible without the generous funding from Novartis AG. For this, I would like to thank Dr Berthold Schenkel to have been instrumental in securing this funding and setting up the goals for this project. I am deeply thankful for your long-lasting support and guidance and hope the output of this work matches your expectations.

As importantly, I would like to express my sincere gratitude to Dr Joerg Sedelmeier for being a wonderful mentor and having believed in me since my early steps as a chemist. I could never thank you enough for the relentless motivation and support you offered me over the past six years. Fortunately, we can continue this scientific journey together and I am looking forward to the next adventure!

From the Novartis team, I would also like to thank Dr Gottfried Sedelmeier for sharing his ideas and expertise throughout this project. I wish you will enjoy reading this thesis.

This experience has also been particularly successful and pleasant as a result my interactions with the experienced and inspiring members of the Ley group, for this I would like to thank: Duc Tran, Mikhail Kabeshov, Gina Musio, Jian Siang Poh, Andreas Hafner, Ricardo Labes, Claudio Bomio, Zoe Wilson, Lorène Crespín, Andreas Greb, Stephen Wallace, Upendra Sharma and Paul Dingwall for their supportive help and guidance at various stages of my PhD project. I learned a lot from working with you all!

I would also like to thank the students I supervised during this the last one and half year: Sandra Johannsen, Lars Grunenberg and Mohamed Husaini. You all have done an excellent job and I wish you the best for your future careers as chemists.

I am particularly thankful to Claudio Bomio, Jian Siang Poh, Holly Davies and Zoe Wilson for taking the time to proof-read this thesis.

More personally, I would like to thank the friends I made in Cambridge. Without you, this experience would not have been the same! First, my soul brother chemist, Alexandre Genoux, I would never have gone through my first year without you being (always) with me in the lab (often late at night) and in the pub afterwards. You are an admirable chemist and person and I am glad to count you as one of my closest friend, I am looking forward to our next adventures in Switzerland! Second, my family here in Cambridge, Hippolyte Astier and Hugo Poplimont, I think 60,000 words would not be enough to summarise the letters of Glisson road and the tales from the Grove and I need to save some space to talk about what I was supposed to do in the lab. We still have many more chapters to write and exciting experiences together ahead of us. It will be really difficult to leave you in a few months but be sure that our next “Dîner du respect” will be with a grand cru de Bordeaux (*i.e.* an expensive Claret). Third, Victor Allard and Jérémy Vey, I will never forget our late nights out, ending up playing the guitar and talking till dawn, I hope we will continue to see each other as much as we can.

The most important person I met in Cambridge is without any doubt my girlfriend Fiona. Je suis le plus heureux des hommes depuis que je t’ai rencontré, je ne pourrais jamais te remercier assez pour toute l’aide que tu m’as apporté pendant mon doctorat. Je t’aime.

Pour finir, je tiens à remercier ma famille pour leurs soutiens inconditionnels dans toutes les étapes de ma vie. Maman, Papa, je sais que vous êtes fiers de moi mais je tiens aussi à vous dire que je suis fière d’être votre fils et de la famille que vous avez construite. J’espère rester digne de l’image que vous avez de moi et des valeurs que vous m’avez transmises. Mes frères, je vous dédie cette thèse en espérant que cela vous inspire dans les grandes entreprises de vos vies. Si j’ai bien compris quelque chose grâce à mon parcours c’est que RIEN n’est impossible tant que l’on est prêt à travailler dur pour l’avoir, saisissez les opportunités qui s’offrent à vous et n’oubliez jamais vos rêves ! Je vous aime et je veux que vous n’oubliez jamais que je serais toujours là pour vous.

Abstract

In recent years, photoredox catalysis emerged as a privileged tool for small molecules activation *via* single-electron transfer mechanisms. Despite their ubiquity as reagents in organic synthesis, the use of boronic acid derivatives to generate carbon-centred radicals remains elusive. This dissertation explores the utilisation of photoredox catalysis to generate carbon radicals from boronic acid derivatives and subsequently engage them in C–C cross-coupling reactions.

In the first chapter, an introduction to photoredox catalysis and organoboron reagents is provided, as well as a discussion on the key mechanistic aspects of photoredox catalysed C–C cross-coupling reactions.

The second chapter presents our initial coupling strategy and how it evolved in understanding that pinacol boronic ester species can be used as a source of carbon radicals *via* single-electron oxidation from a photoredox catalyst. Coordination of the boronic esters with Lewis basic species was identified as a fundamental activating interaction. The synthetic utility of this discovery was highlighted by performing a wide range of photoredox catalysed arylations of pinacol boronic esters.

The third chapter builds on our mechanistic understanding to identify a set of Lewis base catalysts that conveniently activates boronic esters and acids towards single-electron oxidation. The usefulness of this improved set of conditions was demonstrated by alkylating a wide range of boronic acid derivatives.

The fourth chapter describes the application of this methodology in synthesising four active pharmaceutical ingredients from the GABA family. An emphasis was made on developing an efficient flow process and “transition metal free” conditions to survey the attractiveness of the method for the pharmaceutical industry.

Finally, the fifth chapter describes the experimental procedures relevant to the results described in chapters 2 to 4.

Abbreviations

δ	chemical shift in parts per million
Δ	heat
$\tilde{\nu}$	wavenumber
A	single-electron acceptor
Ac	acetyl
acac	acetylacetonate
AIBN	azobis(isobutyronitrile)
API	active pharmaceutical ingredient
Ar	undefined aryl substituent
ATR	attenuated total reflection
BDE	bond dissociation energy
BI	benziodoxolone
Bn	benzyl
Boc	<i>tert</i> -butyloxycarbonyl
bpm	2,2'-bipyrimidine
BPR	back-pressure regulator
bpy	2,2'-bipyridine
bpz	2,2'-bipyrazine
br	broad (NMR spectroscopy)
CAM	ceric (IV) ammonium molybdate (stain)
cat	catechol
COD	1,5-cyclooctadiene
COSY	correlation spectroscopy
d	doublet (NMR spectroscopy)

D	single-electron donor
DABCO	1,4-diazabicyclo[2.2.2]octane
DBN	1,5-diazabicyclo[4.3.0]non-5-ene
DBU	1,8-diazabicyclo[5.4.0]undec-7-ene
DEPT	distortionless enhancement by polarisation transfer
dF(CF ₃)ppy	2-(2,4-difluorophenyl)-5-trifluoromethyl pyridine
DFT	density functional theory
DIPEA	diisopropylethylamine
DMA	<i>N,N</i> -dimethylacetamide
DMAP	4-(dimethylamino)pyridine
DMF	<i>N,N</i> -dimethyl formamide
DMSO	dimethylsulfoxide
dtbpy	4,4'-di- <i>tert</i> -butyl-2,2'-bipyridine
E	electrophile
EDG	electron-donating group
<i>e.g.</i>	<i>exempli gratia</i>
E _g	energy gap between HOMO and LUMO
ESI	electrospray ionisation
EWG	electron-withdrawing group
FT-IR	Fourier transform infrared spectroscopy
FDA	food and drug administration
FEP	fluorinated ethylene propylene
GABA	γ -amino butyric acid
GP	general procedure
HAS	homolytic aromatic substitution
HAT	hydrogen atom transfer

HILIC	hydrophilic interaction liquid chromatography
HMBC	heteronuclear multiple bond coherence
HMDS	hexamethyldisilazane
HOMO	highest occupied molecular orbital
HRMS	high-resolution mass spectrometry
HSQC	heteronuclear simple quantum correlation
IR	infrared
ISC	inter-system crossing
IUPAC	international union of pure and applied chemistry
<i>J</i>	nuclear spin-spin coupling constant
LB	Lewis base
LED	light-emitting diode
LG	leaving group
LUMO	lowest unoccupied molecular orbital
M	mol per litre
m	multiplet (NMR spectroscopy)
Me	methyl
MLCT	metal to ligand charge transfer
mol%	mole percentage
MS	mass spectroscopy
MTBE	methyl <i>tert</i> -butyl ether
MVK	methyl vinyl ketone
NMR	nuclear magnetic resonance
NHPI	<i>N</i> -hydroxyphthalimide
Nu	nucleophile
OA	oxidative addition
ODG	<i>ortho</i> -directing group

p	pentet (NMR spectroscopy)
PBS	phosphate buffered solution (pH 7)
PE	<i>iso</i> -hexane (b.p. 40–60°C)
phen	1,10-phenanthroline
pin	pinacol
pnd	(–)-pinanediol
ppm	parts per million
ppy	2-phenylpyridine
PRE	persistent radical effect
psi	pound(s) per square inch
PTOC	pyridine-2-thione- <i>N</i> -oxycarbonyl
q	quartet (NMR spectroscopy)
QP-TSA	toluene sulfonic acid resin from QuadraPure®
R	undefined alkyl substituent
RE	reductive elimination
R _f	retention factor (thin layer chromatography)
s	singlet (NMR spectroscopy)
S ₁	singlet excited state
SC	standard conditions
SCE	saturated calomel electrode
<i>sec</i>	secondary
sept	septet (NMR spectroscopy)
SET	single-electron transfer
SMD	solvation model based on density
STY	space time yield
t	triplet (NMR spectroscopy)
T ₁	triplet excited state

temp.	temperature
TEMPO	(2,2,6,6-tetramethylpiperidin-1-yl)oxyl
<i>tert</i>	tertiary
Tf	trifluoromethanesulfonyl
THF	tetrahydrofuran
TLC	thin layer chromatography
TM	transmetallation
TMEDA	<i>N,N,N',N'</i> -tetramethyl-1,2-ethylenediamine
TMG	1,1,3,3-tetramethylguanidine
TMS	trimethylsilyl
TOF	time of flight
τ	time of residence

Technology diagrams



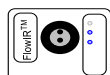
Peristaltic pump (Vapourtec SF-10 type)



T-piece mixer

100 psi

Back-pressure regulator



Mettler Toledo FlowIR[®] in-line IR spectrometer



Vapourtec UV-150 LED photoreactor (17 W at 420 nm)



Thorlabs blue LEDs (253 mW at 450 nm)



Ledxon blue LED strip (14.4 W at 450 nm)



Compact fluorescent lamp (26 W)

Table of contents

Declaration	I
Acknowledgements	III
Abstract.....	V
Abbreviations	VI
Technology diagrams.....	XI
Table of contents	XII
1 Introduction.....	1
1.1 Visible light photoredox catalysis	1
1.1.1 Photocatalysis in chemical synthesis.....	2
1.1.2 Mechanisms underlying photoredox catalysis.....	3
1.1.3 Practical photoredox catalysis	5
1.2 Strategies for photoredox C–C cross-couplings	10
1.2.1 A parallel with palladium-catalysed cross-couplings.....	10
1.2.2 Carbon radical generation.....	12
1.2.3 Redox-neutral photoredox C–C cross-couplings.....	16
1.3 Organoboron reagents.....	29
1.3.1 Properties and preparation of organoboron compounds.....	29
1.3.2 Organoboron compounds as reactants in C–C cross-couplings	32
1.4 Summary and project overview	38
2 Photoredox arylations: from trifluoroborates to boronic esters	41
2.1 A redox-neutral coupling: proof-of-concept.....	41
2.1.1 Optimisation	42
2.1.2 Scope of the transformation.....	43
2.1.3 Mechanism	47
2.1.4 Summary.....	48
2.2 Boronic esters as electron donors	49
2.2.1 Optimisation: from batch to flow	50
2.2.2 Scope investigation.....	52
2.2.3 Larger scale reaction.....	56
2.2.4 Mechanistic investigation using DFT [§]	57
2.3 Aryl bromide electrophiles: a Lewis base additive.....	64
2.3.1 Optimisation	64

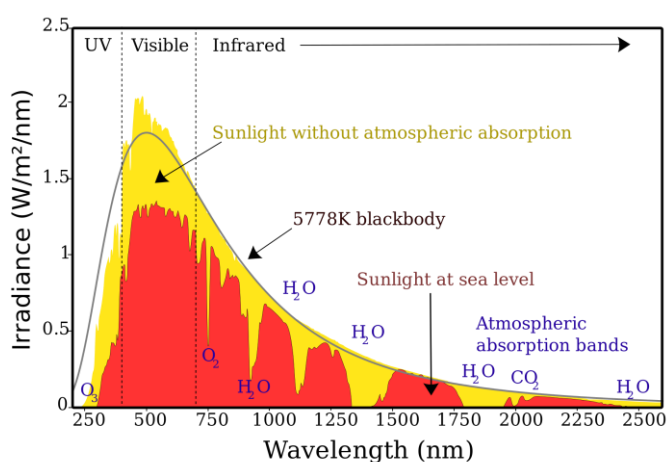
2.3.2	Scope of the transformation.....	67
2.3.3	Mechanistic experiments for DMAP activation	69
2.3.4	Proposed mechanism	72
2.3.5	Summary and conclusions	73
3	Photoredox alkylations of boronic esters and acids: a Lewis base catalyst.....	75
3.1	Optimisation	75
3.2	Scope of the transformation.....	80
3.2.1	Scope of alkenes	80
3.2.2	Scope of boronic esters.....	82
3.2.3	Scope of boronic acids.....	84
3.3	Mechanistic understanding	87
3.3.1	Mechanistic experiments	87
3.3.2	Proposed mechanism	92
3.4	Summary and conclusions	93
4	Applications to APIs synthesis in flow	95
4.1	Synthetic studies towards γ -amino acids	95
4.1.1	Introduction to GABAs	95
4.1.2	Proposed synthesis strategy	95
4.1.3	Photoredox coupling optimisation.....	98
4.1.4	Workup procedure optimisation towards a flow process	100
4.1.5	A batch route	105
4.2	Organic photoredox catalysis	106
4.2.1	Photocatalyst optimisation.....	107
4.2.2	Organic dye performance assessment	109
4.2.3	A residence time “simulation” method.....	111
4.2.4	Organic catalyst for APIs synthesis in flow	112
4.3	Summary and conclusions	116
5	Experimental	117
5.1	General information.....	117
5.1.1	General experimental and analytical methods.....	117
5.1.2	Photochemical and optimisation experiments	119
5.1.3	Computational methods.....	120
5.1.4	Electrochemical measurements	121
5.2	Experimental data for Chapter 2.....	122
5.2.1	Synthetic procedures and characterisation for starting materials	122
5.2.2	Synthetic procedures and characterisation for coupling products.....	131
5.3	Experimental data for Chapter 3.....	152
5.3.1	Synthetic procedures and characterisation for starting materials	152

5.3.2 Synthetic procedures and characterisation for coupling products	155
5.4 Experimental data for Chapter 4.....	183
5.4.1 Synthetic procedures and characterisation for organic dyes	183
5.4.2 Synthetic procedures and characterisation for starting materials	186
5.4.3 Synthetic procedures and characterisation for γ -amino butyric acid analogues	190
6 References	199
7 Appendices (NMR spectra)	212
7.1 Spectra for Chapter 2	212
7.1.1 Starting materials spectra	212
7.1.2 Coupling products spectra	234
7.2 Spectra for Chapter 3	273
7.2.1 Starting materials spectra	273
7.2.2 Coupling products spectra	280
7.3 Spectra for Chapter 4	330
7.3.1 Organic dyes spectra.....	330
7.3.2 Starting materials spectra	333
7.3.3 Coupling products and final APIs spectra	337

1 Introduction

1.1 Visible light photoredox catalysis

Achieving the conversion of abundant solar energy into useful chemical energy has been a long-standing objective of scientists from all disciplines over the past 100 years.^[1] It is commonly accepted that harnessing even a fraction of the power delivered by the sun to earth would enable the humanity to live sustainably without relying on fossil fuels.^[2] At the beginning of the 20th century, Ciamician realised the immense power of solar light to drive chemical processes.^[3] By reporting the first documented photochemical organic reactions, he paved the way to UV light photochemistry which ultimately led to the discovery of a wealth of new chemical reactivity.^[4] The concept was revolutionary at the time, but if one wants to harness the full power of the sun, the entire spectrum of emission has to be captured.



Graph 1 – Solar emission spectrum received on earth.^[5]

From **Graph 1**, it can be seen that the low UV-content of sunlight (only 3%) does not make it an efficient light source to photoactivate UV-absorbing organic molecules. On the other hand, with 44% of the overall irradiation from the sun received on earth, visible light constitutes a much more attractive frequency window to be used to perform photochemistry.^[6] Therefore, the use of photocatalysts which absorb visible light to

mediate photochemical reactions is highly attractive as a more efficient solar energy harnessing process.

1.1.1 Photocatalysis in chemical synthesis

In general, visible light photoredox catalysis describes the use of low energy visible light (380 nm – 750 nm) to drive otherwise energetically disfavoured chemical redox reactions. The development of modern transition metal-based catalysts (such as $[\text{Ru}(\text{bpy})_3]^{2+}$) with efficient absorption properties and long-lived excited states has enabled the development of efficient visible light induced photoreactions. The opportunity to use natural sunlight for chemical transformations introduces new possibilities to transfer and store energy in a sustainable manner, such as the production of hydrogen by water-splitting or solar fuels from carbon dioxide, which encourages significant scientific understanding and progress in this field.^[7–10]

Although pioneering applications of this principle in organic synthesis date back to the work of Kellogg *et al.* in 1978,^[11] it took three decades for the organic synthetic community to realise the full synthetic potential of these methods. The year 2008 marked a clear resurgence of interest in this field with the landmark work of Yoon^[12] and MacMillan^[13] shortly followed by Stephenson^[14].

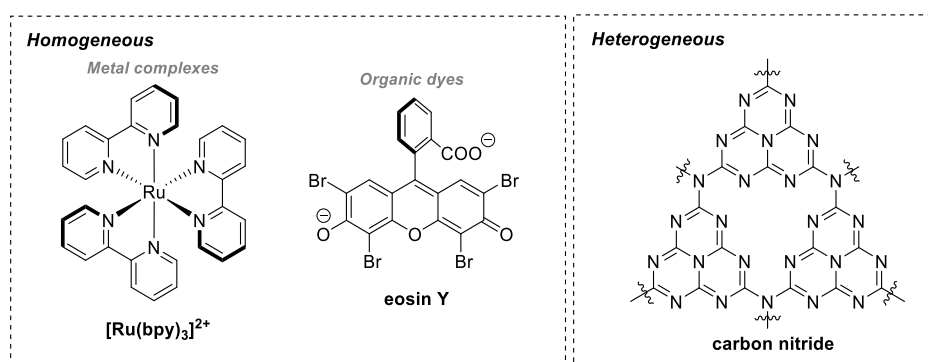


Figure 1 – Examples of commonly employed homogeneous and heterogeneous photocatalysts.

This approach has now been used in a wide variety of transformations in organic synthesis, including C–C or C–X bond forming reactions, cycloadditions, oxidations, and reductions with applications ranging from complex natural product synthesis to late-stage functionalisation of pharmaceutical compounds.^[15–18] The majority of these protocols make use of homogeneous iridium- or ruthenium-based transition metal complexes as

photocatalysts (such as $[\text{Ru}(\text{bpy})_3]^{2+}$ in **Figure 1**). Organic dyes, such as **eosin Y**, represent an interesting alternative to transition metal based photocatalysts for industrial applications where the purity of the products needs to comply with residual transition metal limits (permitted daily exposure (PDE) $\Sigma(\text{Ir, Os, Rh, Ru}) \leq 100 \mu\text{g/day}$).^[17,19,20] A recent demonstration of organic photocatalysis on an industrial scale was made by Sanofi to produce the anti-malarial drug artemisinin (35 tonnes/year in 2013).^[21–23]

Apart from organic photocatalysts, inorganic semiconductors, such as TiO_2 , carbon nitride or CdS , can act as heterogeneous photocatalysts.^[7,9] While these offer the obvious benefits of being non-miscible, their efficiency is limited by the absorption properties of the material, light scattering, surface defects, and the diffusion rate of electron/hole pairs towards the surface of the material.^[24] Because homogeneous transition metal photocatalysts are less influenced by these factors, they are often preferred for developing new catalytic reactions. Although heterogeneous photocatalysts hold great promise for more sustainable solar synthetic chemistry, the work presented in this thesis will focus on the development of new catalytic methods for small molecule activation and will consequently make use of (so far) more efficient homogeneous photoredox catalysts.

1.1.2 Mechanisms underlying photoredox catalysis

Despite the high structural and physical diversity of the photocatalysts described in the literature, every photoredox reaction relies on the absorption of light energy by the ground state catalyst, leading to long-lived photoexcited states that are both more oxidising and reducing than the ground state species.^[16]

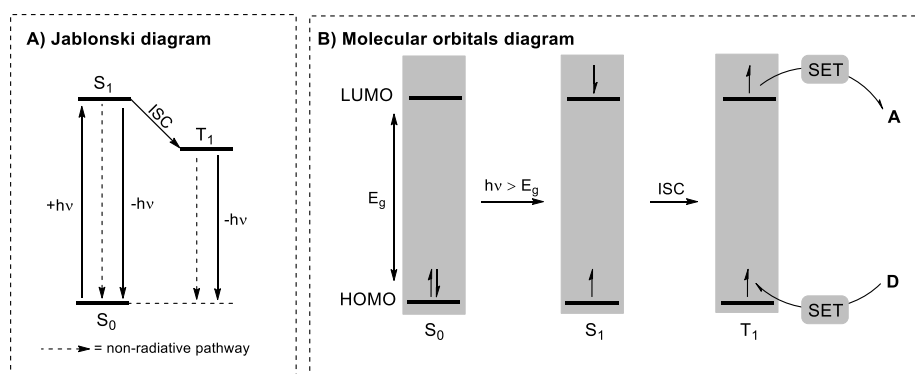


Figure 2 – Photophysical processes of photoredox catalysts.^[17]

Photons with higher energy than the energy gap (E_g) initially excite the catalyst to its singlet excited state (S_1 , **Figure 2**) by the excitation of an electron from the highest

occupied molecular orbital (HOMO) to the lowest unoccupied molecular orbital (LUMO). Because the transition is performed under spin retention of the excited electron, the excited catalyst can return in a spin-allowed recombination of the electron/hole pair to its ground state (S_0) by either radiative (fluorescence) or non-radiative transition (internal conversion). Another possible pathway involves the transition to its triplet excited state (T_1) by intersystem crossing (ISC). Due to its symmetry forbidden relaxation to the ground state, T_1 is the longest-lived excited state. Although both excited states (S_1 and T_1) can react by single-electron transfer (SET) with other substrates, for example, with single-electron acceptors (**A**) or single-electron donors (**D**), SET events are limited by the average lifetime of the excited states. Whereas the singlet excited state lifetime lies in the nanoseconds range, the T_1 state can last up to several microseconds (depending on the catalyst) and therefore is more available for SET between substrates and the photocatalyst.^[16,17] With their long-lived triplet excited states, transition metal-based photocatalysts often offer better reactivity for bimolecular quenching events.^[18]

Considering that the excited states can both act as a reductant or oxidant, two different catalytic cycles are possible once the excited species has been formed. These two modes of action are summarised in **Figure 3**.

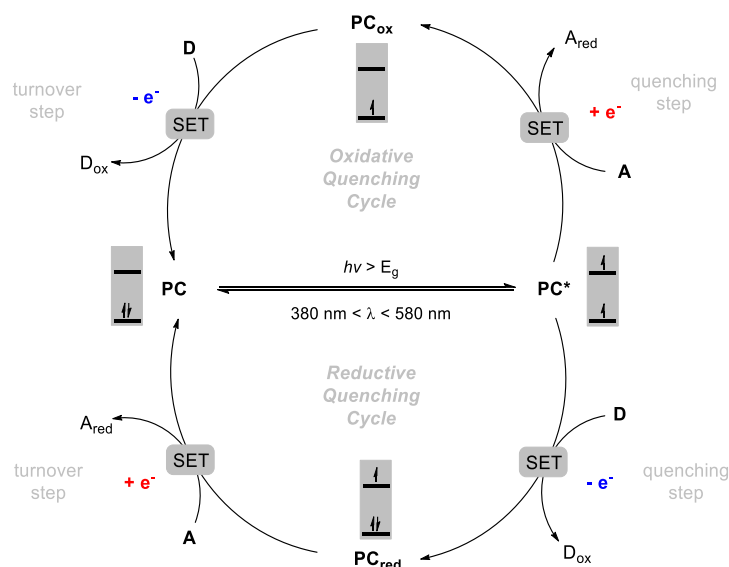


Figure 3 – Reductive and oxidative quenching cycles of the excited photocatalyst (PC^*).

If the excited PC^* (either S_1 or T_1) species is first quenched by an electron acceptor (**A**) it will be an oxidative quenching cycle (from the point of view of the catalyst). Alternatively, in the reductive quenching cycle, the excited species first abstracts an

electron from an electron donor (**D**). In each case, the quenching step of the excited **PC*** species generates a highly oxidised **PC_{ox}** or reduced **PC_{red}** species that requires a subsequent reduction or oxidation respectively (turnover step) to regenerate the ground state **PC**.^[16]

Both an electron donor (**D**) and an electron acceptor (**A**) need to be present to allow catalytic reactions to take place. The photoredox catalyst is a single-electron mediator that will help to transfer an electron from a donor to an acceptor in order to generate highly reactive open-shell species.^[25,26]

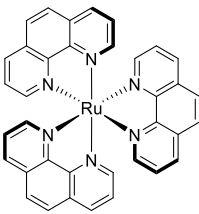
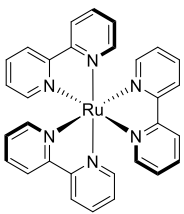
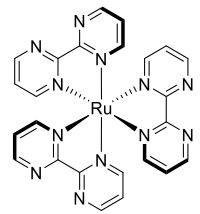
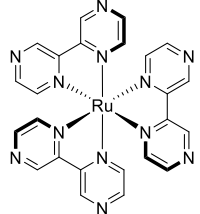
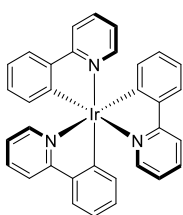
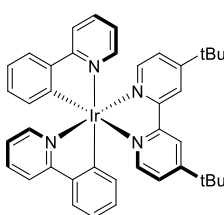
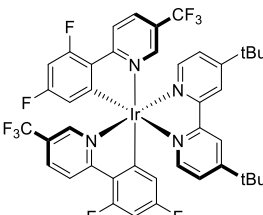
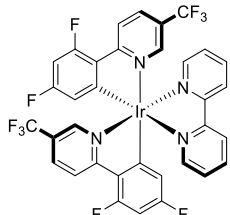
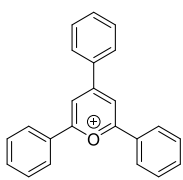
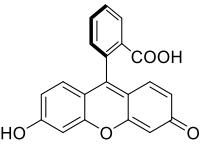
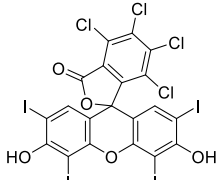
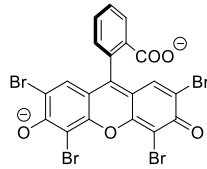
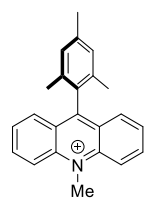
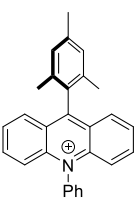
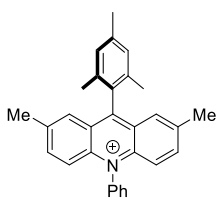
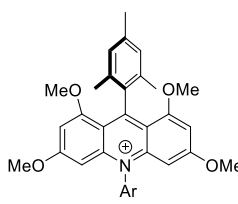
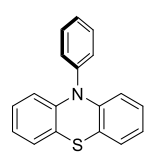
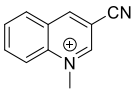
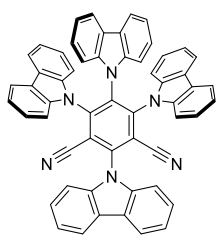
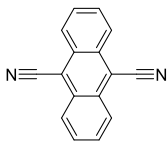
1.1.3 Practical photoredox catalysis

1.1.3.1 Photocatalyst selection

A crucial factor in the development of new photoredox methods is the catalyst selection. Appropriate catalysts can be selected based on the redox potentials needed to oxidise/reduce the desired species (**A** and **D**). Irradiation wavelength (and thus light source selection) is then fixed according to the absorption region of the ground state species of the chosen catalyst. If no absorption data is available, the colour of the catalyst itself can serve as a guide for light source selection. Bright yellow to light orange powders will absorb better in the blue light region (*e.g.* ruthenium and iridium complexes), darker orange to red will preferably absorb green light (*e.g.* eosin Y) and blue catalysts absorb red light preferentially (*e.g.* methylene blue).

Examples of commonly used photocatalysts are presented in **Table 1**. Although other transition metal complexes can be used as photosensitisers,^[27] ruthenium and iridium polypyridyl complexes are by far the most employed catalysts in synthetic photoredox catalysis. Indeed, these complexes both combine visible light absorption, long excited state lifetimes and high ISC yields. However, there are some differences between the two most used metal complexes. Using iridium instead of ruthenium allows the production of stronger oxidising species. This is because iridium needs to be at the +III oxidation state to reach the low-spin d^6 configuration to allow octahedral ligand substitution, whereas ruthenium must be at the +II oxidation state. Also because of its higher oxidation state, iridium is capable of accommodating orthometallated ppy-derived ligands (LX type) to compensate its electron-deficiency.^[28]

Table 1 – Commonly employed visible light absorbing homogeneous photocatalysts.

Transition metal based photocatalysts			
 <p>[Ru(phen)₃]²⁺ = Ru-1 $E_{1/2}^{ox/*} = -0.87$ V $E_{1/2}^{*/red} = +0.82$ V</p>	 <p>[Ru(bpy)₃]²⁺ = Ru-2 $E_{1/2}^{ox/*} = -0.81$ V $E_{1/2}^{*/red} = +0.77$ V</p>	 <p>[Ru(bpm)₃]²⁺ = Ru-3 $E_{1/2}^{ox/*} = -0.21$ V $E_{1/2}^{*/red} = +0.99$ V</p>	 <p>[Ru(bpz)₃]²⁺ = Ru-4 $E_{1/2}^{ox/*} = -0.26$ V $E_{1/2}^{*/red} = +1.45$ V</p>
 <p>fac-Ir(ppy)₃ = Ir-1 $E_{1/2}^{ox/*} = -1.73$ V $E_{1/2}^{*/red} = +0.31$ V</p>	 <p>[Ir(ppy)₂dtbpy]⁺ = Ir-2 $E_{1/2}^{ox/*} = -0.96$ V $E_{1/2}^{*/red} = +0.66$ V</p>	 <p>[Ir(dF(CF₃)ppy)₂dtbpy]⁺ = Ir-3 $E_{1/2}^{ox/*} = -0.89$ V $E_{1/2}^{*/red} = +1.21$ V</p>	 <p>[Ir(dF(CF₃)ppy)₂bpy]⁺ = Ir-4 $E_{1/2}^{ox/*} = -1.00$ V $E_{1/2}^{*/red} = +1.32$ V</p>
Organic dyes			
 <p>Triphenylpyrylium = TPP $E_{1/2}^{gd/red} = -0.32$ V $E_{1/2}^{*/red} = +2.55$ V</p>	 <p>Fluorescein = FL $E_{1/2}^{gd/red} = -1.17$ V $E_{1/2}^{*/red} = +1.25$ V</p>	 <p>Rose bengal = RB $E_{1/2}^{gd/red} = -0.99$ V $E_{1/2}^{*/red} = +1.18$ V</p>	 <p>Eosin Y = EY $E_{1/2}^{gd/red} = -1.08$ V $E_{1/2}^{*/red} = +1.23$ V</p>
 <p>Mes-Acr-1 $E_{1/2}^{gd/red} = -0.57$ V $E_{1/2}^{*/red} = +2.08$ V</p>	 <p>Mes-Acr-2 $E_{1/2}^{gd/red} = -0.57$ V $E_{1/2}^{*/red} = +2.08$ V</p>	 <p>Mes-Acr-3 $E_{1/2}^{gd/red} = -0.57$ V $E_{1/2}^{*/red} = +1.90$ V</p>	 <p>Ar = 3,5-dimethoxyphenyl Mes-Acr-4 $E_{1/2}^{gd/red} = -0.82$ V $E_{1/2}^{*/red} = +1.65$ V</p>
 <p>10-phenyl-phenothiazine $E_{1/2}^{ox/*} = -2.1$ V $E_{1/2}^{ox/gd} = +0.68$ V</p>	 <p>3-cyano-1-methylquinolinium $E_{1/2}^{gd/red} = -0.60$ V $E_{1/2}^{*/red} = +2.72$ V</p>	 <p>4CzIPN $E_{1/2}^{gd/red} = -1.21$ V $E_{1/2}^{*/red} = +1.35$ V</p>	 <p>dicyanoanthracene = DCA $E_{1/2}^{gd/red} = -0.91$ V $E_{1/2}^{*/red} = +1.99$ V</p>

Finally, iridium complexes can be heteroleptic without losing their photoactivity. This property allows them to separate, in space, the HOMO and LUMO of the complex more efficiently and thus enables the variation of one potential without affecting the other. For these reasons, iridium complexes are more tuneable catalysts and will be able to achieve more challenging oxidations and reductions than the homoleptic ruthenium-based polypyridine complexes. Substituents on ligands also alter redox potentials. As a general rule, electron-donating substituents on the ligands render the complex more strongly reducing, while electron-withdrawing substituents cause the complex to be more strongly oxidising.

Organic dye photocatalysts are rising competitors to commonly used transition metal ones, they also feature a high structural diversity and therefore interesting optimisation possibilities.^[17] Despite their usually shorter excited state lifetimes, they show an impressive range of redox potential windows. There are few strongly reducing dyes, with 10-phenyl-phenothiazine most likely being the best example of this family.^[29] Fluorescein to Eosin Y^[30–32] and the more recently developed donor-acceptor scaffolds such as 4CzIPN^[33] offer a well-balanced and large redox window comparable to the commonly used **Ir-3** and **Ir-4** catalysts. Another class of donor-acceptor scaffold is the strongly oxidising mesityl-acridinium dyes family. The 9-mesityl-10-methylacridinium (**Mes-Acr-1**) was originally developed by Fukuzumi^[34] and further optimised by Nicewicz (**Mes-Acr-2** to **Mes-Acr-4**)^[35]. The strongest single-electron-oxidant is probably 3-cyano-1-methylquinolinium^[36] that can be used to perform extremely challenging oxidations.

1.1.3.2 Standard reduction potential notation and uses

Standard reduction potentials are commonly used to assess the thermodynamic feasibility of the single-electron transfer (SET) reactions studied.^[17] In the general notation, $E_{1/2}^{\text{ox/red}}$ is the electrochemical reduction potential of the half reaction written in the direction of the reduction: $\text{ox} + e^- \rightarrow \text{red}$. This value is given in volts against the saturated calomel electrode (SCE), usually measured in acetonitrile.^[37]

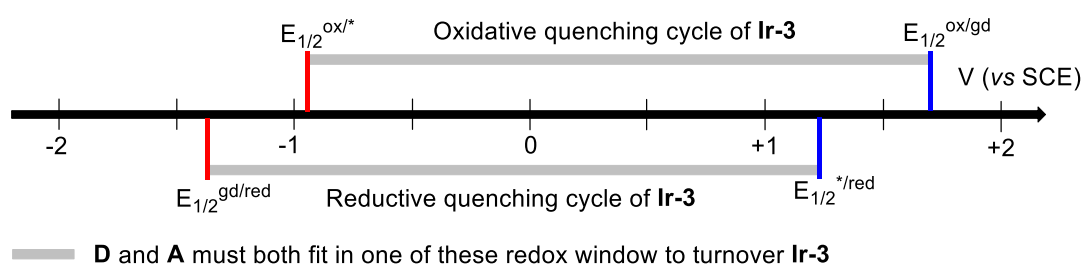
For photocatalysts, the full notation will be employed to avoid confusion between the four species that can exist. For example, in a reductive quenching cycle, the potential associated with the half reaction: $\text{PC}^* + e^- \rightarrow \text{PC}_{\text{red}}$ is written as $E_{1/2}^{*/\text{red}}(\text{PC})$ and the

potential for the consecutive turnover reaction $\text{PC} + e^- \rightarrow \text{PC}_{\text{red}}$ is written as $E_{1/2}^{\text{gd/red}}$ (**PC**) (where “gd” stands for ground state).

For electron acceptors (**A**) and donors (**D**), a simpler notation will be employed. The standard reduction potential associated with the reaction $\text{A} + e^- \rightarrow \text{A}_{\text{red}}$ is written E_{red} (**A**) to shorten the expression $E_{1/2}^{\text{A/A}_{\text{red}}}$, this can also be read as “reduction potential of **A**”. For electron donors, the reaction potential associated with the reaction $\text{D}_{\text{ox}} + e^- \rightarrow \text{D}$ is referred to as E_{ox} (**D**) ($= E_{\text{red}}(\text{D}_{\text{ox}})$) to simplify the $E_{1/2}^{\text{D}_{\text{ox}}/\text{D}}$ notation, this could also be read as “oxidation potential of **D**”.

To approximate the thermodynamic feasibility of an electron transfer reaction, the simplification of the Gibbs free energy of electron transfer equation can be used.^[17] By neglecting the electrostatic work, the relation $E_{1/2}^{\text{ox1/red1}} > E_{1/2}^{\text{ox2/red2}}$ means a negative variation of Gibbs free energy for the reaction $\text{ox1} + \text{red2} \rightarrow \text{ox2} + \text{red1}$ that will be thermodynamically favoured in the forward direction.

Using this rule, one can draw the redox potentials of a photocatalyst on a linear axis to visually “predict” the thermodynamic feasibility of electron transfer reactions (**Scheme 1**). The resulting grey area is where both E_{red} (**A**) and E_{ox} (**D**) must lie to successfully quench and turnover the photoredox catalyst. This is a convenient approach to think about these electron transfer reactions since reduction potentials are measurable (using electrochemical measurements) and many research groups publish these values against reference electrodes.^[37]



Scheme 1 – Reduction potential axis picturing the redox window of the Ir-3 catalyst in its oxidative and reductive quenching cycles.

Notably, we can see that the oxidative quenching cycle generates a highly oxidised PC_{ox} species that is a better oxidant than PC^* ($E_{1/2}^{\text{ox/gd}} > E_{1/2}^{\text{*/red}}$). The same observation can be made for the reducing quenching cycle where the highly reduced PC_{red} is a more potent reducer than PC^* ($E_{1/2}^{\text{ox/*}} > E_{1/2}^{\text{gd/red}}$). Also, more difficult oxidations or reductions can be performed with these more reactive species and the potentials of these should be

considered when planning a photoredox reaction. If the redox potentials of the species used do not fit in either of these windows, a triplet-triplet energy transfer pathway can be suggested.^[16] This process, however, accounts for a minority of the reactivities observed using photoredox catalysis and is not easy to prove experimentally. Therefore, this process will not be described in further detail in this thesis.

1.1.3.3 Overall redox balance

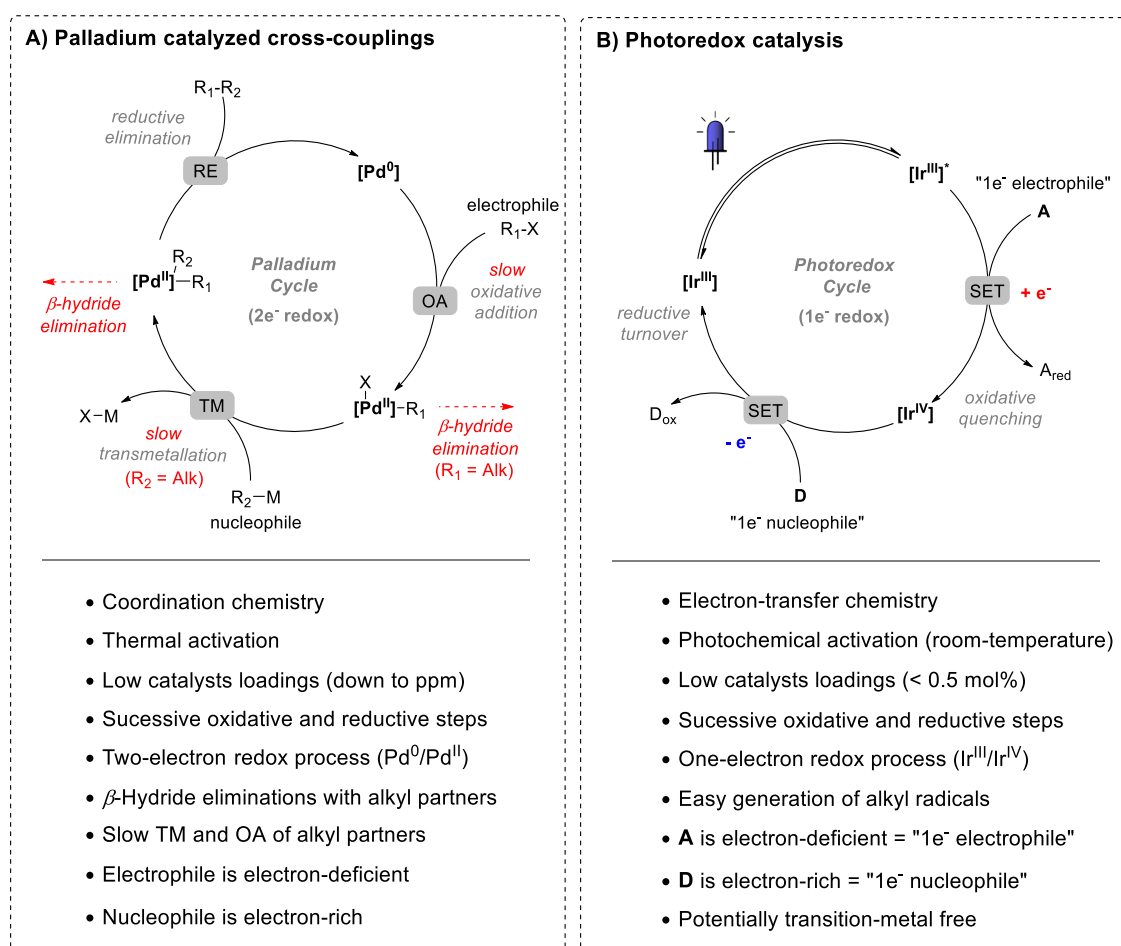
With these considerations in mind, the last thing to rationalise before engaging in the development of a photoredox reaction is the overall redox balance of the transformation. Photoredox reactions fall into three categories: net oxidative, net reductive, and net redox-neutral reactions. In fact, the desired reactive species may not fit in either of the reductive or oxidative redox windows of the catalyst. In this case, an external oxidant (**D**) or reductant (**A**) can be used to initially quench **PC*** and generate the highly oxidised (**PC_{ox}**) or reduced (**PC_{red}**) species. If the only purpose of **D** or **A** is to quench (or turnover) the photocatalyst (*i.e.* sacrificial purpose) the transformation will be categorised as respectively net oxidative or net reductive. In general, these transformations could be achieved without using photoredox catalysis by stoichiometric single-electron transfer reagents^[38] or electrochemical^[39] methods.

Net redox-neutral reactions, on the other hand, are much more challenging to achieve without the tool of photoredox catalysis. As opposed to the other two categories, they do not require any sacrificial oxidant or reductant to turn the photocatalytic cycle over. They are more attractive in the sense that all electron transfer events are synthetically relevant and therefore do not conceptually generate stoichiometric waste products. Even though net redox-neutral transformations can present a considerable number of productive radical chains,^[40] they remain the most synthetically interesting class of photoredox reactions.

1.2 Strategies for photoredox C–C cross-couplings

1.2.1 A parallel with palladium-catalysed cross-couplings

Throughout this project, we have been interested in assessing the potential of photoredox catalysis to achieve predictable and scalable C–C cross-couplings. Therefore, it seemed legitimate to compare its mode of action to one of the most widely used C–C bond forming process, namely: the Nobel-awarded palladium-catalysed cross-coupling paradigm. Even though they both rely on a distinct class of interaction with the substrates (coordination chemistry vs. electron-transfer chemistry), it is instructive to compare their catalytic cycles side-by-side (**Scheme 2**).



Scheme 2 – Comparison of palladium and photoredox catalytic cycles.

On the left side, palladium cross-couplings rely on a thermally activated catalytic cycle involving coordination chemistry and organometallic species. Extensive optimisation possibilities combined with intensive development over decades resulted in fine-tuned

conditions for a virtually infinite number of coupling-partners.^[41] However, common hurdles to these palladium-catalysed methodologies remain, such as the involvement of C(*sp*³) nucleophiles and electrophiles. Alkyl substrates are usually associated with slow transmetallation and oxidative addition steps.^[42] Additionally, the presence of β -hydrogens allows competitive β -hydride elimination and thereby compromising the outcome of these coupling reactions. To tackle these issues innovative approaches have been implemented, including Fu's impressive work.^[43] For example, he uses nickel catalysts able to react *via* single-electron transfers to cross-couple C(*sp*³) electrophiles, thereby circumventing the slow oxidative addition step. Faster "one-electron" transmetallation steps are also observed in nickel couplings with C(*sp*³) nucleophiles able to generate carbon radicals.^[44,45]

On the right side of **Scheme 2**, we see a chance in photoredox catalysis to aid these alkyl partner coupling issues. Just like nickel, photoredox catalysis enables single-electron transfer reactions. The conditions are synthetically extremely interesting since it only requires a minute amount of a photocatalyst to proceed at room temperature with only visible light irradiation. Interestingly, like the palladium cycle, it also consists of successive oxidative and reductive steps with the distinction that they are one-electron redox steps instead of two. Another similarity is the electronic-demand of the substrates that interact in the catalytic cycles. The electron acceptor (**A**) is an electron-deficient species able to accept an electron and could therefore be considered as a "one-electron electrophile". In parallel, the electron donor (**D**) is an electron-rich species and could be referred as a "one-electron nucleophile". In a redox-neutral setting, this paradigm could be used to cross-couple one-electron electrophilic entities to one-electron nucleophilic ones. This process could somehow mimic the mode of action of the palladium-catalysed cross-couplings in a "one-electron" fashion, provided that selective mechanisms allow their combinations. During the course of this writing, reports of visible light-triggered excited state palladium and copper catalysis enabled challenging alkyl electrophile substrates to be engaged in cross-coupling reactions *via* electron-transfer.^[46-48] These recent communications further demonstrate the growing importance of electron-transfer processes in cross-couplings.

Finally, another drive for exploring these reactions is the possibility of using photoredox reactions under strictly "transition metal free" conditions. Indeed, the electron transfer mechanisms of the catalytic cycles do not require the employment of transition metals

and could, therefore, become a cleaner and more sustainable alternative to the classic transition metal-based chemistry.

1.2.2 Carbon radical generation

With this hypothesis in mind, we need to be more specific about the nature of the electron donors and acceptors that will be used in the photoredox catalysis cycle. When thinking of performing C–C coupling reactions using single-electron transfer chemistry, the reactive intermediates must be open-shell carbon species. This means intermediates involved in these reactions would either be carbon radical cations, carbon radical anions or neutral carbon radicals. We will refer to them under the more general terms of “carbon-centred radicals” or “carbon radicals”.

Using this rationale, the initial step of a photoredox-based C–C cross-coupling is the generation of a carbon radical from a spin-paired precursor. The nature of these precursors and the mechanisms leading to these reactive intermediates are described in this section (1.2.2). In stark contrast with classic radical generation methods, typically making use of direct photolysis with non-selective UV-irradiation or radical initiators,^[49] photoredox catalysis enables a mild and catalytic generation of radicals. This paradigm shift enables an unprecedented control over these reactive species. Firstly, the catalytic nature of the radical initiator often allows to circumvent commonly observed radical chain terminations like dimerisation or disproportionation side-reactions.^[50,51] Secondly, redox-neutral reactions that cannot sustain a radical chain mechanism are made possible using the photoredox catalyst as the electron mediator.^[52]

Strategies to generate carbon radical intermediates using photoredox catalysis can be categorised in two main groups, carbon radicals formation *via* direct SET with organic substrates (1.2.2.1) or *via* hydrogen atom transfer (HAT) pathway (1.2.2.2).

1.2.2.1 Using single-electron transfer

Before the generalisation of photoredox catalysis, redox methods to generate carbon-radicals were making use of stoichiometric single-electron oxidant/reductants, electrochemical methods or UV light-based photoinduced electron transfers.^[38,49] The extensive amount of existing research in electron transfer chemistry allowed an initial fast progression of the field of photoredox catalysis.^[53] Also, by providing a simple setup and

rationale to predict these reactions and carry them out selectively, photoredox catalysis enabled a multitude of new applications building on these previous discoveries. This section presents the redox methods commonly used to generate carbon radicals using photoredox catalysis.

The generation of carbon radicals by direct SET can be organised in two subgroups: organic radicals produced *via* a single-electron oxidation of electron donors (left part in **Figure 4**) and carbon radicals generated *via* a single-electron reduction of electron acceptors (right part in **Figure 4**).^[54–56]

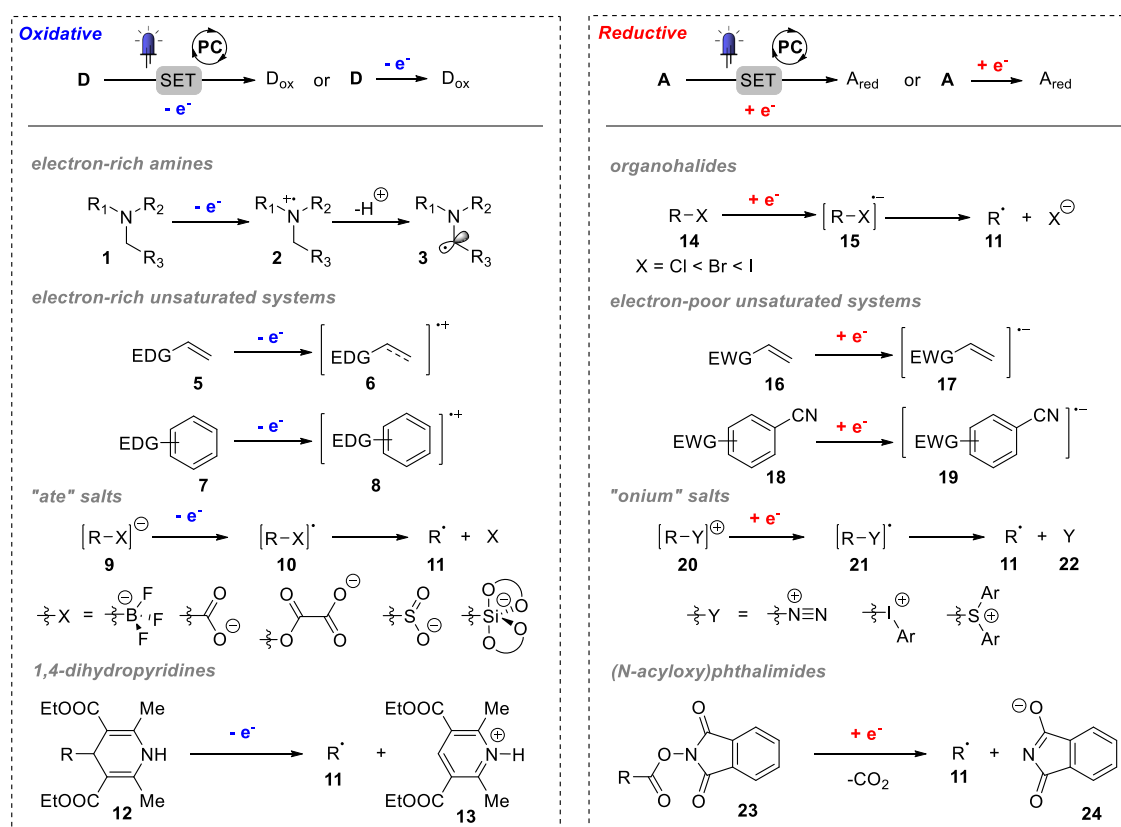


Figure 4 – Common oxidative and reductive approaches to carbon radicals using photoredox catalysis.

The first group (on the left) is composed of electron-rich organic molecules that readily donate an electron to the photoredox catalyst. Electron-rich tertiary amines (**1**) are good single-electron donors and will readily give an electron (typically $E_{\text{ox}}(\mathbf{1}) = +0.7 - +1.0 \text{ V}$)^[57] to generate an amino radical cation (**2**) which can rearrange upon deprotonation to form a neutral α -amino radical (**3**). Extensive chemistry involving these radical intermediates has been developed, marking a new era for amine α -functionalisation.^[58] Although being typically challenging ($E_{\text{ox}}(\mathbf{5} \text{ or } \mathbf{7}) = +1.5 -$

+2.5 V)^[37], the direct oxidation of electron-rich unsaturated systems (**5** and **7**) has been increasingly used, especially since the rise of strongly oxidative mesityl acridinium dyes.

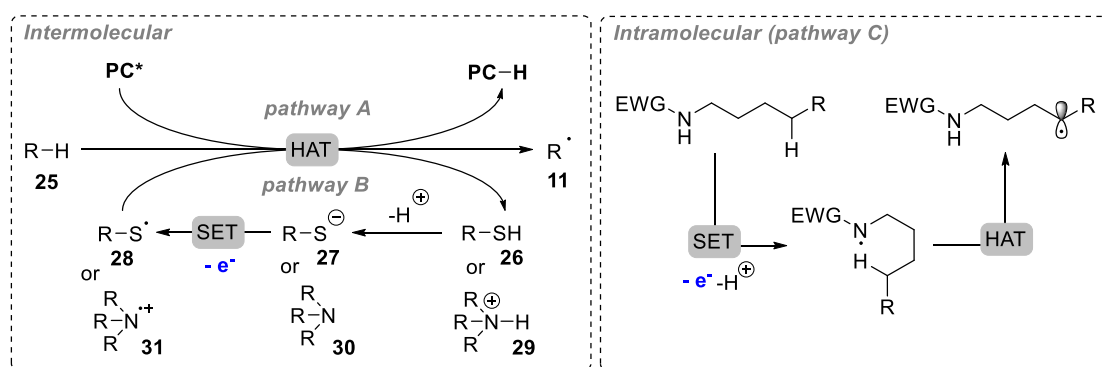
This strategy enables interesting transformations such as cycloadditions^[12,59] and anti-Markovnikov hydrofunctionalisations^[60] using **6** intermediates and arylations of amines using **8** intermediates^[61]. A more common strategy to oxidatively generate carbon radicals is to single-electron oxidise electron-rich “ate” salts (**9**), such as organoborates^[62], carboxylates^[63], oxalates,^[64] sulfonates^[65,66] or silicates^[67,68]. The transient neutral radical (**10**) generated undergoes a C–X cleavage to produce a carbon radical (**11**) that can be used to conduct alkylation reactions. This method is often used to produce reactive C(*sp*³) radicals from less “electronically biased” starting materials since they usually do not require extra electron-donating substituents.^[55] This approach will be described in more detail in the following section (*cf.* 1.2.3). Finally, 1,4-dihydropyridines (**12**) represent a neutral functional group alternative to this practice. Similarly, they can undergo single-electron oxidation ($E_{\text{ox}}(\mathbf{12}) = +1.05 \text{ V}$) to generate a neutral carbon radical (**11**) and a protonated pyridine (**13**).^[69,70]

The second group is composed of electron-poor organic substrates that can potentially accept an electron from the photocatalyst. Organohalides (**14**) have been widely used, for example, generating a transient radical anion (**15**) which subsequently eliminates a halide anion to produce neutral alkyl or aryl radicals (**11**).^[71–73] The ease of reduction increases descending in the halogen series (Cl < Br < I). Electron-deficient unsaturated systems (**16** and **18**) can also be single-electron reduced, an interesting example being the reduction of electron-deficient cyanoarenes ($E_{\text{red}}(\mathbf{18}) = -2.4 - -1.61 \text{ V}$)^[37] that have been widely exploited for arylation chemistries^[74–76] and will be discussed in more detail in the following section (1.2.3). Electrophilic “onium” salts (**20**), can also easily accept an electron to generate a transient radical (**21**) prone to eliminate a spin-paired leaving group (**22**) and produce a carbon-centred radical (**11**). This strategy can be used to generate aryl radicals from aryl diazonium salts ($E_{\text{red}} = -0.1 \text{ V}$)^[77,78] or diaryliodonium salts^[79] and the trifluoromethyl radical from Umemoto’s reagent ($E_{\text{red}} = -0.4 \text{ V}$)^[80,81]. To finish, (N-acyloxy)phthalimides (**23**) or N-hydroxyphthalimide esters (NHPI) have been longstanding alkyl radical precursors using photoredox systems.^[82] Upon one-electron reduction of the phthalimide moiety ($E_{\text{red}}(\mathbf{23}) = -1.2 \text{ V}$), they rapidly undergo a decarboxylative collapse leaving behind the desired carbon radical (**11**).

1.2.2.2 Using hydrogen atom transfer

The formal transfer of a hydrogen atom has also been used as a strategy to form carbon-centred radicals with photoredox catalysis. Among the other atom transfer processes, hydrogen atom transfer is the most synthetically interesting since it enables a formal C–H functionalisation. This process relies on the ability of some radical species to abstract homolytically a weakly bonded hydrogen atom, the driving force being the resulting stronger bond created in the process.

Some specific photocatalysts such as tetrabutylammonium decatungstate can directly abstract hydrogen atoms from their excited states (*pathway A* in **Scheme 3**).^[83] Another approach making use of simple HAT co-catalysts have been developed by the MacMillan group (*pathway B* in **Scheme 3**). Commonly used HAT co-catalysts are thiols (**26**)^[76,84,85] or quinuclidine (**30**)^[86] derived and are compatible with photoredox cycles.



Scheme 3 - Hydrogen Atom Transfer (HAT) mechanisms.

The mechanism starts with the single-electron oxidation of the HAT co-catalyst (**27** and **30**) by the photoredox catalyst to generate either a thiyl radical (**28**) or an amine radical cation (**31**). These radicals are known to be involved in the homolytic cleavage of weak C–H bonds (from **25**) *via* hydrogen atom abstraction, generating the desired carbon-centred radical (**11**). The protonated co-catalysts (**26** and **29**) are then reactivated by the simple action of a base. Prediction of the feasibility of hydrogen atom abstractions can be carried out using bond dissociation energies (BDE) of C–H bonds.^[76] Intramolecular variants of this process have recently flourished, allowing the generation of carbon radicals at distal positions of nitrogen atoms (pathway C).^[87,88] These methods offer complementary approaches to the direct SET activation of organic substrates to generate carbon-centred radicals.

1.2.3 Redox-neutral photoredox C–C cross-couplings

Now that the nature of the precursors and the mechanisms underlying carbon radicals generation have been presented, the subsequent engagement of these species in C–C cross-couplings is described. Since net redox-neutral conditions are synthetically the most interesting ones and the most specific to photoredox systems, it was decided to limit this brief review to this category of transformations.

1.2.3.1 Carbon radical reactivities

In a general sense, intermolecular C–C bond forming reactions with radical intermediates are challenging tasks.^[89] The intermediacy of the species involved coupled to the concentration effects, arising from the bimolecular nature of the coupling, makes it more laborious than intramolecular reactions.^[90] In order to successfully engage carbon radicals in cross-couplings, it is important to understand their reactivity.

Carbon-radicals are generally highly reactive species, but this does not mean that they cannot operate selectively. A general rule is that they proceed towards the formation of the strongest bonds (thermodynamic control).^[91] Also, as neutral species, radicals are not affected much by coulombic interactions, making their addition to polarised groups unfavourable. In analogy to “soft” nucleophiles and electrophiles, the chemical reactivity of radicals is mostly dictated by frontier orbitals interactions.^[92] A typical example is the different reactivity trends observed for the additions of carbon radicals to olefins. Carbon radicals can be stabilised by both adjacent electron-withdrawing and donating groups. These groups are directly affecting the energy levels of the singly occupied molecular orbitals (SOMOs) of these reactive species, resulting in a different “character” of the radicals (**Figure 5**).^[93]

As observed in this figure, the low-energy SOMO of **33** resulting from an adjacent electron-withdrawing group have a better overlap with the HOMO of an electron-rich alkene (**32**), making **33** an “electrophilic” radical. On the other hand, the high-energy SOMO of **34** can favourably interact with the LUMO of an electron-deficient alkene (**35**), resulting in a “nucleophilic” character of the radical **34**. This principle of radical “characters” will further help us to rationalise successful radical coupling reactions based on the nature of the radicals employed.

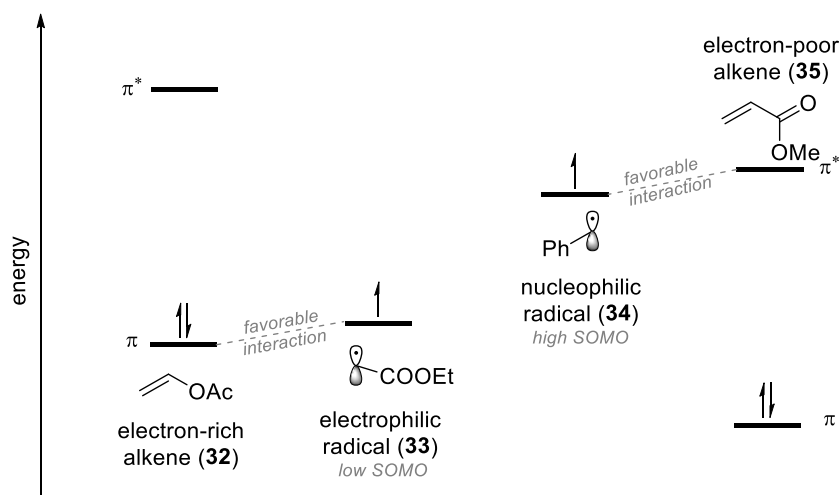


Figure 5 – Frontier orbital diagram explaining the reactivity preferences of different carbon radicals.^[93]

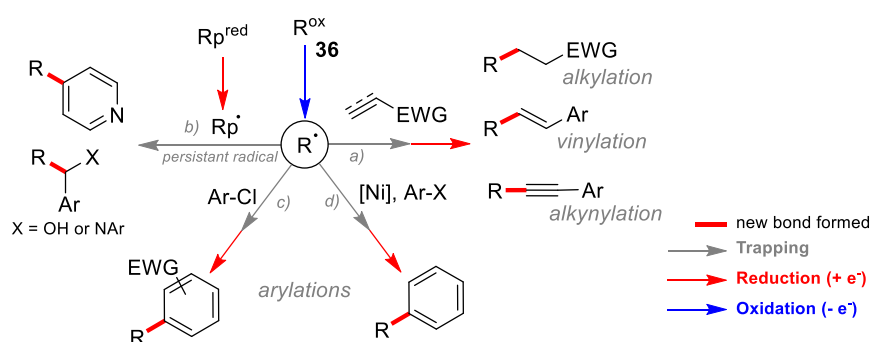
An important consequence of these unequal energy levels are the different redox potentials of nucleophilic and electrophilic radicals. Because of this, radical intermediates can be subject to single-electron transfers in photoredox catalysis cycles. This phenomenon is generally referred as a radical-polar crossover event, where radicals are transformed into ionic closed-shell species. An electron-rich benzylic radical (**34**), for example, is easily oxidised ($E_{\text{ox}}(\mathbf{34}) = +0.8 \text{ V}$) to its corresponding carbocation and the electrophilic α -ester radical is easily reduced ($E_{\text{red}}(\mathbf{33}) = -0.6 \text{ V}$) to its corresponding carbanion.^[89] These common reactivities need to be thoroughly considered in order to plan successful coupling strategies.

1.2.3.2 Neutral couplings using oxidative radical precursors

The following redox-neutral strategies for photoredox C–C coupling reactions are organised based on the nature of the radical precursors (pro-oxidative = R^{ox} or pro-reductive = R^{red}). This organisation is used since the strategy is usually fixed based on the choice of the radical precursor. This classification only clashes if the radical selectively couples to another transiently generated radical, which is commonly disregarded as a productive approach.^[16] However, this does not exclude the possibility for this transient (short-lived) radical to couple with a persistent (long-lived) radical as it will be discussed in the next section (1.2.3.2). In the latter case, the transient radical precursor will be considered as the reference radical precursor. Finally, generation of radicals using HAT

catalysts formally falls under the category of “oxidative radical precursors” since the HAT catalysts are oxidatively activated (*cf.* **Scheme 3**).

Net redox-neutral photoredox couplings strategies relying on an oxidative carbon radical formation are described in **Scheme 4**. Once the oxidative generation (blue arrow) of the carbon radical from **36** (pro-oxidative carbon-radical precursor) is achieved, an effective trapping method (grey arrows) needs to be employed to selectively couple the carbon-radical intermediate. In order to neutrally close the redox cycle, a complementary single-electron reduction (red arrow) needs to take place. This interdependent step can be used to activate the other coupling partner when the transient radical is coupled with a persistent radical (b), or to regenerate a closed shell-species after the trapping of the radical (a, c, or d).



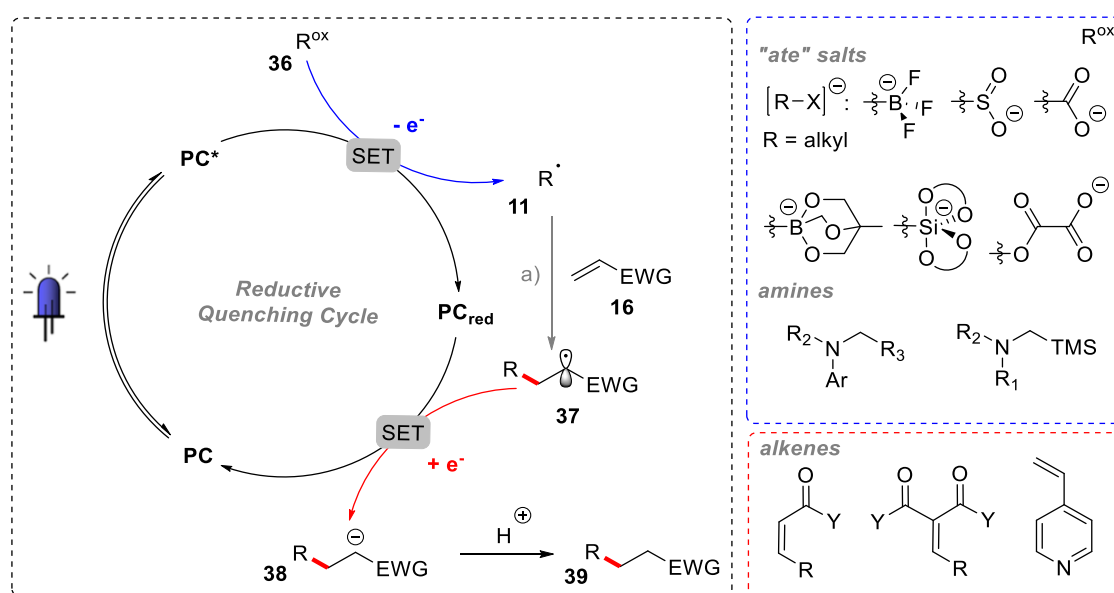
Scheme 4 – Redox-neutral photoredox C–C coupling using oxidative radical precursors (R^{ox}).

a) Addition to C–C multiple bonds

Even though this is not a general rule, oxidatively generated carbon radicals tend to be nucleophilic. This is often the case because oxidation sensitive substrates have to be electron-rich, also if the substrate keeps its electron rich-character at the radical stage, the corresponding radical will be nucleophilic. Therefore, an effective way to trap oxidatively generated radicals intermolecularly is to use electrophilic olefins with a low lying LUMO (*cf.* **Figure 5**). These trapping methods have been one of the most used redox-neutral photoredox C–C cross-coupling procedures (**Scheme 5**).

Radical couplings with electron-deficient olefins are often referred as “Giese-type” additions. They have been exemplified through a wide range of oxidative alkyl radical precursors including trifluoroborates and trialkoxyborates,^[80,94,95] carboxylates,^[96] oxalates,^[64] silicates,^[67] and sulfinates^[65] but also electron-rich tertiary amines^[97] or α -silylamines^[98]. The catalysts used for these couplings are usually strong oxidants such as

Ir-3, **Ir-4** or **Mes-Acr-1**, often proceeding *via* a reductive quenching cycle. The mechanism starts with the single-electron oxidation of the radical precursor (**36**) to lead to a neutral carbon radical (**11**).



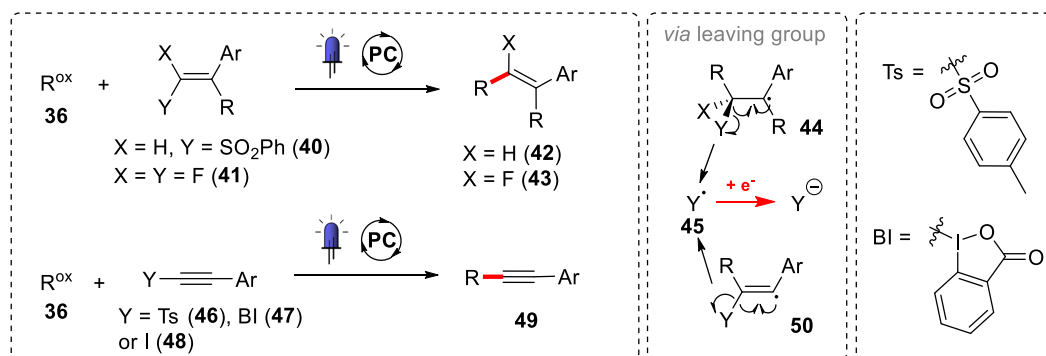
Scheme 5 – Mechanism for photoredox-catalysed alkylation with electron-deficient olefins.

This nucleophilic radical is subsequently trapped by an electron-deficient olefin (**16**), which is often used in excess. The resulting electrophilic radical (**37**) can then undergo a selective reduction to regenerate the ground state photocatalyst (**PC**) and a carbanion (**38**) that is quenched by a proton source to deliver the coupling product (**39**). The reaction proceeds with a wide range of alkyl residues from unactivated primary to tertiary alkanes or activated, α -heteroatom and benzylic positions. Asymmetric variants of this reaction have been successfully developed by Yoon^[99] and Meggers^[100] using a chiral Lewis acid catalyst and by Melchiorre^[101] making use of a chiral iminium olefin acceptors.

Apart from alkylations, radical addition to C–C multiple bonds can also lead to useful vinylation and alkynylation reactions. For example, olefins bearing a sulfonyl group (**40** in **Scheme 6**) can successfully trap nucleophilic radicals generated from carboxylic acids^[102] or tertiary amines^[103].

The radical initially attacks the carbon bearing the sulfone to generate a stabilised benzylic radical (**44**) from which the sulfonyl group can act as a radical leaving group to generate a vinylated product (**42**).^[104] The resulting “open-shell nucleofuge” (**45**) can then be single-electron reduced to close the redox cycle. A similar process making use of *gem*-

difluoro styrenes (**41**) has been recently described leading to interesting mono-fluoroalkenylated products (**43**).^[105]



Scheme 6 – Vinylation and alkynylation reactions based on leaving group strategy.

Based on a similar mechanism, alkynes bearing tosyl (Ts, **46**)^[68], benziodoxolone (BI, **47**)^[106] and iodo (**48**)^[107] leaving groups were successfully employed to deliver alkynylated products (**49**) in a redox-neutral fashion.

b) Coupling with a persistent radical

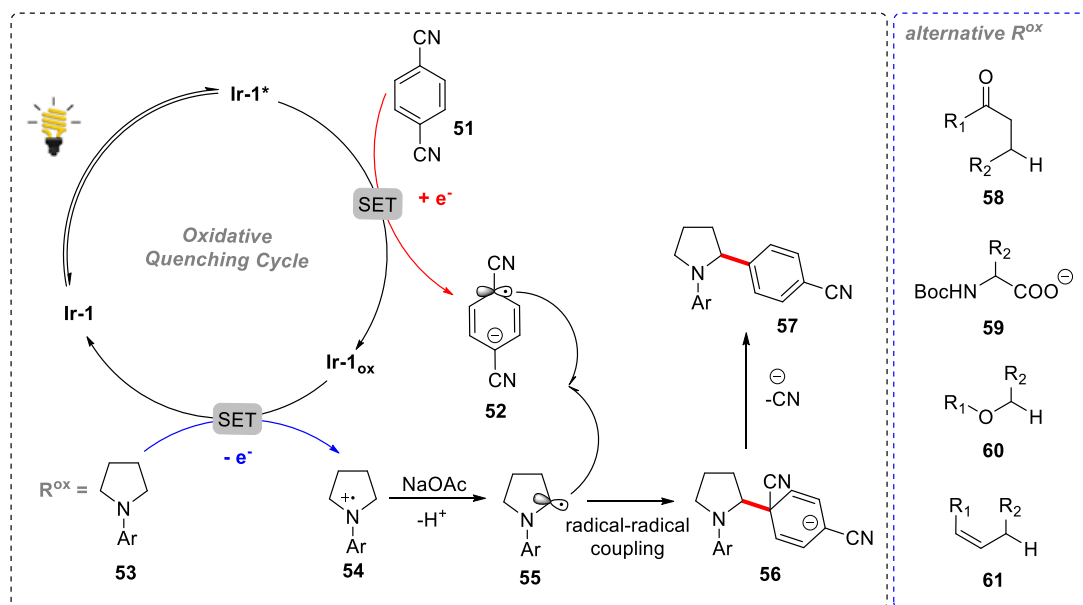
Another approach to engaging radicals in selective bimolecular couplings makes use of the persistent radical effect (PRE).^[108] This kinetic effect demonstrates that if two radicals are generated at the same rate, selective heterocoupling occurs (preferentially to homocoupling) if one of the radical is significantly longer-lived than the other.^[109]

The concept was introduced in the field of photoredox catalysis by MacMillan and co-workers in 2011 to perform selective C–H α -arylation of electron-rich tertiary amines with cyanoarenes.^[74] The proposed mechanism for this arylation (**Scheme 7**) starts with the absorption of a photon by the ground state **Ir-1** to generate the active triplet state **Ir-1***.

This triplet state has a low enough reduction potential ($E_{1/2}^{\text{ox}/*}(\text{Ir-1}) = -1.73 \text{ V}$) to reduce the 1,4-dicyanobenzene ($E_{\text{red}}(\mathbf{51}) = -1.61 \text{ V}$) and form a long-lived radical anion (**52**). **Ir-1_{ox}** ($E_{1/2}^{\text{ox}/\text{gd}} = +0.77 \text{ V}$) which can then oxidise the electron-rich tertiary amine (**53**) leading to the α -amino radical (**55**) after deprotonation. Shortly after its generation, **55** can selectively engage in bimolecular radical-radical coupling with the stabilised radical anion (**52**). The resulting anion (**56**) can then eliminate cyanide to deliver the coupling product (**57**).

This fundamental work led to an extensive development of photoredox arylations by the MacMillan group. The challenging β -arylation of ketones and aldehydes (**58**) was realised

by the single-electron oxidation of their corresponding enamines.^[110] Boc-protected amino acids (**59**) were also successfully engaged in decarboxylative arylations using the same principle.^[63] By making use of a HAT co-catalyst, it was possible to engage weak C–H bonds from ethers (**60**)^[84] or allylic (**61**)^[76] positions in redox-neutral arylations.

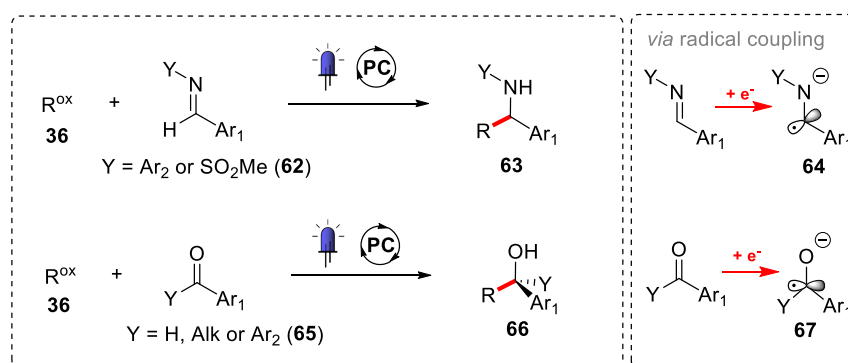


Scheme 7 – Photoredox arylation via a radical-radical coupling with persistent radicals from cyanoarenes.

Inspired by these effective arylation methods, other persistent radicals were engaged in bimolecular radical coupling using similar mechanisms (**Scheme 8**).

Shiff bases derived from benzaldehydes (**62**) are subject to single-electron reduction to generate persistent radical anions (**64**). These were selectively coupled to transiently generated radicals from ethers,^[85] amines,^[111] and silicates^[112], leading to elaborated benzylamines (**63**). The concept was amenable to an enantioselective radical-radical cross-coupling using a chiral Brønsted acid catalyst supposedly forming a chiral radical ion pair with the **64** intermediate.^[113]

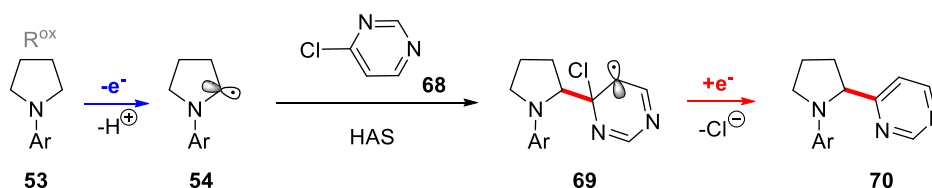
Aldehydes and ketones (**65**) also generate long-lived radical anions (**67**) upon single-electron reduction. Using this reactivity, transient radicals generated from enamines^[114] and tertiary amines^[111] were transformed into benzyl alcohols (**66**). An asymmetric variant of this transformation was also described by Meggers, using a chiral Lewis acid and an iridium-based photocatalyst.^[115]



Scheme 8 – Persistent-radical couplings of imines, aldehydes, and ketones.

c) Homolytic Aromatic Substitution

Homolytic Aromatic Substitution (HAS) is another synthetically interesting redox-neutral cross-coupling strategy. This mechanism is more prevalent in reductive precursors as we will see in the next paragraph (1.2.3.3). However, some examples of this mechanism from oxidative radical precursors have been described. For example, a complementary method for amine C–H α -arylation has been reported by MacMillan using a wider variety of electron-deficient chloroarenes (**Scheme 9**).^[116] In this case, a HAS mechanism is proposed because of the thermodynamic impossibility of reducing the corresponding chloro heteroarenes (**68**) with the iridium photocatalyst **Ir-2** (in contrast to cyanoarenes). The reaction is expected to start with the generation of the α -amino radical (**54**) that can add to the electrophilic heteroarene (**68**) to form a neutral radical (**69**). This radical could be reduced by the photocatalyst to eliminate chloride and deliver the coupling product (**70**).



Scheme 9 – Example of a redox-neutral HAS coupling from an oxidative radical precursor.

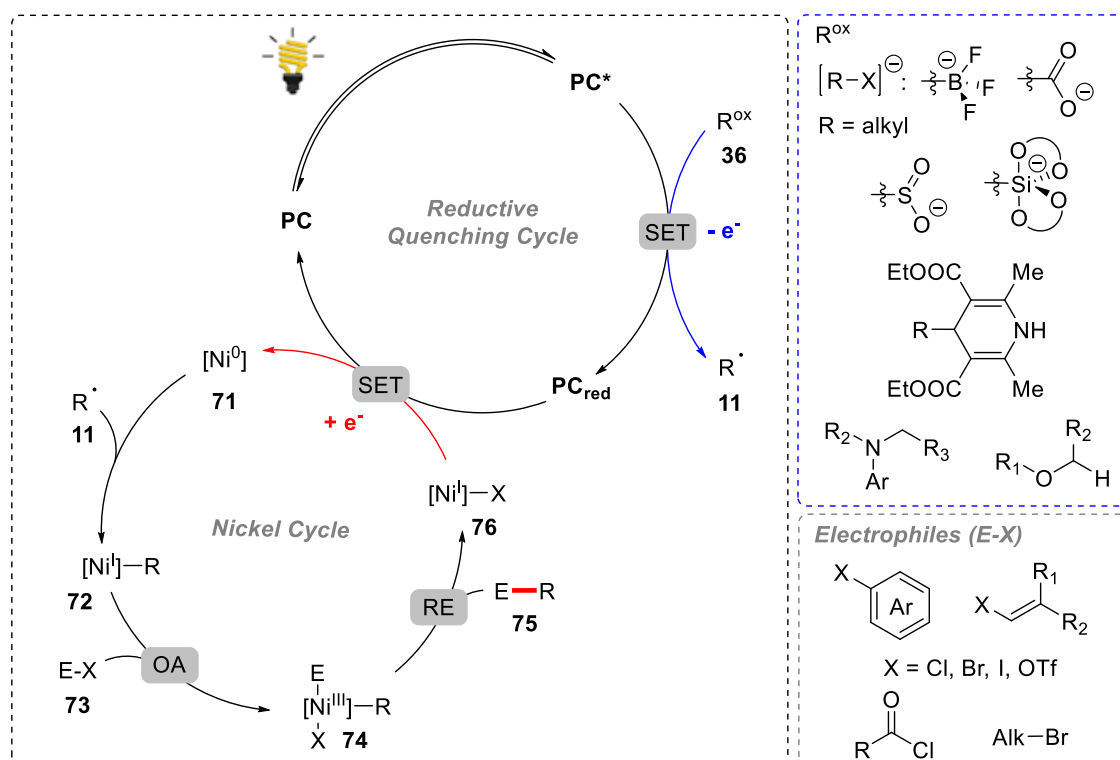
A similar reaction has been disclosed by Weaver and co-workers, however, no postulate on the mechanism was made.^[117]

d) Nickel co-catalysis

While previous coupling strategies were solely relying on the use of a photoredox catalyst, emerging cross-coupling methods make use of an additional nickel

catalyst.^[51,118,119] These methods take advantage of the mild generation of reactive radical intermediates *via* photoredox methods and the ability of nickel to capture nucleophilic radical species (**11**) and perform oxidative addition of two-electron electrophiles (**73**). Using this strategy, Molander^[45] and MacMillan^[44] simultaneously reported a “single-electron transmetalation” of C(*sp*³) radicals on nickel centres in 2014. In these processes, they could couple alkyl trifluoroborates (Molander) or carboxylates (MacMillan) with aryl halides at room temperature to deliver a wide range of C(*sp*²)–C(*sp*³) cross-coupled products.

The general mechanism is depicted in **Scheme 10**: it starts with the reductive quenching of the excited photocatalyst (**PC**^{*}) to deliver a carbon radical (**11**) in an oxidative fragmentation of **36**. This radical (**11**) is then captured by the Ni⁰ complex (**71**) in a so-called “single-electron transmetalation” step. The alkylated Ni^I complex (**72**) can then favourably engage in an oxidative addition of the two-electron electrophile (**73**) to lead to a pentavalent Ni^{III} complex (**74**).^[120] Reductive elimination can then occur from this highly oxidised Ni^{III} (**74**) to deliver the coupling product (**75**) and a Ni^I complex (**76**) that can accept an electron from the **PC**_{red} to restore both the active Ni⁰ species (**71**) and the ground state photocatalyst (**PC**).

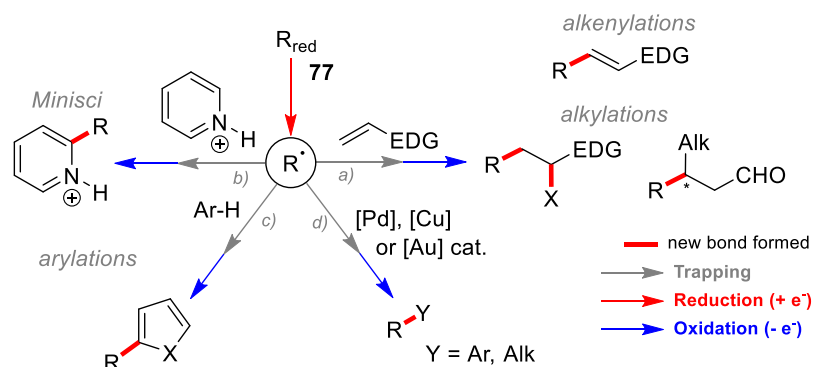


Scheme 10 – General mechanism of the dual nickel and photoredox catalysis paradigm.

Since being reported in 2014, this new paradigm was rapidly applied to a wide variety of coupling partners. The range of oxidative carbon radical precursors (R^{ox} , **36**) was progressively extended, notably to silicates,^[68,121,122] sulfinates,^[66] 1,4-dihydropyridines,^[123] amines,^[124] and ethers^[125] allowing the generation of $C(sp^3)$ radicals from primary^[122], secondary^[126] and tertiary^[127] carbon centres. Alternative two-electron electrophiles (**73**) such as alkenyl,^[121,128,129] acyl,^[130] and even alkyl halides^[131,132] were also successfully engaged using this dual catalysed cross-coupling principle. Finally, this process could be made enantioselective by using chiral ligands to coordinate the nickel centre.^[45,133]

1.2.3.3 Neutral couplings using reductive radical precursors

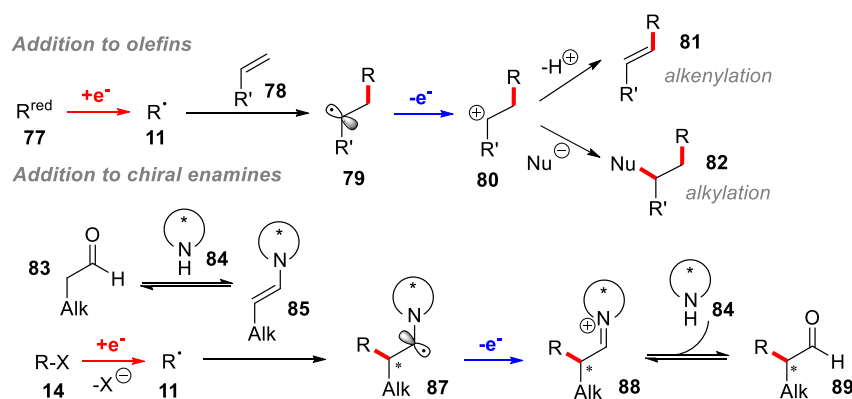
Reductive radical precursors are less common in redox-neutral photoredox C–C couplings. This can be due to the fewer number of reductive radical sources compatible with photoredox catalysts or the lack of compatibility of these with redox-neutral coupling methods. The main strategies employed to couple reductively generated radicals in a redox-neutral setting are summarised in **Scheme 11**.



Scheme 11 – Redox-neutral photoredox C–C coupling from reductive radical precursors.

a) Addition to C–C multiple bonds

Reductively generated radicals can also undergo additions to C–C multiple bonds (**Scheme 12**). In parallel to our observation on oxidatively generated radicals (*cf.* 1.2.3.2 a), reductively generated radicals will tend to be electrophilic. Consequently, most efficient trapping agents often are electron-rich to electron-neutral olefins.



Scheme 12 – Examples of a redox-neutral radical addition processes to electron-rich olefins/enamines.

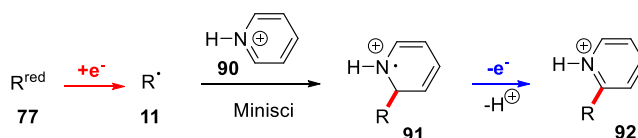
The general process starts with the addition of the reductively generated radical (**11**) into the electron-rich olefin (**78**). The resulting electron rich radical (**79**) can then be

successively oxidised to a cation (**80**) in a radical-polar cross-over step. From there, the cation can either be trapped by a nucleophile to lead to alkylated products (**82**),^[81,134,135] or deprotonation can occur to lead to the alkenylated product (**81**)^[136].

Inspired by this reactivity, MacMillan and Nicewicz reported the use of an imidazolidone chiral organocatalyst (**84**) able to condense with enolisable aldehydes (**83**) to generate *in situ* chiral enamines (**85**). This enamine could efficiently trap electrophilic radicals (**11**) from alkyl halides (**14**) with facial selectivity.^[71,137,138] The α -amino radical intermediate (**87**) resulting from this addition can then be further oxidised to an iminium (**88**), which can liberate an enantioenriched alkylated aldehyde (**89**).

b) Addition to electron-deficient aromatic rings: the Minisci reaction

Also known as the Minisci reaction,^[139] the addition of nucleophilic radicals to electron-deficient protonated heterocycles is a powerful arylation method.^[140] Despite the large number of reports of net oxidative photoredox Minisci reactions,^[141–143] these are not easily achieved in a redox-neutral setting (**Scheme 13**). Indeed, once the carbon radical (**11**) has attacked the protonated ring (**90**), the intermediate radical cation (**91**) needs to be further oxidised to restore the aromaticity (**92**).



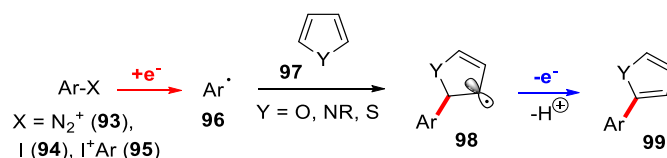
Scheme 13 – Example of a redox-neutral photoredox Minisci coupling.

This means that reductive radical precursors (**77**) must be used to keep an overall redox-neutral balance. Unfortunately, most of the reductively generated radicals fall into the category of electrophilic radicals, making them unsuited for the attack on an electron-deficient aromatic ring (electronic mismatch). As a result, the only examples of redox-neutral Minisci reactions reported were making use of aryl diazonium salts^[144] or more recently alkyl N-hydroxyphthalimide esters^[145] that could reductively produce nucleophilic radicals.

c) Addition to electron-rich aromatic rings

As discussed previously, the mostly “electrophilic” character of reductively generated radicals makes them easier to trap with electron-rich aromatic rings. König and co-workers pioneered using these methods to achieve photoredox arylations of

aryldiazonium salts (**93**)^[30,77,146] and aryl iodide (**94**)^[147] (**Scheme 14**). These were followed by reports using diaryliodonium salts (**95**) as reductive radical precursors.^[79,148]

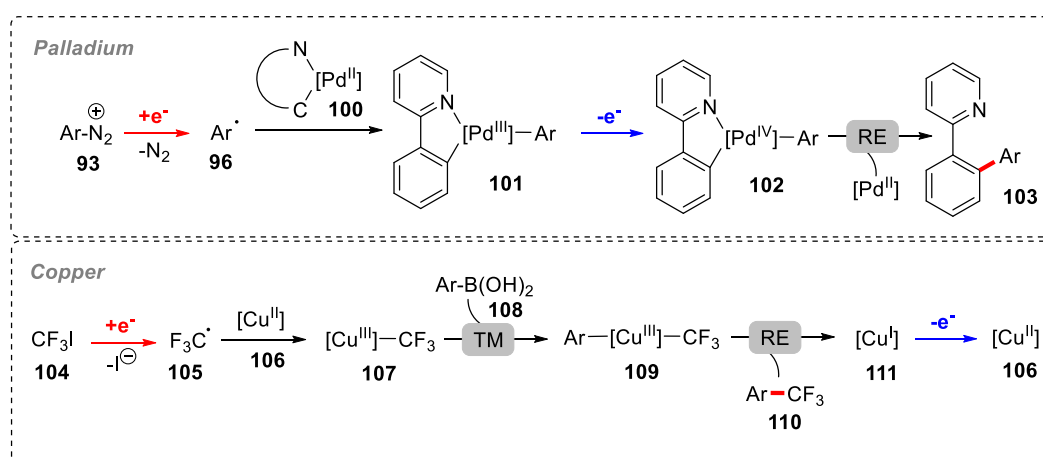


Scheme 14 – Example of a redox-neutral arylation with an electron-rich aromatic ring.

The mechanism follows a similar path to the Minisci reaction, addition of the radical (**96**) to **97** and oxidation of **98** to deliver the coupling product (**99**). It can be noted that by measuring the quantum yields of these reactions, a significant number of radical chains were found to be responsible for the product formation.^[149]

d) Transition metal co-catalysis

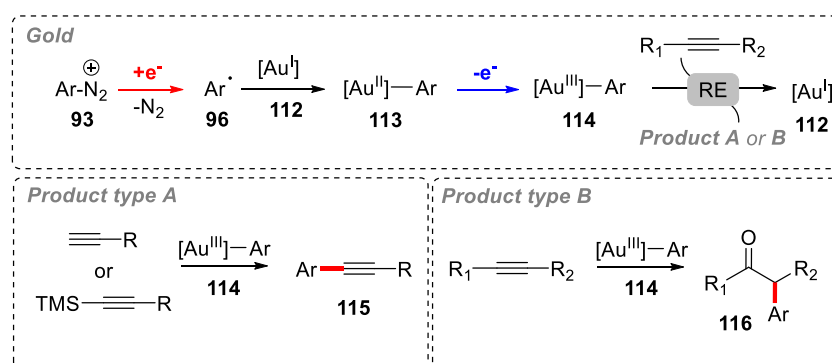
Dual catalysis methods were also applied to reductive radical precursors.^[150] In 2011, Sanford described a merger of palladium-catalysed C–H activation with photoredox catalysis (**Scheme 15**).^[78] In this process, aryl radicals (**96**) generated by the reductive fragmentation of aryl diazonium salts undergo addition to the Pd^{II} C–H activation complex (**100**) to generate a Pd^{III} species (**101**). The consecutive single-electron oxidation is believed to help the metal to reach the highly oxidised Pd^{IV} species (**102**) from which reductive elimination can easily occur to regenerate the palladium catalyst and the arylated product (**103**).



Scheme 15 – Dual catalysed photoredox and Pd or Cu cross-couplings by Sanford.

Building on the success of this concept, a year later the Sanford group disclosed a merger of photoredox and copper catalysis for the trifluoromethylation of aryl boronic acids

(108).^[151] The method relies on the reductive formation of the trifluoromethyl radical (105) from trifluoroiodomethane (104). This radical is trapped by the active Cu^{II} species (106) to generate a trifluoromethylated Cu^{III} species (107) on which the aryl boronic acid (108) can transmetallate. This step is followed by a reductive elimination delivering the trifluoromethylated product (110) and the Cu^I species (111) that can be reactivated to the Cu^{II} (106) active catalyst by the complementary single-electron oxidation.



Scheme 16 – Example of dual catalysed Au and photoredox cross-couplings.

Following these successes with palladium and copper, Glorius and Toste probed the possibility to interlock the photoredox catalytic cycle with a gold catalyst (**Scheme 16**). They discovered that the reductively generated aryl radicals (96) could be intercepted by a Au^I complex (112) to generate a Au^{II} organogold species (113). Upon a successive single-electron oxidation, a highly electrophilic Au^{III} organogold complex (114) is generated.^[152] This reactive organogold species could be intercepted with electron-rich C–C triple bonds to deliver alkynylated (115)^[153,154] or alkylated (116)^[155] cross-coupled products.

1.3 Organoboron reagents

1.3.1 Properties and preparation of organoboron compounds

1.3.1.1 General properties and definitions

Boron is the fifth element in the periodic table and occurs with an abundance of 0.001% in the Earth's crust, prevalently in form of its oxides. Its three valence electrons allow it to form three covalent bonds in the neutral form and adopt a trigonal planar geometry with a vacant *p*-orbital.^[156] Organic compounds that possess at least one C–B bond are commonly referred to as organoboron compounds (**117–121**, **Figure 6**).

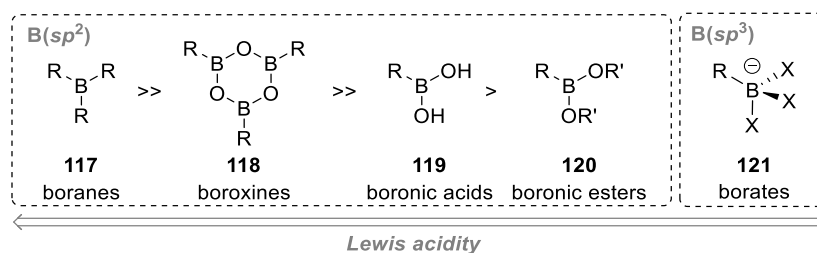


Figure 6 – Commonly encountered organoboron compounds arranged by their Lewis acidity.

Molecules from the first group (**117–120**) have an sp^2 hybridised boron centre, with a vacant *p*-orbital, making these Lewis acidic. The most Lewis acidic members of this family are boranes (**117**), they are highly reactive and air-sensitive reagents making them difficult to be isolated and stored. Boronic acid derivatives (**118–120**) have a boron atom bonded to a carbon and two oxygen atoms, decreasing their Lewis acidity by lone-pair donation. They are the most commonly used organoboron reagents.^[157] Boroxines (**118**) are trimeric boronic acid species, formed by dehydration of boronic acids (**119**) (**Scheme 17**). These compounds are quite strongly Lewis acidic and a high proportion of them can be found when employing boronic acids in non-aqueous media. With similarity to boronic acids, the Lewis acidity of boronic esters (**120**) is weakened by the stronger conjugation of the oxygen lone pairs towards the boron centre, which results in higher stability of these compounds.^[158] Most boronic esters are stable under neutral aqueous conditions, their stability is influenced by steric and entropic effects.^[157] Cyclic esters like the 1,2-ethanediol esters (**124**, **Figure 7**) are entropically stabilised, their hydrolysis

releases only one molecule of ethandiol whereas two molecules of water are consumed. Pinacol (**125**) and pinanediol esters (**126**) are stabilised by the extra steric shielding provided by the adjacent alkyl groups, protecting them against the attack of water or other nucleophiles, they are some of the most stable esters.

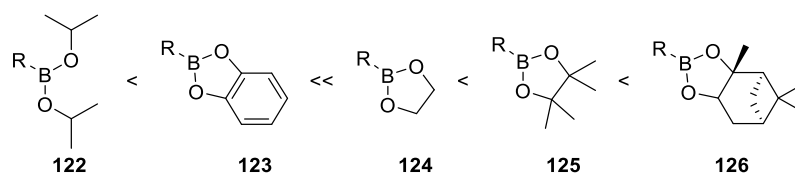


Figure 7 – Stability of various boronic esters against hydrolysis.^[157]

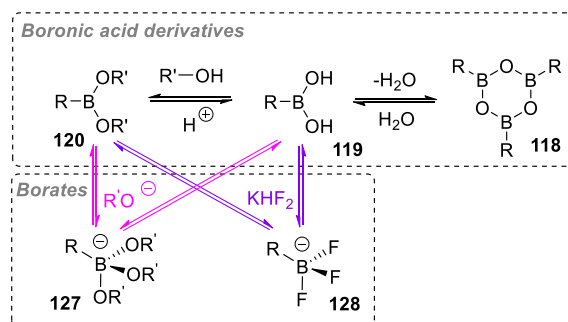
Unfortunately, the exceptional stability of pinanediol esters (**126**) is often linked to a reduced reactivity. On the other hand, boronic pinacol esters (**125**), often have an advantageous balance between stability and reactivity. These reagents are preferentially chosen, especially if their corresponding boronic acids are known for their chemical instability.^[158] Additionally, boronic esters are soluble in apolar solvents and can be purified either by distillation or silica gel chromatography, making them convenient reagents for organic synthesis.^[157]

Borates (**121**, **Figure 6**) are tetra-coordinated and negatively charged organoboron compounds. Since they are not Lewis acidic, they are stable against aerobic oxidation. However, because of their salt nature, borates are often less soluble in apolar solvents, which requires the use of undesirable highly polar and water-miscible solvents.^[157,158]

1.3.1.2 Preparation of organoboron compounds

Interchanging between boronic acid derivatives is relatively straightforward (**Scheme 17**). Boroxines (**118**) are obtained by forcing the dehydration of boronic acids (**119**), for example with the azeotropic distillation of water in toluene, using a Dean-Stark apparatus.^[159] Boronic esters (**120**) are readily prepared by esterification of boronic acids (**119**) with an excess of the desired alcohol, this can be done at room temperature in the presence of a drying agent or using azeotropic distillation.^[157] Borates (**127** and **128**) are prepared by successive nucleophilic attacks on the trivalent boron species. Boronic acid derivatives treated with an excess of alkoxide or fluoride are transformed to their corresponding trialkoxyborate (**127**) or trifluoroborates (**128**) respectively. Since these

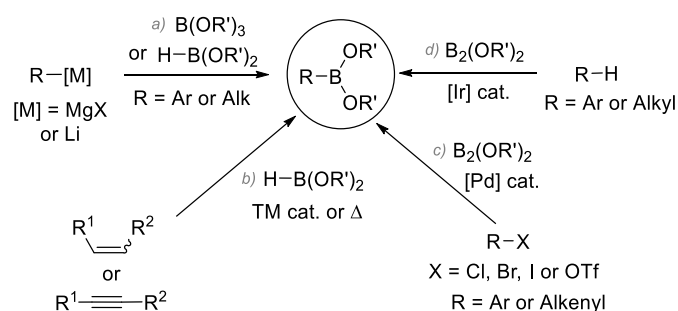
transformations are equilibria, these can be simply and efficiently driven in the desired direction.



Scheme 17 – Boronic acid derivative equilibria.

Due to the widespread use of boronic acid derivatives in organic synthesis, intensive research efforts have been made to efficiently introduce boron atoms into organic compounds (**Scheme 18**). The reactions presented do not consist of a comprehensive list of borylation methods but represent the main strategies employed to introduce boron atoms into organic scaffolds. Most of the time these methods introduce a boronic ester group, requiring further manipulation if a different boronic species is to be used.^[157]

The most common approach is the transmetalation of nucleophilic organomagnesium^[160] or organolithium^[161] species with electrophilic boronic species (**Scheme 18 a**). This method allows an easy and cheap access to aryl or alkyl boronic esters, but the use of reactive organometallic species intermediate species limit its functional group tolerance and often requires cryogenic temperatures. Hydroboration of alkynes or alkenes is probably the most effective method to access alkyl boronic esters (**Scheme 18 b**).^[162]



Scheme 18 – Common routes to boronic acid derivatives.

While hydroboration with dialkyl boranes happens spontaneously at low temperatures, the lowered reactivity of oxygenated borane reagents often requires the use of transition

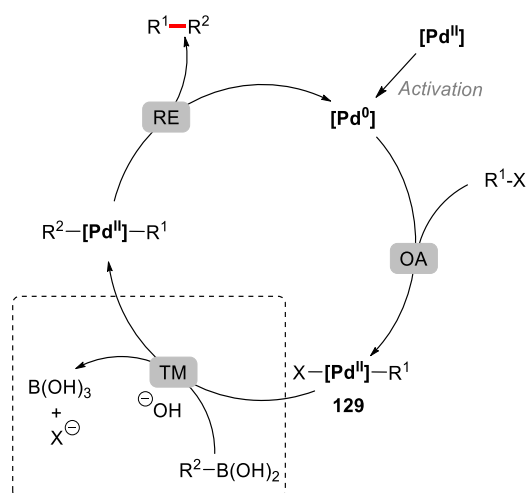
metal catalysts or elevated temperatures.^[163,164] Regio-selectivity and limited substrate scope are common issues with these methods.

Transition-metal-catalysed borylation reactions have emerged as an alternative and powerful tool to produce boronic acid derivatives.^[165] The mildest and most versatile method to access functionalised aryl boronic acid derivatives is the Miyaura borylation (**Scheme 18 c**).^[166–168] This method relies on the engagement of aryl or alkenyl halides in palladium-catalysed cross-couplings with diboron compounds. Pioneered by Hartwig and Smith, more recent transition metal (mainly iridium) catalysed methods allow direct C–H borylation of arene or alkyl groups (**Scheme 18 d**).^[169]

1.3.2 Organoboron compounds as reactants in C–C cross-couplings

1.3.2.1 By transmetalation with transition metals

As mildly nucleophilic and non-toxic organometallic species, organoboron compounds have found tremendous applications based on their ability to transmetalate with various transition metals.^[157] Importantly, this property propelled them as first choice nucleophilic partners for palladium-catalysed C–C cross-coupling reactions.^[170] For developing this transformation, Suzuki shared the 2010 Nobel Prize in Chemistry, further outlining the key role of organoboron reagents in modern organic synthesis (**Scheme 19**).^[42,171]



Scheme 19 – A generalised mechanism of Suzuki-Miyaura cross-coupling reactions.^[158]

Although a range of different organoboron reagents undergo rapid transmetallation (TM) with the active Pd^{II} complex (**129**), the choice of the exact species to employ is influenced by their stability under aerobic conditions, accessibility, and price. Boranes are easily produced by the hydroboration of olefins but are sensitive to oxidation by oxygen, and dehydroboration by water.^[157] Best results in transmetallation are given by using boronic acids and their corresponding boroxines.^[158] A range of different aryl boronic acids are commercially available, but many electron-deficient aryl boronic acids and alkyl boronic acids are sensitive to oxidation or protodeboronation under reaction conditions.^[156,157,172] To circumvent this issue, boronic acids can be transformed into their more stable ester or trifluoroborate salt analogues.^[157,158] Trifluoroborate salts are hydrolysed to the corresponding boronic acids under protic conditions, however releasing toxic and corrosive hydrofluoric acid. Finally, despite the great utility of Suzuki couplings to form biaryl products, challenges to cross-couple alkyl partners still remain (*cf.* 1.2.1).^[42]

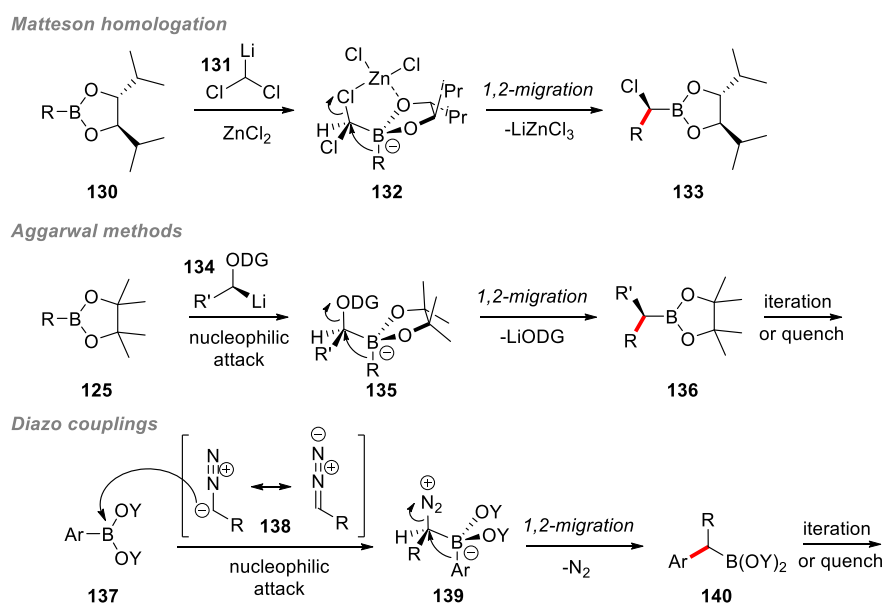
1.3.2.2 By 1,2-migration from ate-complexes

Another remarkable property of organoboron compounds is their ability to undergo stereospecific 1,2-metallate rearrangements (or 1,2-migrations) from tetra-coordinated ate-complexes (**Scheme 20**). This synthetically powerful transformation was first discovered by Matteson in 1980.^[173,174] He could perform a one-carbon homologation of a chiral boronic ester with ZnCl₂ and (dichloromethyl)lithium with high diastereoselectivity (**Scheme 20**).^[173,175]

In the first step, the ate-complex **132** is formed by a nucleophilic attack of (dichloromethyl)lithium (**131**) on a chiral boronic ester (**130**). Although different isomers of the intermediate **132** can be formed, the configuration of the isomer depicted is favoured due to the lower steric repulsion with the coordinating ZnCl₂.^[176] 1,2-migration of the alkyl group from the boron centre with the concomitant anti-periplanar elimination of a chloride substituent affords the homologated boronic ester (**133**) in high diastereomeric ratios. Coordination of the zinc chloride additive not only aids in the elimination of chloride by stabilising the antiperiplanar orientation in the transition state **132** but also promotes the process by weakening the C–Cl bond.

The stereospecific nature of these transformations later inspired Aggarwal to conduct a series of homologations employing chiral organolithium nucleophiles (**134**) accessed *via*

enantioselective deprotonation of Hoppe carbamates.^[177] Their addition to alkyl boronic esters allows a chiral ate-complex (**135**) to form, which, upon further warming of the reaction mixture, undergoes a stereospecific 1,2-migration, leading to the boronic ester **136** with a high degree of enantiomeric control. Interestingly this process could be repeated up to nine times, providing a conceptually powerful method for assembling C–C bonds in an iterative fashion with absolute stereocontrol at each homologated carbon.^[178] Since their initial work, other coupling methods employing chiral boronic esters were further developed by his group, also relying on the 1,2-migration principle.^[179,180]



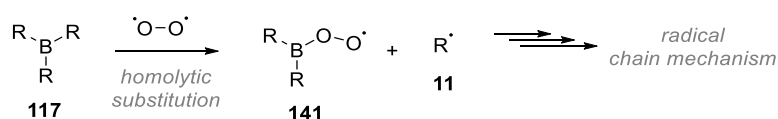
Scheme 20 – C–C cross-couplings of organoboron reagents relying on a 1,2-migration mechanism.

The coupling of diazo compounds with organoboron reagents^[181] was initially reported by Hooz in 1968 with trialkyl boranes and further popularised by Barluenga in 2009 with aryl boronic acids.^[182] These transformations also rely on a 1,2-migration mechanism, with the nucleophilic species being a zwitterionic diazo compound (**138**). Its attack is favoured on highly Lewis acidic organoboron compounds (**137**) such as boroxines.^[183] This attack leads to the formation of a zwitterionic ate-complex (**139**) that can easily undergo 1,2-migration by eliminating nitrogen and leaving behind a highly reactive boronic acid derivative (**140**), that can be oxidised, protodeborylated or further homologated.^[184,185]

1.3.2.3 As carbon radical precursors

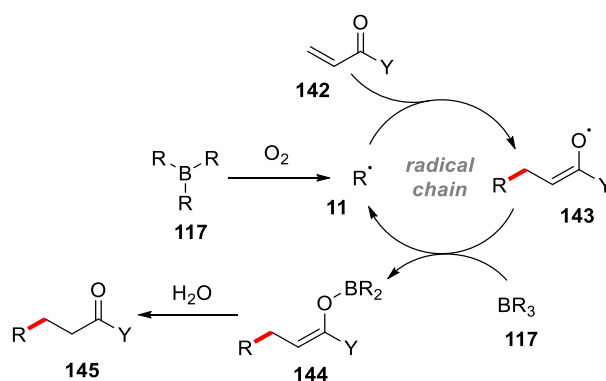
A less recognised reactivity of organoboron compounds is the possibility to use them as carbon radical precursors.^[49] The low polarity of the C–B bond allows it to be cleaved homolytically. Such reactions are usually thermodynamically favoured by the formation of strong B–O (~124 kcal/mol) or B–N (~100 kcal/mol) bonds at the expense of the weaker B–C bond (~81 kcal/mol).^[186]

Trialkyl boranes (**117**) were first used as carbon-centred radical (**11**) precursors in 1967.^[187] Due to their ability to spontaneously react with molecular oxygen (**Scheme 21**), they have been widely used as convenient low-temperature radical initiators.^[186]



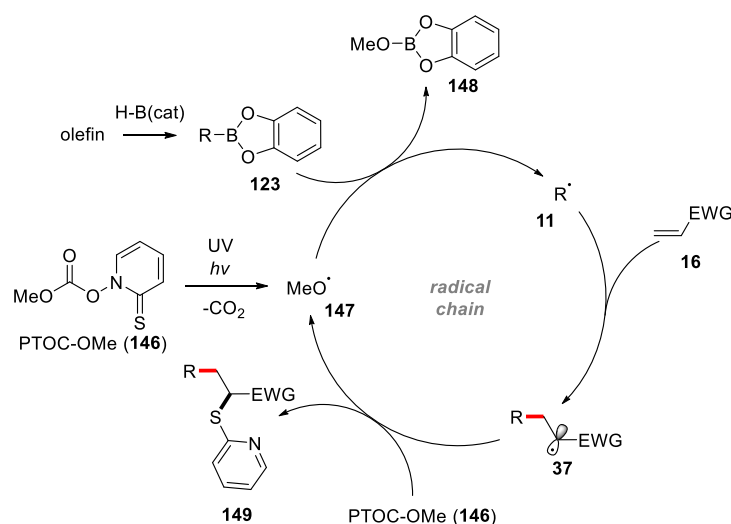
Scheme 21 – Generation of carbon-centred radicals from trialkyl boranes.^[186,188]

This property was discovered by Brown and Suzuki, reporting the use of trialkyl boranes (**117**) as substrates in radical conjugate additions to electron-deficient olefins.^[187] The proposed mechanism for this conjugate addition (**Scheme 22**) starts with the oxygen-mediated formation of a carbon-centred radical (**11**) which adds an olefin (**142**) to form a radical enolate (**143**). Due to the strong B–O bond energy, the intermediate **143** propagates the radical chain mechanism with a second equivalent of borane (**117**) to form a boron enolate (**144**), which releases the addition product (**145**) after aqueous workup.^[188,189]



Scheme 22 – Brown's radical chain mechanism of trialkyl borane conjugate addition.^[189]

To circumvent the lack of selectivity in the cleavage of unsymmetrical trialkyl boranes, in 1999 the Renaud group reported the use of catechol boronic esters (**123**) as radical precursors.^[190] In analogy to their trialkyl borane homologs, these highly Lewis acidic boronic esters are sensitive to radical displacement with oxygen-centred radicals. However, less efficient chain propagation requires the use of a radical chain carrier, such as the Barton carbonate (PTOC-OMe, **146**), to enable efficient radical addition to a wide range of Michael acceptors (**Scheme 23**).^[191] In the absence of oxygen, the Barton carbonate (**146**) served as a radical initiator, generating the oxygen-centred radical (**147**) upon UV light irradiation. This radical is efficiently engaged in a homolytic substitution with a catechol boronic ester (**123**) to liberate a carbon-centred radical (**11**) that efficiently adds to an electron-deficient olefin (**16**). The intermediate radical **37** can then be trapped by the Barton carbonate (**146**) to provide the coupled product (**149**) and regenerate the oxygen-centred radical (**147**).

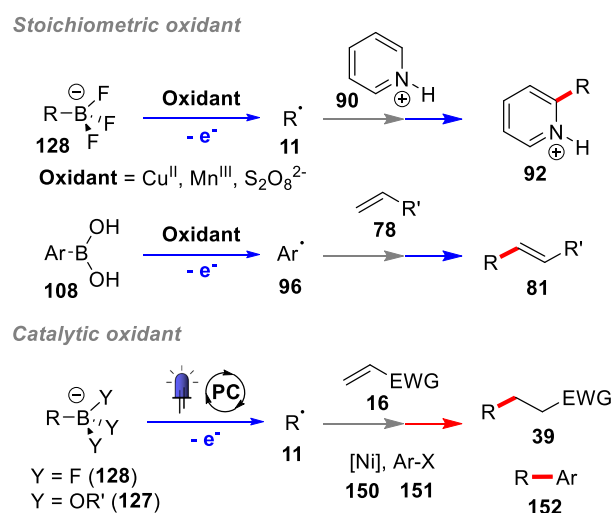


Scheme 23 – Mechanism of Renaud's modification of the Brown reaction.

However, in these processes, oxygen sensitive organoboron starting materials (**123**) required an *in situ* generation method with a hydroboration step, thereby limiting the full synthetic potential of these reactions.^[190,192]

A major paradigm shift in the use of bench-stable organoboron compounds as radical precursors was the discovery that electron-rich organoborates are readily single-electron oxidised.^[193,194] It was only between 2010 and 2011 that this property was identified as a useful synthetic approach by Fensterbank and Molander.^[195,196] Both groups reported the

use stoichiometric metallic oxidants (Cu^{II} and Mn^{III}) to single-electron oxidise trifluoroborate salts (**128**, **Scheme 24**). In a separate report, strong stoichiometric oxidants were employed to generate aryl radicals (**96**) from aryl boronic acids (**108**), although the mechanism underlying this fragmentation was not fully described.^[196–202] The radicals thus generated (**96**) could be further engaged in net-oxidative transformations such as oxidative additions to olefins (**78**) or aromatic systems (**90**).



Scheme 24 – Single-electron oxidation of organoborates and aryl boronic acids and their coupling reactions.

In 2012, Akita demonstrated the compatibility of the single-electron oxidation of organoborates with photoredox catalysis.^[62] Using the **Ir-3** photocatalyst, he could generate alkyl and aryl radicals from a variety of trifluoroborate (**128**) and trialkoxylborate (**127**) salts without using stoichiometric metallic oxidants. These radicals could be trapped with TEMPO or engaged in redox-neutral couplings with electron-deficient olefins (**16**, *cf.* 1.2.3.2 a). In 2014, the Molander group reported a nickel/photoredox dual catalysed $\text{C}(sp^2)\text{--C}(sp^3)$ cross-coupling of benzylic trifluoroborate salts with aryl halides (**151**, *cf.* 1.2.3.2 d), further highlighting the synthetic potential of these methods.^[45]

These seminal reports revived the interest in using organoboron reagents as easily accessible radical precursors.^[203,204] However, the synthetic utility of this concept can still be improved. Due to the low oxidation potentials of common photoredox catalysts, only organoborates can be activated using photoinduced single-electron oxidation. Extending this approach to a wider range of commercially available organoboron reagents would be

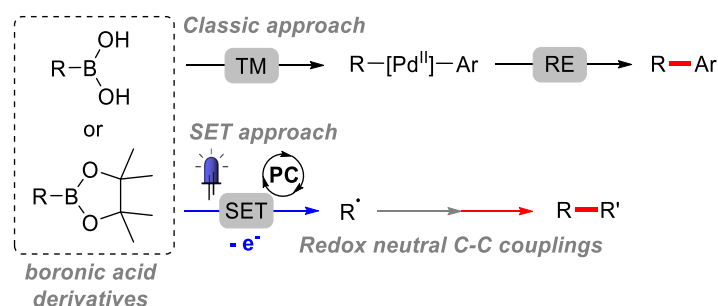
attractive – especially as the low solubility of organoborate salts in common organic solvents limits the scale-up capabilities of the current methods for industrial processes.

1.4 Summary and project overview

Organoboron reagents have shown their synthetic utility as “two-electron nucleophiles” with the immense success of the Suzuki-Miyaura cross-coupling that is often considered as the most used C–C coupling method (*cf.* 1.3.2.1).^[170] While this method is particularly powerful for C(*sp*²)–C(*sp*²) couplings, its extension to C(*sp*³) nucleophiles is still a challenge (*cf.* 1.2.1).^[42] For these reasons, alkyl couplings are often performed with alkyl zinc or Grignard reagents lacking a broad functional group tolerance.^[43] As a result, finding selective and general methods to couple bench-stable C(*sp*³) organoboron reagents is still of high interest.

As thoroughly discussed in 1.2.3, photoredox catalysis has become a method of choice to perform C–C cross-coupling reactions of pro-oxidative or pro-reductive carbon radical precursors in a redox-efficient manner. In this context, finding alternative widely commercially available starting materials able to act as a “radical reservoir” (*cf.* 1.2.2) is of high importance for these methodologies to be applied by a wider synthetic audience.

Organoboron reagents are becoming more commonly used as oxidative carbon radical precursors (*cf.* 1.3.2.3). While this discovery was initially made with unstable organoboranes, bench stable trifluoroborate salts are now increasingly used as radical precursors under photoredox-catalysed conditions.^[203]



Scheme 25 – A single-electron transfer activation of boronic acid derivatives for C–C couplings.

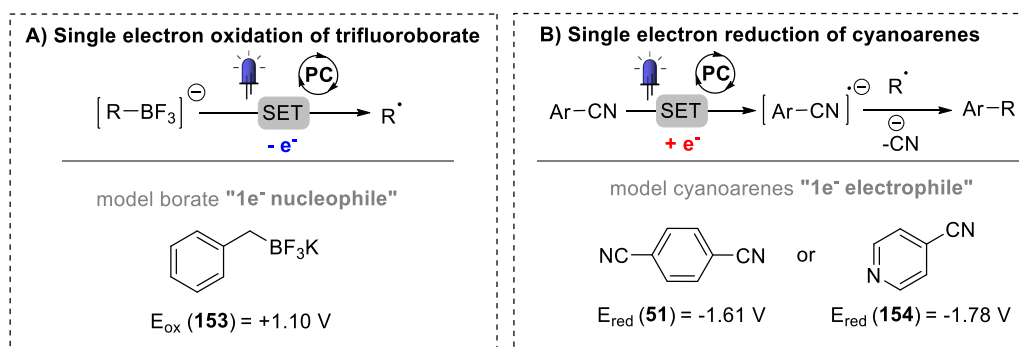
In this thesis, we present our work towards using more commonly available boronic acid derivatives as reagents in photoredox-catalysed C–C cross-couplings (**Scheme 25**).

Chapter 2 presents our original discovery that pinacol boronic esters can be activated under photoredox-catalysed conditions and used in $C(sp^2)$ – $C(sp^3)$ cross-couplings. Based on our mechanistic understanding, Chapter 3 focuses on the use of a Lewis base catalyst to promote the photoinduced single-electron oxidation of boronic esters and acids and their efficient alkylations. Finally, Chapter 4 describes the application of these methods for the efficient synthesis of active pharmaceutical ingredients and our work in finding suitable organic dye catalyst to perform these reactions without using a transition metal-based catalyst.

2 Photoredox arylations: from trifluoroborates to boronic esters

2.1 A redox-neutral coupling: proof-of-concept

We decided to start investigating net-neutral photoredox coupling procedures with organoboron reagents that were already known for their reactivity towards photoinduced single-electron transfer. The success of Akita's and Molander's procedures, relying on the formation of alkyl radicals using single-electron oxidation of alkyl trifluoroborates,^[45,62,126,205,206] encouraged us to use these as model organoboron reagents (**Scheme 26, A**).



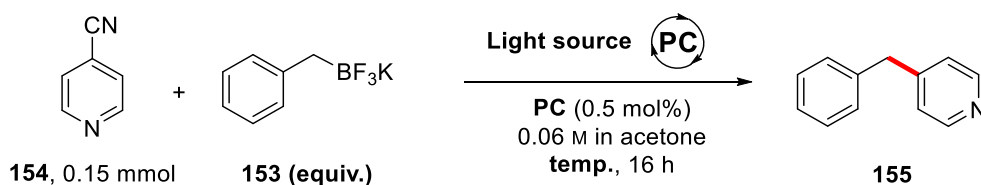
Scheme 26 – Starting idea: oxidise a trifluoroborate and reduce a cyanoarene.

To arylate these radicals in a redox-neutral fashion, we were naturally attracted to the recent work of MacMillan describing the coupling of various carbon-centred radicals to electron-poor aromatic nitriles used as electron acceptors *via* a radical-radical coupling.^[74,76,84,114,207] With two complementary substrates, one that can provide an electron (benzyl trifluoroborate, "1e⁻ nucleophile") and another that can accept an electron (cyanoarene, "1e⁻ electrophile"), it is conceptually possible to perform a net neutral photoredox coupling of these two entities (*cf.* 1.2.3.2 b). We started to investigate this concept using trifluoroborate **153** and cyanoarene **154** as model coupling partners with known complementary reactivity in photoredox-catalysed reactions.

2.1.1 Optimisation

Photocatalyst selection was the initial step of this optimisation. The important redox potential difference between the two reagents (2.7 V) encouraged us to investigate photocatalysts associated with a wide redox window (**Table 2**, entries 1–4). This initial screening allowed us to identify the strong excited state oxidant **Ir-3** ($E_{1/2}^{*/red} = +1.21$ V) as the most promising catalyst, leading to 58% yield in coupling product as the initial result (entry 1). This is not surprising given the high oxidation potential of the benzyl trifluoroborate (E_{ox} (**153**) = +1.10 V)^[45], requiring a strongly oxidising photocatalyst. Surprisingly, the potent oxidants **Mes-Acr-1** ($E_{1/2}^{*/red} = +2.08$ V, entry 2) and **Ru-4** ($E_{1/2}^{*/red} = +1.45$ V, entry 3) did not provide a good conversion of **154**.

Table 2 – Optimisation of photoredox coupling of benzyl trifluoroborate (**153**) with 4-cyanopyridine (**154**).



Entry	PC	Light source	temp.	equiv. ^a	Yield ^b
1	Ir-3	LED ₄₇₀	30°C	0.625	58%
2	Mes-Acr-1	LED ₄₇₀	30°C	0.625	13%
3	Ru-4	LED ₄₇₀	30°C	0.625	0%
4	Ir-1	LED ₄₇₀	30°C	0.625	3%
5	Ir-3	LED _{white}	35°C	0.625	23%
6	Ir-3	Intense bulb	90°C	0.625	6%
7	Ir-3	CFL bulb	40°C	0.625	42%
8 ^c	Ir-3	LED ₄₇₀	30°C	0.625	5%
9	Ir-3	no light	25°C	0.625	0%
10	Ir-3	LED ₄₇₀	30°C	1.2	72%
11^d	Ir-3	LED₄₇₀	30°C	1.2	85% (81%)

Reactions carried out by adapting **GP(II)** to the conditions described. ^aEquivalents of **153** used. ^bYield in **155** determined by ¹H-NMR analysis of crude reaction mixture using CH₂Br₂ as an internal standard. Isolated yield in parentheses. ^cWith 2.0 equiv. of TEMPO. ^dIrradiated 48 h instead of 16 h. Isolated yield in parentheses.

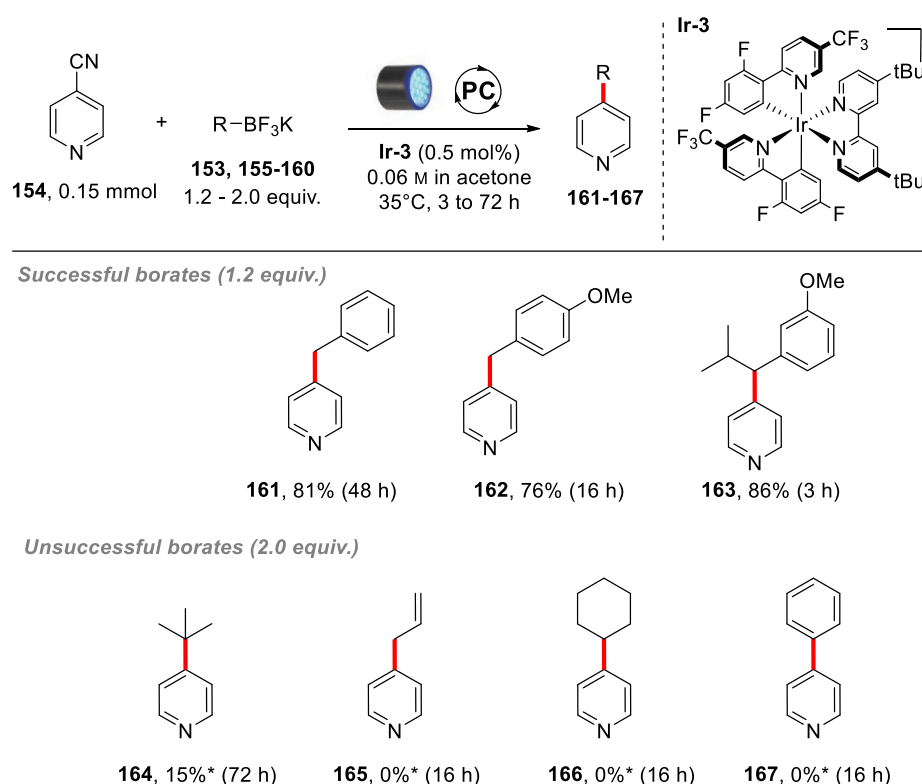
This is probably because of their lower reducing abilities ($E_{1/2}^{\text{gd/red}}$ (**Mes-Acr-1**) = -0.57 V and $E_{1/2}^{\text{gd/red}}$ (**Ru-4**) = -0.80 V) preventing them to reduce **154** (E_{red} = -1.78 V). Finally, the strong excited state reducer **Ir-1** ($E_{1/2}^{\text{ox/*}}$ = -1.73 V) was not effective in this reaction (entry 4). With a suitable catalyst in hand, the influence of light source on the reaction was investigated (entries 5–7 vs. entry 1). Notably, the nature of the light source influenced the temperature of the reaction. While the LEDs and the CFL light bulb provided irradiation at just above ambient temperature (30°C to 40°C), using a more powerful bulb, heated the reactor up to 90°C and led to the degradation of the catalyst (entry 6). Blue LEDs (Thorlabs, λ_{max} = 470 nm, 2 x 253 mW) provided the most efficient irradiation by only emitting within the absorption spectrum of the catalyst (λ_{max} (**Ir-3**) = 380 nm). In contrast, white LEDs emit a smaller proportion of light that can be absorbed by the catalyst, making them less efficient. Interestingly, a simple household CFL light bulb could be used as a cheap irradiation device, only giving a slightly lower yield than the blue LEDs (42% vs. 58%). Control experiments were then carried out. Addition of the persistent radical TEMPO (entry 8) suppresses the reaction as expected, due to the trapping of the postulated radical intermediate (TEMPO adduct detected by MS). No reaction was observed when stirring the mixture in the absence of light (entry 9). The influence of the stoichiometry of the reaction was then examined (entry 1 vs. entry 10). The limiting reagent was changed from **153** to **154** with a significant enhancement of the yield in the coupling product (58% to 72%). Since **154** was not fully converted, irradiating the mixture for 48 h instead of 16 h allowed the reaction to reach full conversion of **154**, resulting in 85% of the coupling product (entry 11).

2.1.2 Scope of the transformation

With optimised conditions in hand, the scope of potassium trifluoroborates was investigated using 4-cyanopyridine (**154**) as model coupling partner (**Table 3**). As observed during the optimisation, electron-neutral benzyl trifluoroborate (**153**) required 48 h of irradiation to afford 81% isolated yield. However, the more activated 4-methoxybenzyl trifluoroborate (**155**) delivered a high yield of coupling product **162** after only 16 h of irradiation, probably because of an easier single-electron-oxidation step. The more electron-rich secondary benzyl trifluoroborate (**156**) was fully converted within 3 h and was transformed in high yield to the hetero-arylated product (**163**). The regioselectivity of this coupling product is interesting since rearrangement of the

postulated benzyl radical can occur to generate a tertiary alkyl radical *via* 1,2-hydrogen atom shift. Moreover, it is a more challenging substrate to engage using a Suzuki-Miyaura coupling procedure, with the possibility of β -hydride elimination after the transmetallation step.

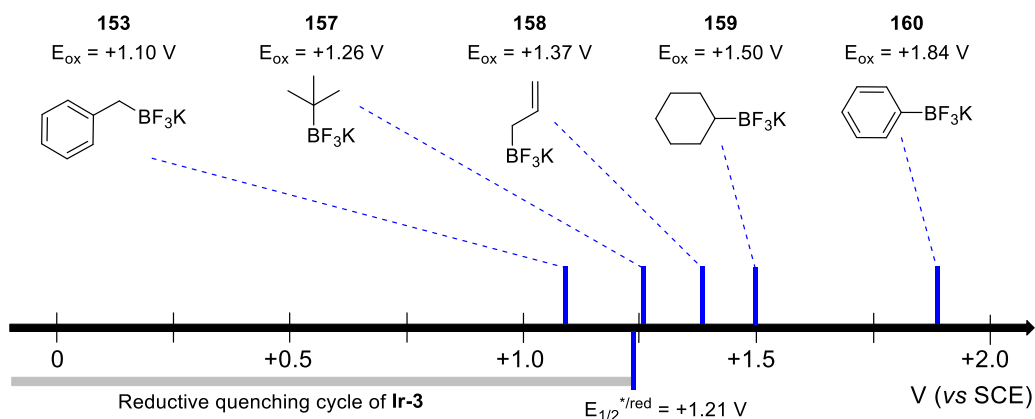
Table 3 – Scope of alkyl and aryl potassium trifluoroborates coupled to 4-cyanopyridine (**154**).



Reactions carried out by following **GP(II)**. Isolated yields unless otherwise stated. *Yield determined by $^1\text{H-NMR}$ analysis (tentative assignment) of crude reaction mixture using CH_2Br_2 as an internal standard.

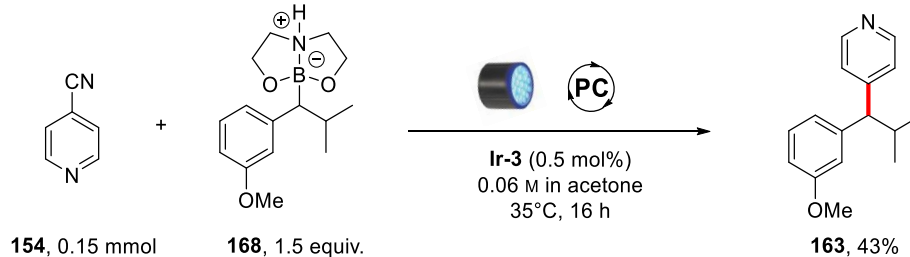
Three other classes of trifluoroborate salts were then tested: allyl, alkyl and aryl trifluoroborates (**157–160**). From these, only *tert*-butylated pyridine (**164**) could be obtained in a low 15% yield after 72 h of irradiation. No reaction was observed using allyl, cyclohexyl or phenyl trifluoroborates (**165–167**). The reason for these results is presumably the higher oxidation potential of those less activated trifluoroborates that are unable to quench the excited **Ir-3*** photocatalyst. To verify this hypothesis, we plotted the measured redox potentials (**Scheme 27**) of these trifluoroborate species against the reduction potential of **Ir-3*** ($E_{1/2}^{*/\text{red}} = +1.21$ V). These values show that only benzyl (**153**) and *tert*-butyl trifluoroborates (**157**) can fit in the reductive quenching redox window of

Ir-3. This reactivity cut-off is therefore correlated with the redox potentials cut-off, suggesting that a reductive quenching cycle of **Ir-3** is probably operative.



Scheme 27 – Oxidation potentials of trifluoroborate species versus the reductive quenching cycle of **Ir-3**.

In addition to reactivity issues, problems solubilising these anionic starting materials in acetone were also observed, even under very dilute conditions (0.06 M). Solubility issues limit the productivity of the reaction and hinder the light absorption by the photocatalyst by light-scattering from the insoluble particles. As the reaction proceeds, potassium salt precipitation also occurs, making process intensification difficult. To investigate more soluble borate salt alternatives, the secondary benzyl diethanolamine borate (**168**) analogue of the highest yielding benzyl trifluoroborate (**156**), was tested under the optimised conditions (**Scheme 28**). This zwitterionic compound only yielded 43% of **163** after 16 h of irradiation and is consequently less reactive than its trifluoroborate analogue (86% in 3 h). Although no report has been made about the photoredox activation of these uncommon organoborates we did not optimise these results further due to commercial unavailability of these reagents.

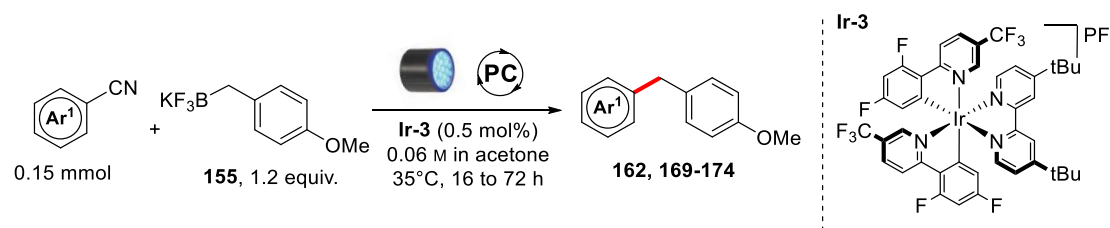


Scheme 28 – Alternative diethanolamine borate salt investigation (following **GP(II)**).

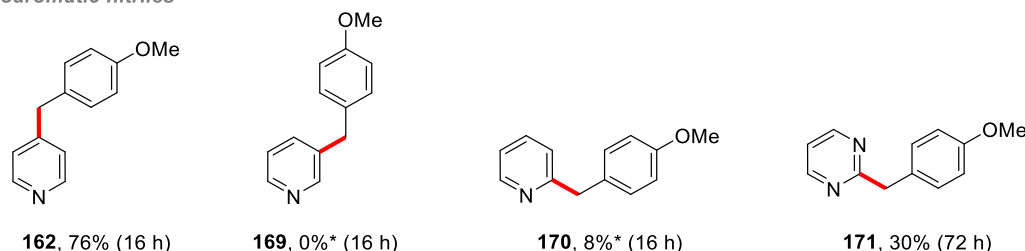
The scope of cyanoarenes was then investigated using 4-methoxybenzyl trifluoroborate (**155**) as coupling partner (**Table 4**). Heteroaromatic nitriles were initially tested. Among

cyanopyridines, only the 4-cyanopyridine (**154**) gave the desired product (**162**) in a productive yield, the more electron-rich 3-position (**169**) did not react under these conditions and 2-cyanopyridine only provided 8% of **170**. The two-nitrogen-containing 2-pyrimidine resulted in a slightly higher yield of the coupling product (**171**), 30% after 72 h.

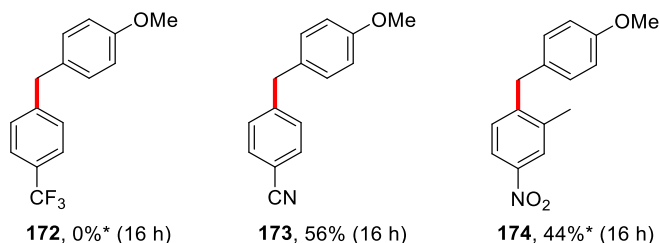
Table 4 – Scope of cyanoarenes partners with benzylic trifluoroborate salt **155**.



Heteroaromatic nitriles



Aromatic nitriles

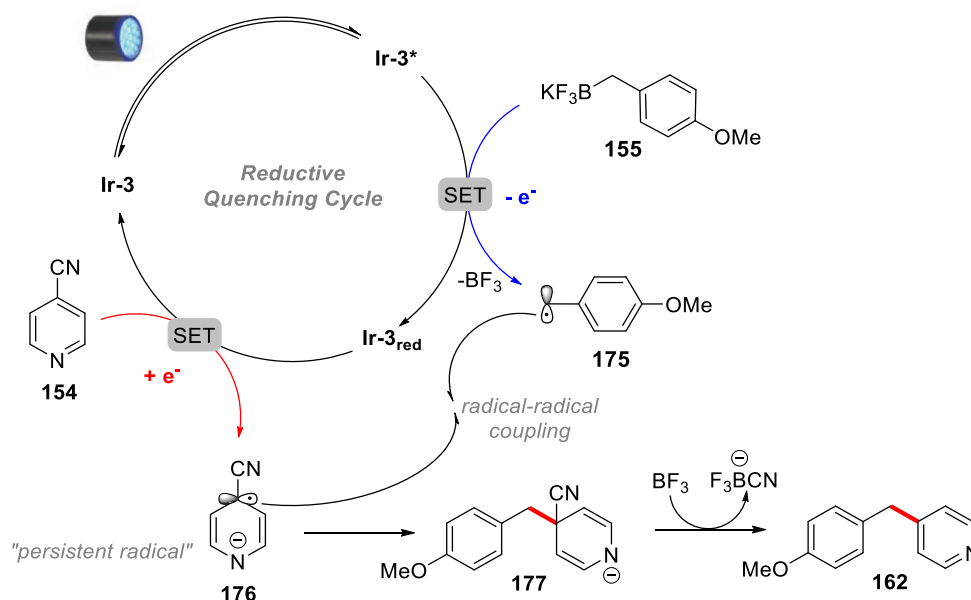


Reactions carried out by following **GP(II)**. Isolated yields unless otherwise stated. *Yield determined by $^1\text{H-NMR}$ analysis (tentative assignment) of crude reaction mixture using CH_2Br_2 as an internal standard.

Non-heteroaromatic nitrile coupling partners were then examined. Electron-deficient benzonitriles were considered as the best potential substrates to start. Unfortunately, the 4-trifluoromethane benzonitrile (**172**) was left unreacted using the optimised reaction conditions. On the other hand, the 4-cyano and 4-nitro benzonitriles (**173** and **174**) were found to have partially reacted under the standard conditions. As a result, the scope was limited to specific cyanoarenes able to engage in single-electron reduction. These observations are in line with the previously observed scope of cyanoarenes using a postulated radical-radical coupling strategy.^[74]

2.1.3 Mechanism

Based on the known oxidative carbon-centred radical generation from organoborates^[45,62] and reductive generation of radicals from electron-deficient cyanoarenes^[74] the following reaction mechanism was suggested (**Scheme 29**).

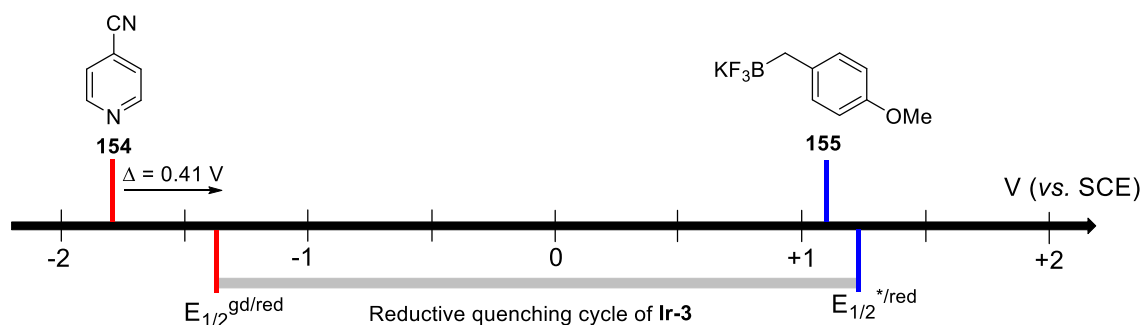


Scheme 29 – Suggested mechanism for the arylation of benzyl trifluoroborates.

The reaction starts with the visible light excitation of the photocatalyst to create a highly oxidative Ir-3^* species ($E_{1/2}^{*\text{red}} = +1.21 \text{ V}$). Based on the redox potential cut-off observed, this stable triplet state can then be reductively quenched by the electron-donor benzyl trifluoroborate ($E_{\text{ox}}(\mathbf{155}) = +1.10 \text{ V}$)^[45] generating a stabilised benzyl radical ($\mathbf{175}$) and liberating BF_3 . In this process, the reduced Ir-3_{red} ($E_{1/2}^{\text{gd/red}} = -1.37 \text{ V}$) is generated. This potent one electron reducing species is then believed to donate an electron to the 4-cyanopyridine ($\mathbf{154}$) to generate the stabilised radical anion ($\mathbf{176}$) and ensure the turnover of the catalyst. The persistent radical anion ($\mathbf{176}$)^[74] can then engage in bimolecular radical-radical coupling with the benzyl radical ($\mathbf{175}$) to form the coupling product ($\mathbf{162}$) after the elimination of cyanide sequestered by BF_3 . The stability of the radical anion intermediate ($\mathbf{176}$) is enhanced in the case of *para*-substitution of the aromatic ring by strongly electron-withdrawing groups or the presence of a nitrogen atom in a suitable position allowing mesomeric delocalisation of the negative charge. This would explain, at least partially, the electronic effects observed by changing the substituents on the cyanoarenes. Improvement of the kinetics of the reaction by

employing more electron-rich benzyl trifluoroborates can also be rationalised by the fact that they will be more readily oxidised by the **Ir-3***. This is also a sign that this initial step might be the rate-limiting one.

However, there is an issue with the proposed mechanism. Although a match with the oxidation potential of the trifluoroborate and **Ir-3*** is observed (blue lines, **Scheme 30**), the oxidation potential of **Ir-3_{red}** ($E_{1/2}^{gd/red} = -1.37$ V) is not high enough to enable the reduction of **154** ($E_{red} = -1.78$ V), as a gap of 0.41 V is separating the two (red lines).



Scheme 30 – Redox potentials of the species involved in the trifluoroborates arylation process relative to the reductive quenching cycle redox window of **Ir-3**.

As far as the redox potential model is concerned, we are confident that it can serve well to illustrate the thermodynamic feasibility of electron transfer mechanisms. Consequently, we believe that activation of the 4-cyanopyridine (**154**) will be required to lead to a thermodynamically feasible reduction. This aspect will be discussed in a following section (*cf.* 2.2.4).

2.1.4 Summary

In summary, we have investigated a proof-of-concept of a redox-neutral arylation between an electron donor and organoboron acceptor using photoredox catalysis. Based on known literature examples, we could cross-couple an organoborate “1e⁻ nucleophile” and a “1e⁻ electrophile” by the use of a photoredox catalyst, mimicking the concept of palladium-catalysed cross-couplings.

However, as only a limited number of synthetically useful examples could be obtained with this method, we decided to further investigate the nucleophiles and electrophiles that could be engaged using this rationale.

2.2 Boronic esters as electron donors

We initially investigated the replacement of the trifluoroborate electron donors by more attractive boronic esters in our developed redox-neutral coupling (**Figure 8**). Due to solubility issues associated with the use of trifluoroborate salts, the use of polar aprotic solvents or solvent mixtures (such as DMF or DMSO) at low concentrations (typically < 0.05 M) is often required to avoid clogging issues. These diluted conditions result in long reaction times (24 to 48 h), low throughput and scale-up difficulties. Moreover, these water-soluble, high boiling point solvents pose issues for downstream processing.^[208] A more soluble source of the organic radical species in a more acceptable solvent would be beneficial.^[209]

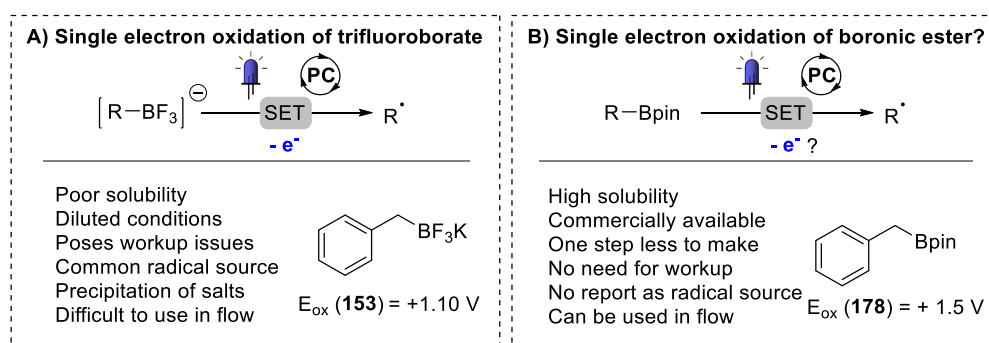


Figure 8 – Comparison between trifluoroborates and boronic esters as electron donors.

Boronic esters are suitable precursors as they are widely available, both from commercial or synthetic sources.^[184,210–214] Although organoboron species have been described as a tin-free source of alkyl radicals,^[186] only a limited number of studies have been focused on the use of boronic esters as carbon radical precursors, with only catechol boronic esters being investigated.^[191,215] Despite the growing interest in generating carbon radicals using trifluoroborate salts, no reports to date for the activation of boronic esters using photoredox catalysis have been made.^[204]

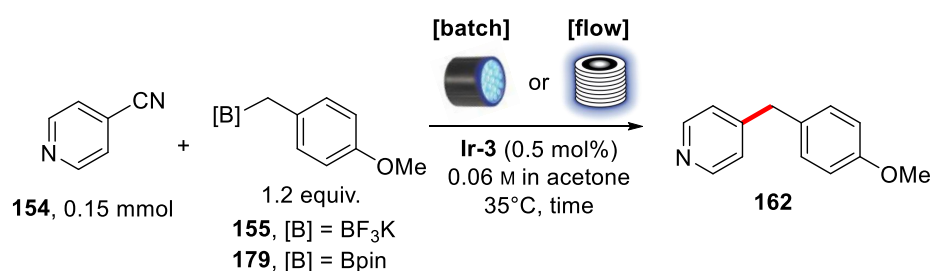
Importantly, solving solubility issues associated with these anionic starting materials would enable the use of continuous processing methods which could provide other advantages. For instance, more efficient irradiation with microchannel devices and better temperature control has been seen to result in faster and cleaner photoreactions in flow.^[216–219] Additionally, due to the inherent limitation of photon attenuation through absorbing media, resulting in a small light penetration depth,^[216] batch photoreactors will often become inefficient when scaled-up.^[220]

2.2.1 Optimisation: from batch to flow

To improve the process productivity, we were interested in irradiating the reaction mixture in a flow reactor. We initially tested the reaction developed with the trifluoroborate salts (*cf.* 2.1) in a Vapourtec UV-150 module equipped with blue LEDs (17 W at 420 nm). Using the trifluoroborate salt (**155**), clogging issues were immediately observed in the flow equipment due to the rapid precipitation of insoluble potassium salts (**Table 5**). We therefore turned our attention towards the more soluble boronic pinacol ester analogue.

Initial test of the boronic ester starting material (**179**) in batch revealed the possibility of using it as a replacement for trifluoroborate salts. Despite the low yielding reaction (23% after 24 h), we were pleased to observe the desired reactivity. More importantly, the fully homogeneous solution of the boronic ester (**179**) in acetone could be eluted through the flow photoreactor without blockages, resulting in better result in less time (32% in 100 min). The faster reaction is not only due to the better design of the reactor but also to the significant difference in the light intensity of the two light sources (253 mW in batch *vs* 17 W in flow). Also, the rest of the mass balance was unreacted starting material, making further optimisation possible.

Table 5 – Initial comparison between batch and flow photochemical reactors using **155** and **179**.



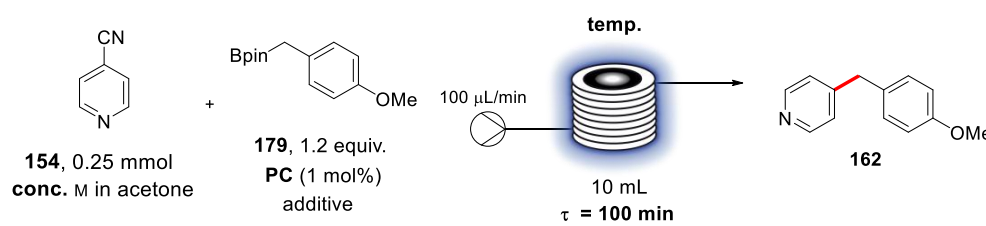
[B]	[batch] ^a	[flow] ^b
BF ₃ K (155)	76% in 16 h	<i>Clogging of the reactor</i>
Bpin (179)	23% in 24 h	32% in 100 min

^aReactions carried out by adapting **GP(II)** to the conditions described. ^bReactions carried out by adapting **GP(III)** to the conditions described.

Based on these preliminary results, we continued the optimisation of this reaction in the flow reactor. The desired premixed reaction mixture was eluted at 100 μ L/min through a 10 mL FEP tubing reactor coil^[221] irradiated by 17 W blue LEDs at 420 nm (**Table 6**). The

reaction slug was then collected and concentrated to determine the yield by crude $^1\text{H-NMR}$, using CH_2Br_2 as an internal standard. Previously optimised conditions were used as a starting point using 100 min residence time (maximum possible using this reactor, *cf.* 4.2.4). The effect of concentration was dramatic (*cf.* 2.2.4) with a doubling of the yield by changing from 0.06 M to 0.25 M (entry 1 *vs.* entry 2). One additional feature of this flow setup is the higher degree of temperature control that is not easily achieved with a batch photoreactor. Increasing the temperature from 35°C to 60°C (entries 2–4) allowed us to bring the reaction to completion at a fixed time of residence and concentration. Entry 4 describes optimised conditions yielding 88% of product after 100 min of irradiation. Selection of the photocatalyst was also a crucial parameter with the most oxidising photocatalysts being more potent.

Table 6 – Optimisation experiments for the coupling of boronic ester **179** with **154** in flow.



Entry	conc.	temp.	PC	additive	Yield ^a
1	0.06 M	35°C	Ir-3	-	32%
2	0.25 M	35°C	Ir-3	-	68%
3	0.25 M	45°C	Ir-3	-	77%
4	0.25 M	60°C	Ir-3	-	88% (81%)
5	0.25 M	80°C	Ir-3	-	88%
6	0.25 M	60°C	Ir-2	-	10%
7	0.25 M	60°C	Mes-Acr-1	-	84%
8	0.25 M	60°C	-	-	0%
9 ^b	0.25 M	60°C	Ir-3	-	0%
10	0.25 M	60°C	Ir-3	TEMPO (2.0 equiv.)	0%
11	0.25 M	60°C	no PC	AIBN (2.0 equiv.)	0%

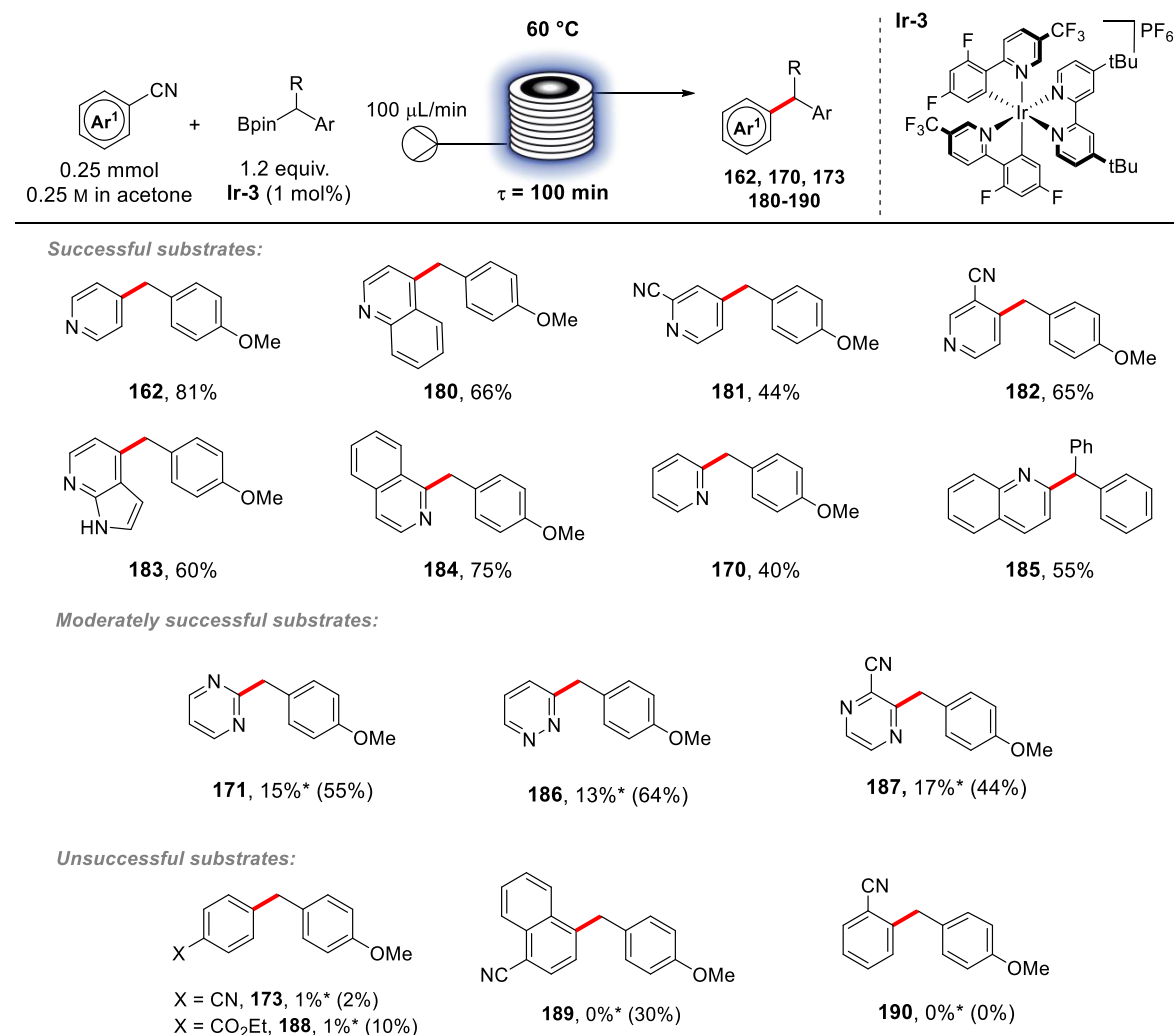
Reactions carried out by adapting **GP(III)** to the conditions described. ^aYield in **162** determined by $^1\text{H-NMR}$ analysis of crude reaction mixture using CH_2Br_2 as an internal standard. ^bIn the dark. Isolated yield in parentheses.

Interestingly the organic dye **Mes-Acr-1** provided **162** in high yield but was less general than the iridium-based **Ir-3** (see comparison on different substrates in **Table 8**). Control experiments confirmed the necessity of the photocatalyst (entry 8) and light (entry 9) to obtain conversion. Stable TEMPO radical additive (entry 10) also inhibited the supposed radical reaction and radical initiator AIBN could not trigger a radical chain reaction (entry 11).

2.2.2 Scope investigation

The scope of this new reaction was then explored starting with the problematic cyanoarenes scope observed previously (**Table 7**). The model substrate, 4-cyanopyridine was the most successful cyanoarene of those examined (**162**). Pleasingly, in addition to cyanopyridine, our transformation was successfully applied to several other *N*-heterocycles. Variations around the 4-cyanopyridine scaffold were possible with 4-cyanoquinoline (**180**) and other nitrile substituted 4-cyanopyridine derivatives (**181** and **182**) giving coupled products with selective coupling at the most electron-deficient 4-position. In these cases, the rest of the mass balance was unreacted cyanoarene. The unprotected 4-cyano-7-azaindole (**183**), commonly used as a bioactive scaffold,^[222] was also tolerated. The 2-pyridyl position was also reactive with 1-cyanoisoquinoline, 2-cyanoquinoline and 2-cyanopyridine all providing synthetically useful yields (**170**, **184** and **185**).

However, only limited success was obtained with diazines, with pyrimidine, pyridazine, and pyrazine (**171**, **186** and **187**) failing to deliver productive yields. Non-nitrogen-containing cyanoarenes were not coupled (**173**, **188–190**), leaving both the starting materials unreacted. Interestingly, *N*-heterocycles are generally seen as catalyst inhibitors for palladium-catalysed cross-couplings^[42] but proved to be crucial in our reaction (*cf.* 2.2.4).

Table 7 – Scope of cyanoarenes investigated to arylate boronic esters.

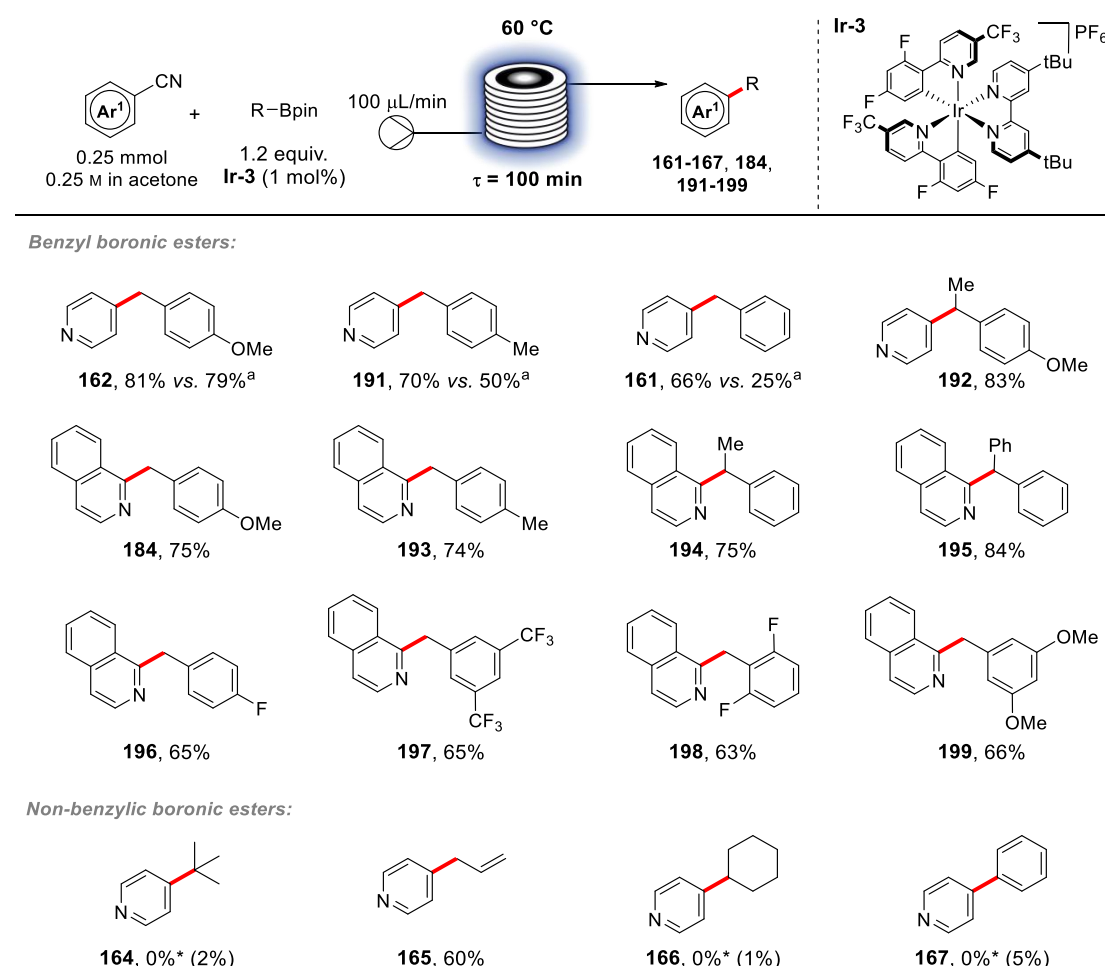
Reactions carried out by following **GP(III)**. Isolated yields unless otherwise stated. *Yield determined by ¹H-NMR analysis (tentative assignment) of crude reaction mixture using CH₂Br₂ as an internal standard. Conversion of the corresponding cyanoarene in parentheses.

The scope of boronic pinacol esters was then investigated. All the primary benzyl boronic esters tested were successfully coupled to 4-cyanopyridine (**154**). We compared the efficiency of the organic dye **Mes-Acr-1** on three examples (**161**, **162** and **191**), showing the lower efficiency of the dye when less reactive boronates were used (**161** and **191**). The low conversions associated with these reactions in addition to the discolouration (photobleaching) of the solutions appeared to suggest that instability of the dye is responsible for its lower activity. Hence, we continued investigating the scope with the more stable **Ir-3** catalyst. In addition to 4-cyanopyridine (**154**), the 1-cyanoisoquinoline (**184**) resulted in comparable isolated yields of coupling products. More challenging

secondary benzylic boronic esters also proceeded in high yields (**192**, **194** and **195**). In addition to the electron-rich methoxy and methyl groups, the benzyl boronates could be substituted with electron-withdrawing fluoro and trifluoromethyl groups in the *para*, *meta*, and *ortho* position of the $-\text{CH}_2\text{Bpin}$ without losing reactivity (**196** to **198**).

We then explored the reactivity of non-benzylic boronic esters and found that unlike with trifluoroborate salts (*cf.* **Table 3**), allyl boronic pinacol ester (**165**) was reactive under these reaction conditions. However, less activated cyclohexyl and *tert*-butyl boronic esters (**164** and **166**) were unreactive under these reaction conditions. The same observation was found for phenyl pinacol boronic ester (**167**), which did not react after 100 min of irradiation.

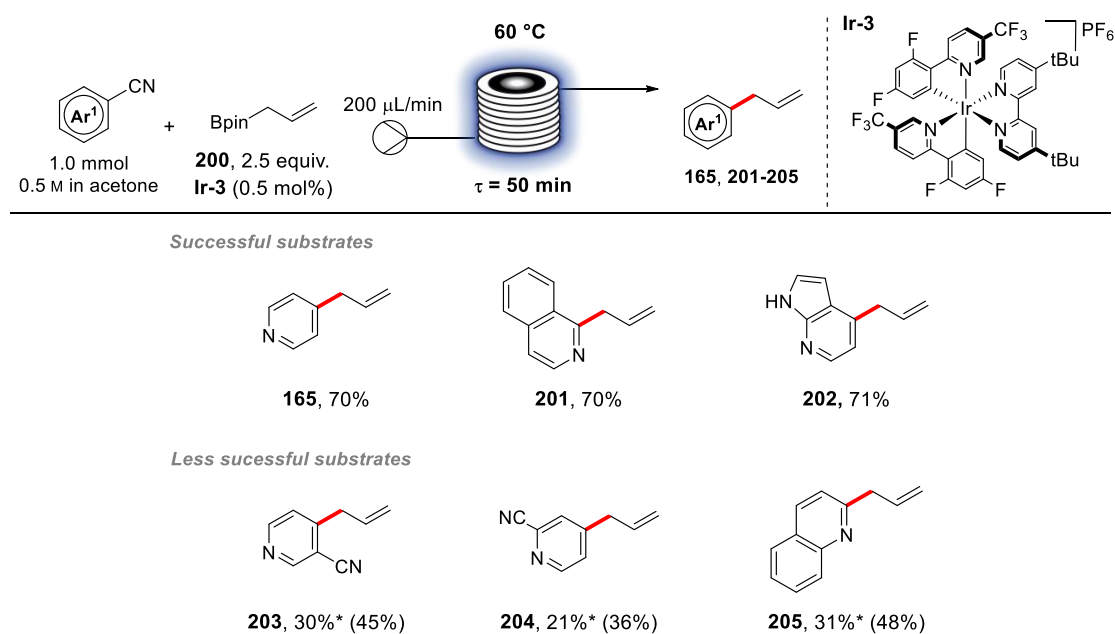
Table 8 – Scope of boronic esters to be arylated.



Reactions carried out by following **GP(III)**. Isolated yields unless otherwise stated. *Yield determined by $^1\text{H-NMR}$ analysis (tentative assignment) of crude reaction mixture using CH_2Br_2 as an internal standard. ^a**Mes-Acr-1** was used instead of **Ir-3**. Conversion of the corresponding cyanoarene in parentheses.

Starting from this observation, we could develop an optimised allylation protocol of heteroaromatic nitriles after optimisation of concentration, stoichiometry and residence time. This reaction would be problematic using an electrophilic allylation approach of a metallated aromatic ring due to the electron-deficiencies of the 2 and 4 positions of the pyridine rings and the competitive nucleophilicity of nitrogen-containing heterocycles. Using commercially available allyl boronic pinacol ester, the efficient synthesis of allylated heterocycles could be performed in only 50 min residence time (**Table 9**). Surprisingly only two protocols were described^[223,224] for the synthesis of 4-allylpyridine (**165**, sold at more than \$1500/g)^[225] and no protocol for the preparation of **201** and **202** could be found. Our method allowed the synthesis of these three allylated heterocycles in 70% yield.

Table 9 – Scope of cyanoarenes allylation in flow.

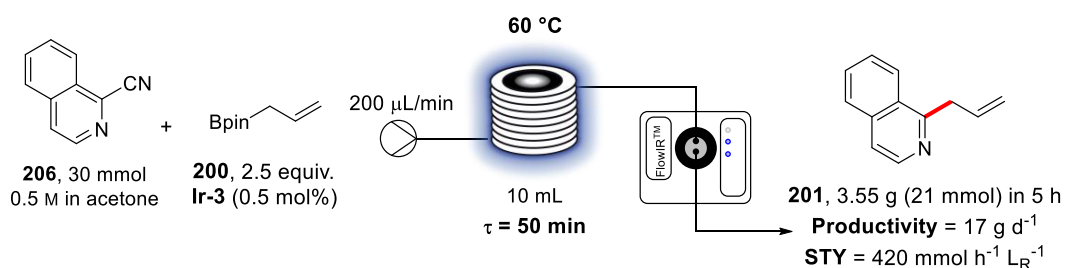


Reactions carried out by following **GP(IV)**. Isolated yields unless otherwise stated. *Yield determined by ¹H-NMR (tentative assignment) analysis of crude reaction mixture using CH₂Br₂ as an internal standard. Conversion of the corresponding cyanoarene in parentheses.

However, some substrates that were found suitable for the benzylation protocol were less successful partners using this allylation method (**203–205**). The reason for this is probably the longer irradiation time required to fully convert these less reactive starting materials. We did not further optimise the reaction conditions to accommodate these less reactive partners.

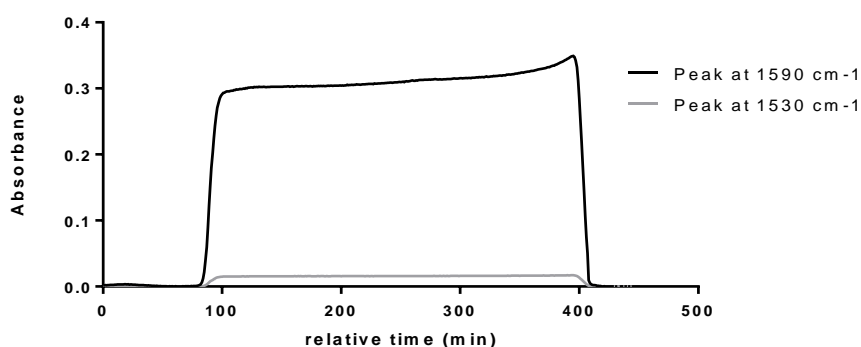
2.2.3 Larger scale reaction

Intensified conditions obtained with the optimised allylation protocol (0.5 M concentration and 50 min residence time) encouraged us to investigate the stability of the process when running the reaction for a longer time (**Scheme 31**).



Scheme 31 – Larger scale reaction conditions and setup (adapting **GP(IV)**).

Using the optimised conditions on 30 mmol scale, by eluting 60 mL of the reaction solution for 5 hours, 3.55 g of the allylated product was obtained. In theory, this process could deliver a throughput of 17 g d^{-1} of **201** using a 10 mL reactor. This productivity translates to a space-time yield (STY) of 420 $\text{mmol h}^{-1} \text{L}_R^{-1}$ meaning that using a visible light-modified Firefly reactor (120 mL internal volume) could potentially deliver a reasonable 200 g (or 1.2 mol) of product per day.^[226]

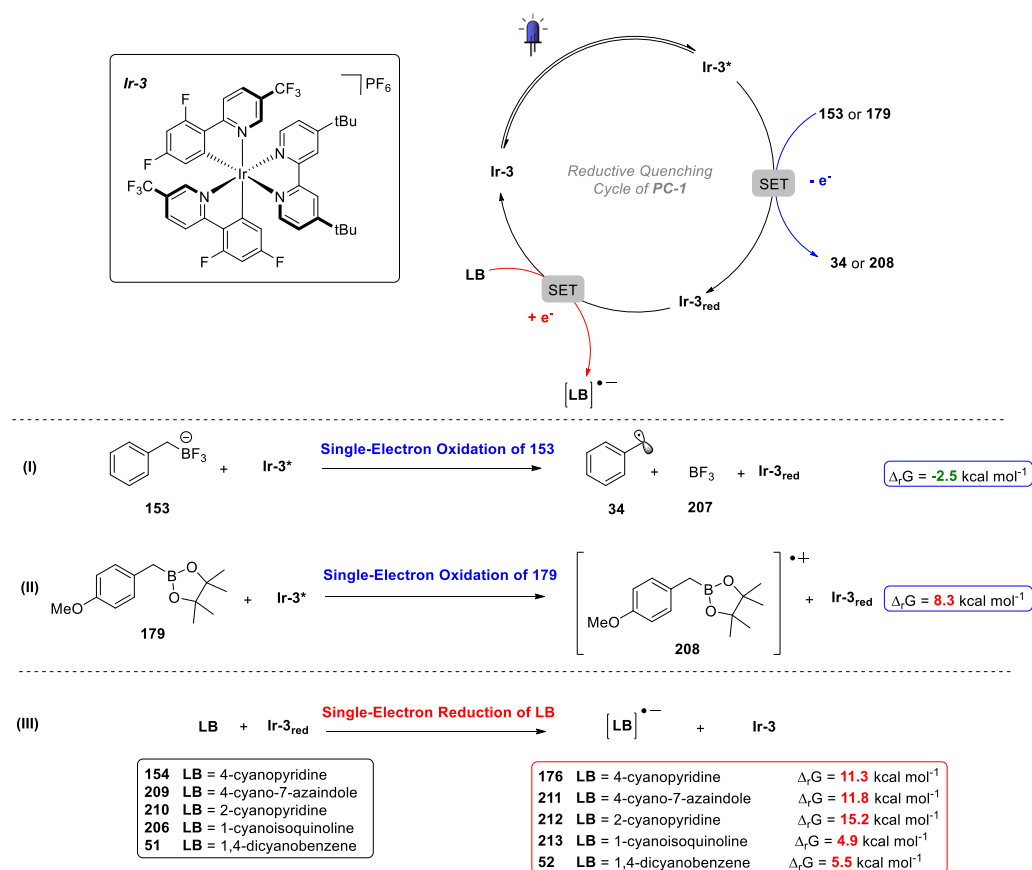


Graph 2 – In-line IR reaction monitoring spectra (1590 cm^{-1} for **201** and 1530 cm^{-1} for **206**).

The consistency of the production could be monitored by in-line IR spectroscopy (**Graph 2**).^[227] Product formation was observed with an intense band at 1590 cm^{-1} (aromatic C=C stretching of **201**) while no substantial residual cyanoarene starting material was observed (little peak at 1530 cm^{-1} accounting for the aromatic C=C stretching of **206**). No pressure issues were seen, and no particle generation was observed. Consequently, this process could be considered as stable and potentially scalable.

2.2.4 Mechanistic investigation using DFT[§]

To gain a better understanding of the mechanism of this new reaction we decided to investigate the feasibility of this transformation using calculations performed at DFT level.



Scheme 32 – The single-electron oxidation/reduction reactions of starting materials used with Ir-3 (Gibbs energies for single-electron transfer reactions).

Our starting hypothesis is that the photocatalyst Ir-3 reacts as an excited state oxidant. This is, in fact, often postulated^[62,118] as Ir-3 is a strong single-electron oxidant ($E_{1/2}^{*/red}(\text{Ir-3}) = +1.21 \text{ V}$) at the excited state and a poorer single-electron reductant ($E_{1/2}^{OX/*}(\text{Ir-3}) = -0.89 \text{ V}$). In this system, we are not using a single-electron donor capable to oxidise Ir-3* (e.g. 4-cyanopyridine, $E_{red}(\text{154}) = -1.78 \text{ V}$). We therefore initially postulated that Ir-3 follows a reductive quenching cycle, being quenched by good single-electron donors present in solution, as we postulated with the benzyl trifluoroborate salts previously ($E_{ox}(\text{153}) = +1.10 \text{ V}$).

Using this rationale, we initially calculated the standard reaction Gibbs energy for SET events of the starting materials (51, 153, 154, 179, 206, 209 and 210) with iridium species

[§]This work was conducted in the Lev Group in collaboration with Dr. Mikhail Kabeshov.

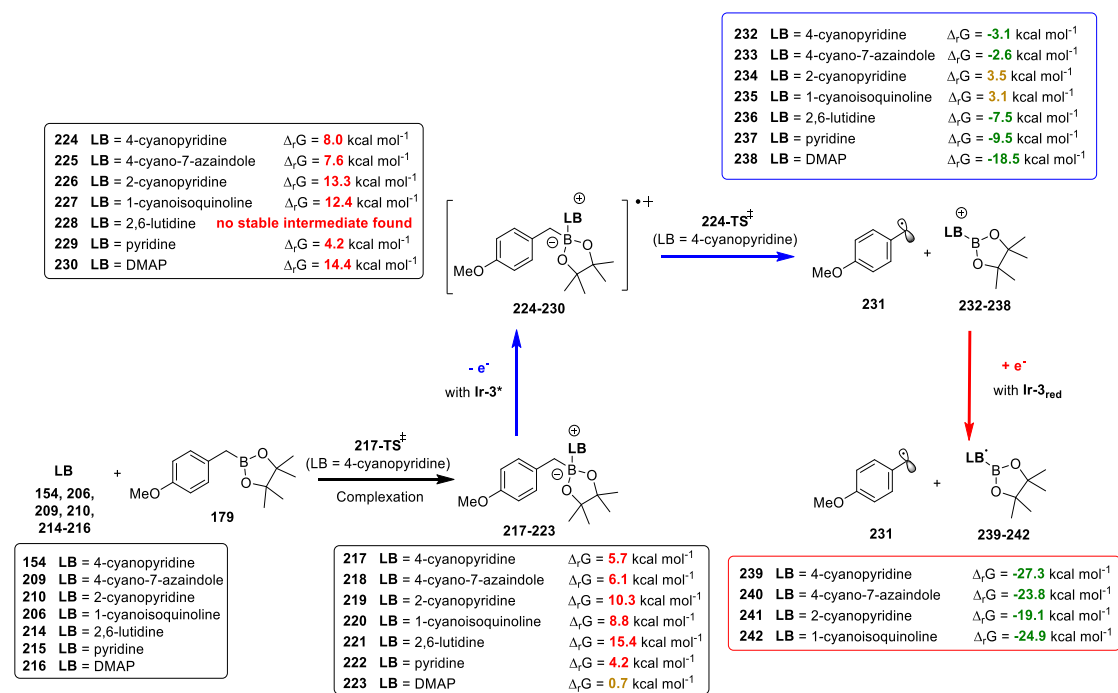
from the reductive quenching cycle of **Ir-3** (**Scheme 32**). Single-electron oxidation of boronic species (in blue) was initially investigated. Equation (**I**) shows that our model predicts the thermodynamic feasibility (negative Δ_rG) of the reductive quenching of **Ir-3*** with trifluoroborate salt (**153**) to spontaneously generate the dissociated benzyl radical **34** and BF_3 (**207**). However, under the same conditions, the single-electron oxidation of benzyl pinacol boronic ester **179** (equation (**II**)) was not calculated to lead to a dissociation and was attributed with a positive reaction Gibbs energy, meaning that the process is not thermodynamically favourable.

On the single-electron reduction side (in red), all cyanoarenes computed (**51**, **154**, **206**, **209** and **210**) are unable to accept an electron from the highly reducing **Ir-3_{red}** (equation (**III**)). It can be noted that in his arylation methods employing cyanoarenes, MacMillan employed the more potent single-electron donors such as **Ir-1**^[74,96] to reduce similar cyanoarenes ($E_{1/2}^{\text{ox}/*}(\text{Ir-1}) = -1.73 \text{ V}$ for $E_{\text{red}}(\text{51}) = -1.61 \text{ V}$).

These initial calculations informed us that the starting materials used cannot react favourably in SET reactions with the photoredox catalyst as such. These calculations are also in line with the redox potential comparison method that would predict the same outcome. Also, we started to think of more favourable reaction pathways.

When investigating the scope of this transformation (**Table 7**), we observed that only nitrogen-containing cyanoarenes were reactive in couplings with **179**. We consequently proposed that interactions between the heterocyclic compounds and the boronic ester (**179**) could be responsible for this significant reactivity difference. The reactive characteristic of the boronic ester functional group is its Lewis acidity (*cf.* 1.3.1). Since nitrogen-containing heteroaromatics are Lewis basic, we postulated that a Lewis acid-base adduct could be formed between the two starting materials and result in their activation towards single-electron transfers.

Complexations of model boronic ester (**179**) with various Lewis bases, either cyanoarenes used in the reaction (**LB = 154, 206, 209, 210**) or other pyridine derived Lewis bases (**LB = 214–216**), were then modelled (**Scheme 33**).



Scheme 33 – A favourable single-electron oxidation/reduction cascade pathway (reaction Gibbs energies for single-electron transfer reactions; mixture **179** + **LB** is set as a ground state for all the transformation).

Ease of complex formation (**217–223**) greatly depended on the Lewis basicity of pyridine-derived ring. With respect to **179**, the most favourable calculated complexation partner is the electron-rich DMAP (*cf.* **223** in **Figure 9**) and the least favourable is the sterically hindered 2,6-lutidine (**221**) whose 2- and 6-methyl groups clash with the methyl groups of the pinacol ligand of **179**.

Complexation events, although being endergonic, are equilibria and could be driven forward if consecutive reactions are favourable. We therefore calculated the Gibbs energies for single-electron oxidations of the complexes instead of **179** alone (blue arrow). Despite the instability of the intermediate radical cation produced (**224–230**), these oxidations allow a subsequent thermodynamically favourable C–B cleavage to the radical **7** and the cationic intermediates (**232–238**). C–B bond cleavage is characterised by a low barrier (1.7 kcal mol⁻¹ for **LB** = 4-cyanopyridine, **224-TS**[±]) thus occurring spontaneously after the single-electron oxidation step. These possible dissociations significantly transform the reaction energy profile of the oxidation (blue sequence) compared to the non-activated case (**(II)** in **Scheme 32** vs. **231** + **232–238** in **Scheme 33**).

Complex formation equilibria will then be driven forward as a result of the thermodynamically favourable C–B cleavage to the radical **231**. As the formation of **231** + **238** is the most favourable ($\Delta_r G = -18.5$ kcal mol⁻¹), DMAP is expected to be the

most efficient Lewis base among those tested to activate **179** towards single-electron oxidation.

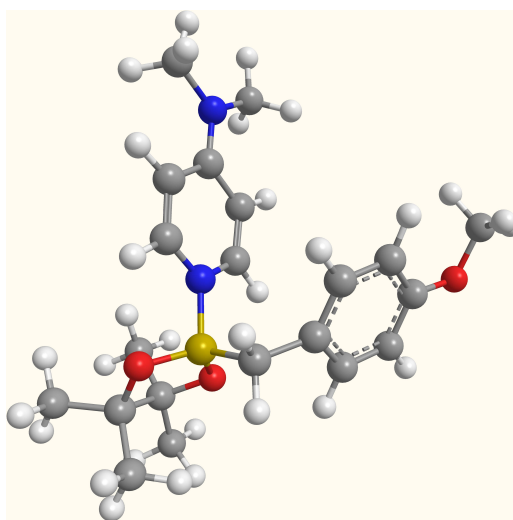


Figure 9 – Calculated structure of the complex **223** between **179** and DMAP.

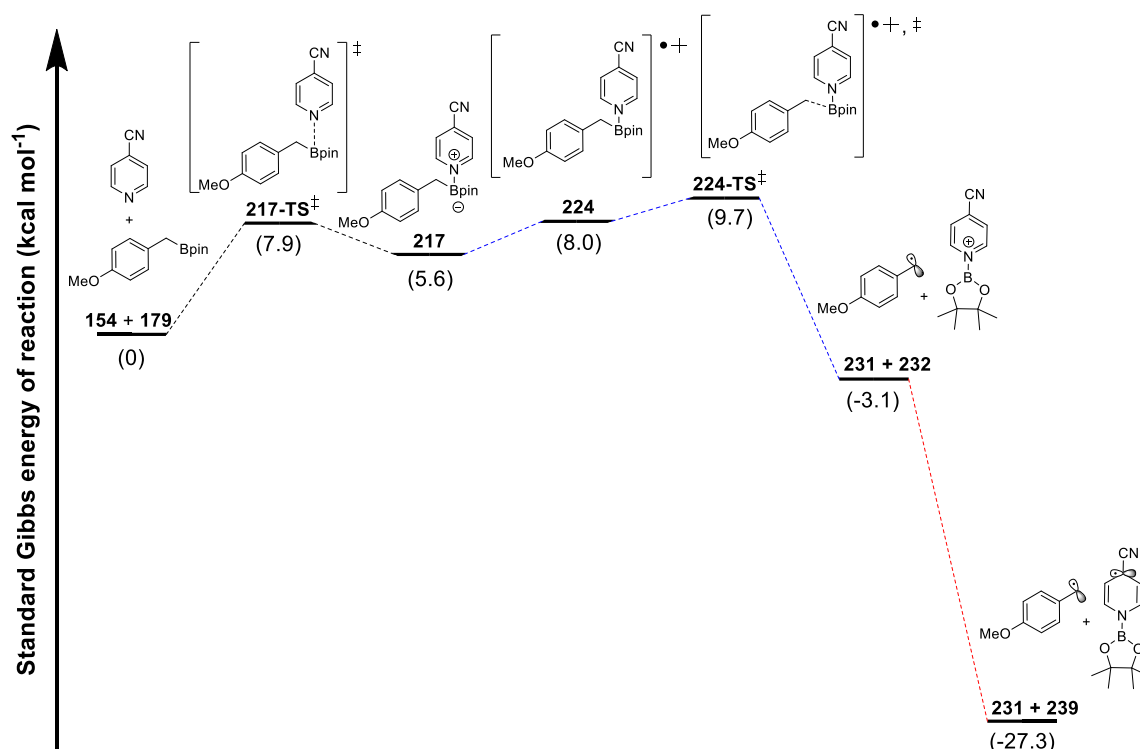
This pathway also produces heterocyclic cationic adducts **232–235** (after C–B cleavage), which are more electron-deficient and consequently easier to reduce than the neutral cyanoarenes. Therefore, we tested a subsequent single-electron reduction from the **Ir-3_{red}** species (red arrow). Formation of the radicals **239–242** from the cationic intermediates **232–235** was calculated to be extremely favourable (**Scheme 32**).

As a result, complex formation not only activated the boronic ester towards single-electron oxidation but also significantly activated Lewis basic cyanoarenes towards single-electron reduction.

To better illustrate the transformation, potential energy surface for the reaction of **179** with **154** was plotted representing the energies of all the intermediates and transition states involved in the calculated mechanism (**Scheme 35**). No transition states for pure single-electron transfer events (**217** to **224** and **231** + **232** to **231** + **239**) were located as these steps only consist of a pure vertical excitation with minimal nuclear rearrangements.

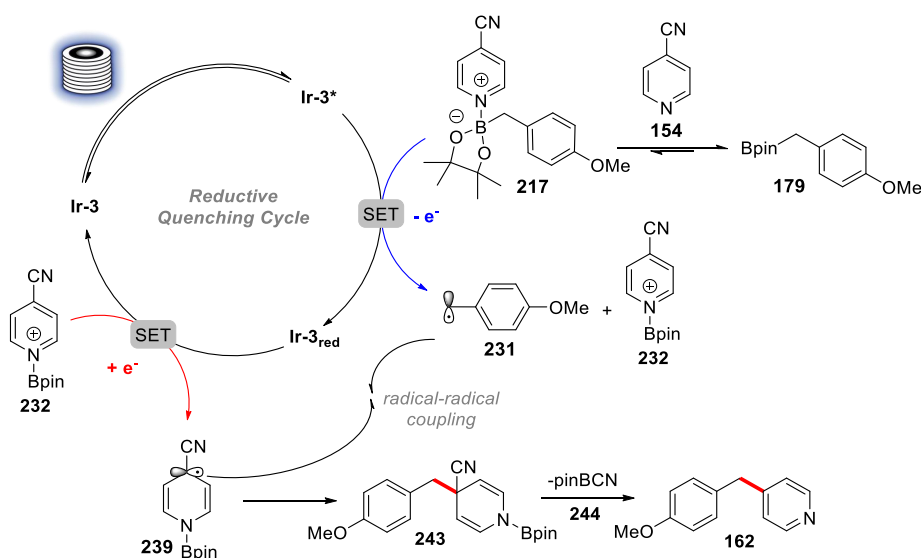
From this diagram, it can be seen that the oxidative fragmentation of the complex (**217** to **231** + **232**) is the rate-determining step of the reaction (**224-TS[‡]** having the highest energy on the potential energy surface). Both the initial complex formation and electronics of the boronic species will play a role in this critical step. Subsequent single-electron reduction from the pyridinium intermediate (**232**) is favourable (red dotted line), leading to two radicals (**231** + **239**) that can engage in radical-radical coupling to finally lead to the coupling product. These final steps will be exergonic from the radical intermediates.

With this model in mind, we can try to explain the effects observed earlier. Increase in the concentration of starting materials would increase the concentration of the complex **217** involved in the rate determining step (*cf.* **Table 6**). Temperature increase leads to increasing reaction rate to allow completion within the residence time of the reactor (*cf.* **Table 6**). Less Lewis basic heterocycles lead to less efficient couplings because of poorer complex formation, whilst and non-Lewis basic ones are not coupled at all due to the absence of the redox-activating adduct formation (*cf.* **Table 7**).



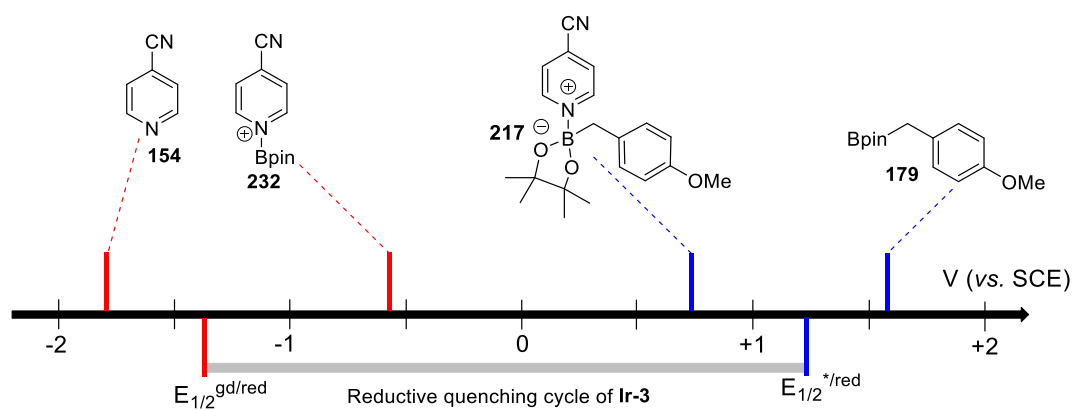
Scheme 34 – Potential energy surface of reaction between **179** and **154**.

To see if the rationalisation using redox potentials is also applicable, we estimated the standard reduction potentials of the species involved in the mechanism. This was achieved by calibrating the computed Gibbs reaction energies for electron transfer reactions against measured redox potentials of potassium benzyl trifluoroborate (E_{ox} (**153**) = +1.10 V)^[62] and 1,4-dicyanobenzene (E_{red} (**51**) = -1.61 V)^[74] as two structurally similar experimental reference points. Using these estimated potentials, we could describe the thermodynamic feasibility of the coupling between 4-cyanopyridine (**154**) and the boronic ester (**179**) using the calculated redox potentials (**Scheme 35**).



Scheme 35 – Proposed mechanistic description for the photoredox net-neutral coupling of cyanoarenes with boronic esters.

As described earlier, **154** and **179** can form a complex **217** (**Scheme 35**). This complex formation facilitates the single-electron oxidation of **179** ($E_{\text{ox}}(\mathbf{217}) = +0.73 \text{ V vs. } E_{\text{ox}}(\mathbf{179}) = +1.57 \text{ V}$). This value makes this SET event possible within the reductive quenching cycle of **Ir-3**. Based on our assumption, the excited **Ir-3*** species ($E_{1/2}^{*/\text{red}} = +1.21 \text{ V}$)^[228] is first quenched by **217** ($E_{\text{ox}} = +0.73 \text{ V}$) leading, after rapid C–B bond cleavage ($1.7 \text{ kcal mol}^{-1}$ barrier), to a carbon-centred radical **231** and the pyridinium **232**. The **Ir-3_{red}** ($E_{1/2}^{\text{gd/red}} = -1.37 \text{ V}$)^[228] species thus generated can reduce the activated pyridinium **232** ($E_{\text{red}} = -0.32 \text{ V}$) in a cascade fashion, generating the radical **239** that quickly couples with **231** to form an intermediate (**243**) that eliminates a boron-cyano species (**244**) to give the coupled product (**162**). The aqueous washing layer of the reaction workup was tested negative to cyanide with a commercial Quantofix® cyanide test (1 mg/L lower sensitivity).

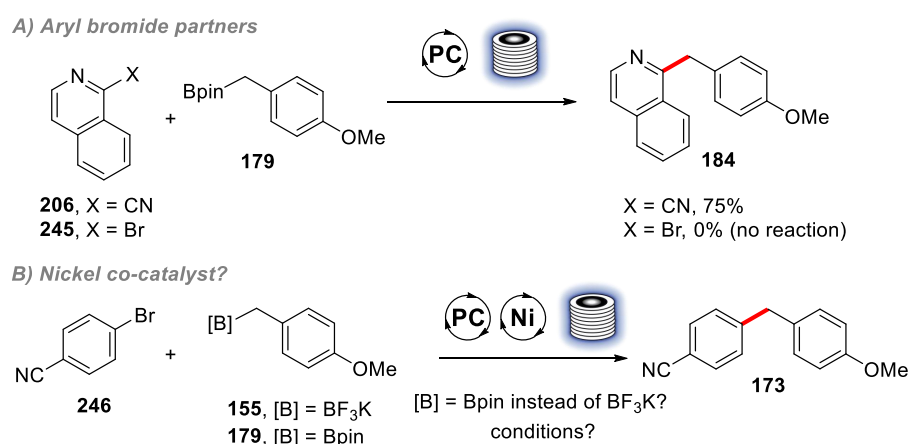


Scheme 36 – Calculated reduction potentials of the species involved in the boronic ester arylation against the reductive quenching cycle redox window of **Ir-3**.

Again, the redox window of the reductive quenching cycle of **Ir-3** is depicted in **Scheme 36** to better visualise the feasibility of the transformations described. The discovery that pyridinium species (**232**) are more easily reduced suggests that the 0.41 V difference observed in the trifluoroborate arylation (*i.e.* **Scheme 30**) could be easily overcome by complexation of the 4-cyanopyridine with BF_3 (liberated by oxidation of **155**).

2.3 Aryl bromide electrophiles: a Lewis base additive

We were interested to investigate if our newly discovered photoredox activation of boronic esters could be used with a wider range of aryl electrophiles. Scope limitations associated with cyanoarene coupling partners encouraged us to investigate aryl bromides as alternative electrophilic coupling partners. However, it was initially observed that they could not be engaged as “one-electron electrophiles” using the conditions previously developed for their cyanoarene homologues (**Scheme 37, A**). To cope with this reactivity mismatch, we decided to investigate the conditions used by Molander^[45] making use of an additional nickel catalyst to activate aryl bromides in a two-electron fashion (**Scheme 37, B** and 1.2.3.2 d).



Scheme 37 – Proposed rationale to use aryl bromides as alternative electrophilic partners.

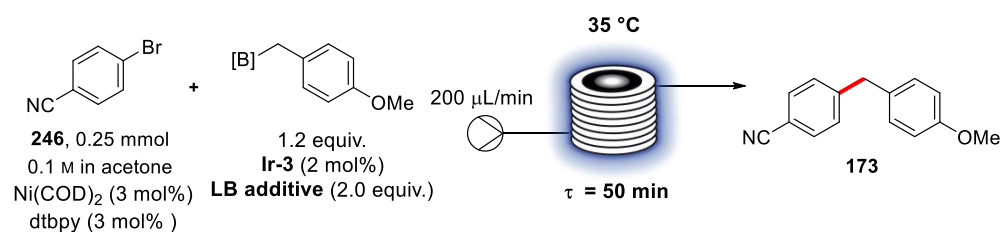
2.3.1 Optimisation

To begin this study, reaction conditions similar to those reported by Molander^[45] were examined with the exception that **Ir-3** was used instead of **Ir-4** as the initial photoredox catalyst in acetone (**Table 10**). Using the trifluoroborate salt (**155**), clogging issues were immediately observed in the flow equipment due to the rapid precipitation of insoluble potassium salts (entry 1). When switching to the commercial boronic pinacol ester (**179**), a fully homogeneous solution in acetone was obtained, but we failed to observe any cross-coupling product with the model aryl bromide (**246**). (entry 2).

Based on our calculations unveiling the effect of Lewis acid-base complexations on boronic ester single-electron oxidation (*cf.* 2.2.4), we changed the predicted non-active 2,6-lutidine additive (used by Molander) to a more coordinating Lewis base. Again, we

could observe a dramatic effect of the pyridine-derived Lewis base on the yield of the reaction. Without any base additive (entry 3) or using 2,6-lutidine (entry 2), no product formation was observed, while using the less sterically hindered pyridine or the more electron-rich DMAP resulted in a greatly enhanced formation of product (entries 4 and 5).

Table 10 – Effect of the pyridine-derived base additive on the dual Ir/Ni-catalysed cross-coupling using benzyl boronic esters in flow.



Entry	[B]	LB additive	K_{eq}^a	Yield ^b
1	BF ₃ K	2,6-lutidine	n/a	clogging
2	Bpin	2,6-lutidine	5.1×10^{-12}	0%
3	Bpin	none	n/a	0%
4	Bpin	Pyridine	8.1×10^{-4}	47%
5	Bpin	DMAP	0.30	87% (82%)

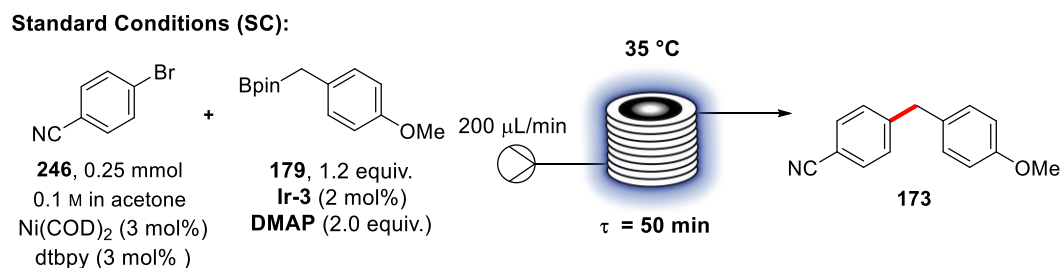
Reactions carried out by adapting **GP(V)** to the conditions described. ^aCalculated equilibrium constant between **179** ([B] = Bpin) and the base additive at 298 K in acetone using ωB97xD/cc-PVTZ+SMD-solvation level of theory (cf. 2.2.4). ^bYield in **173** determined by ¹H-NMR analysis of crude reaction mixture using CH₂Br₂ as an internal standard. Isolated yield in parentheses.

This behaviour correlates with our postulate that a Lewis acid-base adduct needs to form between the Lewis base additive and **179** to enable reactivity. We could estimate equilibrium constants of the corresponding Lewis bases complexing with **179** using the $\Delta_rG = -RT \ln(K_{eq})$ relationship with the computed complexation reactions (column 4). With these values, it becomes more apparent that complexation is playing a critical role in this transformation. Additionally, *in silico* studies of the resulting complexes confirmed, that complexation of **179** with pyridine or DMAP has a favourable single-electron oxidation pathway with Ir-3* (cf. 236–238 in Scheme 33).

Since we were satisfied with the 82% isolated yield in **173** using the boronic ester **179**, we have not re-optimised all parameters that were previously optimised by Molander.

As control experiments, Ni(acac)₂ could be used as a more practical nickel source (entry 2, **Table 11**) but resulted in a lower conversion after 50 min (rest of the mass balance being unreacted **246**).

Table 11 – Control experiments for the dual Ir/ Ni-catalysed benzyl pinacol ester arylation with aryl bromides in flow.



Entry	Variation from SC	Yield ^a
1	none	87%
2	Ni(acac) ₂ instead of Ni(COD) ₂	56%
3	no Ni(COD) ₂	0%
4	no Ir-3	0%
5	no light	0%
6	no dtbpy	52%

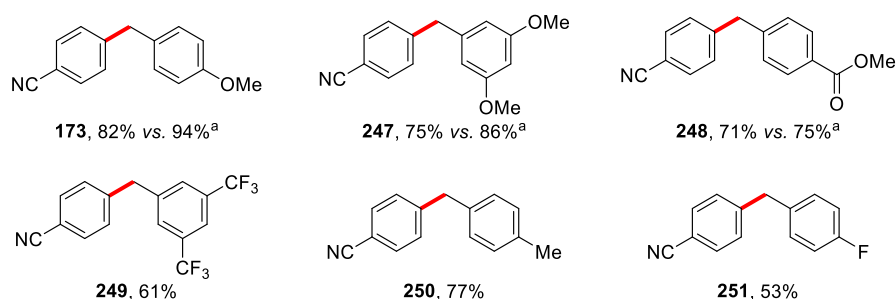
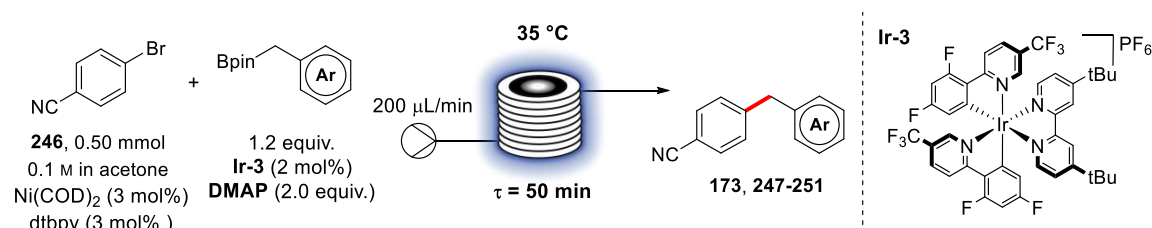
Reactions carried out by adapting **GP(V)** to the conditions described. ^aYield in **173** determined by ¹H-NMR analysis of crude reaction mixture using CH₂Br₂ as an internal standard.

Control experiments were then carried out. The absence of nickel, photocatalyst or light led to no product formation (entry 3 to 5). It was possible to observe a substantial amount of product without dtbpy probably because DMAP can act as a ligand (albeit less effective) to stabilise the Ni⁰ active species (entry 6).

2.3.2 Scope of the transformation

Based on these promising preliminary results, we explored the scope of boronic esters to be arylated with this method and compared it with the existing batch method^[45] using trifluoroborate salts (**Table 12**).

Table 12 – Scope of the dual Ir/Ni-catalysed benzyl boronic ester arylation in flow (boronate partner).



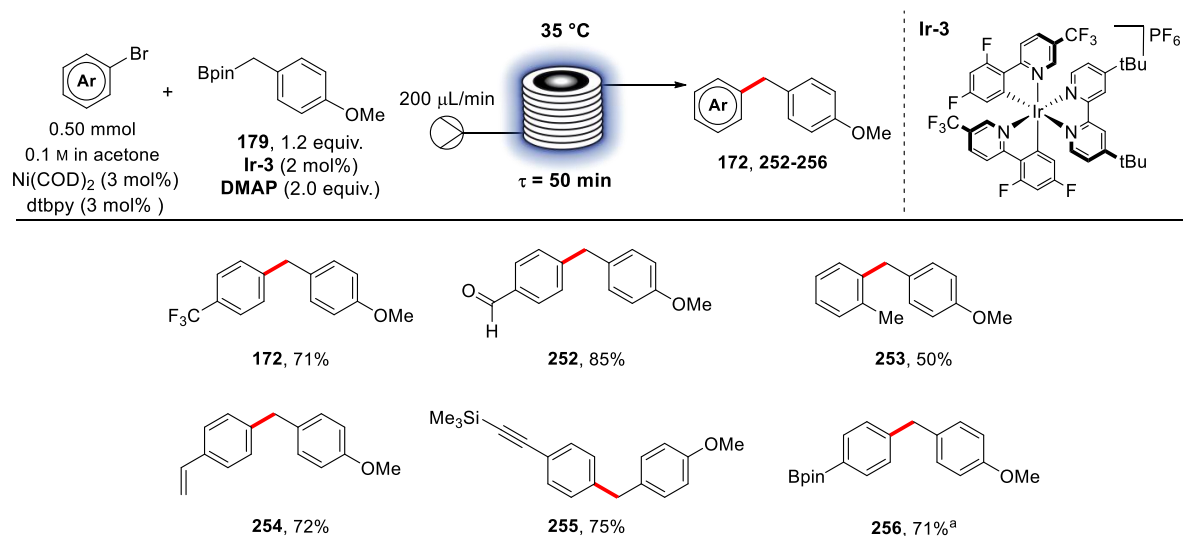
Reactions carried out by following **GP(V)**. Isolated yields. ^aIsolated yield reported by Molander for the product.^[45]

In general, the flow process using boronic esters resulted in slightly lower yields than the previously reported examples (**173**, **247** and **248**). However, the reaction time is dramatically decreased, from 24 h in batch (with trifluoroborate salts)^[45] to 50 min in flow, thus significantly increasing the productivity. As an example, space-time-yield (STY) of **173** with regard to the batch conditions is 2 mmol.h⁻¹.L⁻¹ (with 26 W CFL lamp) whereas the use of a flow photoreactor, allows us to reach an increased STY of 100 mmol.h⁻¹.L⁻¹ in **173**. This clearly shows the intensification of the process due to the improved solubility and more efficient light absorption.

The reaction scope revealed that electron-rich organoboron compounds proceeded in good to excellent yields (**173**, **247** and **250**) whereas compounds bearing electron-withdrawing substituents were associated with slightly lower isolated yields of coupled products (**248**, **249** and **251**). This observation is consistent with the putative single-

electron oxidation mechanism since higher electron-density will make the boronates more reactive towards oxidation.

Table 13 – Scope of the dual Ir/Ni-catalysed benzyl boronic ester arylation in flow (aryl bromide partner).



Reactions carried out by following **GP(V)**. Isolated yields. ^aIsolated as the phenol (**257**) after oxidation of the aryl boronic pinacol ester with H₂O₂/NaOH (**256** was difficult to purify using standard silica gel column chromatography).

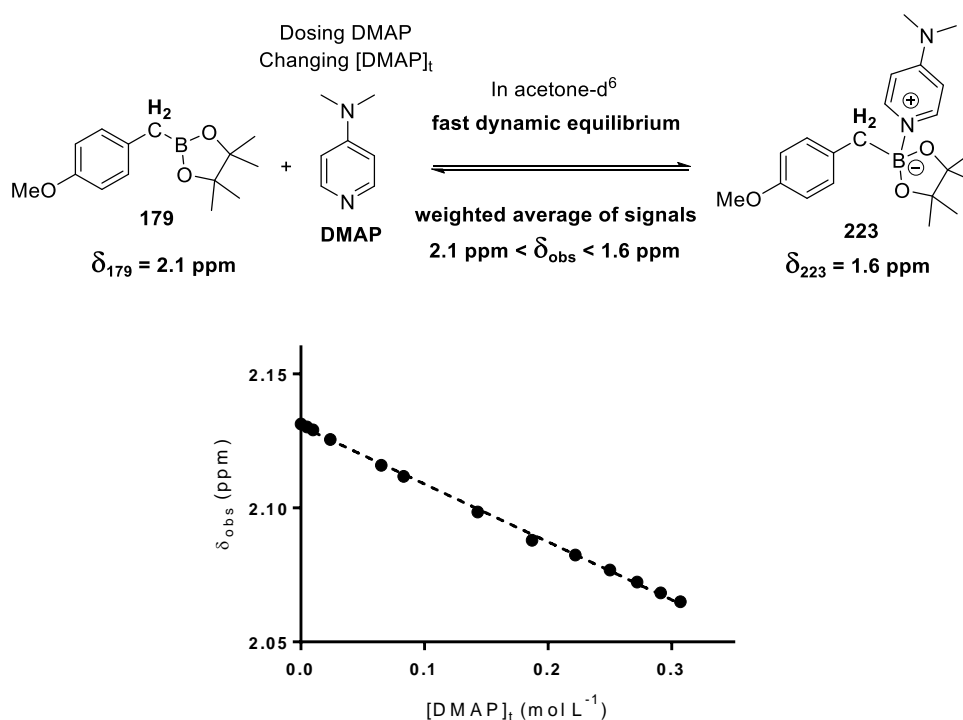
The aryl bromide coupling partners could also be varied, (**Table 13**) tolerating the presence of sensitive aldehyde (**252**), alkene (**254**) and alkyne (**255**) groups. Remarkably an *ortho*-substituent (**253**) is also well tolerated. The use of a boronic ester containing an aryl bromide (**256**) served to confirm the orthogonality between the C(*sp*²) and the C(*sp*³) coupling events. This observation means that subsequent orthogonal cross-couplings become a possible strategy.^[229]

2.3.3 Mechanistic experiments for DMAP activation

To validate our postulate of Lewis base activation discovered with DFT calculations, we decided to study experimentally the complex formation and the change of redox potentials that it induces.

2.3.3.1 Complexation study using NMR

A complexation study was carried out using ^1H -NMR spectroscopy. When studying the ^1H -NMR spectrum of the mixture **179** and DMAP in acetone- d_6 , we could observe that gradually increasing the total concentration of DMAP ($[\text{DMAP}]_t$) had a shielding effect on the signals of **179**, in particular for the benzylic CH_2 signal (δ_{obs} in **Graph 3**). This is an evidence for a fast, dynamic complex formation where weighted average signals of the complex **223** and independent **179** and DMAP signals are observed.^[230] We also tried to separate signals at a lower temperature (at 228 K and 213 K) but signals were still fully averaged at this temperature meaning that the equilibrium is faster than the timescale of NMR measurement, even at these low temperatures.



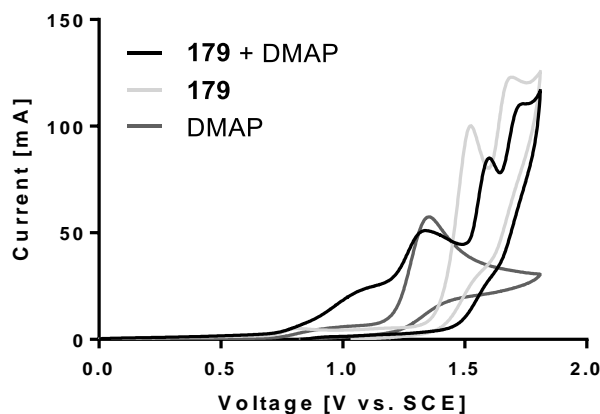
Graph 3 – Complexation study between **179** and DMAP using ^1H -NMR.

Following the protocol described by Espenson,^[230] we were able to extrapolate the equilibrium constant ($K_{\text{measured}} = 0.8$ vs. $K_{\text{calculated}} = 0.3$) and the chemical shift of the complex ($\delta_{223} = 1.6$ ppm). This experiment allowed us to validate the theory that complex formation was occurring in the reaction solvent between the boronic ester starting material (**179**) and Lewis base activator (DMAP). This also informs us that this equilibrium is fast compared to the time needed for the reaction to complete. Therefore, more of the complex will rapidly form when consumed to drive the reaction forward.

2.3.3.2 Redox study using cyclic voltammetry

The DFT calculations previously performed (2.2.4) predicted that the oxidation potential of the boronic ester **179** would be significantly reduced by the coordination of DMAP. Cyclic voltammetry measurements were then carried out to study the effect of the Lewis base complexation on the redox potential of the boronic pinacol ester (**Graph 4**).

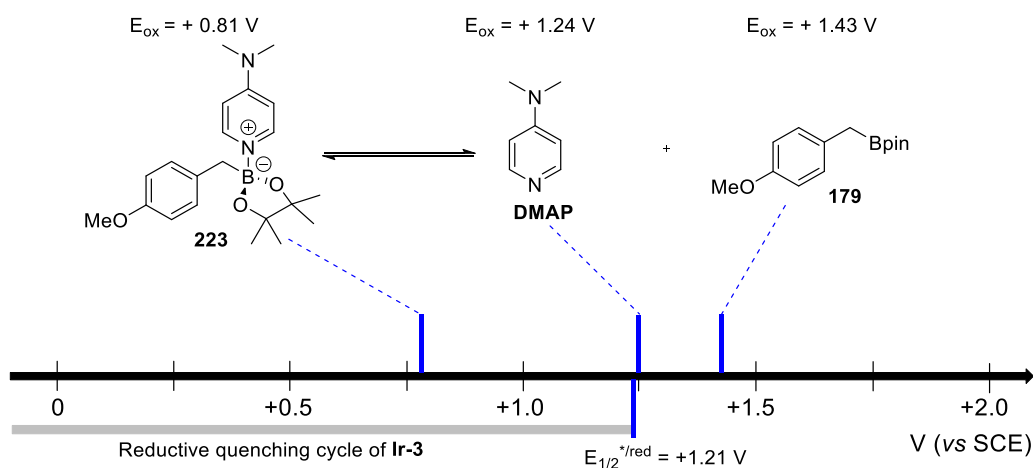
Due to the generation of radicals during oxidation of the analytes, which undergo further reactions, all cyclic voltammograms showed an asymmetric shape describing the irreversibility of the oxidation. Small deviations of the oxidation traces from the baseline (DMAP and **179** measurements) were justified as an effect of the electrolyte solution.



Graph 4 – Oxidation traces of the cyclic voltammograms with boronic ester **179** and DMAP.

The redox potentials of DMAP ($E_{\text{ox}} = +1.24$ V) and the model boronic ester ($E_{\text{ox}}(\mathbf{179}) = +1.43$ V) were initially quantified (dark and light grey lines respectively). The first maximum in the measurement with the ester **179** corresponds to the formation of the benzylic radical and the second maximum is assumed to refer to its oxidation to the

benzylic cation.^[231] Then a 1:1 mixture of DMAP and the boronic ester **179** was measured (black curve). Apart from the oxidation waves of residual DMAP and **179** there is a new local maximum at a lower potential, which could be attributed to the oxidation of the **223** zwitterionic complex in the mixture. The measured potential (E_{ox}) for this maximum is +0.81 V and corresponds to the previously calculated value for a similar complex in acetone (E_{ox} (**227**) = +0.73 V). The appearance of this new maximum in addition to the NMR complexation study consequently confirms the calculations previously described.

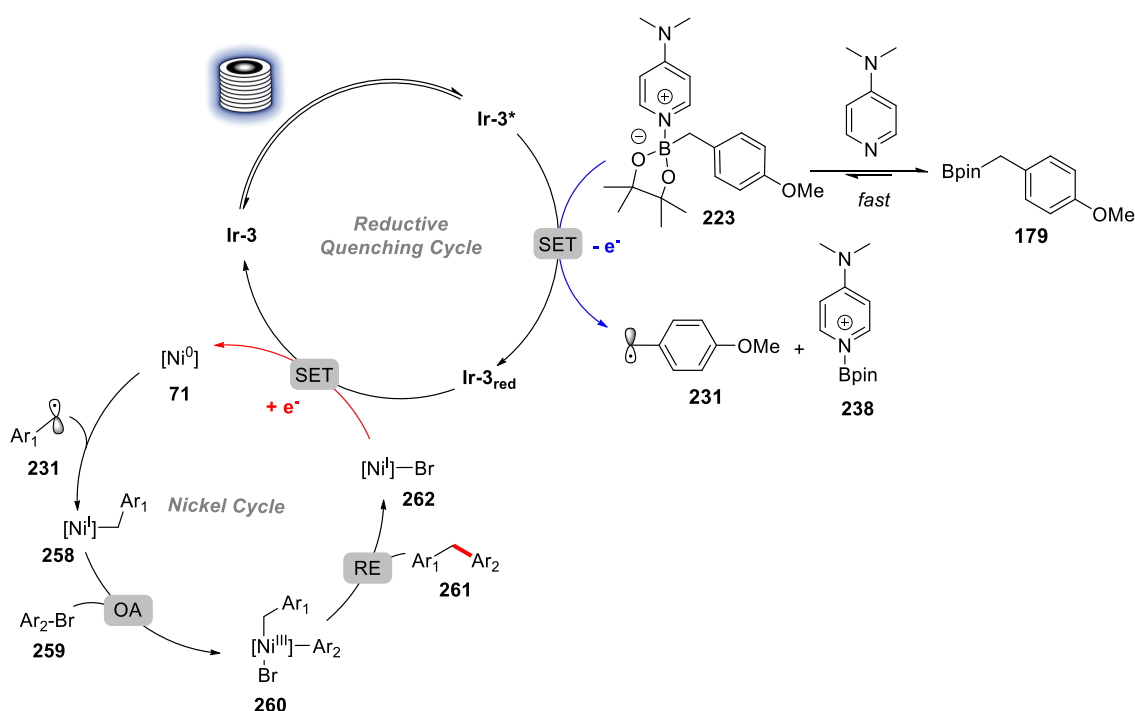


Scheme 38 – Oxidation potentials of the species resulting from the **179** and DMAP mixture versus the reductive quenching cycle of **Ir-3**.

The presence of DMAP in the mixture allows the formation of a more readily oxidised complex (**223**, **Scheme 38**). The excited state of the photocatalyst ($E_{1/2}^{*/\text{red}}$ (**Ir-3**) = +1.21 V)^[228] can be preferentially quenched with **223** (E_{ox} = +0.81 V) and not **179** (E_{ox} = +1.43 V) nor DMAP (E_{ox} = +1.24 V) to initiate the radical reaction. It can be noted that this oxidation potential is even lower than the trifluoroborate equivalent (E_{ox} (**153**) = +1.10 V) making boronic ester complexes more reactive than commonly used trifluoroborate salts.

2.3.4 Proposed mechanism

This transformation is believed to proceed *via* a similar mechanism as the one using trifluoroborate salts disclosed by Molander.^[45] The main difference comes from the initial radical formation, as observed in the NMR experiment, a fast, dynamic complexation happens in solution between the DMAP additive and **179**. The resulting complex is then readily oxidised by the **Ir-3*** excited photoredox catalyst to form the radical **231** and the pyridinium **238** as previously explained in 2.3.3.



Scheme 39 – Proposed mechanistic description for the dual nickel and photoredox-catalysed coupling of aryl bromides with boronic esters.

This radical (**231**) is then engaged in a “one-electron transmetalation” with the Ni⁰ species (**71**) to lead to a Ni^I complex (**258**), which is able to undergo oxidative addition with an aryl bromide (**259**).^[120] The Ni^{III} complex (**260**) can then undergo reductive elimination to provide the coupled product (**261**). This process generates a Ni^I species (**262**) that is reduced back to the active Ni⁰ catalyst (**71**) by the action of the Ir-3_{red} complex, thereby closing both catalytic cycles by regenerating the nickel and iridium catalysts.

2.3.5 Summary and conclusions

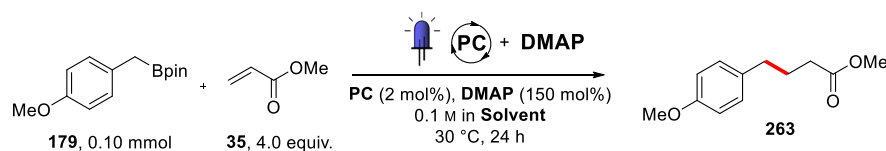
In summary, we have demonstrated a new activation mode of boronic esters that allow them to react under photoredox conditions by the formation of a complex with a pyridine-based Lewis base. This modification not only enhanced the existing chemistry with trifluoroborate salts but also facilitated its application to flow chemistry. These results enabled the development of a new and efficient $C(sp^2)-C(sp^3)$ photoredox coupling process using heteroaromatic nitriles and pinacol boronic esters, whereby no additive other than the photoredox catalyst is required.^[232] This method allowed us to identify nitrogen-containing heteroarenes as key activators of the boronic ester partners. An external Lewis base additive (*e.g.* DMAP) could be used to activate benzylic boronic esters towards photoredox methods. However, this additive is used in stoichiometric quantities and is not “redox-innocent” (*cf.* 2.3.3.2). Further development of this method is therefore desirable to access a wider range of coupled products.

3 Photoredox alkylations of boronic esters and acids: a Lewis base catalyst

3.1 Optimisation

Having proved that alkyl boronic esters were conveniently arylated in a redox-neutral setting, we decided to investigate if these could be efficiently alkylated using photoredox catalysis. The addition of electron-rich carbon-centred radicals onto electron-deficient olefins, also known as “Giese-type” additions, is a powerful method to form C–C bonds in a redox-neutral fashion (*cf.* 1.2.3.2 a). We initially subjected the model boronic ester (**179**) to an excess of methyl acrylate (**35**) in the presence of 1.5 equiv. of DMAP additive and the Ir-3 photoredox catalyst (**Table 14**) that was already shown to be quenched by DMAP activated **179** (*cf.* 2.3.3).

Table 14 – Solvent and catalyst optimisation for radical addition to methyl acrylate (**35**).



Entry	PC	Solvent	Yield ^a
1	Ir-3	Acetone	54%
2	Ir-3	Acetonitrile	62%
3	Ir-3	MeOH	74% (69%)
4	Ir-3	Acetone:MeOH (95:5)	66%
5	Ir-3	Acetone:MeOH (1:1)	77% (74%)
6	Ir-4	Acetone:MeOH (1:1)	86% (75%)
7	Ir-2	Acetone:MeOH(1:1)	71%
8	Ir-1	Acetone:MeOH(1:1)	0%
9	Mes-Acr-1	Acetone:MeOH(1:1)	23%

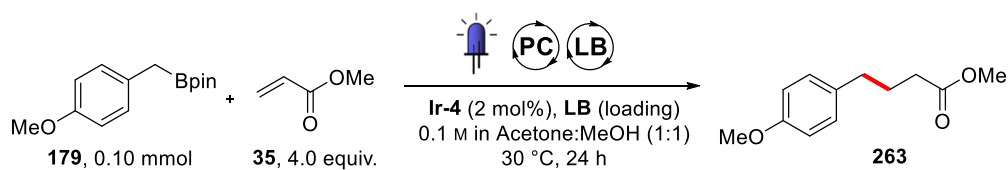
Reactions carried out by adapting **GP(VI)** as described. ^aYield in **263** determined by ¹H-NMR analysis of crude reaction mixture using CH₂Br₂ as an internal standard. Isolated yields in parentheses.

Irradiation of this mixture in acetone with blue LEDs for 24 h readily led to 54% yield of the coupling product (**263**) (**Table 14**, entry 1). Initial solvent screening revealed that the use of methanol provided a clean reaction (entry 3 vs. entries 1 and 2). This solvent was mixed with acetone in 1:1 proportions to obtain the best solvent system (entry 5). The photocatalyst also played a key role in the outcome of the reaction. While strongly oxidative iridium catalysts (**Ir-3** and **Ir-4**, entries 5 and 6) revealed to be the most efficient of the ones tested, the strongly reducing **Ir-1** could not catalyse the reaction at all (entry 8). The **Mes-Acr-1** organic dye (entry 9) was not suitable for this transformation either.

Despite having selective reaction conditions to perform this radical addition, the reaction conditions still use 150 mol% of DMAP additive to activate the boronic ester (**179**). In order to improve the practicality of the reaction conditions, we considered reducing the amount of Lewis base additive used. Lewis base catalysis was introduced as a concept by Denmark to enhance the reactivity of electrophilic n^* , π^* and σ^* orbitals.^[233] Based on this knowledge, we hypothesised that the use of a catalytic amount of an organic Lewis base would be a viable option for the photoredox activation of boronic esters. In fact, activation of diboron compounds using Lewis base catalysts have already been reported,^[234] however, the concept has never been applied for the activation of organoboron compounds.

Pleasingly, reducing DMAP catalyst loading to 20 mol% still provided 75% yield of **263** (**Table 15**, entry 1), with the remaining mass balance resulting from oligomerisation due to multiple acrylate additions. Pleased by this level of catalytic activity, we decided to investigate a wider range of Lewis bases (**Table 16**).

According to Denmark's theory, n - n^* interactions are the most productive type of interactions for a Lewis base catalyst activity,^[233] so a range of commercial neutral Lewis bases with an available non-bonding n orbital was screened at 20 to 50 mol% loading (**Table 15**). While other members of the pyridine family performed poorly (entries 2 and 3), quinine and quinidine delivered synthetically interesting yields (entries 4 and 5). This finding led us to screen other bases having a strongly Lewis basic^[235] quinuclidine-like scaffold. In this family, DABCO, quinuclidine, and quinuclidin-3-ol were identified as excellent catalysts, leading up to 80% yield of **263** (entries 6 to 8).

Table 15 – Lewis base catalyst optimisation.

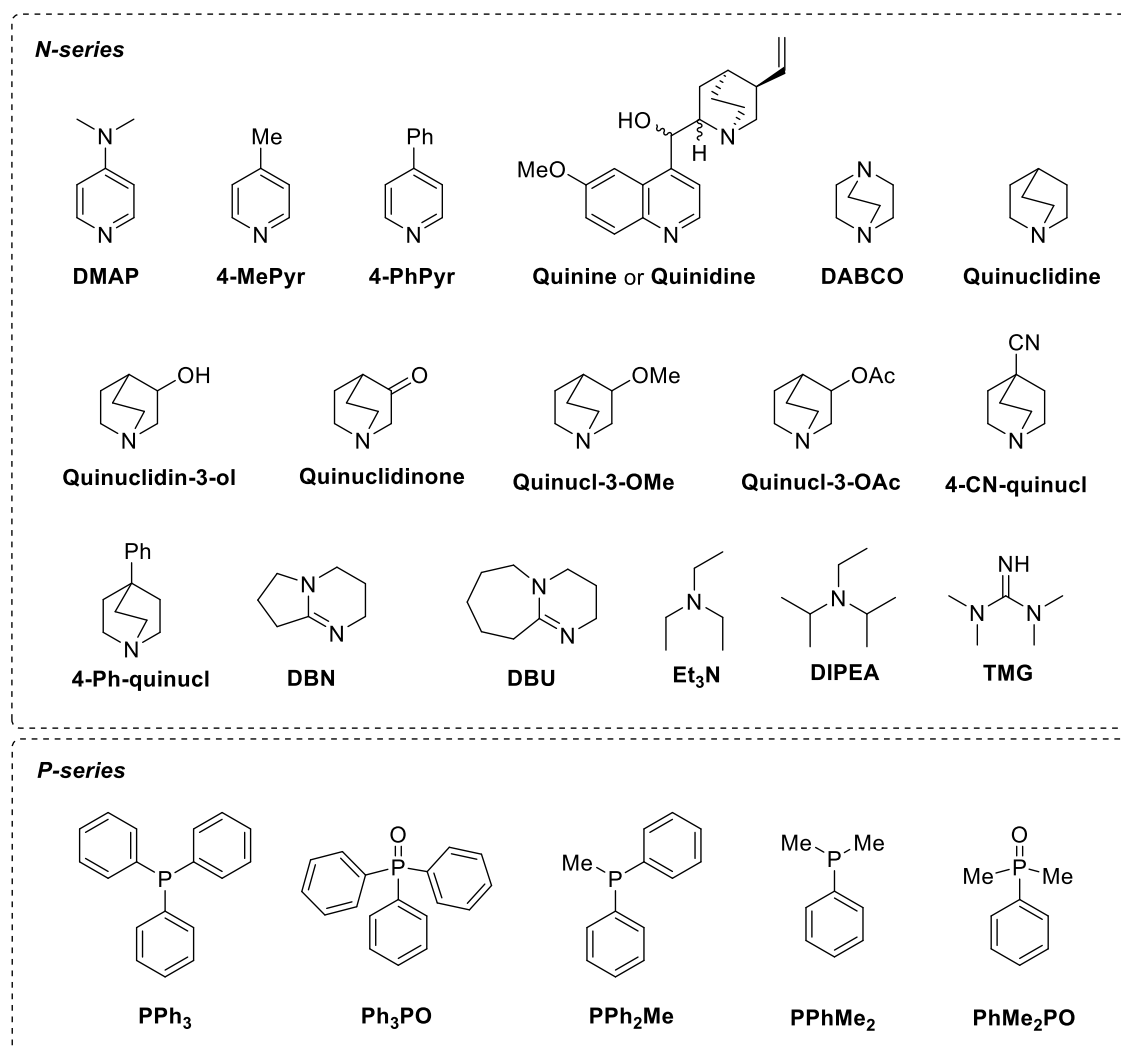
Entry	Lewis Base (LB)	Loading	Yield ^a
1	DMAP	20 mol%	75%
2	4-MePyr	20 mol%	7%
3	4-PhPyr	20 mol%	12%
4	Quinine	20 mol%	65%
5	Quinidine	20 mol%	53%
6	DABCO	20 mol%	65%
7	Quinuclidine	20 mol%	77%
8	Quinuclidin-3-ol	20 mol%	80%
9	Quinuclidinone	20 mol%	43%
10	Quinucl-3-OMe	20 mol%	7%
11	Quinucl-3-OAc	20 mol%	65%
12	4-CN-quinucl	20 mol%	42%
13	4-Ph-quinucl	20 mol%	73%
14	DBN	50 mol%	54%
15	DBU	50 mol%	16%
16	Et ₃ N	50 mol%	44%
17	DIPEA	50 mol%	22%
18	TMG	50 mol%	0%
19	PPh₃	20 mol%	75%
20	Ph ₃ PO	20 mol%	0%
21	PPh ₂ Me	20 mol%	53%
22	PPhMe₂	20 mol%	80%
23	PhMe ₂ PO	20 mol%	0%

Reactions carried out by adapting **GP(VI)** to the conditions described. ^aYield in **263** determined by ¹H-NMR analysis of crude reaction mixture using CH₂Br₂ as an internal standard.

Other commonly employed nitrogenous bases were tested (entries 14 to 18) but did not show comparable activity, probably because of their lower Lewis basicity.^[235]

Phosphine-derived Lewis bases were then investigated with triphenylphosphine (PPh₃) and dimethylphenylphosphine (PPhMe₂) showing both good activities (entries 19 and 22). However, the ease of oxidation of PPhMe₂ coupled to the inactivity of its corresponding phosphine oxide (entry 23) led us to consider other Lewis bases as cheap and easily handled catalysts.

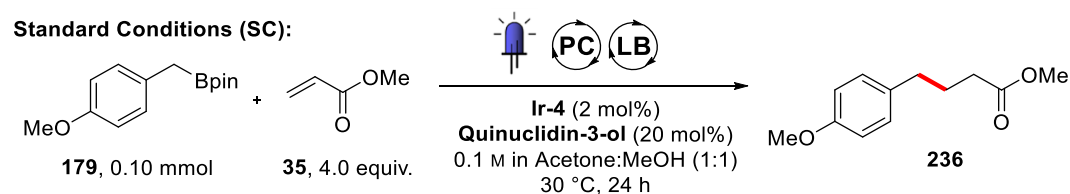
Table 16 – Structures and names of Lewis base catalysts investigated.



Once suitable Lewis bases were identified, a final optimisation was performed against our best conditions using quinuclidin-3-ol as the Lewis base catalyst (**Table 17**). While increasing the photocatalyst loading to 3 mol% slightly increased the reaction yield from 80% to 84% (entry 2 vs. entry 1), a photocatalyst loading of 2 mol% was utilised for the

remaining experiments to conserve the precious iridium photocatalyst. **Ir-3** could also be used instead of **Ir-4** without a major effect on the reaction yield (entry 3).

Table 17 – Final optimisation and control experiments for the Lewis base-catalysed alkylation of boronic esters.



Entry	Variation from SC	Yield ^a
1	none	80% (75%)
2	3 mol% Ir-4	83%
3	Ir-3 instead of Ir-4	79%
4	Acetone as solvent	8% (20% conv.)
5	Acetone:MeOH (9:1) as solvent	42% (54% conv.)
6	non-degassed	40%
7	0.2 mmol of 35	65%
8	10 mol% Quinuclidin-3-ol	71%
9	5 mol% Quinuclidin-3-ol	53%
10	reaction time = 6 h	73% (92% conv.)
11	no photocatalyst	0%
12	no light	0%
13	no Lewis base	0%

Reactions carried out by adapting **GP(VI)** to the conditions described.^aYield in **263** determined by ¹H-NMR analysis of crude reaction mixture using CH₂Br₂ as an internal standard. Isolated yield or conversion in parentheses.

Interestingly, the use of acetone as the only solvent resulted in only 20% of conversion of **179** and a poor reaction yield (entry 4). This observation suggested that the methanol is important for turnover of the Lewis base catalyst since 20 mol% of Lewis base catalyst resulted in 20% conversion without methanol. Degassing of the solvents was identified as a critical parameter to efficiently reproduce the results, probably because of competitive quenching of the photocatalyst by dioxygen (entry 6). Reducing the amount of olefin (entry 7) or Lewis base catalyst (entries 8 and 9) was not beneficial either. Finally, control

experiments revealed the independent importance of the photocatalyst, light and Lewis base for the reaction to lead to any product formation (entries 11 to 13).

3.2 Scope of the transformation

With an optimised set of reaction conditions identified, we then investigated the scope of this optimised transformation (**Figure 10**). To perform this reaction scope, we kept in mind that various Lewis bases were identified as powerful catalysts at 20 mol% loading and could perform differently when using different boronic esters.

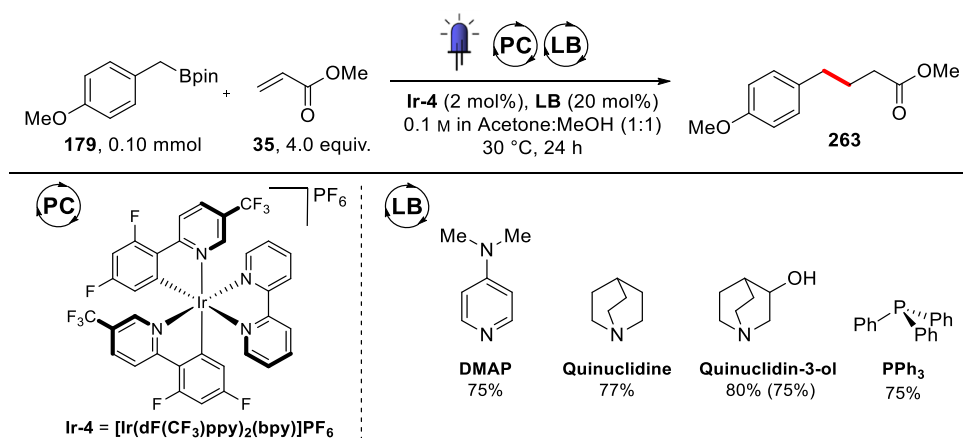
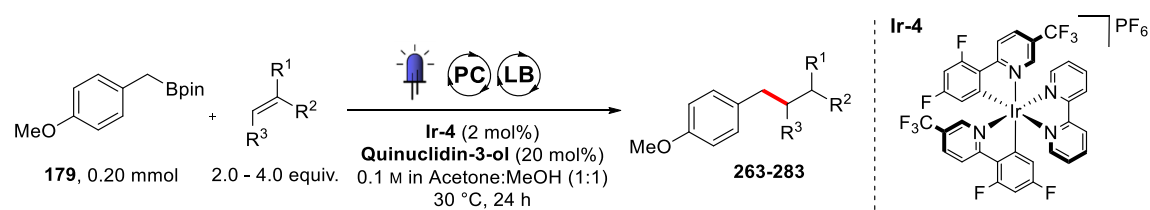
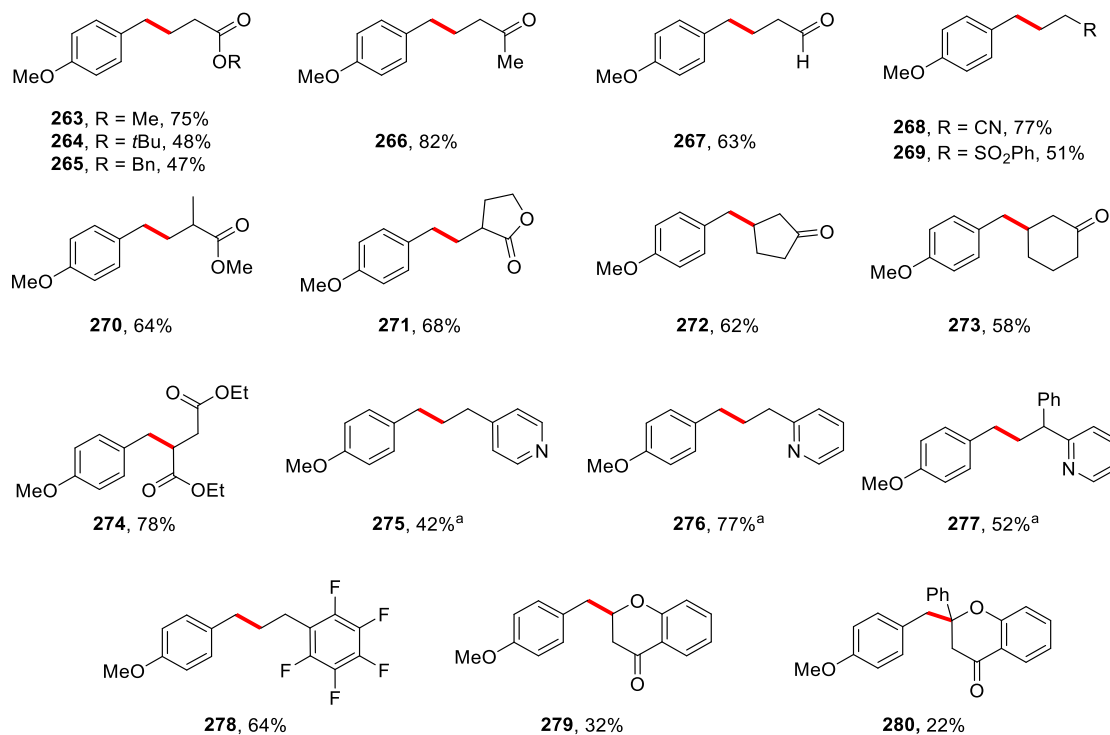
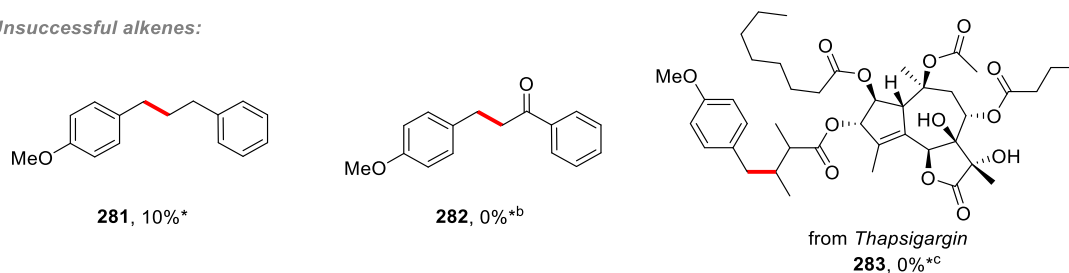


Figure 10 – Optimised conditions summary for “Giese-type” addition of boronic ester **179** on **35** including selected Lewis base catalysts (LB).

3.2.1 Scope of alkenes

We initially assessed the scope of alkenes to be engaged in radical coupling with boronic ester **179** using quinuclidin-3-ol as the Lewis base catalyst (**Table 18**). In addition to methyl acrylate, *tert*-butyl and benzyl acrylates were also successful coupled partners (**263–265**). Methyl vinyl ketone (MVK) was identified as the best coupling partner with conjugate addition product isolated in 82% yield (**266**). Pleasingly, acrolein and acrylonitrile coupled products (**267** and **268**) were also obtained in high yields, thereby expanding the range of functional groups tolerated with this method. *gem*-Disubstituted olefins also reacted in a radical conjugate addition fashion, with methyl methacrylate (**270**), a conjugated lactam (**271**) and two cyclic enones (**272** and **273**) selectively coupled in 58% to 68% yield.

Table 18 – Scope of alkenes to couple with boronic ester **179**.*Successful alkenes:**Unsuccessful alkenes:*

Reactions carried out by following **GP(VI)**. Isolated yields. ^aSimilar yields were obtained without **LB**. ^bfrom TMS-enol ether. ^c*Z/E* isomerisation of the double bond of thapsigargin was observed as the only product. *Yield determined by ¹H-NMR analysis (tentative assignment) of crude reaction mixture using CH₂Br₂ as an internal standard.

Interestingly, 2- and 4-vinyl pyridines were successfully alkylated at the β -carbon (**275** and **276**) providing examples of challenging *N*-heteroaromatics. These results could be extended to a 2-pyridyl-containing 1,1-disubstituted olefin partner (**277**), showcasing the possibility to generate pheniramine analogues and the potential application of the method

for antihistaminic drug discovery.^[236] Pentafluoro styrene was also identified as a successful olefinic trap (**278**). Flavone-derived molecules could be alkylated, albeit in lower yields (**279** and **280**).

By investigating this scope, we could confirm that only electron-deficient olefins were successfully alkylated, probably because of the nucleophilic nature of the carbon radical intermediate (*cf.* 1.2.3.1). Indeed, electron-neutral styrene resulted in a disappointing 10% yield of the coupled product **281** and the more electron-rich silyl enol ether was unable to form any coupling product **282**. Finally, we tested the natural product thapsigargin as a radical trap, but the angelate residue failed to trap any radical (**283**). Instead, *E/Z* isomerisation of the angelate double bond was observed presumably *via* a triplet-triplet energy transfer from the photoredox catalyst.

3.2.2 Scope of boronic esters

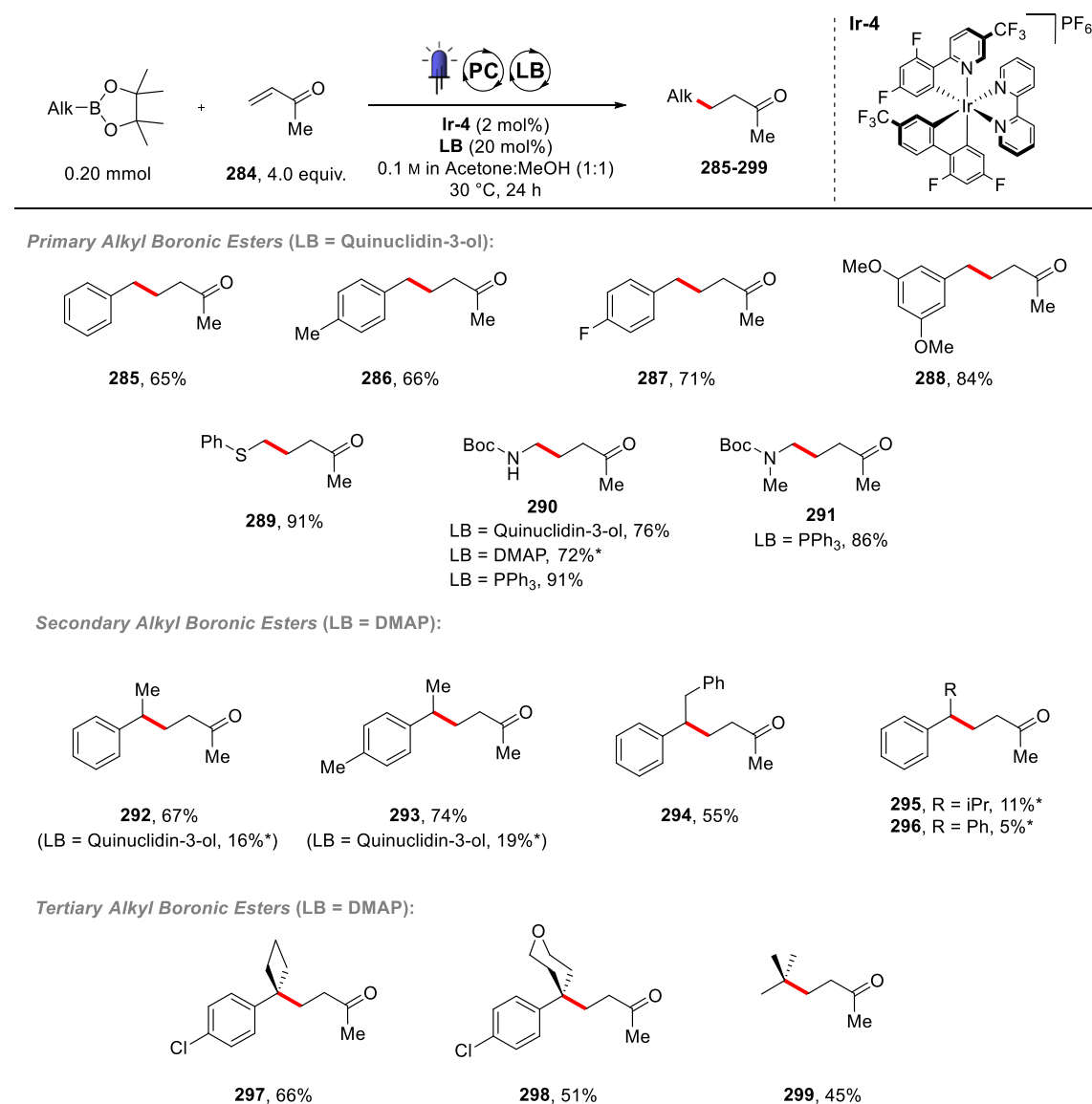
We next turned our attention to establishing the scope of boronic ester coupling partners using methyl vinyl ketone (MVK, **284**) as a radical trap (**Table 19**).

All the primary benzylic pinacol esters tested were selectively coupled to MVK using quinuclidin-3-ol as the Lewis base catalyst (**285–288**). Interestingly, primary alkyl boronic esters α to heteroatoms were also coupled in high yields (**289–291**, 86% to 91%). For α -amino products (**290** and **291**), triphenylphosphine was identified as the most efficient Lewis base catalyst.

More sterically demanding secondary benzylic esters were more complicated partners. Initial treatment of these with the standard quinuclidin-3-ol Lewis base only resulted in poor conversions and low yields (**292** and **293** with LB = quinuclidin-3-ol). When changing the Lewis base to the comparatively flatter DMAP, significantly higher yields were obtained. These observations highlight the effect of the steric hindrance on the required initial complexation between boronic esters and Lewis base. While methyl (**292** and **293**) and benzyl (**294**) were well tolerated, the presence of larger isopropyl (**295**) group led to less efficient couplings. In this case (**295**), only low conversion of the boronic ester starting material was observed presumably because of the poorer coordination of DMAP to the boron atom. The phenyl group (**296**) was also identified as a poor substituent, but for a different reason. The diphenyl boronic ester starting material was fully converted but the mixture contained over 70% of protodeborylated starting

material. In this case, the radical intermediate probably formed but its doubly stabilised character (doubly benzylic position) resulted in a significantly lowered nucleophilic character and a less efficient trapping with MVK. Therefore, the long-lived radical could be reduced to the anion by the photocatalyst and protonated by methanol to lead to the protodeborylated product.

Table 19 – Scope of boronic pinacol esters to couple with alkene **284**.



Reactions carried out by following **GP(VII)**. Isolated yields. Isolated yields. *Yield determined by ¹H-NMR analysis (tentative assignment) of crude reaction mixture using CH₂Br₂ as an internal standard.

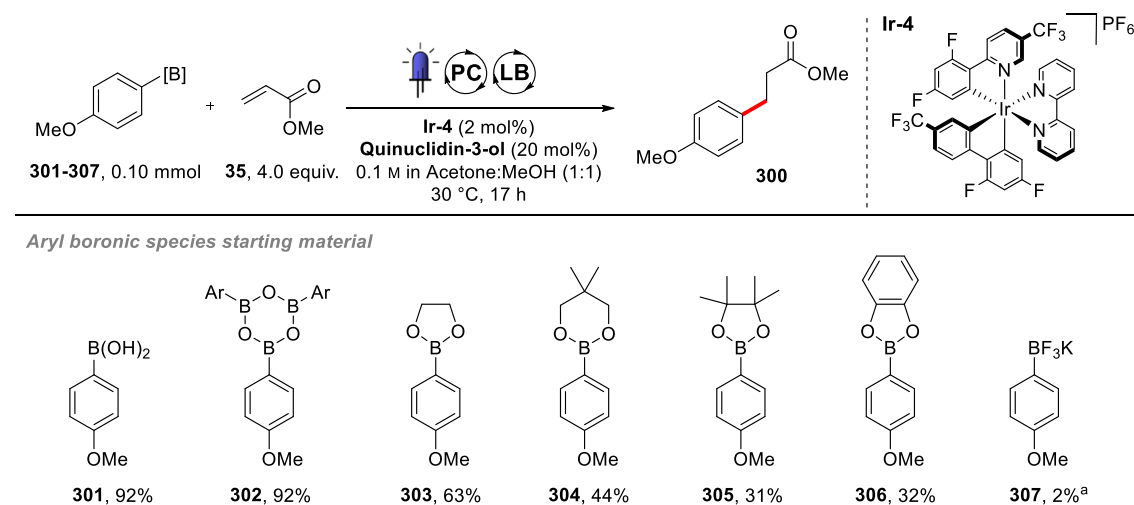
Lastly, tertiary boronic esters were explored (**297–299**). Despite the well-known difficulty of these boronic esters to be efficiently activated and engaged in C–C bond forming

processes,^[64,127] DMAP enabled clean activation to form quaternary carbon centres in respectable yields even from commercial and less activated *tert*-BuBpin (**3pd**).

3.2.3 Scope of boronic acids

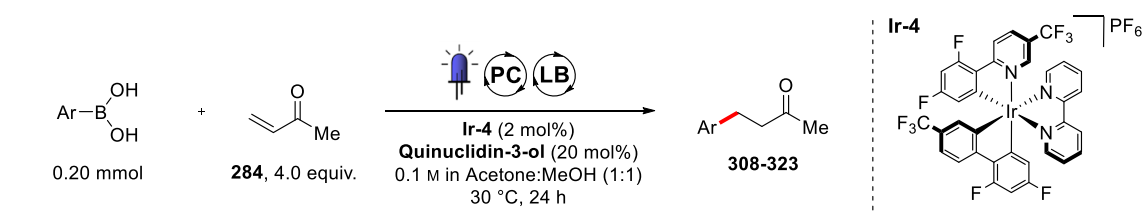
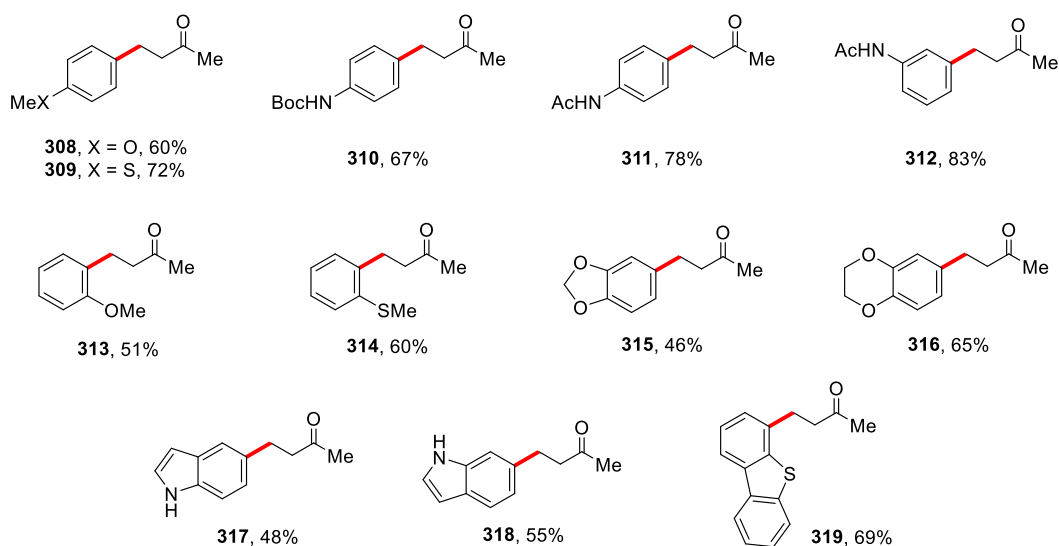
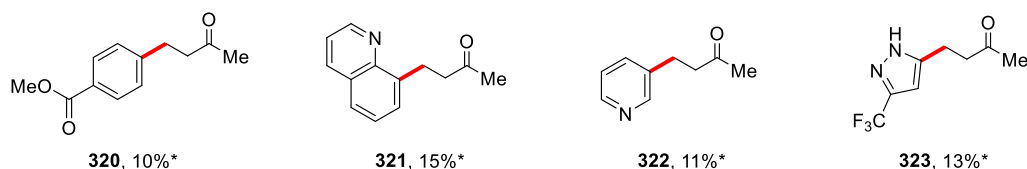
In an effort to extend the scope of boronic esters to react in this radical alkylation reaction, the use of aryl boronic esters was investigated. However, engaging aryl pinacol boronic ester (**305**), in the optimised reaction conditions, only led to a poor conversion (31%) of the starting material after 17 h of irradiation (**Table 20**). This low reactivity led us to survey a wider range of aryl boronic starting materials. As a control, the trifluoroborate salt (**307**) did not show any conversion, confirming the inability of these salts to act as aryl radical precursors.^[62] In the boronic ester series, less hindered neopentyl (**304**) and glycol (**303**) boronic esters were found to be more reactive than their pinacol (**305**) counterpart, probably because of more favoured complexation with the Lewis base catalyst.

Table 20 – Aryl boronic species screening.



Reactions carried out by adapting **GP(VI)** to the conditions described. Conversions determined by ¹H-NMR analysis of crude reaction mixture using CH₂Br₂ as an internal standard. ^aReaction performed without Lewis base.

Unexpectedly, aryl boronic acid (**301**) was identified as the best aryl boronic starting material. The commercial boronic acid (**301**) and its corresponding boroxine (**302**) were both converted efficiently to the coupling product (**300**). This finding led us to assess a series of commercially available boronic acids in this reaction (**Table 21**).

Table 21 – Scope of aryl boronic acids to couple with alkene **284**.*Successful Aryl Boronic Acids :**Unsuccessful Aryl Boronic Acids :*

Reactions carried out by following **GP(VIII)**. Isolated yields. *Yield determined by $^1\text{H-NMR}$ analysis (tentative assignment) of crude reaction mixture using CH_2Br_2 as an internal standard.

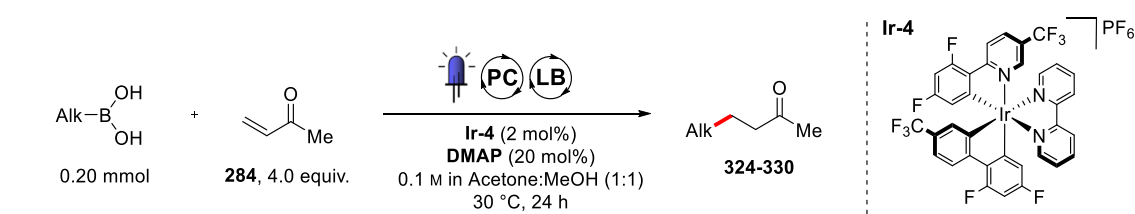
Prior to this study, only strongly oxidising stoichiometric oxidants were employed to oxidise aryl boronic acids (*cf.* 1.3.2.3) with single-electrons. In contrast, this method allows a wide range of electron-rich aryl boronic acids to be oxidised under extremely mild conditions and to be used in a redox-neutral setting.

The reaction tolerates oxygen (**308**), sulphur (**309**) and nitrogen (**310** and **311**) *para*-substituted phenyl boronic acids. *Meta*- and *ortho*-substitution with the same heteroatoms also results in high yields of the alkylated phenyl rings (**312–314**). Oxygen-containing heterocycles derived from catechol could be incorporated into the substrates (**315** and **316**). Unprotected 5- and 6-indoyl boronic acids (**317** and **318**) were also successfully functionalised in the presence of the nucleophilic NH and C3 residues. However, the use

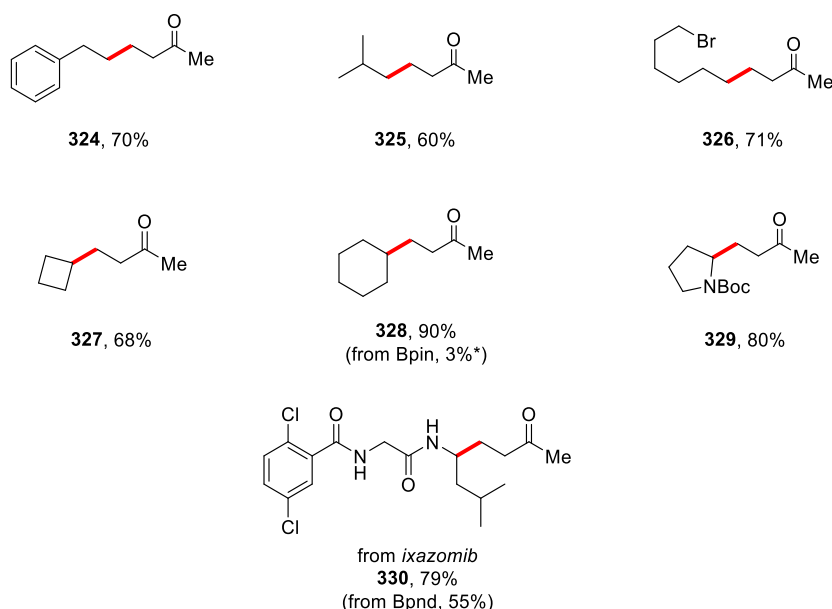
of less electron-rich aryl boronic acids was inefficient, for example, 4-methoxycarbonylphenyl boronic acid and electron-deficient heteroaromatic boronic acids were alkylated in poor yields (**320–323**). Since these less electron-rich starting materials were mostly fully converted, it is believed that the low yields are a result of the reduced nucleophilicity of the radical intermediates, as postulated for **296** (*cf.* **Table 19**).

The enhanced reactivity observed with boronic acids relative to the boronic pinacol esters encouraged us to attempt to use unactivated alkyl boronic acids as starting materials. An initial Lewis base catalyst screening revealed that DMAP gave slightly higher yields than quinuclidin-3-ol with cyclohexyl boronic acid starting material. These conditions were therefore applied to a wider range of commercially available alkyl boronic acids (**Table 22**).

Table 22 – Scope of alkyl boronic acids to couple with alkene **284**.



Successful Alkyl Boronic Acids :



Reactions carried out by following **GP(VIII)**. Isolated yields. *Yield determined by ¹H-NMR analysis of crude reaction mixture using CH₂Br₂ as an internal standard.

Pleasingly, unactivated primary alkyl boronic acids were successfully coupled to MVK (**324–326**), showcasing the utility of the method to generate functional unstabilised alkyl

radicals.^[55] Contrary to their boronic pinacol ester counterparts, secondary alkyl boronic acids were efficiently oxidised and coupled (**327** and **328**). Secondary α -amino boronic acids derived from amino acids^[237] were also well tolerated with proline-derived (**329**) as well as the peptide drug *ixazomib* transformed in high yield (**330**), illustrating the potential application to late-stage functionalisation. In the latter example, starting from the enantiopure boronic acid or pinanediol boronic ester (Bpnd) resulted in a racemic product (**330**). These observations are in line with the postulated radical intermediate and are an area for potential further improvement of this method.

3.3 Mechanistic understanding

Pleased by the generality of our findings, we decided to further explore the mechanism of these transformations with a focus on the unprecedented photoredox activation of boronic acid species.

3.3.1 Mechanistic experiments

Our experience with Lewis acidity of aryl boronic acids led us to propose that the reactive species in solution was more likely to be the trimeric boroxine than the monomeric boronic acid species.^[183] Indeed, complexes of pyridine-derived Lewis bases and aryl boronic acids already have been isolated and characterised.^[238] Moreover, thermodynamic studies of these equilibria in solution are reported and explain the favoured complexation of Lewis bases with boroxines rather than boronic acids.^[239] To study this complexation event, NMR experiments were conducted in the reaction solvent mixture (acetone:methanol (1:1)).

Complexation experiments on aryl boronic acids showed a greater effect than the one on boronic ester **179** (*cf.* 2.3.3.1). Initial ¹H-NMR measurement (**Figure 11**) of commercial 4-methoxyphenyl boronic acid (**301**) in the deuterated reaction solvent mixture revealed the presence of two species in solution, **301** and its corresponding trimeric boroxine **302**. The two distinct set of signals observed for **301** and **302** are a proof of a slow equilibrium (relative to NMR measurement time-scale) between the two species in the solvent mixture.

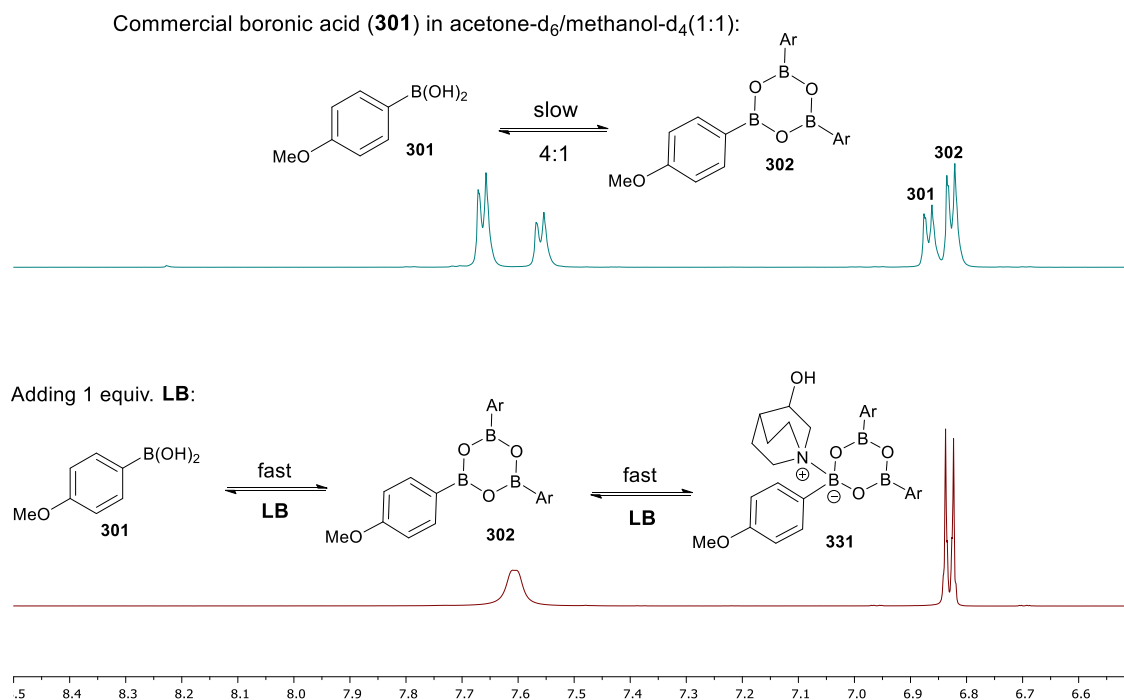


Figure 11 – **301** in acetone- d_6 /methanol- d_4 (1:1) with (red) and without (blue) quinuclidin-3-ol = **LB**.

When adding 1 equiv. of quinuclidin-3-ol (**LB**), all peaks merged into a single set of signals, meaning a fast equilibrium between **301**, **302** and **331** and potentially the boronic acid and quinuclidine-3-ol complex (not shown). As known from previous literature,^[239] the boroxine complex is likely to be more favoured than the complex with monomeric boronic acid (**301**). To check this hypothesis, we developed the following experiments where we could observe equilibrium between the species and the **LB** but no fast equilibrium between **301** and **302**.

To deconvolute the equilibrium between **301** and **302** from the ones involving the Lewis base, we ran the same experiment in acetone- d_6 as sole solvent. The absence of protic solvent was found to suppress the fast equilibrium between **301** and **302** in the presence of **LB**. In this initial measurement (**Figure 12**, blue line), the slow equilibrium between **301** and **302** is still observed (albeit being more shifted on the monomeric boronic acid side).

Addition of 1 equiv. of **LB** (**Figure 12**, green line) only affected the peaks of **302** (in fast equilibrium with the **331** complex) and left the **301** peaks unshifted (despite a change in the proportions of the equilibrium). This suggested that the theoretical complex between

LB and the boronic acid was not forming. Addition of 10 equiv. of methanol- d_4 resulted in a similar result to the red line in **Figure 11**, where all the species are in fast equilibrium.

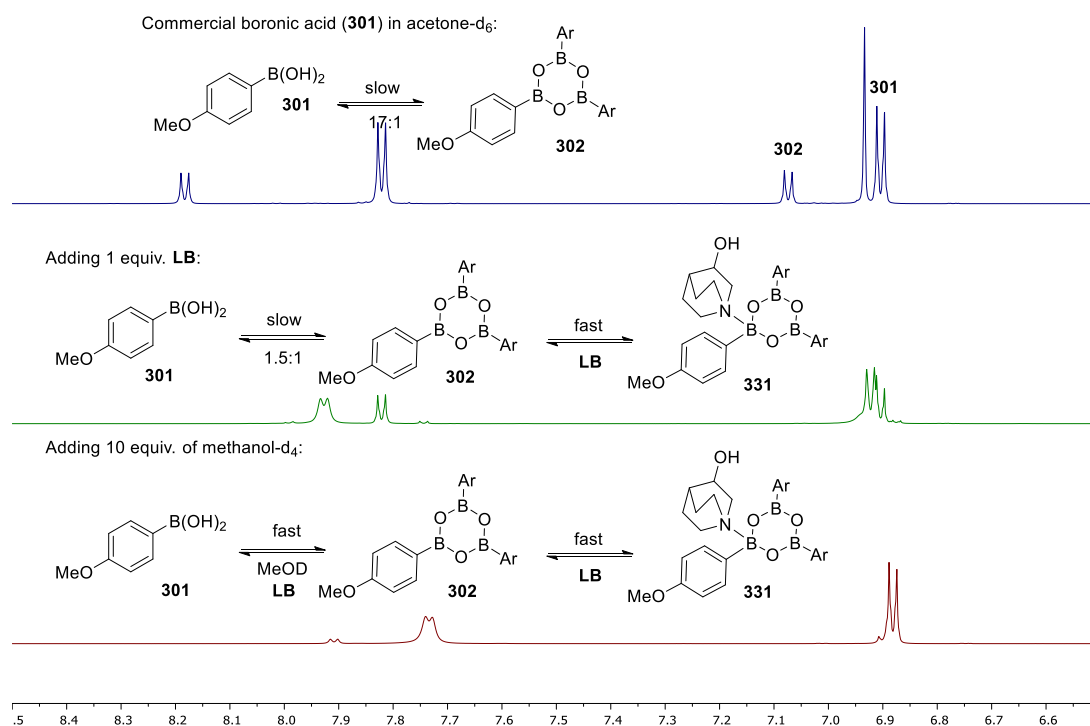


Figure 12 – From top to bottom, **301** in acetone- d_6 , addition of quinuclidin-3-ol = **LB** then methanol- d_4 .

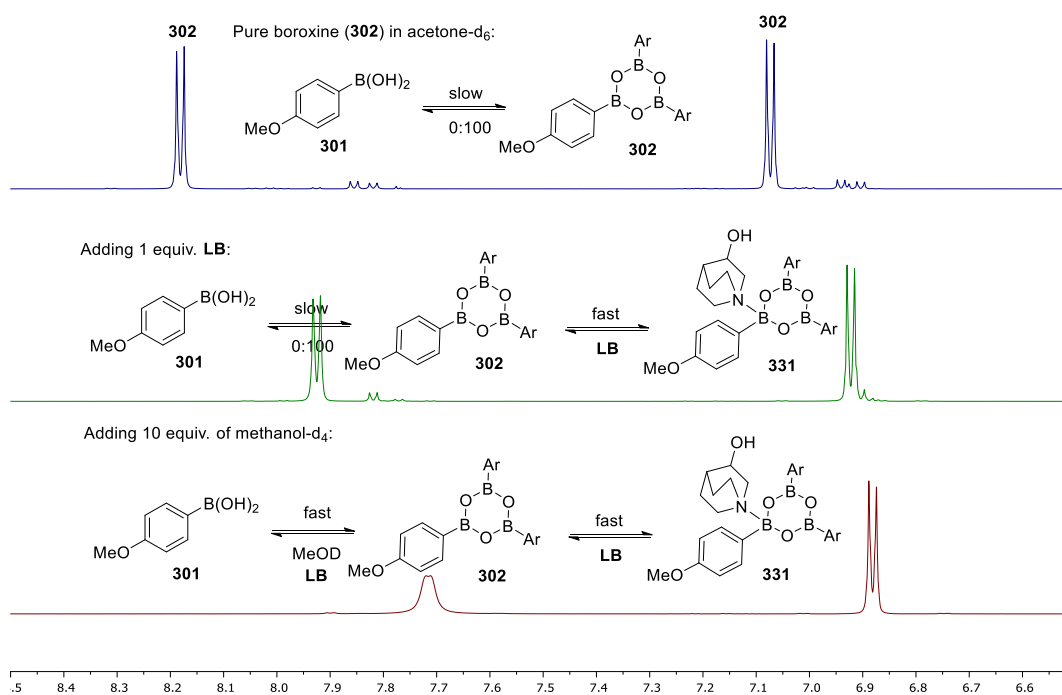
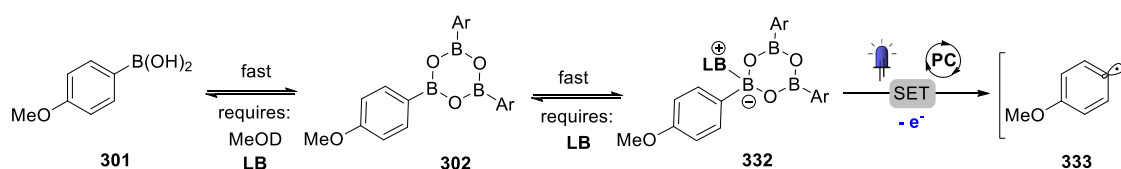


Figure 13 – From top to bottom, **302** in acetone- d_6 , addition of quinuclidin-3-ol = **LB** then methanol- d_4 .

As a control, we performed the same experiment using the pure boroxine (**302**) prepared by azeotropic removal of water from **301** (*cf.* **Figure 13**). In acetone- d_6 , only boroxine peaks were observed (blue line, **Figure 13**). Addition of the **LB** led again to a change in the shift of the boroxine peaks with the formation of **331** (green line). Addition of 10 equiv. of methanol- d_4 resulted in a similar result to the red lines in **Figure 11** and **Figure 12**, where all the species are in fast equilibrium.

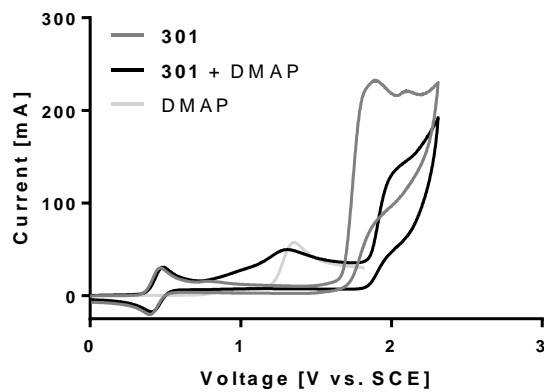
These experiments suggested that in the case of boronic acid starting materials (**301**), complex formation with **LB** is preferred from the most Lewis acidic trimeric boroxine species (**302**). We also observed that methanol acts as a proton source to enable a fast, dynamic equilibrium between **301** and **302** when **LB** is present. This finding explains why starting from only boroxine starting materials gives the same results as the commercial boronic acid (*cf.* **Table 20**) in the reaction conditions where both methanol and **LB** are present.

From these observations, it was postulated that as in the case of the boronic esters (*cf.* 2.3.3.2), this **332** complex will have a lower E_{ox} value than the free boroxine and boronic acid and is the species that undergoes single-electron oxidation by the excited photoredox catalyst (**Scheme 40**).



Scheme 40 – Summary of the postulated boronic acid reactivity in the reaction solvent.

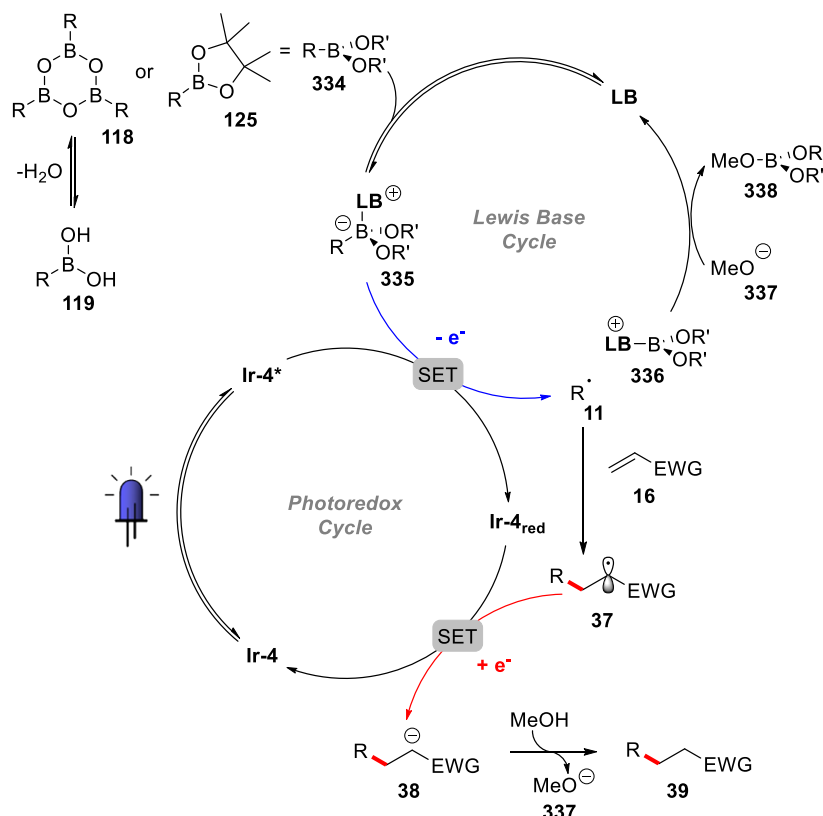
To further confirm this hypothesis, cyclic voltammetry studies on this system were carried out (**Graph 5**). These measurements revealed the presence of a new irreversible oxidation trace of the boronic acid (**301**) when DMAP was added (black curve, **Graph 5**). This trace probably corresponds to the oxidation of the **332** adduct observed by NMR (with **LB** = DMAP instead of quinuclidin-3-ol). However, since three equilibria are now operative in the solution, the oxidation trace is broad and diffuse and does not show a distinct maximum. Due to this broad shape, no value for the oxidation potential could be determined for the boroxine and DMAP adduct **332**, but it appears to be the same range as the boronic ester and DMAP complex (*cf.* 2.3.3.2).



Graph 5 – Oxidation traces of the cyclic voltammograms with boronic acid **301** and DMAP.

3.3.2 Proposed mechanism

According to NMR studies, a fast, dynamic equilibrium occurs between the boroxine (**118**) derived from boronic acid (**119**) or the boronic ester (**125**) and the Lewis base catalyst (**LB**) in the reaction solvent mixture (**Scheme 41**).



Scheme 41 – Proposed mechanistic description for the Lewis base and photoredox-catalysed “Giese-type” addition of boronic acid derivatives.

Cyclic voltammetry measurements informed us that complex **335** undergo single-electron oxidation (E_{ox} (**223**) = +0.81 V) within the reductive quenching cycle of **Ir-4** ($E_{1/2}^{*/\text{red}}$ = +1.21 V). The carbon radical thus generated (**11**) undergoes a radical addition with **16** to form the intermediate radical (**37**), which can then be reduced and quenched by a proton from methanol to lead to coupling product (**39**) (*cf.* 1.2.3.2 a). The resulting methanolate (**337**) can then be used to regenerate the **LB** from **336**. The Lewis base catalyst recycling process is favoured by the formation of a stronger B–O (~124 kcal/mol) in **338** at the expense of the weaker B–N (~100 kcal/mol) in **336**.^[186]

3.4 Summary and conclusions

To conclude, this chapter demonstrates a novel set of reaction conditions to generate primary, secondary and tertiary alkyl or aryl radicals from boronic acid derivatives. Building on our previous study, we could take advantage of the Lewis acidity of boronic esters and boroxines (from boronic acids) to form *in situ* redox-active complexes of these with a Lewis base catalyst. These complexes could undergo single-electron oxidation by a photoredox catalyst to generate carbon radicals. These intermediates were engaged in redox-neutral C–C couplings with electron-deficient olefins forming a wide range of new C(*sp*³)–C(*sp*³) and C(*sp*²)–C(*sp*³) cross-coupled products.^[240] Over 50 examples of structurally and functionally diverse products were successfully synthesised. This new activation method should enable the use of boronic acids and esters in a wide range of other radical-based reactions. Applications and further developments of this method are presented in the next chapter.

4 Applications to APIs synthesis in flow

4.1 Synthetic studies towards γ -amino acids

4.1.1 Introduction to GABAs

γ -amino butyric acid (GABA) is the most important inhibitory neurotransmitter in the human central nervous system. There are two main classes of GABA receptors, GABA_A and GABA_B, both inhibiting signal transduction in the neuronal system (**Figure 14**).^[241]

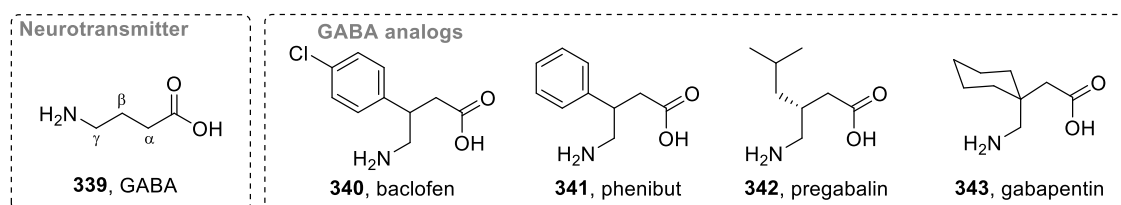


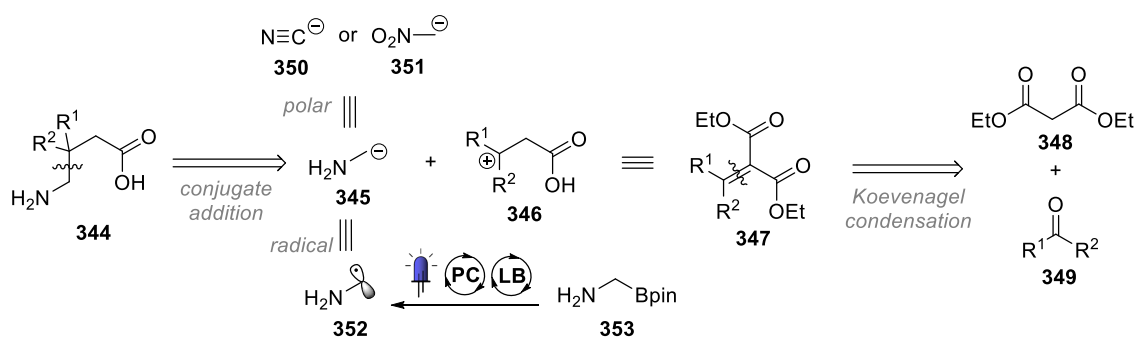
Figure 14 – Structures of GABA and its potent analogues.

Because of the key role of GABA (**339**) in the central nervous system, GABA analogues are forefront pharmaceutical ingredients indicated against neuropathic pain, epilepsy and anxiety.^[242] For example, pregabalin (**342**, Lyrica[®](Pfizer)) was eleventh on the highest selling drugs in the world in 2016.^[243] Other members of this family share the same γ -amino acid backbone: baclofen (**340**, Lioresal[®](Novartis)), gabapentin (**52**, Neurontin[®](Pfizer)), and phenibut (**341**, Anvifen[®](Anvi)). Even though they belong to the same family of GABA derivatives, their pharmacological mode of action is different. Whereas baclofen (**340**) and phenibut (**341**) are GABA_B agonists, the inhibitory effects of pregabalin (**342**) and gabapentin (**343**) are mainly caused by the inhibition of voltage-gated calcium channels, which must be activated for sufficient neurotransmitter release into the synaptic cleft. As a result, these different drugs are prescribed to treat different symptoms.^[244]

4.1.2 Proposed synthesis strategy

A retrosynthetic analysis of the general GABA analogues motif (**344**) is proposed in **Scheme 42**. The β/γ disconnection is a sensible approach to this motif, leading to two

synthons **345** and **346** to be assembled *via* a conjugate addition. While the electrophilic synthon (**347**) is stable, and accessible by Knoevenagel condensation of a carbonyl compound (**349**) with diethyl malonate (**348**), the nucleophilic synthon (**345**) is destabilised by the adjacent donating amino group. Therefore, the common polar approach to this condensation makes use of cyanide (**350**)^[245] or nitromethane anion (**351**)^[246] to introduce the nitrogenous moiety. These highly oxidised groups have to be subsequently reduced to reveal the target amino acid (**344**). On the other hand, when using a radical approach, the α -amino radical species (**352**) is already stabilised and is perfectly suited to engage in radical conjugate addition with these malonate derived olefins (**347**).

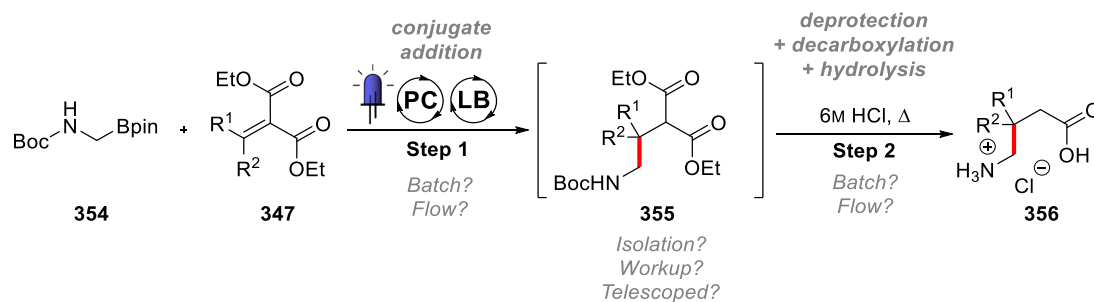


Scheme 42 – Retrosynthetic planning for GABA analogues syntheses.

Using our method, this radical could be derived from a α -amino boronic ester species (**353**). Also, it was decided to test the usefulness of our recently developed coupling method for the synthesis of active pharmaceutical ingredients (APIs) from the GABA family. Although similar radical approaches have already been reported for the synthesis of baclofen^[95] and pregabalin^[96], we aimed to synthesise all four analogues to investigate the robustness and applicability of our photoredox method.

This approach would use the Boc-protected amino boronic ester (**354**) as the amino radical building block (**Scheme 43**). It would undergo our recently developed Lewis base and photoredox dual catalysed addition to diethyl malonate-derived olefins (**347**). The resulting coupled product (**355**) could then be deprotected, hydrolysed and decarboxylated using aqueous 6 M HCl and heating to reveal the amino acid hydrochloride (**356**).^[95]

To be able to compete with the large production volumes of industrial scale processes, we aimed to investigate the potential telescoping (using it without isolation) of the **355** intermediate. This protocol would allow a continuous flow production of these pharmaceutical ingredients by running the two steps consecutively.^[246–248]



Scheme 43 – Proposed protocol for the synthesis of GABA analogues.

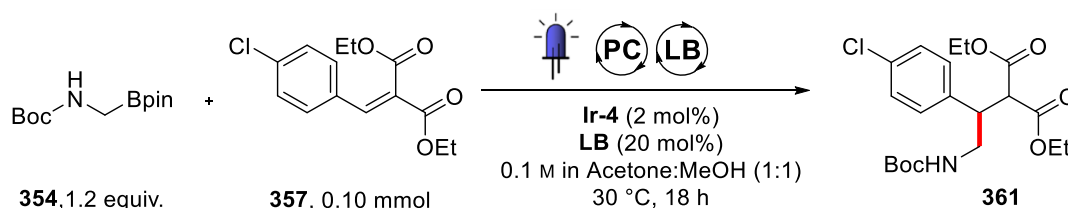
The photochemical nature of the first step means it would highly benefit from being carried out in a micro to meso scale reactor. Shorter path lengths in smaller dimension tubing increase the light harvesting efficiency, leading to higher yields and shortened reaction times in micro-structured reactors.^[216–218,220,249] Also, the second step could benefit from the possibility to use “super-heated” conditions. The high pressures reachable in the flow reactors allows reaching higher temperatures without boiling the solvent off.^[250,251]

To investigate the feasibility of this flow process, the conditions for the photoredox coupling and workup procedures were initially optimised in batch mode.

4.1.3 Photoredox coupling optimisation

The reaction towards the synthesis of baclofen was chosen as a model system to investigate the photoredox coupling reaction (**Table 23**). Only a slight modification from the already optimised conditions (*cf.* 3.1) was made. Since the olefin partner (**357**) is not volatile (*i.e.* not easily removed), it was decided to use it as the limiting reagent with a slight excess of the boronic ester (**354**).

Table 23 – Lewis base screening for baclofen precursor (**361**) synthesis.

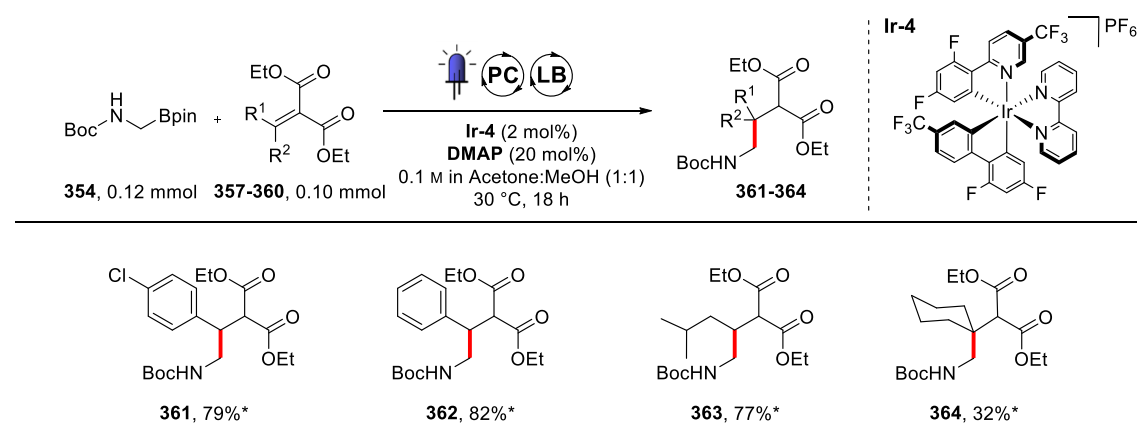


Entry	Lewis base (LB)	Yield ^a
1	Quinuclidin-3-ol	52%
2	Quinuclidine	58%
3	DABCO	44%
4	DMAP	79%
5	PPh ₃	60%

Reactions carried out by adapting **GP(IX)** to the conditions described. ^aYield in **361** determined by ¹H-NMR analysis of crude reaction mixture using CH₂Br₂ as an internal standard.

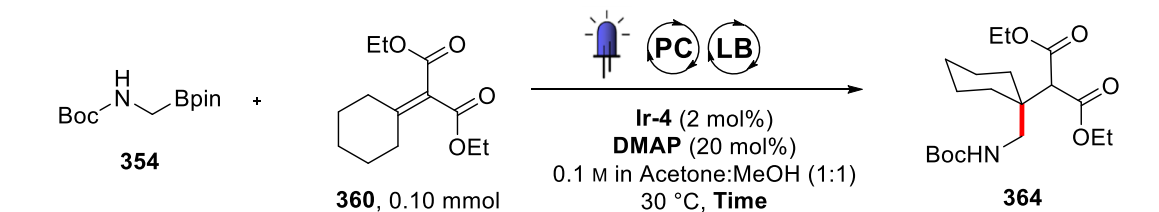
The standard conditions with quinuclidin-3-ol resulted in a decent 52% yield of the coupled product (**361**) with some unconverted alkene (**357**) (entry 1). A Lewis base catalyst screening was then carried out with the selected Lewis bases. While DABCO (entry 3) did not outperform quinuclidin-3-ol; quinuclidine (entry 2), DMAP (entry 4) and PPh₃ (entry 5) all resulted in an enhanced product formation. Because of its significantly higher coupling product yield, DMAP was chosen as the optimised Lewis base catalyst. With this catalyst, full conversion of the alkene (**357**) is observed after the 18 h.

To verify the generality of these reaction conditions, this photoredox coupling was tested for the synthesis of the precursors of phenibut (**362**), pregabalin (**363**) and gabapentin (**364**) (**Table 24**).

Table 24 – NMR yields for drug precursors coupling products (**361–364**).

Reactions carried out by adapting **GP(IX)** to the conditions described. *Yields determined by $^1\text{H-NMR}$ analysis of crude reaction mixture using CH_2Br_2 as an internal standard.

Pleasingly, these optimised conditions efficiently delivered the phenibut and pregabalin precursors (**362** and **363**). However, the quaternary olefin (**360**) only resulted in 32% yield of the gabapentin precursor (**364**). Also, further optimisation of this specific coupling was initiated (**Table 25**).

Table 25 – Optimisation of the gabapentin precursor (**364**) synthesis.

Entry	Loading of 354	Lewis base (LB)	Time	Yield ^a
1	1.2 equiv.	DMAP	18 h	32%
2	1.2 equiv.	DMAP	48 h	50%
3	1.2 equiv.	quinclidin-3-ol	48 h	33%
4	1.2 equiv.	quinuclidine	48 h	56%
5	1.5 equiv.	DMAP	48 h	65%
6	1.5 equiv.	quinuclidine	48 h	60%
7	2.0 equiv.	DMAP	48 h	57%
8	2.0 equiv.	quinuclidine	48 h	66%

Reactions carried out by adapting **GP(IX)** to the conditions described. ^aYield in **364** determined by $^1\text{H-NMR}$ analysis of crude reaction mixture using CH_2Br_2 as an internal standard.

Since the alkene **360** was not fully converted after 18 h, a longer irradiation time was initially tested, resulting in an increased product yield (entry 2). To verify that DMAP was the most active catalyst, further Lewis base screening was conducted. Quinuclidine was identified as a possible replacement for DMAP (entry 4 vs. 2). As we observed that the remaining mass balance still was unreacted alkene (**360**), the stoichiometry of boronic ester (**354**) was gradually increased from 1.2 to 2.0 equivalents (entries 4 to 8) to drive the reaction to completion. The highest yield in the coupling product (**364**) with the least excess of starting materials was obtained using DMAP as Lewis base, 1.5 equiv. of boronic ester (**354**) and 48 h irradiation time (entry 5). Considering that the coupling is forming a quaternary carbon, these conditions delivered a satisfactory 65% yield.

4.1.4 Workup procedure optimisation towards a flow process

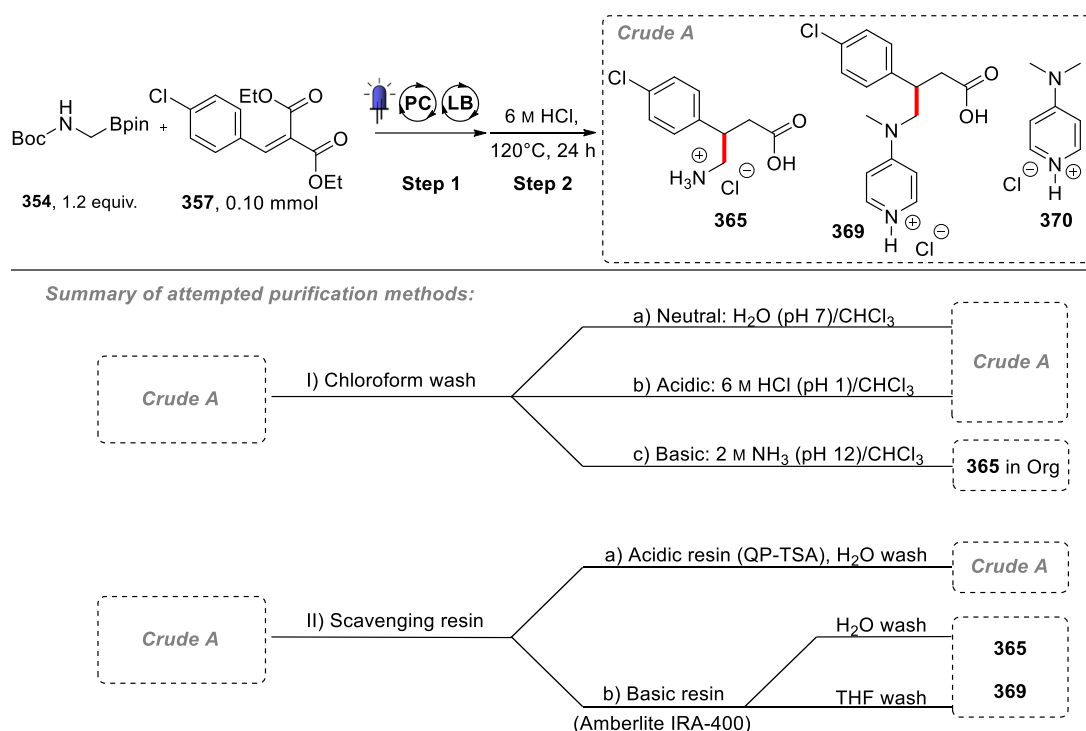
With optimised conditions for all the photoredox couplings in hand, we started to investigate the next step, consisting of successive deprotection, hydrolysis, and decarboxylation. At this stage, the treatment of the crude mixture after the photoredox coupling have to be defined.

4.1.4.1 Telescoped process investigation

To best mimic a flow process, a telescoped approach was initially tested by directly adding an aqueous 6 M HCl solution to the crude photoredox coupling mixture (without intermediate treatment, **Scheme 44**). After refluxing the mixture for 24 h, the solvents were removed under reduced pressure. The residue was suspended in water and the aqueous layer was extracted with chloroform (Ia) to remove non-water-soluble impurities (target product **365** is insoluble in chloroform). Removal of water *in vacuo* afforded a yellow (residual **Ir-4**) sticky residue, whose composition was determined by HRMS and NMR analysis. While the product (**365**) was the main component of the mixture (crude A), it was contaminated with DMAP and traces of a DMAP-adduct (**369**) side-product (**Scheme 44**). This side-product originates from the attack of the DMAP-derived α -amino radical (*cf.* 1.2.2) on the olefin (competitive DMAP attack).

To remove DMAP and the side-product (**369**) from the aqueous layer, both acidic (Ib) and basic (Ic) workup procedures were tested. With a pK_a of 9.7,^[252] the concentration of DMAP in the aqueous layer was significantly reduced under basic conditions, but at the

same time, most of the product (**365**) was lost in the organic layer. Under acidic conditions, DMAP was completely protonated (**370**) and therefore only found in the aqueous layer, but the protonated amino-group ($pK_a = 10.2$) of the coupling product (**365**) prevented it from being sufficiently extracted into the organic layer. Because of the multiple acidities of the product (**365**), none of the tested aqueous workup conditions showed an efficient separation.



Scheme 44 – Fully telescoped process impurities and tested purification methods.

We next attempted to separate the impurities by solid-supported scavenging with ion-exchange resins (II).^[253] These recyclable, polymer-based materials can reversibly bind compounds by ionic interactions and have been widely used in continuous processes to remove trace metals, switch between different solvent systems, or act as solid-supported reagents.^[254,255]

An acidic QP-TSA (TsOH) resin was initially used (Ia). We rationalised that the sulfonate groups could favourably interact with protonated amino residue. The product (**365**) was successfully bound to the resin under acidic conditions, as it was not detected in the obtained eluent fraction. However, some product was already released during the following neutral wash with water. The residual material was released with aqueous 1 M ammonia wash and contained product (**365**), side-product (**369**), and residual DMAP (**370**), which could also interact in their protonated form with the cation-exchanger.

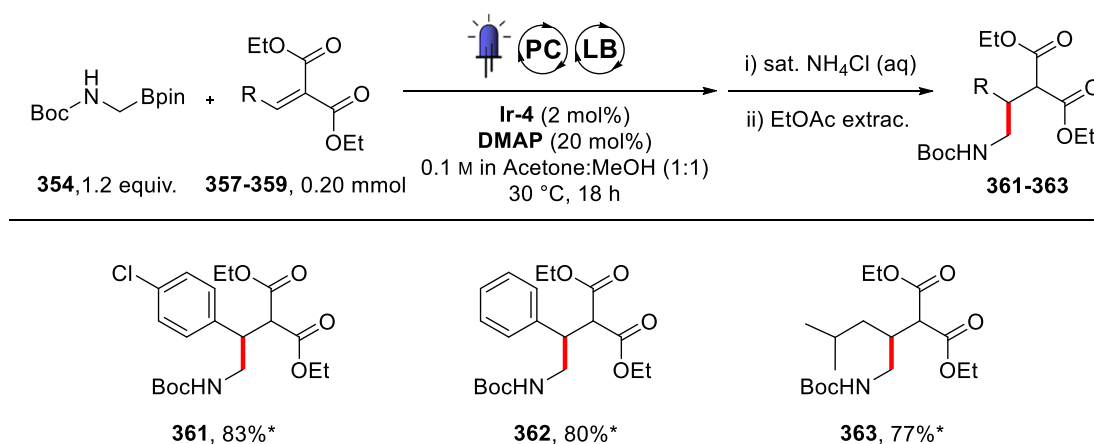
To circumvent this issue, we then used a basic anion-exchanger Amberlite IRA-400 (NR_4^+) (I**b**). This material carries quaternary ammonium functionalities on its surface, which can potentially interact with the negatively charged carboxylate groups ($\text{p}K_{\text{a}} = 4.2$). After the immobilisation on the ion-exchange resin under basic ($\text{pH} = 9.8$) or neutral conditions ($\text{pH} = 7.0$), the product (**365**) did not bind strongly enough to the material and was partially released during the aqueous wash. Changing the washing solvent from water to THF did not result in any improvement. Although DMAP was not present in the release fraction (using 3 M HCl), the product (**365**) was still contaminated with the side-product (**369**), due to their structural similarities.

4.1.4.2 Intermediate treatment investigation

Since, it appeared that purification is a problem at the final product stage, a fully telescoped process cannot provide high-purity product. We decided to test an intermediate aqueous workup to remove the problematic DMAP-impurities before engaging the mixture in the second step. In contrast to chromatographic separation, an aqueous workup could still be integrated into a continuous process by using an in-line phase separator.^[256,257]

Initial investigations showed that DMAP was effectively removed by treating the crude mixture with aqueous ammonium chloride solution ($\text{pH} 5-6$) and extracting the product with ethyl acetate.

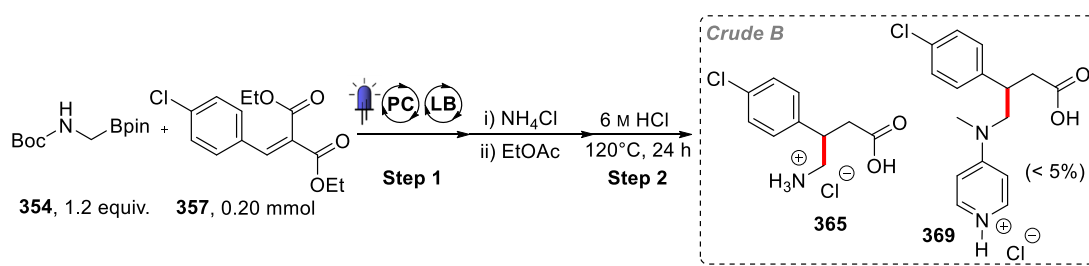
Table 26 – NMR yields for drug precursor coupling products after acidic aqueous workup.



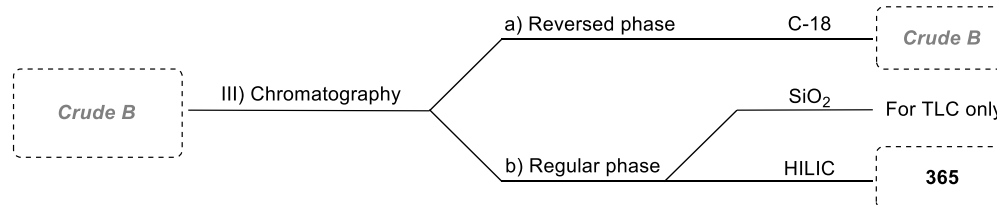
Reactions carried out by adapting **GP(IX)** to the conditions described. *Yield determined by $^1\text{H-NMR}$ analysis of the reaction mixture after an acidic aqueous workup with CH_2Br_2 as an internal standard.

The yields in coupling products after the aqueous workup (**Table 26**) match those obtained without any treatment (*cf.* **Table 24**). This observation suggests that the Boc-amino coupling products are not deprotected using this mildly acidic treatment.

We then turned our attention to the second step using baclofen as the model system (**Scheme 45**). The residue was dissolved in acetone and 6 M HCl before to be refluxed overnight. After solvents removal, the residue was dissolved in water and washed with chloroform to remove non-polar impurities. The ¹H-NMR was clean, with only the side-product (**369** < 5%) as a minor impurity (crude B). Despite its higher purity than in crude A, the amino acid (**365**) did not crystallise from the mixture. Several drying and crystallisation conditions in water, methanol, 2-propanol, CH₂Cl₂ and combinations thereof were tested, but none of them resulted in a crystalline product.



Summary of attempted purification methods:



Scheme 45 – Intermediate workup approach and tested purification methods.

Thus, we decided to subject the crude B to a chromatographic separation. Due to their high polarity, both product (**365**) and side-product (**369**) interact strongly with silica, which makes them unlikely to be separated by regular phase silica chromatography. To be able to visualise product-containing fractions from chromatographic separations with modified silica stationary phases, we tested different polar solvent systems on TLC plates. Neither highly polar solvent mixtures of chloroform and methanol, nor pure methanol or mixtures of *n*-BuOH and acetic acid could elute the compounds on silica gel. Only a complex eluent mixture containing EtOAc, CHCl₃, MeOH, water and formic acid (40:30:20:5:5) resulted in an acceptable separation.^[258] However, this separation was not suitable for isolating the product by preparative TLC.

We further tested conditions for the purification on reverse phase silica (C-18, IIIa). Because of the insolubility of the amino acid product in acetonitrile, we used different concentrations of water in methanol as the mobile phase, but neither highly polar (H₂O:MeOH 80:20) eluent systems, nor pure methanol showed sufficient separation. Instead, the compound mixture was found unseparated in the first few fractions. We concluded that the interaction of the charged compounds with the non-polar phase was too weak in comparison to their high solubility in the solvent system.

We therefore decided to try a more polar solid phase for the separation by hydrophilic interaction liquid chromatography (HILIC).^[259] These materials allow the separation of products with regular phase solvent systems, which are strongly retained on silica and weakly retained under reversed phase conditions. The modified stationary phase strongly interacts with the polar component of the solvent system (usually water), which forms a thin hydrophilic layer on the surface. Hence polar compounds in the mobile phase are retained by both ionic and hydrophilic liquid-liquid interactions.^[260]

Initial tests with EtOAc and MeOH (1:1) as mobile phase on spherical modified silica (Claricep-HILIC[®], Agela) showed promising separation. Further optimisation revealed a mixture of acetonitrile, methanol, and water (90:10:3) as a suitable solvent system and afforded the product **365** (purity > 90% by ¹H-NMR).

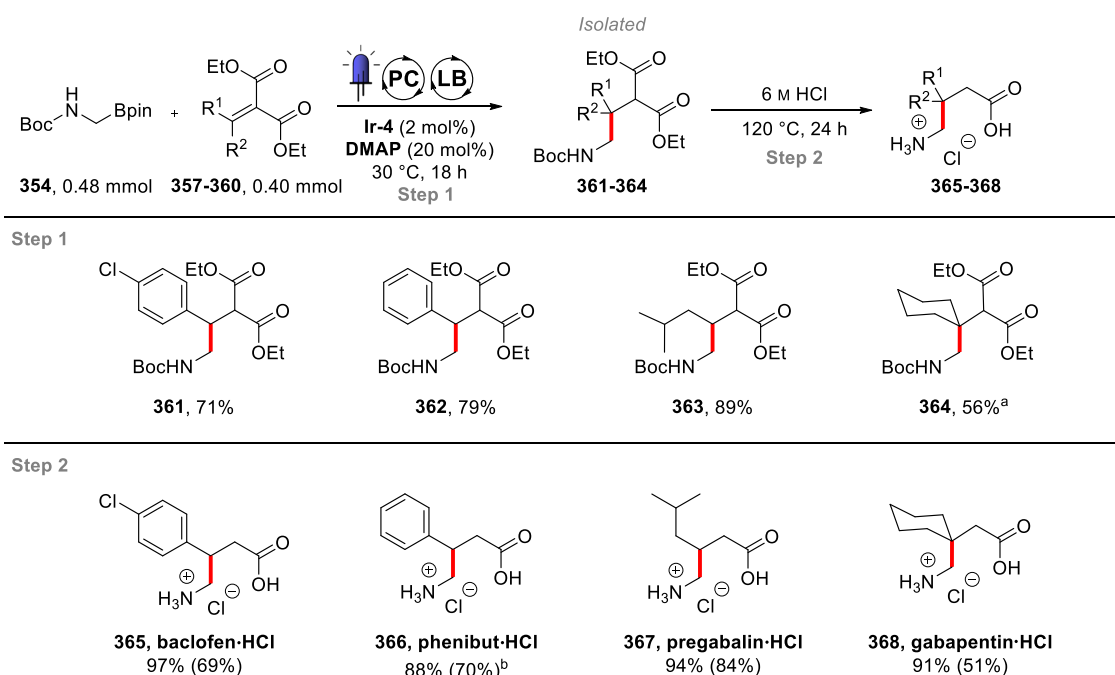
Although suitable conditions for purifying these compounds were finally obtained, we also had to keep the cost efficiency in mind. Besides the valuable separation capacity and recyclability of the HILIC stationary phase, its high price (one thousand pounds per kilogram) limits its larger scale applications.

4.1.5 A batch route

Since an expensive stationary phase was required for the purification of the free amino acid, we decided to divide the synthesis route into a two-step process, with an intermediate purification by silica gel chromatography after the photoredox coupling step (Table 27).

Column chromatography on silica gel afforded the coupling products (**361–364**) in good to excellent yields. The isolated drug precursors were then subjected to deprotection, hydrolysis, and decarboxylation using aqueous 6 M HCl. While phenibut (**366**) was obtained without residual lactam after only 1 h of reflux, the other precursors required prolonged heating (24 h) to fully hydrolyse their corresponding γ -lactams to the final crystalline APIs as hydrochloride salts (**365**, **367**, and **368**).

Table 27 – Isolated yields for the drugs and their precursors in batch.



Step 1 carried out by following **GP(IX)**. Isolated yields. Yields in parentheses are calculated over both steps. ^aDeviating from standard conditions, 0.60 mmol of **354** and 48 h of irradiation. ^bDeviating from standard conditions, only 1 h of refluxing is necessary.

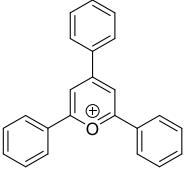
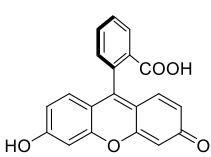
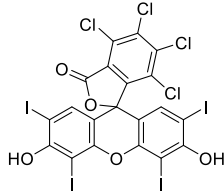
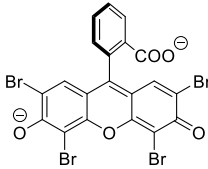
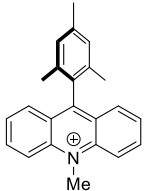
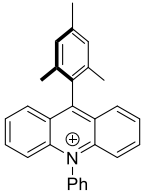
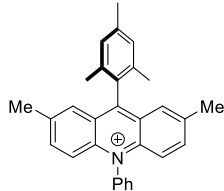
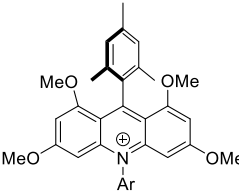
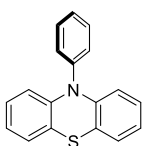
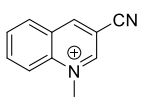
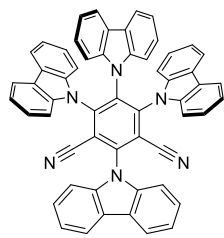
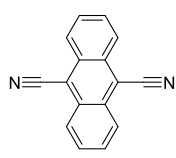
To conclude, we could obtain all desired APIs in a crystalline form with a concise two-steps method using our developed photoredox method as a key step. The yields over the two steps are good to excellent and are competitive with already reported yields for these molecules.^[95,96,246,247]

4.2 Organic photoredox catalysis

The popularity of organic photocatalysts has raised considerably over the past decade, as they hold great promises to replace transition metal based photocatalysts (*cf.* 1.1.3.1).^[17] With the pharmaceutical industry starting to adopt processes based on this technology,^[22,23] we thought it would be desirable to show the possibility to perform our methodologies without any added metal. Our photoredox methods would greatly benefit from such an approach. Firstly, in terms of catalyst costs and secondly in terms of products purifications, circumventing any possibility of residual metal contamination.

Therefore, it was decided to investigate the possible replacement of **Ir-4** photocatalyst in our latest developed method by an organic one (**Table 28**). Furthermore, this organic catalyst could also be tested in the latest developed APIs syntheses (*cf.* **Table 27**) to further highlight the relevance of this method for the pharmaceutical industry.

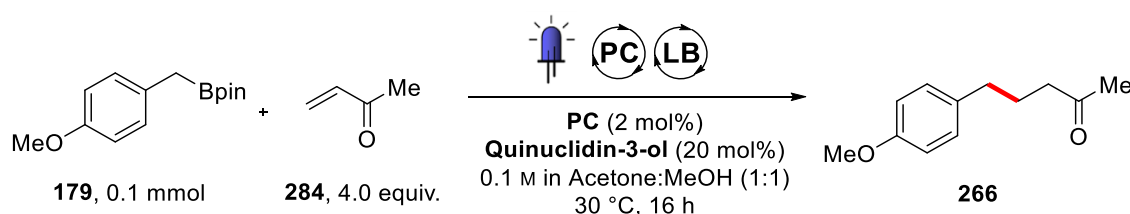
Table 28 – Commonly used organic dyes.

Organic dyes			
 <p>Triphenylpyrylium = TPP $E_{1/2}^{gd/red} = -0.32$ V $E_{1/2}^{*/red} = +2.55$ V</p>	 <p>Fluoreiscein = FL $E_{1/2}^{gd/red} = -1.17$ V $E_{1/2}^{*/red} = +1.25$ V</p>	 <p>Rose bengal = RB $E_{1/2}^{gd/red} = -0.99$ V $E_{1/2}^{*/red} = +1.18$ V</p>	 <p>Eosin Y = EY $E_{1/2}^{gd/red} = -1.08$ V $E_{1/2}^{*/red} = +1.23$ V</p>
 <p>Mes-Acr-1 $E_{1/2}^{gd/red} = -0.57$ V $E_{1/2}^{*/red} = +2.08$ V</p>	 <p>Mes-Acr-2 $E_{1/2}^{gd/red} = -0.57$ V $E_{1/2}^{*/red} = +2.08$ V</p>	 <p>Mes-Acr-3 $E_{1/2}^{gd/red} = -0.57$ V $E_{1/2}^{*/red} = +1.90$ V</p>	 <p>Ar = 3,5-dimethoxyphenyl Mes-Acr-4 $E_{1/2}^{gd/red} = -0.82$ V $E_{1/2}^{*/red} = +1.65$ V</p>
 <p>10-phenyl-phenothiazine $E_{1/2}^{ox/r} = -2.1$ V $E_{1/2}^{ox/gd} = +0.68$ V</p>	 <p>3-cyano-1-methylquinolinium $E_{1/2}^{gd/red} = -0.60$ V $E_{1/2}^{*/red} = +2.72$ V</p>	 <p>4CzIPN $E_{1/2}^{gd/red} = -1.21$ V $E_{1/2}^{*/red} = +1.35$ V</p>	 <p>dicyanoanthracene = DCA $E_{1/2}^{gd/red} = -0.91$ V $E_{1/2}^{*/red} = +1.99$ V</p>

4.2.1 Photocatalyst optimisation

To start this investigation, a range of commercially available or easily accessible visible light absorbing organic photocatalysts (**Table 28**) were screened using a model reaction. Following our optimised conditions (*cf.* **Table 19**), we subjected the boronic ester **179** and the alkene **284** to the series of photoredox catalysts in the presence of catalytic amount of quinuclidin-3-ol and under blue light irradiation to produce the coupled product **266** (**Table 29**).

Table 29 – Organic photocatalyst screening with boronic ester **179**.



Entry	PC	Yield ^a	Comment
1	Ir-4	86%	
2	Ru-2	31%	
3	DCA	0%	Photobleached
4	TPP	0%	Photobleached
5	FL	11%	Photobleached
6	RB	74%	
7 ^b	EY	15%	Photobleached
8	Mes-Acr-1	67%	
9	Mes-Acr-2	58%	Photobleached
10	Mes-Acr-3	62%	
11	Mes-Acr-4	83%	
12	4CzIPN	52%	

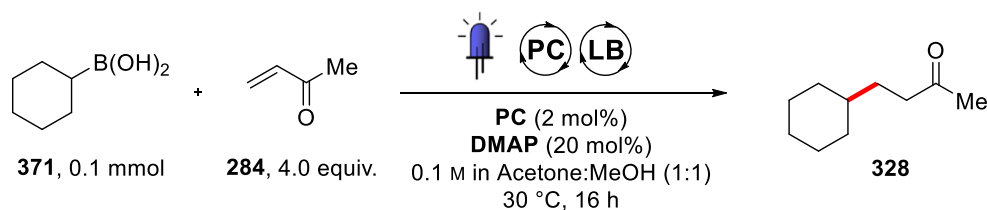
Reactions carried out by adapting **GP(VI)** to the conditions described. ^aYield in **266** determined by ¹H-NMR analysis of crude reaction mixture using CH₂Br₂ as an internal standard. ^bGreen LEDs were used instead (14 W @540 nm).

The results of this screening showed the crucial effect of the photocatalyst on the reaction. Importantly, some dyes were found unstable to the reaction conditions (entries 3

to 5, 7 and 9) as they were decolourised during the irradiation process (photobleached). The reason for this might be the decomposition of the dyes with intense light, or with reactive radical intermediates. We can observe that in this category, only **Mes-Acr-2** resulted in significant product formation (entry 9), the four others producing between 0% (entries 3 and 4) and 15% of product (entry 7). Among the stable dyes, results disparities were also observed. While the ruthenium-based **Ru-2** photocatalyst did not provide efficient yields (entry 2), the donor-acceptor dyes scaffolds (entries 8 to 12) were found to successfully catalyse the transformation. Rose Bengal (**RB**) and the mesityl acridinium dye **Mes-Acr-4** were identified as the best performing organic catalysts of this screening. To our delight, **Mes-Acr-4** yield was comparable (entry 11) to that of our optimised iridium-based catalyst (**Ir-4**).

In order to verify the reproducibility and robustness of this initial screening, we subsequently engaged the stable photocatalysts in a different test reaction. This time, cyclohexyl boronic acid (**371**) was used as a substrate. The results of this second screening are summarised in **Table 30**.

Table 30 – Organic photocatalyst screening with boronic acid **371**.



Entry	PC	Yield ^a
1	Ir-4	90%
2	Ru-2	26%
3	RB	59%
4	Mes-Acr-1	15%
5	Mes-Acr-3	36%
6	Mes-Acr-4	95%
7	4CzIPN	83%

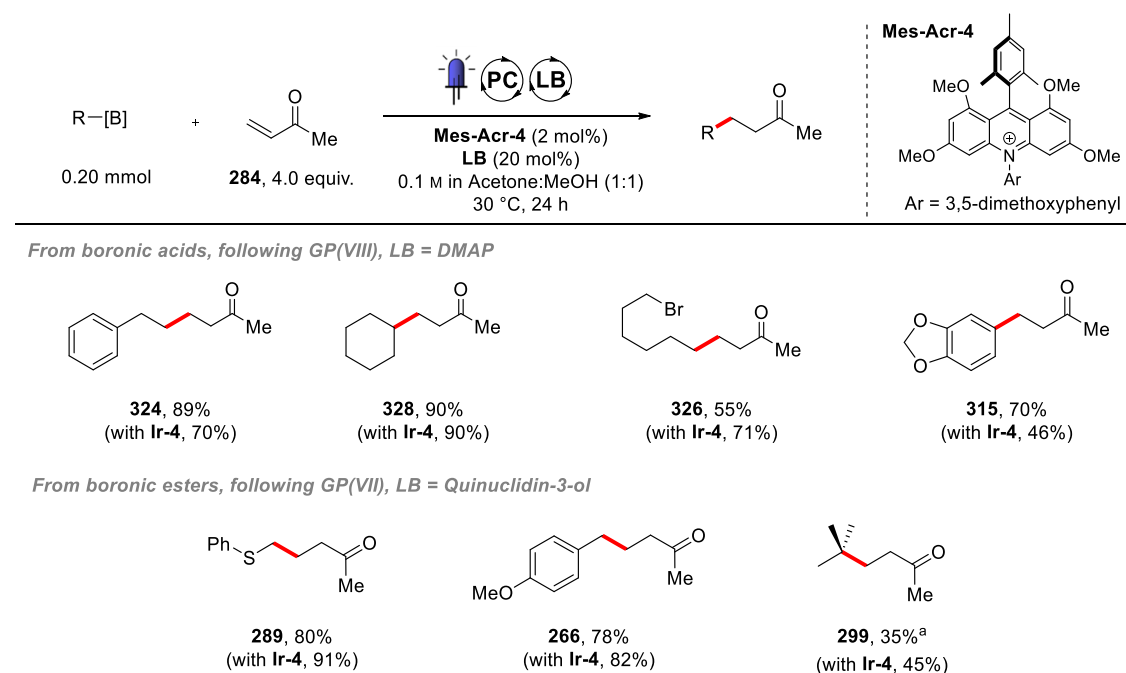
Reactions carried out by adapting **GP(VIII)** to the conditions described. ^aYield in **328** determined by ¹H-NMR analysis of crude reaction mixture using CH₂Br₂ as an internal standard.

Interestingly, a similar reactivity trend was observed with this reaction. This time, **RB** was not as efficient, giving slightly more than 59% yield in **328** (entry 3). Again, **Mes-Acr-4** gave an excellent yield (entries 6). To finish, **4CzIPN** led to comparable results to the iridium-based catalyst (entry 7 vs. 1). To conclude these screenings, we have identified **Mes-Acr-4** as a potential organic-based replacement to **Ir-4** in our latest developed photoredox- and Lewis base-catalysed coupling.

4.2.2 Organic dye performance assessment

To assess the generality of this new catalyst, we initially tested it in a variety of cross-coupling reactions and compared its performance against the previously used **Ir-4** catalyst (Table 31). As far as the cross-coupled products yields are concerned, the performance of the **Mes-Acr-4** dye was often equivalent to the **Ir-4** photocatalyst.

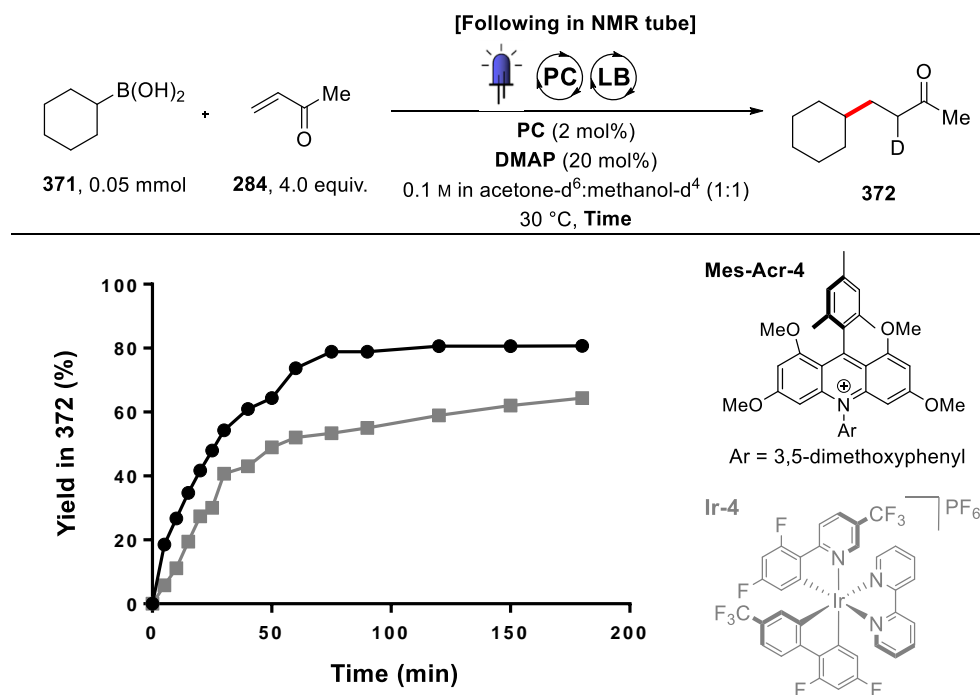
Table 31 – Performance of **Mes-Acr-4** against **Ir-4** for several alkylations of boronic acid derivatives.



Reactions carried out by following **GP(VII)** or **GP(VIII)** using **Mes-Acr-4** instead of **Ir-4**. Isolated yields. ^aDMAP was used as a Lewis base. Yield obtained with **Ir-4** for the same product in parentheses.

While **328** and **266** gave the same isolated yields with both photocatalysts, the organic dye was superior to the iridium one for **324** and **315**. However, in some cases, inferior yields were observed with the organic dye (**326**, **289**, and **299**). Although no apparent correlation between the structure of the boronic acid derivative and their reactivity could be drawn, no reactivity shutdown was observed even in the case of the challenging **299**.

To more finely compare the two catalysts, a reaction profile of the conjugate addition of the cyclohexyl boronic acid (**371**) was recorded by following the reaction using NMR spectroscopy (**Scheme 46**).



Scheme 46 – Reaction following, comparison between **Mes-Ar-4** (dots) and **Ir-4** (squares). Carried out by adapting **GP(VIII)**.

To do this, reagents were dissolved in a deuterated solvent mixture and irradiated inside an NMR tube. At different time points, the light was turned off, thereby putting the reaction on hold to conduct a $^1\text{H-NMR}$ measurement. Using 1,3,5-trimethoxy benzene as an internal standard, it was possible to work out the yield in the deuterated product (**372**) and conversion of starting materials (**371** and **284**) over time. Using this method, we were able to conveniently monitor the reaction progress with minimal material use (0.05 mmol scale).

While the two catalysts performed equally after 24 h of irradiation (*cf.* **Table 31**), they do not share the same kinetic profile (**Scheme 46**). Although the two curves seem to follow a similar initial kinetic (almost linear slope between 0 and 30 min), the **Ir-4** curve “breaks” after 30 min while the other continues to follow a pseudo first-order shape. We believe that this behaviour is a sign of a catalyst deactivation pathway. Radical alkylation of the polypyridyl ligands has already been observed on similar iridium-based photoredox catalysts.^[261] Also bpy ligand removal in acetonitrile solvent was identified as another

deactivation pathway for these photocatalysts.^[262] We therefore believe that strongly nucleophilic DMAP may result in bpy displacement on the iridium centre and lead to catalyst deactivation. Moreover, the **Mes-Acr-4** catalysts have already proven to be stable under similar conditions.^[35]

This deactivation pathway is responsible for a significant rate reduction of the **Ir-4** catalysed reaction. While the full conversion was not reached after 180 min of irradiation with the iridium catalyst, the reaction completed in 70 min with the acridinium dye. Although increasing the **Ir-4** loading could help to cope with this effect, the **Mes-Acr-4** catalyst brings faster kinetics at the same loading and is therefore the most efficient for this reaction.

4.2.3 A residence time “simulation” method

Having developed a straightforward NMR monitoring method, we sought to use it for other purposes. Since we were still interested to perform the photochemical step of the γ -amino acids synthesis in flow, we aimed to develop an expeditious method to determine the residence times needed for these photoreactions to be complete.

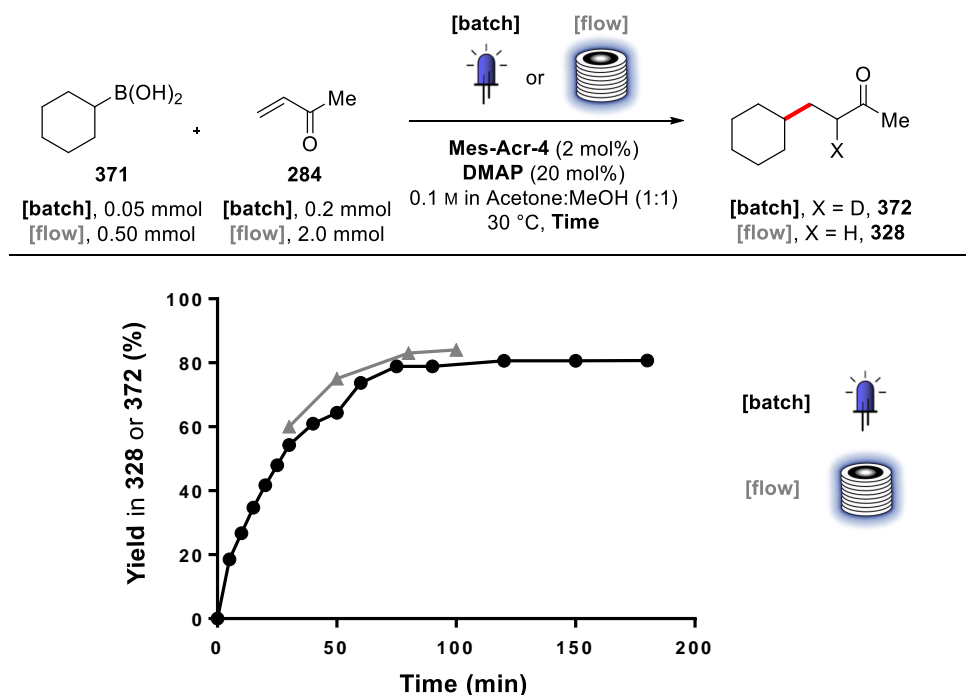
Photoredox reactions are slow reactions, usually requiring from hours to days to complete. Moreover, a continuous flow process productivity decreases with increased reaction time, making this technology less attractive for long reactions (typically exceeding two hours). Therefore, having a knowledge of the residence time needed to perform a reaction is crucial to decide on the viability of a continuous process. This is usually done by testing one residence time at a time for the flow process, or by acquiring the kinetic data and simulating the flow conditions. When working in a chemistry laboratory the first option is often the only one available. This task is often time and material consuming.

In stark contrast, reaction kinetics in the hour range are more efficiently studied with a batch method because only one batch experiment is required to record all the desired time points. However, observed kinetics for photoreactions limited by photon flux are often significantly different in a large batch vessel than in the small channels of a photo flow reactor.^[219]

With these problems in mind, we decided to compare the kinetics observed in the small dimension NMR tube to those observed in the photo flow reactor. If both match, we will

be able to predict the residence time needed for other photo flow reactions to complete by using a simple NMR study.

To test this hypothesis, we compared the reaction yield of our model reaction after a certain residence time (flow mode) and compared this outcome to the reaction profile obtained using the NMR tube (batch mode) method (**Scheme 47**).



Although the flow reaction gave slightly higher yields in **328** at a given time point, this comparison clearly shows a good fitting of the two curves, and hence validates our postulate. While obtaining of the four data points of the flow curve required two days of experimentation and consumed 2.0 mmol of the limiting boronic acid reagent (**371**), the NMR monitoring only required 2.5% of this material demand and half a day of acquisition to optimise the residence time.

4.2.4 Organic catalyst for APIs synthesis in flow

With these encouraging results, we decided to apply this “transition metal free” methodology to the flow synthesis of the active pharmaceutical ingredients (APIs) from the γ -aminobutyric acid (GABA) family. At this point, it must be specified that at a fixed reactor volume, the flow rate determines the residence time of the reaction. However, the

peristaltic pump we are using is not accurate for flow rates under 100 $\mu\text{L}/\text{min}$, indicating that with our largest 10 mL reactor coil, reactions taking longer than 100 minutes are not desirable. Also, with this residence time limitation, the synthesis of the gabapentin precursor (**364**) was impossible to achieve (48 h of irradiation required).

Therefore, we limited our investigation to the synthesis of the three other drug precursors (**361–363**). The suitability of the **Mes-Acr-4** photocatalyst in the synthesis of the phenibut precursor (**362**) was initially investigated in batch (**Table 32**). To our delight, high yields in coupling product (**362**) were also obtained with the organic dye (entry 2 vs. entry 1).

Because of the workup issues posed by DMAP during the previous optimisations (*cf.* **Scheme 44** and **Scheme 45**), we explored again the use of PPh_3 as an alternative Lewis base catalyst (entry 3). We could observe that using PPh_3 , only 82% of the starting material (**358**) was converted after 16 h of irradiation. Increasing the irradiation time to 40 h did not result in a full conversion of **358** either (entry 4).

Table 32 – Initial batch optimisation of phenibut precursor (**362**) synthesis.

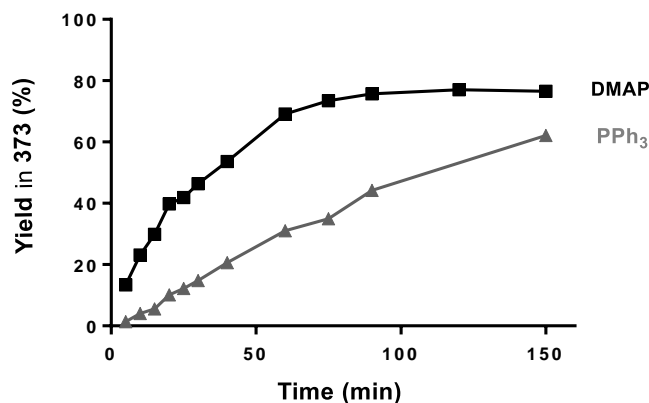
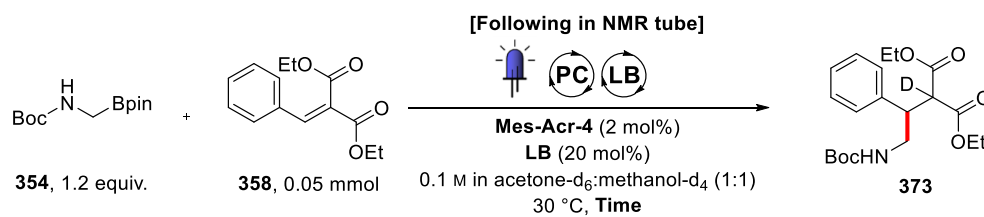
Entry	PC	LB	Time	Yield ^a	Conversion ^a
1	Ir-4	DMAP	16 h	79%	100%
2	Mes-Acr-4	DMAP	16 h	76%	100%
3	Mes-Acr-4	PPh_3	16 h	62%	82%
4	Mes-Acr-4	PPh_3	40 h	77%	89%

Reactions carried out by adapting **GP(IX)** to the conditions described. ^aYield in **362** and conversion of **358** are determined by $^1\text{H-NMR}$ analysis of crude reaction mixture using CH_2Br_2 as an internal standard.

As already mentioned, a fast photoreaction is the key to transferring it in a flow process. Based on these initial results, we compared the reaction profiles obtained with both Lewis bases for this transformation (**Scheme 48**).

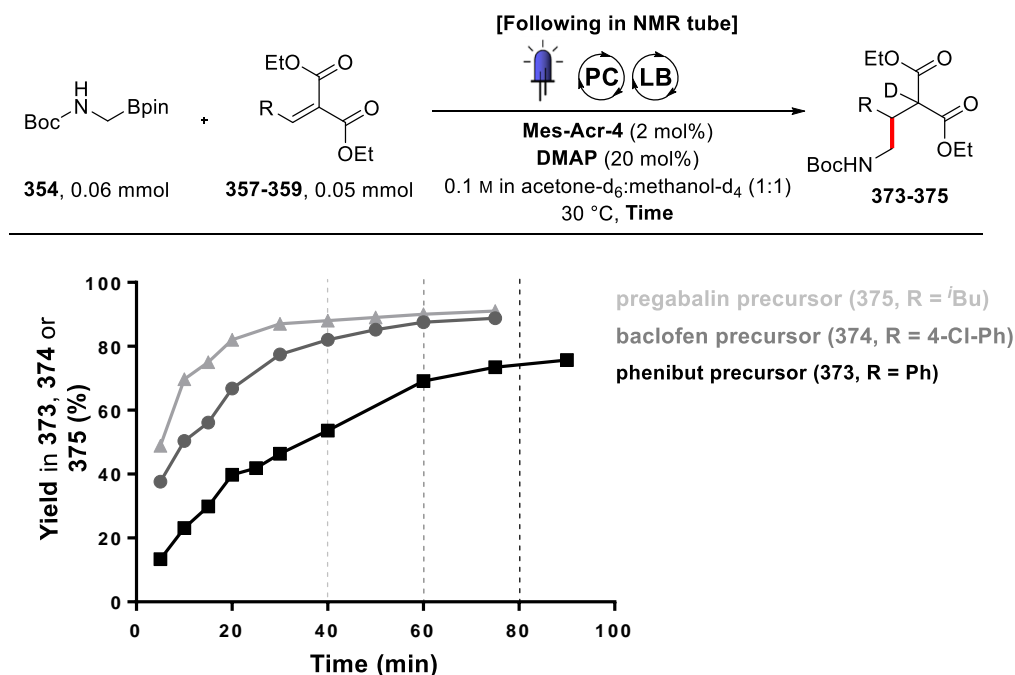
Observing these reaction profiles, it is apparent that DMAP leads to enhanced kinetics. After the 100 min reaction time limit, PPh_3 only delivers 45% of the deuterated product (**373**) while DMAP results in 80% yield of the same product.

Therefore, even if the PPh_3 can result in better yields than DMAP for prolonged irradiations, its use in the continuous flow photoreactor remains inefficient.



Scheme 48 – Lewis base effect, comparison between DMAP (squares) and PPh_3 (triangles) (carried out by adapting **GP(IX)**).

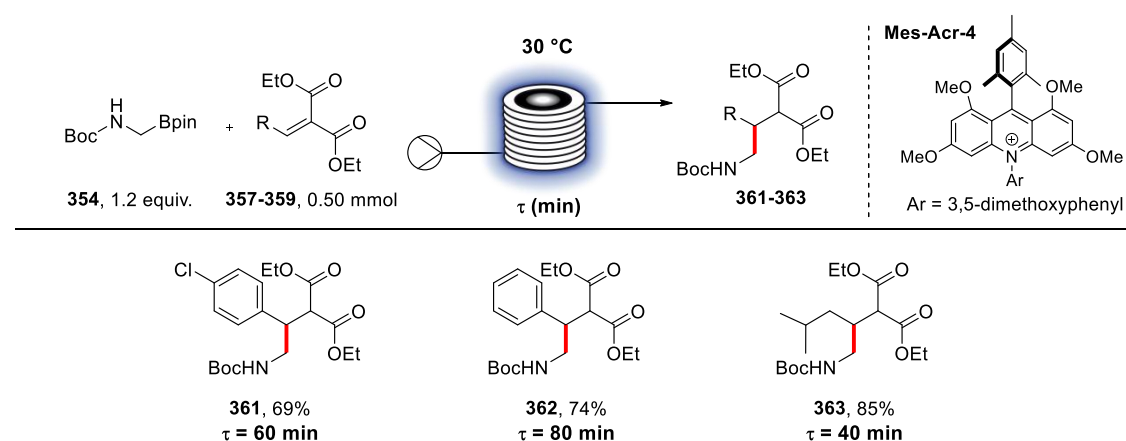
With this final optimised parameter, we could record the reaction profile of the two other targeted drug precursors using the **Mes-Acr-4** and DMAP dual catalysed system (**Scheme 49**). These profiles allowed us to finely tune the residence time needed for each partner. While the deuterated phenibut precursor (**373**) required 80 min of irradiation, the baclofen (**374**) and pregabalin (**375**) ones could be synthesised efficiently in 60 min and 40 min respectively.



Scheme 49 – Coupling kinetics observed in NMR tube for the three APIs precursors (adapting **GP(IX)**).

Using these predicted residence times in a flow photoreactor setup resulted in finely tuned conditions for these APIs precursors coupling reactions (**Table 33**). Pleasingly, all the targeted compounds were successfully obtained in high yields after purification (**361–363**).

Table 33 – Final flow synthesis of drug precursors **361** to **363** with the optimised flow conditions.



Reactions carried out by following **GP(X)**. Isolated yields.

Although yields were consistently lower than those obtained with the batch protocol and the **Ir-4** photocatalyst (*cf.* **Table 27**), these experiments finally confirm the feasibility of the initial photoredox coupling step in a flow reactor.

4.3 Summary and conclusions

As a summary, the synthetic utility of our methodology could be further demonstrated by the two-step syntheses of four approved central nervous system drugs from the GABA family. Utilising **353** in presence of malonate-derived olefins (**357–360** as limiting reagents), we could obtain high yields of the coupled products (**361–364**) in batch mode using the **Ir-4** photocatalyst (*cf.* **Table 27**). All these were deprotected and decarboxylated using 6 M HCl in excellent yields to deliver baclofen, phenibut, pregabalin, and gabapentin as their corresponding hydrochloride salts (**365–368**).

We also identified the organic dye **Mes-Acr-4** as a promising alternative to iridium photocatalyst **Ir-4**. This organic photocatalyst have shown similar to better activity than **Ir-4** in our photoredox couplings as well as enhanced stability under our reaction conditions. **Mes-Acr-4** could also successfully replace **Ir-4** in the synthesis of the pharmaceutical ingredients previously described. Using this “transition metal free” conditions we could carry out the synthesis of the precursors of baclofen, phenibut and pregabalin in a flow photoreactor (**361–364** in **Table 33**). Although telescoping in the second step proved to be problematic, we believe that the first step alone would benefit from being run continuously if a larger amount of these compounds are to be made.

5 Experimental

5.1 General information

5.1.1 General experimental and analytical methods

General methods: All reactions, unless otherwise noted, were performed magnetically stirred under Ar atmosphere using standard Schlenk techniques. Reaction temperatures were electronically monitored as external heating block temperatures. Reagents were purchased from different commercial sources and used without further purification. The removal of solvent under reduced pressure was carried out on a standard rotary evaporator.

Solvents: Et₂O and THF were distilled with sodium and benzophenone under inert gas prior to use. Degassed solvents were degassed by purging with Ar for at least 20 min. Solvents for flash column chromatography and crystallisations were distilled under reduced pressure. *Iso*-hexane mentioned as petrol ether (PE) consist of the boiling fractions between 40 and 50°C.

Chromatography: Analytical thin-layer chromatography (TLC) was carried out on pre-coated glass plates (silica gel 60 F₂₅₄) from Merck. Compound spots were visualised under ultraviolet (UV) light (254 nm or 365 nm for fluorescent compounds), ceric ammonium molybdate (CAM), ninhydrin or KMnO₄ stain solutions. For flash column chromatography silica gel 60 from Merck, with a particle size between 40 and 63 µm, was used. Crudes were often loaded onto columns using dry loading technique with ISOLUTE[®] HM-N.

NMR spectroscopy: ¹H-NMR spectra were recorded on a Bruker Avance DPX-400 or DRX-600 spectrometer at 400 and 600 MHz respectively and are reported as follows: chemical shift δ in ppm (multiplicity, coupling constants *J* in Hz, number of protons, assignment). The multiplicity and shape of the ¹H signals are designated by the following abbreviations: s = singlet, d = doublet, t = triplet, q = quartet, p = pentet, sept = septet, m = multiplet, br = broad, or combinations thereof. These chemical shifts δ are reported to

the nearest 0.01 ppm with the residual solvent peak as the internal reference ($\text{CDCl}_3 = 7.26$ ppm, methanol- $\text{d}_4 = 3.31$ ppm, water- $\text{d}_2 = 4.79$ ppm). ^{13}C -NMR spectra were recorded on the same spectrometers at 100 and 150 MHz with ^1H decoupling. All ^{13}C resonances are reported to the nearest 0.1 ppm with the central resonance of the solvent peak as the internal reference ($\text{CDCl}_3 = 77.16$ ppm, methanol- $\text{d}_4 = 49.00$ ppm). The ^{13}C signal of the carbon bonded to boron was not observed in some cases due to quadrupolar relaxation. ^{19}F -NMR spectra were recorded on a Bruker DPX-400 spectrometer at 376 MHz with ^1H decoupling. All chemical shifts δ are reported to the nearest 0.1 ppm with CFCl_3 as the external standard ($\text{CFCl}_3 = 0.0$ ppm). ^{11}B -NMR NMR spectra were recorded on a Bruker DPX-400 or DRX-600 spectrometer at 128 MHz and 193 MHz respectively with ^1H decoupling. All chemical shifts δ are reported to the nearest 0.1 ppm with $\text{BF}_3 \cdot \text{OEt}_2$ as the external standard ($\text{BF}_3 \cdot \text{OEt}_2 = 0.0$ ppm). Spectra are assigned using ^1H -COSY, ^{13}C -DEPT-135, HSQC and HMBC where appropriate to facilitate structural determination. The numbering of the proton and carbon atoms does not match the IUPAC nomenclature. Diastereotopic protons in the ^1H -NMR spectra are referenced with a and b, nomenclature is arbitrarily and does not correspond to the spin system.

Infrared spectroscopy: Infrared spectra were recorded neat on a Perkin-Elmer Spectrum One FT-IR spectrometer using Universal ATR sampling measuring unit. Selected peaks are reported in wavenumbers (cm^{-1}) of absorption.

High-resolution mass spectrometry (HRMS) was performed using a Waters Micromass LCT PremierTM spectrometer using time of flight (TOF) mass detection and positive ESI ionization method. Unless otherwise stated, reported mass correspond to the parent molecular ion associated with a proton $[\text{M}+\text{H}]^+$ or a sodium cation $[\text{M}+\text{Na}]^+$ (^{23}Na isotope). All m/z values are reported to four decimal places and within ± 5 ppm of the calculated value.

Melting points (m.p.) were recorded on a Stanford Research Systems OptiMelt Automated Melting Point System calibrated against vanillin (m.p. 83°C), phenacetin (m.p. 136°C) and caffeine (m.p. 237°C).

5.1.2 Photochemical and optimisation experiments

Batch photochemical experiments were performed magnetically stirred in 5 mL glass test tubes or microwave vials, sealed with a rubber septum. The tubes/vials were externally irradiated with blue light either using a coiled commercial LED strip (Ledxon, 14.4 W at 470 nm) or a LED torch (Thorlabs, 253 mW at 470 nm). To maintain a constant reaction temperature of 30°C, the setup was cooled by a constant air flow from a clip fan (**Figure 15**).

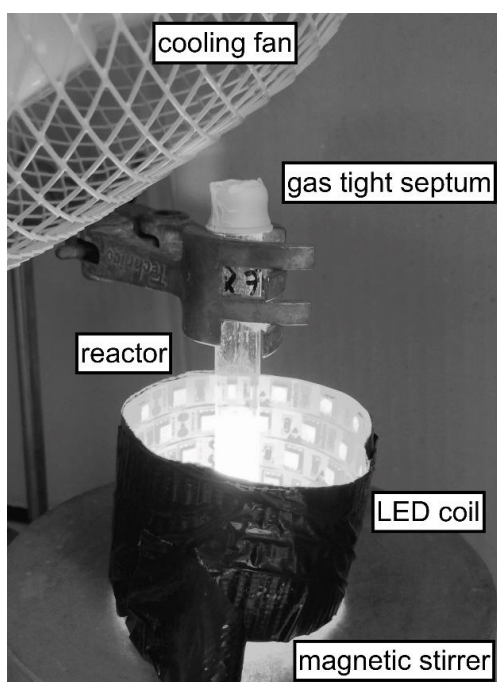


Figure 15 – Typical batch photoreactor setup.

Flow photochemical experiments were performed using a Vapourtec E-series unit equipped with a UV-150 module with blue LEDs (17 W at 420 nm). The pumps used on this equipment are peristaltic pumps (SF-10 type) allowing to deliver accurate flow rates between 100 $\mu\text{L}/\text{min}$ and 10 mL/min . The reactor coil (10 mL) is made of FEP tubing with thin walls (outer diameter: 1.6 mm, inner diameter: 1.3 mm). The system was pressurised at 100 psi by the use of a BPR at the end of the line.

Optimisation experiments were carried out using adapted protocols from the mentioned general procedures (GP). Optimisation yields were determined by using the $^1\text{H-NMR}$ integration of an internal standard as reference, added to the crude mixture after the reaction workup.

NMR following experiments were carried out by adapting the mentioned **GP(n)** to a 0.05 mmol scale, employing the corresponding deuterated solvents and 1,3,5-trimethoxybenzene as internal standard. After being prepared in a separate vial, the reaction mixture was transferred in an NMR tube under argon. An initial $^1\text{H-NMR}$ measurement (time zero) was made before the tube was irradiated. Irradiation times were accurately measured by the use of a stopwatch. Integrating the product and starting material peaks against the internal standard gave access to conversions and yields over time.

5.1.3 Computational methods

Geometries of all structures (minima and saddle points) were optimised at the $\omega\text{B97xd/cc-pVDZ}$ level^[263–265] in acetone as a solvent (using the SMD solvation model^[266] $\epsilon = 20.493$) using Gaussian 09 software (revision D.01)^[267], subsequent vibrational frequency calculations were performed at the same level for all calculated structures. Transition states found possess exactly one negative Hessian eigenvalue, while all other stationary points were confirmed to be genuine minima on the potential energy surface. Intrinsic reaction coordinate analysis was performed to unambiguously assign located transition states when needed. Electronic energies were obtained by performing single point calculations at the $\omega\text{B97xd/cc-pVTZ}$ level in solvent. Gibbs energies were calculated as $\Delta_r G = \Delta_r H - T\Delta_r S$ at 298 K where enthalpies and entropies were obtained by using standard statistical mechanical formulae for the ideal gas, rigid rotor, and harmonic oscillator approximations following the normal-mode analysis in vacuum. A correction of $(1.9 \cdot \Delta n)$ kcal mol⁻¹ (corresponding to the difference between the concentration of the ideal gas at 298 K and 1 atm and its 1 mol L⁻¹ concentration; Δn is the change in number of moles in the reaction) has been applied in order that the computed values refer to 1 mol L⁻¹ standard state.

Calculated redox potentials are relative and were obtained using single-electron oxidation of potassium benzyltrifluoroborate ($E_{\text{ox}} = +1.10$ V)^[62] and single-electron reduction of 1,4-dicyanobenzene ($E_{\text{red}} = -1.61$ V)^[74] as two experimental reference points describing redox properties of the structurally similar compounds.

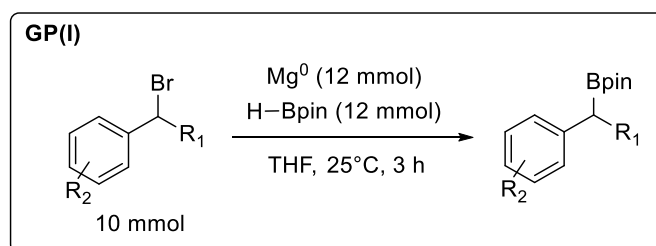
5.1.4 Electrochemical measurements

Cyclic voltammetry experiments were conducted on a Palmstat EmStat 3 potentiostat with a glassy carbon working, a platinum mesh counter and a Ag/AgCl reference electrode, referenced to SCE using ferrocene as an internal standard (0.42 V vs. SCE).^[37] In the standard procedure 0.02 mmol substrate were dissolved in 10 mL of a 0.1 M [N(Bu)₄]PF₆ electrolyte solution in degassed acetonitrile. The reactor was sealed with a rubber septum and degassed by purging the solution with nitrogen for 10 min. Each measurement was conducted with a new glassy carbon working electrode and a scan rate of 100 mV/s at room temperature under nitrogen atmosphere without stirring. The half-peak oxidation potentials ($E_{1/2}$) were determined as the voltage at half the current of the local maximum current using QTI-Plot to analyse the data.^[37] Due to the generation of radicals during oxidation of the analytes, which undergo further reactions, all cyclic voltammograms showed an asymmetric shape describing the irreversibility of the oxidation.

5.2 Experimental data for Chapter 2

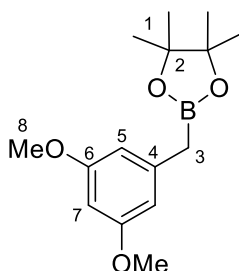
5.2.1 Synthetic procedures and characterisation for starting materials

5.2.1.1 Boronic esters starting materials



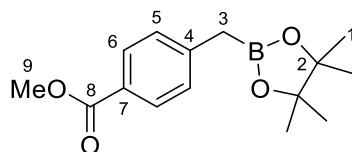
GP(I): A 100 mL round-bottom flask equipped with a magnetic stir bar was charged with magnesium turnings (290 mg, 12 mmol, 1.2 equiv.) and was activated by addition of iodine crystals and warming until iodine sublimed. The flask was cooled to 25°C and was purged with argon. THF (25 mL) was added to the flask, followed by the addition of neat pinacolborane (1.2 mL, 12 mmol, 1.2 equiv.). Benzylic bromide compound (10 mmol, 1.0 equiv.) diluted in 5 mL of THF was then added dropwise over 10 min with constant stirring at 25°C. After stirring the reaction mixture at room temperature for 3 h, it was cooled to 0°C and acidified with 3 M aqueous HCl (15 mL) (Caution, H₂ generation). After 10 min of stirring the reaction mixture was warmed to 25°C and stirred for an additional 30 min. The reaction mixture was then transferred to a separatory funnel and extracted with diethyl ether (3 × 15 mL). The combined organic layers were dried over MgSO₄, filtered, and dried *in vacuo*. Residue was then purified over silica gel flash column chromatography (5% EtOAc in hexane) to deliver the pure boronic ester.

2-(3,5-dimethoxybenzyl)-4,4,5,5-tetramethyl-1,3,2-dioxaborolane

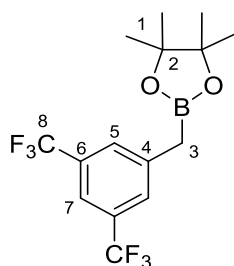


Obtained following **GP(I)** as a colourless oil (1.25 g, 4.47 mmol) in 45% yield. **¹H-NMR (600 MHz, CDCl₃)** δ 6.37 (d, *J* = 2.1 Hz, 2H, H₇), 6.27 (t, *J* = 2.1 Hz, 1H, H₅), 3.78 (s, 6H, H₈), 2.26 (s, 2H, H₃), 1.26 (s, 12H, H₁). **¹³C-NMR (151 MHz, CDCl₃)** δ 160.6 (C₆), 140.9 (C₄), 107.1 (C₅), 97.3 (C₇), 83.4 (C₂), 55.2 (C₈), 24.7 (C₁). **¹¹B-NMR (193 MHz, CDCl₃)** δ 33.1. **IR (ATR – neat)** $\tilde{\nu}$ (cm⁻¹) = 2929, 2222, 1623, 1608, 1508, 1467, 1433, 1376, 1274, 1161, 1116, 898. **HRMS for [C₁₅H₂₄O₄¹¹B]⁺** calculated 279.1762 found 279.1764. **R_f**(1:9 EtOAc/hexane) = 0.19.

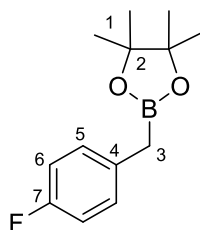
methyl 4-((4,4,5,5-tetramethyl-1,3,2-dioxaborolan-2-yl)methyl)benzoate



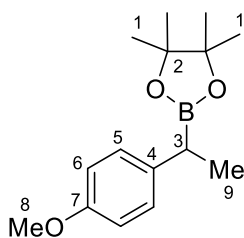
Obtained following **GP(I)** as a colourless oil (1.84 g, 6.65 mmol) in 67% yield. **¹H-NMR (600 MHz, CDCl₃)** δ 7.92 (d, *J* = 8.3 Hz, 2H, H₆), 7.25 (d, *J* = 8.3 Hz, 2H, H₅), 3.89 (s, 3H, H₉), 2.36 (s, 2H, H₃), 1.23 (s, 12H, H₁). **¹³C-NMR (151 MHz, CDCl₃)** δ 167.3 (C₈), 144.7 (C₄), 129.6 (C₆), 128.9 (C₅), 126.9 (C₇), 83.6 (C₂), 51.9 (C₉), 24.7 (C₁). **¹¹B-NMR (193 MHz, CDCl₃)** δ 32.5. **HRMS for [C₁₅H₂₂O₄¹¹B]⁺** calculated 277.1611 found 277.1621. **R_f** (1:4 EtOAc/hexane) = 0.33. Spectroscopic data were consistent with literature values.^[268]

2-(3,5-bis(trifluoromethyl)benzyl)-4,4,5,5-tetramethyl-1,3,2-dioxaborolane

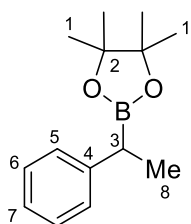
Obtained following **GP(I)** as a colourless oil (1.98 g, 5.98 mmol) in 60% yield. **¹H-NMR (600 MHz, CDCl₃)** δ 7.65 (s, 1H, H₇), 7.64 (s, 2H, H₅), 2.42 (s, 2H, H₃), 1.25 (s, 12H, H₁). **¹³C-NMR (151 MHz, CDCl₃)** δ 141.3 (C₄), 131.2 (q, *J* = 32.8 Hz, C₈), 129.1 (q, *J* = 2.5 Hz, C₅), 123.5 (q, *J* = 270 Hz, C₈), 119.0 (sept, *J* = 3.8 Hz, C₇), 84.0 (C₂), 24.7 (C₁). **¹¹B-NMR (193 MHz, CDCl₃)** δ 32.8. **¹⁹F-NMR (376 MHz, CDCl₃)** δ -62.9. **HRMS for [C₁₅H₁₈O₂¹¹BNa]⁺** calculated 355.1304 found 355.1287. **R_f** (1:9 EtOAc/hexane) = 0.40. Spectroscopic data were consistent with literature values.^[269]

2-(4-fluorobenzyl)-4,4,5,5-tetramethyl-1,3,2-dioxaborolane

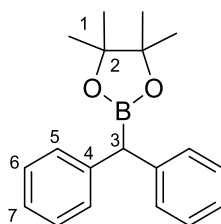
Obtained following **GP(I)** as a colourless oil (1.21 g, 5.09 mmol) in 51% yield. **¹H-NMR (600 MHz, CDCl₃)** δ 7.13 (dd, *J* = 8.3, 5.6 Hz, 2H, H₅), 6.93 (t, *J* = 8.7 Hz, 2H, H₆), 2.26 (s, 2H, H₃), 1.24 (s, 12H, H₁). **¹³C-NMR (151 MHz, CDCl₃)** δ 160.7 (d, *J* = 244 Hz, C₇), 134.1 (d, *J* = 3.1 Hz, C₄), 130.2 (d, *J* = 7.6 Hz, C₅), 114.9 (d, *J* = 21 Hz, C₆), 83.5 (C₂), 24.7 (C₁). **¹¹B-NMR (193 MHz, CDCl₃)** δ 33.1 **¹⁹F-NMR (376 MHz, CDCl₃)** δ -62.90 **HRMS for [C₁₃H₁₉O₂F¹¹B]⁺** calculated 237.1457 found 237.1456. **R_f** (1:9 EtOAc/hexane) = 0.33. Spectroscopic data were consistent with literature values^[212]

2-(1-(4-methoxyphenyl)ethyl)-4,4,5,5-tetramethyl-1,3,2-dioxaborolane

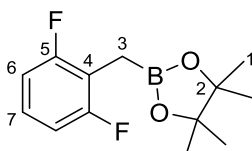
Obtained following **GP(I)** as a colourless oil (2.15 g, 8.21 mmol) in 82% yield. **¹H-NMR (600 MHz, CDCl₃)** δ 7.15 (d, *J* = 8.6 Hz, 2H, H₅), 6.83 (d, *J* = 8.6 Hz, 2H, H₆), 3.79 (s, 3H, H₈), 2.39 (q, *J* = 7.5 Hz, 1H, H₃), 1.31 (d, *J* = 7.5 Hz, 3H, H₉), 1.23 (s, 6H, H₁ or H_{1'}), 1.22 (s, 6H, H₁ or H_{1'}). **¹³C-NMR (151 MHz, CDCl₃)** δ 157.2 (C₇), 137.0 (C₄), 128.6 (C₅), 113.8 (C₆), 83.2 (C₂), 55.2 (C₈), 24.6 (C₁ and C_{1'}), 17.4 (C₉). **¹¹B-NMR (193 MHz, CDCl₃)** δ 32.9. **HRMS for [C₁₅H₂₃O₃¹¹BNa]⁺** calculated 285.1632 found 285.1621. **R_f** (1:9 EtOAc/hexane) = 0.58. Spectroscopic data were consistent with literature values. ^[212]

4,4,5,5-tetramethyl-2-(1-phenylethyl)-1,3,2-dioxaborolane

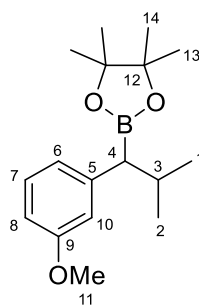
Obtained following **GP(I)** as a colourless oil (1.56 g, 6.71 mmol) in 67% yield. **¹H-NMR (600 MHz, CDCl₃)** δ 7.27 (t, *J* = 7.5 Hz, 2H, H₆), 7.23 (d, *J* = 7.2 Hz, 2H, H₅), 7.14 (t, *J* = 7.2 Hz, 1H, H₇), 2.44 (q, *J* = 7.4 Hz, 1H, H₃), 1.34 (d, *J* = 7.5 Hz, 3H, H₈), 1.22 (s, 6H, H₁ or H_{1'}), 1.21 (s, 6H, H₁ or H_{1'}). **¹³C-NMR (151 MHz, CDCl₃)** δ 145.0 (C₄), 128.3 (C₆), 127.8 (C₅), 125.0 (C₇), 83.3 (C₂), 24.6 (C₁ or C_{1'}), 24.5 (C_{1'} or C₁), 17.0 (C₈). **¹¹B-NMR (193 MHz, CDCl₃)** δ 33.2. **HRMS for [C₁₄H₂₁O₂¹¹B²³Na]⁺** calculated 255.1527 found 255.1515. **R_f** (1:9 EtOAc/hexane) = 0.62. Spectroscopic data were consistent with literature values. ^[211]

2-benzhydryl-4,4,5,5-tetramethyl-1,3,2-dioxaborolane

Obtained following **GP(I)** as a white solid (709 mg, 2.40 mmol) in 24% yield. **¹H-NMR** (600 MHz, CDCl₃) δ 7.30 (br s, 8H, H₆ and H₅), 7.20 (br s, 2H, H₇), 3.91 (s, 1H, H₃), 1.27 (s, 12H, H₁). **¹³C-NMR** (151 MHz, CDCl₃) δ 142.1 (C₄), 129.1 (C₆ or C₅), 128.4 (C₅ or C₆), 125.6 (C₇), 83.7 (C₂), 24.6 (C₁). **¹¹B-NMR** (193 MHz, CDCl₃) δ 33.1. **HRMS** for [C₁₉H₂₃O₂¹¹B²³Na]⁺ calculated 317.1683 found 317.1671. **R_f**(1:9 EtOAc/hexane) = 0.39. **M.p.** 76–78°C. Spectroscopic data were consistent with literature values.^[270]

2-(2,6-difluorobenzyl)-4,4,5,5-tetramethyl-1,3,2-dioxaborolane

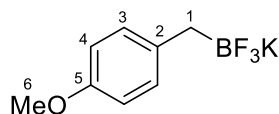
Obtained following **GP(I)** as a yellowish oil (492 mg, 1.93 mmol) in 19% yield. **¹H-NMR** (600 MHz, CDCl₃) δ 7.10 – 7.04 (m, 1H, H₇), 6.83 (t, *J* = 7.5 Hz, 2H, H₆), 2.24 (s, 2H, H₃), 1.25 (s, 12H, H₁). **¹³C-NMR** (151 MHz, CDCl₃) δ 126.1 (C₇), 110.7 (C₆), 110.6 (C₄), 83.7 (C₂), 24.6 (C₁). **¹¹B-NMR** (193 MHz, CDCl₃) δ 33.1 **HRMS** for [C₁₃H₁₈O₂F₂¹¹B]⁺ calculated 255.1362 found 255.1377. **R_f**(1:9 EtOAc/hexane) = 0.47.

2-(1-(3-Methoxyphenyl)-2-methylpropyl)-4,4,5,5-tetramethyl-1,3,2-dioxaborolane

Obtained following **GP(I)** as a colourless (1.23 g, 4.22 mmol) in 42% yield. **¹H-NMR (400 MHz, CDCl₃)** δ 7.15 (t, *J* = 7.8 Hz, 1H, H₇), 6.84 – 6.75 (m, 2H, H₈ and H₁₀), 6.68 (dd, *J* = 8.2, 1.9 Hz, 1H, H₆), 3.78 (s, 3H, H₁₁), 2.16 – 2.03 (m, 1H, H₃), 1.94 (d, *J* = 10.4 Hz, 1H, H₄), 1.20 (s, 6H, H₁₃ or H₁₄), 1.18 (s, 6H, H₁₃ or H₁₄), 1.02 (d, *J* = 6.5 Hz, 3H, H₁ or H₂), 0.74 (d, *J* = 6.5 Hz, 3H, H₁ or H₂). **¹³C-NMR (151 MHz CDCl₃)** δ 159.5 (C₉), 144.1 (C₅), 129.0 (C₇), 121.8(C₆), 114.7 (C₁₀), 110.8 (C₈), 83.3 (C₁₂), 55.1 (C₁₁), 31.1 (C₃), 24.8 (C₁₃ or C₁₄), 24.7 (C₁₃ or C₁₄), 23.2 (C₁ or C₂), 22.1 (C₁ or C₂). **¹¹B-NMR (128 MHz, CDCl₃)** δ 32.9. **IR (ATR – neat)** $\tilde{\nu}$ (cm⁻¹) = 2975, 1598, 1581, 1486, 1465, 1380, 1353, 1318, 1258, 1214, 1139, 1139, 1113, 1047, 971, 865, 848, 777, 714, 694, 672. **HRMS for [C₁₇H₂₈O₃¹¹B]⁺** calculated 291.2126 found 291.2115. **R_f**(1:10 EtOAc/hexane) = 0.57.

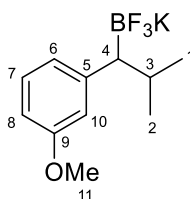
5.2.1.2 Borate starting materials

Potassium trifluoro(4-methoxybenzyl)borate (**155**)



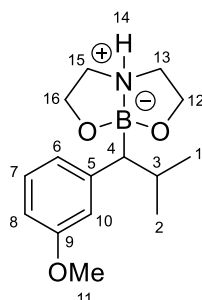
A 100 mL round-bottom flask equipped with a magnetic stir bar was charged with 2-(4-methoxybenzyl)-4,4,5,5-tetramethyl-1,3,2-dioxaborolane (2.16 g, 8.71 mmol, 1.0 equiv.) and THF (20 mL) under air at room temperature, then, KHF_2 (3.85 g, 49.3 mmol, 5.6 equiv.) dissolved in H_2O (10 mL) was added dropwise to the reaction mixture. The resulting reaction solution was stirred at room temperature for 2 hours. The mixture was then concentrated *in vacuo* and dried under high vacuum overnight. The residue was dissolved in hot acetone and filtered. The filtrate was concentrated to yield a mixture of potassium trifluoroborate and pinacol. The crude product was washed with cold ether for several times to afford **155** (1.58 g, 7.00 mmol) as a white solid in 82% yield.

$^1\text{H-NMR}$ (600 MHz, methanol- d_4) δ 7.03 (d, $J = 8.4$ Hz, 2H, H_3), 6.69 (d, $J = 8.6$ Hz, 2H, H_4), 3.72 (s, 3H, H_6), 1.63 (d, $J = 6.5$ Hz, 2H, H_1). $^{13}\text{C-NMR}$ (151 MHz, methanol- d_4) δ 155.9 (C_5), 137.5 (C_2), 129.1 (C_3), 112.6 (C_4), 54.2 (C_6). $^{19}\text{F-NMR}$ (376 MHz, methanol- d_4) δ -143.6. $^{11}\text{B-NMR}$ (128 MHz, methanol- d_4) δ 5.0. HRMS for $[\text{C}_8\text{H}_9\text{O}^{11}\text{BF}_3^{39}\text{KNa}]^+$ calculated 251.0228 found 251.0224. Spectroscopic data were consistent with literature values.^[62]

Potassium trifluoro(1-(3-methoxyphenyl)-2-methylpropyl)borate (156)

A 25 mL round-bottom flask equipped with a magnetic stir bar was charged with 2-(1-(3-methoxyphenyl)-2-methylpropyl)-4,4,5,5-tetramethyl-1,3,2-dioxaborolane (523 mg, 1.8 mmol, 1.0 equiv.) and THF (6.0 mL) under air at room temperature, then, KHF_2 (888 mg, 11.4 mmol, 6.3 equiv.) dissolved in H_2O (3.0 mL) was added dropwise to the reaction mixture. The resulting reaction solution was stirred at room temperature for 14 h. The mixture was then concentrated *in vacuo* and dried under high vacuum overnight. The residue was dissolved in hot acetone and filtered. The filtrate was concentrated to yield a mixture of potassium trifluoroborate and pinacol. The crude product was washed with cold ether for several times to afford **156** (195 mg, 0.72 mmol) as a white solid in 40% yield.

$^1\text{H-NMR}$ (600 MHz, methanol- d_4) δ 7.01 (t, $J = 7.8$ Hz, 1H, H_7), 6.74 – 6.72 (m, 2H, H_8 and H_{10}), 6.54 (ddd, $J = 8.1, 2.6, 0.9$ Hz, 1H, H_6), 3.74 (s, 3H, H_{11}), 1.99 (dsept, $J = 9.1, 6.6$ Hz, 1H, H_3), 1.36 (dd, $J = 8.8$ Hz, $J = 5.5$ Hz, 1H, H_4), 1.01 (d, $J = 6.6$ Hz, 3H, H_1 or H_2), 0.67 (d, $J = 6.6$ Hz, 3H, H_1 or H_2). **$^{13}\text{C-NMR}$ (151 MHz, methanol- d_4)** δ 158.9 (C_9), 151.2 (C_5), 127.3 (C_7), 122.0 (C_6), 114.6 (C_{10}), 108.2 (C_8), 53.9 (C_{11}), 30.4 (C_3), 22.6 (C_1 and C_2). **$^{19}\text{F-NMR}$ (376 MHz, methanol- d_4)** δ -141.8. **$^{11}\text{B-NMR}$ (128 MHz, methanol- d_4)** δ 5.5. **IR (ATR – neat)** $\tilde{\nu}$ (cm^{-1}) = 2984, 2948, 2861, 1604, 1575, 1484, 1263, 1152, 1065, 971, 943, 923, 786, 763, 739, 707. **HRMS for $[\text{C}_{11}\text{H}_{15}\text{O}^{11}\text{BF}_3^{39}\text{KNa}]^+$** calculated 293.0697 found 293.0691. **M.p.** = 165–167°C.

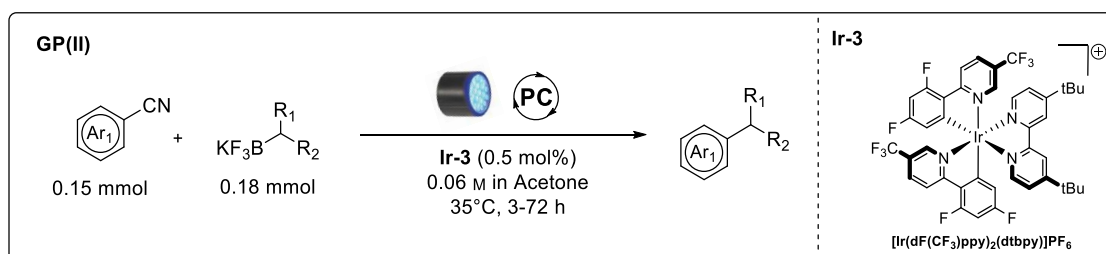
8-(1-(3-methoxyphenyl)-2-methylpropyl)hexahydro-1,3,2-oxazaborolo[2,3-b]-1,3,2-oxazaborol-4-ium-8-uide (168)

A 25 mL round-bottom flask equipped with a magnetic stir bar was charged with 2-(1-(3-methoxyphenyl)-2-methylpropyl)-4,4,5,5-tetramethyl-1,3,2-dioxaborolane (523 mg, 1.8 mmol, 1.0 equiv.) and Et₂O (6.0 mL) under air at room temperature, then diethanolamine (210 mg, 2.0 mmol, 1.1 equiv.) was added in one portion to the reaction mixture. The resulting reaction solution was stirred at room temperature until a white precipitate formed. After 2 h the precipitate was filtered, washed with Et₂O (10 mL) and dried *in vacuo* to afford **168** (448 mg, 1.62 mmol) as a white solid in 90% yield.

¹H-NMR (400 MHz, CDCl₃) δ 7.15 (t, J = 8.0 Hz, 1H, H₇), 6.82 – 6.74 (m, 2H, H₈ and H₁₀), 6.63 (dd, J = 8.0, 3.0 Hz, 1H, H₆), 4.05 – 3.87 (m, 4H, H₁₂ and H₁₆), 3.78 (s, 3H, H₁₁), 3.52 (br s, 1H, H₁₄), 3.22 – 3.06 (m, 1H, H_{13a} or H_{15a}), 2.63 – 2.32 (m, 3H, H_{13b}, H_{15b} and H_{15a} or H_{13a}), 2.17 (dsept, J = 10.5, 6.5 Hz, 1H, H₃), 1.51 (d, J = 10.5 Hz, 1H, H₄), 1.16 (d, J = 6.5 Hz, 3H, H₁ or H₂), 0.71 (d, J = 6.5 Hz, 3H, H₂ or H₁). **¹³C-NMR (151 MHz, CDCl₃)** δ 159.7 (C₉), 151.6 (C₅), 129.4 (C₇), 120.5 (C₆), 113.5 (C₁₀), 109.6 (C₈), 63.3 (C₁₂ or C₁₆), 63.2 (C₁₆ or C₁₂), 55.1 (C₁₁), 52.1 (C₁₃ or C₁₅), 51.8 (C₁₅ or C₁₃), 30.8 (C₃), 23.7 (C₁ or C₂), 23.4 (C₂ or C₁). **¹¹B-NMR (128 MHz, CDCl₃)** δ 13.1. **IR (ATR – neat)** $\tilde{\nu}$ (cm⁻¹) = 3280, 2985, 2945, 1601, 1579, 1485, 1320, 1262, 1152, 1051, 972, 923, 778, 751, 720, 704. **HRMS for [C₁₅H₂₄O₃N¹¹BNa]⁺** calculated 300.1741 found 300.1744. **M.p.** = 157–159°C.

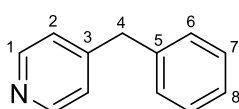
5.2.2 Synthetic procedures and characterisation for coupling products

5.2.2.1 Arylation of benzyl potassium trifluoroborates

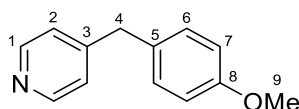


GP(II): A 5 mL microwave vial equipped with a magnetic stir bar was charged with the cyanoarene (0.15 mmol, 1.0 equiv.), the potassium benzyltrifluoroborate salt (0.18 mmol, 1.2 equiv.) and the photoredox catalyst $[\text{Ir}(\text{dF}(\text{CF}_3)\text{ppy})_2(\text{dtbbpy})]\text{PF}_6$ (**Ir-3**, 0.9 mg, 0.5 mol%). The vial was sealed and evacuated/backfilled with argon three times. Then 2.5 mL of degassed acetone was added through the septum to obtain a clear yellow transparent 0.06 M solution. The vial was then irradiated for the indicated time with Thorlab blue LEDs generating about 35°C temperature. The crude mixture was then concentrated *in vacuo* and the residue purified by flash column chromatography on silica gel ($\text{Et}_2\text{O}/\text{EtOAc}/\text{hexane}/\text{Et}_3\text{N}$, 1:1:2:0.04) to yield the pure product.

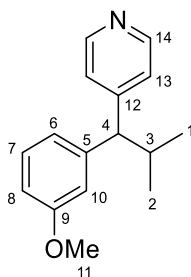
4-benzylpyridine (**161**)



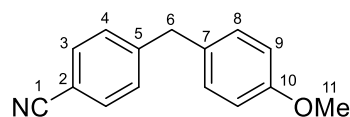
161 was obtained following **GP(II)** as a colourless oil (21 mg, 0.12 mmol) in 81% yield after 48 h of irradiation. $^1\text{H-NMR}$ (600 MHz, CDCl_3) δ 8.53 (br s, 2H, H_1), 7.33 (t, $J = 7.5$ Hz, 2H, H_7), 7.26 (t, $J = 7.4$ Hz, 1H, H_8), 7.18 (d, $J = 7.4$ Hz, 2H, H_6), 7.15 (d, $J = 4.4$ Hz, 2H, H_2), 3.99 (s, 2H, H_4). $^{13}\text{C-NMR}$ (151 MHz, CDCl_3) δ 150.6 (C_1), 149.3 (C_3), 138.7 (C_5), 129.0 (C_6), 128.8 (C_7), 126.7 (C_8), 124.4 (C_2), 41.3 (C_4). **HRMS** for $[\text{C}_{12}\text{H}_{12}\text{N}]^+$ calculated 170.0970 found 170.0977. R_f (1:1 EtOAc/hexane) = 0.12. Spectroscopic data were consistent with literature values.^[207]

4-(4-methoxybenzyl)pyridine (162)

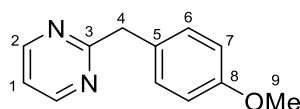
162 was obtained following **GP(II)** as a colourless oil (22 mg, 0.11 mmol) in 76% yield after 16 h of irradiation. **¹H-NMR (600 MHz, CDCl₃)** δ 8.49 (d, *J* = 5.8 Hz, 2H, H₁), 7.13 – 7.07 (m, 4H, H₂ and H₆), 6.86 (d, *J* = 8.7 Hz, 2H, H₇), 3.91 (2H, s, H₄), 3.80 (s, 3H, H₉). **¹³C-NMR (151 MHz, CDCl₃)** δ 158.4 (C₈), 150.6 (C₃), 149.7 (C₁), 130.9 (C₅), 130.0 (C₂), 124.1 (C₆), 114.1 (C₇), 55.3 (C₉), 40.3 (C₄). **HRMS for [C₁₃H₁₄NO]⁺** calculated 200.1075 found 200.1078. **R_f** (1:1 EtOAc/hexane) = 0.13. Spectroscopic data were consistent with literature values.^[271]

4-(1-(3-methoxyphenyl)-2-methylpropyl)pyridine (163)

163 was obtained following **GP(II)** as a yellowish solid (33 mg, 0.14 mmol) in 86% yield after 3 h of irradiation. Also obtained using **168** as starting material in 43% yield. **¹H-NMR (600 MHz, CDCl₃)** δ 8.47 (d, *J* = 5.1 Hz, 2H, H₁₄), 7.23 – 7.18 (m, 3H, H₁₃ and H₇), 6.86 (br d, *J* = 7.7 Hz, 1H, H₆), 6.82 – 6.80 (m, 1H, H₁₀), 6.73 (dd, *J* = 8.2, 2.5, 1H, H₈), 3.78 (s, 3H, H₁₁), 3.36 (d, *J* = 10.8 Hz, 1H, H₄), 2.47 (dsept, *J* = 10.8, 6.6 Hz, 1H, H₃), 0.90 (d, *J* = 6.5 Hz, 3H, H₁ or H₂), 0.87 (d, *J* = 6.5 Hz, 3H, H₁ or H₂). **¹³C-NMR (151 MHz, CDCl₃)** δ 159.7 (C₉), 153.6 (C₅), 149.8 (C₁₄), 144.6 (C₁₂), 129.6 (C₇), 123.4 (C₆), 120.4 (C₁₃), 114.4 (C₁₀), 111.2 (C₈), 60.2 (C₄), 55.1 (C₁₁), 31.4 (C₃), 21.6 (C₁ or C₂), 21.5 (C₁ or C₂). **IR (ATR – neat)** $\tilde{\nu}$ (cm⁻¹) = 2988, 2972, 2902, 1592, 1557, 1484, 1466, 1452, 1438, 1408, 1393, 1385, 1277, 1260, 1242, 1232, 1148, 1066, 1048, 889, 880, 833, 820, 780, 761, 737, 700. **HRMS for [C₁₆H₂₀NO]⁺** calculated 242.1545 found 242.1549. **R_f** (1:1 EtOAc/hexane) = 0.16. **M.p.** = 47–49°C.

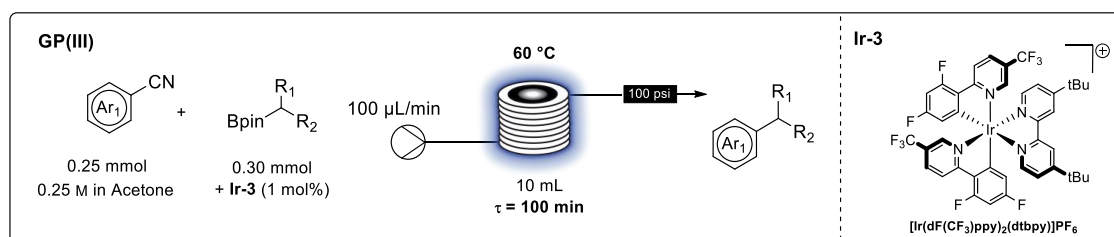
4-(4-methoxybenzyl)benzonitrile (173)

173 was obtained following **GP(II)** as a colourless oil (14 mg, 0.065 mmol) in 43% yield after 16 h of irradiation. **¹H-NMR (600 MHz, CDCl₃)** δ 7.57 (d, J = 8.2 Hz, 2H, H₃), 7.28 (d, J = 8.3 Hz, 2H, H₄), 7.08 (d, J = 8.5 Hz, 2H, H₈), 6.86 (d, J = 8.6 Hz, 2H, H₉), 3.98 (s, 2H, H₆), 3.80 (s, 3H, H₁₁). **¹³C-NMR (151 MHz, CDCl₃)** δ 158.4 (C₁₀), 147.2 (C₇), 132.3 (C₅), 131.4 (C₃), 129.9 (C₄), 129.5 (C₈), 119.0 (C₁), 114.2 (C₉), 109.9 (C₂), 55.3 (C₄), 41.1 (C₆). **HRMS for [C₁₅H₁₄NO]⁺** calculated 224.1075 found 224.1072. **R_f** (1:1 EtOAc/hexane) = 0.51. Spectroscopic data were consistent with literature values.^[271]

2-(4-methoxybenzyl)pyrimidine (171)

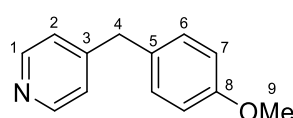
171 was obtained following **GP(II)** as a colourless oil (8.5 mg, 0.042 mmol) in 28% yield after 72 h of irradiation. **¹H-NMR (600 MHz, CDCl₃)** δ 8.68 (d, J = 4.9 Hz, 2H, H₂), 7.29 (d, J = 8.6 Hz, 2H, H₆), 7.12 (t, J = 4.9 Hz, 1H, H₁), 6.86 (d, J = 8.7 Hz, 2H, H₇), 4.24 (s, 2H, H₄), 3.78 (s, 3H, H₉). **¹³C-NMR (151 MHz, CDCl₃)** δ 170.4 (C₃), 158.3 (C₈), 157.3 (C₂), 130.3 (C₅), 130.1 (C₆), 118.6 (C₁), 114.0 (C₇), 55.2 (C₉), 45.2 (C₄). **IR (ATR – neat)** $\tilde{\nu}$ (cm⁻¹) = 2988, 2972, 2902, 1611, 1571, 1561, 1511, 1415, 1394, 1382, 1301, 1248, 1178, 1076, 1066, 1056, 892, 879, 809. **HRMS for [C₁₂H₁₃N₂O]⁺** calculated 201.1028 found 201.1028. **R_f** (1:1 EtOAc/hexane) = 0.09.

5.2.2.2 Arylation of boronic esters with cyanoarenes in flow

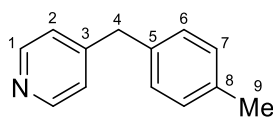


GP(III): A 5 mL conical shape microwave vial was charged with the cyanoarene (0.25 mmol, 1.0 equiv.), the benzyl pinacol boronic ester (0.30 mmol, 1.2 equiv), and the photoredox catalyst $[\text{Ir}(\text{dF}(\text{CF}_3)\text{ppy})_2(\text{dtbbpy})]\text{PF}_6$ (**Ir-3**, 3.0 mg, 1.0 mol%). Then 1.0 mL of acetone was added to obtain a clear yellow transparent 0.25 M solution after sonication for 1 min. The clear yellow solution was then pumped at 100 $\mu\text{L}/\text{min}$ through a Vapourtec UV-150 photochemical reactor (10 mL reactor coil, FEP tubing, $\tau = 100$ min) held at 60°C. Once the reaction mixture has fully be taken up by the pump, the input was swapped to acetone solvent to push the rest of the reaction mixture through the reactor. When the reaction plug was exiting the output stream (yellow to orange colour), the totality of the plug was collected in a vial wrapped in aluminium foil and concentrated *in vacuo*. The residue was then purified by Bioatage flash column chromatography on KP-NH modified silica gel cartridge (0% to 20% EtOAc in hexane gradient) to yield the pure product.

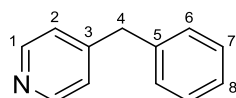
4-(4-methoxybenzyl)pyridine (**162**)



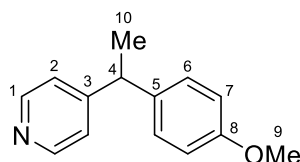
162 was obtained following **GP(III)** as a pale yellow oil (40 mg, 0.20 mmol) in 81% yield. $^1\text{H-NMR}$ (600 MHz, CDCl_3) δ 8.49 (d, $J = 5.8$ Hz, 2H, H_1), 7.13 – 7.07 (m, 4H, H_2 and H_6), 6.86 (d, $J = 8.7$ Hz, 2H, H_7), 3.91 (2H, s, H_4), 3.80 (s, 3H, H_9). $^{13}\text{C-NMR}$ (151 MHz, CDCl_3) δ 158.4 (C_8), 150.6 (C_3), 149.7 (C_1), 130.9 (C_5), 130.0 (C_2), 124.1 (C_6), 114.1 (C_7), 55.3 (C_9), 40.3 (C_4). **HRMS** for $[\text{C}_{13}\text{H}_{14}\text{NO}]^+$ calculated 200.1075 found 200.1078. R_f (1:1 EtOAc/hexane) = 0.13. Spectroscopic data were consistent with literature values.^[271]

4-(4-methylbenzyl)pyridine (191)

191 was obtained following **GP(III)** as a colourless oil (32 mg, 0.17 mmol) in 70% yield. **¹H-NMR (600 MHz, CDCl₃)** δ 8.49 (d, J = 5.3 Hz, 2H, H₁), 7.13 (d, J = 7.8 Hz, 2H, H₇), 7.10 (d, J = 5.5 Hz, 2H, H₂), 7.07 (d, J = 7.8 Hz, 2H, H₆), 3.93 (s, 2H, H₄), 2.34 (s, 3H, H₉). **¹³C-NMR (151 MHz, CDCl₃)** δ 150.3 (C₃), 149.8 (C₁), 136.3 (C₅), 135.8 (C₈), 129.4 (C₇), 128.9 (C₆), 124.1 (C₂), 40.8 (C₄), 21.0 (C₉). **HRMS for [C₁₃H₁₄N]⁺** calculated 184.1121 found 184.117. **R_f** (1:1 EtOAc/hexane) = 0.13. Spectroscopic data were consistent with literature values.^[272]

4-(benzyl)pyridine (161)

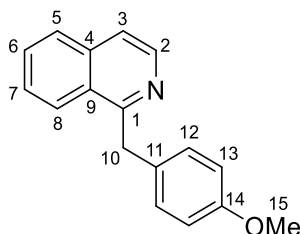
161 was obtained following **GP(III)** as a colourless oil (28 mg, 0.16 mmol) in 66% yield. **¹H-NMR (600 MHz, CDCl₃)** δ 8.53 (br s, 2H, H₁), 7.33 (t, J = 7.5 Hz, 2H, H₇), 7.26 (t, J = 7.4 Hz, 1H, H₈), 7.18 (d, J = 7.4 Hz, 2H, H₆), 7.15 (d, J = 4.4 Hz, 2H, H₂), 3.99 (s, 2H, H₄). **¹³C-NMR (151 MHz, CDCl₃)** δ 150.6 (C₁), 149.3 (C₃), 138.7 (C₅), 129.0 (C₆), 128.8 (C₇), 126.7 (C₈), 124.4 (C₂), 41.3 (C₄). **HRMS for [C₁₂H₁₂N]⁺** calculated 170.0970 found 170.0977. **R_f** (1:1 EtOAc/hexane) = 0.13. Spectroscopic data were consistent with literature values.^[207]

4-(1-(4-methoxyphenyl)ethyl)pyridine (192)

192 was obtained following **GP(III)** as a colourless oil (44 mg, 0.21 mmol) in 83% yield. **¹H-NMR (600 MHz, CDCl₃)** δ 8.49 (d, J = 5.9 Hz, 2H), 7.16 – 7.05 (m, 4H, H₆ and H₂), 6.85 (d, J = 8.6 Hz, 2H, H₇), 4.07 (q, J = 7.2 Hz, 1H, H₄), 3.79 (s, 3H, H₉), 1.61 (d, J = 7.2 Hz, 3H, H₁₀). **¹³C-NMR (151 MHz, CDCl₃)** δ 158.3 (C₈), 155.5 (C₃), 149.8 (C₂), 136.5 (C₅), 128.5 (C₆), 122.9 (C₂), 114.0 (C₇), 55.2 (C₉), 43.4 (C₄), 21.2 (C₁₀). **HRMS for**

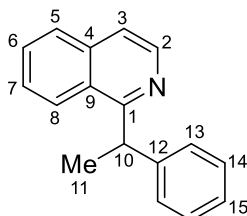
$[\text{C}_{12}\text{H}_{12}\text{N}]^+$ calculated 214.1226 found 214.1220. R_f (1:1 EtOAc/hexane) = 0.12. Spectroscopic data were consistent with literature values.^[273]

1-(4-methoxybenzyl)isoquinoline (184)

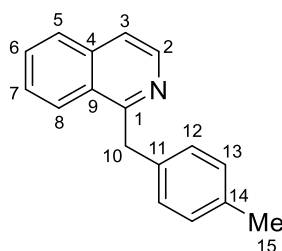


184 was obtained following **GP(III)** as a pale green oil (47 mg, 0.19 mmol) in 75% yield. $^1\text{H-NMR}$ (600 MHz, CDCl_3) δ 8.50 (d, $J = 5.7$ Hz, 1H, H_2), 8.17 (d, $J = 8.5$ Hz, 1H, H_8), 7.81 (d, $J = 8.2$ Hz, 1H, H_5), 7.64 (ddd, $J = 8.1, 7.0, 1.0$ Hz, 1H, H_6), 7.56 (d, $J = 5.7$ Hz, 1H, H_3), 7.53 (ddd, $J = 8.5, 6.9, 1.1$ Hz, 1H, H_7), 7.21 (d, $J = 8.7$ Hz, 2H, H_{12}), 6.80 (d, $J = 8.7$ Hz, 2H, H_{13}), 4.62 (s, 2H, H_{10}), 3.75 (s, 3H, H_{15}). $^{13}\text{C-NMR}$ (151 MHz, CDCl_3) δ 160.5 (C_1), 158.0 (C_{14}), 142.0 (C_2), 136.6 (C_4), 131.6 (C_{11}), 129.8 (C_7), 129.5 (C_{12}), 127.3 (C_6), 127.1 (C_5), 127.0 (C_9), 125.8 (C_8), 119.7 (C_3), 113.9 (C_{13}), 55.2 (C_{15}), 41.2 (C_{10}). **HRMS** for $[\text{C}_{17}\text{H}_{16}\text{ON}]^+$ calculated 250.1226 found 250.1216. R_f (1:1 EtOAc/hexane) = 0.48. Spectroscopic data were consistent with literature values.^[274]

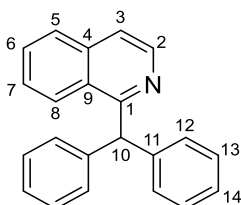
1-(1-phenylethyl)isoquinoline (194)



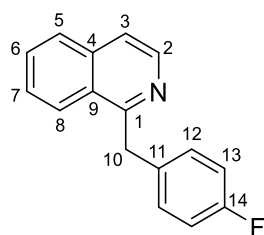
194 was obtained following **GP(III)** as a white solid (44 mg, 0.19 mmol) in 75% yield. $^1\text{H-NMR}$ (600 MHz, CDCl_3) δ 8.59 (d, $J = 5.7$ Hz, 1H, H_2), 8.19 (d, $J = 8.6$ Hz, 1H, H_8), 7.79 (d, $J = 8.2$ Hz, 1H, H_5), 7.60 (t, $J = 7.5$ Hz, 1H, H_6), 7.55 (d, $J = 5.7$ Hz, 1H, H_7), 7.49 (t, $J = 7.8$ Hz, 1H, H_3), 7.33 (d, $J = 7.5$ Hz, 2H, H_{13}), 7.26 (t, $J = 7.6$ Hz, 2H, H_{14}), 7.16 (t, $J = 7.3$ Hz, 1H, H_{15}), 5.10 (q, $J = 7.0$ Hz, 1H, H_{10}), 1.87 (d, $J = 7.0$ Hz, 3H, H_{11}). $^{13}\text{C-NMR}$ (151 MHz, CDCl_3) δ 162.9 (C_1), 145.9 (C_2), 141.7 (C_{12}), 136.5 (C_4), 129.5 (C_6), 128.5 (C_{14}), 127.6 (C_{13}), 127.4 (C_8), 127.0 (C_7), 126.2 (C_{15}), 125.3 (C_5), 120.0 (C_3), 43.2 (C_{10}), 21.9 (C_{11}). **IR** (ATR – neat) $\tilde{\nu}$ (cm^{-1}) = 3060, 3020, 2968, 2925, 1619, 1584, 1560, 1491, 1354, 1140, 876. **HRMS** for $[\text{C}_{17}\text{H}_{16}\text{N}]^+$ calculated 234.1277 found 234.1266. R_f (1:1 EtOAc/hexane) = 0.32. **M.p.** 59–62°C.

1-(4-methylbenzyl)isoquinoline (193)

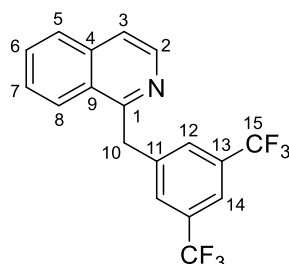
193 was obtained following **GP(III)** as a colourless oil (43 mg, 0.18 mmol) in 74% yield. **¹H-NMR (600 MHz, CDCl₃)** δ 8.51 (d, $J = 5.7$ Hz, 1H, H₂), 8.17 (d, $J = 8.5$ Hz, 1H, H₈), 7.81 (d, $J = 8.2$ Hz, 1H, H₅), 7.63 (t, $J = 7.5$ Hz, 1H, H₆), 7.56 (d, $J = 5.7$ Hz, 1H, H₃), 7.53 (t, $J = 7.6$ Hz, 1H, H₇), 7.19 (d, $J = 7.9$ Hz, 2H, H₁₂), 7.07 (d, $J = 7.9$ Hz, 2H, H₁₃), 4.65 (s, 2H, H₁₀), 2.29 (s, 3H, H₁₅). **¹³C-NMR (151 MHz, CDCl₃)** δ 160.4 (C₁), 142.0 (C₂), 136.6 (C₁₄), 136.4 (C₄), 135.7 (C₁₁), 129.8 (C₇), 129.2 (C₁₃), 128.5 (C₁₂), 127.3 (C₉), 127.2 (C₅), 125.9 (C₈), 119.7 (C₃), 41.7 (C₁₀), 21.0 (C₁₅). **HRMS for [C₁₇H₁₆N]⁺** calculated 234.1277 found 234.1265. **R_f** (1:1 EtOAc/hexane) = 0.34. Spectroscopic data were consistent with literature values.^[275]

1-benzhydrylisoquinoline (195)

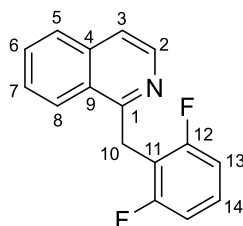
195 was obtained following **GP(III)** as a white solid (62 mg, 0.21 mmol) in 84% yield. **¹H-NMR (600 MHz, CDCl₃)** δ 8.56 (d, $J = 5.7$ Hz, 1H, H₂), 8.27 (d, $J = 8.6$ Hz, 1H, H₈), 7.85 (d, $J = 8.2$ Hz, 1H, H₅), 7.66 (t, $J = 7.5$ Hz, 1H, H₆), 7.57 – 7.54 (m, 2H, H₇ and H₃), 7.34 – 7.31 (m, 4H, H₁₃), 7.29 – 7.23 (m, 6H, H₁₂ and H₁₄), 6.52 (s, 1H, H₁₀). **¹³C-NMR (151 MHz, CDCl₃)** δ 161.9 (C₁), 142.8 (C₁₁), 142.0 (C₂), 136.6 (C₄), 129.6 (C₆), 128.3 (C₁₃), 127.5 (C₁₂), 127.3 (C₈ and C₉), 126.5 (C₇), 125.2 (C₁₄), 119.6 (C₅), 54.8 (C₁₀). **IR (ATR – neat)** $\tilde{\nu}$ (cm⁻¹) = 3056, 3020, 1621, 1586, 1560, 1495, 1447, 1380, 1344, 1156, 1029, 826. **HRMS for [C₂₂H₁₈N]⁺** calculated 296.1434 found 296.1421. **R_f** (1:9 EtOAc/hexane) = 0.16. **M.p.** 89–92°C.

1-(4-fluorobenzyl)isoquinoline (196)

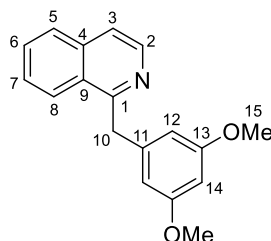
196 was obtained following **GP(III)** as an amorphous white solid (39 mg, 0.16 mmol) in 65% yield. **¹H-NMR (600 MHz, CDCl₃)** δ 8.50 (d, *J* = 5.6 Hz, 1H, H₂), 8.13 (d, *J* = 8.4 Hz, 1H, H₈), 7.83 (d, *J* = 8.1 Hz, 1H, H₅), 7.65 (t, *J* = 7.5 Hz, 1H, H₆), 7.58 (d, *J* = 5.7 Hz, 1H, H₃), 7.55 (t, *J* = 7.6 Hz, 1H, H₇), 7.26 – 7.22 (m, 2H, H₁₂), 6.95 (t, *J* = 8.5 Hz, 2H, H₁₃), 4.65 (s, 2H, H₁₀). **¹³C-NMR (151 MHz, CDCl₃)** δ 161.4. (d, *J* = 244 Hz, C₁₄), 159.9 (C₁), 142.0 (C₂), 136.6 (C₄), 135.0 (d, *J* = 3.2 Hz, (C₁₁), 129.9 (d, *J* = 4.6 Hz, C₁₂), 127.4 (C₅), 127.3 (C₆), 127.1 (C₉), 125.6 (C₈), 119.9 (C₃), 115.3 (d, *J* = 21 Hz, C₁₃), 41.1 (C₁₀). **HRMS for [C₁₆H₁₃NF]⁺** calculated 238.1027 found 238.1025. **R_f**(1:1 EtOAc/hexane) = 0.48. Spectroscopic data were consistent with literature values.^[276]

1-(3,5-bis(trifluoromethyl)benzyl)isoquinoline (197)

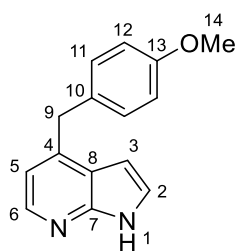
197 was obtained following **GP(III)** as a white solid (48 mg, 0.13 mmol) in 55% yield. **¹H-NMR (600 MHz, CDCl₃)** δ 8.52 (d, *J* = 5.7 Hz, 1H, H₂), 8.10 (d, *J* = 8.5 Hz, 1H, H₈), 7.87 (d, *J* = 8.2 Hz, 1H, H₅), 7.78 (s, 2H, H₁₂), 7.73 (s, 1H, H₁₄), 7.70 (t, *J* = 7.5 Hz, 1H, H₆), 7.63-7.60 (m, 2H, H₇ and H₃), 4.78 (s, 2H, H₁₀). **¹³C-NMR (151 MHz, CDCl₃)** δ 157.9 (C₁), 142.2 (C₂), 141.6 (C₁₁), 136.6 (C₄), 131.6 (q, *J* = 33.2 Hz, C₁₃), 130.2 (C₆), 129.0 (q, *J* = 3.6 Hz, C₁₂), 127.7 (C₅ and C₇), 126.9 (C₉), 124.8 (C₈), 123.3 (q, *J* = 273 Hz, C₁₅) 120.5 (sept, *J* = , 3.8 Hz, C₁₄), 120.4 (C₃), 41.0 (C₁₀). **IR (ATR – neat)** $\tilde{\nu}$ (cm⁻¹) = 3051, 2929, 1621, 1586, 1558, 1506, 1463, 1372, 1280, 1165, 1116, 880, 828. **HRMS for [C₁₈H₁₂NF₆]⁺** calculated 356.0868 found 356.0858. **R_f**(1:1 EtOAc/hexane) = 0.67. **M.p.** 82–84°C.

1-(2,6-difluorobenzyl)isoquinoline (198)

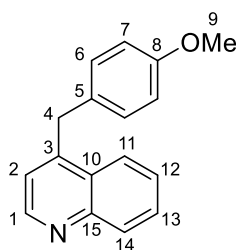
198 was obtained following **GP(III)** as a white solid (40 mg, 0.16 mmol) in 63% yield. **¹H-NMR (600 MHz, CDCl₃)** δ 8.42 (d, *J* = 5.7 Hz, 1H, H₂), 8.30 (d, *J* = 8.4 Hz, 1H, H₈), 7.85 (d, *J* = 8.1 Hz, 1H, H₅), 7.73 – 7.68 (m, 1H, H₆), 7.64 (t, *J* = 7.6 Hz, 1H, H₇), 7.54 (d, *J* = 5.7 Hz, 1H, H₃), 7.27 – 7.20 (m, 1H, H₁₄), 6.94 (t, *J* = 7.8 Hz, 2H, H₁₃), 4.73 (s, 2H, H₁₀). **¹³C-NMR (151 MHz, CDCl₃)** δ 161.7 (dd, *J* = 248 Hz, *J* = 8.7 Hz, C₁₂), 157.6 (C₁), 142.0 (C₂), 136.2 (C₄), 129.8 (C₆), 128.2 (t, *J* = 10.3 Hz, C₁₄), 127.4 (C₈), 127.2 (C₉), 126.9 (C₇), 124.8 (C₅), 119.6 (C₃), 114.8 (t, *J* = 19.9 Hz, C₁₁), 111.1 (dd, *J* = 20.9, 5.1 Hz, C₁₃), 28.4 (C₁₀). **¹⁹F-NMR (376 MHz, CDCl₃)** δ -113.81. **IR (ATR – neat)** $\tilde{\nu}$ (cm⁻¹) = 2924, 2853, 1623, 1590, 1566, 1465, 1380, 1205, 1019, 1003, 860, 743. **HRMS for [C₁₆H₁₂NF₂]⁺** calculated 256.0932 found 256.0927. **R_f** (1:1 EtOAc/hexane) = 0.67. **M.p.** 83–85°C.

1-(3,5-dimethoxybenzyl)isoquinoline (199)

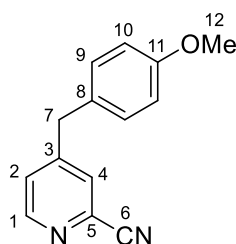
199 was obtained following **GP(III)** as a pale green oil (46 mg, 0.16 mmol) in 66% yield. **¹H-NMR (600 MHz, CDCl₃)** δ 8.51 (d, *J* = 5.7 Hz, 1H, H₂), 8.17 (d, *J* = 8.5 Hz, 1H, H₈), 7.82 (d, *J* = 8.2 Hz, 1H, H₅), 7.65 (t, *J* = 7.5 Hz, 1H, H₆), 7.58 (d, *J* = 5.7 Hz, 1H, H₃), 7.54 (t, *J* = 7.6 Hz, 1H, H₇), 6.46 (s, 2H, H₁₂), 6.30 (s, 1H, H₁₄), 4.62 (s, 2H, H₁₀), 3.73 (s, 6H, H₁₅). **¹³C-NMR (151 MHz, CDCl₃)** δ 160.8 (C₁₃), 159.8 (C₁), 141.9 (C₂), 141.8 (C₁₁), 136.6 (C₄), 129.9 (C₆), 127.3 (C₉ and C₈), 127.2 (C₇), 125.8 (C₅), 119.9 (C₃), 106.9 (C₁₂), 98.1 (C₁₄), 55.2 (C₁₅), 42.3 (C₁₀). **IR (ATR – neat)** $\tilde{\nu}$ (cm⁻¹) = 3056, 3000, 2937, 2837, 1596, 1560, 1500, 1461, 1427, 1383, 1342, 1322, 1288, 1205, 1154, 1058, 822, 789, 747, 730, 684. **HRMS for [C₁₈H₁₈NO₂]⁺** calculated 280.1332 found 280.1328. **R_f** (1:1 EtOAc/hexane) = 0.39.

4-(4-methoxybenzyl)-1H-pyrrolo[2,3-b]pyridine (183)

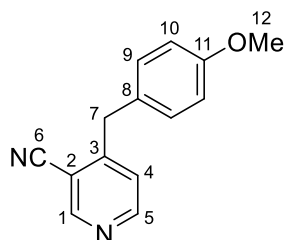
183 was obtained following **GP(III)** (using 3.5 mL of acetone instead of 1.0 mL because of the low starting material solubility) as a brownish solid (36 mg, 0.15 mmol) in 60% yield. $^1\text{H-NMR}$ (600 MHz, CDCl_3) δ 11.12 (s, 1H, H_1), 8.25 (d, $J = 4.8$ Hz, 1H, H_6), 7.32 (d, $J = 3.0$ Hz, 1H, H_2), 7.18 (d, $J = 8.4$ Hz, 2H, H_{11}), 6.87 – 6.84 (m, 3H, H_{12} and H_5), 6.51 (d, $J = 3.3$ Hz, 1H, H_3), 4.23 (s, 2H, H_9), 3.79 (s, 3H, H_{14}). $^{13}\text{C-NMR}$ (151 MHz, CDCl_3) δ 158.2 (C_{13}), 148.7 (C_7), 143.4 (C_6), 142.6 (C_4), 131.4 (C_{10}), 130.0 (C_{11}), 124.6 (C_2), 120.2 (C_8), 116.0 (C_5), 114.0 (C_{12}), 99.3 (C_3), 55.2 (C_{14}), 38.2 (C_9). **IR** (ATR – neat) $\tilde{\nu}$ (cm^{-1}) = 3127, 3000, 2929, 2837, 2762, 1592, 1508, 1439, 1348, 1243, 1181, 1031, 823. **HRMS** for $[\text{C}_{15}\text{H}_{15}\text{ON}_2]^+$ calculated 239.1179 found 239.1179. R_f (1:1 EtOAc/hexane) = 0.19. **M.p.** 116–118°C.

4-(4-methoxybenzyl)quinoline (184)

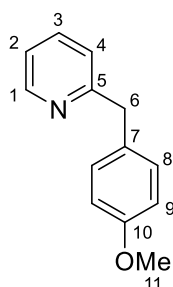
184 was obtained following **GP(III)** as a white solid (41 mg, 0.16 mmol) in 66% yield. $^1\text{H-NMR}$ (600 MHz, CDCl_3) δ 8.84 (d, $J = 4.5$ Hz, 1H, H_1), 8.12 (d, $J = 7.6$ Hz, 1H, H_{11}), 8.07 (d, $J = 7.6$ Hz, 1H, H_{14}), 7.73 (t, $J = 7.6$, 1H, H_{13}), 7.56 (t, $J = 7.6$, 1H, H_{12}), 7.17–7.10 (m, 3H, H_6 and H_2), 6.87 (d, $J = 8.65$ Hz, 2H, H_7), 4.41 (s, 2H, H_4), 3.81 (s, 3H, H_9). $^{13}\text{C-NMR}$ (151 MHz, CDCl_3) δ 158.7 (C_8), 150.1 (C_{15}), 148.1 (C_1), 147.3 (C_3), 130.5 (C_5), 130.0 (C_{13}), 129.9 (C_{14}), 129.2 (C_6), 127.6 (C_{10}), 126.6 (C_{12}), 123.9 (C_{11}), 121.7 (C_2), 114.2 (C_7), 55.3 (C_9), 44.3 (C_4). **HRMS** for $[\text{C}_{17}\text{H}_{16}\text{NO}]^+$ calculated 250.1226 found 250.1227. R_f (1:1 EtOAc/hexane) = 0.75. **M.p.** 79–81°C. Spectroscopic data were consistent with literature values.^[271]

4-(4-methoxybenzyl)picolinonitrile (181)

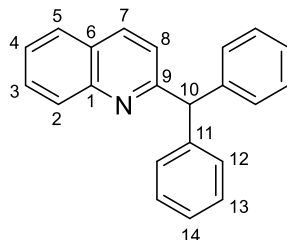
181 was obtained following **GP(III)** as a pale yellow oil (25 mg, 0.11 mmol) in 44% yield. $^1\text{H-NMR}$ (600 MHz, CDCl_3) δ 8.72 (d, $J = 5.0$ Hz, 1H, H_1), 7.34 (d, $J = 5.0$ Hz, 1H, H_2), 7.30 (s, 1H, H_4), 7.17 (d, $J = 8.5$ Hz, 2H, H_9), 6.88 (d, $J = 8.6$ Hz, 2H, H_{10}), 4.16 (s, 2H, H_7), 3.81 (s, 3H, H_{12}). $^{13}\text{C-NMR}$ (151 MHz, CDCl_3) δ 163.3 (C_{11}), 158.6 (C_3), 150.2 (C_1), 130.2 (C_9), 129.9 (C_5), 124.5 (C_2), 122.6 (C_8), 120.8 (C_4), 116.6 (C_6), 114.3 (C_{10}), 55.3 (C_{12}), 43.6 (C_7). **IR** (ATR – neat) $\tilde{\nu}$ (cm^{-1}) = 2956, 2933, 2238, 1609, 1594, 1508, 1461, 1395, 1302, 1243, 1177, 1033, 830, 817, 775. **HRMS** for $[\text{C}_{14}\text{H}_{13}\text{N}_2\text{O}]^+$ calculated 225.1022 found 225.1023. R_f (1:1 EtOAc/hexane) = 0.54.

4-(4-methoxybenzyl)nicotinonitrile (182)

182 was obtained following **GP(III)** as a colourless oil (36 mg, 0.16 mmol) in 65% yield. $^1\text{H-NMR}$ (600 MHz, CDCl_3) δ 8.82 (s, 1H, H_1), 8.65 (d, $J = 5.2$ Hz, 1H, H_5), 7.17 (d, $J = 5.2$ Hz, 1H, H_4), 7.15 (d, $J = 8.7$ Hz, 2H, H_9), 6.88 (d, $J = 8.7$ Hz, 2H, H_{10}), 4.14 (s, 2H, H_7), 3.81 (s, 3H, H_{12}). $^{13}\text{C-NMR}$ (151 MHz, CDCl_3) δ 158.8 (C_{11}), 154.1 (C_3), 153.0 (C_5), 152.8 (C_1), 130.2 (C_9), 128.6 (C_8), 124.1 (C_4), 116.0 (C_6), 114.4 (C_2), 110.3 (C_{10}), 55.3 (C_{12}), 38.9 (C_7). **HRMS** for $[\text{C}_{14}\text{H}_{13}\text{ON}_2]^+$ calculated 225.1022 found 225.1019. R_f (1:1 EtOAc/hexane) = 0.23.

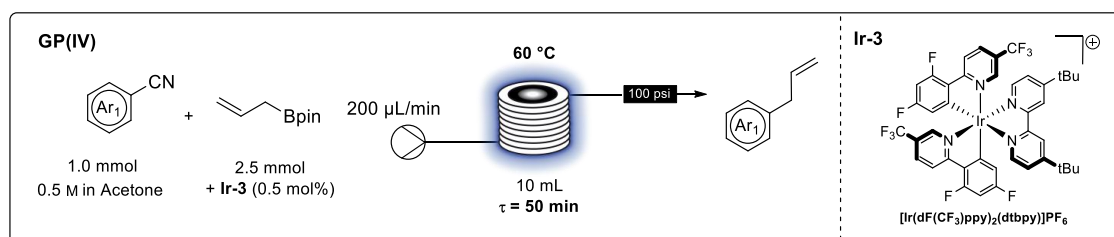
2-(4-methoxybenzyl)pyridine (170)

170 was obtained following **GP(III)** as a pale yellow oil (20 mg, 0.10 mmol) in 40% yield. $^1\text{H-NMR}$ (600 MHz, CDCl_3) δ 8.55 (d, $J = 4.5$ Hz, 1H, H_1), 7.58 (td, $J = 7.7$, 1.2 Hz, 1H, H_3), 7.19 (d, $J = 8.5$ Hz, 2H, H_8), 7.11 (t, $J = 8.2$ Hz, 2H, H_2 and H_4), 6.85 (d, $J = 8.5$ Hz, 2H, H_9), 4.11 (s, 2H, H_6), 3.79 (s, 3H, H_{11}). $^{13}\text{C-NMR}$ (151 MHz, CDCl_3) δ 161.3 (C_{10}), 158.2 (C_5), 149.2 (C_2), 136.6 (C_3), 131.5 (C_7), 130.1 (C_8), 123.0 (C_4), 121.2 (C_2), 114.0 (C_9), 55.2 (C_{11}), 43.7 (C_6). **HRMS** for $[\text{C}_{13}\text{H}_{14}\text{ON}]^+$ 200.1070 found 200.1071. R_f (1:1 EtOAc/hexane) = 0.36. Spectroscopic data were consistent with literature values.^[277]

2-benzhydrylquinoline (185)

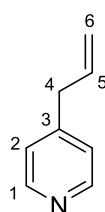
185 was obtained following **GP(III)** as a colourless oil (41 mg, 0.14 mmol) in 55% yield. $^1\text{H-NMR}$ (400 MHz, CDCl_3) δ 8.08 (t, $J = 7.8$ Hz, 2H, H_7 and H_2), 7.79 (dd, $J = 8.1$, 1.1 Hz, 1H, H_5), 7.70 (ddd, $J = 8.5$, 6.9, 1.4 Hz, 1H, H_3), 7.51 (ddd, $J = 8.1$, 7.0, 1.1 Hz, 1H, H_4), 7.33 – 7.27 (m, 5H, H_8 and H_{12}), 7.26 – 7.21 (m, 6H, H_{13} and H_{14}), 5.94 (s, 1H, H_{10}). $^{13}\text{C-NMR}$ (151 MHz, CDCl_3) δ 163.1 (C_9), 147.9 (C_1), 142.6 (C_{11}), 136.4 (C_7), 129.5 (C_3), 129.5 (C_{13}), 129.4 (C_2), 128.4 (C_{12}), 127.5 (C_5), 126.8 (C_6), 126.6 (C_{14}), 126.3 (C_4), 122.0 (C_8), 60.1 (C_{10}). **HRMS** for $[\text{C}_{22}\text{H}_{18}\text{N}]^+$ calculated 296.1434 found 296.1421. R_f (1:1 EtOAc/hexane) = 0.72. Spectroscopic data were consistent with literature values.^[278]

5.2.2.3 Allylation of heterocycles in flow

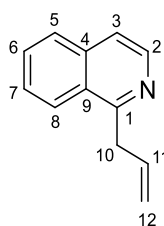


GP(IV): A 5 mL conical shape microwave vial was charged with the cyanoarene (1.0 mmol, 1.0 equiv.), the allyl boronic pinacol ester (2.5 mmol, 2.5 equiv), and the photoredox catalyst $[\text{Ir}(\text{dF}(\text{CF}_3)\text{ppy})_2(\text{dtbbpy})]\text{PF}_6$ (**Ir-3**, 6.0 mg, 0.5 mol%). Then 1.5 mL of acetone was added to obtain a clear yellow transparent 0.5 M solution (2.0 mL overall volume) after sonication for 1 min. The clear yellow solution was then pumped at 200 $\mu\text{L}/\text{min}$ through a Vapourtec UV-150 photochemical reactor (10 mL reactor coil, FEP tubing, $\tau = 50$ min) held at 60°C. Once the reaction mixture has fully be taken up by the pump, the input was swapped to acetone solvent to push the rest of the reaction mixture through the reactor. When the reaction plug was exiting the output stream (yellow to orange colour), the totality of the plug was collected in a vial wrapped in aluminium foil and concentrated *in vacuo*. The residue was then purified by Bioatage flash column chromatography on KP-NH modified silica gel cartridge (0% to 20% EtOAc in hexane gradient) to yield the pure product.

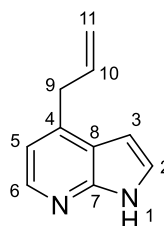
4-allylpyridine (**165**)



165 was obtained following **GP(IV)** as a colourless oil (83 mg, 0.70 mmol) in 70% yield. $^1\text{H-NMR}$ (600 MHz, CDCl_3) δ 8.50 (d, $J = 6.0$ Hz, 2H, H_1), 7.11 (d, $J = 5.8$ Hz, 2H, H_2), 5.92 (ddt, $J = 16.9, 10.1, 6.7$ Hz, 1H, H_5), 5.18 – 5.08 (m, 2H, H_6), 3.37 (d, $J = 6.7$ Hz, 2H, H_4). $^{13}\text{C-NMR}$ (151 MHz, CDCl_3) δ 149.8 (C_1), 148.9 (C_3), 135.1 (C_5), 123.9 (C_2), 117.4 (C_6), 39.3 (C_4). **HRMS** for $[\text{C}_8\text{H}_{10}\text{N}]^+$ calculated 120.0808 found 120.0807. R_f (2:1 EtOAc/hexane) = 0.30. Spectroscopic data were consistent with literature values.^[279]

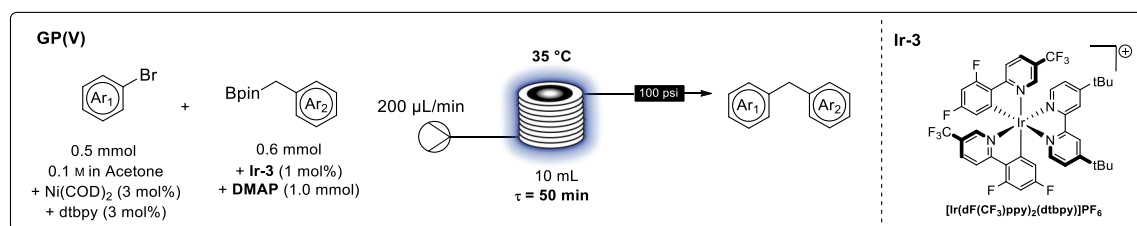
1-allylisoquinoline (201)

201 was obtained following **GP(IV)** as a colourless oil (119 mg, 0.70 mmol) in 70% yield. **¹H-NMR (600 MHz, CDCl₃)** δ 8.46 (d, $J = 5.7$ Hz, 1H, H₂), 8.16 (d, $J = 8.5$ Hz, 1H, H₈), 7.81 (d, $J = 8.2$ Hz, 1H, H₅), 7.67 (t, $J = 7.5$ Hz, 1H, H₆), 7.59 (t, $J = 7.7$ Hz, 1H, H₇), 7.53 (d, $J = 5.7$ Hz, 1H, H₃), 6.22 (ddt, $J = 16.8, 10.1, 6.5$ Hz, 1H, H₁₁), 5.23 – 5.12 (m, 2H, H₁₂), 4.10 (d, $J = 6.5$ Hz, 2H, H₁₀). **¹³C-NMR (151 MHz, CDCl₃)** δ 159.7 (C₁), 142.1 (C₂), 136.3 (C₄), 135.4 (C₁₁), 129.9 (C₆), 127.3 (C₈), 127.1 (C₉), 127.0 (C₇), 125.4 (C₅), 119.6 (C₃), 116.8 (C₁₂), 40.2 (C₁₀). **IR (ATR – neat)** $\tilde{\nu}$ (cm^{-1}) = 3055, 1639, 1623, 1588, 1562, 1500, 1385, 1352, 1340, 1144, 991, 906, 820, 745. **HRMS for [C₁₂H₁₂N]⁺** calculated 170.0964 found 170.0959. **R_f** (EtOAc/hexane, 2:1) = 0.49.

4-allyl-1H-pyrrolo[2,3-b]pyridine (202)

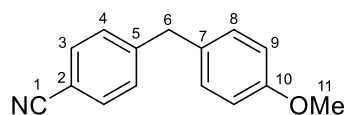
202 was obtained following **GP(IV)** (using 5 mL of acetone instead of 1.5 mL because of the low starting material solubility) as a white solid (113 mg, 0.71 mmol) in 71% yield. **¹H-NMR (600 MHz, CDCl₃)** δ 11.88 (s, 1H, H₁), 8.30 (d, $J = 4.9$ Hz, 1H, H₆), 7.40 (d, $J = 3.2$ Hz, 1H, H₂), 6.96 (d, $J = 4.9$ Hz, 1H, H₅), 6.57 (d, $J = 3.3$ Hz, 1H, H₃), 6.09 (ddt, $J = 16.8, 10.0, 6.7$ Hz, 1H, H₁₀), 5.19 (dd, $J = 25.9, 13.5$ Hz, 2H, H₁₁), 3.71 (d, $J = 6.7$ Hz, 2H, H₉). **¹³C-NMR (151 MHz, CDCl₃)** δ 148.8 (C₇), 142.5 (C₆), 141.9 (C₄), 135.5 (C₁₀), 124.7 (C₂), 120.2 (C₈), 116.8 (C₅), 115.5 (C₁₁), 98.9 (C₃), 37.4 (C₉). **IR (ATR – neat)** $\tilde{\nu}$ (cm^{-1}) = 3079, 2917, 2829, 1637, 1588, 1493, 1433, 1403, 1340, 1302, 1276, 989, 902, 809, 719. **HRMS for [C₁₀H₁₁N₂]⁺** calculated 159.0917 found 159.0915. **R_f** (1:1 EtOAc/hexane) = 0.19. **M.p.** 79–81°C.

5.2.2.4 Arylation of boronic esters with aryl bromides in flow

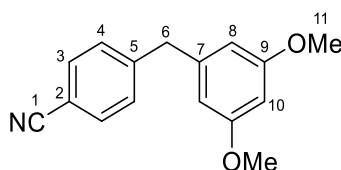


GP(V): A 10 mL microwave vial was charged with the aryl bromide (0.50 mmol, 1.0 equiv.), the photoredox catalyst Ir(dF(CF₃)ppy)₂(dtbpy)]PF₆ (**Ir-3**, 6.0 mg, 1.0 mol%), 4,4'-di-*tert*-butyl-2,2'-bipyridine (6.1 mg, 3 mol%), DMAP (120 mg, 2.0 equiv.) and the benzyl pinacol boronic ester (0.60 mmol, 1.2 equiv). The vial was then transferred in a glovebox where the Ni(COD)₂ (6.0 mg, 3 mol%) was added and sealed with a rubber septum. Then 5.0 mL of acetone was added to obtain a clear yellow to brownish transparent solution after sonication for 1 to 5 min. The clear solution was then pumped at 200 µL/min through a Vapourtec UV-150 photochemical reactor (10 mL reactor coil, FEP tubing, τ = 50 min) held at 35°C. Once the reaction mixture has fully been taken up by the pump, the input was swapped to acetone solvent to push the rest of the reaction mixture through the reactor. When the reaction plug was exiting the output stream (orange colour), the totality of the plug was collected in a vial wrapped in aluminium foil, filtered through a pad of celite[®] and concentrated *in vacuo*. The residue was then immobilised on ISOLUTE[®] HM-N for easy dry loading and purified by Biotage flash column chromatography on a regular silica gel cartridge (0% to 5% EtOAc in hexane gradient) to yield the pure product.

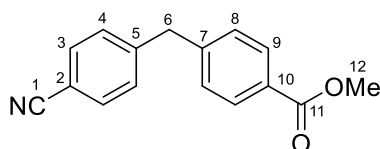
4-(4-methoxybenzyl)benzonitrile (**173**)



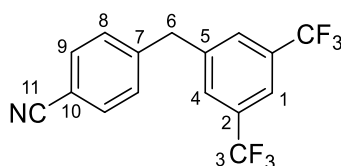
173 was obtained following **GP(V)** as a colourless oil (91 mg, 0.61 mmol) in 82% yield. ¹H-NMR (600 MHz, CDCl₃) δ 7.57 (d, J = 8.2 Hz, 2H, H₃), 7.28 (d, J = 8.3 Hz, 2H, H₄), 7.08 (d, J = 8.5 Hz, 2H, H₈), 6.86 (d, J = 8.6 Hz, 2H, H₉), 3.98 (s, 2H, H₆), 3.80 (s, 3H, H₁₁). ¹³C-NMR (151 MHz, CDCl₃) δ 158.4 (C₁₀), 147.2 (C₇), 132.3 (C₅), 131.4 (C₃), 129.9 (C₄), 129.5 (C₈), 119.0 (C₁), 114.2 (C₉), 109.9 (C₂), 55.3 (C₄), 41.1 (C₆). HRMS for [C₁₅H₁₄NO]⁺ calculated 224.1075 found 224.1077. R_f (1:4 EtOAc/hexane) = 0.29. Spectroscopic data were consistent with literature values.^[271]

4-(3,5-dimethoxybenzyl)benzonitrile (247)

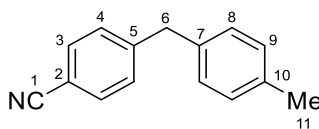
247 was obtained following **GP(V)** as a colourless oil (95 mg, 0.37 mmol) in 75% yield. **¹H-NMR (600 MHz, CDCl₃)** δ 7.58 (d, $J = 8.3$ Hz, 2H, H₃), 7.30 (d, $J = 8.3$ Hz, 2H, H₄), 6.35 (t, $J = 2.2$ Hz, 1H, H₁₀), 6.31 (d, $J = 2.2$ Hz, 2H, H₈), 3.96 (s, 2H, H₆), 3.77 (s, 6H, H₁₁). **¹³C-NMR (151 MHz, CDCl₃)** δ 161.1 (C₉), 146.4 (C₅), 141.5 (C₇), 132.3 (C₃), 129.6 (C₄), 119.0 (C₁), 110.1 (C₂), 107.2 (C₈), 98.3 (C₁₀), 55.3 (C₁₁), 42.1 (C₆). **HRMS for [C₁₆H₁₆NO₂]⁺** calculated 254.1181 found 254.1192. **R_f** (1:4 EtOAc/hexane) = 0.23. Spectroscopic data were consistent with literature values.^[271]

methyl 4-(4-cyanobenzyl)benzoate (248)

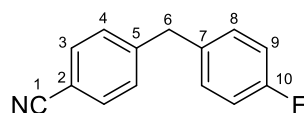
248 was obtained following **GP(V)** as a colourless oil (90 mg, 0.36 mmol) in 71% yield. **¹H-NMR (600 MHz, CDCl₃)** δ 7.99 (d, $J = 8.3$ Hz, 2H, H₉), 7.59 (d, $J = 8.2$ Hz, 2H, H₃), 7.28 (d, $J = 8.3$ Hz, 2H, H₄), 7.24 (d, $J = 8.2$ Hz, 2H, H₈), 4.09 (s, 2H, H₆), 3.91 (s, 3H, H₁₂). **¹³C-NMR (151 MHz, CDCl₃)** δ 166.8 (C₁₁), 145.6 (C₇), 144.5 (C₅), 132.4 (C₃), 130.1 (C₉), 129.7 (C₄), 129.0 (C₁₀), 128.7 (C₈), 118.8 (C₁), 110.4 (C₂), 52.1 (C₁₂), 41.9 (C₆). **HRMS for [C₁₆H₁₄NO₂]⁺** calculated 252.1025 found 252.1029. **R_f** (1:4 EtOAc/hexane) = 0.19. Spectroscopic data were consistent with literature values.^[271]

4-(3,5-bis(trifluoromethyl)benzyl)benzonitrile (249)

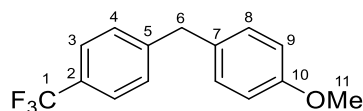
249 was obtained following **GP(V)** as a colourless oil (100 mg, 0.30 mmol) in 61% yield. **¹H-NMR (600 MHz, CDCl₃)** δ 7.78 (s, 1H, H₁), 7.65 (d, J = 8.2 Hz, 2H, H₉), 7.62 (s, 2H, H₄), 7.30 (d, J = 8.2 Hz, 2H, H₈), 4.18 (s, 2H, H₆). **¹³C-NMR (151 MHz, CDCl₃)** δ 144.1 (C₇), 141.7 (C₅), 132.6 (C₉), 132.1 (q, J = 33.4 Hz, C₃), 129.6 (C₄), 129.0 (C₂), 124.0 (C₈), 120.9 (C₁), 118.5 (C₁₁), 111.1 (C₁₀), 41.4 (C₆). **IR (ATR – neat)** $\tilde{\nu}$ (cm^{-1}) = 2929, 2222, 1624, 1607, 1508, 1467, 1433, 1376, 1274, 1161, 1116, 898. **HRMS for [C₁₆H₁₀NF₆]⁺** calculated 330.0717 found 330.0730. **R_f** (1:4 EtOAc/hexane) = 0.17.

4-(4-methylbenzyl)benzonitrile (250)

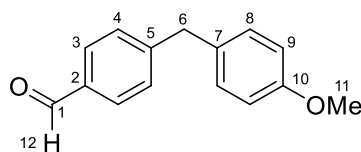
250 was obtained following **GP(V)** as colourless needles (80 mg, 0.38 mmol) in 77% yield. **¹H-NMR (600 MHz, CDCl₃)** δ 7.57 (d, J = 8.3 Hz, 2H, H₃), 7.29 (d, J = 8.3 Hz, 2H, H₄), 7.13 (d, J = 7.9 Hz, 2H, H₈), 7.06 (d, J = 7.9 Hz, 2H, H₉), 4.00 (s, 2H, H₆), 2.34 (s, 3H, H₁₁). **¹³C-NMR (151 MHz, CDCl₃)** δ 147.1 (C₅), 136.3 (C₇ and C₁₀), 132.2 (C₄ and C₃), 129.5 (C₉), 128.8 (C₈), 119.0 (C₁), 109.9 (C₂), 41.6 (C₆), 21.0 (C₁₁). **HRMS for [C₁₅H₁₄N]⁺** calculated 208.1126 found 208.1133. **R_f** (1:4 EtOAc/hexane) = 0.45. **M.p.** 58–60°C. Spectroscopic data were consistent with literature values.^[280]

4-(4-fluorobenzyl)benzonitrile (251)

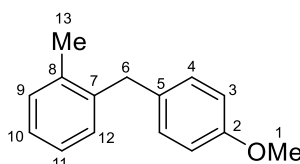
251 was obtained following **GP(V)** as a colourless oil (56 mg, 0.26 mmol) in 53% yield. **¹H-NMR (600 MHz, CDCl₃)** δ 7.59 (d, $J = 8.3$ Hz, 2H, H₃), 7.27 (d, $J = 8.3$ Hz, 2H, H₄), 7.12 (dd, $J = 8.6, 5.4$ Hz, 2H, H₈), 7.01 (t, $J = 8.7$ Hz, 2H, H₉), 4.01 (s, 3H). **¹³C-NMR (151 MHz, CDCl₃)** δ 161.7 (d, $J = 245$ Hz, C₁₀), 146.5 (C₅), 135.0 (d, $J = 3.3$ Hz, C₇), 132.4 (C₃), 130.4 (d, $J = 7.9$ Hz, C₈), 129.5 (C₄), 118.9 (C₁), 115.6, (d, $J = 21$ Hz, C₉), 110.2 (C₂), 41.1 (C₆). **HRMS for [C₁₄H₁₁NF]⁺** calculated 212.0876 found 212.0883. **R_f**(1:4 EtOAc/hexane) = 0.42. Spectroscopic data were consistent with literature values.^[281]

1-methoxy-4-(4-(trifluoromethyl)benzyl)benzene (172)

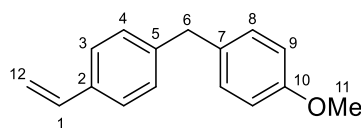
172 was obtained following **GP(V)** as a colourless oil (95 mg, 0.36 mmol) in 71% yield. **¹H-NMR (600 MHz, CDCl₃)** δ 7.55 (d, $J = 8.1$ Hz, 2H, H₃), 7.30 (d, $J = 8.0$ Hz, 2H, H₄), 7.11 (d, $J = 8.7$ Hz, 2H, H₈), 6.87 (d, $J = 8.7$ Hz, 2H, H₉), 3.99 (s, 2H, H₆), 3.81 (s, 3H, H₁₁). **¹³C-NMR (151 MHz, CDCl₃)** δ 158.2 (C₁₀), 145.7 (C₅), 132.1 (C₇), 129.9 (C₈), 129.0 (C₄), 128.4 (q, $J = 32$ Hz, C₂), 125.3 (q, $J = 3.7$ Hz, C₃), 124.2 (q, $J = 272$ Hz, C₁), 114.1 (C₉), 55.6 (C₁₁), 40.8 (C₆). **HRMS for [C₁₅H₁₄OF₃]⁺** calculated 267.0997 found 267.0989. **R_f** (1:4 EtOAc/hexane) = 0.46. Spectroscopic data were consistent with literature values.^[282]

4-(4-methoxybenzyl)benzaldehyde (252)

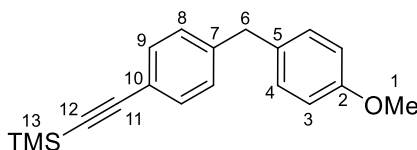
252 was obtained following **GP(V)** as a colourless oil (96 mg, 0.42 mmol) in 85% yield. **¹H-NMR (600 MHz, CDCl₃)** δ 9.98 (s, 1H, H₁₂), 7.81 (d, *J* = 8.0 Hz, 2H, H₃), 7.35 (d, *J* = 8.0 Hz, 2H, H₄), 7.11 (d, *J* = 8.7 Hz, 2H, H₈), 6.86 (d, *J* = 8.7 Hz, 2H, H₉), 4.01 (s, 2H, H₆), 3.80 (s, 3H, H₁₁). **¹³C-NMR (151 MHz, CDCl₃)** δ 192.0 (C₁), 158.3 (C₁₀), 149.0 (C₅), 134.6 (C₅), 131.8 (C₇), 130.0 (C₈), 129.9 (C₃), 129.4 (C₄), 114.1 (C₉), 55.3 (C₁₁), 41.2 (C₆). **HRMS for [C₁₅H₁₅O₂]⁺** calculated 227.1072 found 227.1071. **R_f** (1:4 EtOAc/hexane) = 0.26. Spectroscopic data were consistent with literature values.^[283]

1-(4-methoxybenzyl)-2-methylbenzene (253)

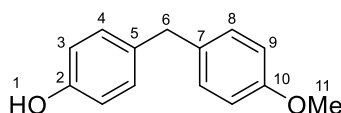
253 was obtained following **GP(V)** as a colourless oil (53 mg, 0.25 mmol) in 50% yield. **¹H-NMR (600 MHz, CDCl₃)** δ 7.20 – 7.13 (m, 3H, H₉, H₁₀ and H₁₁), 7.11 – 7.08 (m, 1H, H₁₂), 7.05 (d, *J* = 8.7 Hz, 2H, H₄), 6.83 (d, *J* = 8.7 Hz, 2H, H₃), 3.94 (s, 2H, H₆), 3.79 (s, 3H, H₁), 2.26 (s, 3H, H₁₃). **¹³C-NMR (151 MHz, CDCl₃)** δ 157.8 (C₂), 139.3 (C₇), 136.5 (C₈), 132.4 (C₅), 130.2 (C₉), 129.8 (C₁₂), 129.7 (C₄), 126.3 (C₁₀), 125.9 (C₁₁), 113.8 (C₃), 55.2 (C₁), 38.5 (C₆), 19.6 (C₁₃). **HRMS for [C₁₅H₁₆O]⁺** calculated 212.1201 found 212.1202. **R_f** (1:4 EtOAc/hexane) = 0.54. Spectroscopic data were consistent with literature values.^[277]

1-methoxy-4-(4-vinylbenzyl)benzene (254)

254 was obtained following **GP(V)** as a colourless oil (81 mg, 0.36 mmol) in 72% yield. $^1\text{H-NMR}$ (600 MHz, CDCl_3) δ 7.36 (d, $J = 8.1$ Hz, 2H, H_3), 7.16 (d, $J = 8.1$ Hz, 2H, H_4), 7.13 (d, $J = 8.7$ Hz, 2H, H_8), 6.86 (d, $J = 8.7$ Hz, 2H, H_9), 6.71 (dd, $J = 17.6, 10.9$ Hz, 1H, H_1), 5.73 (dd, $J = 17.6, 0.7$ Hz, 1H, $\text{H}_{12\text{cis}}$), 5.22 (dd, $J = 10.9, 0.7$ Hz, 1H, $\text{H}_{12\text{trans}}$), 3.94 (s, 2H, H_6), 3.80 (s, 3H, H_{11}). $^{13}\text{C-NMR}$ (151 MHz, CDCl_3) δ 157.9 (C_{10}), 141.3 (C_5), 136.6 (C_1), 135.4 (C_2), 133.1 (C_7), 129.9 (C_8), 129.0 (C_4), 126.3 (C_3), 113.9 (C_9), 113.2 (C_{12}), 55.3 (C_{11}), 40.8 (C_6). **HRMS** for $[\text{C}_{16}\text{H}_{17}\text{O}]^+$ calculated 225.1279 found 225.1274. R_f (1:4 EtOAc/hexane) = 0.51. Spectroscopic data were consistent with literature values.^[284]

((4-(4-methoxybenzyl)phenyl)ethynyl)trimethylsilane (255)

255 was obtained following **GP(V)** as a colourless oil (91 mg, 75% yield). $^1\text{H-NMR}$ (600 MHz, CDCl_3) δ 7.39 (d, $J = 8.2$ Hz, 2H, H_9), 7.11 (d, $J = 8.2$ Hz, 2H, H_8), 7.07 (d, $J = 8.7$ Hz, 2H, H_4), 6.84 (d, $J = 8.7$ Hz, 2H, H_3), 3.92 (s, 2H, H_6), 3.79 (s, 3H, H_1), 0.25 (s, 9H, H_{13}). $^{13}\text{C-NMR}$ (151 MHz, CDCl_3) δ 158.1 (C_2), 142.2 (C_7), 132.6 (C_5), 132.1 (C_9), 129.8 (C_4), 128.7 (C_8), 120.7 (C_{10}), 113.9 (C_3), 105.2 (C_{11}), 93.6 (C_{12}), 55.2 (C_1), 40.9 (C_6), 0.0 (C_{13}). **IR** (ATR – neat) $\tilde{\nu}$ (cm^{-1}) = 2956, 2901, 2155, 1609, 1584, 1510, 1504, 1455, 1441, 1300, 1243, 1175, 1031, 840, 813, 755. **HRMS** for $[\text{C}_{19}\text{H}_{22}\text{OSi}]^+$ calculated 294.1440 found 294.1442. R_f (1:4 EtOAc/hexane) = 0.54.

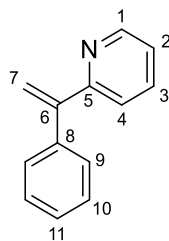
4-(4-methoxybenzyl)phenol (257)

257 was obtained following **GP(V)** using 2-(4-bromophenyl)-4,4,5,5-tetramethyl-1,3,2-dioxaborolane as arylbromide followed by an NaOH/H₂O₂ oxidation of the aryl pinacol ester product as described by Molander.^[229] The corresponding phenol (**257**) was then isolated as a white amorphous solid (76 mg, 0.36 mmol) in 71% yield. **¹H-NMR (600 MHz, CDCl₃)** δ 7.12 (d, *J* = 8.7 Hz, 2H, H₈), 7.06 (d, *J* = 8.5 Hz, 2H, H₄), 6.86 (d, *J* = 8.7 Hz, 2H, H₉), 6.77 (d, *J* = 8.5 Hz, 2H, H₃), 5.31 (br s, 1H, H₁), 3.88 (s, 2H, H₆), 3.81 (s, 3H, H₁₁). **¹³C-NMR (151 MHz, CDCl₃)** δ 157.8 (C₁₀), 153.7 (C₂), 133.8 (C₇ and C₅), 130.0 (C₄), 129.8 (C₈), 115.3 (C₃), 113.9 (C₉), 55.3 (C₁₁), 40.1 (C₆). **HRMS for [C₁₄H₁₄O₂]⁺** calculated 214.0994 found 214.0986. **R_f** (1:4 EtOAc/hexane) = 0.13. Spectroscopic data were consistent with literature values.^[273]

5.3 Experimental data for Chapter 3

5.3.1 Synthetic procedures and characterisation for starting materials

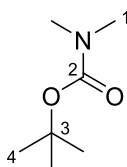
2-(1-phenylvinyl) pyridine



2-benzylpyridine (95 mg, 0.56 mmol, 1.0 equiv.) was loaded in a 20 mL two-necked flask equipped with a reflux condenser along with $\text{Cu}(\text{OAc})_2 \cdot \text{H}_2\text{O}$ (11 mg, 0.056 mmol, 10 mol%), $\text{Na}_2\text{S}_2\text{O}_8$ (266 mg, 1.12 mmol, 2.0 equiv.) and dissolved in DMA (2.5 mL). The resulting mixture was then stirred under argon at 120°C for 4 h. The reaction mixture was then cooled down to room temperature and extracted with ethyl acetate. The organic layer was washed with water (3 x 100 mL), dried over MgSO_4 and solvents removed *in vacuo*. Column chromatography on silica gel (15% EtOAc in hexane) afforded the title compound (65 mg, 0.36 mmol) as a colourless oil in 64% yield.

$^1\text{H-NMR}$ (400 MHz, CDCl_3) δ 8.64 (d, $J = 4.8$ Hz, 1H, H_1), 7.63 (t, $J = 7.7$ Hz, 1H, H_3), 7.35 (s, 5H, $\text{H}_8, \text{H}_9, \text{H}_{10}$ and H_{11}), 7.27 (d, $J = 8.1$ Hz, 1H, H_4), 7.20 (t, $J = 6.3$ Hz, 1H, H_2), 5.99 (s, 1H, H_{7a}), 5.61 (s, 1H, H_{7b}). **$^{13}\text{C-NMR}$ (151 MHz, CDCl_3)** 158.5 (C_5), 149.4 (C_1), 149.2 (C_6), 140.4 (C_8), 136.3 (C_3), 128.4 (C_9), 128.3 (C_{10}), 127.8 (C_{11}), 122.8 (C_4), 122.4 (C_2), 117.7 (C_7). **HRMS for $[\text{C}_{13}\text{H}_{12}\text{N}]^+$** calculated 182.0970 found 182.0966. **R_f** (1:4 EtOAc/PE) = 0.58. Spectroscopic data were consistent with literature values.^[285]

tert-butyl dimethylcarbamate

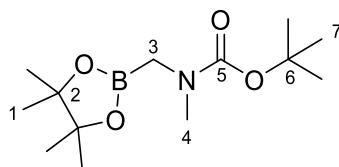


A solution of triethylamine (3.0 mL, 22 mmol, 1.0 equiv.) and dimethylamine (40% in H_2O , 2.7 mL, 22 mmol, 1.0 equiv.) in THF (10 mL) was cooled to 0°C. Boc_2O (5.0 mL, 22 mmol, 1.0 equiv.) was added slowly and the reaction mixture was stirred at

0°C for 10 min. and for an additional 18 h at room temperature. The solvent was removed under reduced pressure and the residue was suspended in water (15 mL). The suspension was extracted with EtOAc (3 x 20 mL), the combined organic extracts were dried over MgSO₄ and concentrated *in vacuo*. Fractional distillation under reduced pressure afforded the title compound (3.1 g, 22 mmol) as a colourless oil in 99% yield.

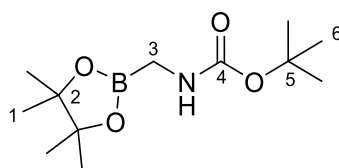
¹H-NMR (600 MHz, CDCl₃) δ 2.85 (s, 6H, H₁), 1.45 (s, 9H, H₄). **¹³C-NMR (151 MHz, CDCl₃)** δ 156.2 (C₂), 79.3 (C₃), 36.3 (C₁), 28.6 (C₄). **HRMS for [C₇H₁₅O₂NNa]⁺** calculated 168.0995 found 168.0991. **B.p.** (12 mTorr) = 40°C. Spectroscopic data were consistent with literature values.^[286]

***tert*-butyl methyl((4,4,5,5-tetramethyl-1,3,2-dioxaborolan-2-yl)methyl)carbamate**



A solution of *tert*-butyl dimethylcarbamate (0.20 g, 1.4 mmol, 1.0 equiv.) and TMEDA (0.40 mL, 2.8 mmol, 2.0 equiv.) in Et₂O (10 mL) was cooled to -78°C. *sec*-BuLi (1.4 M in hexane, 1.2 mL, 1.7 mmol, 1.2 equiv.) was added dropwise and the mixture was stirred at -78°C for 3 h. Then a solution of 2-isopropoxy-4,4,5,5-tetramethyl-1,3,2-dioxaborolane (0.34 mL, 1.7 mmol, 1.2 equiv.) in Et₂O (2 mL) was added. After stirring at -78°C for 1.5 h acetyl chloride (0.12 mL, 1.7 mmol, 1.2 equiv.) was added and the reaction mixture was allowed to warm to room temperature. The reaction mixture was concentrated under reduced pressure and the residue was suspended in 0.1 M PBS (pH 7, 30 mL) and extracted with EtOAc (3 x 40 mL). The combined organic layers were dried over MgSO₄ and the solvents removed *in vacuo*. Column chromatography on oven-dried silica (20% to 25% EtOAc in hexane) afforded the product (0.34 g, 1.2 mmol) as a yellowish oil in 90% yield.

¹H-NMR (600 MHz, CDCl₃) δ 2.77 (s, 3H, H₄), 2.34 (s, 2H, H₃), 1.43 (s, 9H, H₇), 1.14 (s, 12H, H₁) ppm. **¹³C-NMR (151 MHz, CDCl₃)** δ 160.7 (C₅), 84.7 (C₂), 80.7 (C₆), 40.7 (C₃), 34.2 (C₄), 28.4 (C₇), 25.1 (C₁). **¹¹B-NMR (193 MHz, CDCl₃)** δ 17.2. **IR (ATR – neat)** $\tilde{\nu}$ (cm⁻¹) = 2976, 1689, 1367, 1335, 1215, 1160, 1139, 968, 879, 846, 771. **HRMS for [C₁₃H₂₇O₄NB]⁺** calculated 272.2028 found 272.2026. **R_f** (1:1 EtOAc/PE) = 0.35.

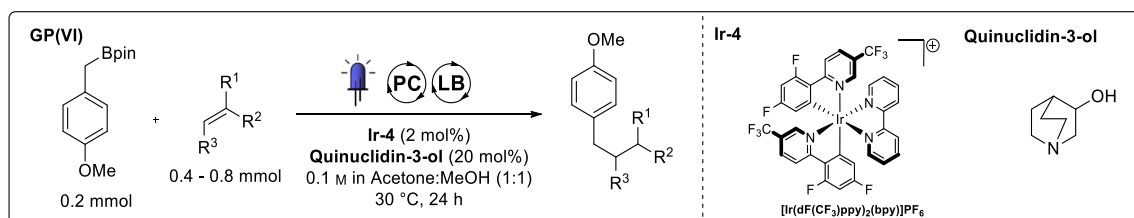
***tert*-butyl ((4,4,5,5-tetramethyl-1,3,2-dioxaborolan-2-yl)methyl)carbamate (1g)**

A solution of NaHMDS (1 M in THF, 5.6 mL, 5.6 mmol, 1.0 equiv.) in THF (30 mL) was cooled to -78°C . 2-(chloromethyl)-4,4,5,5-tetramethyl-1,3,2-dioxaborolane (0.98 g, 5.6 mmol, 1.0 equiv.) in THF (6 mL) was added dropwise and the reaction mixture was stirred at -78°C for 20 min, before it was allowed to warm to room temperature and stirred for additional 2 h. The reaction mixture was then cooled to 0°C before MeOH (0.44 mL, 11 mmol, 2.0 equiv.) was added, the mixture was then stirred at this temperature for 1 h. Boc_2O (1.5 mL, 6.7 mmol, 1.2 equiv.) was then added and the mixture was stirred at room temperature for 72 h. The solvent was evaporated and the crude mixture was loaded on oven dried silica. Column chromatography on oven-dried silica (20% Et_2O in PE) afforded the product (1.1 g, 4.3 mmol) as a colourless oil in 77% yield.

$^1\text{H-NMR}$ (600 MHz, CDCl_3) δ 4.63 (s, 1H, *NH*), 2.77 (d, $J = 4.4$ Hz, 2H, H_3), 1.44 (s, 9H, H_6), 1.27 (s, 12H, H_1). **$^{13}\text{C-NMR}$ (151 MHz, CDCl_3)** δ 157.1 (C_4), 84.2 (C_2), 79.2 (C_5), 28.6 (C_6), 24.9 (C_1). **$^{11}\text{B-NMR}$ (193 MHz, CDCl_3)** δ 32.6. **IR (ATR – neat)** $\tilde{\nu}$ (cm^{-1}) = 3376, 2979, 1697, 1506, 1382, 1367, 1335, 1167, 1141, 968, 845, 780. **HRMS for $[\text{C}_{12}\text{H}_{24}\text{O}_4\text{NBNa}]^+$** calculated 280.1691 found 280.1686. **R_f** (1:1 EtOAc/PE) = 0.28.

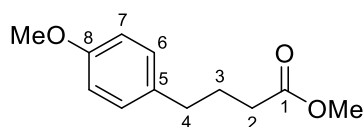
5.3.2 Synthetic procedures and characterisation for coupling products

5.3.2.1 Scope of electron-deficient olefins



GP(VI): A 5 mL glass vial equipped with a magnetic stir bar was charged with 2-(4-methoxybenzyl)-4,4,5,5-tetramethyl-1,3,2-dioxaborolane (50 mg, 0.20 mmol, 1.0 equiv.), the photoredox catalyst $[\text{Ir}(\text{dF}(\text{CF}_3)\text{ppy})_2(\text{bpy})]\text{PF}_6$ (**Ir-4**, 4.0 mg, 2.0 mol%) and quinuclidin-3-ol (5.0 mg, 0.04 mmol, 20 mol%). The vial was then sealed with a rubber septum and evacuated/backfilled with argon three times. The volatile olefin (0.4–0.8 mmol, 2.0–4.0 equiv.) was then added followed by 2.0 mL of a degassed acetone/methanol (1:1) mixture to lead a clear yellow transparent 0.1 M solution. This solution was then stirred while irradiated with a commercial blue LED strip (Ledxon, 14.4 W, 470 nm) for 24 h, the temperature was maintained at 30°C using a desktop fan. The content of the vial was then concentrated *in vacuo* and immobilised on ISOLUTE[®] HM-N for easy dry loading on flash column chromatography to yield the pure product.

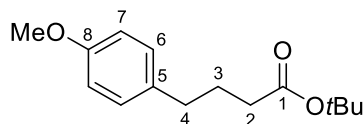
methyl 4-(4-methoxyphenyl)butanoate (**263**)



Obtained following **GP(VI)** at 0.2 mmol scale using 0.8 mmol of methyl acrylate. Purification by column chromatography on silica gel (3% EtOAc in hexane) afforded product **263** (31 mg, 0.15 mmol) as colourless oil in 75% yield. ¹H-NMR (600 MHz, CDCl₃) δ 7.09 (d, *J* = 8.6 Hz, 2H, H₆), 6.83 (d, *J* = 8.6 Hz, 2H, H₇), 3.79 (s, 3H, ArOMe), 3.66 (s, 3H, COOMe), 2.61 – 2.58 (m, 2H, H₂), 2.32 (t, *J* = 7.5 Hz, 2H, H₄), 1.95 – 1.89 (m, 2H, H₃). ¹³C-NMR (151 MHz, CDCl₃) δ 174.0 (C₁), 157.9 (C₈), 133.4 (C₅), 129.4 (C₆), 113.8 (C₇), 55.2 (ArOMe), 51.5 (COOMe), 34.2 (C₄), 33.3 (C₂), 26.7 (C₃). HRMS

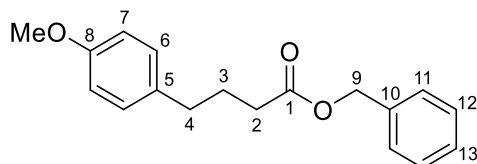
for $[\text{C}_{12}\text{H}_{17}\text{O}_3]^+$ calculated 209.1172 found 209.1163. $R_f(1:4 \text{ EtOAc/PE}) = 0.38$. Spectroscopic data were consistent with literature values.^[287]

***tert*-butyl 4-(4-methoxyphenyl)butanoate (264)**

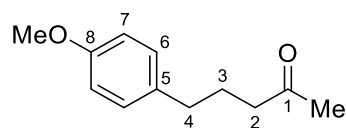


Obtained following **GP(VI)** at 0.2 mmol scale using 0.8 mmol of *tert*-butyl acrylate. Purification by column chromatography on silica gel (7% EtOAc in hexane) afforded product **264** (24 mg, 0.096 mmol) as colourless oil in 48% yield. **¹H-NMR (400 MHz, CDCl₃)** δ 7.10 (d, $J = 8.6$ Hz, 2H, H₆), 6.83 (d, $J = 8.6$ Hz, 2H, H₇), 3.79 (s, 3H, OMe) 2.58 (t, $J = 7.4$ Hz, 2H, H₂), 2.22 (t, $J = 7.5$ Hz, 2H, H₄), 1.88 (q, $J = 7.6$ Hz, 2H, H₃), 1.44 (s, 9H, OtBu). **¹³C-NMR (101 MHz, CDCl₃)** δ 173.0 (C₁), 157.8 (C₈), 133.7 (C₅), 129.4 (C₆), 113.8 (C₇), 80.1 (OC(Me)₃), 55.3 (OMe), 34.9 (C₄), 34.2 (C₂), 28.1 (OC(Me)₃), 27.0 (C₃). **HRMS for $[\text{C}_{15}\text{H}_{23}\text{O}_3\text{Na}]^+$** calculated 273.1464 found 273.1461. $R_f(1:4 \text{ EtOAc/PE}) = 0.60$. Spectroscopic data were consistent with literature values.^[288]

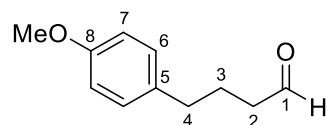
benzyl 4-(4-methoxyphenyl)butanoate (265)



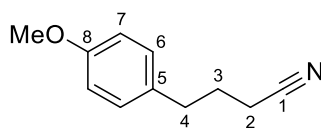
Obtained following **GP(VI)** at 0.2 mmol scale using 0.8 mmol of benzyl acrylate. Purification by column chromatography on silica gel (7% EtOAc in hexane) afforded product **265** (27 mg, 0.10 mmol) as colourless oil in 47% yield. **¹H-NMR (400 MHz, CDCl₃)** δ 7.41 – 7.28 (m, 5H, H₁₁, H₁₂, and H₁₃), 7.07 (d, $J = 8.2$ Hz, 2H, H₆), 6.81 (d, $J = 8.2$ Hz, 2H, H₇), 5.11 (s, 2H, H₉), 3.78 (s, 3H, OMe), 2.58 (t, $J = 7.5$ Hz, 2H, H₄), 2.36 (t, $J = 7.5$ Hz, 2H, H₂), 1.94 (p, $J = 7.5$ Hz, 2H, H₃). **¹³C-NMR (101 MHz, CDCl₃)** δ 173.4 (C₁), 157.9 (C₈), 136.0 (C₁₀), 133.4 (C₅), 129.4 (C₆), 128.6 (C₁₂), 128.2 (C₁₃), 127.7 (C₁₁), 113.8 (C₇), 66.2 (C₉), 55.3 (OMe), 34.2 (C₄), 33.6 (C₂), 26.7 (C₃). **HRMS for $[\text{C}_{18}\text{H}_{21}\text{O}_3\text{Na}]^+$** calculated 308.1385 found 308.1389. $R_f(1:4 \text{ EtOAc/PE}) = 0.82$. Spectroscopic data were consistent with literature values.^[289]

5-(4-methoxyphenyl)pentan-2-one (266)

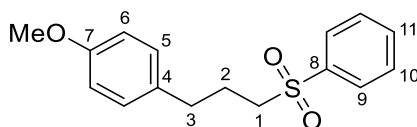
Obtained following **GP(VI)** at 0.2 mmol scale using 0.8 mmol of methyl vinyl ketone. Purification by column chromatography on silica gel (10% EtOAc in hexane) afforded product **266** (32 mg, 0.16 mmol) as colourless oil in 82% yield. Repeating the same procedure with **Mes-Acr-4** instead of **Ir-4** afforded the same product in 78% yield. **¹H-NMR (600 MHz, CDCl₃)** δ 7.08 (d, $J = 8.6$ Hz, 2H, H₆), 6.83 (d, $J = 8.6$ Hz, 2H, H₇), 3.79 (s, 3H, OMe), 2.56 (t, $J = 7.5$ Hz, 2H, H₄), 2.42 (t, $J = 7.5$ Hz, 2H, H₂), 2.11 (s, 3H, COMe), 1.87 (p, $J = 7.5$ Hz, 2H, H₃). **¹³C-NMR (151 MHz, CDCl₃)** δ 209.0 (C₁), 158.0 (C₈), 133.7 (C₅), 129.5 (C₆), 113.9 (C₇), 55.4 (OMe), 42.9 (C₂), 34.2 (C₄), 30.1 (COMe), 25.6 (C₃). **HRMS for [C₁₂H₁₇O₂]⁺** calculated 193.1223 found 193.1228. **R_f** (1:4 EtOAc/PE) = 0.38. Spectroscopic data were consistent with literature values.^[287]

4-(4-methoxyphenyl)butanal (267)

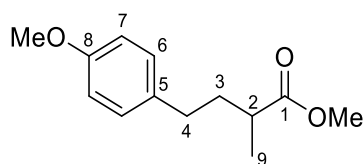
Obtained following **GP(VI)** at 0.2 mmol scale using 0.4 mmol of acrolein. Purification by column chromatography on silica gel (10% EtOAc in hexane) afforded product **267** (22 mg, 0.16 mmol) as colourless oil in 63% yield. **¹H-NMR (400 MHz, CDCl₃)** δ 9.75 (s, 1H, CHO), 7.09 (d, $J = 8.2$ Hz, 2H, H₆), 6.83 (d, $J = 8.2$ Hz, 2H, H₇), 3.79 (s, 3H, OMe), 2.60 (t, $J = 7.5$ Hz, 2H, H₂), 2.44 (t, $J = 7.5$ Hz, 1H, H₄), 1.93 (p, $J = 7.5$ Hz, 2H, H₃). **¹³C-NMR (101 MHz, CDCl₃)** δ 202.5 (C₁), 158.0 (C₈), 133.3 (C₅), 129.4 (C₆), 113.9 (C₇), 55.3 (OMe), 43.1 (C₂), 34.1 (C₄), 23.9 (C₃). **HRMS for [C₁₁H₁₅O₂]⁺** calculated 179.1067 found 179.1060. **R_f** (1:4 EtOAc/PE) = 0.30. Spectroscopic data were consistent with literature values.^[290]

4-(4-methoxyphenyl)butanenitrile (268)

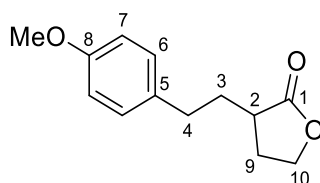
Obtained following **GP(VI)** at 0.2 mmol scale using 0.8 mmol of acrylonitrile. Purification by column chromatography on silica gel (10% EtOAc in hexane) afforded product **268** (27 mg, 0.15 mmol) as colourless oil in 77% yield. **¹H-NMR (400 MHz, CDCl₃)** δ 7.10 (d, $J = 8.2$ Hz, 2H, H₆), 6.85 (d, $J = 8.2$ Hz, 2H, H₇), 3.79 (s, 3H, OMe), 2.72 (t, $J = 7.4$ Hz, 2H, H₄), 2.30 (t, $J = 7.1$ Hz, 2H, H₂), 1.94 (p, $J = 7.3$ Hz, 2H, H₃). **¹³C-NMR (101 MHz, CDCl₃)** δ 158.3 (C₈), 131.7 (C₅), 129.4 (C₆), 119.6 (C₁), 114.1 (C₇), 55.3 (OMe), 33.5 (C₄), 27.1 (C₃), 16.3 (C₂). **HRMS for [C₁₁H₁₄NO]⁺** calculated 176.1070 found 176.1077. **R_f** (1:4 EtOAc/PE) = 0.50. Spectroscopic data were consistent with literature values.^[287]

1-methoxy-4-(3-(phenylsulfonyl)propyl)benzene (269)

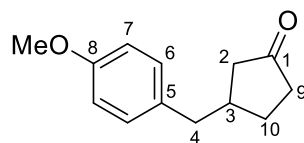
Obtained following **GP(VI)** at 0.2 mmol scale using 0.4 mmol of acrylonitrile. Purification by column chromatography on silica gel (12% EtOAc in hexane) afforded product **269** (30 mg, 0.10 mmol) as white solid in 51% yield. **¹H-NMR (400 MHz, CDCl₃)** δ 7.88 (d, $J = 7.6$ Hz, 2H, H₉), 7.65 (t, $J = 7.5$ Hz, 1H, H₁₁), 7.56 (t, $J = 7.6$ Hz, 2H, H₁₀), 7.01 (d, $J = 8.1$ Hz, 2H, H₅), 6.80 (d, $J = 8.1$ Hz, 2H, H₆), 3.78 (s, 3H, OMe), δ 3.11 – 3.01 (m, 1H, H₁), 2.64 (t, $J = 7.5$ Hz, 2H, H₃), 2.01 (p, $J = 7.6$ Hz, 2H, H₂). **¹³C-NMR (101 MHz, CDCl₃)** δ 158.2 (C₇), 139.1 (C₈), 133.6 (C₄), 131.8 (C₁₁), 129.3 (C₅), 129.3 (C₆), 128.0 (C₁₉), 114.0 (C₆), 55.4 (C₁), 55.3 (OMe), 33.2 (C₃), 24.4 (C₂). **HRMS for [C₁₆H₁₉O₃S]⁺** calculated 291.1049 found 291.1044. **R_f** (1:4 EtOAc/PE) = 0.25. **M.p.** 60–62°C. Spectroscopic data were consistent with literature values.^[9]

methyl 4-(4-methoxyphenyl)-2-methylbutanoate (270)

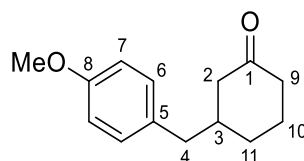
Obtained following **GP(VI)** at 0.2 mmol scale using 0.8 mmol of methyl methacrylate. Purification by column chromatography on silica gel (10% EtOAc in hexane) afforded product **270** (28 mg, 0.13 mmol) as colourless oil in 64% yield. **¹H-NMR (600 MHz, CDCl₃)** δ 7.10 (d, $J = 8.5$ Hz, 2H, H₇), 6.83 (d, $J = 8.5$ Hz, 2H, H₆), 3.79 (s, 3H, OMe), 3.68 (s, 3H, COOMe), 2.56 (t, $J = 7.9$ Hz, 2H, H₄), 2.48 (h, $J = 7.0$ Hz, 1H, H₂), 2.04 – 1.94 (m, 1H, H₃), 1.69 (dq, $J = 14.2, 7.7$ Hz, 1H, H₃), 1.19 (d, $J = 7.0$ Hz, 3H, H₇). **¹³C-NMR (151 MHz, CDCl₃)** δ 177.0 (C₁), 157.8 (C₈), 133.7 (C₅), 129.3 (C₆), 113.8 (C₇), 55.2 (OMe), 51.5 (COMe), 38.9 (C₂), 35.6 (C₄), 32.5 (C₃), 17.1 (C₉). **HRMS for [C₁₃H₁₉O₃]⁺** calculated 223.1329 found 223.1328. **R_f** (1:4 EtOAc/PE) = 0.31. Spectroscopic data were consistent with literature values.^[287]

3-(4-methoxyphenethyl) dihydrofuran-2(3H)-one (271)

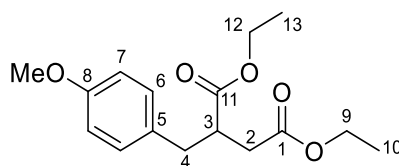
Obtained following **GP(VI)** at 0.2 mmol scale using 0.8 mmol of 3-methylenedihydrofuran-2(3H)-one. Purification by column chromatography on silica gel (10% EtOAc in hexane) afforded product **271** (28 mg, 0.13 mmol) as colourless oil in 68% yield. **¹H-NMR (600 MHz, CDCl₃)** δ 7.11 (d, $J = 8.6$ Hz, 2H, H₇), 6.83 (d, $J = 8.6$ Hz, 2H, H₆), 4.33 (td, $J = 8.8, 2.8$ Hz, 1H, H_{10a}), 4.15 (td, $J = 9.4, 6.7$ Hz, 1H, H_{10b}), 3.78 (s, 3H, OMe), 2.70-2.77 (m, 1H, H_{4a}), 2.69 – 2.61 (m, 1H, H_{4b}), 2.53 – 2.44 (m, 1H, H₂), 2.40 – 2.33 (m, 1H, H_{9a}), 2.16-2.23 (m, 1H, H_{9b}), 1.94 (ddd, $J = 18.6, 12.5, 10.0$ Hz, 1H, H_{3a}), 1.72 (dtd, $J = 14.6, 8.9, 5.9$ Hz, 1H, H_{3b}). **¹³C-NMR (151 MHz, CDCl₃)** δ 179.5 (C₁), 158.1 (C₈), 132.8 (C₅), 129.4 (C₆), 114.0 (C₇), 66.5 (C₁₀), 55.3 (OMe), 38.4 (C₂), 32.5 (C₄), 32.2 (C₃), 28.9 (C₉). **IR (ATR – neat)** $\tilde{\nu}$ (cm⁻¹) 2914, 1763, 1611, 1510, 1374, 1243, 1023, 824. **HRMS for [C₁₃H₁₇O₃]⁺** calculated 221.1172 found 221.1156. **R_f** (1:4 EtOAc/PE) = 0.32.

2-(4-methoxybenzyl)cyclopentanone (272)

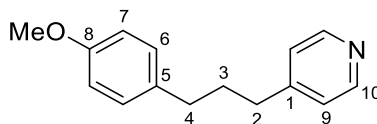
Obtained following **GP(VI)** at 0.2 mmol scale using 0.8 mmol of cyclopent-2-en-1-one. Purification by column chromatography on silica gel (15% EtOAc in hexane) afforded product **272** (25 mg, 0.12 mmol) as yellowish oil in 62% yield. **¹H-NMR (400 MHz, CDCl₃)** δ 7.08 (d, $J = 8.2$ Hz, 2H, H₆), 6.84 (d, $J = 8.2$ Hz, 2H, H₇), 3.79 (s, 3H, OMe), 2.68 (d, $J = 6.2$ Hz, 2H, H₄), 2.44 (sept, $J = 7.3$ Hz, 1H, H₃), 2.31 (ddd, $J = 16.6, 10.0, 6.7$ Hz, 2H, H_{2a}, H_{9a}), 2.21–2.00 (m, 2H, H_{9b}, H_{10a}), 1.90 (dd, $J = 18.0, 9.7$ Hz, 1H, H_{2b}), 1.67 – 1.54 (m, 1H, H_{10b}). **¹³C-NMR (101 MHz, CDCl₃)** δ 219.4 (C₁), 158.1 (C₈), 132.1 (C₅), 129.7 (C₆), 113.8 (C₇), 55.3 (OMe), 44.9 (C₄), 40.6 (C₂), 39.0 (C₉), 38.3 (C₃), 29.0 (C₁₀). **IR (ATR – neat)** $\tilde{\nu}$ (cm⁻¹) = 2920, 1691, 1603, 1460, 1116, 892, 765. **HRMS for [C₁₃H₁₇O₂]⁺** calculated 205.1223 found 205.1220. **R_f** (1:4 EtOAc/PE) = 0.57.

3-(4-methoxybenzyl)cyclohexanone (273)

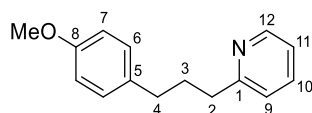
Obtained following **GP(VI)** at 0.2 mmol scale using 0.8 mmol of cyclohex-2-en-1-one. Purification by column chromatography on silica gel (15% EtOAc in hexane) afforded product **273** (25 mg, 0.12 mmol) as yellowish oil in 58% yield. **¹H-NMR (400 MHz, CDCl₃)** δ 7.04 (d, $J = 8.1$ Hz, 2H, H₆), 6.83 (d, $J = 8.1$ Hz, 2H, H₇), 3.79 (s, 3H, OMe), 2.57 (d, $J = 4.8$ Hz, 2H, H₄), 2.39–2.21 (m, 3H, H_{2a}, H₃, H_{9a}), 2.10–1.96 (m, 3H, H_{2b}, H_{9a}, H_{11a}), 1.92–1.81 (m, 1H, H_{10a}), 1.63–1.54 (m, 1H, H_{10b}), 1.40–1.30 (m, 1H, H_{11b}). **¹³C-NMR (101 MHz, CDCl₃)** δ 211.8 (C₁), 158.0 (C₈), 131.5 (C₅), 130.0 (C₆), 113.8 (C₇), 55.3 (OMe), 47.8 (C₂), 42.0 (C₉), 41.4 (C₄), 41.1 (C₃), 30.8 (C₁₁), 25.1 (C₁₀). **HRMS for [C₁₄H₁₉O₂]⁺** calculated 219.1380 found 219.1375. **R_f** (1:4 EtOAc/PE) = 0.58. Spectroscopic data were consistent with literature values.^[287]

diethyl 2-(4-methoxybenzyl)succinate (274)

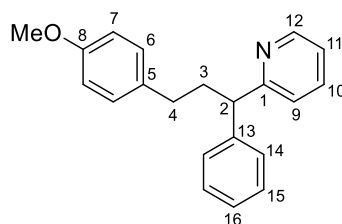
Obtained following **GP(VI)** at 0.2 mmol scale using 0.8 mmol of diethyl fumarate. Purification by column chromatography on silica gel (10% EtOAc in hexane) afforded product **274** (46 mg, 0.16 mmol) as yellowish oil in 78% yield. **¹H-NMR (400 MHz, CDCl₃)** δ 7.08 (d, *J* = 8.6 Hz, 2H, H₆), 6.82 (d, *J* = 8.6 Hz, 2H, H₇), 4.12 (q, *J* = 7.1 Hz, 2H, H₉ or H₁₂), 4.09 (q, *J* = 7.1 Hz, 2H, H₁₂ or H₉), 3.78 (s, 3H, OMe), 3.06 (dddd, *J* = 9.2, 8.1, 6.5, 4.9 Hz, 1H, H₂), 2.98 (dd, *J* = 13.6, 6.5 Hz, 1H, H_{4a}), 2.75 – 2.59 (m, 2H, H_{4b} and H_{2a}), 2.38 (dd, *J* = 16.7, 5.0 Hz, 1H, H_{2b}), 1.22 (t, *J* = 7.1 Hz, 3H, H₁₀ or H₁₃), 1.20 (t, *J* = 7.1 Hz, 3H, H₁₃ or H₁₀). **¹³C-NMR (101 MHz, CDCl₃)** δ 174.3 (C₁₁), 171.9 (C₁), 158.4 (C₈), 130.3 (C₅), 130.0 (C₆), 113.9 (C₇), 60.7 (C₁₂ or C₉), 60.6 (C₉ or C₁₂), 55.3 (OMe), 43.3 (C₃), 37.0 (C₄), 35.2 (C₂), 14.2 (C₁₀ or C₁₃), 14.1 (C₁₃ or C₁₀). **HRMS for [C₁₆H₂₃O₅]⁺** calculated 295.1540 found 295.1543. **R_f** (1:4 EtOAc/PE) = 0.50. Spectroscopic data were consistent with literature values.^[292]

4-(3-(4-methoxyphenyl)propyl)pyridine (275)

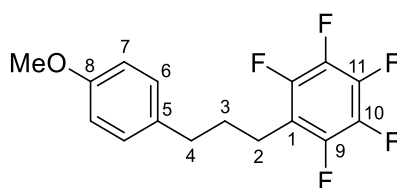
Obtained following **GP(VI)** at 0.2 mmol scale using 0.8 mmol of 4-vinyl pyridine. Purification by column chromatography on silica gel (15% EtOAc in hexane) afforded product **275** (20 mg, 0.09 mmol) as colourless oil in 45% yield. **¹H-NMR (600 MHz, CDCl₃)** δ 8.49 (d, *J* = 6.1 Hz, 2H, H₁₀), 7.13 – 7.07 (m, 4H, H₆ and H₉), 6.84 (d, *J* = 8.6 Hz, 2H, H₇), 3.79 (s, 3H, OMe), 2.62 (t, *J* = 7.7 Hz, 2H, H₄), 2.60 (t, *J* = 7.7 Hz, 2H, H₂), 1.94 (p, *J* = 7.7 Hz, 2H, H₃). **¹³C-NMR (151 MHz, CDCl₃)** δ 157.9 (C₈), 151.3 (C₁), 149.6 (C₁₀), 133.6 (C₅), 129.3 (C₆), 123.9 (C₉), 113.8 (C₇), 55.2 (OMe), 34.5 (C₂), 34.3 (C₄), 32.0 (C₃). **HRMS for [C₁₅H₁₈NO]⁺** calculated 228.1383 found 228.1380. **R_f** (1:4 EtOAc/PE) = 0.50. Spectroscopic data were consistent with literature values.^[287]

2-(3-(4-methoxyphenyl)propyl)pyridine (276)

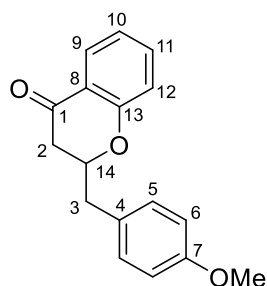
Obtained following **GP(VI)** at 0.2 mmol scale using 0.4 mmol of 2-vinyl pyridine. Purification by column chromatography on silica gel (20% EtOAc in hexane) afforded product **276** (35 mg, 0.15 mmol) as yellowish oil in 77% yield. **¹H-NMR (400 MHz, CDCl₃)** δ 8.53 (ddd, $J = 4.9, 1.7, 0.8$ Hz, 1H, H₁₂), 7.58 (td, $J = 7.6, 1.9$ Hz, 1H, H₁₀), 7.16 – 7.06 (m, 4H, H₆, H₉ and H₁₁), 6.82 (d, $J = 8.6$ Hz, 2H, H₇), 3.78 (s, 3H, OMe), 2.81 (t, $J = 7.8$ Hz, 2H, H₄), 2.63 (t, $J = 7.5$ Hz, 2H, H₂), 2.03 (p, $J = 7.8$ Hz, 2H, H₃). **¹³C-NMR (101 MHz, CDCl₃)** δ 162.0 (C₁), 157.7 (C₈), 149.2 (C₁₂), 136.3 (C₁₀), 134.2 (C₅), 129.3 (C₆), 122.8 (C₉), 121.0 (C₁₁), 113.7 (C₇), 55.3 (OMe), 37.8 (C₂), 34.6 (C₄), 31.7 (C₃). **IR (ATR – neat)** $\tilde{\nu}$ (cm^{-1}) = 2926, 2854, 1510, 1434, 1242, 1176, 1035, 828, 748. **HRMS for [C₁₅H₁₈NO]⁺** calculated 228.1383 found 228.1382. **R_f** (1:4 EtOAc/PE) = 0.30.

2-(3-(4-methoxyphenyl)-1-phenylpropyl)pyridine (277)

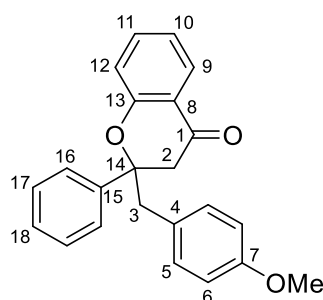
Obtained following **GP(VI)** at 0.2 mmol scale using 0.4 mmol of 2-(1-phenylvinyl) pyridine (**2o**). Purification by column chromatography on silica gel (7% EtOAc in hexane) afforded product **277** (32 mg, 0.10 mmol) as colourless oil in 52% yield. **¹H-NMR (400 MHz, CDCl₃)** δ 8.57 (d, $J = 4.8$ Hz, 1H, H₁₂), 7.55 (t, $J = 7.7$ Hz, 1H, H₁₀), 7.37 – 7.26 (m, 4H, H₉, H₁₁ and H₁₅), 7.19 (t, $J = 7.0$ Hz, 1H, H₁₆), 7.13 (d, $J = 7.9$ Hz, 1H, H_{14a}), 7.10 – 7.04 (m, 3H, H₆ and H_{14b}), 6.81 (d, $J = 8.1$ Hz, 2H, H₇), 4.06 (t, $J = 7.4$ Hz, 1H, H₂), 3.78 (s, 3H, OMe), 2.59 – 2.49 (m, 3H, H₄, H_{3a}), 2.38 (dd, $J = 11.7, 7.5$ Hz, 2H, H_{3b}). **¹³C-NMR (101 MHz, CDCl₃)** δ 163.7 (C₁), 157.7 (C₈), 149.3 (C₁₂), 143.6 (C₁₃), 136.4 (C₁₀), 134.1 (C₅), 129.4 (C₆), 128.5 (C₁₁), 128.1 (C₁₅), 126.4 (C₁₄), 122.8 (C₁₆), 121.3 (C₉), 113.7 (C₇), 55.3 (OMe), 52.9 (C₂), 36.8 (C₄), 33.0 (C₃). **IR (ATR – neat)** $\tilde{\nu}$ (cm^{-1}) = 3003, 2929, 2833, 1610, 1568, 1431, 1242, 1176, 1033, 827, 746, 699, 536. **HRMS for [C₂₁H₂₂NO]⁺** calculated 304.1696 found 304.1694. **R_f** (1:4 EtOAc/PE) = 0.80.

1,2,3,4,5-pentafluoro-6-(3-(4-methoxyphenyl)propyl)benzene (278)

Obtained following **GP(VI)** at 0.2 mmol scale using 0.4 mmol of 1,2,3,4,5-pentafluoro-6-vinylbenzene. Purification by column chromatography on silica gel (5% EtOAc in hexane) afforded product **278** (40 mg, 0.13 mmol) as colourless oil in 64% yield. **¹H-NMR (400 MHz, CDCl₃)** δ 7.09 (d, $J = 8.6$ Hz, 2H, H₆), 6.83 (d, $J = 8.6$ Hz, 2H, H₇), 3.79 (s, 3H, OMe), 2.71 (t, $J = 7.7$ Hz, 2H, H₂), 2.61 (t, $J = 7.8$ Hz, 2H, H₄), 1.88 (p, $J = 7.7$ Hz, 2H, H₃). **¹³C-NMR (101 MHz, CDCl₃)** δ 157.9 (C₈), 144.9 (dd, $J = 247, 12$ Hz, C₉), 139.4 (d, $J = 249$ Hz, C₁₁), 137.4 (dt, $J = 249, 15$ Hz, C₁₀), 133.2 (C₅), 129.2 (C₆), 115.2 (t, $J = 19$ Hz, C₁), 113.8 (C₇), 55.2 (OMe), 34.5 (C₄), 30.9 (C₃), 22.0 (C₂). **HRMS for [C₁₆H₁₄F₅O]⁺** calculated 317.0959 found 317.0962. **R_f** (1:4 EtOAc/PE) = 0.20. Spectroscopic data were consistent with literature values.^[293]

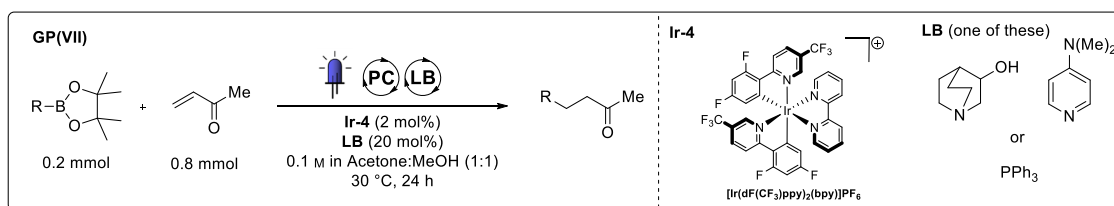
3-(4-methoxybenzyl) chroman-4-one (279)

Obtained following **GP(VI)** at 0.2 mmol scale using 0.4 mmol of 4*H*-chromen-4-one. Purification by column chromatography on silica gel (10% EtOAc in hexane) afforded product **279** (17 mg, 0.064 mmol) as yellowish oil in 32% yield. **¹H-NMR (400 MHz, CDCl₃)** δ 7.86 (dd, $J = 7.8, 1.8$ Hz, 1H, H₉), 7.47 (ddd, $J = 8.6, 7.2, 1.8$ Hz, 1H, H₁₁), 7.17 (d, $J = 8.6$ Hz, 2H, H₅), 7.03 – 6.96 (m, 2H, H₁₀ and H₁₂), 6.87 (d, $J = 8.6$ Hz, 2H, H₆), 4.68 – 4.59 (m, 1H, H₁₄), 3.80 (s, 3H, OMe), 3.15 (dd, $J = 14.1, 6.2$ Hz, 1H, H_{3a}), 2.99 (dd, $J = 14.1, 6.5$ Hz, 1H, H_{2a}), 2.70 – 2.62 (m, 2H, H_{2b} and H_{3b}). **¹³C-NMR (101 MHz, CDCl₃)** δ 192.4 (C₁), 161.5 (C₁₃), 158.6 (C₇), 136.0 (C₁₁), 130.6 (C₄), 128.1 (C₉), 126.9 (C₈), 121.3 (C₁₀), 118.0 (C₁₂), 114.0 (C₆), 78.5 (C₁₄), 55.3 (OMe), 42.1 (C₂), 40.3 (C₃). **IR (ATR – neat)** $\tilde{\nu}$ (cm⁻¹) = 2909, 1736, 1651, 1507, 1132, 1100, 981, 699. **HRMS for [C₁₇H₁₇O₃]⁺** calculated 269.1172 found 269.1175. **R_f** (1:4 EtOAc/PE) = 0.50.

3-(4-methoxybenzyl)-2-phenylchroman-4-one (280)

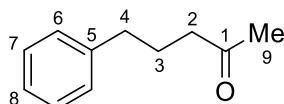
Obtained following **GP(VI)** at 0.2 mmol scale using 0.8 mmol of 3-phenyl-4*H*-chromen-4-one. Purification by column chromatography on silica gel (10% EtOAc in hexane) afforded product **280** (17 mg, 0.064 mmol) as yellowish oil in 22% yield. **¹H-NMR (400 MHz, CDCl₃)** δ 7.69 (d, $J = 7.8$ Hz, 1H, H₉), 7.45 (t, $J = 7.8$ Hz, 1H, H₁₁), 7.31-7.26 (m, 2H, H₁₆), 7.26 – 7.15 (m, 3H, H₁₇ and H₁₈), 7.09 (d, $J = 8.3$ Hz, 1H, H₁₀), 6.90 (d, $J = 8.2$ Hz, 3H, H₅ and H₁₂), 6.75 (d, $J = 8.2$ Hz, 2H, H₆), 3.77 (s, 3H, OMe), 3.31 (d, $J = 14.1$ Hz, 1H, H_{3a}), 3.23 (d, $J = 16.5$ Hz, 1H, H_{2a}), 3.11 (d, $J = 14.1$ Hz, 1H, H_{3b}), 3.08 (d, $J = 16.5$ Hz, 1H, H_{2b}). **¹³C-NMR (101 MHz, CDCl₃)** δ 191.8 (C₁), 159.9 (C₁₃), 158.6 (C₇), 141.1 (C₁₅), 136.1 (C₄), 131.8 (C₅), 128.4 (C₁₁), 127.7 (C₁₇), 127.2 (C₁₆), 126.5 (C₉), 126.2 (C₁₈), 121.4 (C₈), 121.0 (C₁₀), 118.3 (C₁₂), 113.4 (C₆), 85.0 (C₁₄), 55.2 (OMe), 48.7 (C₂), 45.2 (C₃). **IR (ATR – neat)** $\tilde{\nu}$ (cm^{-1}) = 2914, 1687, 1605, 1459, 1302, 1176, 1030, 734, 696. **HRMS for [C₂₃H₂₁O₃]⁺** calculated 345.1485 found 345.1480. **R_f** (1:4 EtOAc/PE) = 0.54.

5.3.2.2 Scope of boronic esters

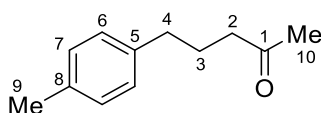


GP(VII): A 5 mL glass vial equipped with a magnetic stir bar was charged with the desired boronic ester (0.20 mmol, 1.0 equiv.), the photoredox catalyst [Ir(dF(CF₃)ppy)₂(bpy)]PF₆ (**Ir-4**, 4.0 mg, 2 mol%) and the Lewis base catalyst (**LB**, 0.04 mmol, 20 mol%). The vial was then sealed with a rubber septum and evacuated/backfilled with argon three times. Methyl vinyl ketone (66 μ L, 0.8 mmol, 4.0 equiv.) was then added followed by 2.0 mL of a degassed acetone/methanol (1:1) mixture to lead a clear yellow transparent 0.1 M solution. This solution was then stirred while irradiated with a commercial blue LED strip (Ledxon, 14.4 W, 470 nm) for 24 hours, the temperature was maintained at 30°C using a desktop fan. The content of the vial was then concentrated *in vacuo* and immobilised on ISOLUTE[®] HM-N for easy dry loading on flash column chromatography to yield the pure product.

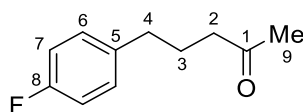
5-phenylpentan-2-one (**285**)



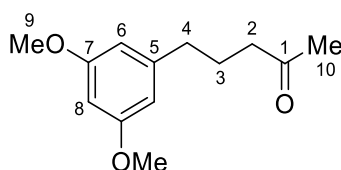
Obtained following **GP(VII)** using 2-benzyl-4,4,5,5-tetramethyl-1,3,2-dioxaborolane (44 mg, 0.20 mmol) and quinuclidin-3-ol (5.0 mg, 40 μ mol, 20 mol%) as Lewis base catalyst. Purification by column chromatography on silica gel (0% to 5% EtOAc in hexane) afforded product **285** (21 mg, 0.13 mmol) as a colourless oil in 65% yield. ¹H-NMR (600 MHz, CDCl₃) δ 7.29 (t, J = 7.6 Hz, 2H, H₇), 7.22 – 7.15 (m, 3H, H₆, H₈), 2.62 (t, J = 7.5 Hz, 2H, H₄), 2.44 (t, J = 7.5 Hz, 2H, H₂), 2.12 (s, 3H, H₉), 1.91 (p, J = 7.5 Hz, 2H, H₃). ¹³C-NMR (151 MHz, CDCl₃) δ 208.9 (C₁), 141.7 (C₅), 128.6 (C₈), 128.5 (C₇), 126.1 (C₆), 43.0 (C₂), 35.2 (C₄), 30.1 (C₉), 25.3 (C₃). HRMS for [C₁₁H₁₅O]⁺ calculated 163.1117 found 163.1121. R_f (1:4 EtOAc/PE) = 0.54. Spectroscopic data were consistent with literature values.^[294]

5-(*p*-tolyl)pentan-2-one (286)

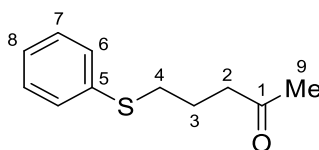
Obtained following **GP(VII)** using 4,4,5,5-tetramethyl-2-(4-methylbenzyl)-1,3,2-dioxaborolane (46 mg, 0.20 mmol) and quinuclidin-3-ol (5.0 mg, 40 μ mol, 20 mol%) as Lewis base catalyst. Purification by column chromatography on silica gel (0% to 5% EtOAc in hexane) afforded product **286** (23 mg, 0.13 mmol) as a colourless oil in 66% yield. **$^1\text{H-NMR}$ (600 MHz, CDCl_3)** δ 7.10 (d, $J = 7.9$ Hz, 2H, H_7), 7.06 (d, $J = 7.9$ Hz, 2H, H_6), 2.59 (t, $J = 7.5$ Hz, 2H, H_4), 2.43 (t, $J = 7.5$ Hz, 2H, H_2), 2.32 (s, 3H, H_9), 2.12 (s, 3H, H_{10}), 1.89 (p, $J = 7.5$ Hz, 2H, H_3). **$^{13}\text{C-NMR}$ (151 MHz, CDCl_3)** δ 209.0 (C_1), 138.6 (C_5), 135.5 (C_8), 129.2 (C_7), 128.5 (C_6), 43.0 (C_2), 34.7 (C_4), 30.1 (C_{10}), 25.4 (C_3), 21.1 (C_9). **HRMS for $[\text{C}_{12}\text{H}_{17}\text{O}]^+$** calculated 177.1274 found 177.1278. **R_f** (1:4 EtOAc/PE) = 0.56. Spectroscopic data were consistent with literature values.^[295]

5-(4-fluorophenyl)pentan-2-one (287)

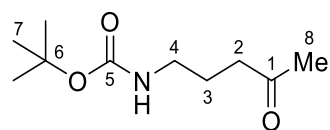
Obtained following **GP(VII)** using 2-(4-fluorobenzyl)-4,4,5,5-tetramethyl-1,3,2-dioxaborolane (47 mg, 0.20 mmol) and quinuclidin-3-ol (5.0 mg, 40 μ mol, 20 mol%) as Lewis base catalyst. Purification by column chromatography on silica gel (0% to 5% EtOAc in hexane) afforded product **287** (28 mg, 0.15 mmol) as a colourless oil in 71% yield. **$^1\text{H-NMR}$ (600 MHz, CDCl_3)** δ 7.12 (m, 2H, H_6), 6.96 (m, 2H, H_7), 2.59 (t, $J = 7.5$ Hz, 2H, H_4), 2.42 (t, $J = 7.5$ Hz, 2H, H_2), 2.12 (s, 3H, H_9), 1.88 (p, $J = 7.5$ Hz, 2H, H_3). **$^{13}\text{C-NMR}$ (151 MHz, CDCl_3)** δ 208.7 (C_1), 161.5 (d, $J = 244$ Hz, C_8), 137.3 (d, $J = 3.3$ Hz, C_5), 129.9 (d, $J = 7.8$ Hz, C_6), 115.3 (d, $J = 21$ Hz, C_7), 42.8 (C_2), 34.3 (C_4), 30.1 (C_9), 25.4 (C_3). **$^{19}\text{F-NMR}$ (376 MHz, CDCl_3)** δ -117.6. **HRMS for $[\text{C}_{11}\text{H}_{14}\text{OF}]^+$** calculated 181.1023 found 181.1022. **R_f** (1:4 EtOAc/PE) = 0.41. Spectroscopic data were consistent with literature values.^[296]

5-(3,5-dimethoxyphenyl)pentan-2-one (288)

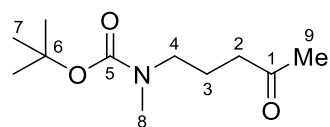
Obtained following **GP(VII)** using 2-(3,5-dimethoxybenzyl)-4,4,5,5-tetramethyl-1,3,2-dioxaborolane (56 mg, 0.20 mmol) and quinuclidin-3-ol (5.0 mg, 40 μ mol, 20 mol%) as Lewis base catalyst. Purification by column chromatography on silica gel (5% to 10% EtOAc in hexane) afforded product **288** (36 mg, 0.13 mmol) as a colourless oil in 63% yield. **$^1\text{H-NMR}$ (600 MHz, CDCl_3)** δ 6.32 (d, $J = 2.3$ Hz, 2H, H₆), 6.30 (t, $J = 2.3$ Hz, 1H, H₈), 3.77 (s, 6H, H₉), 2.56 (t, $J = 7.4$ Hz, 2H, H₄), 2.43 (t, $J = 7.4$ Hz, 2H, H₂), 2.11 (s, 3H, H₁₀), 1.89 (p, $J = 7.4$ Hz, 2H, H₃). **$^{13}\text{C-NMR}$ (151 MHz, CDCl_3)** δ 208.9 (C₁), 160.9 (C₇), 144.1 (C₅), 106.6 (C₆), 98.0 (C₈), 55.4 (C₉), 42.9 (C₂), 35.4 (C₄), 30.1 (C₁₀), 25.0 (C₃). **IR (ATR – neat)** $\tilde{\nu}$ (cm^{-1}) = 3002, 2925, 1713, 1594, 1460, 1428, 1354, 1203, 1147, 1056, 830, 695. **HRMS for $[\text{C}_{13}\text{H}_{19}\text{O}_3]^+$** calculated 223.1329 found 223.1328. **R_f** (1:4 EtOAc/PE) = 0.28.

5-(phenylthio)pentan-2-one (289)

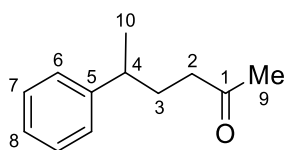
Obtained following **GP(VII)** using 4,4,5,5-tetramethyl-2-((phenylthio)methyl)-1,3,2-dioxaborolane (50 mg, 0.20 mmol) and quinuclidin-3-ol (5.0 mg, 40 μ mol, 20 mol%) as Lewis base catalyst. Purification by column chromatography on silica gel (5% to 7% EtOAc in hexane) afforded product **289** (35 mg, 0.18 mmol) as a colourless oil in 91% yield. Repeating the same procedure with **Mes-Acr-4** instead of **Ir-4** afforded the same product in 80% yield. **$^1\text{H-NMR}$ (600 MHz, CDCl_3)** δ 7.35 – 7.31 (m, 2H, H₆), 7.30 – 7.26 (m, 2H, H₇), 7.20 – 7.14 (m, 1H, H₈), 2.94 (t, $J = 7.0$ Hz, 2H, H₄), 2.60 (t, $J = 7.0$ Hz, 2H, H₂), 2.12 (s, 3H, H₉), 1.90 (p, $J = 7.0$ Hz, 2H, H₃). **$^{13}\text{C-NMR}$ (151 MHz, CDCl_3)** δ 208.1 (C₁), 136.2 (C₅), 129.3 (C₆), 129.0 (C₇), 126.1 (C₈), 42.0 (C₂), 33.1 (C₄), 30.1 (C₉), 23.1 (C₃). **HRMS for $[\text{C}_{11}\text{H}_{15}\text{OS}]^+$** calculated 195.0844 found 195.0838. **R_f** (1:4 EtOAc/PE) = 0.43. Spectroscopic data were consistent with literature values.^[297]

***tert*-butyl (4-oxopentyl)carbamate (290)**

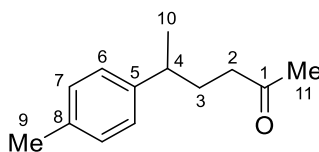
Obtained following **GP(VII)** using *tert*-butyl ((4,4,5,5-tetramethyl-1,3,2-dioxaborolan-2-yl)methyl)carbamate (51 mg, 0.20 mmol, 1.0 equiv.) and PPh₃ (10 mg, 40 μmol, 20 mol%) as Lewis base catalyst. Purification by column chromatography on silica gel (10% to 60% EtOAc and 1% Et₃N in hexane) afforded product **290** (37 mg, 0.19 mmol) as a colourless oil in 91% yield. **¹H-NMR (600 MHz, CDCl₃)** δ 4.60 (s, 1H, NH), 3.13 (m, 2H, H₄), 2.49 (t, *J* = 7.1 Hz, 2H, H₂), 2.16 (s, 3H, H₈), 1.76 (p, *J* = 7.1 Hz, 2H, H₃), 1.44 (s, 9H, H₇). **¹³C-NMR (151 MHz, CDCl₃)** δ 208.6 (C₁), 156.2 (C₅), 79.4 (C₆), 40.9 (C₂), 40.1 (C₄), 30.1 (C₈), 28.6 (C₇), 24.2 (C₃). **HRMS for [C₁₀H₁₉O₃NNa]⁺** calculated 224.1257 found 224.1258. **R_f** (1:1 EtOAc/PE) = 0.50. Spectroscopic data were consistent with literature values.^[95]

***tert*-butyl methyl(4-oxopentyl)carbamate (291)**

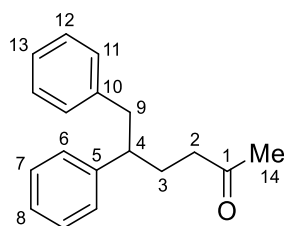
Obtained following **GP(VII)** using *tert*-butyl methyl((4,4,5,5-tetramethyl-1,3,2-dioxaborolan-2-yl)methyl)carbamate (54 mg, 0.20 mmol) and PPh₃ (10 mg, 40 μmol, 20 mol%) as Lewis base catalyst. Purification by column chromatography on silica gel (10% EtOAc and 1% Et₃N in hexane) afforded product **291** (35 mg, 0.16 mmol) as a colourless oil in 86% yield. **¹H-NMR (600 MHz, CDCl₃)** δ 3.19 (t, *J* = 7.1 Hz, 2H, H₄), 2.80 (s, 3H, H₈), 2.41 (t, *J* = 7.1 Hz, 2H, H₂), 2.12 (s, 3H, H₉), 1.75 (p, *J* = 7.1 Hz, 2H, H₃), 1.43 (s, 9H, H₇). **¹³C-NMR (151 MHz, CDCl₃)** δ 208.2 (C₁), 156.0 (C₅), 79.4 (C₆), 47.9 (C₄), 40.5 (C₂), 34.1 (C₈), 30.1 (C₉), 28.6 (C₇), 21.8 (C₃). **HRMS for [C₁₁H₂₁O₃N]⁺** calculated 215.1521 found 215.1519. **R_f** (1:4 EtOAc/PE) = 0.32. Spectroscopic data were consistent with literature values.^[298]

5-phenylhexan-2-one (292)

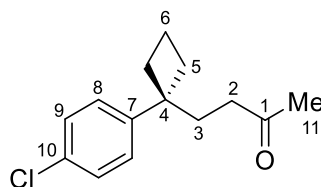
Obtained following **GP(VII)** using 4,4,5,5-tetramethyl-2-(1-phenylethyl)-1,3,2-dioxaborolane (46 mg, 0.20 mmol) and DMAP (4.8 mg, 40 μ mol, 20 mol%) as Lewis base catalyst. Purification by column chromatography on silica gel (0% to 5% EtOAc in hexane) afforded product **292** (24 mg, 0.13 mmol) as a colourless oil in 67% yield. **¹H-NMR (600 MHz, CDCl₃)** δ 7.30 (t, $J = 7.6$ Hz, 2H, H₇), 7.23 – 7.18 (m, 1H, H₈), 7.18 – 7.14 (m, 2H, H₆), 2.74 – 2.64 (m, 1H, H₄), 2.40 – 2.23 (m, 2H, H₂), 2.05 (s, 3H, H₉), 1.91 (ddd, $J = 13.8, 9.3, 6.0$ Hz, 1H, H_{3a}), 1.86 – 1.78 (m, 1H, H_{3b}), 1.26 (d, $J = 6.9$ Hz, 3H, H₁₀). **¹³C-NMR (151 MHz, CDCl₃)** δ 209.1 (C₁), 146.6 (C₅), 128.6 (C₇), 127.1 (C₆), 126.3 (C₈), 42.0 (C₂), 39.5 (C₄), 32.0 (C₃), 30.1 (C₉), 22.6 (C₁₀). **HRMS for [C₁₂H₁₇O]⁺** calculated 177.1274 found 177.1276. **R_f** (1:4 EtOAc/PE) = 0.64. Spectroscopic data were consistent with literature values.^[299]

5-(*p*-tolyl)hexan-2-one (293)

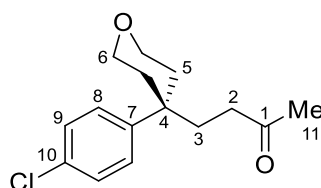
Obtained following **GP(VII)** using 4,4,5,5-tetramethyl-2-(1-(*p*-tolyl)ethyl)-1,3,2-dioxaborolane (50 mg, 0.20 mmol) and DMAP (4.8 mg, 40 μ mol, 20 mol%) as Lewis base catalyst. Purification by column chromatography on silica gel (0% to 5% EtOAc in hexane) afforded product **293** (28 mg, 0.15 mmol) as a colourless oil in 74% yield. **¹H-NMR (600 MHz, CDCl₃)** δ 7.11 (d, $J = 8.0$ Hz, 2H, H₇), 7.06 (d, $J = 8.0$ Hz, 2H, H₆), 2.69 – 2.61 (m, 1H, H₄), 2.36 – 2.23 (m, 5H, H₂ and H₉), 2.06 (s, 3H, H₁₁), 1.89 (m, 1H, H_{3a}), 1.84 – 1.76 (m, 1H, H_{3b}), 1.25 (d, $J = 6.9$ Hz, 3H, H₁₀). **¹³C-NMR (151 MHz, CDCl₃)** δ 209.1 (C₁), 143.5 (C₅), 135.7 (C₈), 129.3 (C₇), 127.0 (C₆), 42.0 (C₂), 39.1 (C₄), 32.0 (C₃), 30.1 (C₁₁), 22.7 (C₁₀), 21.1 (C₉). **HRMS for [C₁₃H₁₉O]⁺** calculated 191.1430 found 191.1429. **R_f** (1:4 EtOAc/PE) = 0.49. Spectroscopic data were consistent with literature values.^[300]

5,6-diphenylhexan-2-one (294)

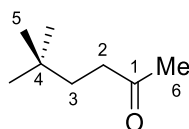
Obtained following **GP(VII)** using 2-(1,2-diphenylethyl)-4,4,5,5-tetramethyl-1,3,2-dioxaborolane (62 mg, 0.20 mmol) and DMAP (4.8 mg, 40 μ mol, 20 mol%) as Lewis base catalyst. Purification by column chromatography on silica gel (0% to 5% EtOAc in hexane) afforded product **294** (27 mg, 0.11 mmol) as a colourless oil in 55% yield. **¹H-NMR (600 MHz, CDCl₃)** δ 7.30 – 7.24 (m, 2H, H₁₂), 7.22 – 7.17 (m, 3H, H₆, H₈), 7.16 – 7.12 (m, 1H, H₁₃), 7.11 – 7.08 (m, 2H, H₇), 7.05 – 7.02 (m, 2H, H₁₁), 2.95 – 2.84 (m, 2H, H₉), 2.79 (m, 1H, H₄), 2.30 – 2.16 (m, 2H, H₂), 2.06 – 1.97 (m, 4H, H₁₄ and H_{3a}), 1.85 (dddd, J = 14.2, 10.7, 8.9, 5.8 Hz, 1H, H_{3b}). **¹³C-NMR (151 MHz, CDCl₃)** δ 208.9 (C₁), 144.2 (C₁₀), 140.4 (C₅), 129.2 (C₁₁), 128.6 (C₁₂), 128.2 (C₆), 127.9 (C₇), 126.5 (C₈), 126.0 (C₁₃), 47.4 (C₄), 44.1 (C₉), 41.9 (C₂), 30.0 (C₁₄), 29.3 (C₃). **IR (ATR – neat)** $\tilde{\nu}$ (cm^{-1}) = 3002, 2923, 1713, 1495, 1452, 1358, 1158, 758, 698. **HRMS for [C₁₈H₂₁O]⁺** calculated 253.1587 found 253.1586. **R_f** (1:4 EtOAc/PE) = 0.58.

4-(1-(4-chlorophenyl)cyclobutyl)butan-2-one (297)

Obtained following **GP(VII)** at 0.2 mmol scale using DMAP (4.8 mg, 40 μ mol, 20 mol%) as Lewis base catalyst. Purification by column chromatography on silica gel (2% EtOAc in hexane) afforded product **297** (32 mg, 0.13 mmol) as a colourless oil in 66% yield. **¹H-NMR (600 MHz, CDCl₃)** δ 7.26 (d, J = 7.9 Hz, 2H, H₉), 7.03 (d, J = 8.1 Hz, 2H, H₈), 2.36 – 2.26 (m, 2H, H_{5a}), 2.18 – 2.03 (m, 7H, H_{5b}, H_{6b}, H₃ and H₂), 2.03 (s, 3H, H₁₁), 1.89 – 1.79 (m, 1H, H_{6a}). **¹³C-NMR (151 MHz, CDCl₃)** δ 208.8 (C₁), 147.8 (C₇), 131.2 (C₁₀), 128.2 (C₉), 127.1 (C₈), 45.3 (C₄), 39.2 (C₂), 35.7 (C₃), 32.5 (C₅), 29.9 (C₁₁), 15.8 (C₆). **IR (ATR – neat)** $\tilde{\nu}$ (cm^{-1}) = 2976, 2952, 2853, 1715, 1491, 1364, 1245, 1161, 1092, 1013, 828, 721. **HRMS for [C₁₄H₁₈OCl]⁺** calculated 237.1046 found 237.1037. **R_f** (1:4 EtOAc/PE) = 0.47.

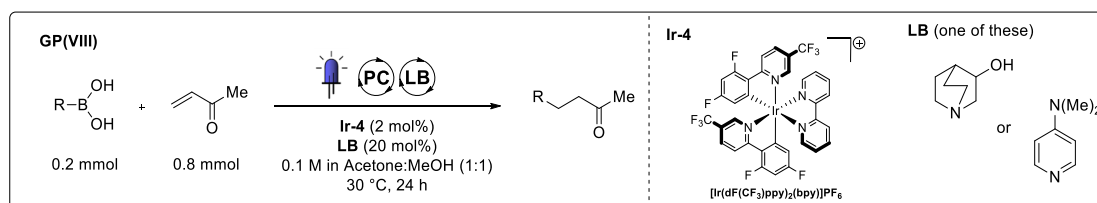
4-(4-(4-chlorophenyl)tetrahydro-2H-pyran-4-yl)butan-2-one (298)

Obtained following **GP(VII)** at 0.2 mmol scale using DMAP (4.8 mg, 40 μmol , 20 mol%) as Lewis base catalyst. Purification by column chromatography on silica gel (10% EtOAc in hexane) afforded product **298** (27 mg, 0.10 mmol) as a colourless oil in 51% yield. **$^1\text{H-NMR}$ (600 MHz, CDCl_3)** δ 7.33 (d, $J = 8.6$ Hz, 2H, H_9), 7.19 (d, $J = 8.6$ Hz, 2H, H_8), 3.80 – 3.76 (m, 2H, H_{6a}), 3.55 – 3.51 (m, 2H, H_{6b}), 2.10 – 2.03 (m, 4H, H_2 and H_{5a}), 2.00 (s, 3H, H_{11}), 1.91 – 1.87 (m, 2H, H_3), 1.83 – 1.78 (m, 2H, H_{5b}). **$^{13}\text{C-NMR}$ (151 MHz, CDCl_3)** δ 208.2 (C_1), 143.2 (C_7), 132.0 (C_{10}), 128.7 (C_9), 128.2 (C_8), 64.1 (C_6), 38.4 (C_2), 37.8 (C_3), 36.2 (C_4), 36.1 (C_5), 29.9 (C_{11}). **IR (ATR – neat)** $\tilde{\nu}$ (cm^{-1}) = 2948, 2857, 1714, 1494, 1360, 1241, 1114, 1094, 1012, 824. **HRMS for $[\text{C}_{15}\text{H}_{20}\text{O}_2\text{Cl}]^+$** calculated 267.1152 found 267.1149. **R_f** (1:4 EtOAc/PE) = 0.14.

5,5-dimethylhexan-2-one (299)

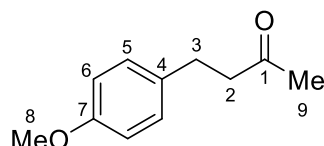
Obtained following **GP(VII)** at 0.2 mmol scale using DMAP (4.8 mg, 40 μmol , 20 mol%) as Lewis base catalyst. Purification by column chromatography on silica gel (5% Et_2O in pentane) afforded product **299** (11 mg, 0.09 mmol) as a colourless oil in 45% yield. Repeating the same procedure with **Mes-Acr-4** instead of **Ir-4** afforded the same product in 35% yield. **$^1\text{H-NMR}$ (600 MHz, CDCl_3)** δ 2.42 – 2.36 (m, 2H, H_3), 2.15 (s, 3H, H_6), 1.50 – 1.45 (m, 2H, H_2), 0.88 (s, 9H, H_5). **$^{13}\text{C-NMR}$ (151 MHz, CDCl_3)** δ 209.8 (C_1), 39.7 (C_2), 37.5 (C_3), 30.1 (C_4), 30.0 (C_6), 29.3 (C_5). **HRMS for $[\text{C}_8\text{H}_{17}\text{O}]^+$** calculated 129.1274 found 129.1269. **R_f** (1:4 EtOAc/PE) = 0.66. Spectroscopic data were consistent with literature values.^[301]

5.3.2.3 Scope of boronic acids

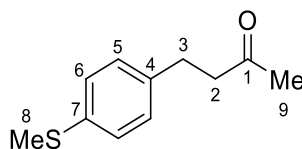


GP(VIII): A 5 mL glass vial equipped with a magnetic stir bar was charged with the desired boronic acid (0.20 mmol, 1.0 equiv.), the photoredox catalyst $[\text{Ir}(\text{dF}(\text{CF}_3)\text{ppy})_2(\text{bpy})]\text{PF}_6$ (**Ir-4**, 2.0 mg, 2.0 mol%) and the Lewis base catalyst (0.04 mmol, 20 mol%). The vial was then sealed with a rubber septum and evacuated/backfilled with argon three times. Methyl vinyl ketone (66 μL , 0.8 mmol, 4.0 equiv.) was then added followed by 2.0 mL of a degassed acetone/methanol (1:1) mixture to lead a clear yellow transparent 0.1 M solution. This solution was then stirred while irradiated with a commercial blue LED strip (Ledxon, 14.4 W, 470 nm) for 24 hours, the temperature was maintained at 30°C using a desktop fan. The content of the vial was then concentrated *in vacuo* and immobilised on ISOLUTE[®] HM-N for easy dry loading on flash column chromatography to yield the pure product.

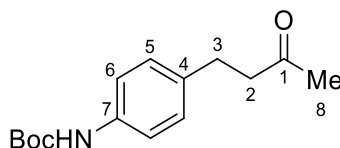
4-(4-methoxyphenyl)butan-2-one (**308**)



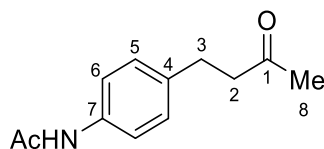
Obtained following **GP(VIII)** at 0.2 mmol scale using quinuclidin-3-ol (5.0 mg, 40 μmol , 20 mol%) as Lewis base catalyst. Purification by column chromatography on silica gel (3% EtOAc in hexane) afforded product **308** (21 mg, 0.12 mmol) as a colourless oil in 60% yield. ¹H-NMR (600 MHz, CDCl₃) δ 7.10 (d, J = 8.6 Hz, 2H, H₅), 6.82 (d, J = 8.6 Hz, 2H, H₆), 3.78 (s, 3H, H₈), 2.83 (t, J = 7.6 Hz, 2H, H₃), 2.72 (t, J = 7.6 Hz, 2H, H₂), 2.13 (s, 3H, H₉). ¹³C-NMR (151 MHz, CDCl₃) δ 208.2 (C₉), 158.1 (C₇), 133.1 (C₄), 129.3 (C₅), 114.0 (C₆), 55.4 (C₈), 45.6 (C₂), 30.2 (C₃), 29.0 (C₉). IR (ATR – neat) $\tilde{\nu}$ (cm^{-1}) = 3004, 2921, 2833, 1713, 1611, 1510, 1362, 1300, 1241, 1179, 1157, 1033, 820. HRMS for $[\text{C}_{11}\text{H}_{14}\text{O}_2]^+$ calculated 178.0994 found 178.0987. R_f (1:4 EtOAc/PE) = 0.25.

4-(4-(methylthio)phenyl)butan-2-one (309)

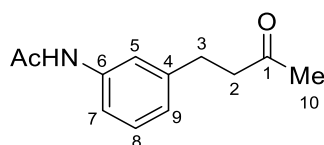
Obtained following **GP(VIII)** at 0.2 mmol scale using quinuclidin-3-ol (5.0 mg, 40 μ mol, 20 mol%) as Lewis base catalyst. Purification by column chromatography on silica gel (3% EtOAc in hexane) afforded product **309** (28 mg, 0.144 mmol) as a pinkish oil in 72% yield. **$^1\text{H-NMR}$ (600 MHz, CDCl_3)** δ 7.16 (d, $J = 8.3$ Hz, 2H, H_6), 7.08 (d, $J = 8.2$ Hz, 2H, H_5), 2.82 (d, $J = 7.6$ Hz, 2H, H_3), 2.71 (t, $J = 7.6$ Hz, 2H, H_2), 2.43 (s, 3H, H_8), 2.11 (s, 3H, H_9). **$^{13}\text{C-NMR}$ (151 MHz, CDCl_3)** δ 207.7 (C_1), 138.0 (C_4), 135.7 (C_7), 128.8 (C_5), 127.1 (C_6), 45.0 (C_2), 30.0 (C_3), 29.1 (C_9), 16.1 (C_8). **IR (ATR – neat)** $\tilde{\nu}$ (cm^{-1}) = 2988, 2921, 1715, 1495, 1439, 1407, 1360, 1161, 1096, 1017, 967, 807. **HRMS for $[\text{C}_{11}\text{H}_{14}\text{O}_2]^+$** calculated 194.0765 found 194.0761. **R_f** (1:4 EtOAc/PE) = 0.34.

tert-butyl (4-(3-oxobutyl)phenyl)carbamate (310)

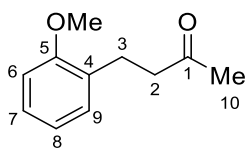
Obtained following **GP(VIII)** at 0.2 mmol scale using quinuclidin-3-ol (5.0 mg, 40 μ mol, 20 mol%) as Lewis base catalyst. Purification by column chromatography on silica gel (15% EtOAc in hexane) afforded product **310** (35 mg, 0.13 mmol) as white needles in 67% yield. **$^1\text{H-NMR}$ (600 MHz, CDCl_3)** δ 7.26 (d, $J = 8.2$ Hz, 2H, H_6), 7.08 (d, $J = 8.2$ Hz, 2H, H_5), 6.55 (bs, 1H, NHBoc), 2.82 (t, $J = 7.6$ Hz, 2H, H_3), 2.71 (t, $J = 7.6$ Hz, 2H, H_2), 2.11 (s, 3H, H_8), 1.50 (s, 9H, NHCOOtBu). **$^{13}\text{C-NMR}$ (151 MHz, CDCl_3)** δ 208.2 (C_1), 153.0 (NHCOOtBu), 136.6 (C_7), 135.7 (C_4), 128.9 (C_5), 118.9 (C_6), 80.5 ($\text{NHCOOC}(\text{CH}_3)_3$), 45.3 (C_2), 30.2 (C_3), 29.2 (C_8), 28.4 ($\text{NHCOOC}(\text{CH}_3)_3$). **IR (ATR – neat)** $\tilde{\nu}$ (cm^{-1}) = 3675, 3333, 2972, 2925, 1709, 1598, 1526, 1413, 1366, 1314, 1235, 1157, 1056, 819, 773. **HRMS for $[\text{C}_{15}\text{H}_{21}\text{NO}_3]^+$** calculated 263.1521 found 263.1511. **R_f** (2:3 EtOAc/PE) = 0.48. **M.p.** = 96–98°C

N-(4-(3-oxobutyl)phenyl)acetamide (311)

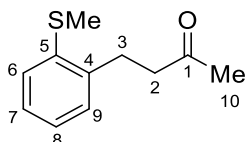
Obtained following **GP(VIII)** at 0.2 mmol scale using quinuclidin-3-ol (5.0 mg, 40 μ mol, 20 mol%) as Lewis base catalyst. Purification by column chromatography on silica gel (60% EtOAc in hexane) afforded product **311** (32 mg, 0.16 mmol) as white needles in 78% yield. **$^1\text{H-NMR}$ (600 MHz, CDCl_3)** δ 7.63 (bs, 1H, NHAc), 7.39 (d, $J = 8.5$ Hz, 2H, H₆), 7.10 (d, $J = 8.4$ Hz, 2H, H₅), 2.84 (t, $J = 7.5$ Hz, 2H, H₂), 2.72 (t, $J = 7.5$ Hz, 2H, H₃), 2.13 (s, 3H, H₈), 2.12 (s, 3H, NHCOMe). **$^{13}\text{C-NMR}$ (151 MHz, CDCl_3)** 208.3 (C₁), 168.6 (NHCOMe), 137.0 (C₇), 136.2 (C₄), 128.9 (C₅), 120.3 (C₆), 45.2 (C₂), 30.2 (C₃), 29.2 (C₈), 24.6 (NHCOMe). **IR (ATR – neat)** $\tilde{\nu}$ (cm^{-1}) = 3294, 3123, 3060, 2937, 1711, 1665, 1606, 1534, 1514, 1411, 1370, 1316, 1263, 1161, 819. **HRMS for $[\text{C}_{12}\text{H}_{15}\text{NO}_2]^+$** calculated 205.1103 found 205.1099. **R_f** (EtOAc) = 0.33. **M.p.** = 104–106°C.

N-(3-(3-oxobutyl)phenyl)acetamide (312)

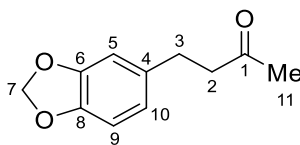
Obtained following **GP(VIII)** at 0.2 mmol scale using quinuclidin-3-ol (5.0 mg, 40 μ mol, 20 mol%) as Lewis base catalyst. Purification by column chromatography on silica gel (40% EtOAc in hexane) afforded product **312** (34 mg, 0.17 mmol) as a colourless oil in 83% yield. **$^1\text{H-NMR}$ (600 MHz, CDCl_3)** δ 7.38 (br s, 1H, NHAc), 7.36 – 7.27 (m, 2H, H₅ and H₇), 7.21 (t, $J = 7.8$ Hz, 1H, H₈), 6.92 (d, $J = 7.6$ Hz, 1H, H₉), 2.87 (t, $J = 7.5$ Hz, 2H, H₃), 2.75 (t, $J = 7.5$ Hz, 2H, H₂), 2.16 (s, 3H, H₁₁), 2.13 (s, 3H, H₁₀). **$^{13}\text{C-NMR}$ (151 MHz, CDCl_3)** δ 208.3 (C₁), 168.6 (NHCOMe), 142.1 (C₄), 138.1 (C₆), 129.2 (C₈), 124.4 (C₉), 119.8 (C₅), 117.7 (C₇), 45.1 (C₂), 30.3 (C₃), 29.7 (C₁₀), 24.8 (NHCOMe). **IR (ATR – neat)** $\tilde{\nu}$ (cm^{-1}) = 3298, 2964, 2929, 1713, 1669, 1611, 1594, 1552, 1491, 1437, 1421, 1372, 1314, 1262, 1161, 789, 698. **HRMS for $[\text{C}_{12}\text{H}_{15}\text{NO}_2]^+$** calculated 205.1103 found 205.1097. **R_f** (Et₂O) = 0.40.

4-(2-methoxyphenyl)butan-2-one (313)

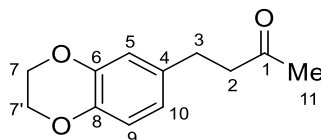
Obtained following **GP(VIII)** at 0.2 mmol scale using quinuclidin-3-ol (5.0 mg, 40 μ mol, 20 mol%) as Lewis base catalyst. Purification by column chromatography on silica gel (5% EtOAc in hexane) afforded product **313** (18 mg, 0.10 mmol) as a colourless oil in 51% yield. **$^1\text{H-NMR}$ (600 MHz, CDCl_3)** δ 7.19 (t, $J = 7.8$ Hz, 1H, H₇), 7.13 (d, $J = 7.4$ Hz, 1H, H₉), 6.87 (t, $J = 7.4$ Hz, 1H, H₈), 6.84 (d, $J = 7.8$ Hz, 1H, H₆), 3.82 (s, 3H, OMe), 2.88 (t, $J = 7.7$ Hz, 2H, H₃), 2.72 (t, $J = 7.7$ Hz, 2H, H₂), 2.14 (s, 3H, H₁₀). **$^{13}\text{C-NMR}$ (151 MHz, CDCl_3)** δ 208.8 (C₁), 157.5 (C₅), 130.0 (C₉), 129.4 (C₄), 127.6 (C₇), 120.6 (C₈), 110.3 (C₆), 55.3 (OMe), 43.8 (C₂), 30.0 (C₁₀), 25.1 (C₃). **IR (ATR – neat)** $\tilde{\nu}$ (cm^{-1}) = 3004, 2956, 2933, 2837, 1713, 1602, 1588, 1494, 1465, 1441, 1358, 1241, 1161, 1116, 1035, 753. **HRMS for $[\text{C}_{11}\text{H}_{14}\text{O}_2]^+$** calculated 178.0994 found 178.0988. **R_f** (1:4 EtOAc/PE) = 0.36.

4-(2-(methylthio)phenyl)butan-2-one (314)

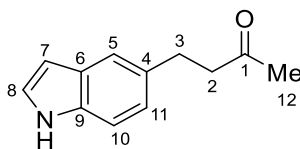
Obtained following **GP(VIII)** at 0.2 mmol scale using quinuclidin-3-ol (5.0 mg, 40 μ mol, 20 mol%) as Lewis base catalyst. Purification by column chromatography on silica gel (3% EtOAc in hexane) afforded product **314** (23 mg, 0.12 mmol) as a colourless oil in 60% yield. **$^1\text{H-NMR}$ (600 MHz, CDCl_3)** δ 7.24 – 7.18 (m, 2H, H₆ and H₇), 7.15 (d, $J = 8.0$ Hz, 1H, H₉), 7.09 (ddd, $J = 8.0, 6.0, 2.6$ Hz, 1H; H₈), 2.99 (dd, $J = 8.6, 6.9$ Hz, 2H, H₃), 2.78 (dd, $J = 8.5, 7.0$ Hz, 2H, H₂), 2.47 (s, 3H, SMe), 2.16 (s, 3H, H₁₀). **$^{13}\text{C-NMR}$ (151 MHz, CDCl_3)** δ 208.0 (C₁), 138.7 (C₅), 137.1 (C₄), 129.2 (C₉), 127.0 (C₆), 125.6 (C₇), 125.1 (C₈), 43.5 (C₂), 29.9 (C₃), 27.9 (C₁₀), 15.7 (SMe). **IR (ATR – neat)** $\tilde{\nu}$ (cm^{-1}) = 3060, 2921, 1715, 1590, 1471, 1439, 1358, 1286, 1159, 1068, 967, 957, 747. **HRMS for $[\text{C}_{11}\text{H}_{15}\text{OS}]^+$** calculated 195.0844 found 195.0838. **R_f** (1:4 EtOAc/PE) = 0.40.

4-(benzo[d][1,3]dioxol-5-yl)butan-2-one (315)

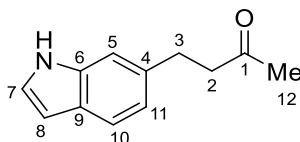
Obtained following **GP(VIII)** at 0.2 mmol scale using quinuclidin-3-ol (5.0 mg, 40 μ mol, 20 mol%) as Lewis base catalyst. Purification by column chromatography on silica gel (5% EtOAc in hexane) afforded product **315** (18 mg, 0.092 mmol) as an amorphous solid in 46% yield. Repeating the same procedure with **Mes-Acr-4** instead of **Ir-4** afforded the same product in 70% yield. **$^1\text{H-NMR}$ (600 MHz, CDCl_3)** δ 6.71 (d, $J = 7.9$ Hz, 1H, H_9), 6.66 (d, $J = 1.7$ Hz, 1H, H_5), 6.61 (dd, $J = 8.0, 1.7$ Hz, 1H, H_{10}), 5.90 (s, 2H, H_7), 2.80 (t, $J = 7.6$ Hz, 2H, H_3), 2.70 (t, $J = 7.6$ Hz, 2H, H_2), 2.12 (s, 3H, H_{11}). **$^{13}\text{C-NMR}$ (151 MHz, CDCl_3)** δ 208.0 (C_1), 147.7 (C_6), 145.9 (C_8), 134.9 (C_4), 121.1 (C_{10}), 108.9 (C_5), 108.3 (C_9), 100.9 (C_7), 45.5 (C_2), 30.2 (C_3), 29.6 (C_{11}). **IR (ATR – neat)** $\tilde{\nu}$ (cm^{-1}) = 2921, 2897, 2782, 1713, 1504, 1489, 1443, 1360, 1245, 1187, 1159, 1096, 1035, 922, 803, 773. **HRMS for $[\text{C}_{11}\text{H}_{12}\text{O}_3]^+$** calculated 192.0786 found 192.0782. **R_f** (1:4 EtOAc/PE) = 0.27.

4-(2,3-dihydrobenzo[b][1,4]dioxin-6-yl)butan-2-one (316)

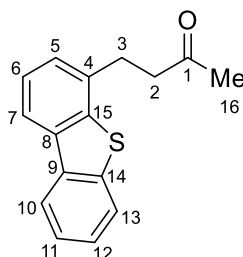
Obtained following **GP(VIII)** at 0.2 mmol scale using quinuclidin-3-ol (5.0 mg, 40 μ mol, 20 mol%) as Lewis base catalyst. Purification by column chromatography on silica gel (5% EtOAc in hexane) afforded product **316** (27 mg, 0.13 mmol) as an amorphous solid in 65% yield. **$^1\text{H-NMR}$ (600 MHz, CDCl_3)** δ 6.76 (d, $J = 8.0$ Hz, 1H, H_9), 6.68 (d, $J = 2.1$ Hz, 1H, H_5), 6.64 (dd, $J = 8.2, 2.2$ Hz, 1H, H_{10}), 4.26 – 4.17 (m, 4H, H_7 and $\text{H}_{7'}$), 2.78 (t, $J = 7.5$ Hz, 2H, H_3), 2.70 (t, $J = 7.5$ Hz, 2H, H_2), 2.13 (s, 3H, H_{11}). **$^{13}\text{C-NMR}$ (151 MHz, CDCl_3)** δ 208.1 (C_1), 143.4 (C_6), 141.9 (C_8), 134.3 (C_4), 121.3 (C_{10}), 117.3 (C_9), 117.0 (C_5), 64.5 (C_7 or $\text{C}_{7'}$), 64.4 (C_7 or $\text{C}_{7'}$), 45.4 (C_2), 30.2 (C_3), 29.1 (C_{11}). **IR (ATR – neat)** $\tilde{\nu}$ (cm^{-1}) = 2976, 2925, 2873, 1715, 1590, 1508, 1431, 1364, 1308, 1282, 1259, 1205, 1161, 1126, 1066, 1050, 918, 888, 807. **HRMS for $[\text{C}_{12}\text{H}_{14}\text{O}_3]^+$** calculated 206.0942 found 206.0934. **R_f** (1:4 EtOAc/PE) = 0.24.

4-(1H-indol-5-yl)butan-2-one (317)

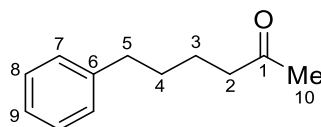
Obtained following **GP(VIII)** at 0.2 mmol scale using quinuclidin-3-ol (5.0 mg, 40 μ mol, 20 mol%) as Lewis base catalyst. Purification by column chromatography on silica gel (15% EtOAc in hexane) afforded product **317** (18 mg, 0.096 mmol) as a colourless oil in 48% yield. **$^1\text{H-NMR}$ (600 MHz, CDCl_3)** δ 8.18 (bs, 1H, NH), 7.45 (s, 1H, H₅), 7.31 (d, $J = 8.3$ Hz, 1H, H₁₀), 7.18 (t, $J = 2.8$ Hz, 1H, H₈), 7.03 (dd, $J = 8.3, 1.7$ Hz, 1H; H₁₁), 6.50 (ddd, $J = 3.1, 2.0, 0.9$ Hz, 1H, H₇), 3.01 (t, $J = 7.7$ Hz, 2H, H₃), 2.81 (t, $J = 7.7$ Hz, 2H, H₂), 2.15 (s, 3H, H₁₂). **$^{13}\text{C-NMR}$ (151 MHz, CDCl_3)** δ 208.9 (C₁), 134.6 (C₉), 132.4 (C₄), 128.2 (C₆), 124.6 (C₈), 122.8 (C₁₁), 119.9 (C₅), 111.1 (C₁₀), 102.3 (C₇), 46.3 (C₂), 30.3 (C₁₂), 30.1 (C₃). **IR (ATR – neat)** $\tilde{\nu}$ (cm^{-1}) = 3675, 3400, 2996, 2972, 1707, 1479, 1413, 1362, 1221, 1161, 1066, 729. **HRMS for $[\text{C}_{12}\text{H}_{13}\text{NO}]^+$** calculated 187.0997 found 187.0992. **R_f** (2:3 EtOAc/PE) = 0.52.

4-(1H-indol-6-yl)butan-2-one (318)

Obtained following **GP(VIII)** at 0.2 mmol scale using quinuclidin-3-ol (5.0 mg, 40 μ mol, 20 mol%) as Lewis base catalyst. Purification by column chromatography on silica gel (15% EtOAc in hexane) afforded product **318** (20 mg, 0.11 mmol) as a colourless oil in 55% yield. **$^1\text{H-NMR}$ (600 MHz, CDCl_3)** δ 8.23 (bs, 1H, NH), 7.57 (d, $J = 8.1$ Hz, 1H, H₁₀), 7.20 (dt, $J = 1.6, 0.8$ Hz, 1H, H₅), 7.14 (dd, $J = 3.2, 2.4$ Hz, 1H, H₇), 6.97 (dd, $J = 8.1, 1.5$ Hz, 1H, H₁₁), 6.52 (ddd, $J = 3.1, 2.0, 1.0$ Hz, 1H, H₈), 3.02 (t, $J = 7.7$ Hz, 2H, H₃), 2.82 (t, $J = 7.7$ Hz, 2H, H₂), 2.14 (s, 3H, H₁₂). **$^{13}\text{C-NMR}$ (151 MHz, CDCl_3)** δ 208.8 (C₁), 136.2 (C₆), 134.9 (C₄), 126.3 (C₉), 124.1 (C₇), 120.7 (C₁₁), 120.6 (C₁₀), 110.7 (C₅), 102.4 (C₈), 46.0 (C₃), 30.3 (C₁₂), 30.3 (C₃). **IR (ATR – neat)** $\tilde{\nu}$ (cm^{-1}) = 3400, 2960, 2921, 2853, 1703, 1625, 1510, 1455, 1403, 1346, 1274, 1249, 1161, 1092, 896, 866, 807, 769, 725. **HRMS for $[\text{C}_{12}\text{H}_{13}\text{NO}]^+$** calculated 187.0997 found 187.0992. **R_f** (2:3 EtOAc/PE) = 0.49.

4-(dibenzo[b,d]thiophen-4-yl)butan-2-one (319)

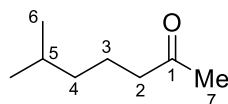
Obtained following **GP(VIII)** at 0.2 mmol scale using quinuclidin-3-ol (5.0 mg, 40 μ mol, 20 mol%) as Lewis base catalyst. Purification by column chromatography on silica gel (10% EtOAc in hexane) afforded product **319** (35 mg, 0.14 mmol) as a yellowish solid in 69% yield. **$^1\text{H-NMR}$ (600 MHz, CDCl_3)** δ 8.16 – 8.08 (m, 1H, H₁₀), 8.01 (d, $J = 7.7$ Hz, 1H, H₇), 7.90 – 7.82 (m, 1H, H₁₃), 7.48 – 7.43 (m, 2H, H₁₁ and H₁₂), 7.41 (t, $J = 7.6$ Hz, 1H, H₆), 7.28 (d, $J = 7.2$ Hz, 1H, H₅), 3.18 (t, $J = 7.7$ Hz, 2H, H₃), 2.93 (t, $J = 7.7$ Hz, 2H, H₂), 2.17 (s, 3H, H₁₆). **$^{13}\text{C-NMR}$ (151 MHz, CDCl_3)** δ 207.6 (C₁), 139.0 (C₁₄ or C₁₅), 138.9 (C₁₅ or C₁₄), 136.2 (C₈ or C₉), 135.9 (C₉ or C₈), 135.2 (C₄), 126.8 (C₁₂), 126.3 (C₅), 125.0 (C₆), 124.5 (C₁₁), 122.9 (C₁₀), 121.8 (C₁₃), 119.7 (C₇), 42.7 (C₂), 30.1 (C₃), 29.0 (C₁₆). **IR (ATR – neat)** $\tilde{\nu}$ (cm^{-1}) = 3063, 2905, 1713, 1582, 1443, 1403, 1356, 1161, 1054, 1021, 791, 706. **HRMS for [C₁₆H₁₅O³²S]⁺** calculated 255.0838 found 255.0834. **R_f** (2:3 EtOAc/PE) = 0.60. **M.p.** = 85–87°C

6-phenylhexan-2-one (324)

Obtained following **GP(VIII)** at 0.2 mmol scale using DMAP (4.8 mg, 40 μ mol, 20 mol%) as Lewis base catalyst. Purification by column chromatography on silica gel (3% EtOAc in hexane) afforded product **324** (25 mg, 0.14 mmol) as colourless oil in 70% yield. Repeating the same procedure with **Mes-Acr-4** instead of **Ir-4** afforded the same product in 89% yield. **$^1\text{H-NMR}$ (600 MHz, CDCl_3)** δ 7.31 – 7.26 (m, 2H, H₈), 7.21 – 7.16 (m, 3H, H₇ and H₉), 2.67 – 2.60 (m, 2H, H₅), 2.48 – 2.42 (m, 2H, H₂), 2.13 (s, 3H, H₁₀), 1.67 – 1.60 (m, 4H, H₂ and H₃). **$^{13}\text{C-NMR}$ (151 MHz, CDCl_3)** δ 208.9 (C₁), 142.2 (C₆), 128.4 (C₇), 128.3 (C₈), 125.7 (C₉), 43.6 (C₂), 35.7 (C₅), 30.9 (C₁₀), 29.9 (C₄), 23.5 (C₃). **IR (ATR – neat)** $\tilde{\nu}$ (cm^{-1}) = 2989, 2922,

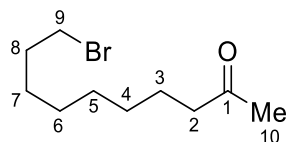
1712, 1454, 1356, 1159, 1031, 745, 699. **HRMS for [C₁₂H₁₇NO]⁺** calculated 177.1279 found 177.1279. **R_f** (1:4 EtOAc/PE) = 0.43.

6-methylheptan-2-one (325)

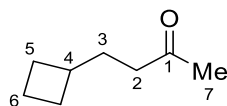


Obtained following **GP(VIII)** at 0.2 mmol scale using DMAP (4.8 mg, 40 μ mol, 20 mol%) as Lewis base catalyst. Purification by column chromatography on silica gel (10% Et₂O in pentane) afforded product **325** (15 mg, 0.12 mmol) as colourless oil in 60% yield. **¹H-NMR (600 MHz, CDCl₃)** δ 2.40 (t, J = 7.5 Hz, 2H, H₂), 2.13 (s, 3H, H₇), 1.60 – 1.54 (m, 3H, H₃ and H₅), 1.19 – 1.08 (m, 2H, H₄), 0.87 (d, J = 6.6 Hz, 6H, H₆). **¹³C-NMR (151 MHz, CDCl₃)** δ 209.4 (C₁), 44.0 (C₂), 38.4 (C₄), 29.8 (C₅), 27.8 (C₇), 22.5 (C₆), 21.7 (C₃). **HRMS for [C₈H₁₇O]⁺** calculated 129.1274 found 129.1268. **R_f** (1:4 EtOAc/PE) = 0.43. Spectroscopic data were consistent with literature values.^[302]

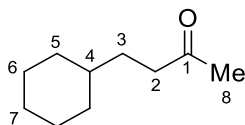
10-bromodecan-2-one (326)



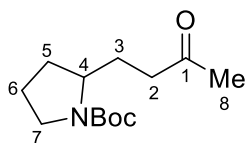
Obtained following **GP(VIII)** at 0.2 mmol scale using DMAP (4.8 mg, 40 μ mol, 20 mol%) as Lewis base catalyst. Filtration on silica gel (5% EtOAc in hexane) afforded product **326** (33 mg, 0.14 mmol) as colourless oil in 71% yield. Repeating the same procedure with **Mes-Acr-4** instead of **Ir-4** afforded the same product in 55% yield. **¹H-NMR (600 MHz, CDCl₃)** δ 3.39 (t, J = 6.8 Hz, 2H, H₉), 2.41 (t, J = 7.4 Hz, 2H, H₂), 2.12 (s, 3H, H₁₀), 1.84 (p, J = 7.0 Hz, 2H, H₈), 1.60 – 1.49 (m, 2H, H₃), 1.44 – 1.38 (m, 2H, H₇), 1.34 – 1.26 (m, 6H, H₄, H₅ and H₆). **¹³C-NMR (151 MHz, CDCl₃)** δ 209.2 (C₁), 43.7 (C₂), 34.0 (C₉), 32.7 (C₈), 29.9 (C₁₀), 29.2 (C₅), 29.0 (C₆), 28.5 (C₄), 28.1 (C₇), 23.7 (C₃). **HRMS for [C₁₀H₂₀OBr]⁺** calculated 235.0698 found 235.0693. **R_f** (1:4 EtOAc/PE) = 0.44. Spectroscopic data were consistent with literature values.^[303]

4-cyclobutylbutan-2-one (327)

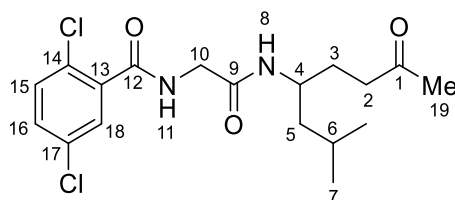
Obtained following **GP(VIII)** at 0.2 mmol scale using DMAP (4.8 mg, 40 μmol , 20 mol%) as Lewis base catalyst. Purification by column chromatography on silica gel (5% Et_2O in pentane) afforded product **327** (17 mg, 0.14 mmol) as colourless oil in 68% yield. $^1\text{H-NMR}$ (600 MHz, CDCl_3) δ 2.31 (t, $J = 7.6$ Hz, 2H, H_2), 2.25 – 2.16 (m, 1H, H_4), 2.11 (s, 3H, H_8), 2.05 – 1.97 (m, 2H, H_{5a}), 1.86 – 1.74 (m, 2H, H_{5b}), 1.64 (q, $J = 7.6$ Hz, 2H, H_3), 1.56 (pd, $J = 8.8, 2.6$ Hz, 2H, H_6). $^{13}\text{C-NMR}$ (151 MHz, CDCl_3) δ 209.3 (C_1), 41.4 (C_2), 35.4 (C_3), 30.9 (C_7), 29.8 (C_4), 27.9 (C_5), 18.2 (C_6). IR (ATR – neat) $\tilde{\nu}$ (cm^{-1}) = 2956, 2925, 2857, 1719, 1441, 1411, 1358, 1241, 1169. HRMS for $[\text{C}_8\text{H}_{15}\text{O}]^+$ calculated 127.1117 found 127.1112. R_f (1:4 EtOAc/PE) = 0.45.

4-cyclohexylbutan-2-one (328)

Obtained following **GP(VIII)** at 0.2 mmol scale using DMAP (4.8 mg, 40 μmol , 20 mol%) as Lewis base catalyst. Filtration on silica gel (10% Et_2O in pentane) afforded product **328** (28 mg, 0.18 mmol) as colourless oil in 90% yield. Repeating the same procedure with **Mes-Acr-4** instead of **Ir-4** afforded the same product in 90% yield. $^1\text{H-NMR}$ (600 MHz, CDCl_3) δ 2.43 (t, $J = 7.8$ Hz, 2H, H_2), 2.14 (s, 3H, H_8), 1.72 – 1.63 (m, 5H, H_{5a} , H_{6a} and H_{7a}), 1.50 – 1.43 (m, 2H, H_3), 1.26 – 1.08 (m, 4H, H_4 , H_{6b} and H_{7b}), 0.93 – 0.84 (m, 2H, H_{5b}). $^{13}\text{C-NMR}$ (151 MHz, CDCl_3) δ 209.6 (C_1), 41.4 (C_8), 37.2 (C_4), 33.1 (C_5), 31.2 (C_3), 29.8 (C_8), 26.5 (C_7), 26.2 (C_6). HRMS for $[\text{C}_{10}\text{H}_{19}\text{O}]^+$ calculated 155.1430 found 155.1428. R_f (1:4 EtOAc/PE) = 0.51. Spectroscopic data were consistent with literature values.^[67]

tert-butyl 2-(3-oxobutyl)pyrrolidine-1-carboxylate (329)

Obtained following **GP(VIII)** at 0.2 mmol scale using DMAP (4.8 mg, 40 μmol , 20 mol%) as Lewis base catalyst. Purification by column chromatography on silica gel (10% EtOAc in hexane) afforded product **329** (38 mg, 0.16 mmol) as colourless oil in 80% yield. **$^1\text{H-NMR}$ (600 MHz, CDCl_3)** δ 3.93 – 3.59 (m, 1H, H₄), 3.46 – 3.22 (m, 2H, H₇), 2.51 – 2.32 (m, 2H, H₂), 2.11 (s, 3H, H₈), 1.92 – 1.71 (m, 4H, H_{3a}, H_{5a} and H₆), 1.64 – 1.52 (m, 2H, H_{3b} and H_{5b}), 1.42 (s, 9H, NBoc). **$^{13}\text{C-NMR}$ (151 MHz, CDCl_3)** δ 208.5 (C₁), 154.8 (COOC(CH₃)₃), 79.1 (COOC(CH₃)₃), 56.5 (C₄), 46.2 (C₇), 40.6 (C₂), 30.5 (C₅), 29.8 (C₈), 28.6 (C₃), 28.5 (COOC(CH₃)₃), 23.3 (C₆). **IR (ATR – neat)** $\tilde{\nu}$ (cm^{-1}) = 2968, 2933, 2873, 1715, 1685, 1391, 1364, 1253, 1167, 1102, 1124, 939, 864, 775. **HRMS for [C₁₃H₂₄NO₃]⁺** calculated 242.1756 found 242.1749. **R_f** (1:4 EtOAc/PE) = 0.20.

2,5-dichloro-N-(2-((2-methyl-7-oxooctan-4-yl)amino)-2-oxoethyl)benzamide (330)

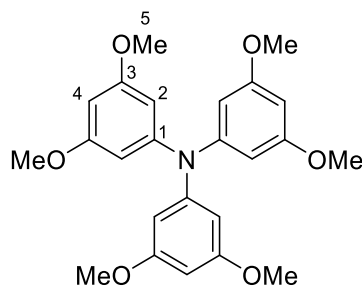
Obtained following **GP(VIII)** at 0.2 mmol scale using DMAP (4.8 mg, 40 μmol , 20 mol%) as Lewis base catalyst. Purification by column chromatography on silica gel (50% EtOAc in hexane) afforded product **330** (61 mg, 0.158 mmol) as yellowish oil in 79% yield. **$^1\text{H-NMR}$ (600 MHz, CDCl_3)** δ 7.61 (bt, J = 1.6 Hz, 1H, H₁₈), 7.36 – 7.34 (m, 3H, H₁₁, H₁₅ and H₁₆), 6.43 (d, J = 9.2 Hz, 1H, H₈), 4.17 – 4.07 (m, 2H, H₁₀), 3.98 (qt, J = 9.2, 4.6 Hz, 1H, H₄), 2.57 – 2.44 (m, 2H, H₂), 2.11 (s, 3H, H₁₉), 1.85 – 1.74 (m, 1H, H_{3a}), 1.65 – 1.54 (m, 2H, H_{3b} and H₆), 1.35 (ddd, J = 14.5, 9.1, 5.6 Hz, 1H, H_{5a}), 1.29 – 1.23 (m, 1H, H_{5b}), 0.89 (d, J = 6.6 Hz, 3H, H_{7a}), 0.88 (d, J = 6.6 Hz, 3H, H_{7b}). **$^{13}\text{C-NMR}$ (151 MHz, CDCl_3)** δ 208.8 (C₄), 167.8 (C₉), 165.4 (C₁₂), 135.5 (C₁₃), 133.2 (C₁₄), 131.6 (C₁₅ or C₁₆), 131.5 (C₁₆ or C₁₅), 129.9 (C₁₈), 129.2 (C₁₇), 47.6 (C₄), 44.7 (C₅), 43.8 (C₁₀), 40.1 (C₂), 30.1 (C₁₉), 29.3 (C₃), 24.9 (C₆), 23.0 (C_{7a}), 22.1 (C_{7b}). **IR (ATR – neat)** $\tilde{\nu}$ (cm^{-1}) = 3298, 3075, 2952, 2929, 2869, 1711, 1643, 1530,

1463, 1368, 1292, 1257, 1167, 1098, 1046, 912, 819, 729. **HRMS for [C₁₈H₂₅N₂O₃Cl₂]⁺**
calculated 387.1242 found 387.1237. **R_f** (1:1 EtOAc/PE) = 0.19.

5.4 Experimental data for Chapter 4

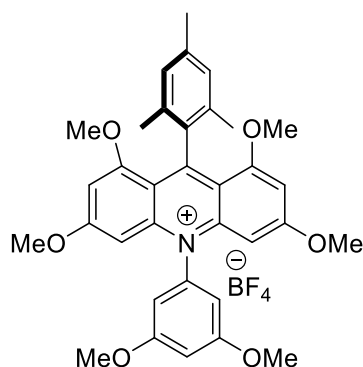
5.4.1 Synthetic procedures and characterisation for organic dyes

tris(3,5-dimethoxyphenyl)amine



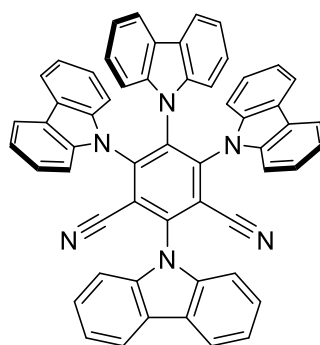
In a 250 mL two-necked round-bottom flask equipped with a magnetic stir bar were placed 3,5-dimethoxyaniline (1.75 g, 11.4 mmol, 1.0 equiv.), 1-bromo-3,5-dimethoxybenzene (4.96 g, 22.8 mmol, 2.0 equiv.), and chloro[(tri-*tert*-butylphosphine)-2-(2-aminobiphenyl)]palladium(II) (168.8 mg, 0.34 mmol, 3.0 mol%). The headspace was purged with argon and the solid content dissolved with THF (40 mL). A 2.0 M solution of sodium *tert*-butoxide in THF (23 mL, 46 mmol, 4.0 equiv.) was then added in one portion under argon, and the reaction mixture was heated to 70°C. After 24 h, the reaction mixture was cooled down to room temperature. The THF solution was filtered through a pad of celite® and concentrated *in vacuo*. Residue was dissolved with 100 mL of water and 50 mL of MTBE. Layers were separated and aqueous layer extracted with MTBE (3 x 50 mL). Combined organic layers were washed with brine and dried over MgSO₄. Further removal of the solvent *in vacuo* resulted in tris(3,5-dimethoxyphenyl)amine (4.80 g, 11.3 mmol) as a brown amorphous solid in 99% yield.

¹H-NMR (600 MHz, CDCl₃) δ 6.26 (d, *J* = 2.3 Hz, 6H, H₂), 6.17 (t, *J* = 2.3 Hz, 3H, H₄), 3.71 (s, 12H, H₅). **¹³C-NMR (151 MHz, CDCl₃)** δ 161.1 (C₃), 149.1 (C₁), 103.1 (C₂), 95.5 (C₄), 55.3 (C₅). **HRMS for [C₂₄H₂₈NO₆]⁺** calculated 426.1911 found 426.1916. **R_f** (1:1 EtOAc/PE) = 0.38. Spectroscopic data were consistent with literature values.^[35]

10-(3,5-dimethoxyphenyl)-9-mesityl-1,3,6,8-tetramethoxyacridin-10-ium tetrafluoroborate (Mes-Acr-4)

In a 250 mL round-bottom flask equipped with a magnetic stir bar were placed tris(3,5-dimethoxyphenyl)amine (4.80 g, 11.3 mmol, 1.0 equiv.) and 2,4,6-trimethylbenzoyl chloride (4.0 mL, 24 mmol, 2.1 equiv.) followed by chlorobenzene (60 mL). Triflic acid (950 μ L, 11.3 mmol, 1.0 equiv.) was then added slowly and the mixture heated to 90°C. After 24 h the reaction mixture was cooled to room temperature and washed with aqueous 0.2 M NaBF₄ solution (3 \times 30 mL) and water (2 \times 60 mL). To the organic layer was then dried over MgSO₄ and concentrated *in vacuo* and cold MTBE (200 mL) was added slowly until a precipitate started to form. An additional 400 mL of MTBE was added slowly and the mixture was stirred at 0°C for 2 h. The orange precipitate was then filtered-off and the solid was washed with cold MTBE (200 mL). This brown-orange solid was then purified by column chromatography (CH₂Cl₂) to afford **Mes-Acr-4** (3.75 g, 6.77 mmol) as a bright orange solid in 60% yield.

¹H-NMR (600 MHz, CDCl₃) δ 6.91 (s, 2H), 6.83 (t, J = 2.2 Hz, 1H), 6.63 (d, J = 2.1 Hz, 2H), 6.49 (d, J = 2.3 Hz, 2H), 6.19 (d, J = 2.3 Hz, 2H), 3.93 (s, 6H), 3.86 (s, 6H), 3.49 (s, 6H), 2.38 (s, 3H), 1.84 (s, 6H). **¹³C-NMR (151 MHz, CDCl₃)** δ 168.22, 163.14, 162.22, 160.68, 144.76, 139.81, 136.43, 131.99, 127.03, 113.32, 105.56, 102.81, 97.62, 92.67, 57.04, 56.49, 56.21, 21.10, 20.16. **HRMS for [C₃₄H₃₇NO₆¹¹BF₄]⁺** calculated 554.2537 found 554.2542. **R_f** (CH₂Cl₂) = 0.08. Spectroscopic data were consistent with literature values.^[35]

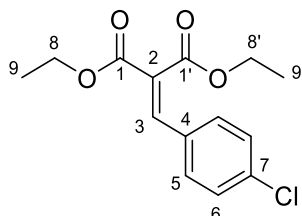
2,4,5,6-tetra(9*H*-carbazol-9-yl)isophthalonitrile (4CzIPN)

In a 250 mL round-bottom flask equipped with a magnetic stir bar was added carbazole (3.67 g, 21.9 mmol, 4.4 equiv.). The flask was sealed with a rubber septum and flushed with argon. THF (44 mL) was then added, and the solution was cooled to 0°C. The flask was then charged with a 1.0 M NaHMDS solution in THF (20.9 mL, 20.9 mmol, 4.2 equiv.). The resulting orange-brown solution was then allowed to warm to room temperature and stirred for 1 h. The flask was then charged with tetrafluoroisophthalonitrile (1.00 g, 5.0 mmol, 1.0 equiv.) and equipped with a reflux condenser. The solution was heated at 70°C under argon for 72 h. The brown mixture with yellow precipitate was then allowed to cool to room temperature and filtered. The resulting yellow solid was successively washed with Et₂O (200 mL) and cold CHCl₃ (300 mL). The yellow filtrate was then purified by column chromatography (50% CH₂Cl₂ in PE) to deliver **4CzIPN** (2.2 g, 2.76 mmol) as a bright yellow solid in 55% yield.

¹H-NMR (600 MHz, CDCl₃) δ 8.23 (d, *J* = 7.7 Hz, 2H), 7.75 – 7.68 (m, 8H), 7.53 (t, *J* = 7.2 Hz, 2H), 7.34 (d, *J* = 7.5 Hz, 2H), 7.25 – 7.21 (m, 4H), 7.13 – 7.06 (m, 8H), 6.83 (t, *J* = 8.0 Hz, 4H), 6.65 (t, *J* = 7.7 Hz, 2H). **¹³C-NMR (151 MHz, CDCl₃)** δ 145.2, 144.6, 140.0, 138.2, 136.9, 134.7, 126.9, 125.8, 124.9, 124.7, 124.5, 123.8, 122.4, 121.9, 121.4, 121.0, 120.4, 119.6, 116.3, 111.6, 109.9, 109.5, 109.4. **HRMS for [C₅₆H₃₃N₆]⁺** calculated 789.2761 found 789.2770. **R_f** (1:1 CH₂Cl₂/PE) = 0.19. Spectroscopic data were consistent with literature values.^[112]

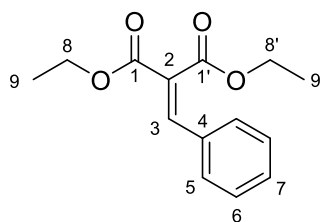
5.4.2 Synthetic procedures and characterisation for starting materials

diethyl 2-(4-chlorobenzylidene)malonate (**357**)



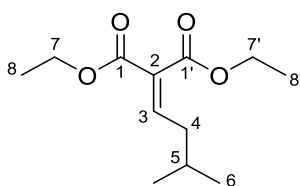
4-Chlorobenzaldehyde (7.00 g, 50.0 mmol, 1.0 equiv.) was added to a solution of diethyl malonate (6.3 mL, 42.0 mmol, 0.8 equiv.) and piperidine (0.5 mL, 5.0 mmol, 0.1 equiv.) in toluene (25 mL). Glacial acetic acid (0.3 mL, 5.0 mmol, 0.1 equiv.) was added and the reaction mixture was heated to 160°C for 24 h with a Dean-Stark apparatus. The solvent was evaporated under reduced pressure and the orange residue was diluted with EtOAc (30 mL). The organic phase was washed with water (30 mL), aqueous 1 M HCl (30 mL), saturated aqueous NaHCO₃ (30 mL) and brine (30 mL). The organic phase was then dried over MgSO₄ and the solvents removed *in vacuo*. Column chromatography on silica gel (15% EtOAc in PE) afforded product **357** (4.10 g, 14.5 mmol) as a yellowish oil in 29% yield.

¹H-NMR (600 MHz, CDCl₃) δ 7.69 (s, 1H, H₃), 7.41 (d, *J* = 8.6 Hz, 2H, H₅), 7.37 (d, *J* = 8.6 Hz, 2H, H₆), 4.35 (q, *J* = 7.1 Hz, 2H, H₈), 4.32 (q, *J* = 7.1 Hz, 2H, H_{8'}), 1.35 (t, *J* = 7.1 Hz, 3H, H₉), 1.31 (t, *J* = 7.1 Hz, 3H, H_{9'}). **¹³C-NMR (151 MHz, CDCl₃)** δ 166.4 (C₁), 163.9 (C_{1'}), 140.6 (C₃), 136.6 (C₇), 131.4 (C₄), 130.7 (C₅), 129.1 (C₆), 126.9 (C₂), 61.8 (C₈), 61.8 (C_{8'}), 14.1 (C₉), 13.9 (C_{9'}). **HRMS for [C₁₄H₁₅O₄ClNa]⁺** calculated 305.0551 found 305.0540. **R_f** (2:1 EtOAc/PE) = 0.50. Spectroscopic data were consistent with literature values.^[95]

diethyl 2-benzylidenemalonate (358)

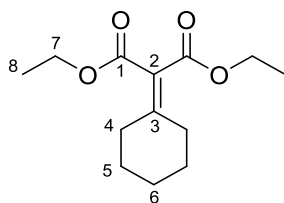
A solution of diethylmalonate (3.8 mL, 25 mmol, 1.0 equiv.), benzaldehyde (2.4 mL, 24 mmol, 1.0 equiv.), piperidine (0.40 mL, 4.0 mmol, 0.2 equiv.) and benzoic acid (0.32 g, 2.6 mmol, 0.1 equiv.) in toluene (25 mL) was heated to 130°C for 21 h with a Dean-Stark apparatus. The reaction mixture was then washed with water (25 mL), aqueous 1 M HCl (25 mL), saturated aqueous NaHCO₃ (25 mL) and brine (25 mL). The organic phase was then dried with MgSO₄ and the solvents were removed *in vacuo*. Column chromatography (0% to 5% EtOAc in hexane) afforded the product **358** (5.4 g, 22 mmol) as a yellowish oil in 91% yield.

¹H-NMR (600 MHz, CDCl₃) δ 7.74 (s, 1H, H₃), 7.45 (dd, *J* = 7.7, 2.0 Hz, 2H, H₅), 7.41 – 7.36 (m, 3H, H₆ and H₇), 4.34 (q, *J* = 7.1 Hz, 2H, H₈), 4.31 (q, *J* = 7.1 Hz, 2H, H_{8'}), 1.33 (t, *J* = 7.1 Hz, 3H, H₉), 1.28 (t, *J* = 7.1 Hz, 3H, H_{9'}). **¹³C-NMR (151 MHz, CDCl₃)** δ 166.8 (C₁), 164.3 (C_{1'}), 142.3 (C₃), 133.1 (C₄), 130.7 (C₆), 129.6 (C₅), 128.9 (C₇), 126.5 (C₂), 61.8 (C₈ and C_{8'}), 14.3 (C₉), 14.0 (C_{9'}). **HRMS for [C₁₄H₁₅O₄]⁺** calculated 247.0965 found 247.0978. **R_f** (1:4 EtOAc/PE) = 0.53. Spectroscopic data were consistent with literature values.^[304]

1,3-diethyl 2-(3-methylbutylidene)propanedioate (359)

A solution of diethyl malonate (7.6 mL, 50 mmol, 1.0 equiv.) and piperidine (0.5 mL, 5.0 mmol, 0.1 equiv.) in heptane (25 mL) was mixed with glacial acetic acid (0.3 mL, 5.0 mmol, 0.1 equiv.) and *iso*-valeraldehyde (5.3 mL, 50 mmol, 1.0 equiv.). The solution was heated to 160°C for 24 h using a Dean-Stark apparatus. Water (15 mL) and diethyl ether (15 mL) were then added and the phases separated. The organic phase was washed with saturated aqueous NaHCO₃ (15 mL), brine (15 mL), water (15 mL), and dried over MgSO₄. Solvents were then removed *in vacuo*. Column chromatography on silica gel (5% EtOAc in PE) afforded product **359** (5.00 g, 21.9 mmol) as a colourless oil in 44% yield.

¹H-NMR (600 MHz, CDCl₃) δ 7.01 (t, *J* = 8.0 Hz, 1H, H₃), 4.30 (q, *J* = 7.1 Hz, 2H, H₇), 4.23 (q, *J* = 7.1 Hz, 2H, H_{7'}), 2.20 – 2.16 (m, 2H, H₄), 1.86 – 1.76 (m, 1H, H₅), 1.32 (t, *J* = 7.1 Hz, 3H, H₈), 1.29 (t, *J* = 7.1 Hz, 3H, H_{8'}), 0.93 (d, *J* = 6.7 Hz, 6H, H₆). **¹³C-NMR (151 MHz, CDCl₃)** δ 165.7 (C₁), 164.0 (C_{1'}), 148.3 (C₃), 129.3 (C₂), 61.2 (C₇), 61.1 (C_{7'}), 38.5 (C₄), 28.2 (C₅), 22.4 (C₆), 14.2 (C₈), 14.1 (C_{8'}). **HRMS for [C₁₂H₂₁O₄]⁺** calculated 229.1434 found 229.1437. **R_f** (1:4 EtOAc/PE) = 0.58. Spectroscopic data were consistent with literature values.^[305]

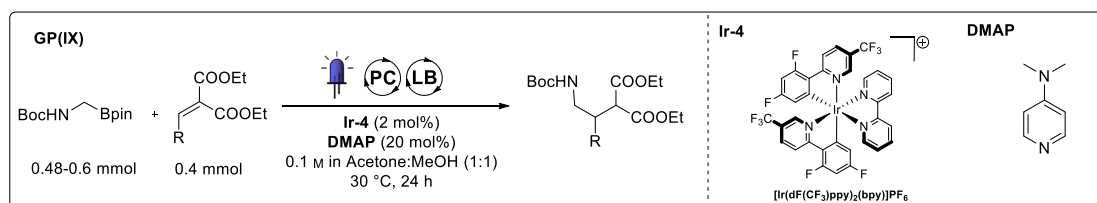
diethyl 2-cyclohexylidenemalonate (360)

A mixture of THF (18 mL) and CH₂Cl₂ (56 mL) was cooled to 0°C and TiCl₄ (5.3 mL, 48 mmol, 1.9 equiv.) was added dropwise. Diethylmalonate (3.8 mL, 25 mmol, 1.0 equiv.) and cyclohexanone (2.7 mL, 29 mmol, 1.2 equiv.) were then added portionwise. The slurry was diluted by the addition of CH₂Cl₂ (30 mL), allowed to warm to room temperature and stirred for 18 h. The reaction mixture was washed with water (2 x 40 mL), the organic layer was dried over MgSO₄ and concentrated *in vacuo*. Column

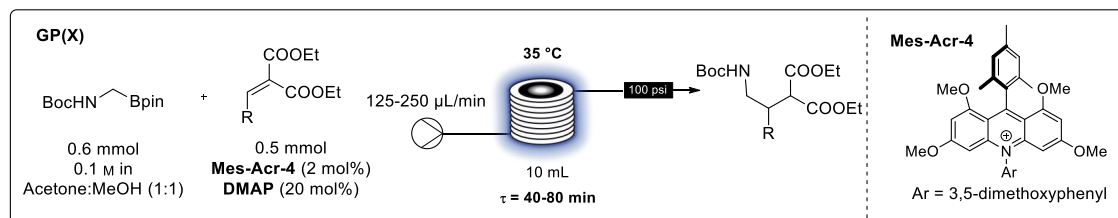
chromatography on silica gel (0% to 5% EtOAc in hexane) afforded the product **360** (3.2 g, 14 mmol) as a yellowish oil in 54% yield.

¹H-NMR (600 MHz, CDCl₃) δ 4.22 (q, *J* = 7.1 Hz, 4H, H₇), 2.59 – 2.43 (m, 4H, H₄), 1.75 – 1.65 (m, 4H, H₅), 1.65 – 1.53 (m, 2H, H₆), 1.28 (t, *J* = 7.1 Hz, 6H, H₈). **¹³C-NMR (151 MHz, CDCl₃)** δ 165.9 (C₁), 161.7 (C₃), 121.9 (C₂), 61.0 (C₇), 32.7 (C₄), 28.3 (C₅), 26.2 (C₆), 14.2 (C₈). **HRMS for [C₁₃H₂₀O₄Na]⁺** calculated 263.1259 found 263.1245. **R_f** (1:4 EtOAc/PE) = 0.63. Spectroscopic data were consistent with literature values.^[306]

5.4.3 Synthetic procedures and characterisation for γ -amino butyric acid analogues



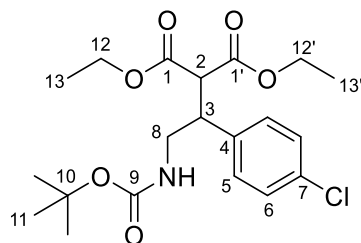
GP(IX): A 10 mL microwave vial was charged with the desired alkene (0.4 mmol, 1.0 equiv.), *tert*-butyl((4,4,5,5-tetramethyl-1,3,2-dioxaborolan-2-yl)methyl)carbamate (0.48–0.60 mmol, 1.2–1.5 equiv.), the photoredox catalyst [Ir(dF(CF₃)ppy)₂(bpy)]PF₆ (**Ir-4**, 8.0 mg, 2.0 mol%) and DMAP (9.6 mg, 80 μ mol, 20 mol%) as Lewis base catalyst. The vial was then capped, evacuated and backfilled with argon three times before 4.0 mL of a degassed acetone/methanol (1:1) mixture was added to obtain a clear yellow transparent 0.1 M solution. This solution was then stirred while irradiated with a commercial blue LED strip (Ledxon, 14.4 W, 470 nm) for 24 hours, the temperature was maintained at 30°C using a desktop fan. The content of the vial was then concentrated *in vacuo* and purified by flash column chromatography to yield the pure product.



GP(X): A 10 mL microwave vial was charged with the desired alkene (0.5 mmol, 1.0 equiv.), *tert*-butyl((4,4,5,5-tetramethyl-1,3,2-dioxaborolan-2-yl)methyl)carbamate (0.15 g, 0.60 mmol, 1.2 equiv.), the photoredox catalyst **Mes-Acr-4** (5.5 mg, 2.0 mol%) and DMAP (12 mg, 100 μ mol, 20 mol%) as Lewis base catalyst. The vial was then capped, evacuated and backfilled with argon three times before 4.0 mL of a degassed acetone/methanol (1:1) mixture was added to obtain a clear yellow transparent 0.1 M solution. The clear solution was then pumped at 125 to 250 μ L/min through a Vapourtec UV-150 photochemical reactor (10 mL reactor coil, FEP tubing, τ = 40 to 80 min) held at 35°C. Once the reaction mixture has fully been taken up by the pump, the input was swapped to acetone:methanol (1:1) solvent to push the rest of the reaction mixture through the reactor. When the reaction plug was exiting the output stream (yellow

colour), the totality of the plug was collected in a vial wrapped in aluminium foil and concentrated *in vacuo* before being purified by flash column chromatography to yield the pure product.

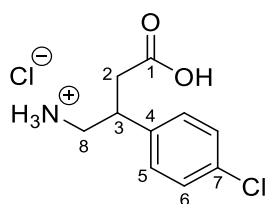
diethyl 2-((tert-butoxycarbonyl)amino)-1-(4-chlorophenyl)ethylmalonate (361)



Obtained following **GP(IX)** using diethyl 2-(4-chlorobenzylidene) malonate (0.11 g, 0.40 mmol) as olefin and *tert*-butyl ((4,4,5,5-tetramethyl-1,3,2-dioxaborolan-2-yl)methyl)carbamate (0.12 g, 0.48 mmol, 1.2 equiv.). Purification by column chromatography on silica gel (7% to 10% EtOAc and 1% Et₃N in hexane) afforded product **361** (0.11 g, 0.28 mmol) as a white solid in 71% yield.

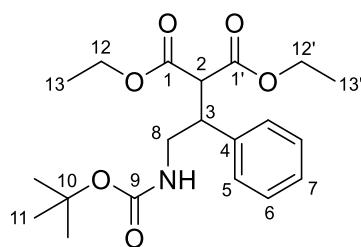
Also obtained following **GP(X)** using diethyl 2-(4-chlorobenzylidene) malonate (0.14 g, 0.50 mmol) and 60 min residence time. Purification by column chromatography on silica gel (7% to 10% EtOAc and 1% Et₃N in hexane) afforded product **361** (0.13 g, 0.35 mmol) as a white solid in 69% yield.

¹H-NMR (600 MHz, CDCl₃) δ 7.26 (d, *J* = 8.3 Hz, 2H, H₅), 7.16 (d, *J* = 8.3 Hz, 2H, H₆), 4.52–4.37 (m, 1H, NH), 4.23 (q, *J* = 7.1 Hz, 2H, H₁₂), 3.97 – 3.88 (m, 2H, H_{12'}), 3.66 (d, *J* = 10.3 Hz, 1H, H₂), 3.62 – 3.54 (m, 1H, H₃), 3.49 (m, 1H, H_{8a}), 3.37 (m, 1H, H_{8b}), 1.36 (s, 9H, H₁₁), 1.27 (t, *J* = 7.1 Hz, 3H, H₁₃), 0.99 (t, *J* = 7.1 Hz, 3H, H_{13'}). **¹³C-NMR (151 MHz, CDCl₃)** δ 168.3 (C₁), 167.7 (C_{1'}), 155.8 (C₉), 137.8 (C₄), 133.6 (C₇), 130.1 (C₆), 129.0 (C₅), 79.8 (C₁₀), 62.2 (C₁₂), 61.8 (C_{12'}), 55.8 (C₂), 45.2 (C₃), 44.1 (C₈), 28.6 (C₁₁), 14.4 (C₁₃), 14.1 (C_{13'}). **HRMS for [C₂₀H₂₈NO₆ClNa]⁺** calculated 436.1497 found 436.1483. **R_f** (1:1 Et₂O:PE) = 0.45. **M.p.** = 105–106°C. Spectroscopic data were consistent with literature values.^[95]

baclofen·HCl (365)

diethyl 2-(2-((*tert*-butoxycarbonyl)amino)-1-(4-chlorophenyl)ethyl)malonate (**361**, 0.11 g, 0.28 mmol.) was dissolved in aqueous 6 M HCl (3.0 mL) and heated to 120°C for 24 h in a sealed vial. The solvent was removed under reduced pressure, the residue was dissolved in water (6.0 mL) and washed with Et₂O (2 x 8 mL). Removal of the solvent *in vacuo* afforded the amino acid hydrochloride **365** (67 mg, 0.27 mmol) as white crystals in 97% yield.

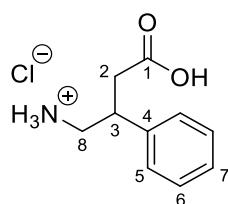
¹H-NMR (600 MHz, D₂O) δ 7.47 (d, *J* = 8.5 Hz, 2H, H₅), 7.36 (d, *J* = 8.5 Hz, 2H, H₆), 3.48 (m, 1H, H₃), 3.40 (dd, *J* = 12.9, 5.0 Hz, 1H, H_{8a}), 3.27 (dd, *J* = 12.9, 10.6 Hz, 1H, H_{8b}), 2.90 (dd, *J* = 16.0, 5.8 Hz, 1H, H_{2a}), 2.80 (dd, *J* = 16.0, 9.4 Hz, 1H, H_{2b}). **¹³C-NMR (151 MHz, D₂O)** δ 173.9 (C₁), 136.8 (C₄), 133.4 (C₇), 129.4 (C₆), 129.2 (C₅), 43.5 (C₈), 39.4 (C₃), 38.1 (C₂). **HRMS for [C₁₀H₁₃NO₂Cl]⁺** calculated 214.0629 found 214.0629. **M.p.** 195–198°C. Spectroscopic data were consistent with literature values.^[246]

diethyl 2-(2-((tert-butoxycarbonyl)amino)-1-phenylethyl)malonate (362)

Obtained following **GP(IX)** using diethyl 2-benzylidenemalonate (0.10 g, 0.41 mmol) as olefin and *tert*-butyl((4,4,5,5-tetramethyl-1,3,2-dioxaborolan-2-yl)methyl)carbamate (0.12 g, 0.48 mmol, 1.2 equiv.). Purification by column chromatography on silica gel (5% to 10% EtOAc and 1% Et₃N in hexane) afforded product **362** (0.12 g, 0.32 mmol) as an amorphous white solid in 79% yield.

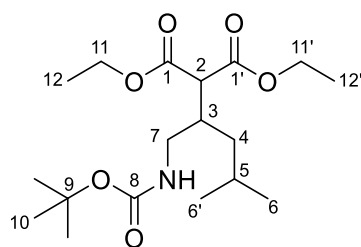
Also obtained following **GP(X)** using diethyl 2-benzylidenemalonate (0.12 g, 0.50 mmol) as olefin and 80 min residence time. Purification by column chromatography on silica gel (5% to 10% EtOAc and 1% Et₃N in hexane) afforded product **362** (0.14 g, 0.37 mmol) as an amorphous white solid in 74% yield.

¹H-NMR (600 MHz, CDCl₃) δ 7.32 – 7.27 (m, 2H, H₆), 7.25 – 7.18 (m, 3H, H₆, H₇), 4.42 (s, 1H, NH), 4.24 (q, *J* = 7.2 Hz, 2H, H₁₂), 3.96 – 3.85 (m, 2H, H_{12'}), 3.70 (d, *J* = 10.4 Hz, 1H, H₂), 3.64 – 3.58 (m, 1H, H₃), 3.53 (dt, *J* = 13.0, 6.2 Hz, 1H, H_{8a}), 3.45 – 3.34 (m, 1H, H_{8b}), 1.37 (s, 9H, H₁₁), 1.28 (t, *J* = 7.2 Hz, 3H, H₁₃), 0.95 (t, *J* = 7.1 Hz, 3H, H_{13'}). **¹³C-NMR (151 MHz, CDCl₃)** δ 168.3 (C₁), 167.6 (C_{1'}), 155.7 (C₉), 139.0 (C₄), 128.7 (C₆), 128.5 (C₅), 127.6 (C₇), 79.4 (C₁₀), 61.9 (C₁₂), 61.5 (C_{12'}), 55.9 (C₂), 45.5 (C₃), 44.1 (C₈), 28.4 (C₁₁), 14.2 (C₁₃), 13.8 (C_{13'}). **HRMS for [C₂₀H₂₉NO₆Na]⁺** calculated 402.1887 found 402.1875. **R_f**(1:1 Et₂O:PE) = 0.45. Spectroscopic data were consistent with literature values.^[95]

phenibut·HCl (366)

diethyl 2-(2-((tert-butoxycarbonyl)amino)-1-phenylethyl)malonate (**362**, 0.12 g, 0.32 mmol) was dissolved in aqueous 6 M HCl (3.0 mL) and heated to 120°C for 1 h. A small amount of active charcoal was added and the mixture was heated to 120°C for 20 min. The mixture was allowed to cool to room temperature and filtered. Removal of the solvent *in vacuo* afforded the amino acid hydrochloride (61 mg, 0.28 mmol) as colourless crystals in 88% yield.

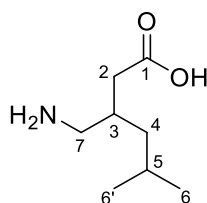
¹H-NMR (600 MHz, D₂O) δ 7.47 (t, *J* = 7.6 Hz, 2H, H₆), 7.40 (d, *J* = 7.6 Hz, 3H, H₅ and H₇), 3.50 – 3.37 (m, 2H, H₇, H_{8a}), 3.33 – 3.23 (m, 1H, H_{8b}), 2.92 – 2.86 (m, 1H, H_{2a}), 2.80 (dd, *J* = 16.1, 8.8 Hz, 1H, H_{2b}). **¹³C-NMR (151 MHz, D₂O)** δ 175.5 (C₁), 138.3 (C₄), 129.3 (C₆), 128.3 (C₇), 127.8 (C₅), 43.8 (C₈), 39.9 (C₃), 38.2 (C₂). **HRMS for [C₁₀H₁₄NO₂]⁺** calculated 180.1019 found 180.1021. **M.p.** 185–188°C. Spectroscopic data were consistent with literature values.^[246]

diethyl 2-(1-((tert-butoxycarbonyl)amino)-4-methylpentan-2-yl)malonate (363)

Obtained following **GP(IX)** using diethyl 2-(3-methylbutylidene)malonate (91 mg, 0.40 mmol) as olefin and *tert*-butyl ((4,4,5,5-tetramethyl-1,3,2-dioxaborolan-2-yl)methyl)carbamate (0.12 g, 0.48 mmol, 1.2 equiv.). Purification by column chromatography on silica gel (0% to 7% EtOAc and 1% Et₃N in hexane) afforded product **363** (0.13 g, 0.35 mmol) as a colourless oil in 89% yield.

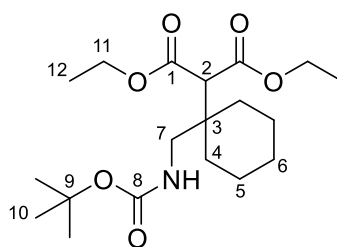
Also obtained following **GP(IX)** using diethyl 2-(3-methylbutylidene)malonate (0.11 g, 0.40 mmol) as olefin and 40 min residence time. Purification by column chromatography on silica gel (0% to 7% EtOAc and 1% Et₃N in hexane) afforded product **363** (0.15 g, 0.42 mmol) as a colourless oil in 85% yield.

¹H-NMR (600 MHz, CDCl₃) δ 4.82 (t, *J* = 6.5 Hz, 1H, NH), 4.27 – 4.14 (m, 4H, H₄, H₁₁ and H_{11'}), 3.38 (d, *J* = 6.6 Hz, 1H, H₂), 3.26 (dt, *J* = 14.3, 5.4 Hz, 1H, H_{7a}), 3.18 (dt, *J* = 14.3, 6.8 Hz, 1H, H_{7b}), 2.40 (m, 1H, H₃), 1.68 (m, 1H, H₅) 1.41 (s, 9H, H₁₀), 1.29 – 1.21 (m, 7H, H_{4a}, H₁₂ and H_{12'}), 1.11 (ddd, *J* = 13.8, 8.6, 5.2 Hz, 1H, H_{4b}), 0.95 – 0.81 (m, 6H, H₆ and H_{6'}). **¹³C-NMR (151 MHz, CDCl₃)** δ 169.1 (C₁ and C_{1'}), 156.0 (C₈), 79.2 (C₉), 61.5 (C₁₁ and C_{11'}), 54.3 (C₂), 41.7 (C₇), 39.3 (C₄), 37.0 (C₃), 28.5 (C₁₀), 25.4 (C₅), 23.4 (C₆), 22.1 (C_{6'}), 14.2 (C₁₂ and C_{12'}). **HRMS for [C₁₈H₃₃NO₆Na]⁺** calculated 382.2200 found 382.2188. **R_f**(1:1 Et₂O:PE) = 0.58. Spectroscopic data were consistent with literature values.^[96]

pregabalin (342)

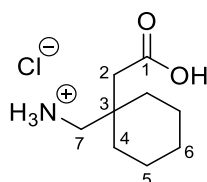
diethyl 2-(1-((*tert*-butoxycarbonyl)amino)-4-methylpentan-2-yl)malonate (**363**, 89 mg, 0.24 mmol) was dissolved in aqueous 6 M HCl (3.0 mL) and heated to 125°C for 24 h. Removal of the solvent *in vacuo* at 60°C for 2 h afforded the amino acid hydrochloride **367** (65 mg, 0.33 mmol) as a sticky residue in 94% yield. For the preparation of crystalline material, which was used for characterization, a sample of the hydrochloride was dissolved in water, neutralised with aqueous 1 M NaOH to pH 7 and recrystallised from a mixture of *iso*-PrOH (30%) in H₂O to afford colourless crystals of pregabalin **342** as the free amino acid.

¹H-NMR (600 MHz, D₂O) δ 2.99 (m, 2H, H_{7a} and H_{7b}), 2.38 – 2.29 (m, 1H, H_{4a}), 2.24 (m, 1H, H_{4b}), 2.21 – 2.13 (m, 1H, H₃), 1.72 – 1.56 (m, 1H, H₅), 1.23 (t, *J* = 7.2 Hz, 2H, H₂), 1.02 – 0.82 (m, 6H, H₆ and H_{6'}). **¹³C-NMR (151 MHz, D₂O)** δ 181.1 (C₁), 43.7 (C₇), 40.7 (C₄), 40.6 (C₂), 31.7 (C₃), 24.4 (C₅), 22.0 (C₆), 21.5 (C_{6'}). **HRMS for [C₈H₁₈NO₂]⁺** calculated 160.1332 found 160.1334. **M.p.** 167–168°C. Spectroscopic data were consistent with literature values.^[96]

diethyl 2-(1-((tert-butoxycarbonyl)amino)cyclohexyl)malonate (364)

Obtained following **GP(IX)** using diethyl 2-cyclohexylidenemalonate (96 mg, 0.40 mmol) as olefin and *tert*-butyl ((4,4,5,5-tetramethyl-1,3,2-dioxaborolan-2-yl)methyl)carbamate (0.15 g, 0.60 mmol, 1.5 equiv.). Purification by column chromatography on silica gel (5% to 10% EtOAc in hexane) afforded product **364** (89 mg, 0.24 mmol) as a colourless oil in 56% yield.

¹H-NMR (600 MHz, CDCl₃) δ 5.36 (t, *J* = 6.6 Hz, 1H, NH), 4.22 – 4.15 (m, 4H, H₁₁), 3.52 (s, 1H, H₂), 3.37 (d, *J* = 6.6 Hz, 2H, H₇), 1.63 – 1.44 (m, 9H, H₄, H₅ and H_{6a}), 1.42 (s, 9H, H₁₀), 1.37 – 1.29 (m, 1H, H_{6b}), 1.27 (t, *J* = 7.1 Hz, 6H, H₁₂). **¹³C-NMR (151 MHz, CDCl₃)** δ 168.7 (C₁), 156.5 (C₈), 79.0 (C₉), 61.4 (C₁₁), 57.5 (C₂), 44.4 (C₇), 40.9 (C₃), 32.2 (C₄), 28.5 (C₁₀), 25.7 (C₆), 21.4 (C₅), 14.2 (C₁₂). **IR (ATR – neat)** $\tilde{\nu}$ (cm⁻¹) = 3420, 1752, 1716, 1511, 1454, 1366, 1240, 1095, 1031, 758. **HRMS for [C₁₉H₃₃NO₆Na]⁺** calculated 394.2200 found 394.2188. **R_f** (1:1 Et₂O:PE) = 0.56.

gabapentin·HCl (368)

diethyl 2-(1-((tert-butoxycarbonyl)amino)cyclohexyl)malonate (**364**, 89 mg, 0.24 mmol) was dissolved in aqueous 6 M HCl (3.0 mL) and heated to 120°C for 24 h. The solvent was removed under reduced pressure, the residue was dissolved in water (6.0 mL) and washed with Et₂O (2 x 8 mL). Removal of the solvent *in vacuo* afforded the amino acid hydrochloride **368** (45 mg, 0.22 mmol) as white crystals in 91% yield.

¹H-NMR (600 MHz, D₂O) δ 3.12 (s, 2H, H₇), 2.55 (s, 2H, H₂), 1.56 – 1.34 (m, 10H, H₄, H₅ and H₆). **¹³C-NMR (151 MHz, D₂O)** δ 176.1 (C₁), 46.6 (C₇), 38.8 (C₂), 34.6 (C₃), 32.8 (C₄), 25.0 (C₆), 20.5 (C₅). **HRMS for [C₉H₁₈NO₂]⁺** calculated 172.1332

found 172.1334. **M.p.** 116–118°C. Spectroscopic data were consistent with literature values.^[307]

6 References

- [1] V. Balzani, A. Credi, M. Venturi, *ChemSusChem* **2008**, *1*, 26–58.
- [2] N. Armaroli, V. Balzani, *Angew. Chem. Int. Ed.* **2007**, *46*, 52–66.
- [3] G. Ciamician, *Science* **1912**, *36*, 385–394.
- [4] G. Ciamician, P. Silber, *Chem. Ber.* **1908**, *41*, 1928–1935.
- [5] “Solar_spectrum_en.svg (CC BY-SA 3.0),” can be found under <https://en.wikipedia.org/wiki/Sunlight>, last consulted in January **2018**.
- [6] D. M. Schultz, T. P. Yoon, *Science* **2014**, *343*, 1239176.
- [7] Q. Li, B. Guo, J. Yu, J. Ran, B. Zhang, H. Yan, J. R. Gong, *J. Am. Chem. Soc.* **2011**, *133*, 10878–10884.
- [8] H. Ahmad, S. K. Kamarudin, L. J. Minggu, M. Kassim, *Renew. Sustain. Energy Rev.* **2015**, *43*, 599–610.
- [9] S. N. Habisreutinger, L. Schmidt-Mende, J. K. Stolarczyk, *Angew. Chem. Int. Ed.* **2013**, *52*, 7372–7408.
- [10] A. Albini, *Photochemistry: Past, Present and Future*, Springer, Berlin, **2015**.
- [11] D. M. Hedstrand, W. H. Kruijzinga, R. M. Kellogg, *Tetrahedron Lett.* **1978**, *19*, 1255–1258.
- [12] M. A. Ischay, M. E. Anzovino, J. Du, T. P. Yoon, *J. Am. Chem. Soc.* **2008**, *130*, 12886–12887.
- [13] D. A. Nicewicz, D. W. C. MacMillan, *Science* **2008**, *322*, 77–80.
- [14] J. M. R. Narayanam, J. W. Tucker, C. R. J. Stephenson, *J. Am. Chem. Soc.* **2009**, *131*, 8756–8757.
- [15] M. H. Shaw, J. Twilton, D. W. C. MacMillan, *J. Org. Chem.* **2016**, *81*, 6898–6926.
- [16] C. K. Prier, D. A. Rankic, D. W. C. MacMillan, *Chem. Rev.* **2013**, *113*, 5322–5363.
- [17] N. A. Romero, D. A. Nicewicz, *Chem. Rev.* **2016**, *116*, 10075–10166.
- [18] J. W. Tucker, C. R. J. Stephenson, *J. Org. Chem.* **2012**, *77*, 1617–1622.
- [19] M. Majek, A. Jacobi von Wangelin, *Angew. Chem. Int. Ed.* **2015**, *54*, 2270–2274.
- [20] N. G. Anderson, *Practical Process Research and Development: A Guide for Organic Chemists*, Academic Press, Oxford, **2012**.
- [21] F. Lévesque, P. H. Seeberger, *Angew. Chem. Int. Ed.* **2012**, *51*, 1706–1709.
- [22] Z. Amara, J. F. B. Bellamy, R. Horvath, S. J. Miller, A. Beeby, A. Burgard, K. Rossen, M. Poliakoff, M. W. George, *Nat. Chem.* **2015**, *7*, 489–495.
- [23] J. Turconi, F. Grioret, R. Guevel, G. Oddon, R. Villa, A. Geatti, M. Hvala, K. Rossen, R. Göller, A. Burgard, *Org. Process Res. Dev.* **2014**, *18*, 417–422.
- [24] V. W. Lau, I. Moudrakovski, T. Botari, S. Weinberger, M. B. Mesch, V. Duppe, J.
-

- Senker, V. Blum, B. V. Lotsch, *Nat. Commun.* **2016**, *7*, 12165.
- [25] Y. Xi, H. Yi, A. Lei, *Org. Biomol. Chem.* **2013**, *11*, 2387–2403.
- [26] M. A. Ischay, T. P. Yoon, *Eur. J. Org. Chem.* **2012**, 3359–3372.
- [27] M. Parasram, V. Gevorgyan, *Chem. Soc. Rev.* **2017**, *46*, 6227–6240.
- [28] I. M. Dixon, J.-P. Collin, J.-P. Sauvage, L. Flamigni, S. Encinas, F. Barigelletti, *Chem. Soc. Rev.* **2000**, *29*, 385–391.
- [29] J. Read de Alaniz, E. H. Discekici, N. Treat, S. O. Poelma, K. M. Mattson, Z. M. Hudson, Y. Luo, C. J. Hawker, *Chem. Commun.* **2015**, *51*, 11705–11708.
- [30] D. P. Hari, B. König, *Angew. Chem. Int. Ed.* **2013**, *52*, 4734–4743.
- [31] D. P. Hari, B. König, *Chem. Commun.* **2014**, *50*, 6688–6699.
- [32] D. A. Nicewicz, T. M. Nguyen, *ACS Catal.* **2014**, *4*, 355–360.
- [33] J. Luo, J. Zhang, *ACS Catal.* **2016**, *6*, 873–877.
- [34] S. Fukuzumi, H. Kotani, K. Ohkubo, S. Ogo, N. V. Tkachenko, H. Lemmetyinen, *J. Am. Chem. Soc.* **2004**, *126*, 1600–1601.
- [35] A. Joshi-Pangu, F. Lévesque, H. G. Roth, S. F. Oliver, L. C. Campeau, D. Nicewicz, D. A. DiRocco, *J. Org. Chem.* **2016**, *81*, 7244–7249.
- [36] K. Ohkubo, T. Kobayashi, S. Fukuzumi, *Angew. Chem. Int. Ed.* **2011**, *50*, 8652–8655.
- [37] H. G. Roth, N. A. Romero, D. A. Nicewicz, *Synlett* **2016**, *27*, 714–723.
- [38] N. Zhang, S. R. Samanta, B. M. Rosen, V. Percec, *Chem. Rev.* **2014**, *114*, 5848–5958.
- [39] M. Yan, Y. Kawamata, P. S. Baran, *Chem. Rev.* **2017**, *117*, 13230–13319.
- [40] M. A. Cismesia, T. P. Yoon, *Chem. Sci.* **2015**, *6*, 5426–5434.
- [41] M. Busch, M. D. Wodrich, C. Corminboeuf, *ACS Catal.* **2017**, *7*, 5643–5653.
- [42] A. De Meijere, F. Diederich, *Metal-Catalyzed Cross-Coupling Reactions*, Wiley-VCH, Weinheim, **2004**.
- [43] J. Choi, G. C. Fu, *Science* **2017**, *356*, 152–160.
- [44] Z. Zuo, D. T. Ahneman, L. Chu, J. A. Terrett, A. G. Doyle, D. W. C. MacMillan, *Science* **2014**, *437*, 437–440.
- [45] J. C. Tellis, D. N. Primer, G. A. Molander, *Science* **2014**, *345*, 433–436.
- [46] G.-Z. Wang, R. Shang, W.-M. Cheng, Y. Fu, *J. Am. Chem. Soc.* **2017**, *139*, 18307–18312.
- [47] C. D. Matier, J. Schwaben, J. C. Peters, G. C. Fu, *J. Am. Chem. Soc.* **2017**, *139*, 17707–17710.
- [48] J. M. Ahn, J. C. Peters, G. C. Fu, *J. Am. Chem. Soc.* **2017**, *139*, 18101–18106.
- [49] P. Renaud, M. P. Sibi, *Radicals in Organic Synthesis*, Wiley-VCH, Weinheim, **2001**.
- [50] S. P. Pitre, C. D. McTiernan, J. C. Scaiano, *Acc. Chem. Res.* **2016**, *49*, 1320–1330.
-

- [51] J. K. Matsui, S. B. Lang, D. R. Heitz, G. A. Molander, *ACS Catal.* **2017**, *7*, 2563–2575.
- [52] A. Studer, D. P. Curran, *Angew. Chem. Int. Ed.* **2016**, *55*, 58–102.
- [53] C. Chatgililoglu, A. Studer, *Encyclopedia of Radicals in Chemistry, Biology and Materials*, John Wiley & Sons Ltd, Chichester, **2012**.
- [54] J.-P. Goddard, C. Ollivier, L. Fensterbank, *Acc. Chem. Res.* **2016**, *49*, 1924–1936.
- [55] S. Roslin, L. R. Odell, *Eur. J. Org. Chem.* **2017**, 1993–2007.
- [56] T. Koike, M. Akita, *Inorg. Chem. Front.* **2014**, *1*, 562–576.
- [57] D. D. M. Wayner, J. J. Dannenberg, D. Griller, *Chem. Phys. Lett.* **1986**, *131*, 189–191.
- [58] J. Hu, J. Wang, T. H. Nguyen, N. Zheng, *Beilstein J. Org. Chem.* **2013**, *9*, 1977–2001.
- [59] M. A. Ischay, Z. Lu, T. Yoon, *J. Am. Chem. Soc.* **2010**, *132*, 8572–8574.
- [60] K. A. Margrey, D. A. Nicewicz, *Acc. Chem. Res.* **2016**, *49*, 1997–2006.
- [61] K. A. Margrey, J. B. McManus, S. Bonazzi, F. Zecri, D. A. Nicewicz, *J. Am. Chem. Soc.* **2017**, *139*, 11288–11299.
- [62] Y. Yasu, T. Koike, M. Akita, *Adv. Synth. Catal.* **2012**, *354*, 3414–3420.
- [63] Z. Zuo, D. W. C. MacMillan, *J. Am. Chem. Soc.* **2014**, *136*, 5257–5260.
- [64] C. C. Nawrat, C. R. Jamison, Y. Slutskyy, D. W. C. MacMillan, L. E. Overman, *J. Am. Chem. Soc.* **2015**, *137*, 11270–11273.
- [65] A. Gualandi, D. Mazzarella, A. Ortega-Martínez, L. Mengozzi, F. Calcinelli, E. Matteucci, F. Monti, N. Armaroli, L. Sambri, P. G. Cozzi, *ACS Catal.* **2017**, *7*, 5357–5362.
- [66] T. Knauber, R. Chandrasekaran, J. W. Tucker, J. M. Chen, M. Reese, D. A. Rankic, N. Sach, C. Helal, *Org. Lett.* **2017**, *19*, 6566–6569.
- [67] V. Corcé, L. M. Chamoreau, E. Derat, J. P. Goddard, C. Ollivier, L. Fensterbank, *Angew. Chem. Int. Ed.* **2015**, *54*, 11414–11418.
- [68] C. Lévêque, L. Cheneberg, V. Corcé, C. Ollivier, L. Fensterbank, *Chem. Commun.* **2016**, *52*, 9877–9880.
- [69] J. C. Tellis, J. K. Matsui, B. A. Vara, G. A. Molander, *ACS Catal.* **2016**, *6*, 8004–8008.
- [70] L. Buzzetti, A. Prieto, S. Raha Roy, P. Melchiorre, *Angew. Chem. Int. Ed.* **2017**, *56*, 15039–15043.
- [71] D. A. Nicewicz, D. W. C. MacMillan, *Science* **2008**, *322*, 77–80.
- [72] Y. Zhu, L. Zhang, S. Luo, Y. Zhu, L. Zhang, S. Luo, *J. Am. Chem. Soc.* **2014**, *136*, 14642–14645.
- [73] I. Ghosh, T. Ghosh, J. I. Bardagi, B. König, *Science* **2014**, *346*, 725–728.
- [74] A. McNally, C. K. Prier, D. W. C. MacMillan, *Science* **2011**, *334*, 1114–1117.
- [75] J. Jin, D. W. C. MacMillan, *Angew. Chem. Int. Ed.* **2015**, *127*, 1585–1589.
-

- [76] J. D. Cuthbertson, D. W. C. MacMillan, *Nature* **2015**, *519*, 74–77.
- [77] D. P. Hari, P. Schroll, B. König, *J. Am. Chem. Soc.* **2012**, *134*, 2958–2961.
- [78] D. Kalyani, K. B. McMurtrey, S. R. Neufeldt, M. S. Sanford, *J. Am. Chem. Soc.* **2011**, *133*, 18566–18569.
- [79] Y. X. Liu, D. Xue, J. Di Wang, C. J. Zhao, Q. Z. Zou, C. Wang, J. Xiao, *Synlett* **2013**, *24*, 507–513.
- [80] Y. Yasu, T. Koike, M. Akita, *Angew. Chem. Int. Ed.* **2012**, *51*, 9567–9571.
- [81] T. Koike, M. Akita, *Chem* **2017**, *4*, DOI: 10.1016/j.chempr.2017.11.004.
- [82] K. Okada, K. Okamoto, M. Oda, *J. Am. Chem. Soc.* **1988**, *110*, 8736–8738.
- [83] S. Montanaro, D. Ravelli, D. Merli, M. Fagnoni, A. Albini, *Org. Lett.* **2012**, *14*, 4218–4221.
- [84] K. Qvortrup, D. A. Rankic, D. W. C. MacMillan, *J. Am. Chem. Soc.* **2013**, *136*, 626–629.
- [85] D. Hager, D. W. C. MacMillan, *J. Am. Chem. Soc.* **2014**, *136*, 16986–16989.
- [86] M. H. Shaw, V. W. Shurtleff, J. A. Terrett, J. D. Cuthbertson, D. W. C. Macmillan, *Science* **2016**, *352*, 1304–1308.
- [87] G. J. Choi, Q. Zhu, D. C. Miller, C. J. Gu, R. R. Knowles, *Nature* **2016**, *539*, 268–271.
- [88] J. C. K. Chu, T. Rovis, *Nature* **2016**, *539*, 272–275.
- [89] D. Ravelli, S. Protti, M. Fagnoni, *Chem. Rev.* **2016**, *116*, 9850–9913.
- [90] J. Xie, H. Jin, A. S. K. Hashmi, *Chem. Soc. Rev.* **2017**, *46*, 5193–5203.
- [91] F. De Vleeschouwer, V. Van Speybroeck, M. Waroquier, P. Geerlings, F. De Proft, *Org. Lett.* **2007**, *9*, 2720–2724.
- [92] I. Fleming, *Molecular Orbitals and Organic Chemical Reactions*, John Wiley & Sons Ltd, Chichester, **2010**.
- [93] J. Clayden, N. Greeves, S. Warren, *Organic Chemistry*, Oxford University Press, Oxford, **2012**.
- [94] Y. Li, K. Miyazawa, T. Koike, M. Akita, *Org. Chem. Front.* **2015**, *2*, 319–323.
- [95] K. Miyazawa, T. Koike, M. Akita, *Adv. Synth. Catal.* **2014**, *356*, 2749–2755.
- [96] L. Chu, C. Ohta, Z. Zuo, D. W. C. MacMillan, *J. Am. Chem. Soc.* **2014**, *136*, 10886–10889.
- [97] Y. Miyake, K. Nakajima, Y. Nishibayashi, *J. Am. Chem. Soc.* **2012**, *134*, 3338–3341.
- [98] Y. Miyake, Y. Ashida, K. Nakajima, Y. Nishibayashi, *Chem. Commun.* **2012**, *48*, 6966–6968.
- [99] L. Ruiz Espelt, I. S. McPherson, E. M. Wiensch, T. P. Yoon, *J. Am. Chem. Soc.* **2015**, *137*, 2452–2455.
- [100] H. Huo, K. Harms, E. Meggers, *J. Am. Chem. Soc.* **2016**, *138*, 6936–6939.
- [101] J. J. Murphy, D. Bastida, S. Paria, M. Fagnoni, P. Melchiorre, *Nature* **2016**, *532*,
-

- 218–222.
- [102] D. R. Heitz, K. Rizwan, G. A. Molander, *J. Org. Chem.* **2016**, *81*, 7308–7313.
- [103] A. Noble, D. W. C. MacMillan, *J. Am. Chem. Soc.* **2014**, *136*, 11602–11605.
- [104] A. P. Schaffner, V. Darmency, P. Renaud, *Angew. Chem. Int. Ed.* **2006**, *45*, 5847–5849.
- [105] J. Xie, J. Yu, M. Rudolph, F. Rominger, A. S. K. Hashmi, *Angew. Chem. Int. Ed.* **2016**, *55*, 9416–9421.
- [106] Q. Q. Zhou, W. Guo, W. Ding, X. Wu, X. Chen, L. Q. Lu, W. J. Xiao, *Angew. Chem. Int. Ed.* **2015**, *54*, 11196–11199.
- [107] J. Xie, S. Shi, T. Zhang, N. Mehrkens, M. Rudolph, A. S. K. Hashmi, *Angew. Chem. Int. Ed.* **2015**, *54*, 6046–6050.
- [108] H. Fischer, *Chem. Rev.* **2001**, *101*, 3581–3610.
- [109] A. Studer, *Chem. Soc. Rev.* **2004**, *33*, 267–273.
- [110] M. T. Pirnot, D. A. Rankic, D. B. C. Martin, D. W. C. MacMillan, *Science* **2013**, *339*, 1593–1596.
- [111] E. Fava, A. Millet, M. Nakajima, S. Loescher, M. Rueping, *Angew. Chem. Int. Ed.* **2016**, *55*, 6776–6779.
- [112] N. R. Patel, C. B. Kelly, A. P. Siegenfeld, G. A. Molander, *ACS Catal.* **2017**, *7*, 1766–1770.
- [113] D. Uraguchi, N. Kinoshita, T. Kizu, T. Ooi, *J. Am. Chem. Soc.* **2015**, *137*, 13768–13771.
- [114] F. R. Petronijević, M. Nappi, D. W. C. MacMillan, *J. Am. Chem. Soc.* **2013**, *135*, 18323–18326.
- [115] C. Wang, J. Qin, X. Shen, R. Riedel, K. Harms, E. Meggers, *Angew. Chem. Int. Ed.* **2015**, *55*, 685–688.
- [116] C. K. Prier, D. W. C. MacMillan, *Chem. Sci.* **2014**, *5*, 4173–4178.
- [117] A. Singh, A. Arora, J. D. Weaver, *Org. Lett.* **2013**, *15*, 5390–5393.
- [118] J. C. Tellis, C. B. Kelly, D. N. Primer, M. Jouffroy, N. R. Patel, G. A. Molander, *Acc. Chem. Res.* **2016**, *49*, 1429–1439.
- [119] L. N. Cavalcanti, G. A. Molander, *Top. Curr. Chem.* **2016**, *374*, 1–23.
- [120] O. Gutierrez, J. C. Tellis, D. N. Primer, G. A. Molander, M. C. Kozlowski, *J. Am. Chem. Soc.* **2015**, *137*, 4896–4899.
- [121] N. R. Patel, C. B. Kelly, M. Jouffroy, G. A. Molander, *Org. Lett.* **2016**, *18*, 764–767.
- [122] M. Jouffroy, D. N. Primer, G. A. Molander, *J. Am. Chem. Soc.* **2015**, *138*, 475–478.
- [123] Á. Gutiérrez-Bonet, J. C. Tellis, J. K. Matsui, B. A. Vara, G. A. Molander, *ACS Catal.* **2016**, *6*, 8004–8008.
- [124] D. T. Ahneman, A. G. Doyle, *Chem. Sci.* **2016**, *7*, 7002–7006.
- [125] B. J. Shields, A. G. Doyle, *J. Am. Chem. Soc.* **2016**, *138*, 12719–12722.
-

- [126] D. N. Primer, I. Karakaya, J. C. Tellis, G. A. Molander, *J. Am. Chem. Soc.* **2015**, *137*, 2195–2198.
- [127] D. N. Primer, G. A. Molander, *J. Am. Chem. Soc.* **2017**, *139*, 9847–9850.
- [128] A. Noble, S. J. McCarver, D. W. C. MacMillan, *J. Am. Chem. Soc.* **2015**, *137*, 624–627.
- [129] Y.-Y. Gui, L.-L. Liao, L. Sun, Z. Zhang, J.-H. Ye, G. Shen, Z.-P. Lu, W.-J. Zhou, D.-G. Yu, *Chem. Commun.* **2017**, *111*, 1315–1345.
- [130] J. Amani, E. Sodagar, G. A. Molander, *Org. Lett.* **2016**, *18*, 732–735.
- [131] C. P. Johnston, R. T. Smith, S. Allmendinger, D. W. C. MacMillan, *Nature* **2016**, *536*, 322–325.
- [132] L. G. Fensterbank, C. Ollivier, C. Lévêque, V. Corcé, L. Chenneberg, *Eur. J. Org. Chem.* **2017**, 2118–2121.
- [133] Z. Zuo, H. Cong, W. Li, J. Choi, G. C. Fu, D. W. C. MacMillan, *J. Am. Chem. Soc.* **2016**, *138*, 1832–1835.
- [134] J. D. Nguyen, J. W. Tucker, M. D. Konieczynska, C. R. J. Stephenson, *J. Am. Chem. Soc.* **2011**, *133*, 4160–4163.
- [135] C. J. Wallentin, J. D. Nguyen, P. Finkbeiner, C. R. J. Stephenson, *J. Am. Chem. Soc.* **2012**, *134*, 8875–8884.
- [136] P. Schroll, D. P. Hari, B. König, *ChemistryOpen* **2012**, *1*, 130–133.
- [137] D. A. Nagib, M. E. Scott, D. W. C. MacMillan, *J. Am. Chem. Soc.* **2009**, *131*, 10875–10877.
- [138] H. W. Shih, M. N. Vander Wal, R. L. Grange, D. W. C. MacMillan, *J. Am. Chem. Soc.* **2010**, *132*, 13600–13603.
- [139] F. Minisci, F. Bertini, R. Galli, M. Perchinijmmo, *Tetrahedron* **1971**, *27*, 3575–3579.
- [140] J. Tauber, D. Imbri, T. Opatz, *Molecules* **2014**, *19*, 16190–16222.
- [141] D. A. DiRocco, K. Dykstra, S. Krska, P. Vachal, D. V. Conway, M. Tudge, *Angew. Chem. Int. Ed.* **2014**, *53*, 4802–4806.
- [142] G.-X. Li, C. A. Morales-Rivera, Y. Wang, F. Gao, G. He, P. Liu, G. Chen, *Chem. Sci.* **2016**, *7*, 6407–6412.
- [143] J. Jin, D. W. C. MacMillan, *Angew. Chem. Int. Ed.* **2015**, *54*, 1565–1569.
- [144] D. Xue, Z.-H. Jia, C.-J. Zhao, Y.-Y. Zhang, C. Wang, J. Xiao, *Chem. Eur. J.* **2014**, *20*, 2960–5.
- [145] W. M. Cheng, R. Shang, Y. Fu, *ACS Catal.* **2017**, *7*, 907–911.
- [146] F. Gomes, V. Narbonne, F. Blanchard, G. Maestri, M. Malacria, *Org. Chem. Front.* **2015**, 464–469.
- [147] I. Gosh, T. Gosh, J. I. Bardagi, B. König, *Science* **2014**, *346*, 725–728.
- [148] M. Tobisu, T. Furukawa, N. Chatani, *Chem. Lett.* **2013**, *42*, 1203–1205.
- [149] M. Majek, F. Filace, A. J. von Wangelin, *Beilstein J. Org. Chem.* **2014**, *10*, 981–989.
-

- [150] J. Twilton, C. C. Le, P. Zhang, M. H. Shaw, R. W. Evans, D. W. C. MacMillan, *Nat. Rev. Chem.* **2017**, *1*, 52.
- [151] Y. Ye, M. S. Sanford, *J. Am. Chem. Soc.* **2012**, *134*, 9034–9037.
- [152] M. N. Hopkinson, A. Tlahuext-Aca, F. Glorius, *Acc. Chem. Res.* **2016**, *49*, 2261–2272.
- [153] S. Kim, J. Rojas-Martin, F. D. Toste, *Chem. Sci.* **2016**, *7*, 85–88.
- [154] A. Tlahuext-Aca, M. N. Hopkinson, B. Sahoo, F. Glorius, *Chem. Sci.* **2016**, *7*, 89–93.
- [155] A. Tlahuext-Aca, M. N. Hopkinson, R. Aleyda Garza-Sanchez, F. Glorius, *Chem. Eur. J.* **2016**, *22*, 5909–5913.
- [156] R. Steudel, *Chemistry of the Non-Metals With an Introduction to Atomic Structure and Chemical Bonding*, De Gruyter, Berlin, **2014**.
- [157] D. G. Hall, *Structure, Properties, and Preparation of Boronic Acid Derivatives. Overview of Their Reactions and Applications*, Wiley-VCH, Weinheim, **2006**.
- [158] A. J. J. Lennox, G. C. Lloyd-Jones, *Chem. Soc. Rev.* **2014**, *43*, 412–443.
- [159] R. Crampton, S. Woodward, M. Fox, *Adv. Synth. Catal.* **2011**, *353*, 903–906.
- [160] X. J. Wang, X. Sun, L. Zhang, Y. Xu, D. Krishnamurthy, C. H. Senanayake, *Org. Lett.* **2006**, *8*, 305–307.
- [161] W. Li, D. P. Nelson, M. S. Jensen, R. S. Hoerner, D. Cai, R. D. Larsen, P. J. Reider, *J. Org. Chem.* **2002**, *67*, 5394–5397.
- [162] B. M. Trost, Z. T. Ball, *Synthesis* **2005**, 853–887.
- [163] D. A. Evans, G. C. Fu, A. H. Hoveyda, *J. Am. Chem. Soc.* **1992**, *114*, 6671–6679.
- [164] I. Beletskaya, A. Pelter, *Tetrahedron* **1997**, *53*, 4957–5026.
- [165] T. Ishiyama, N. Miyaura, *Chem. Rec.* **2004**, *3*, 271–280.
- [166] G. A. Molander, S. L. J. Trice, S. D. Dreher, *J. Am. Chem. Soc.* **2010**, *132*, 17701–17703.
- [167] P. Merino, T. Tejero, *Angew. Chem. Int. Ed.* **2010**, *49*, 7164–7165.
- [168] S. R. Gurung, C. Mitchell, J. Huang, M. Jonas, J. D. Strawser, E. Daia, A. Hardy, E. O'Brien, F. Hicks, C. D. Papageorgiou, *Org. Process Res. Dev.* **2017**, *21*, 65–74.
- [169] I. A. I. Mkhaliid, J. H. Barnard, T. B. Marder, J. M. Murphy, J. F. Hartwig, *Chem. Rev.* **2009**, *110*, 890–931.
- [170] N. Miyaura, A. Suzuki, *Chem. Rev.* **1995**, *95*, 2457–2483.
- [171] X. F. Wu, P. Anbarasan, H. Neumann, M. Beller, *Angew. Chem. Int. Ed.* **2010**, *49*, 9047–9050.
- [172] P. A. Cox, M. Reid, A. G. Leach, A. D. Campbell, E. J. King, G. C. Lloyd-Jones, *J. Am. Chem. Soc.* **2017**, *139*, 13156–13165.
- [173] D. S. Matteson, K. M. Sadhu, *J. Am. Chem. Soc.* **1983**, *105*, 2077–2078.
- [174] D. S. Matteson, R. Ray, *J. Am. Chem. Soc.* **1980**, *102*, 7590–7591.
-

- [175] D. S. Matteson, *J. Org. Chem.* **2013**, *78*, 10009–10023.
- [176] E. J. Corey, D. Barnes-Seeman, T. W. Lee, *Tetrahedron: Asymmetry* **1997**, *8*, 3711–3713.
- [177] D. Leonori, V. K. Aggarwal, *Acc. Chem. Res.* **2014**, *47*, 3174–3183.
- [178] M. Burns, S. Essafi, J. R. Bame, S. P. Bull, M. P. Webster, S. Balieu, J. W. Dale, C. P. Butts, J. N. Harvey, V. K. Aggarwal, *Nature* **2014**, *513*, 183–188.
- [179] C. Sandford, V. K. Aggarwal, *Chem. Commun.* **2017**, *53*, 5481–5494.
- [180] D. Leonori, V. K. Aggarwal, *Angew. Chem. Int. Ed.* **2015**, *54*, 1082–1096.
- [181] M. Paraja, M. Plaza, *Synlett* **2017**, *28*, 2373–2389.
- [182] J. Barluenga, M. Tomás-Gamasa, F. Aznar, C. Valdés, *Nat. Chem.* **2009**, *1*, 494–499.
- [183] C. Bomio, M. A. Kabeshov, A. R. Lit, S.-H. Lau, J. Ehlert, C. Battilocchio, S. V. Ley, *Chem. Sci.* **2017**, *8*, 6071–6075.
- [184] C. Battilocchio, F. Feist, A. Hafner, M. Simon, D. N. Tran, D. M. Allwood, D. C. Blakemore, S. V. Ley, *Nat. Chem.* **2016**, *8*, 360–367.
- [185] A. Greb, J.-S. Poh, S. Greed, C. Battilocchio, P. Pasau, D. C. Blakemore, S. V. Ley, *Angew. Chem. Int. Ed.* **2017**, *56*, 16602–16605.
- [186] C. Ollivier, P. Renaud, *Chem. Rev.* **2001**, *101*, 3415–3434.
- [187] A. Suzuki, A. Arase, H. Matsumoto, M. Itoh, H. C. Brown, M. M. Rogić, M. W. Rathke, *J. Am. Chem. Soc.* **1967**, *89*, 5708–5709.
- [188] H. C. Brown, M. M. Midland, *Angew. Chem. Int. Ed.* **1972**, *11*, 692–700.
- [189] G. W. Kabalka, H. C. Brown, A. Suzuki, S. Honma, A. Arase, M. Itoh, *J. Am. Chem. Soc.* **1970**, *92*, 710–712.
- [190] C. Ollivier, P. Renaud, *Chem. Eur. J.* **1999**, 1468–1473.
- [191] C. Ollivier, P. Renaud, *Angew. Chem. Int. Ed.* **2000**, *39*, 925–928.
- [192] A. P. Schaffner, P. Renaud, *Eur. J. Org. Chem.* **2004**, 2291–2298.
- [193] L. A. Shundrin, V. V. Bardin, H. J. Frohn, *Zeitschrift für Anorg. und Allg. Chemie* **2004**, *630*, 1253–1257.
- [194] G. B. Schuster, *Pure Appl. Chem.* **1990**, *62*, 1565–1572.
- [195] G. Sorin, R. Martinezmallorquin, Y. Contie, A. Baralle, M. Malacria, J. P. Goddard, L. Fensterbank, *Angew. Chem. Int. Ed.* **2010**, *49*, 8721–8723.
- [196] G. A. Molander, V. Colombel, V. A. Braz, *Org. Lett.* **2011**, *13*, 1852–1855.
- [197] A. S. Demir, Ö. Reis, M. Emrullahoglu, *J. Org. Chem.* **2003**, *68*, 578–580.
- [198] A. Dickschat, A. Studer, *Org. Lett.* **2010**, *12*, 3972–3974.
- [199] S. K. Guchhait, M. Kashyap, S. Saraf, *Synthesis* **2010**, 1166–1170.
- [200] J. W. Lockner, D. D. Dixon, R. Risgaard, P. S. Baran, *Org. Lett.* **2011**, *13*, 5628–5631.
- [201] I. B. Seiple, S. Su, R. A. Rodriguez, R. Gianatassio, Y. Fujiwara, A. L. Sobel, P. S. Baran, *J. Am. Chem. Soc.* **2010**, *132*, 13194–13196.
-

- [202] G. Yan, M. Yang, X. Wu, *Org. Biomol. Chem.* **2013**, *11*, 7999–8008.
- [203] T. Koike, M. Akita, *Org. Biomol. Chem.* **2016**, *14*, 6886–6890.
- [204] G. Duret, R. Quinlan, P. Bissereet, N. Blanchard, *Chem. Sci.* **2015**, *6*, 5366–5382.
- [205] T. Chinzei, K. Miyazawa, Y. Yasu, T. Koike, M. Akita, *RSC Adv.* **2015**, *5*, 21297–21300.
- [206] I. Karakaya, D. N. Primer, G. A. Molander, *Org. Lett.* **2015**, *17*, 3294–3297.
- [207] T. Hoshikawa, M. Inoue, *Chem. Sci.* **2013**, *4*, 3118–3123.
- [208] L. Delhaye, A. Ceccato, P. Jacobs, C. K ttgen, A. Merschaert, *Org. Process Res. Dev.* **2007**, *11*, 160–164.
- [209] P. Isnard, E. Guntrum, T. Senac, P. Cruciani, *Org. Process Res. Dev.* **2013**, *17*, 1517–1525.
- [210] T. C. Atack, R. M. Lecker, S. P. Cook, *J. Am. Chem. Soc.* **2014**, *136*, 9521–9523.
- [211] J. W. Clary, T. J. Rettenmaier, R. Snelling, W. Bryks, J. Banwell, W. T. Wipke, B. Singaram, *J. Org. Chem.* **2011**, *76*, 9602–9610.
- [212] H. Li, L. Wang, Y. Zhang, J. Wang, *Angew. Chem. Int. Ed.* **2012**, *51*, 2943–2946.
- [213] W. N. Palmer, J. V. Obligacion, I. Pappas, P. J. Chirik, *J. Am. Chem. Soc.* **2016**, *138*, 766–769.
- [214] H. Li, L. Wang, Y. Zhang, J. Wang, *Angew. Chem.* **2012**, *124*, 2997–3000.
- [215] C. Ollivier, *Angew. Chem.* **2000**, *112*, 946–949.
- [216] Y. Su, N. J. W. Straathof, V. Hessel, T. No l, *Chem. Eur. J.* **2014**, *20*, 10562–10589.
- [217] M. Neumann, K. Zeitler, *Org. Lett.* **2012**, *14*, 2658–2661.
- [218] J. W. Beatty, C. R. J. Stephenson, *J. Am. Chem. Soc.* **2014**, *136*, 10270–10273.
- [219] D. Cambi , C. Bottecchia, N. J. W. Straathof, V. Hessel, T. No l, *Chem. Rev.* **2016**, *116*, 10276–10341.
- [220] K. Loubi re, M. Oelgem ller, T. Aillet, O. Dechy-Cabaret, L. Prat, *Chem. Eng. Process.* **2016**, *104*, 120–132.
- [221] B. D. A. Hook, W. Dohle, P. R. Hirst, M. Pickworth, M. B. Berry, K. I. Booker-Milburn, *J. Org. Chem.* **2005**, *70*, 7558–7564.
- [222] J. Y. M rour, F. Buron, K. Pl , P. Bonnet, S. Routier, *Molecules* **2014**, *19*, 19935–19979.
- [223] S. Panda, A. Coffin, Q. N. Nguyen, D. J. Tantillo, J. M. Ready, *Angew. Chem. Int. Ed.* **2016**, *55*, 2205–2209.
- [224] M. Ishikura, M. Kamada, I. Oda, T. Ohta, M. Terashima, *J. Heterocycl. Chem.* **1987**, *24*, 377–386.
- [225] “Buy 4-allyl-pyridine,” can be found under <http://www.accelpharmtech.com/product/76419.html>, last consulted in January **2018**.
- [226] L. D. Elliott, M. Berry, B. Harji, D. Klauber, J. Leonard, K. I. Booker-Milburn, *Org. Process Res. Dev.* **2016**, *20*, 1806–1811.
-

- [227] C. F. Carter, H. Lange, S. V. Ley, I. R. Baxendale, B. Wittkamp, J. G. Goode, N. L. Gaunt, *Org. Process Res. Dev.* **2010**, *14*, 393–404.
- [228] K. Teegardin, J. I. Day, J. Chan, J. Weaver, *Org. Process Res. Dev.* **2016**, *20*, 1156–1163.
- [229] Y. Yamashita, J. C. Tellis, G. A. Molander, *Proc. Natl. Acad. Sci. U.S.A.* **2015**, *112*, 12026–12029.
- [230] W. D. Wang, J. H. Espenson, *J. Am. Chem. Soc.* **1998**, *120*, 11335–11341.
- [231] K. Ohtsuka, S. Inagi, T. Fuchigami, *ChemElectroChem* **2016**, 183–187.
- [232] F. Lima, M. A. Kabeshov, D. N. Tran, C. Battilocchio, J. Sedelmeier, G. Sedelmeier, B. Schenkel, S. V. Ley, *Angew. Chem. Int. Ed.* **2016**, *55*, 14085–14089.
- [233] S. E. Denmark, G. L. Beutner, *Angew. Chem. Int. Ed.* **2008**, *47*, 1560–1638.
- [234] A. H. Hoveyda, H. Wu, S. Radomkit, J. M. Garcia, F. Haeffner, K. Lee, *Lewis Base Catalysis in Organic Synthesis*, Wiley-VCH, Weinheim, **2016**.
- [235] C. Laurence, J.-F. Gal, *Lewis Basicity and Affinity Scales*, John Wiley & Sons Ltd, Chichester, **2010**.
- [236] L. Capaldo, M. Fagnoni, D. Ravelli, *Chem. Eur. J.* **2017**, *23*, 6527–6530.
- [237] C. Li, J. Wang, L. M. Barton, S. Yu, M. Tian, D. S. Peters, M. Kumar, A. W. Yu, K. A. Johnson, A. K. Chatterjee, et al., *Science* **2017**, *356*, 6342.
- [238] H. R. Snyder, M. S. Konecky, W. J. Lennarz, *J. Am. Chem. Soc.* **1958**, *80*, 3611–3615.
- [239] A. L. Korich, P. M. Iovine, *Dalt. Trans.* **2010**, *39*, 1423–1431.
- [240] F. Lima, U. K. Sharma, L. Grunenberg, D. Saha, S. Johannsen, J. Sedelmeier, E. V. Van der Eycken, S. V. Ley, *Angew. Chem. Int. Ed.* **2017**, *56*, 15136–15140.
- [241] M. Pokorski, *Neurotransmitter Interactions and Cognitive Function*, Springer, Berlin, Heidelberg, **2014**.
- [242] G. J. Sills, *Curr. Opin. Pharmacol.* **2006**, *6*, 108–113.
- [243] G. Sedelmeier, J. Sedelmeier, *Chim. Int. J. Chem.* **2017**, *71*, 730.
- [244] J. Egebjerg, A. Schousboe, P. Krogsgaard-Larsen, *Glutamate and GABA Receptors and Transporters: Structure, Function and Pharmacology*, Taylor & Francis, London, **2001**.
- [245] T. M. Grote, B. K. Huckabee, T. Mulhern, D. M. Sobieray, R. D. Titus, *Method of Making (S)-3-(Aminomethyl)-5-Methylhexanoic Acid*, **1997**, US5637767 A.
- [246] D. Ghislieri, K. Gilmore, P. H. Seeberger, *Angew. Chem. Int. Ed.* **2015**, *54*, 678–682.
- [247] H. Ishitani, K. Kanai, Y. Saito, T. Tsubogo, S. Kobayashi, *Eur. J. Org. Chem.* **2017**, 6491–6494.
- [248] R. Porta, M. Benaglia, A. Puglisi, *Org. Process Res. Dev.* **2016**, *20*, 2–25.
- [249] D. Cambié, C. Bottecchia, N. J. W. Straathof, V. Hessel, T. Noël, *Chem. Rev.* **2016**, *116*, 10276–10341.
-

- [250] M. B. Plutschack, B. Pieber, K. Gilmore, P. H. Seeberger, *Chem. Rev.* **2017**, *117*, 11796–11893.
- [251] M. Movsisyan, E. I. P. Delbeke, J. K. E. T. Berton, C. Battilocchio, S. V. Ley, C. V. Stevens, *Chem. Soc. Rev.* **2016**, *45*, 4892–4928.
- [252] G. Höfle, W. Steglich, H. Vorbrüggen, *Angew. Chem. Int. Ed.* **1978**, *17*, 569–583.
- [253] R. Chenevert, M. Desjardins, *Can. J. Chem.* **1994**, *72*, 2312–2317.
- [254] S. V. Ley, I. R. Baxendale, R. N. Bream, P. S. Jackson, A. G. Leach, D. A. Longbottom, M. Nesi, J. S. Scott, R. I. Storer, S. J. Taylor, *J. Chem. Soc. Perkin Trans. 1* **2000**, 3815–4195.
- [255] S. V. Ley, D. E. Fitzpatrick, R. J. Ingham, R. M. Myers, *Angew. Chem. Int. Ed.* **2015**, *54*, 3449–3464.
- [256] D. X. Hu, M. O'Brien, S. V. Ley, *Org. Lett.* **2012**, *14*, 4246–4249.
- [257] C. H. Hornung, M. R. Mackley, I. R. Baxendale, S. V. Ley, *Org. Process Res. Dev.* **2007**, *11*, 399–405.
- [258] C. O. Europe, *European Pharmacopoeia*, Renouf Publishing Company Limited, Ottawa, **2005**.
- [259] L. K. Sorensen, J. B. Hasselstrom, *J. Anal. Toxicol.* **2014**, *38*, 177–183.
- [260] B. Buszewski, S. Noga, *Anal. Bioanal. Chem.* **2012**, *402*, 231–247.
- [261] J. J. Devery III, J. J. Douglas, J. D. Nguyen, K. P. Cole, R. A. Flowers II, C. R. J. Stephenson, *Chem. Sci.* **2015**, *6*, 537–541.
- [262] I. N. Mills, J. A. Porras, S. Bernhard, *Acc. Chem. Res.* **2018**, DOI: 10.1021/acs.accounts.7b00375.
- [263] J. Da Chai, M. Head-Gordon, *Phys. Chem. Chem. Phys.* **2008**, *10*, 6615–6620.
- [264] S. Schenker, C. Schneider, S. B. Tsogoeva, T. Clark, *J. Chem. Theory Comput.* **2011**, *7*, 3586–3595.
- [265] M. A. Kabeshov, O. Kysilka, L. Rulisek, Y. V. Suleimanov, M. Bella, A. V. Malkov, P. Kocovsky, *Chem. Eur. J.* **2015**, *21*, 12026–12033.
- [266] A. V. Marenich, C. J. Cramer, D. G. Truhlar, *J. Phys. Chem. B* **2009**, *113*, 6378–6396.
- [267] J. N. M. J. Frisch, G. W. Trucks, H. B. Schlegel, G. E. Scuseria, M. A. Robb, J. R. Cheeseman, G. Scalmani, V. Barone, B. Mennucci, G. A. Petersson, H. Nakatsuji, M. Caricato, X. Li, H. P. Hratchian, A. F. Izmaylov, J. Bloino, G. Zheng, J. L. Sonnenberg, M. Had, J. V. O. J. C. K. Raghavachari, A. Rendell, J. C. Burant, S. S. Iyengar, J. Tomasi, M. Cossi, N. Rega, J. M. Millam, M. Klene, J. E. Knox, J. B. Cross, V. Bakken, C. Adamo, J. Jaramillo, R. Gomperts, R. E. Stratmann, O. Yazyev, A. J. Austin, R. Cammi, C. Pomelli, J. W., D. J. Fox, “Gaussian 09, Revision D.01,” **2013**.
- [268] M. A. Larsen, C. V. Wilson, J. F. Hartwig, *J. Am. Chem. Soc.* **2015**, *137*, 8633–8643.
- [269] Z.-C. Cao, F.-X. Luo, W.-J. Shi, Z.-J. Shi, *Org. Chem. Front.* **2015**, *2*, 1505–1510.
- [270] S. Roesner, C. A. Brown, M. Mohiti, A. P. Pulis, R. Rasappan, D. J. Blair, S.
-

- Essafi, D. Leonori, V. K. Aggarwal, *Chem. Commun.* **2014**, 50, 4053–4055.
- [271] S. Duez, A. K. Steib, S. M. Manolikakes, P. Knochel, *Angew. Chem. Int. Ed.* **2011**, 50, 7686–7690.
- [272] M.-J. Shiao, W.-L. Chia, *Synth. Commun.* **1991**, 21, 401–406.
- [273] X. Li, Y. Feng, L. Lin, G. Zou, *J. Org. Chem.* **2012**, 77, 10991–10995.
- [274] D. Collado, E. Perez-Inestrosa, R. Suau, *J. Org. Chem.* **2003**, 68, 3574–84.
- [275] E. Reimann, A. Höglmüller, *Arch. Pharm.* **1985**, 318, 487–495.
- [276] S. Thapa, A. Kafle, S. K. Gurung, A. Montoya, P. Riedel, R. Giri, *Angew. Chem. Int. Ed.* **2015**, 54, 8236–8240.
- [277] X.-X. Wang, M.-J. Luo, J.-M. Lu, *Org. Biomol. Chem.* **2015**, 13, 4925–4930.
- [278] G. Song, Y. Su, X. Gong, K. Han, X. Li, *Org. Lett.* **2011**, 13, 1968–1971.
- [279] S. Panda, A. Coffin, Q. N. Nguyen, D. J. Tantillo, J. M. Ready, *Angew. Chem. Int. Ed.* **2015**, 55, 2205–2209.
- [280] R. B. Bedford, E. Carter, P. M. Cogswell, N. J. Gower, M. F. Haddow, J. N. Harvey, D. M. Murphy, E. C. Neeve, J. Nunn, *Angew. Chem. Int. Ed.* **2013**, 52, 1285–1288.
- [281] S. Bernhardt, Z. L. Shen, P. Knochel, *Chem. Eur. J.* **2013**, 19, 828–833.
- [282] D. Saha, R. Ghosh, A. Sarkar, *Tetrahedron* **2013**, 69, 3951–3960.
- [283] R. Kuwano, M. Yokogi, *Org. Lett.* **2005**, 7, 945–947.
- [284] I. Erol, L. Özcan, S. Yurdakal, *J. Therm. Anal. Calorim.* **2013**, 114, 377–385.
- [285] M. Itoh, K. Hirano, T. Satoh, M. Miura, *Org. Lett.* **2014**, 16, 2050–2053.
- [286] R. K. Dieter, S. Li, *J. Org. Chem.* **1997**, 62, 7726–7735.
- [287] N. El Achi, M. Penhoat, Y. Bakkour, C. Rolando, L. Chausset-Boissarie, *Eur. J. Org. Chem.* **2016**, 4284–4288.
- [288] X. J. Dai, H. Wang, C. J. Li, *Angew. Chem. Int. Ed.* **2017**, 56, 6302–6306.
- [289] E. E. Finney, K. A. Ogawa, A. J. Boydston, *J. Am. Chem. Soc.* **2012**, 134, 12374–12377.
- [290] M. Shimogaki, M. Fujita, T. Sugimura, *Angew. Chem. Int. Ed.* **2016**, 55, 15797–15801.
- [291] G. C. Tsui, M. Lautens, *Angew. Chem. Int. Ed.* **2010**, 49, 8938–8941.
- [292] M. H. Wang, D. T. Cohen, C. B. Schwamb, R. K. Mishra, K. A. Scheidt, *J. Am. Chem. Soc.* **2015**, 137, 5891–5894.
- [293] H. Jiang, W. Yang, H. Chen, J. Li, W. Wu, *Chem. Commun.* **2014**, 50, 7202–7204.
- [294] K. M. M. Huihui, J. A. Caputo, Z. Melchor, A. M. Olivares, A. M. Spiewak, K. A. Johnson, T. A. Dibenedetto, S. Kim, L. K. G. Ackerman, D. J. Weix, *J. Am. Chem. Soc.* **2016**, 138, 5016–5019.
- [295] N. Kise, T. Mano, T. Sakurai, *J. Org. Chem.* **1994**, 62, 1407–1413.
- [296] F. Berthiol, H. Doucet, M. Santelli, *Synthesis* **2005**, 3589–3602.
-

- [297] F. Chen, B. Mudryk, T. Cohen, *Tetrahedron* **1999**, *55*, 3291–3304.
- [298] R. K. Dieter, C. W. Alexander, L. E. Nice, *Tetrahedron* **2000**, *56*, 2767–2778.
- [299] P. Wipf, W. Xu, J. H. Smitrovich, R. Lehmann, L. M. Venanzi, *Tetrahedron* **1994**, *50*, 1935–1954.
- [300] K. Adachi, *Nippon Kagaku Kaishi* **1972**, 985–987.
- [301] W. Kerr, R. Mudd, J. Brown, *Chem. Eur. J.* **2016**, *22*, 4738–4742.
- [302] M. B. Reardon, M. Xu, Q. Tan, P. G. Baumgartel, D. J. Augur, S. Huo, C. E. Jakobsche, *J. Org. Chem.* **2016**, *81*, 10964–10974.
- [303] D. A. Chaudhari, R. A. Fernandes, *J. Org. Chem.* **2016**, *81*, 2113–2121.
- [304] J. X. Gu, H. L. Holland, *Synth. Commun.* **1998**, *28*, 3305–3315.
- [305] S. Mohanty, A. K. Roy, G. Sandeep Reddy, K. P. Vinay Kumar, B. Ramadevi, G. Bhargavi, A. C. Karmakar, *Tetrahedron Lett.* **2015**, *56*, 2564–2567.
- [306] G. Griffiths, H. Mettler, L. S. Mills, F. Previdoli, *Helv. Chim. Acta* **1991**, *74*, 309–314.
- [307] M. Nagatomo, H. Nishiyama, H. Fujino, M. Inoue, *Angew. Chem. Int. Ed.* **2015**, *54*, 1537–1541.
-

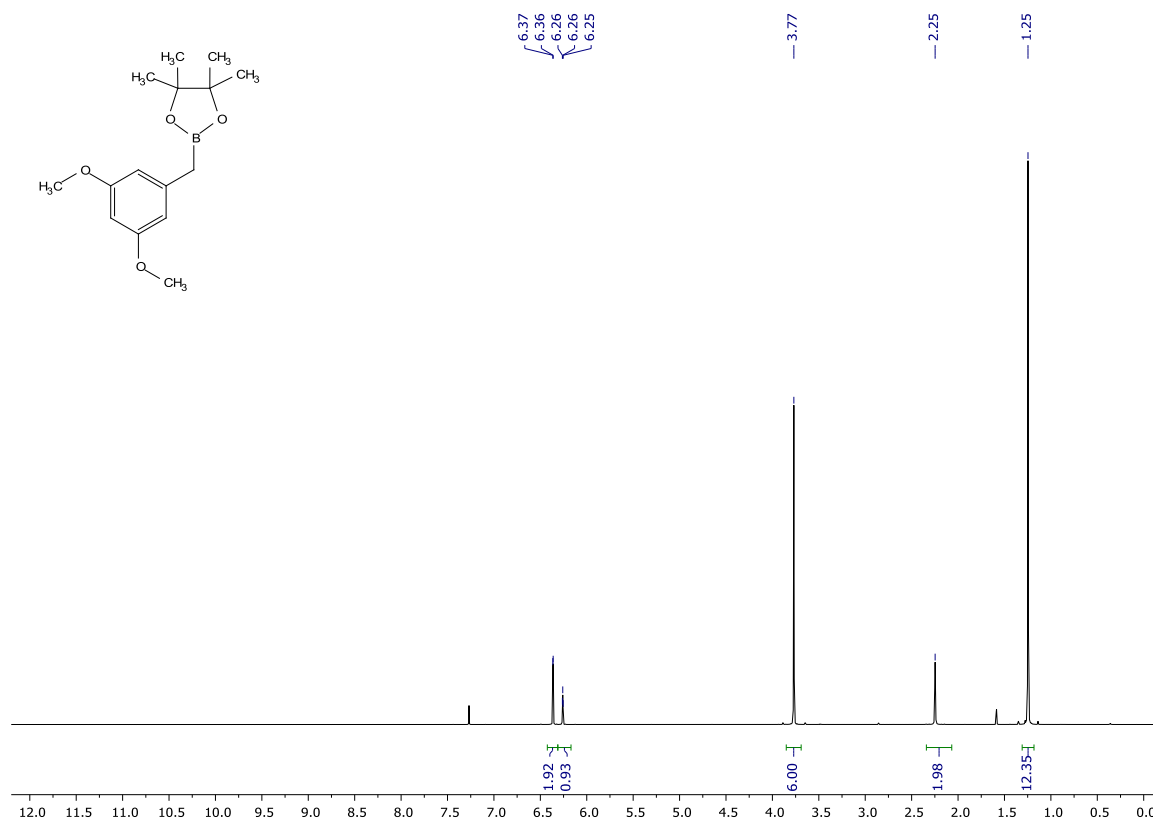
7 Appendices (NMR spectra)

7.1 Spectra for Chapter 2

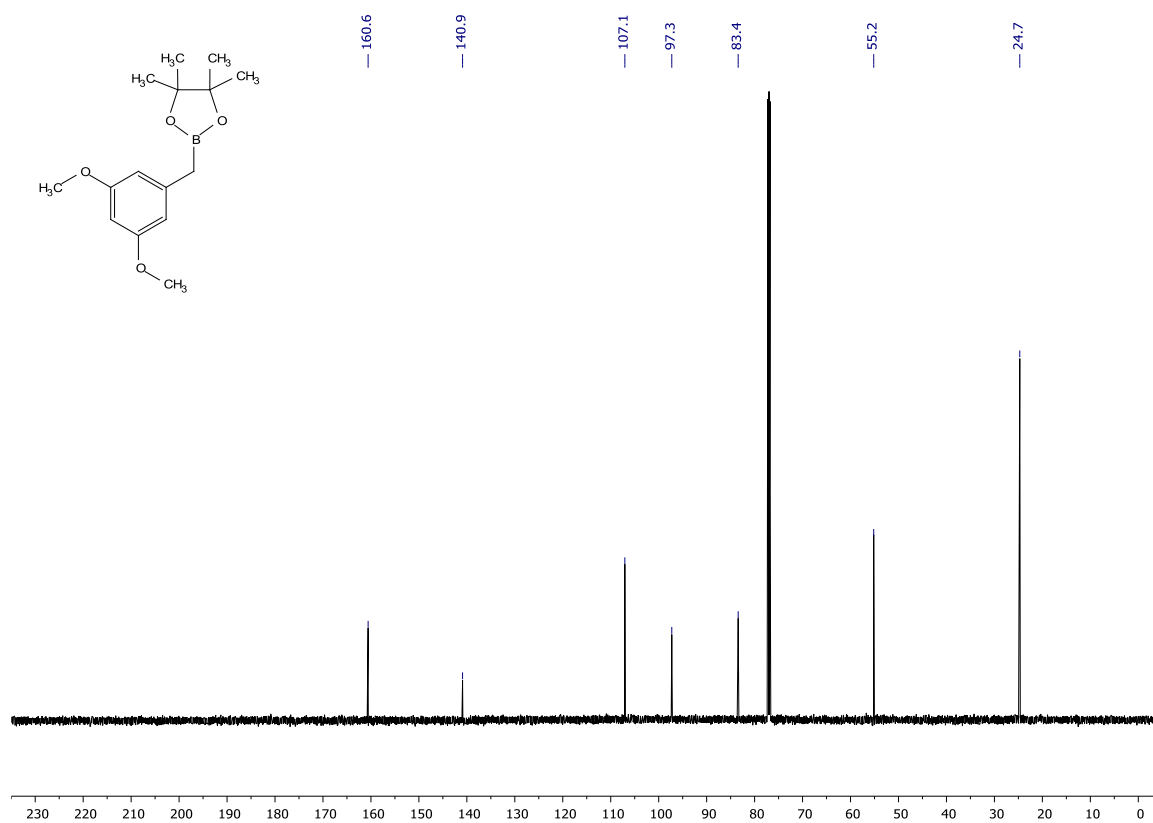
7.1.1 Starting materials spectra

2-(3,5-dimethoxybenzyl)-4,4,5,5-tetramethyl-1,3,2-dioxaborolane

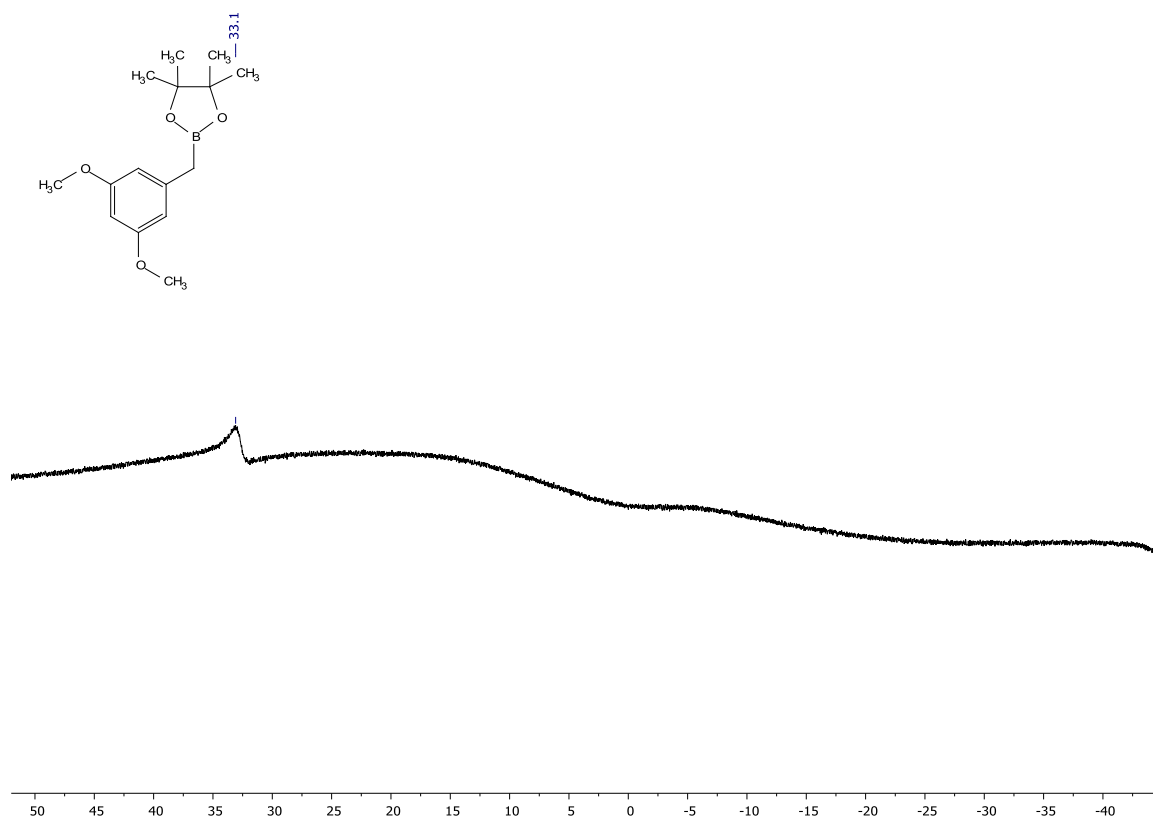
$^1\text{H-NMR}$ (600 MHz, CDCl_3)

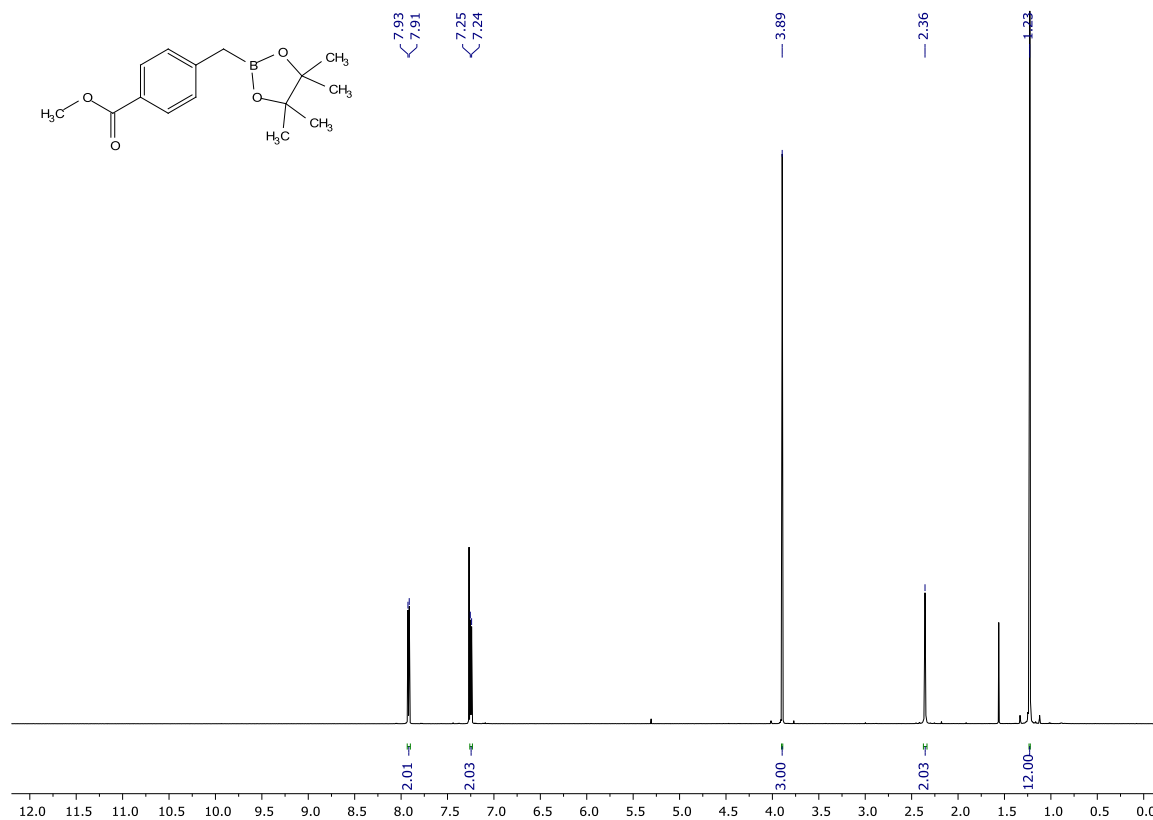
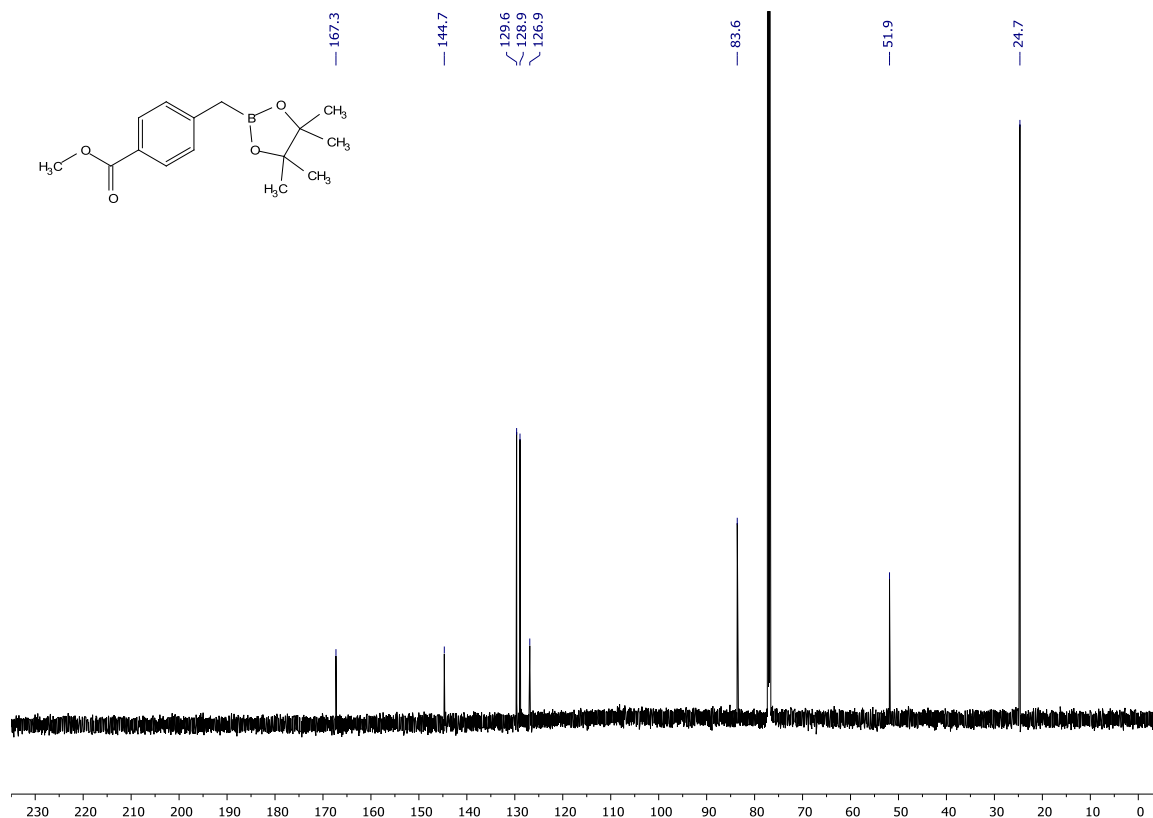


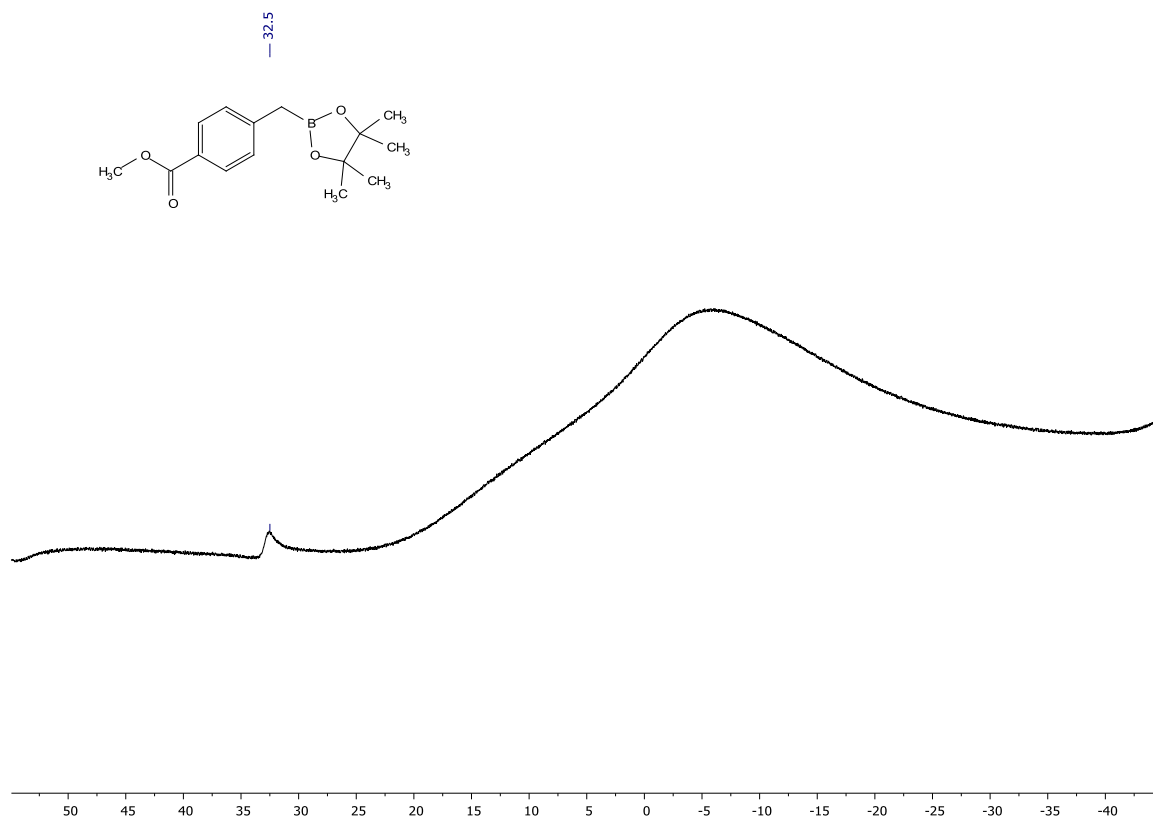
¹³C-NMR (151 MHz, CDCl₃)

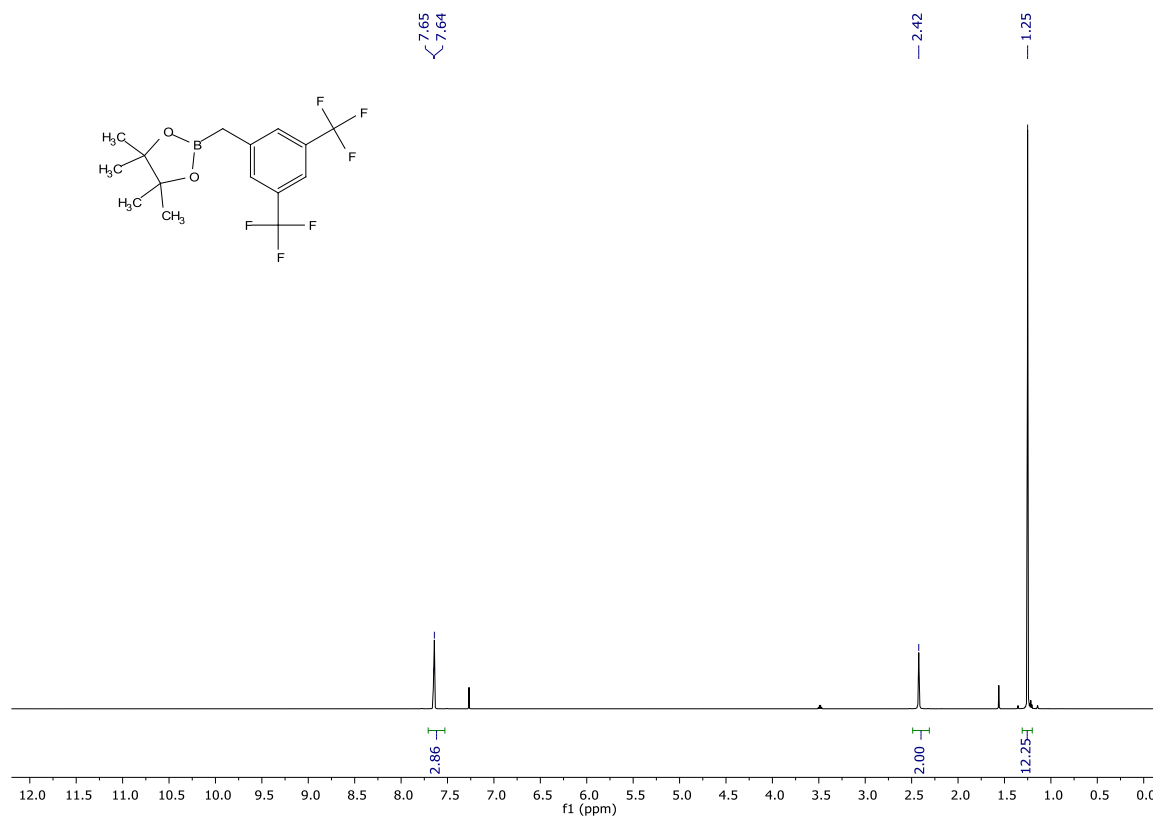
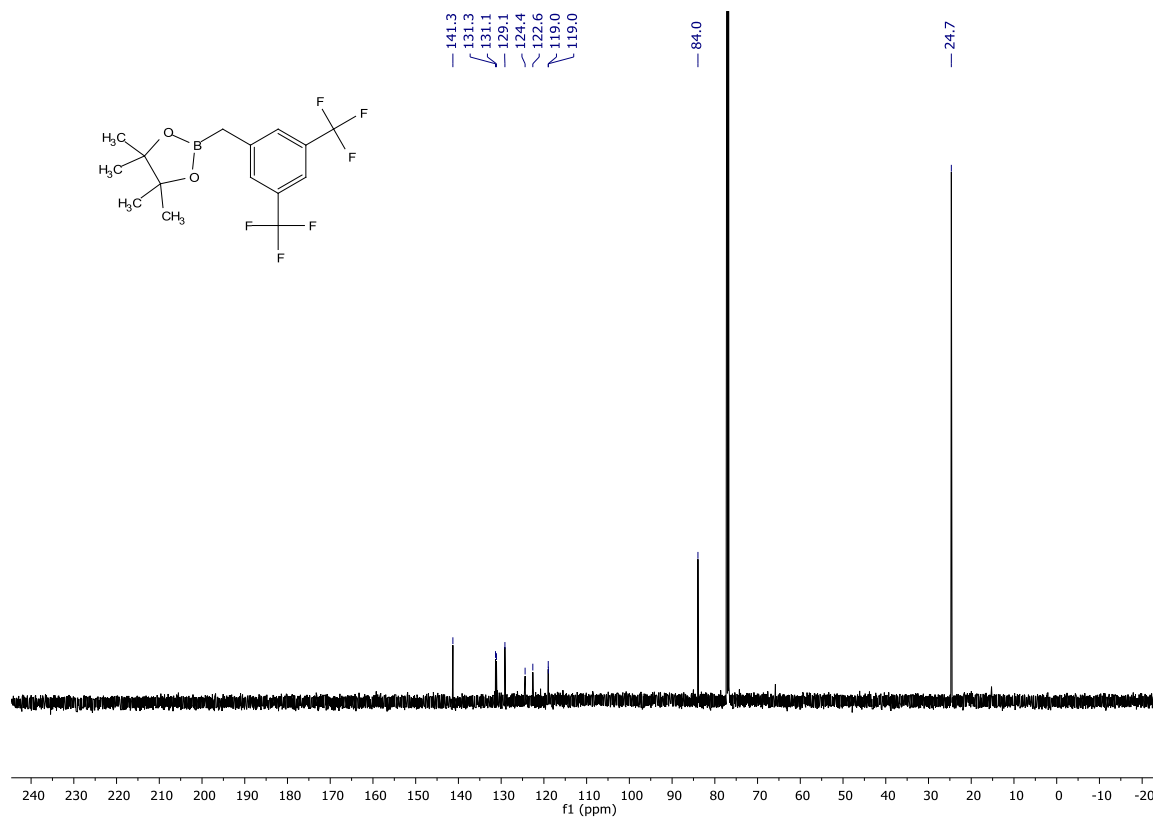


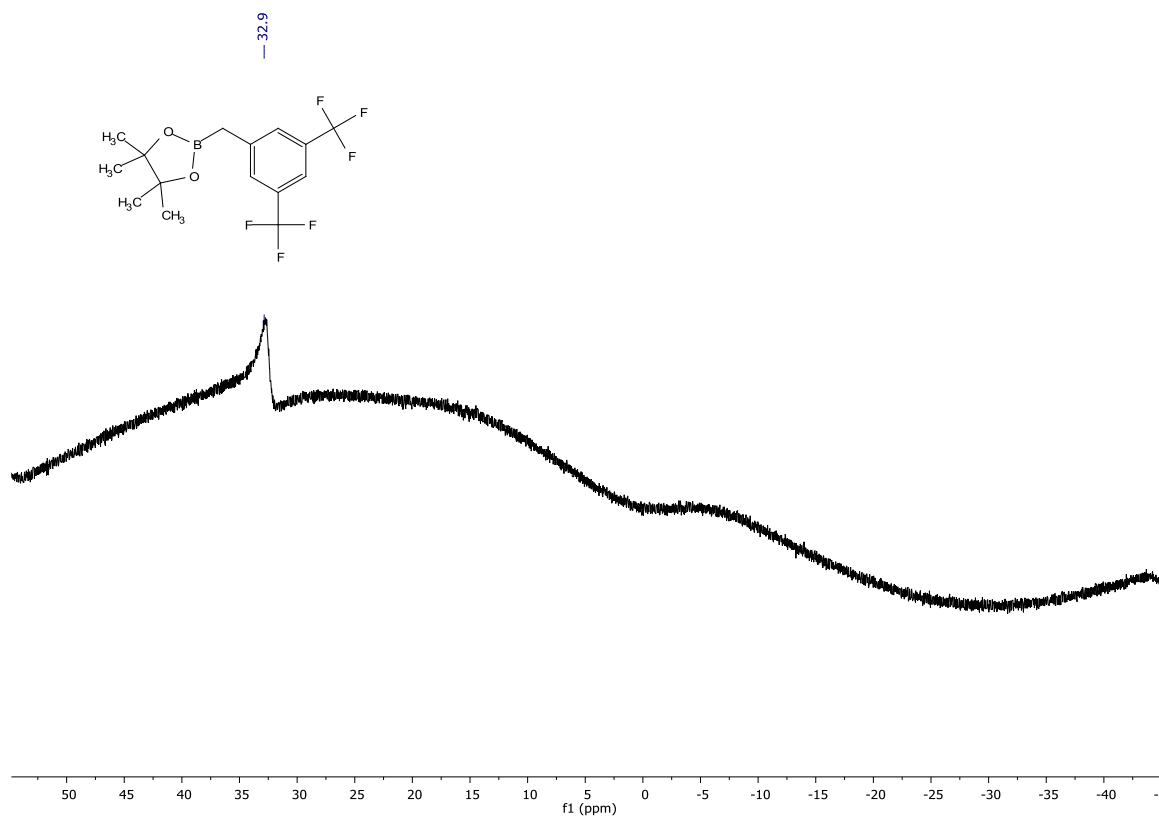
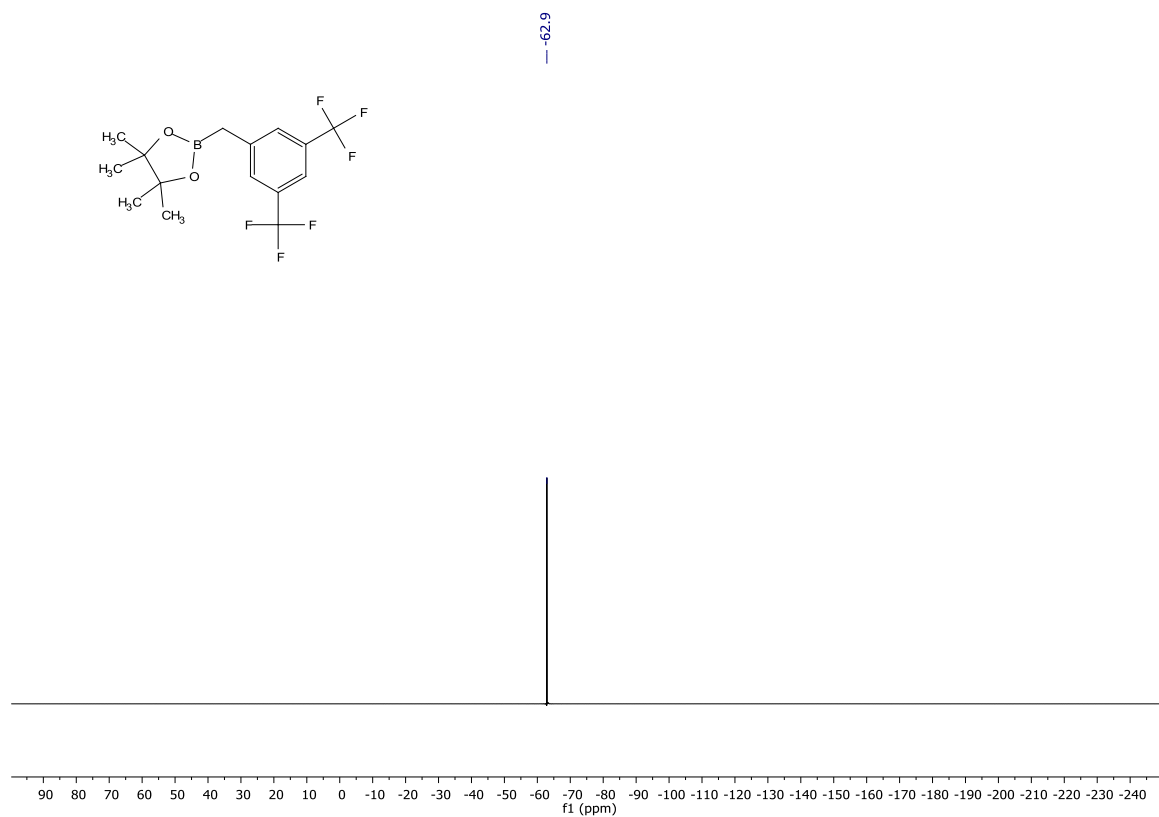
¹¹B-NMR (193 MHz, CDCl₃)

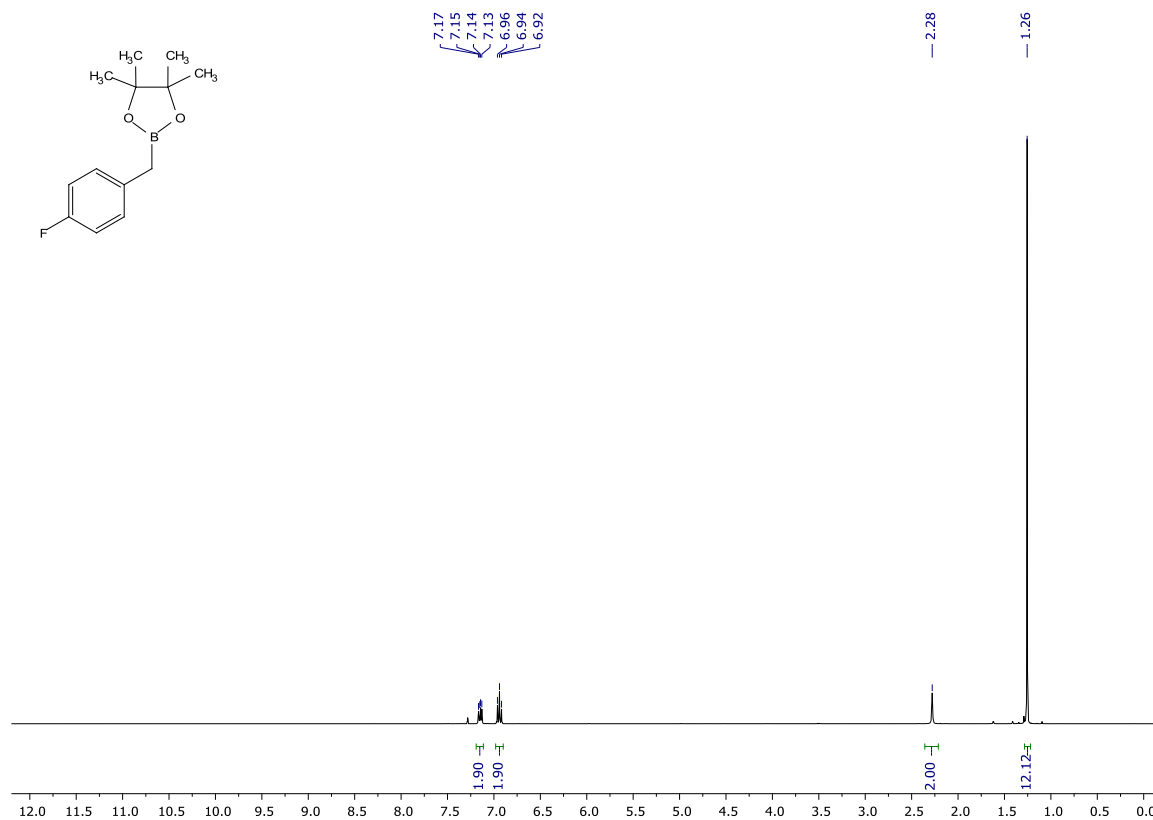
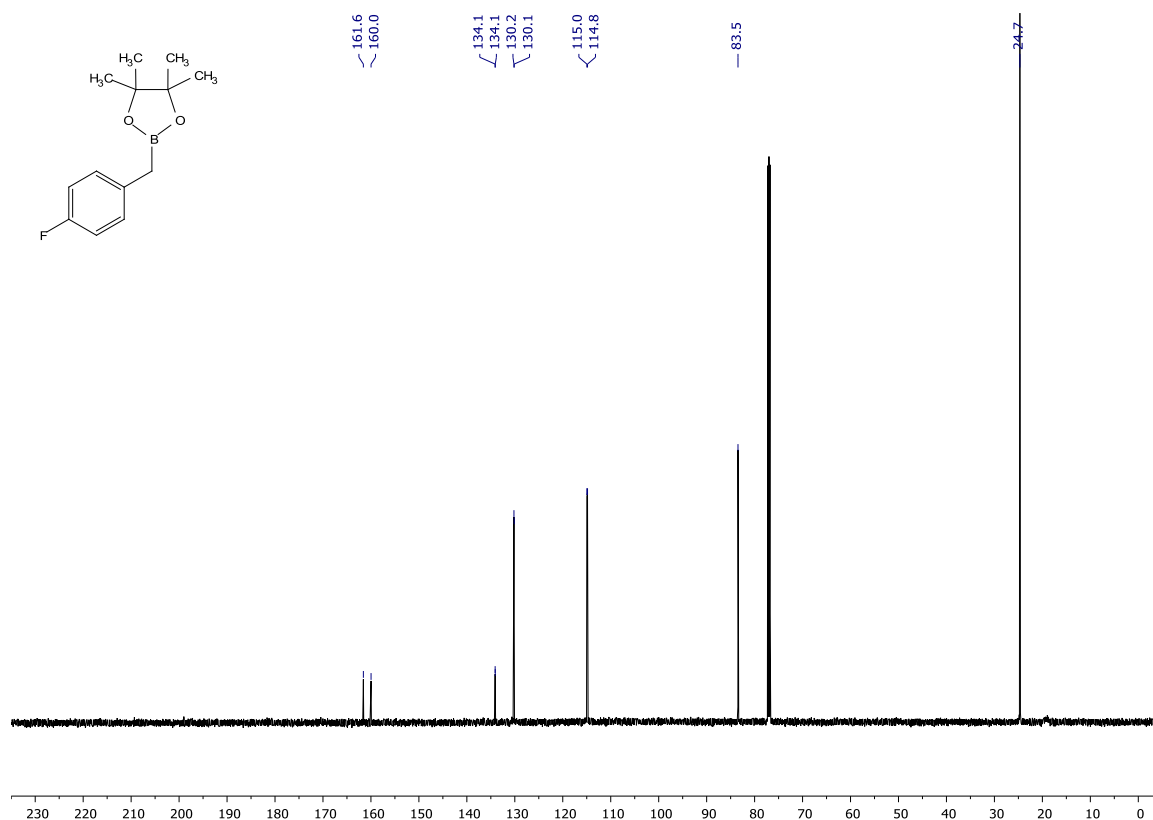


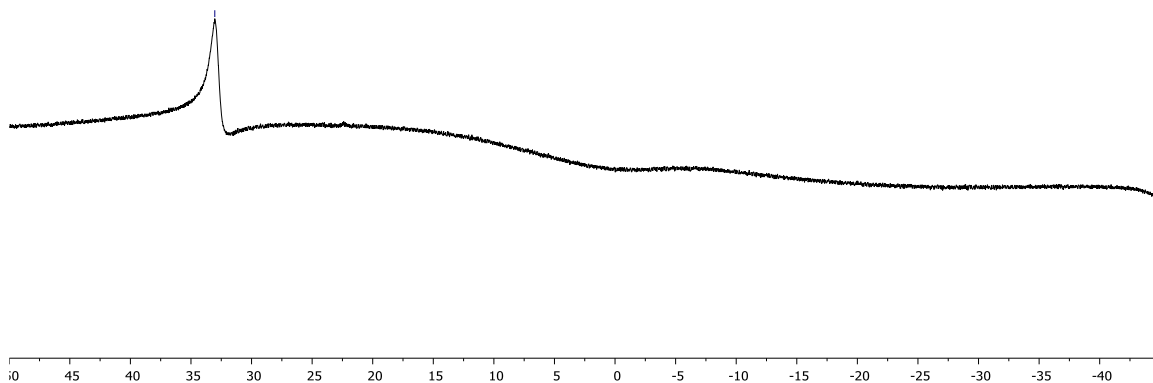
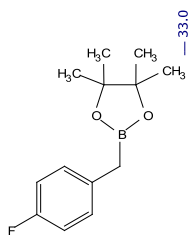
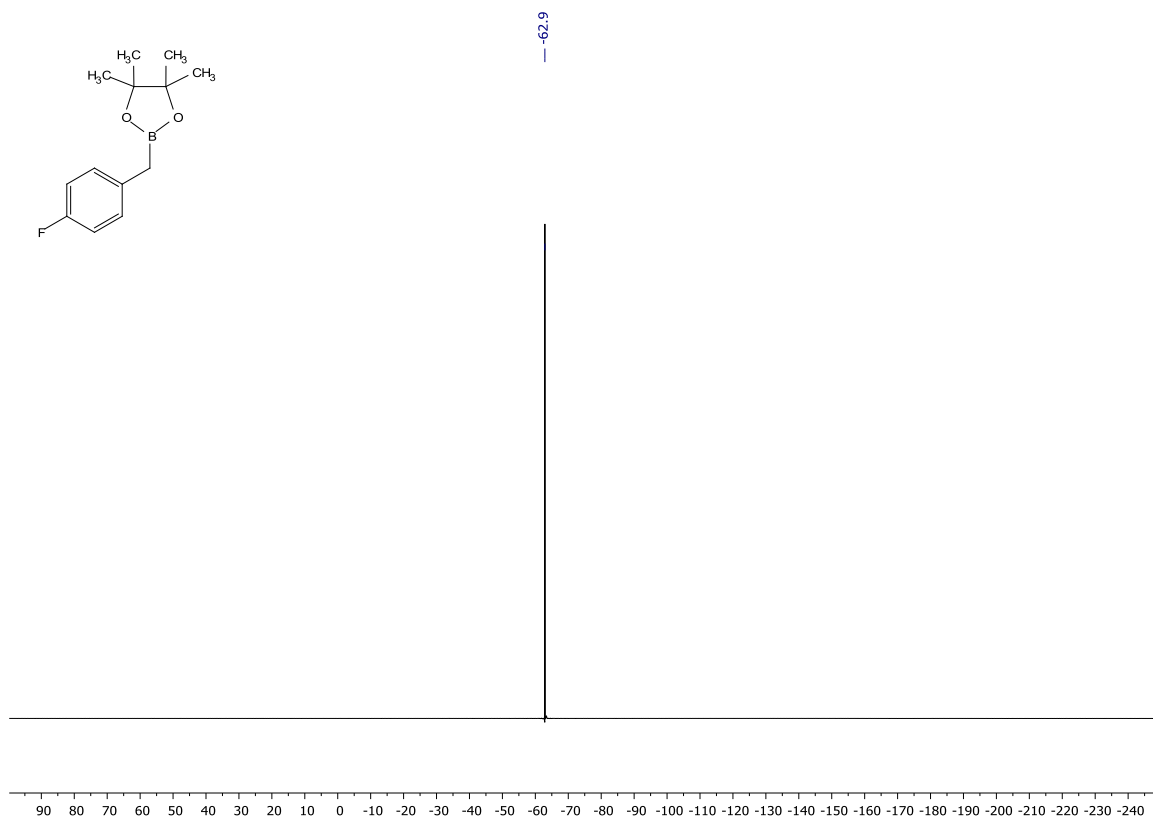
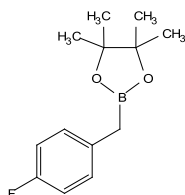
methyl 4-((4,4,5,5-tetramethyl-1,3,2-dioxaborolan-2-yl)methyl)benzoate**¹H-NMR (600 MHz, CDCl₃)****¹³C-NMR (151 MHz, CDCl₃)**

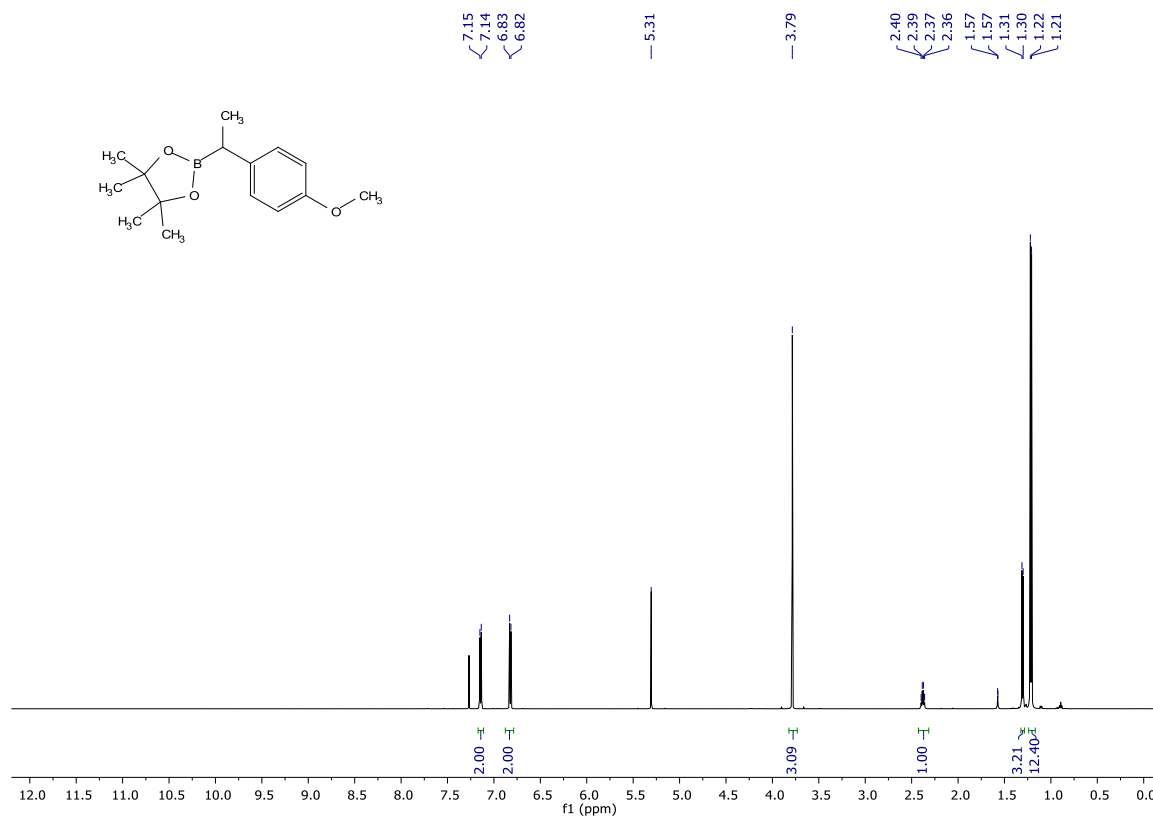
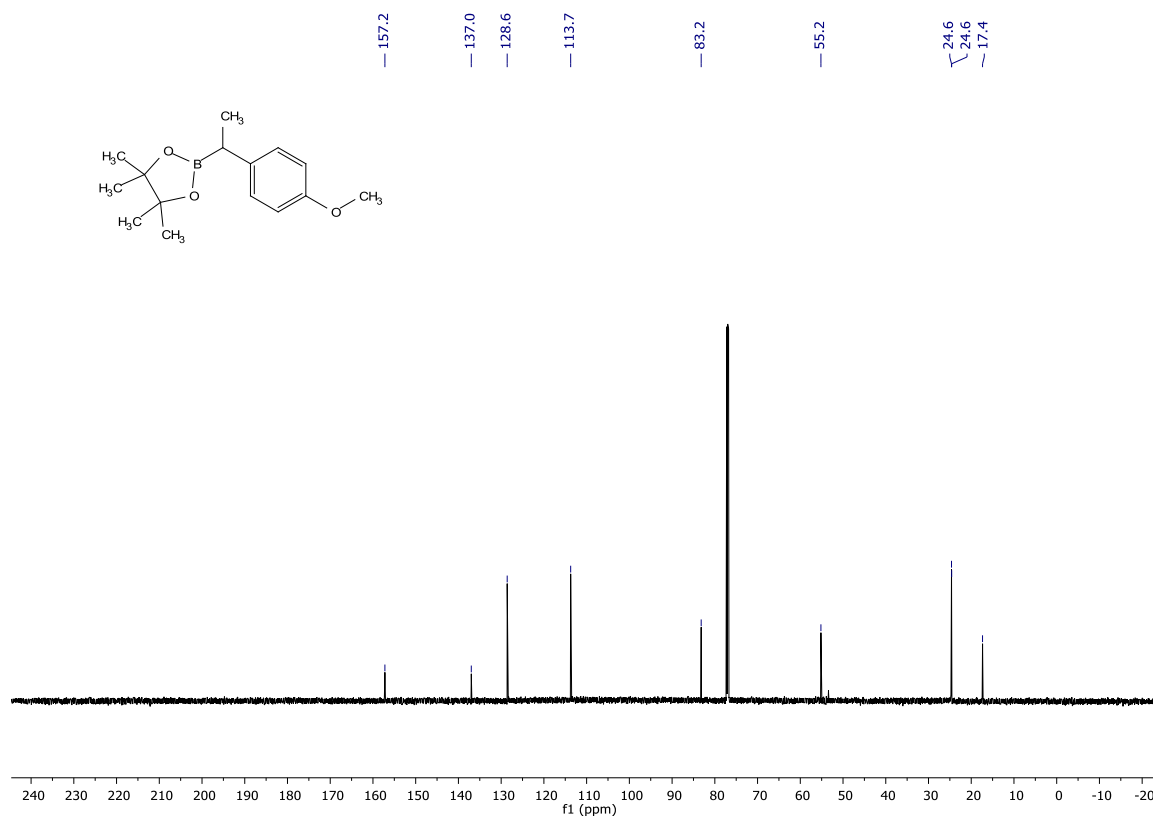
^{11}B -NMR (193 MHz, CDCl_3)

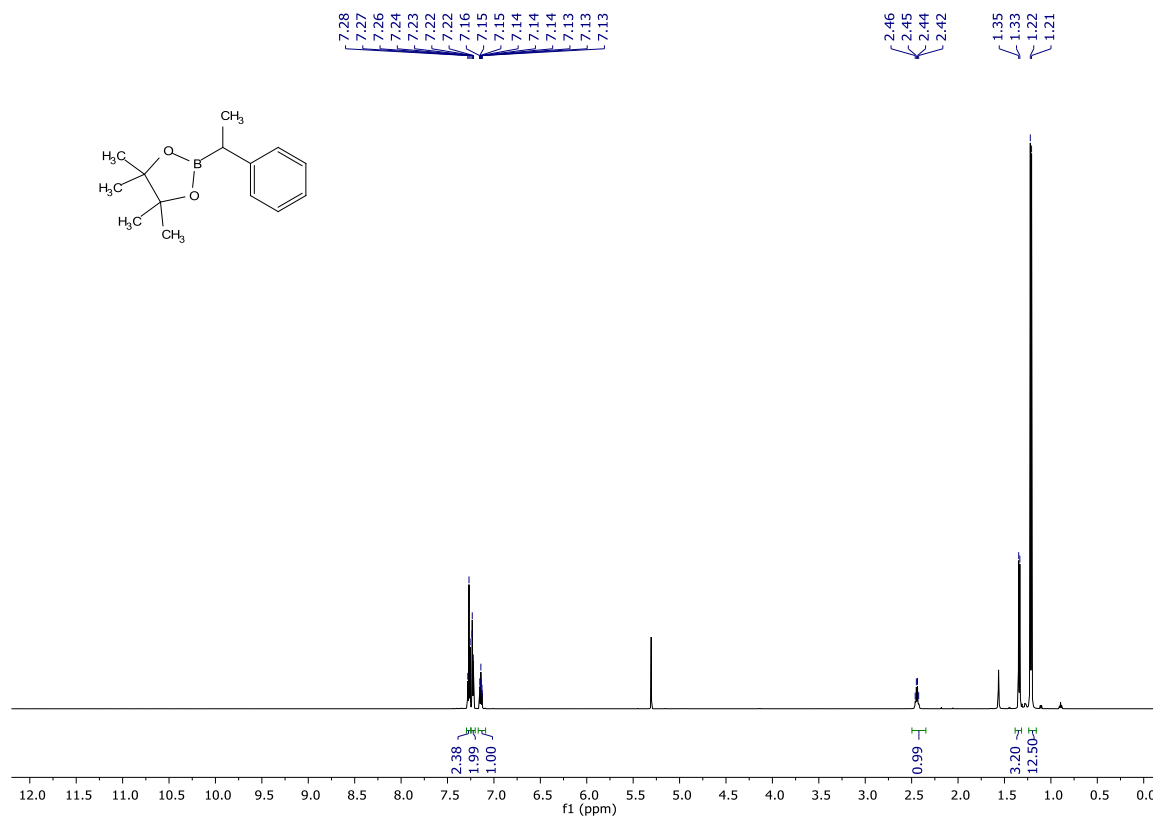
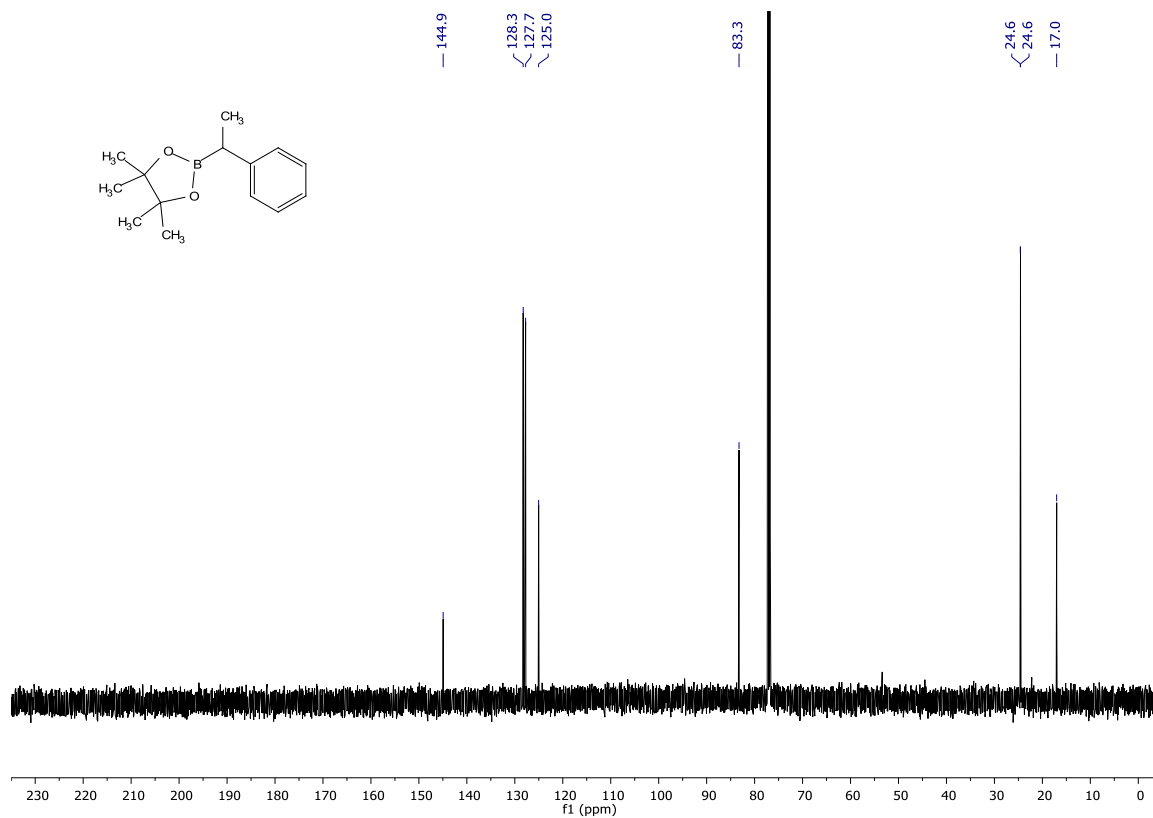
2-(3,5-bis(trifluoromethyl)benzyl)-4,4,5,5-tetramethyl-1,3,2-dioxaborolane**¹H-NMR (600 MHz, CDCl₃)****¹³C-NMR (151 MHz, CDCl₃)**

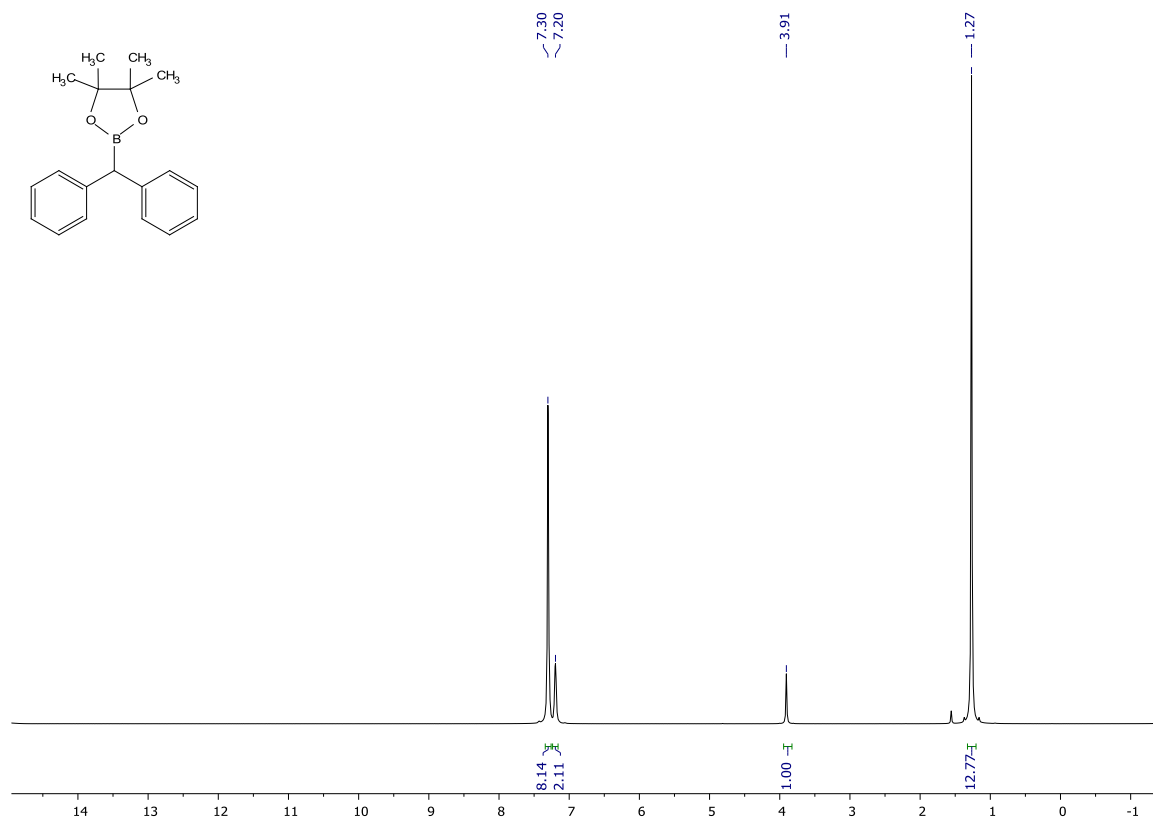
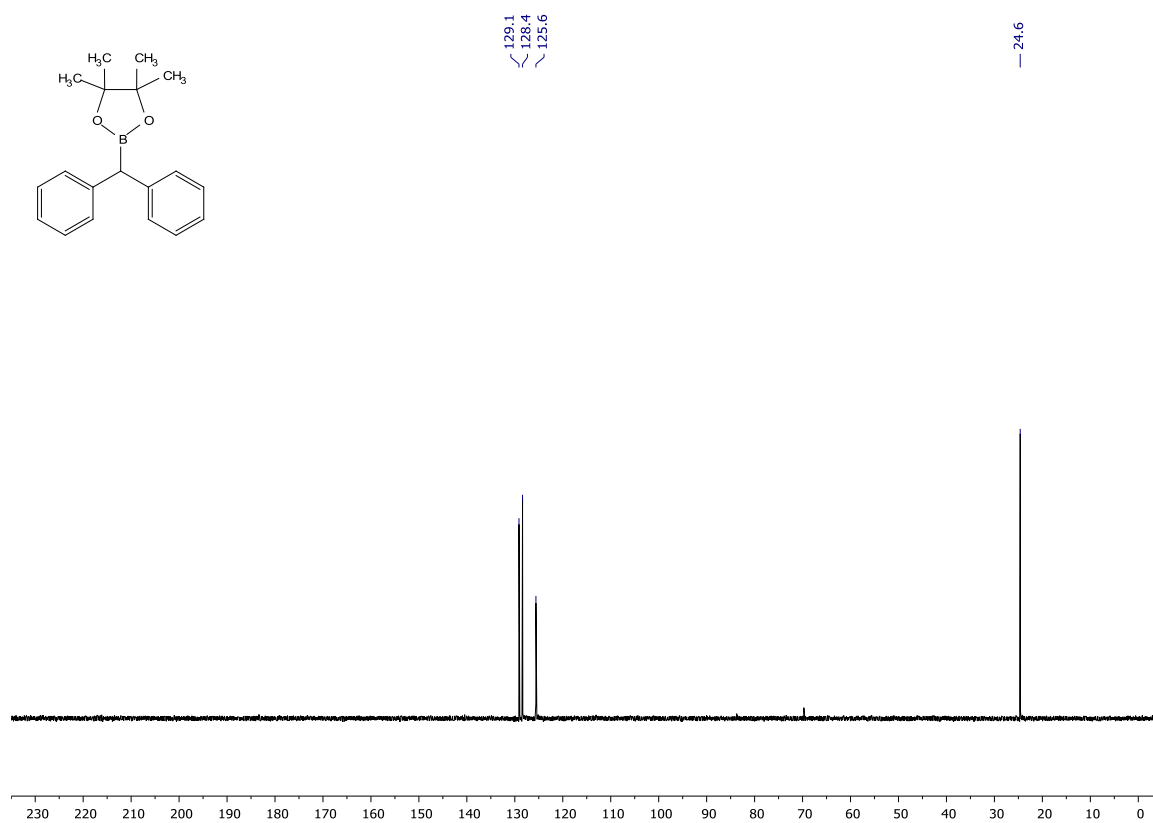
^{11}B -NMR (193 MHz, CDCl_3) **^{19}F -NMR (376 MHz, CDCl_3)**

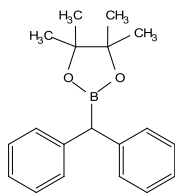
2-(4-fluorobenzyl)-4,4,5,5-tetramethyl-1,3,2-dioxaborolane **$^1\text{H-NMR}$ (600 MHz, CDCl_3)** **$^{13}\text{C-NMR}$ (151 MHz, CDCl_3)**

^{11}B -NMR (193 MHz, CDCl_3) **^{19}F -NMR (376 MHz, CDCl_3)**

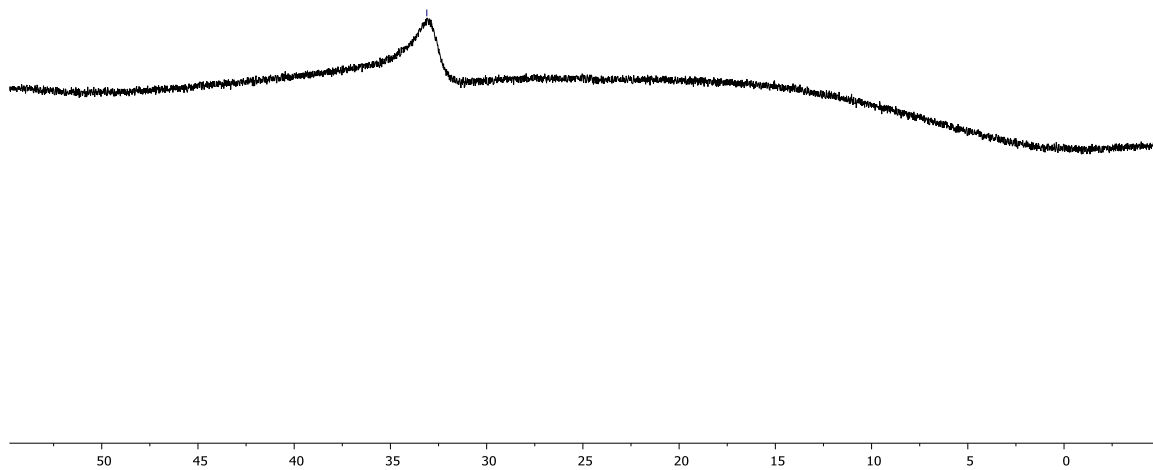
2-(1-(4-methoxyphenyl)ethyl)-4,4,5,5-tetramethyl-1,3,2-dioxaborolane**¹H-NMR (600 MHz, CDCl₃)****¹³C-NMR (151 MHz, CDCl₃)**

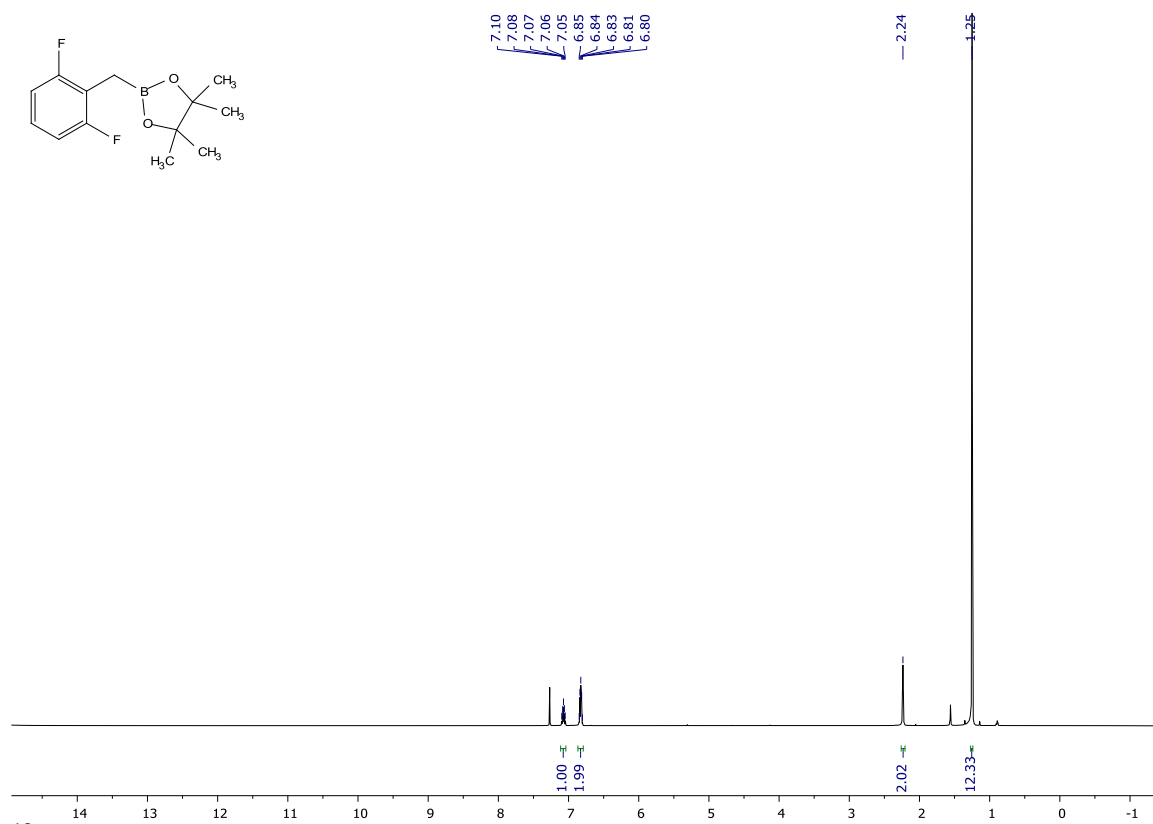
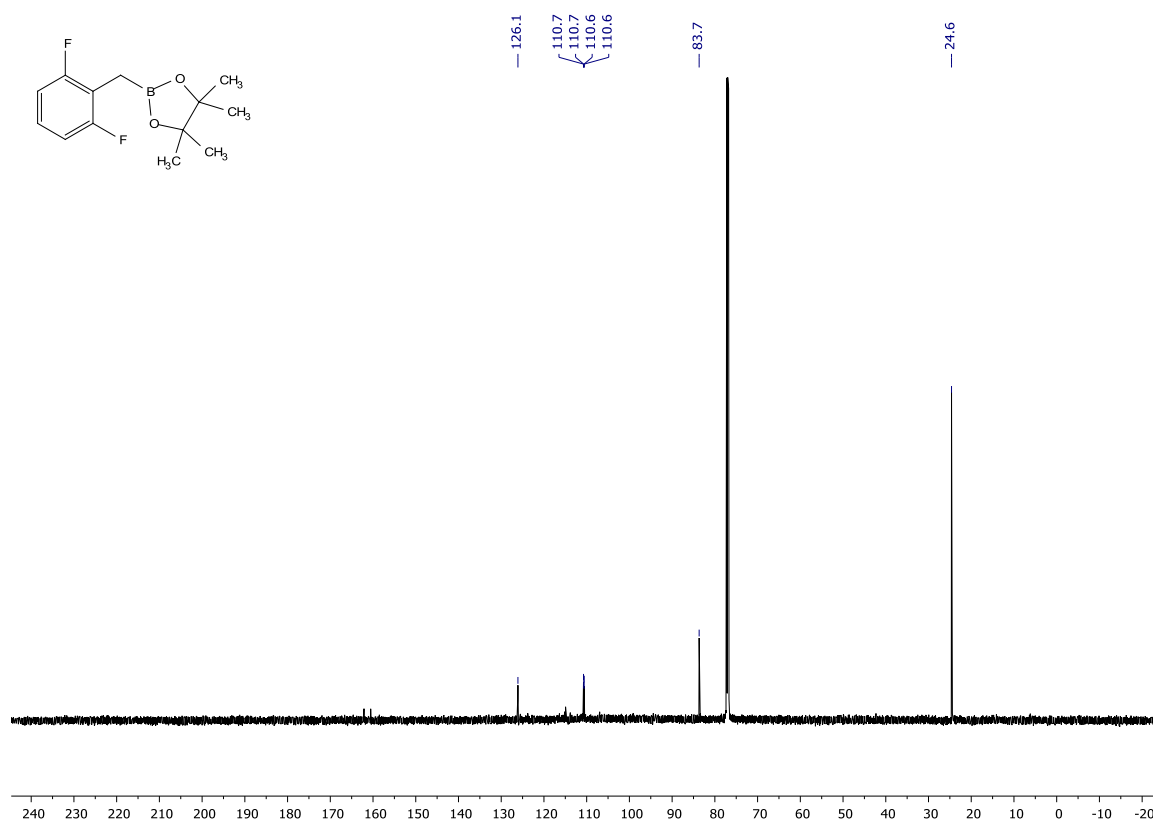
4,4,5,5-tetramethyl-2-(1-phenylethyl)-1,3,2-dioxaborolane**¹H-NMR (600 MHz, CDCl₃)****¹³C-NMR (151 MHz, CDCl₃)**

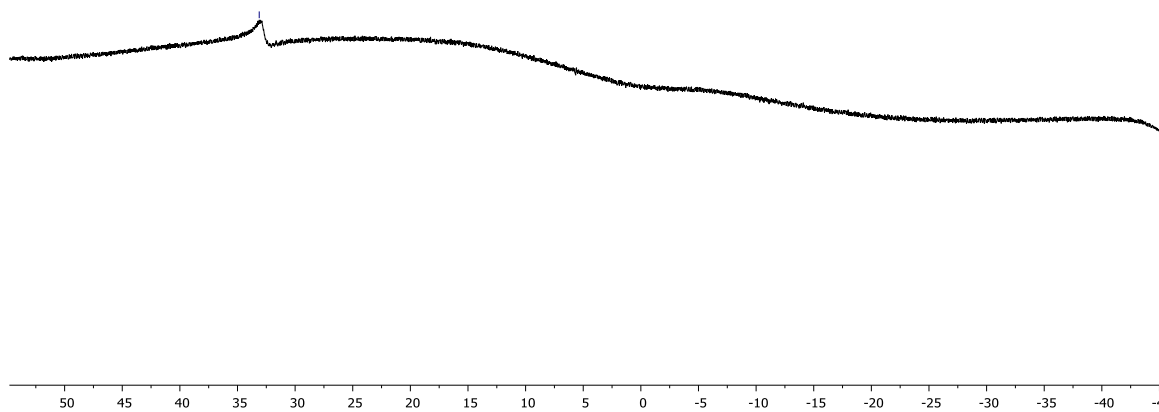
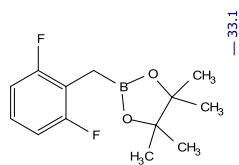
2-benzhydryl-4,4,5,5-tetramethyl-1,3,2-dioxaborolane **$^1\text{H-NMR}$ (600 MHz, CDCl_3)** **$^{13}\text{C-NMR}$ (151 MHz, CDCl_3)**

^{11}B -NMR (193 MHz, CDCl_3)

- 33.1

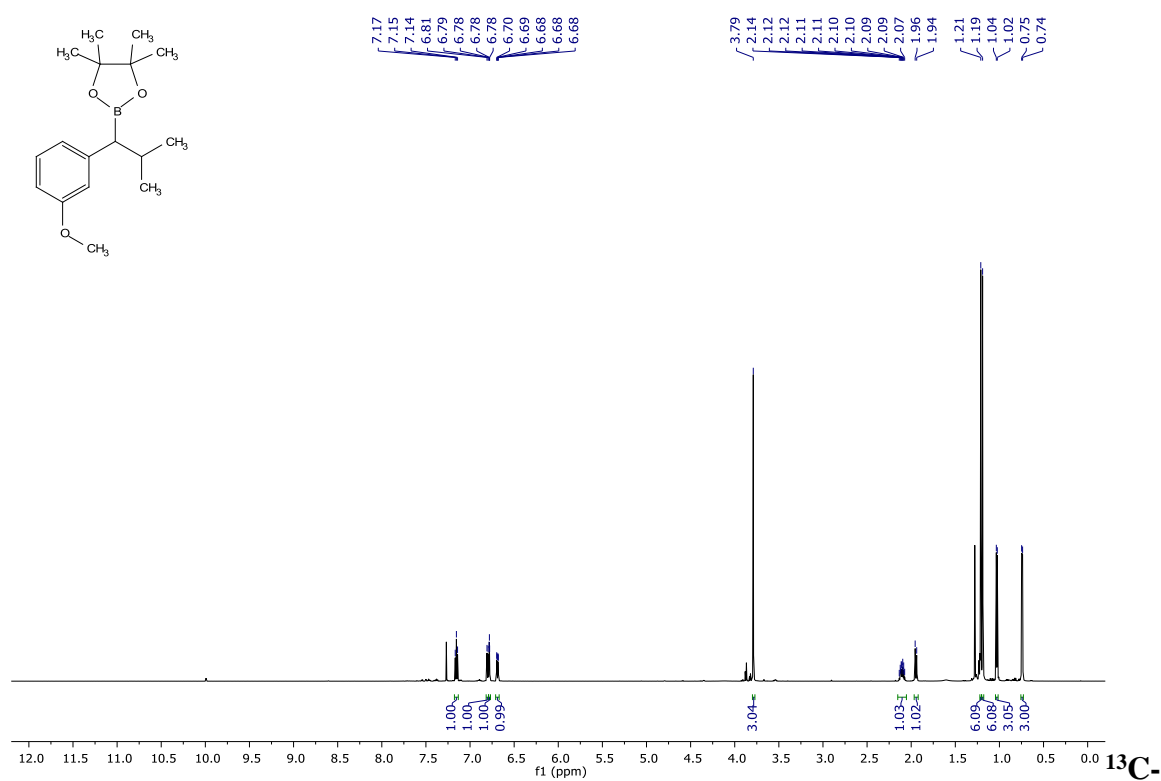


2-(2,6-difluorobenzyl)-4,4,5,5-tetramethyl-1,3,2-dioxaborolane **$^1\text{H-NMR}$ (600 MHz, CDCl_3)** **$^{13}\text{C-NMR}$ (151 MHz, CDCl_3)**

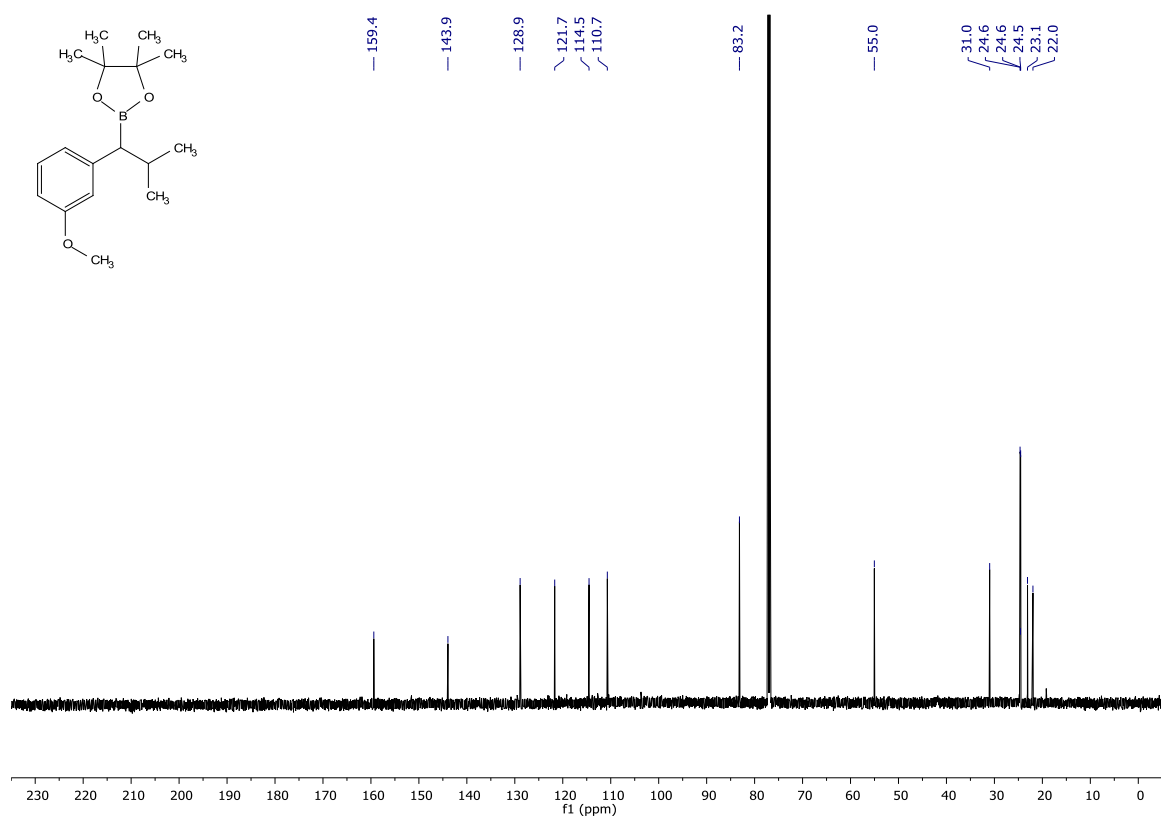
^{11}B -NMR (193 MHz, CDCl_3)

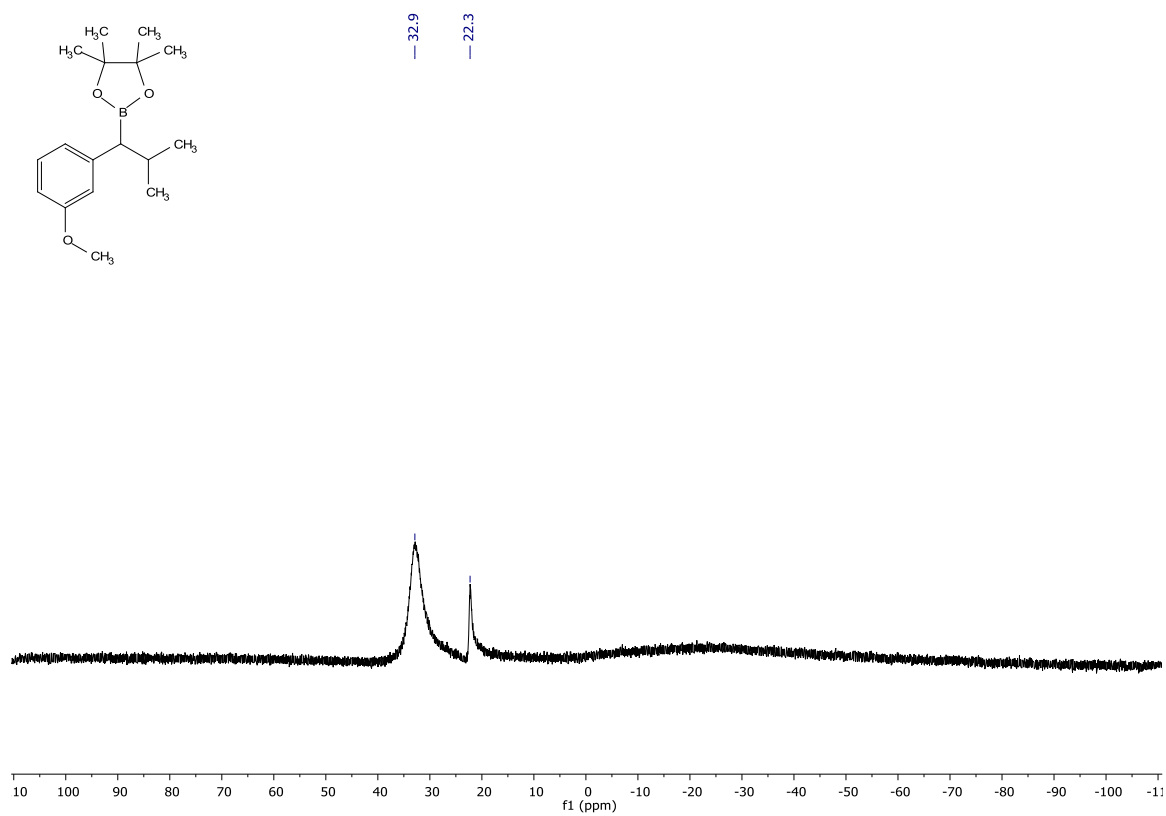
2-(1-(3-Methoxyphenyl)-2-methylpropyl)-4,4,5,5-tetramethyl-1,3,2-dioxaborolane

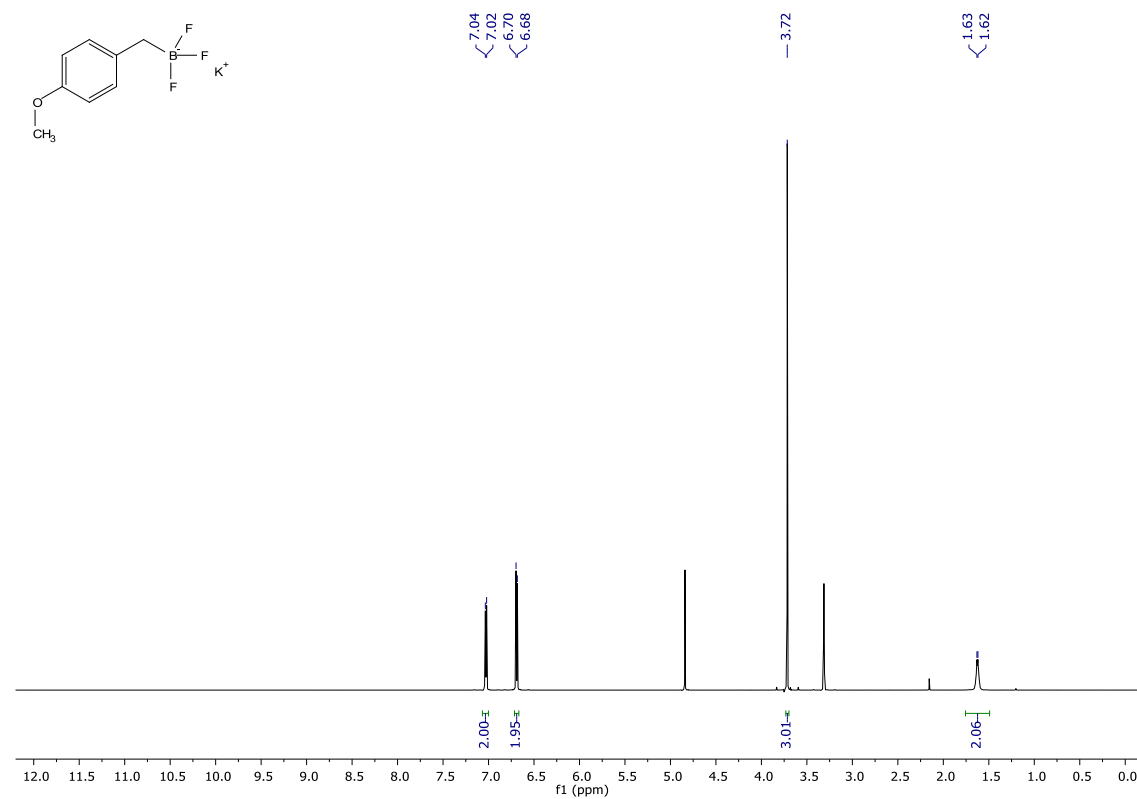
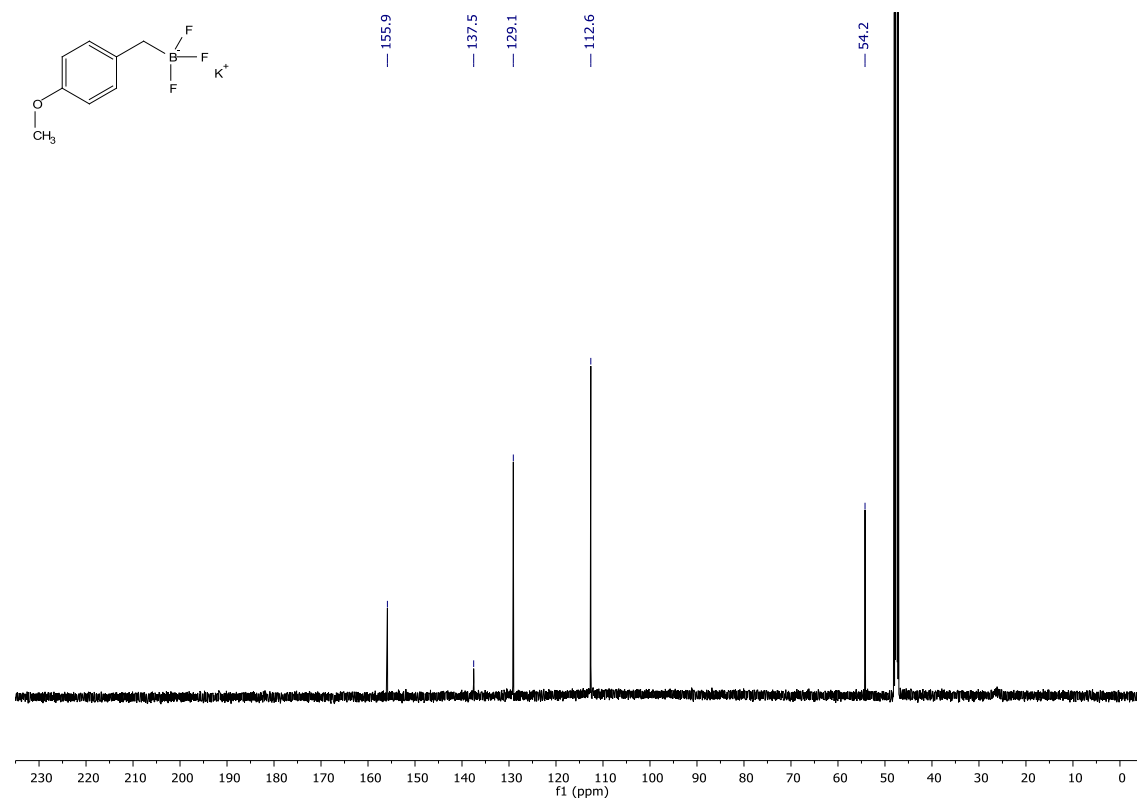
$^1\text{H-NMR}$ (400 MHz, CDCl_3)

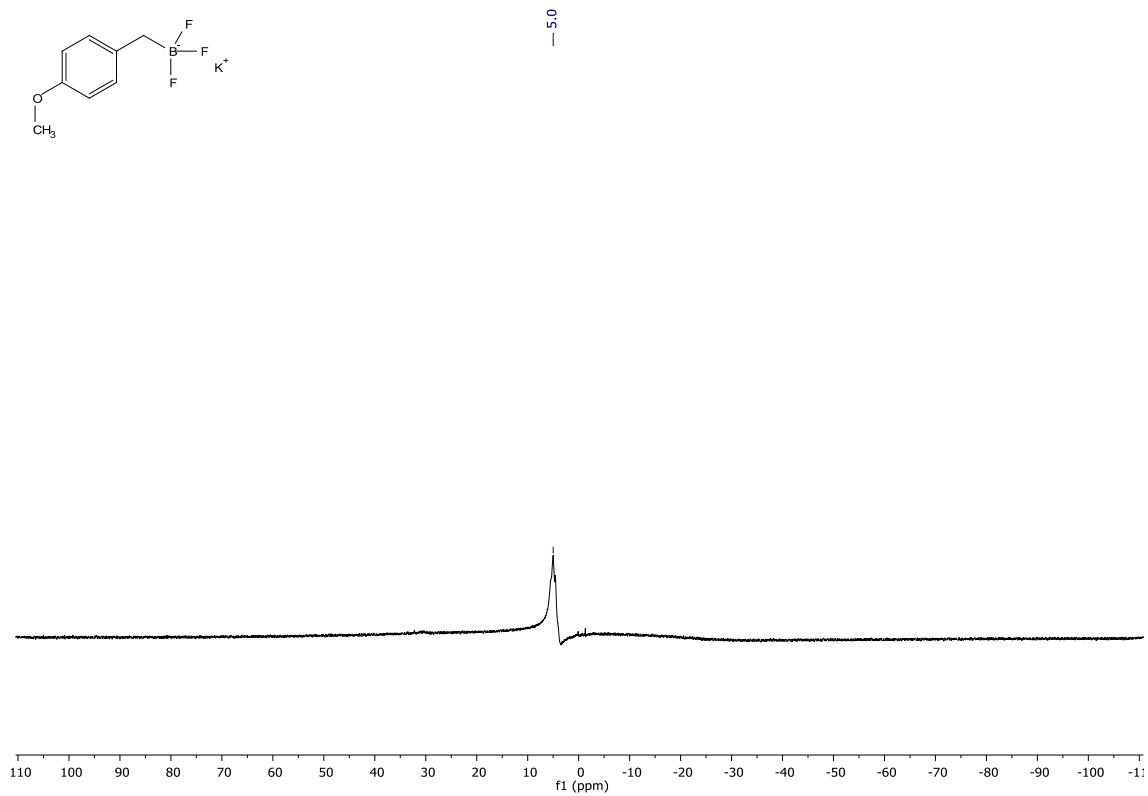
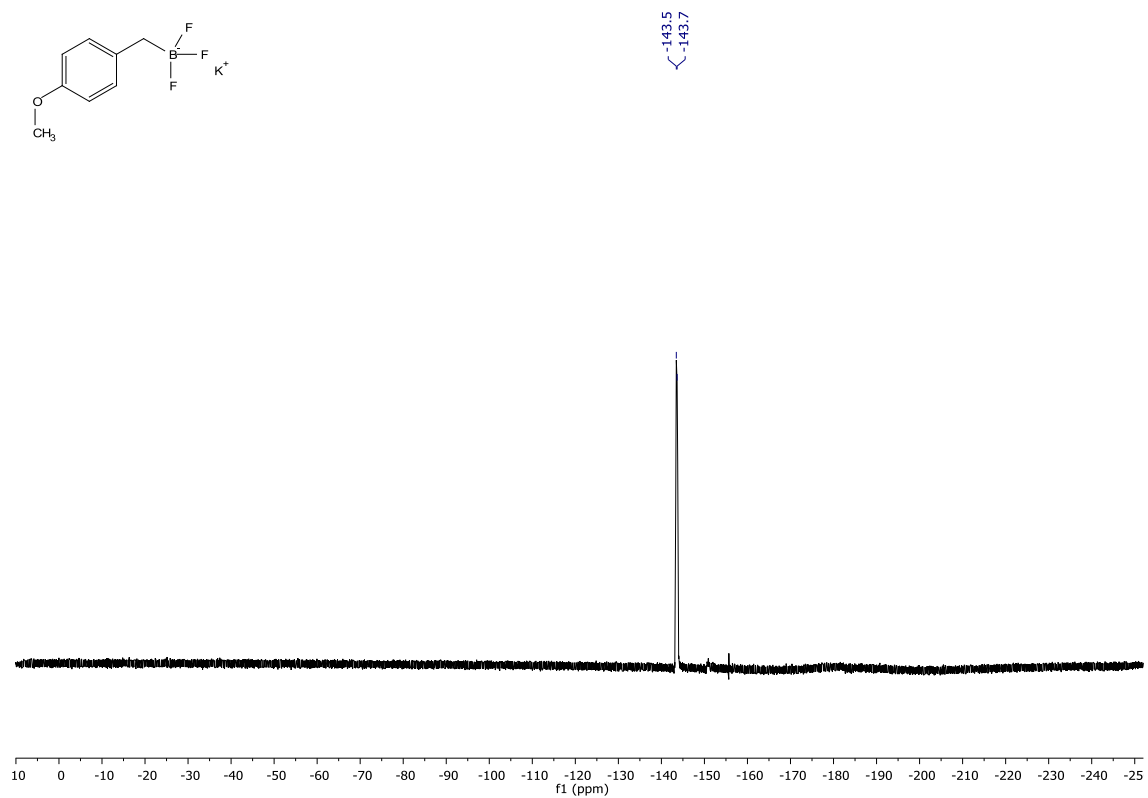


$^{13}\text{C-NMR}$ (151 MHz CDCl_3)



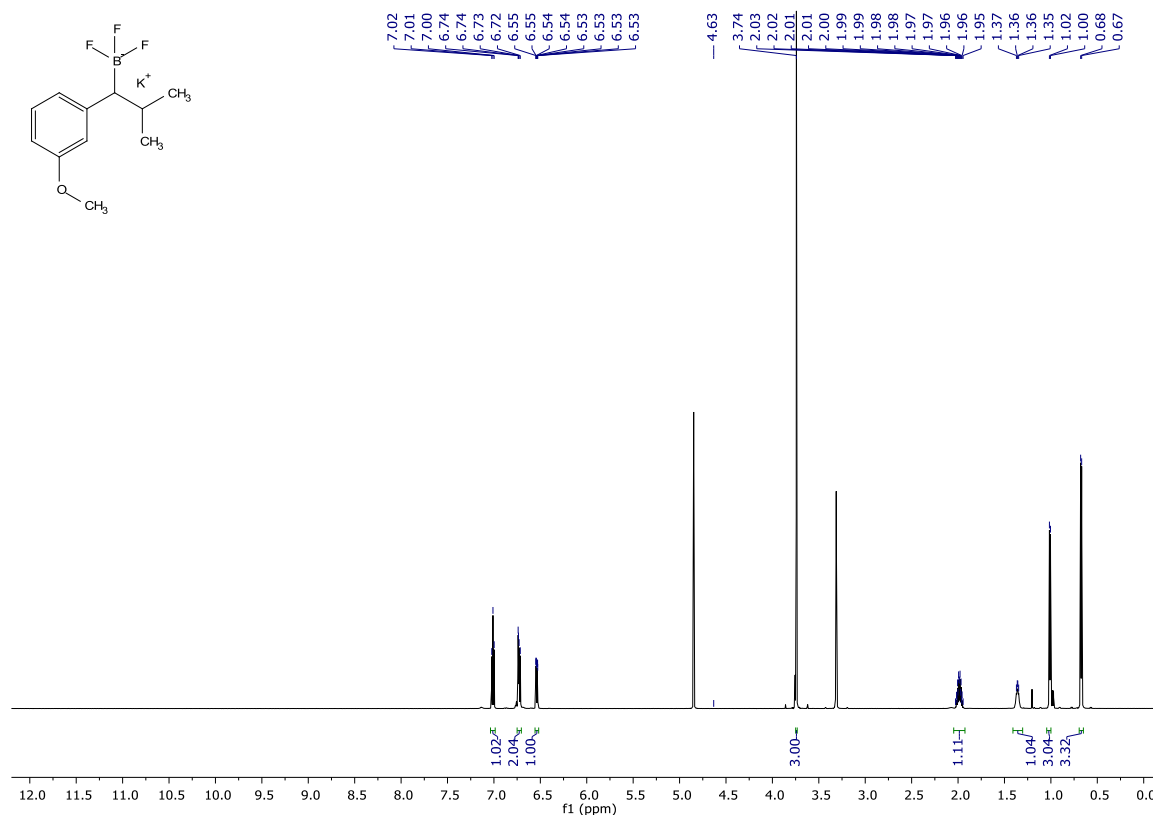
^{11}B -NMR (128 MHz, CDCl_3)

Potassium trifluoro(4-methoxybenzyl)borate (155) **$^1\text{H-NMR}$ (600 MHz, methanol- d_4)** **$^{13}\text{C-NMR}$ (151 MHz, methanol- d_4)**

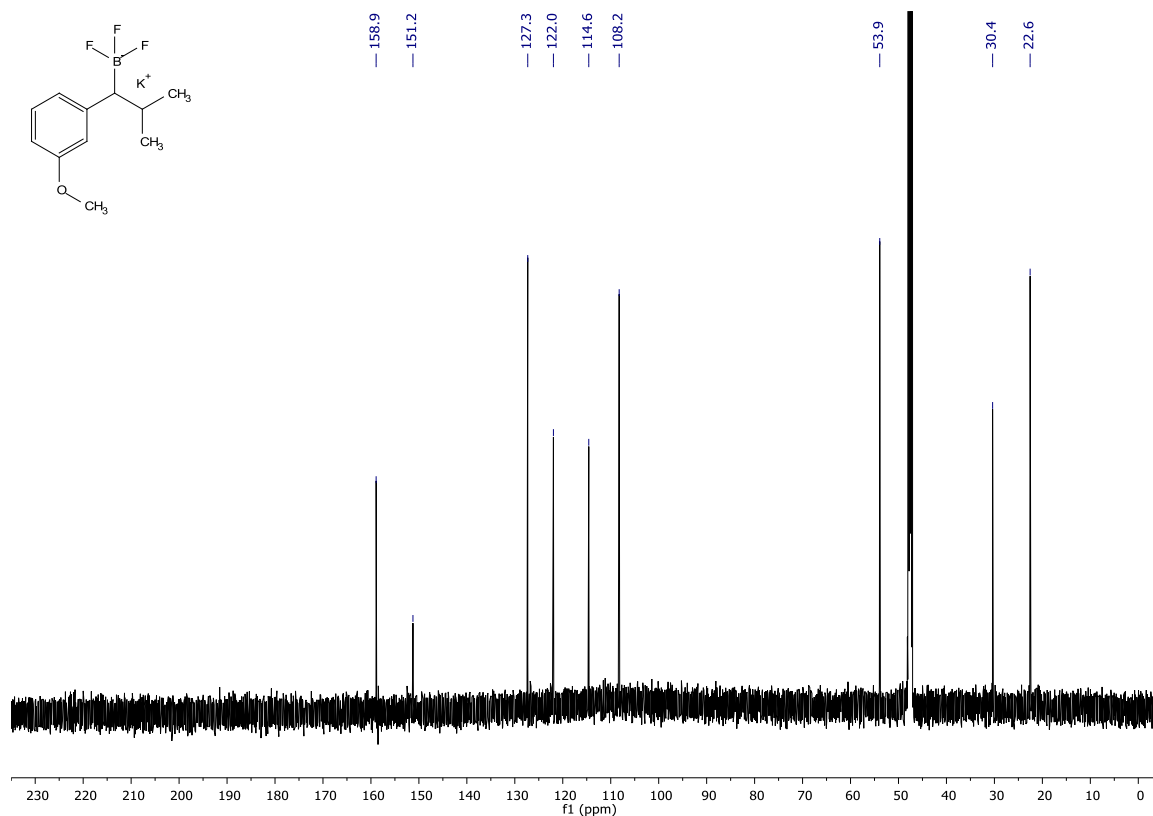
^{11}B -NMR (128 MHz, methanol- d_4) **^{19}F -NMR (376 MHz, methanol- d_4)**

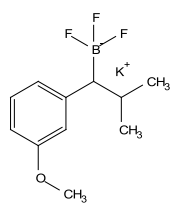
Potassium trifluoro(1-(3-methoxyphenyl)-2-methylpropyl)borate (156)

¹H-NMR (600 MHz, methanol-d₄)

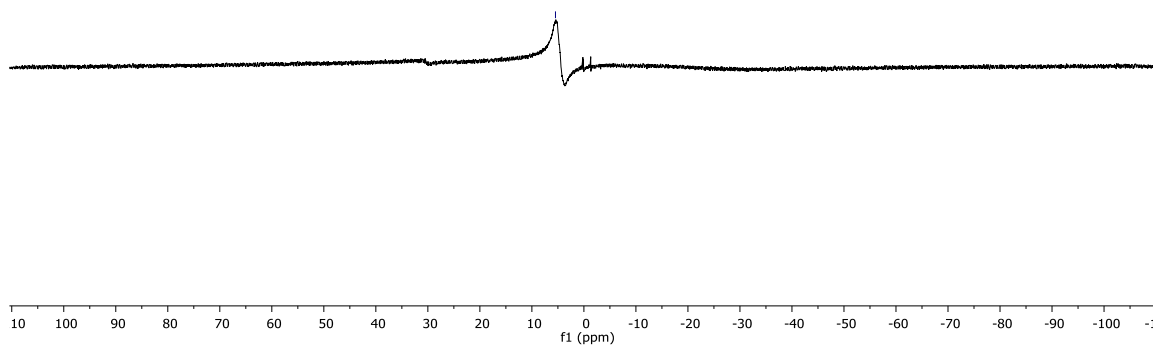
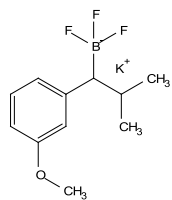


¹³C-NMR (151 MHz, methanol-d₄)

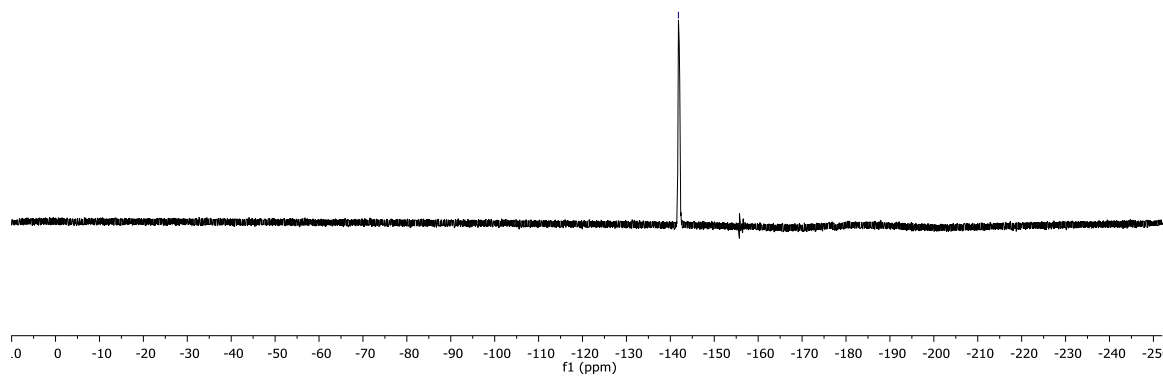


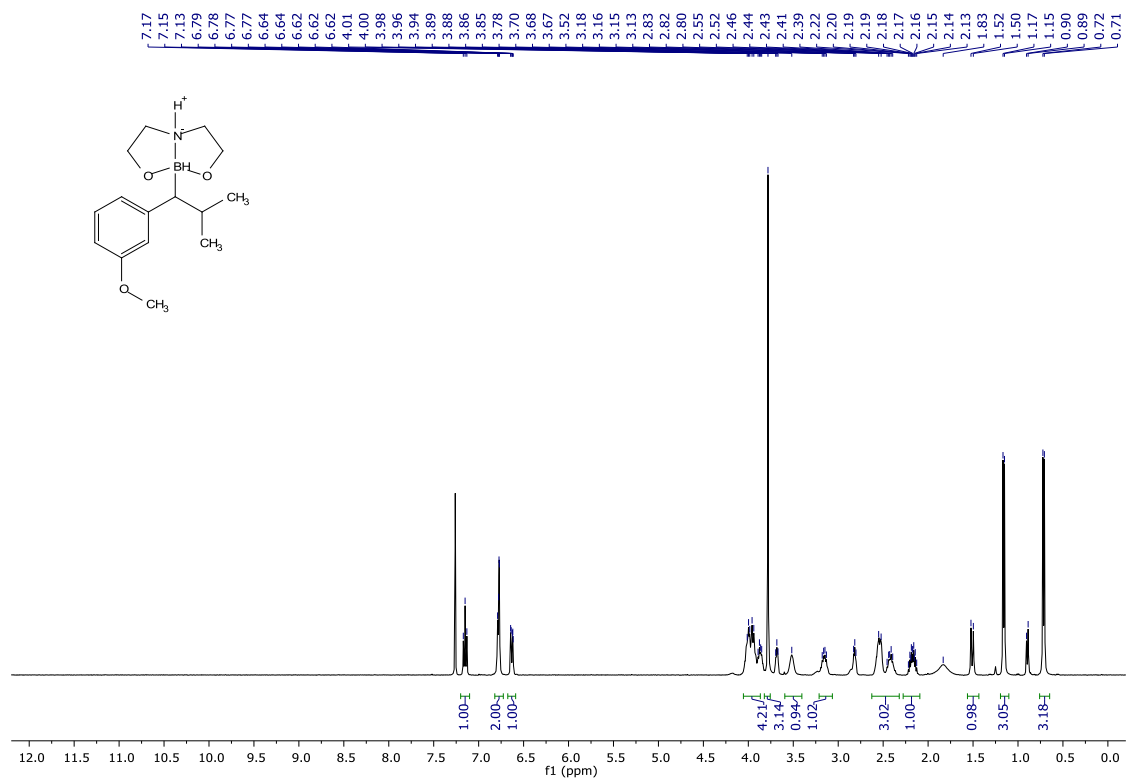
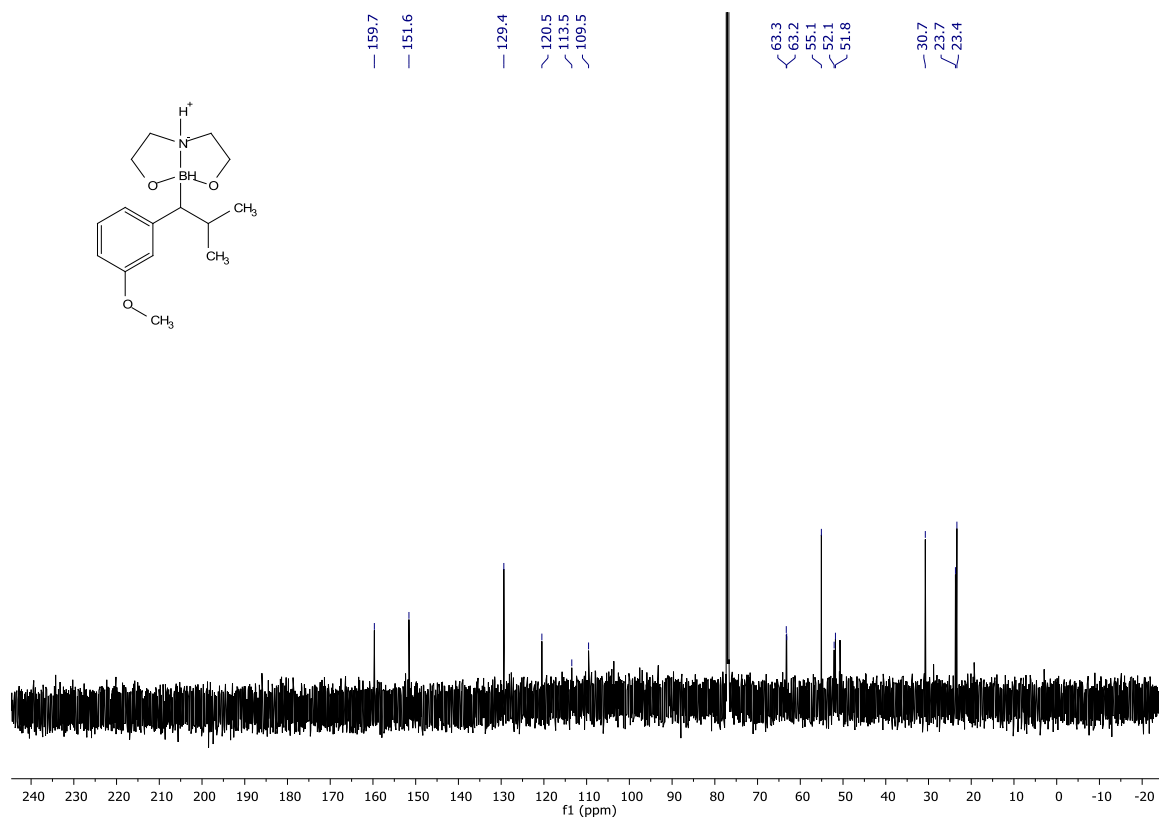
^{11}B -NMR (128 MHz, methanol- d_4)

-5.5

 **^{19}F -NMR (376 MHz, methanol- d_4)**

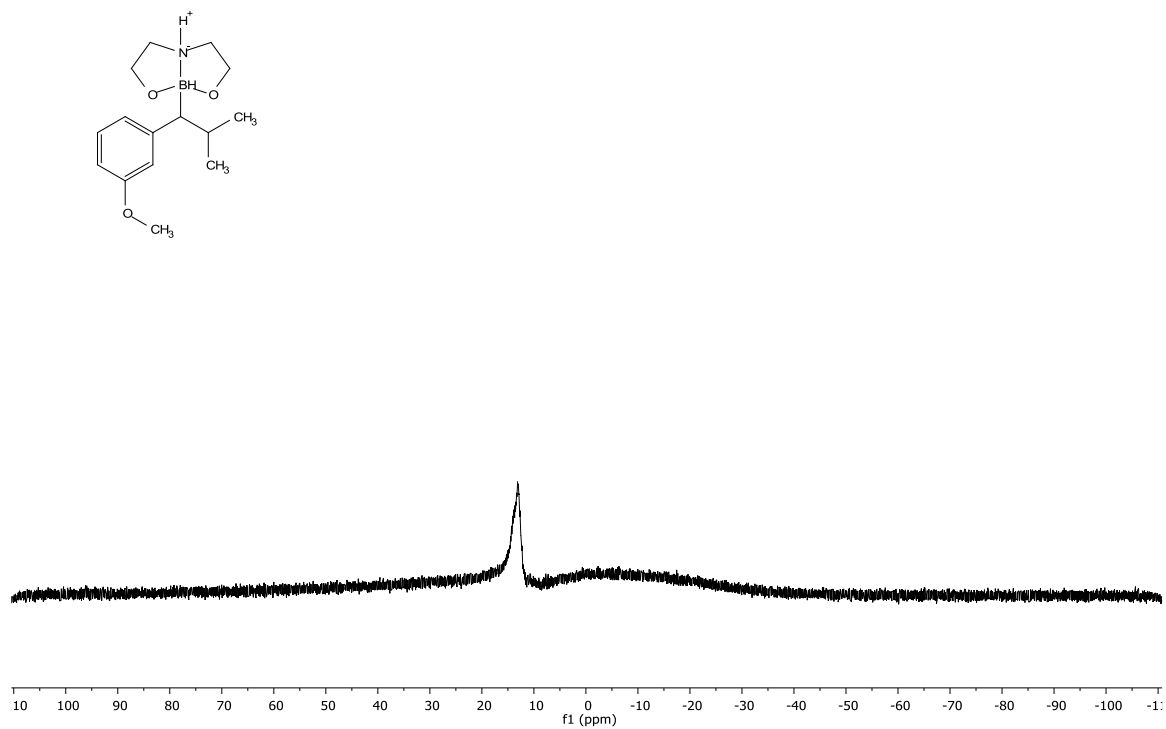
-141.8



8-(1-(3-methoxyphenyl)-2-methylpropyl)hexahydro-1,3,2-oxazaborolo[2,3-b]-1,3,2-oxazaborol-4-ium-8-uide (168)**¹H-NMR (400 MHz, CDCl₃)****¹³C-NMR (151 MHz, CDCl₃)**

^{11}B -NMR (128 MHz, CDCl_3)

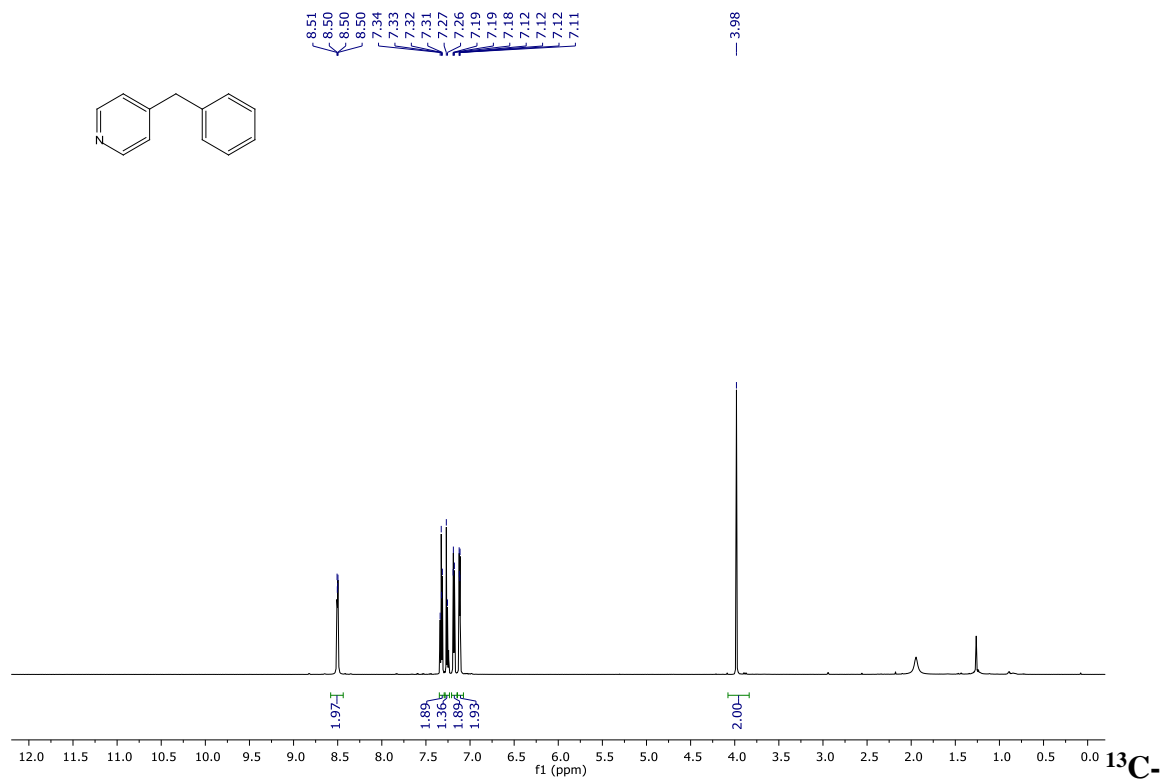
-13.1



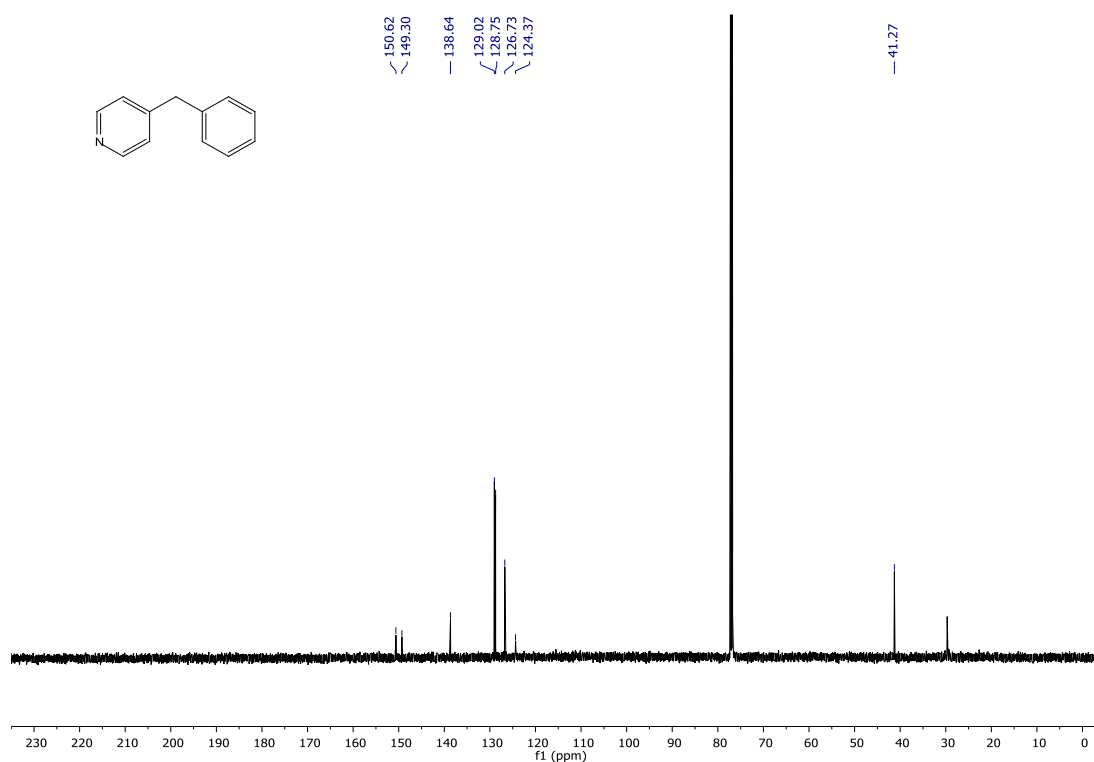
7.1.2 Coupling products spectra

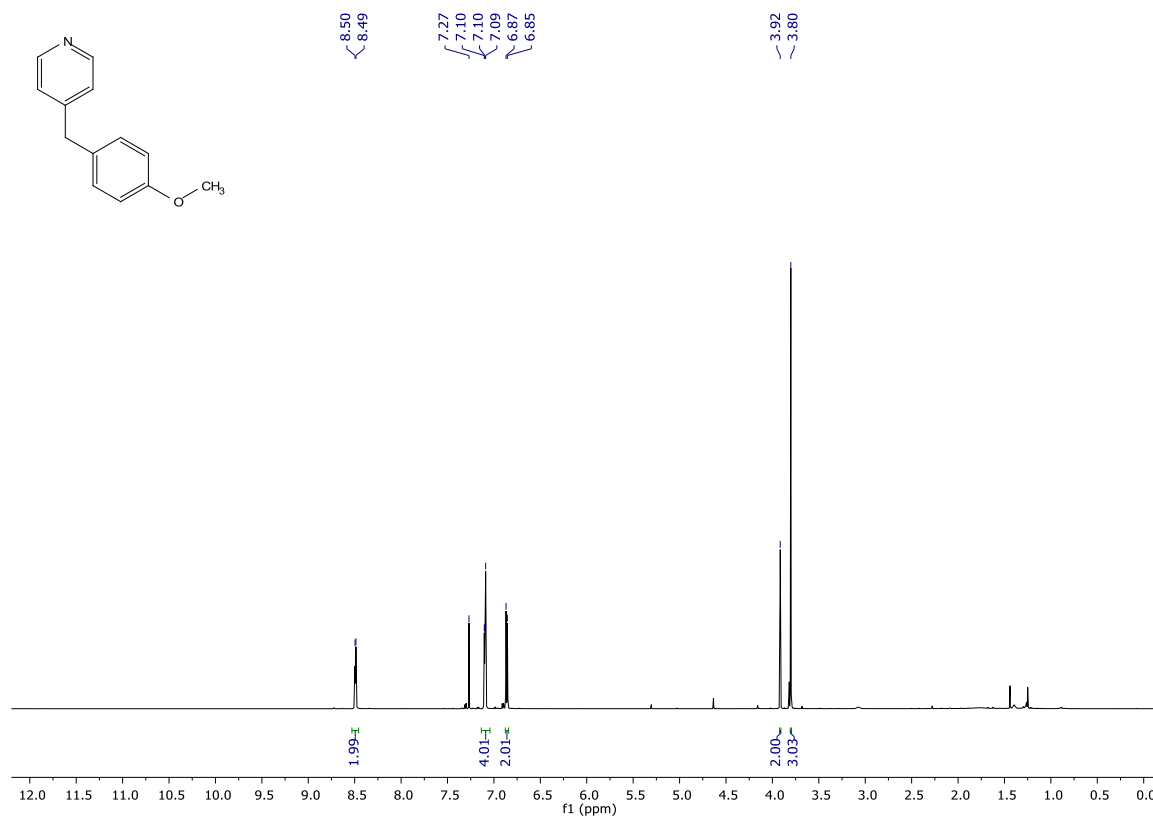
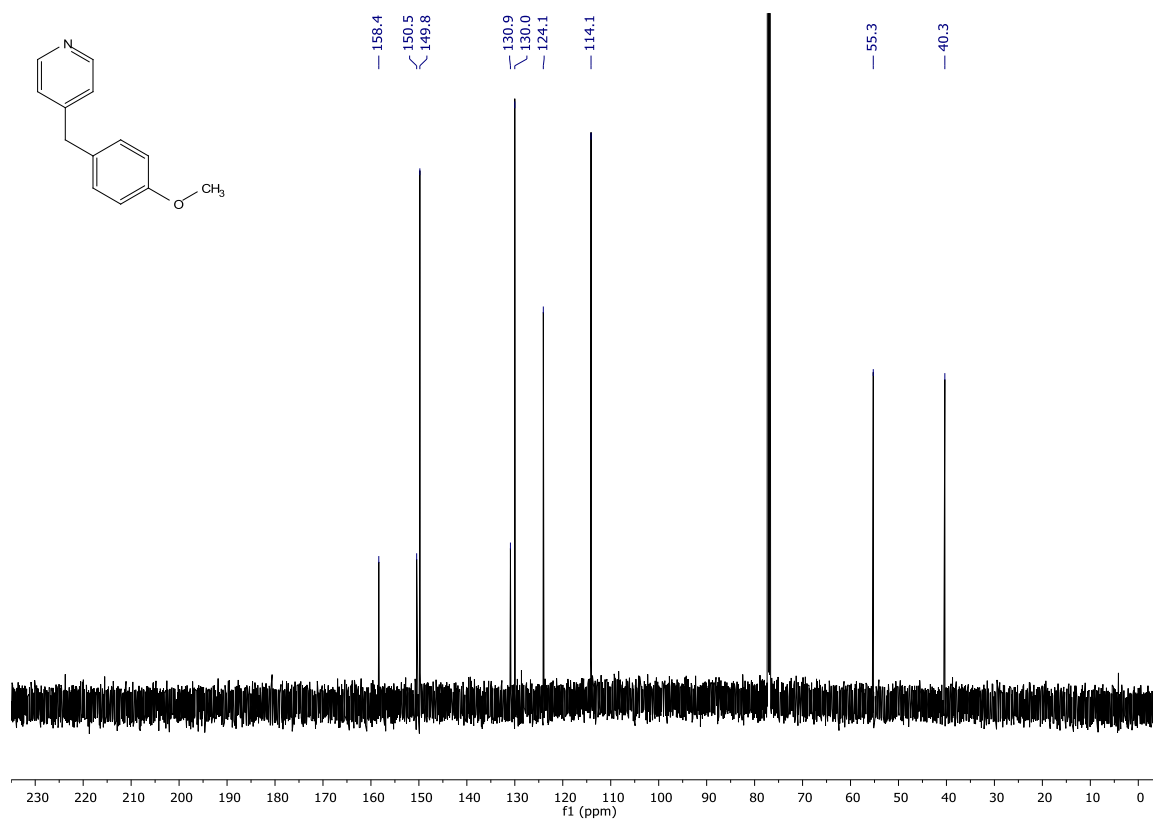
4-(benzyl)pyridine (161)

$^1\text{H-NMR}$ (600 MHz, CDCl_3)



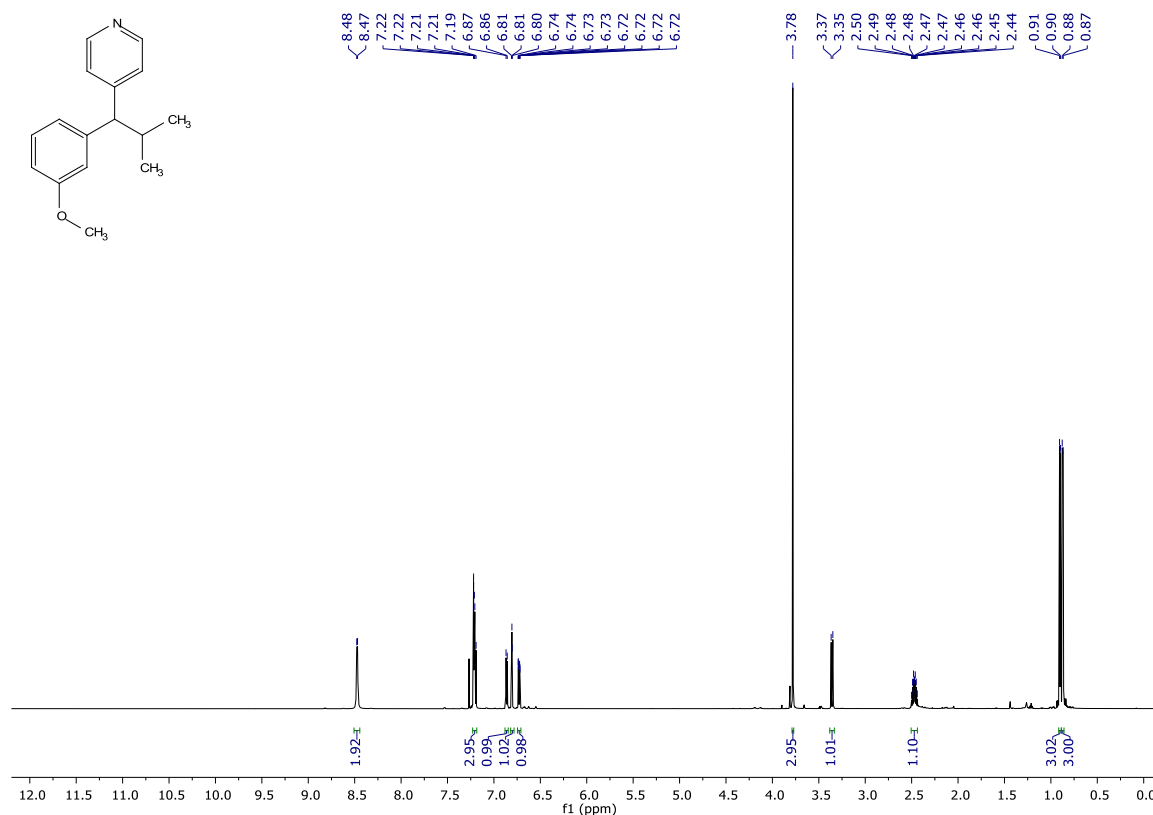
$^{13}\text{C-NMR}$ (151 MHz, CDCl_3)



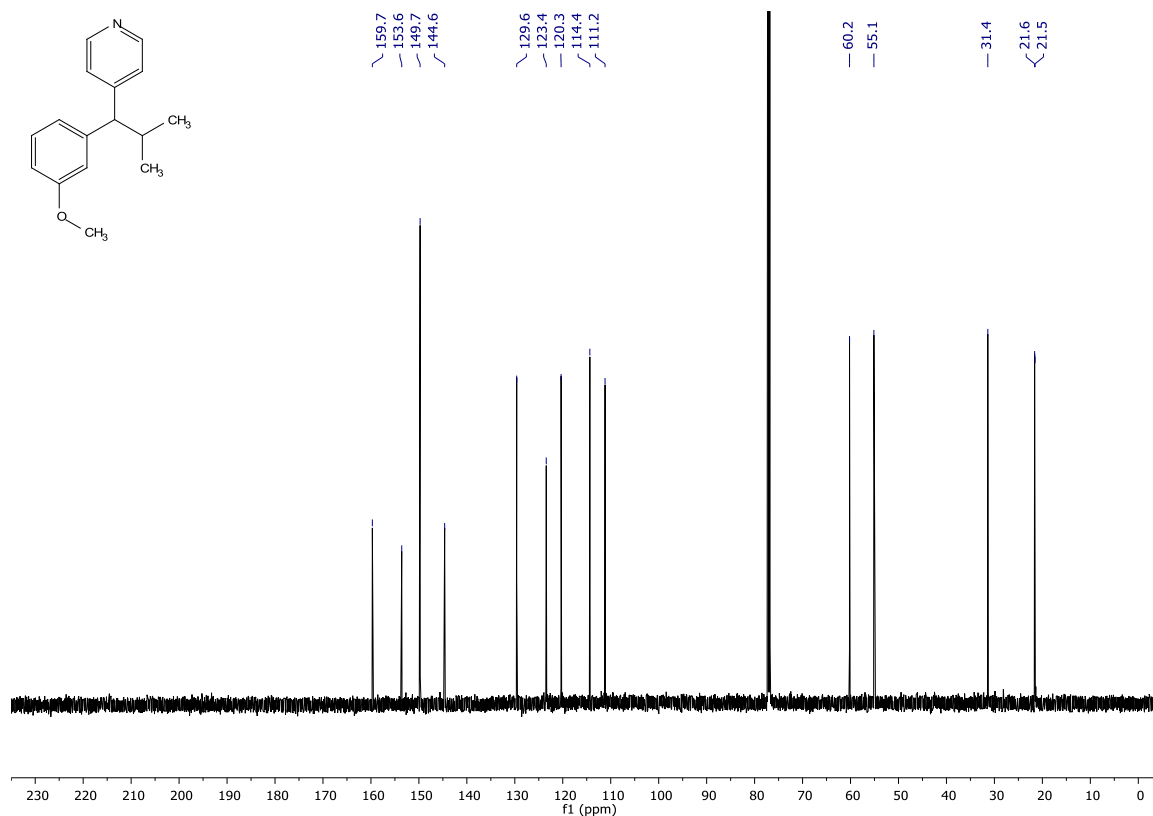
4-(4-methoxybenzyl)pyridine (162)**¹H-NMR (600 MHz, CDCl₃)****¹³C-NMR (151 MHz, CDCl₃)**

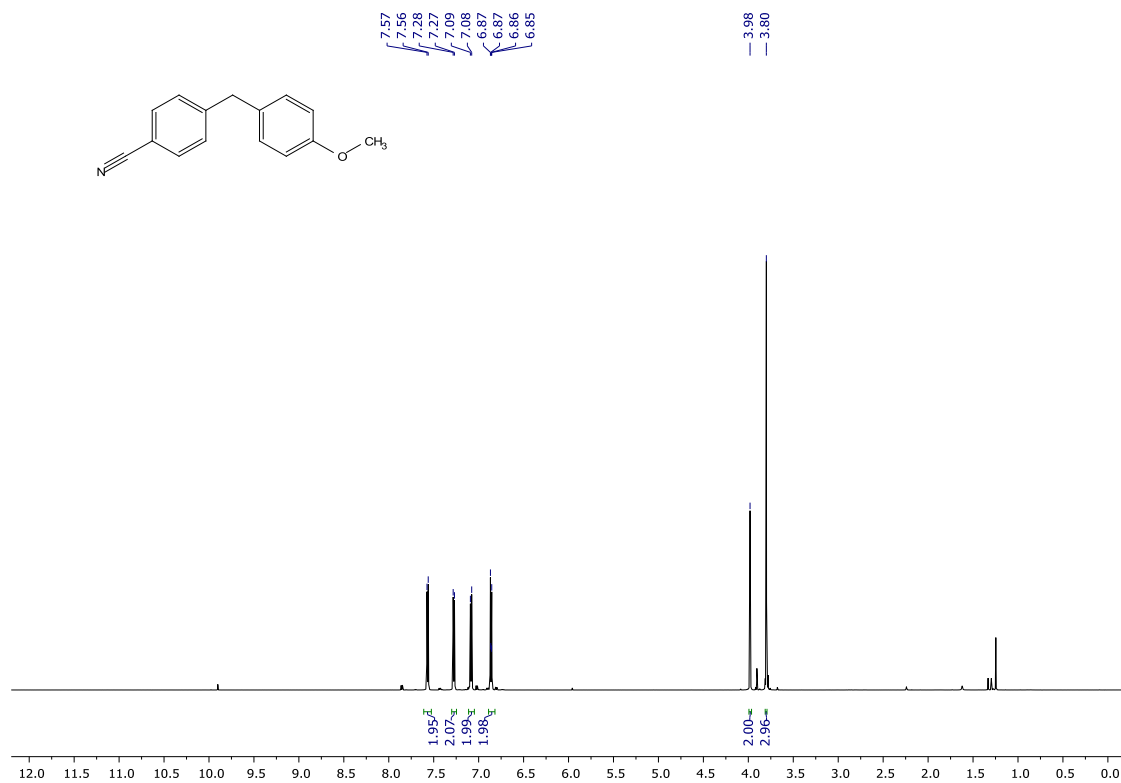
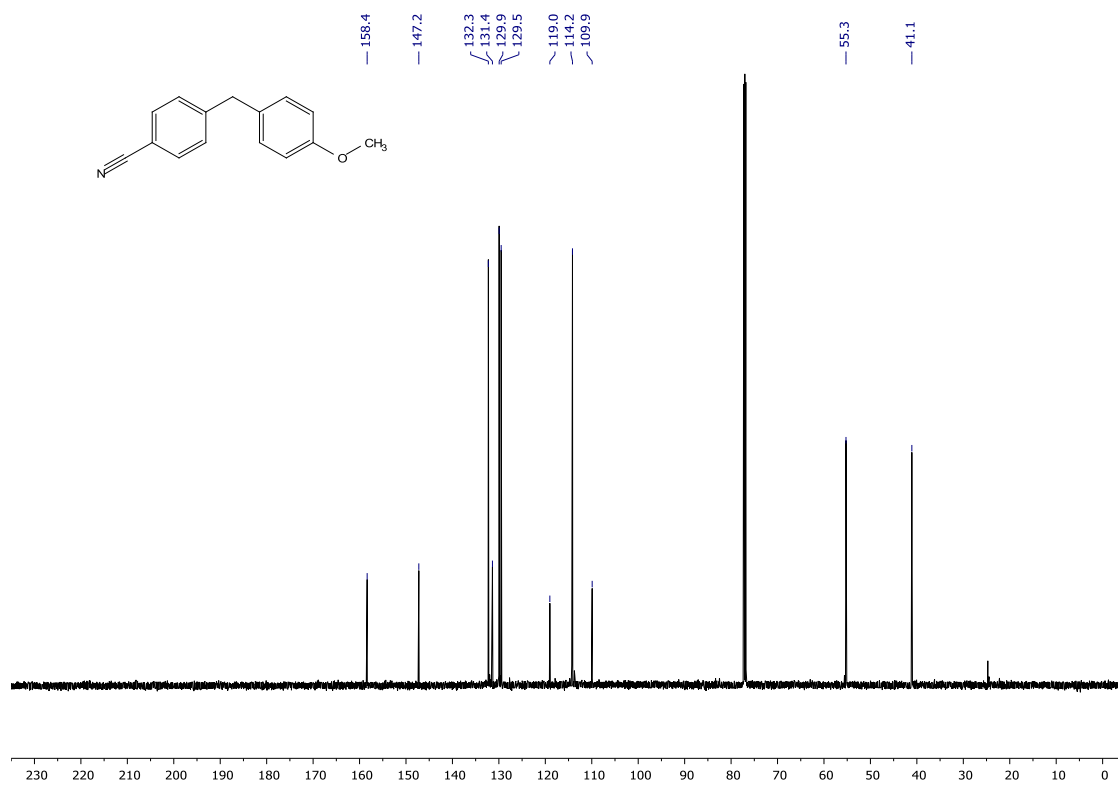
4-(1-(3-methoxyphenyl)-2-methylpropyl)pyridine (163)

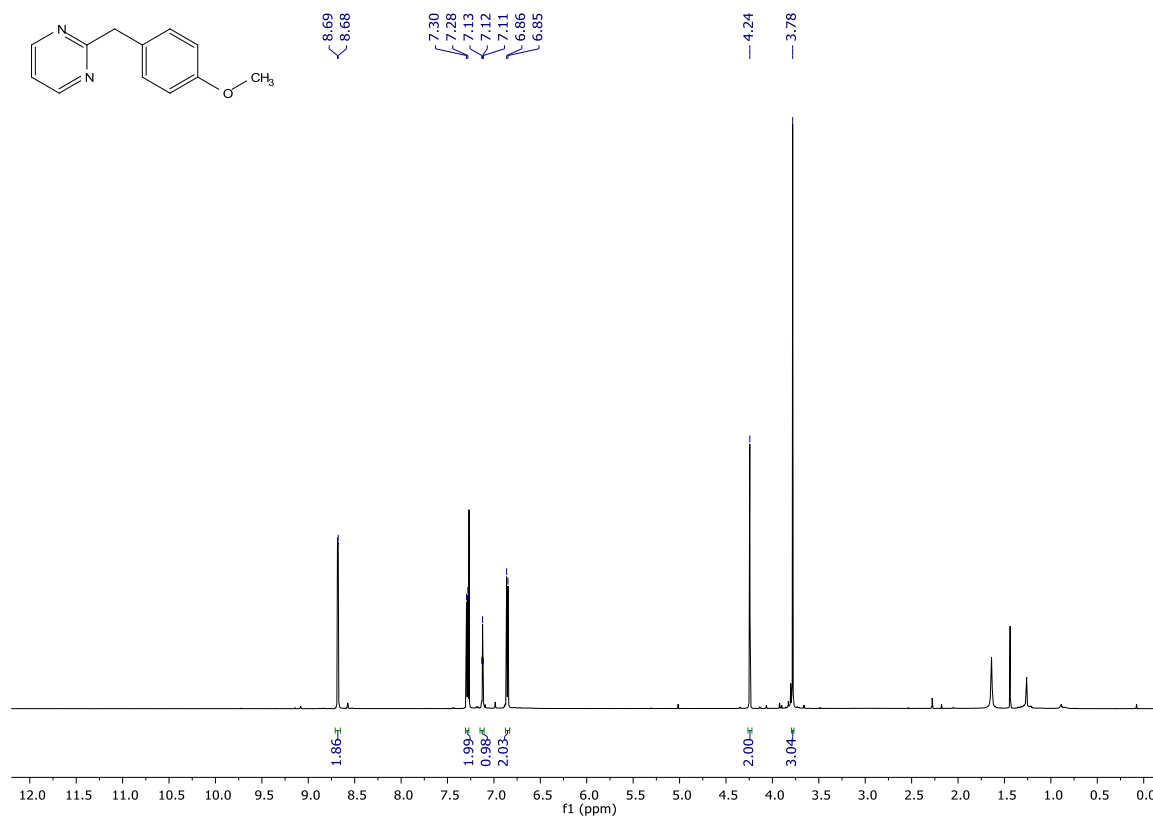
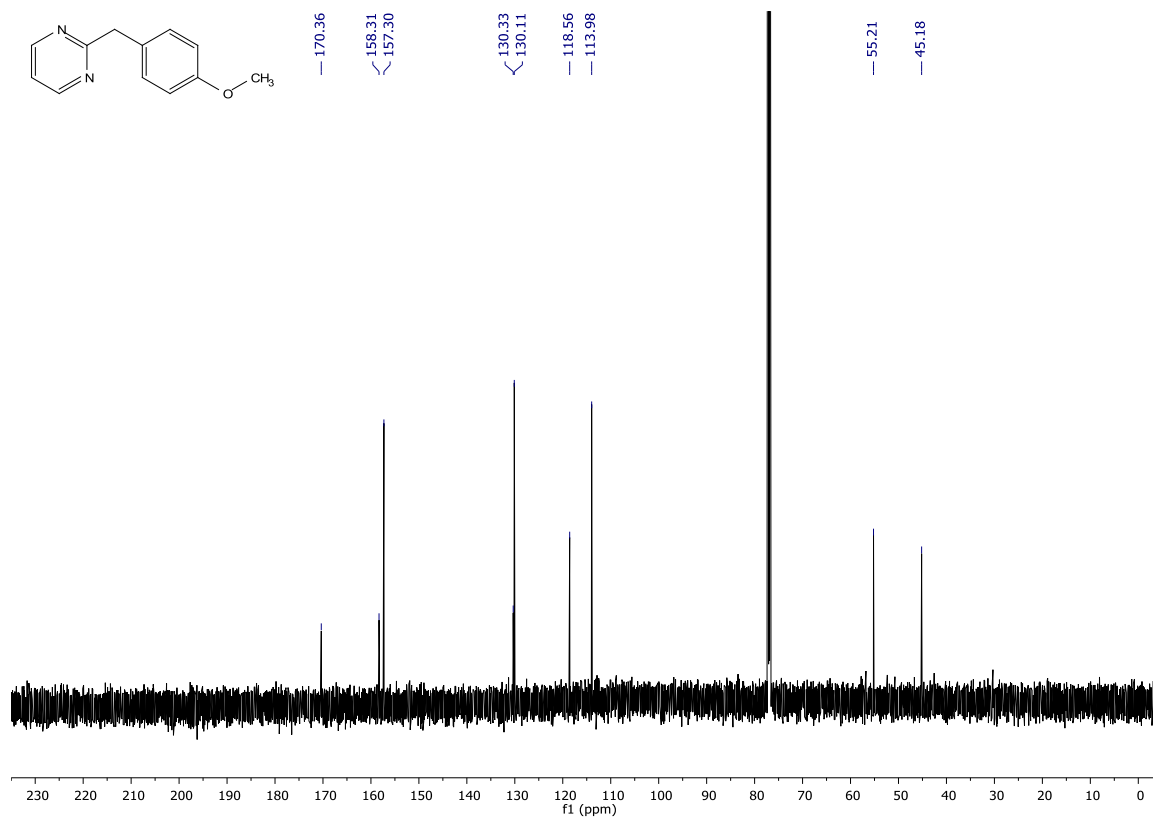
¹H-NMR (600 MHz, CDCl₃)

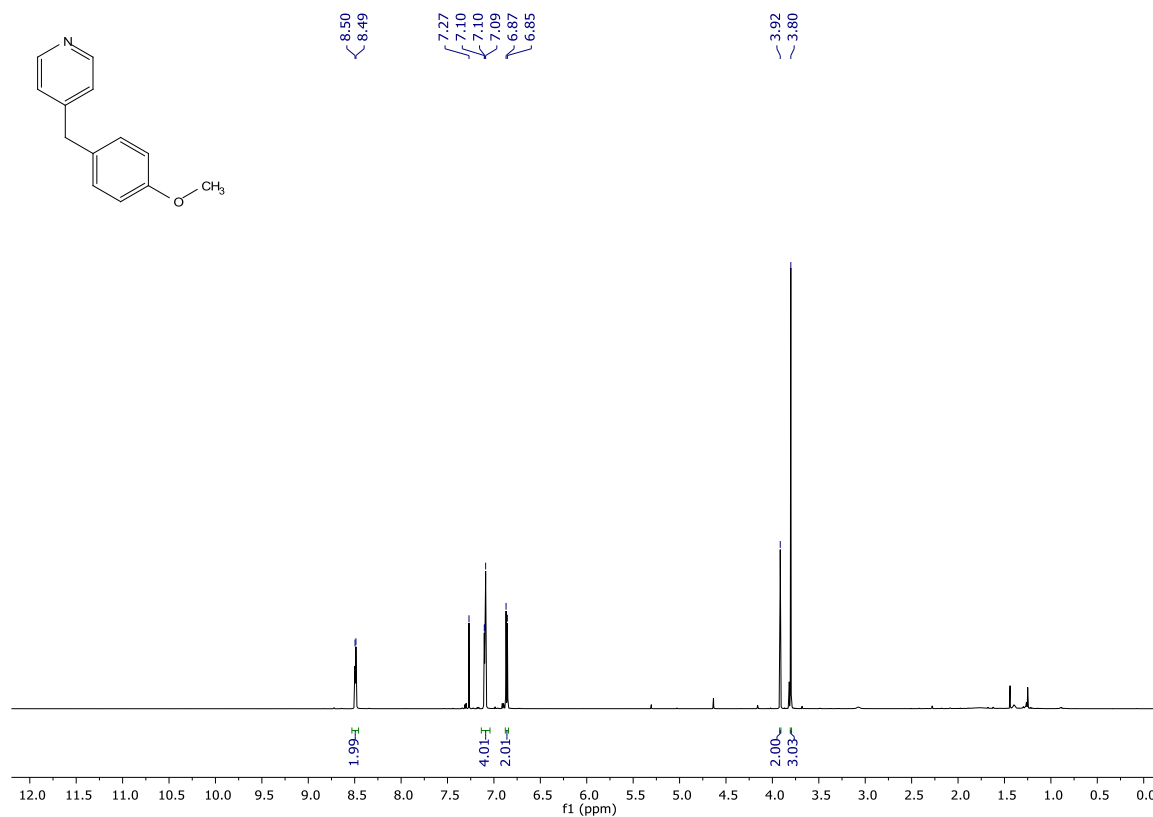
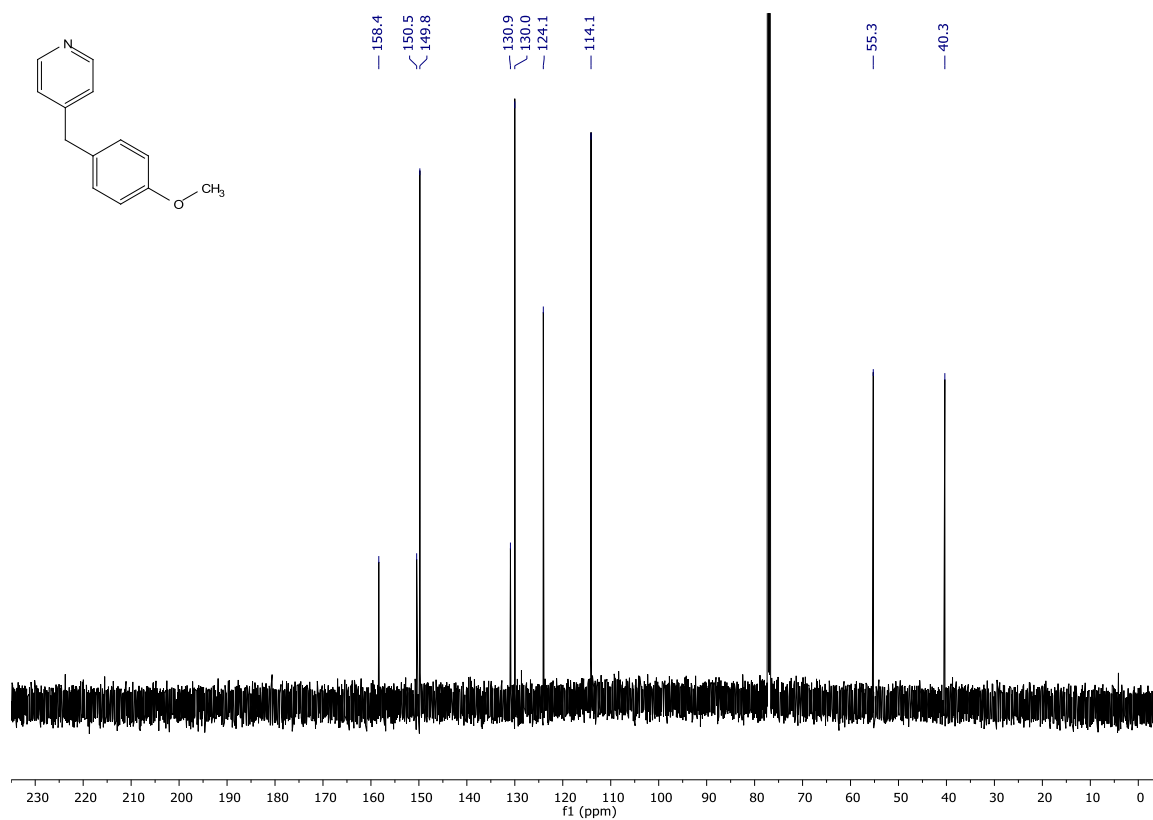


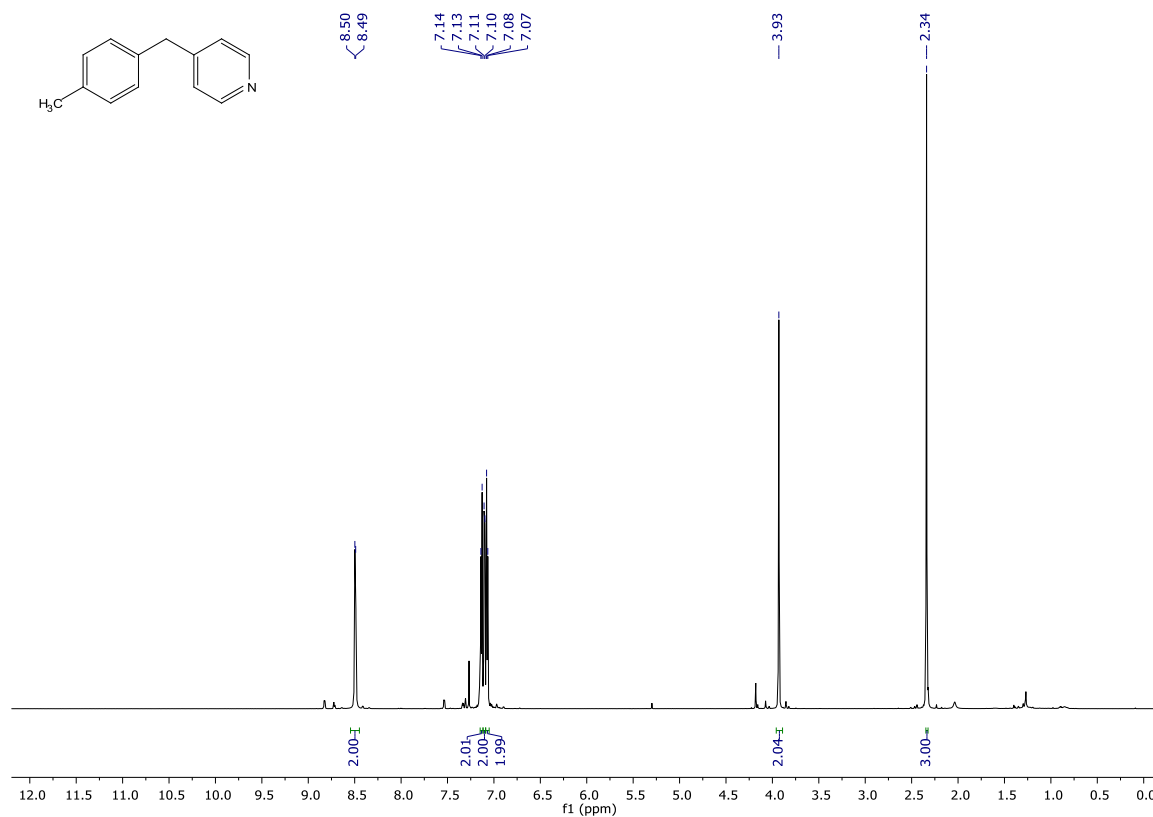
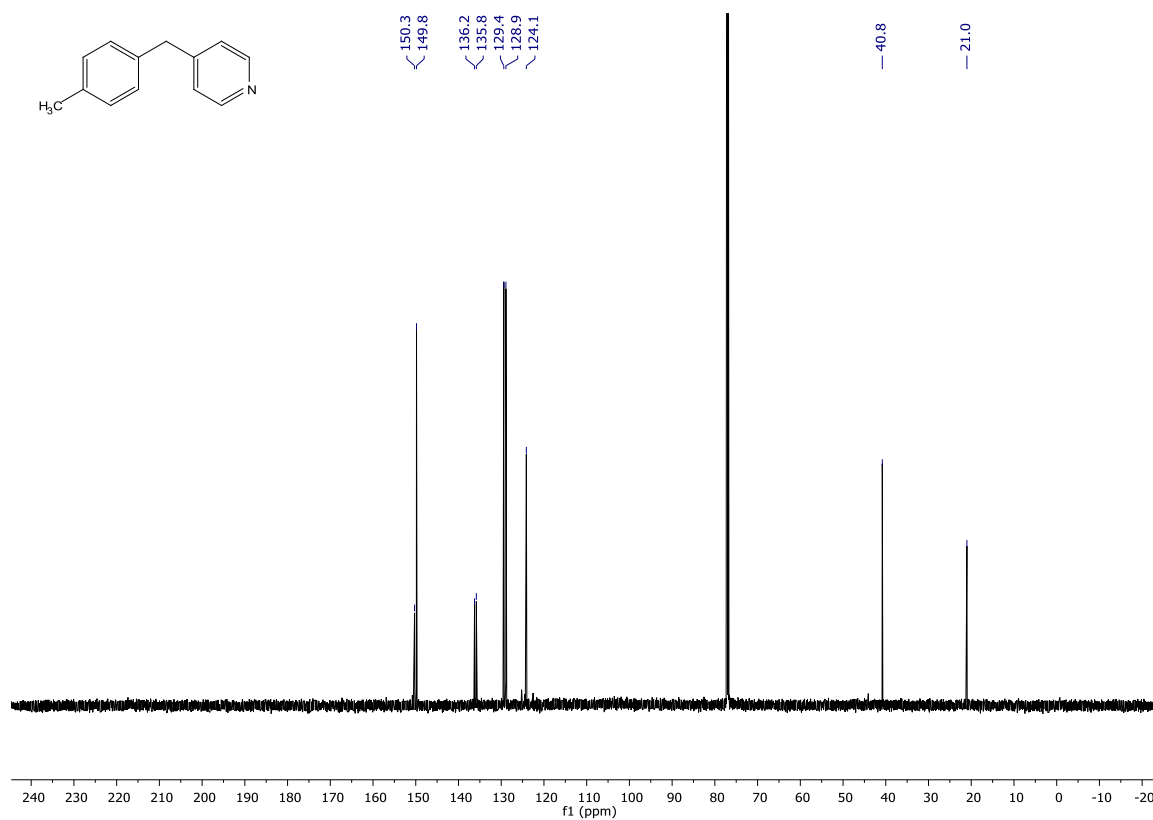
¹³C-NMR (151 MHz, CDCl₃)



4-(4-methoxybenzyl)benzonitrile (173)**¹H-NMR (600 MHz, CDCl₃)****¹³C-NMR (151 MHz, CDCl₃)**

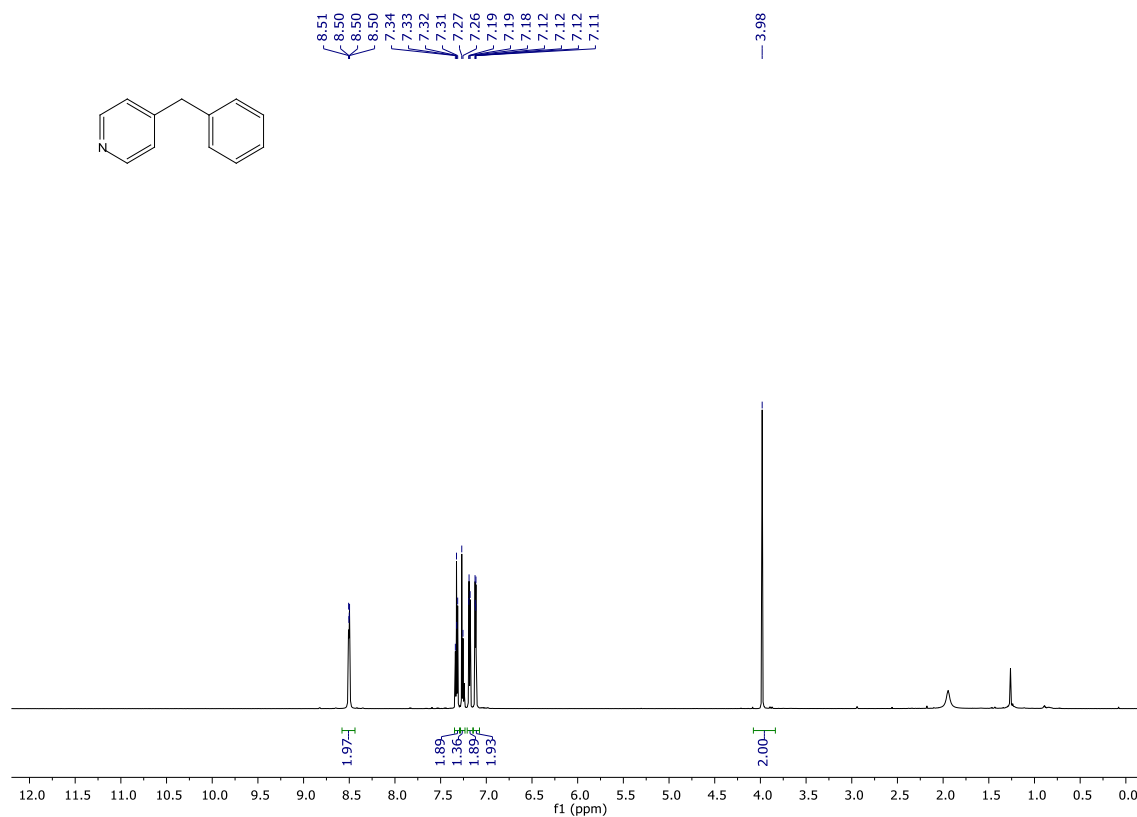
2-(4-methoxybenzyl)pyrimidine (171)**¹H-NMR (600 MHz, CDCl₃)****¹³C-NMR (151 MHz, CDCl₃)**

4-(4-methoxybenzyl)pyridine (162)**¹H-NMR (600 MHz, CDCl₃)****¹³C-NMR (151 MHz, CDCl₃)**

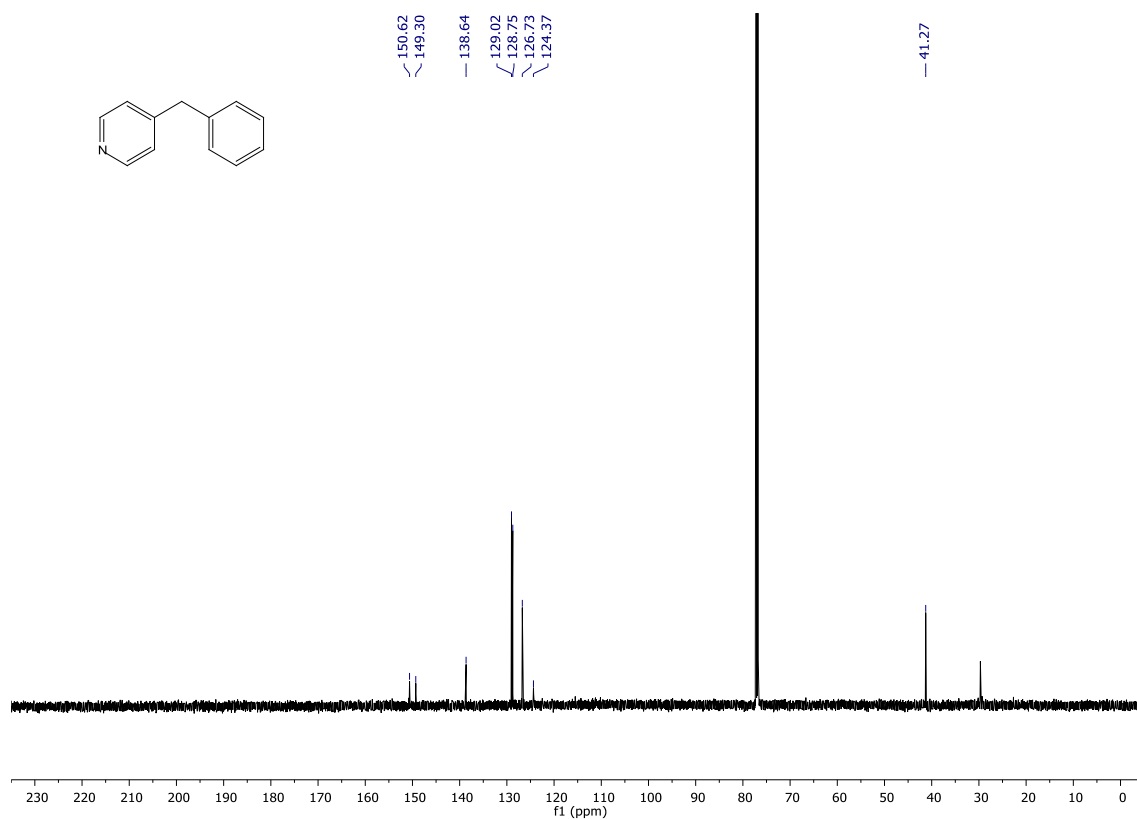
4-(4-methylbenzyl)pyridine (191)**¹H-NMR (600 MHz, CDCl₃)****¹³C-NMR (151 MHz, CDCl₃)**

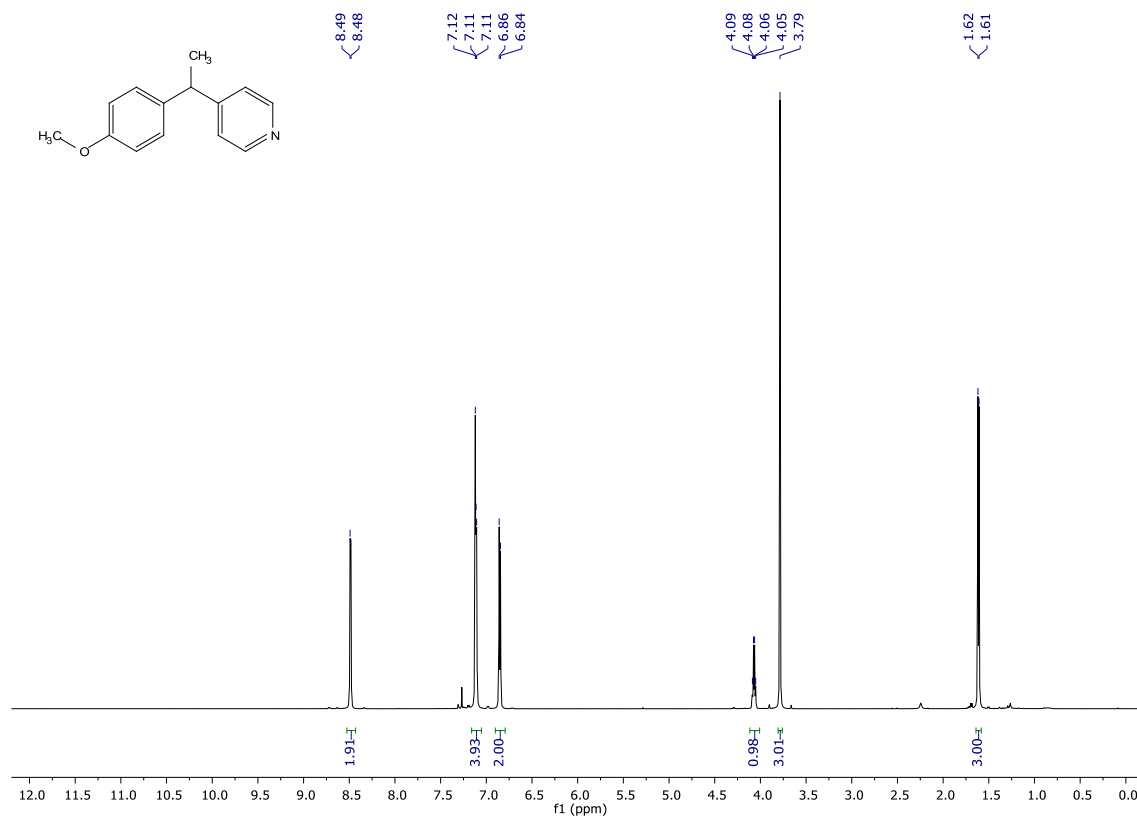
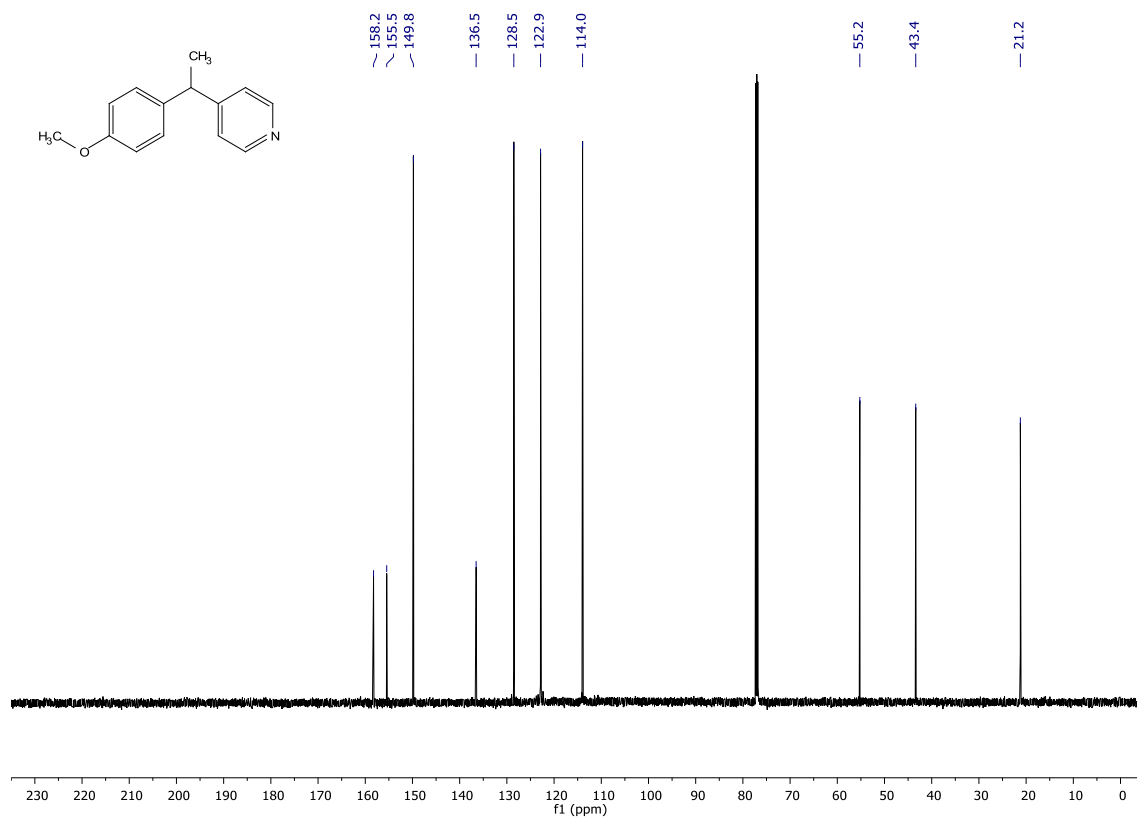
4-(benzyl)pyridine (161)

¹H-NMR (600 MHz, CDCl₃)



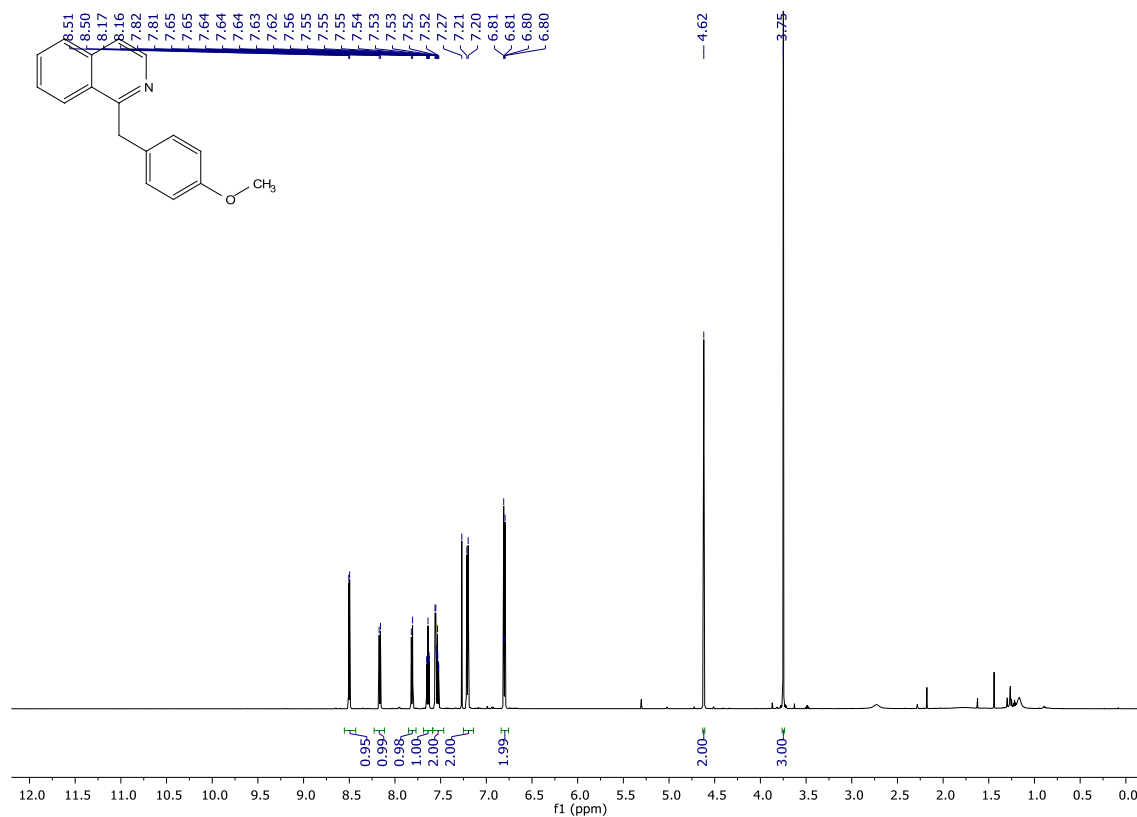
¹³C-NMR (151 MHz, CDCl₃)



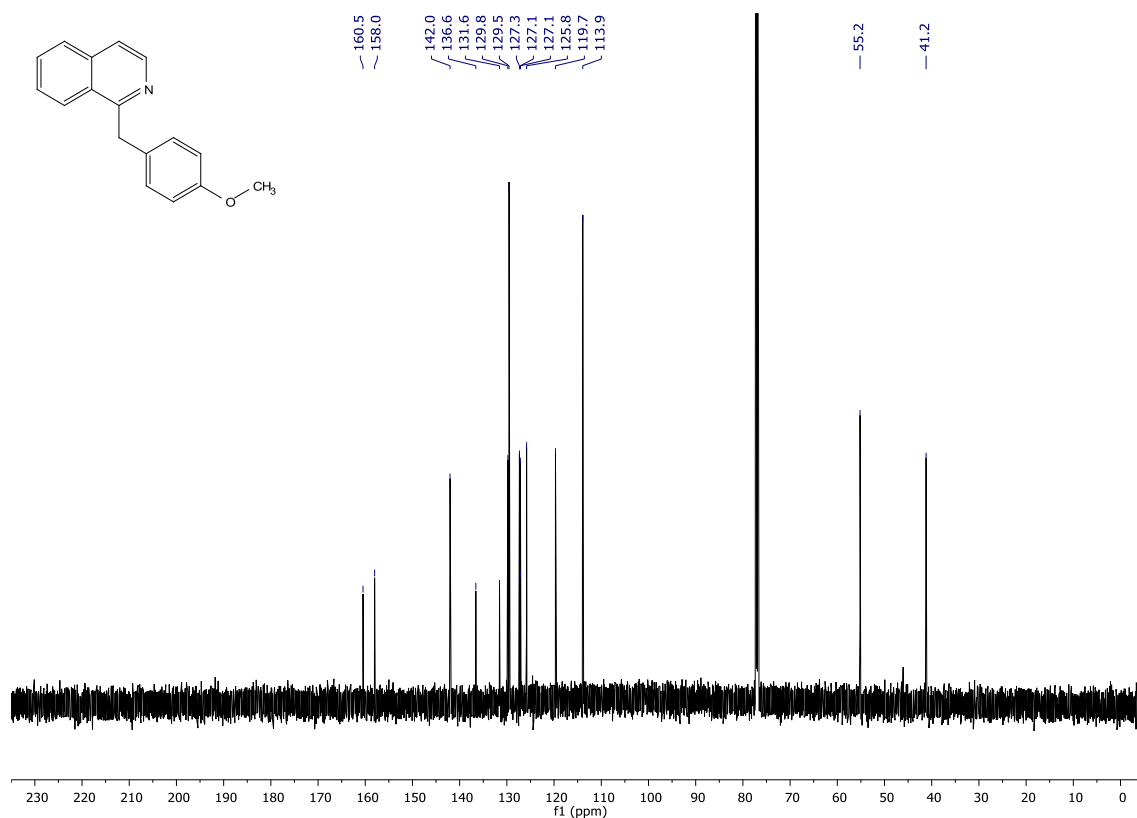
4-(1-(4-methoxyphenyl)ethyl)pyridine (192) **$^1\text{H-NMR}$ (600 MHz, CDCl_3)** **$^{13}\text{C-NMR}$ (151 MHz, CDCl_3)**

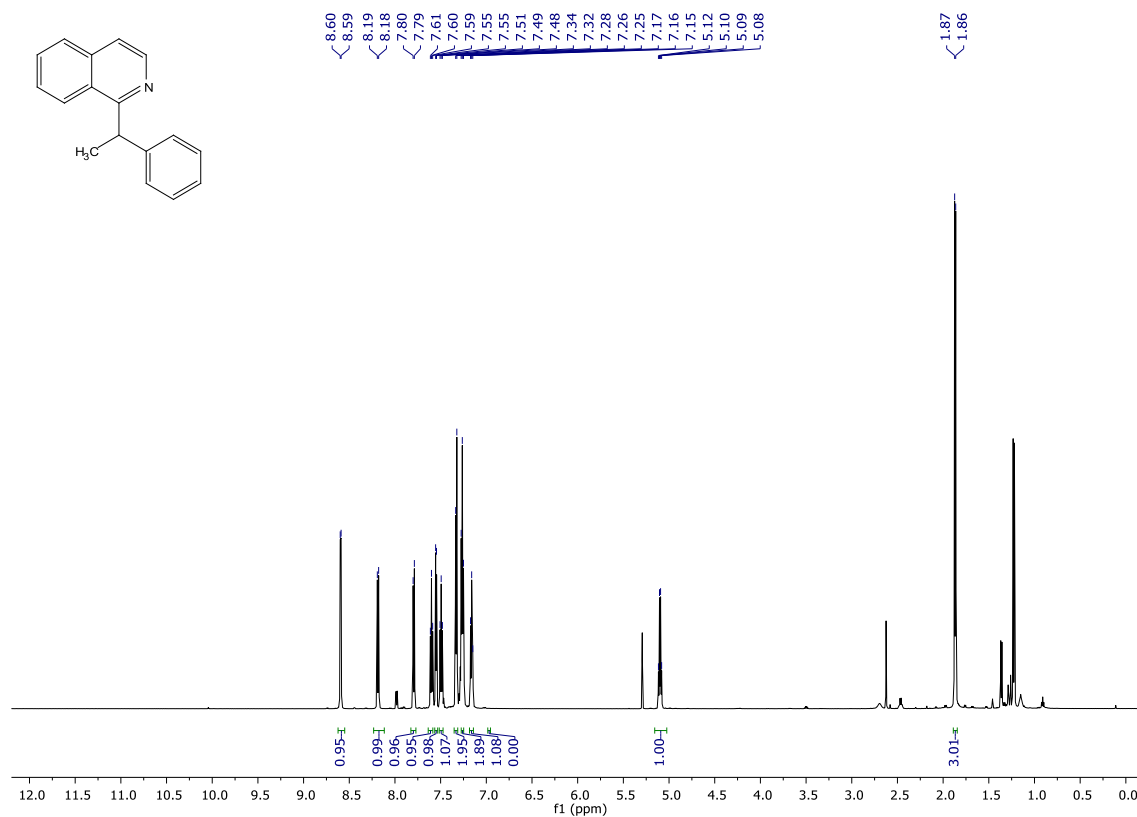
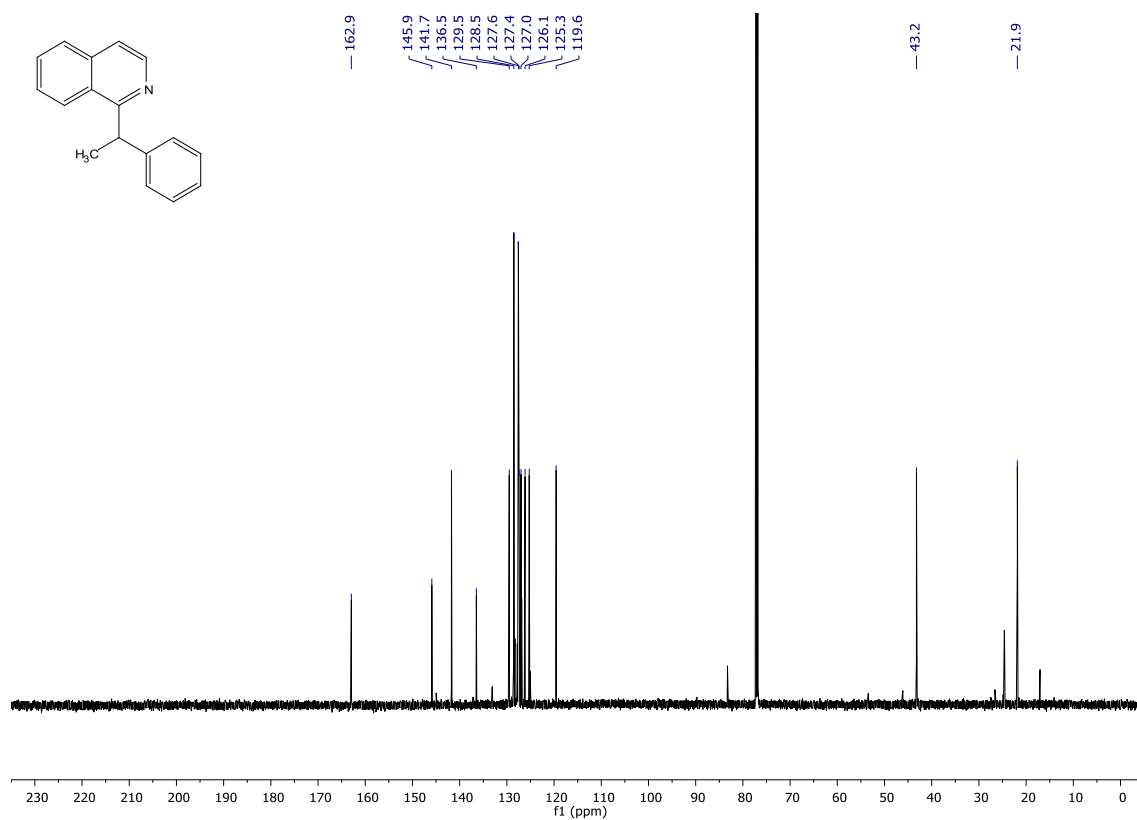
1-(4-methoxybenzyl)isoquinoline (184)

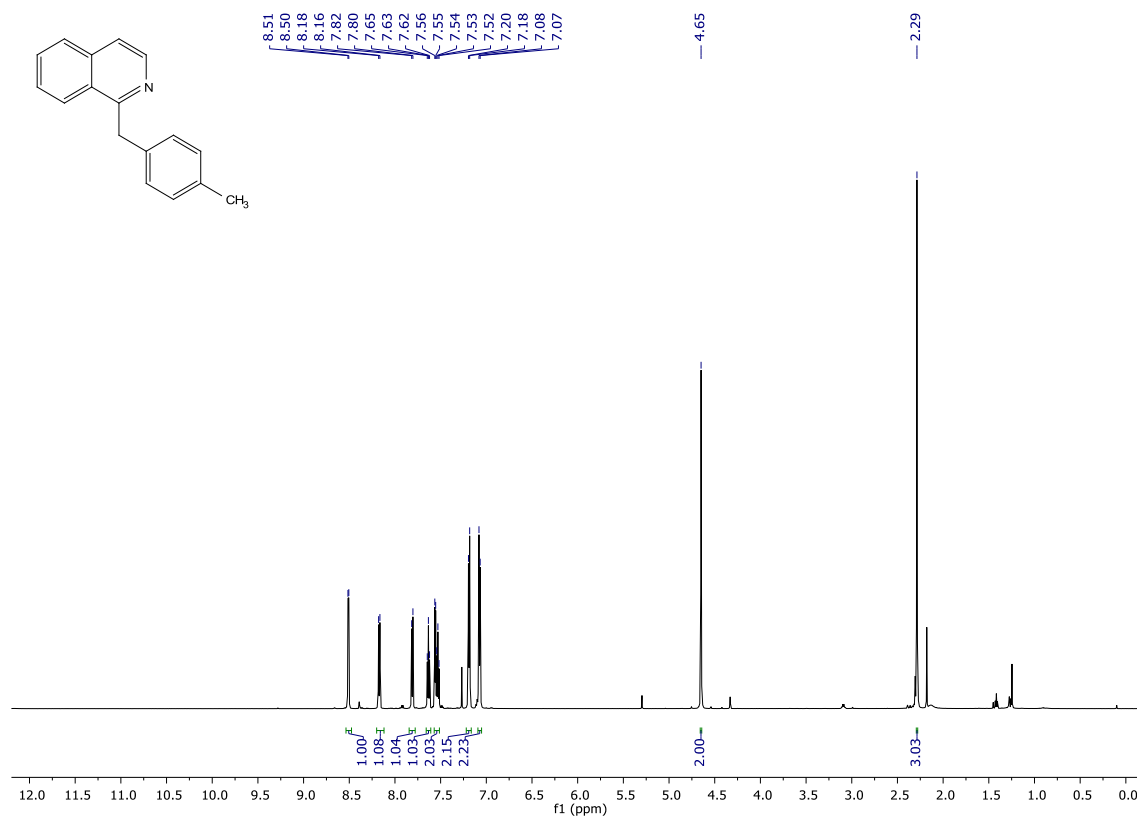
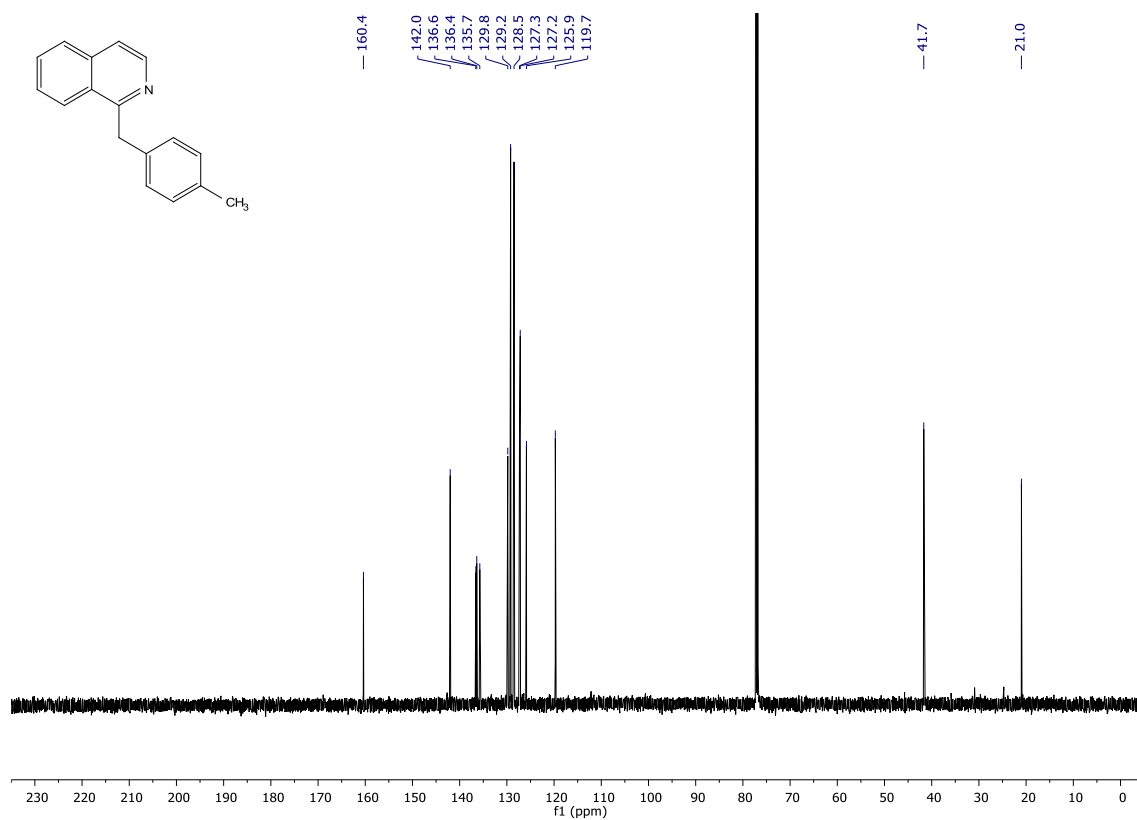
¹H-NMR (600 MHz, CDCl₃)

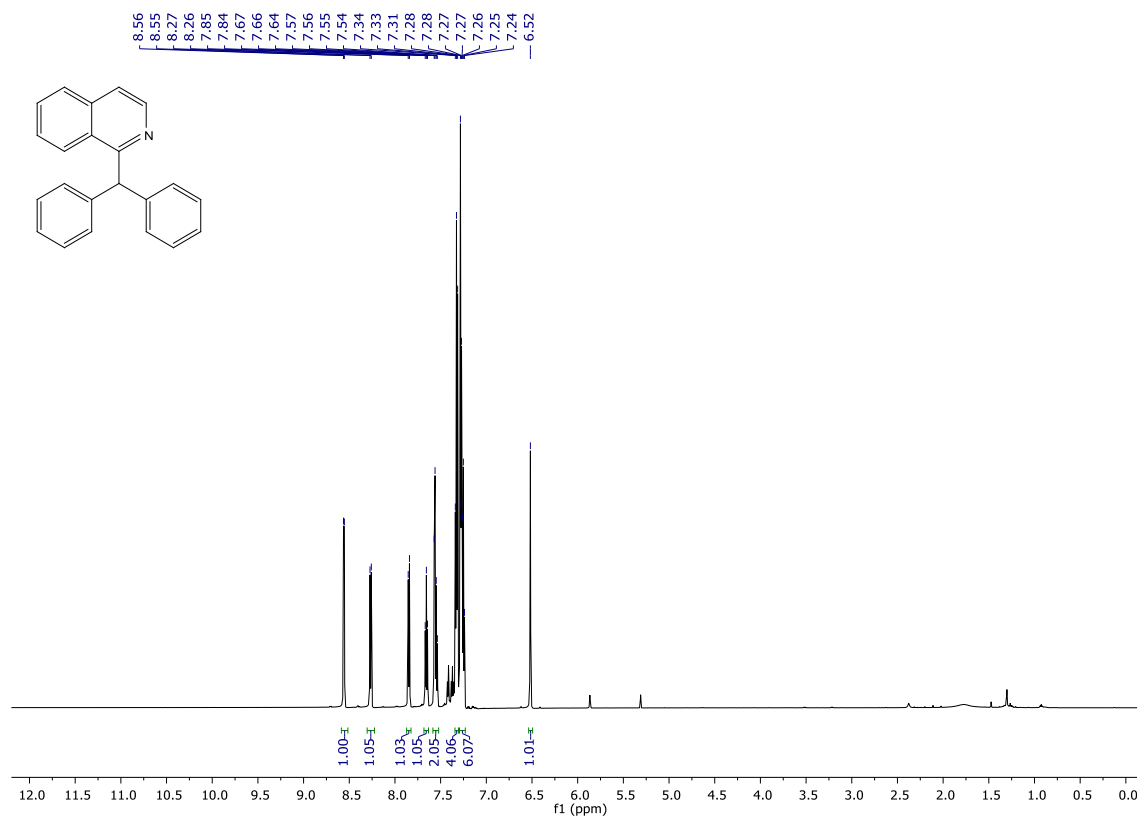
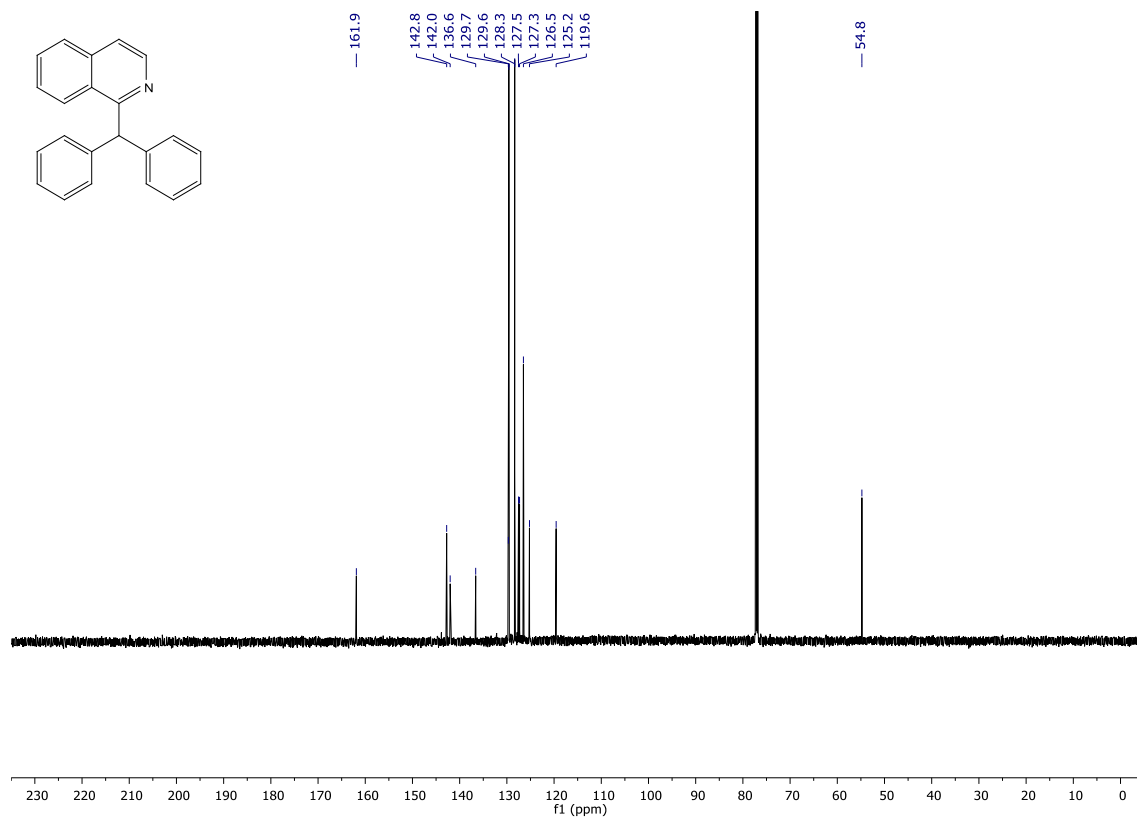


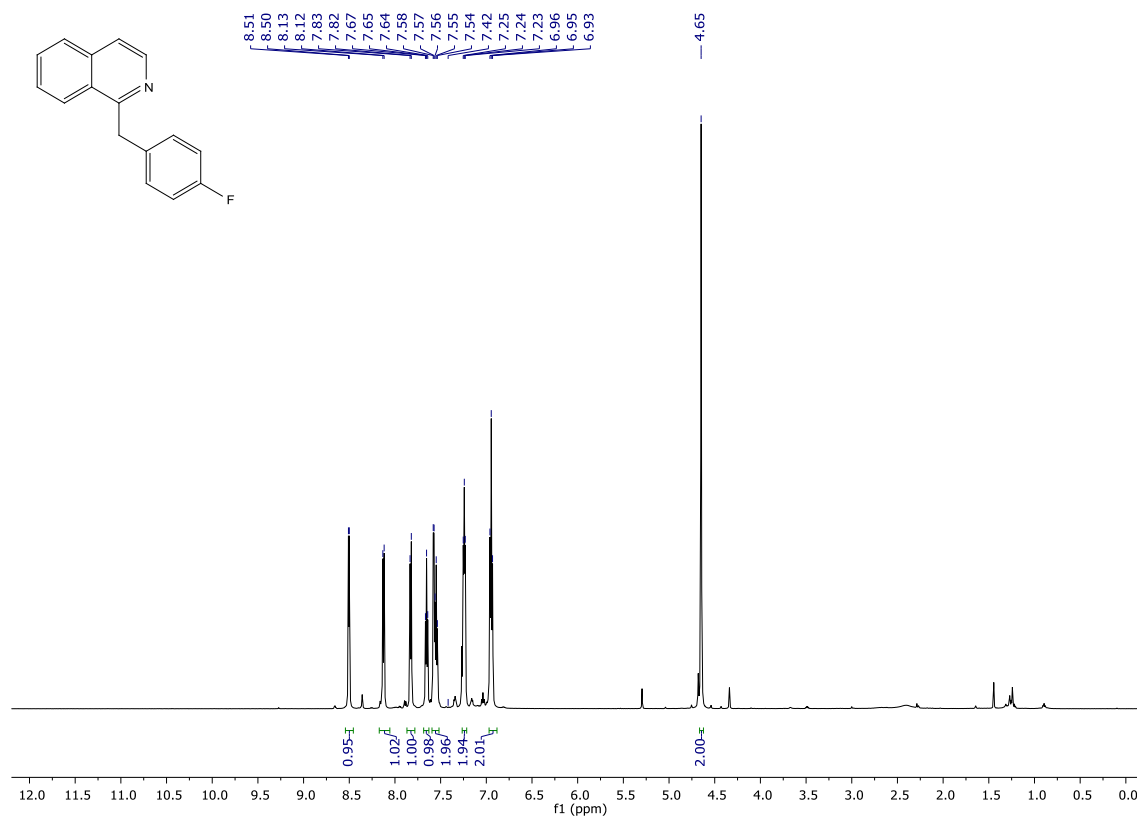
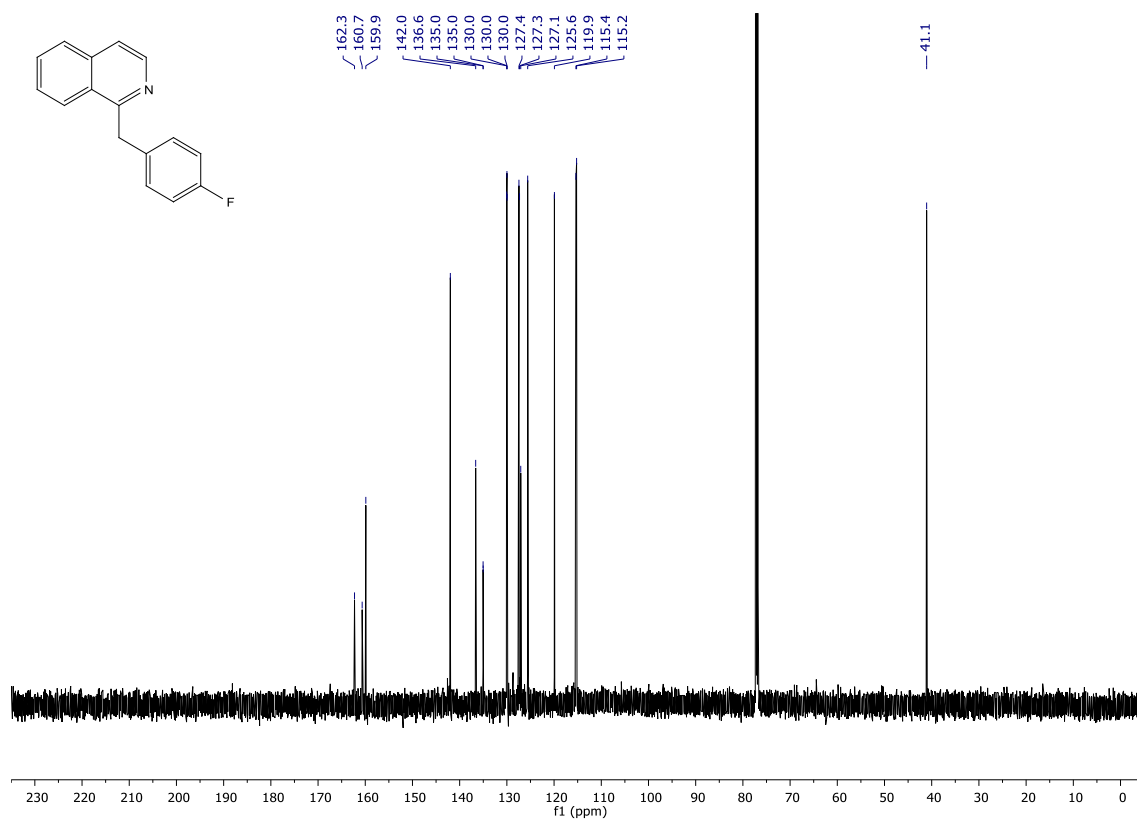
¹³C-NMR (151 MHz, CDCl₃)

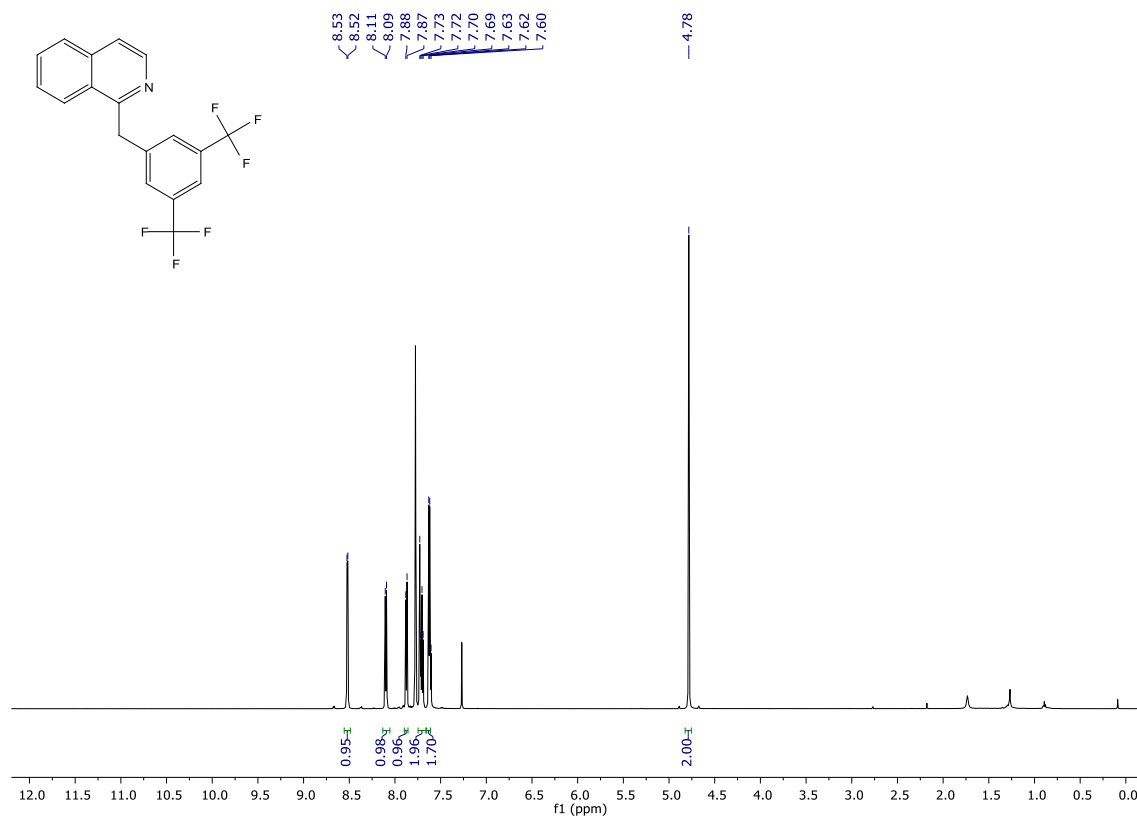
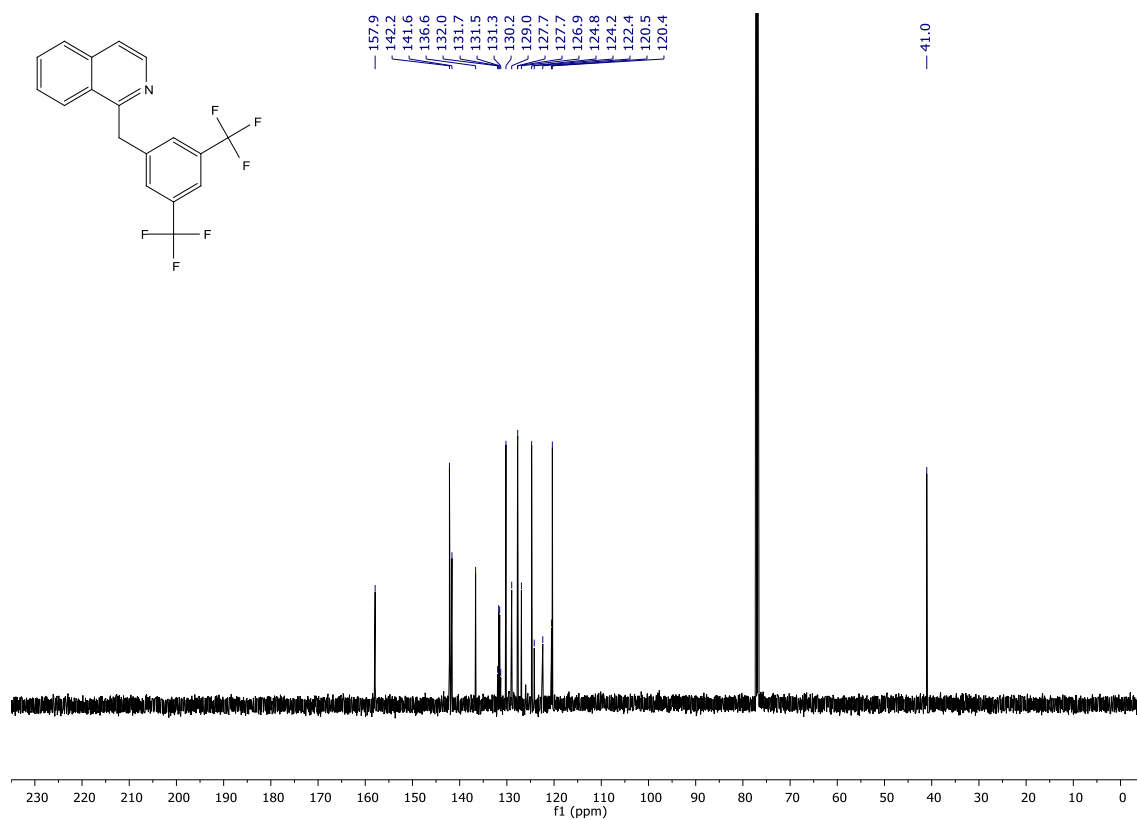


1-(1-phenylethyl)isoquinoline (194) **$^1\text{H-NMR}$ (600 MHz, CDCl_3)** **$^{13}\text{C-NMR}$ (151 MHz, CDCl_3)**

1-(4-methylbenzyl)isoquinoline (193) **$^1\text{H-NMR}$ (600 MHz, CDCl_3)** **$^{13}\text{C-NMR}$ (151 MHz, CDCl_3)**

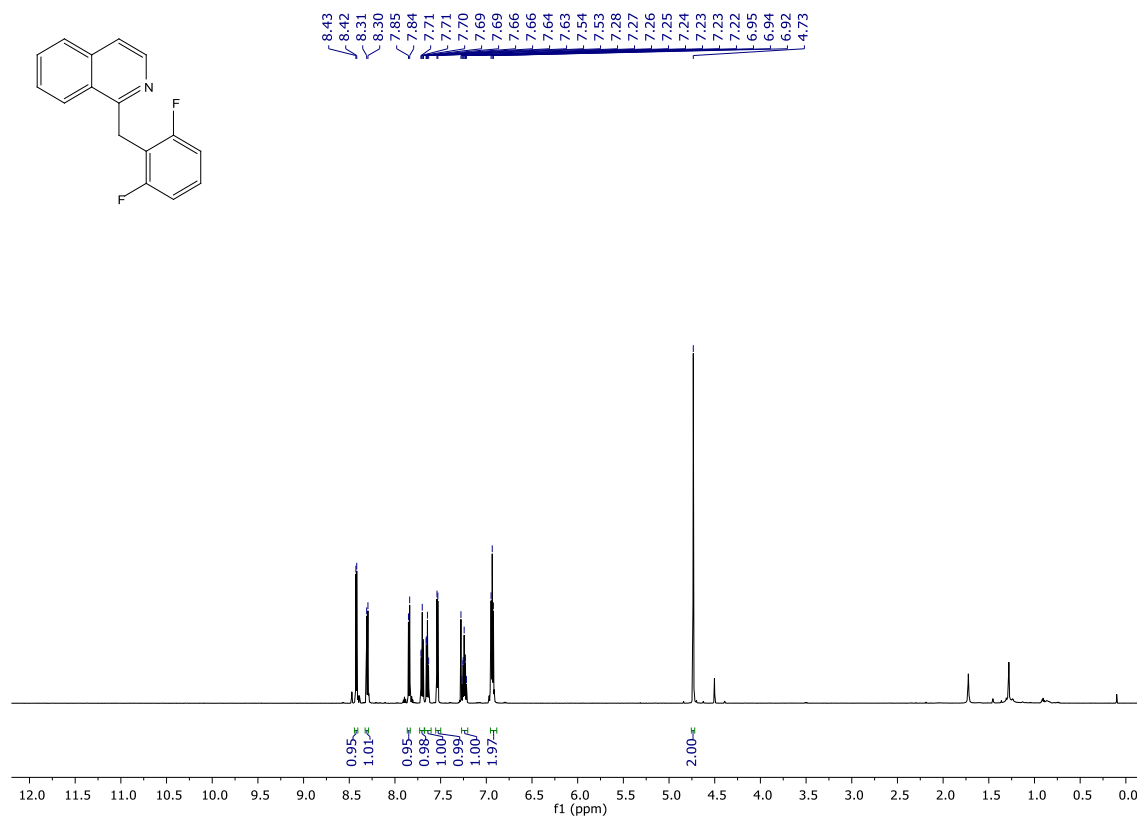
1-benzhydrylisoquinoline (195) **$^1\text{H-NMR}$ (600 MHz, CDCl_3)** **$^{13}\text{C-NMR}$ (151 MHz, CDCl_3)**

1-(4-fluorobenzyl)isoquinoline (196) **$^1\text{H-NMR}$ (600 MHz, CDCl_3)** **$^{13}\text{C-NMR}$ (151 MHz, CDCl_3)**

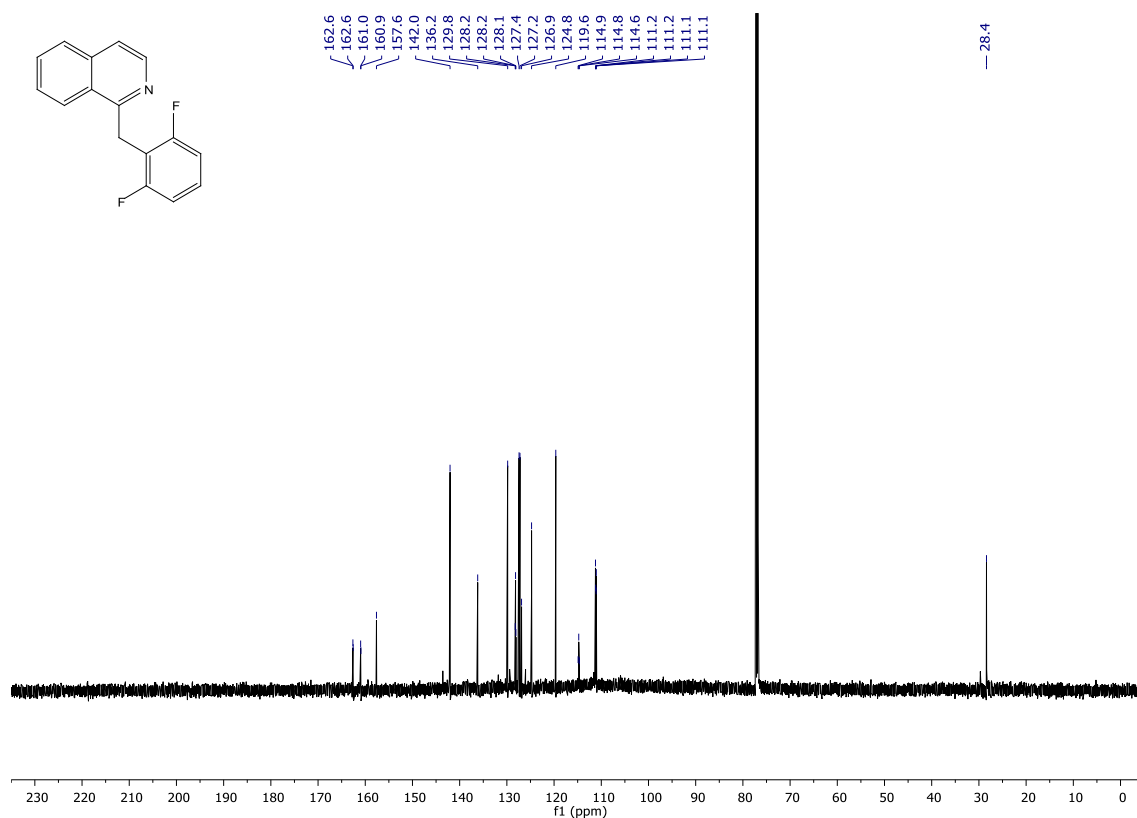
1-(3,5-bis(trifluoromethyl)benzyl)isoquinoline (197) **$^1\text{H-NMR}$ (600 MHz, CDCl_3)** **$^{13}\text{C-NMR}$ (151 MHz, CDCl_3)**

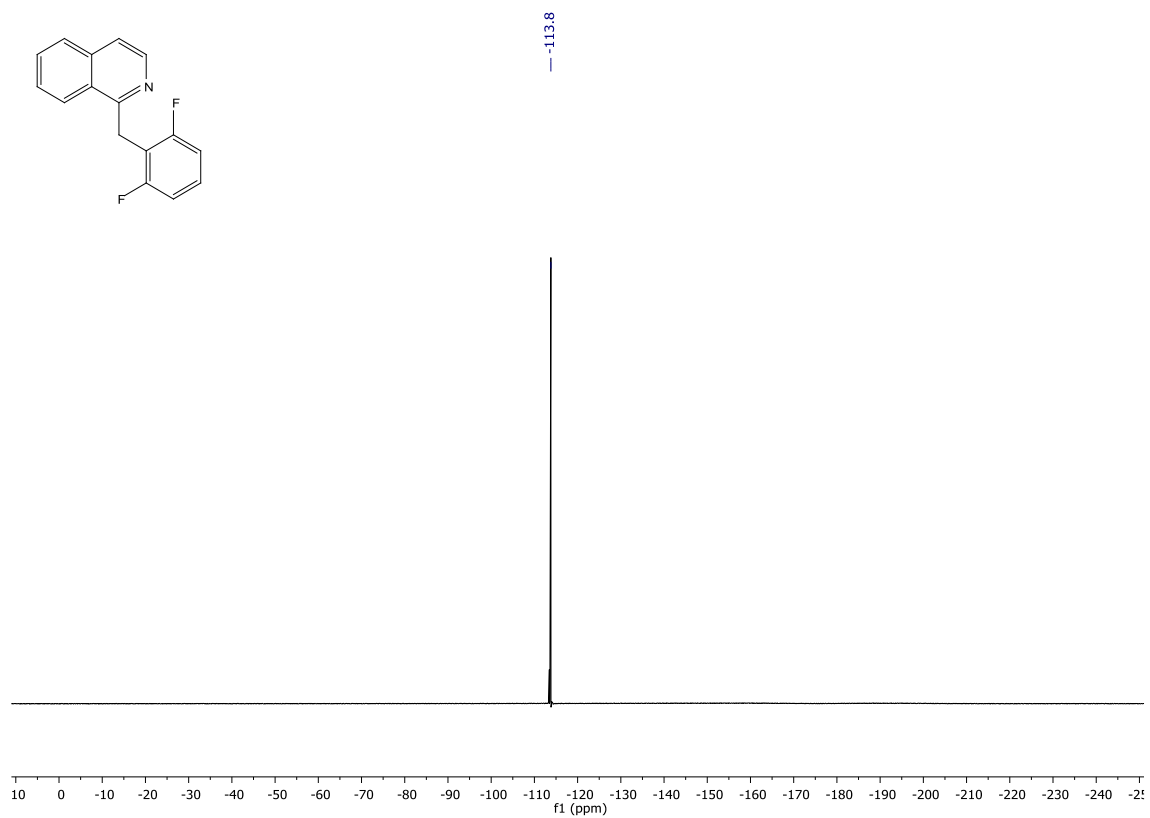
1-(2,6-difluorobenzyl)isoquinoline (198)

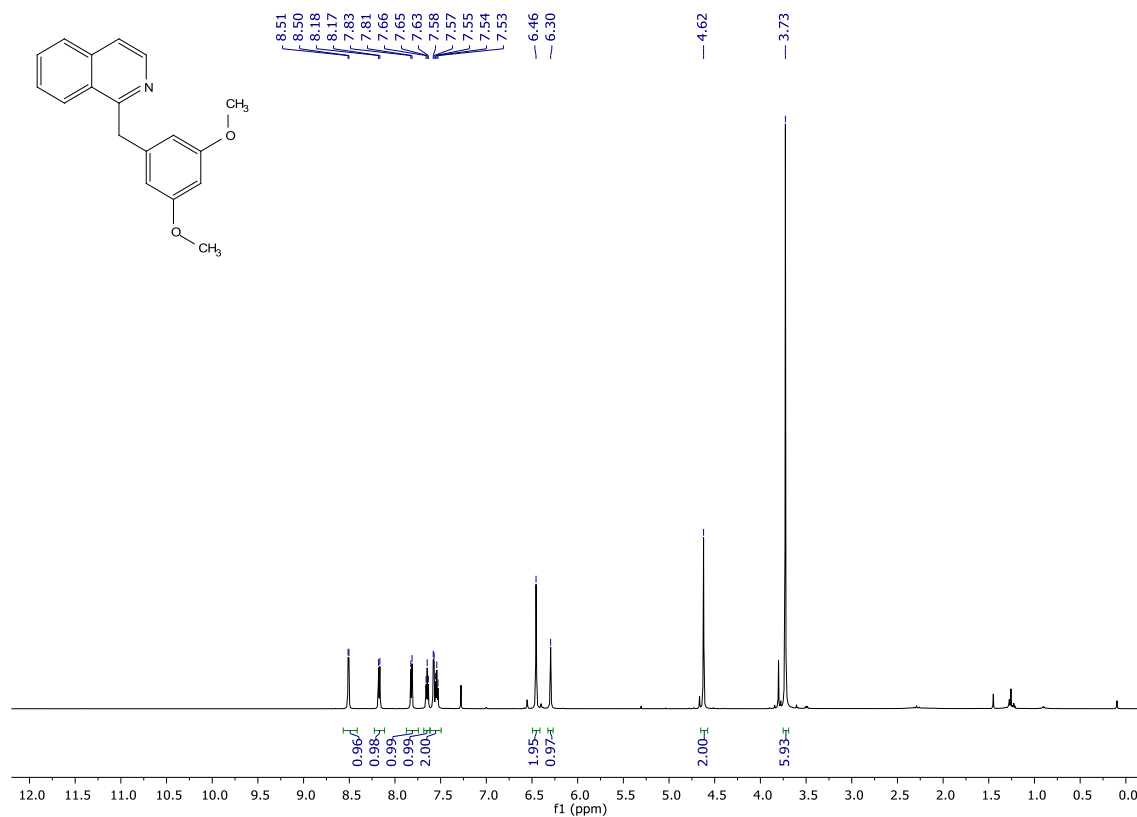
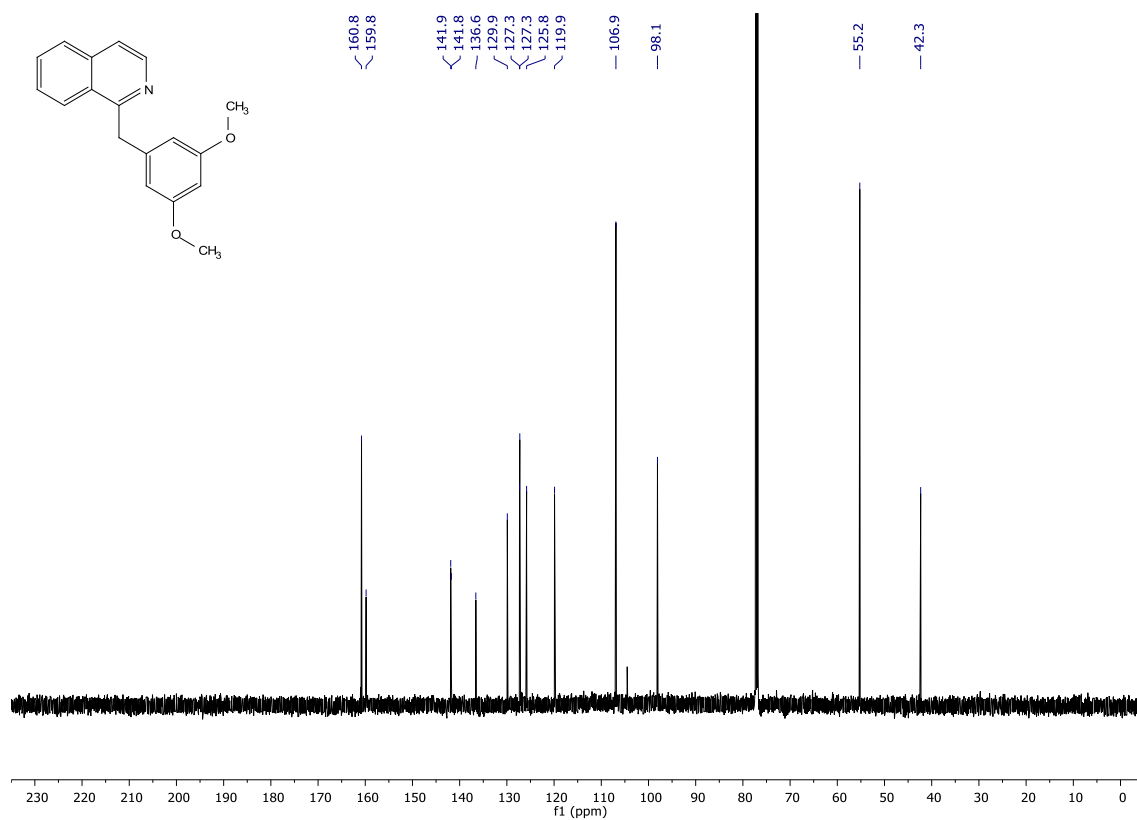
¹H-NMR (600 MHz, CDCl₃)

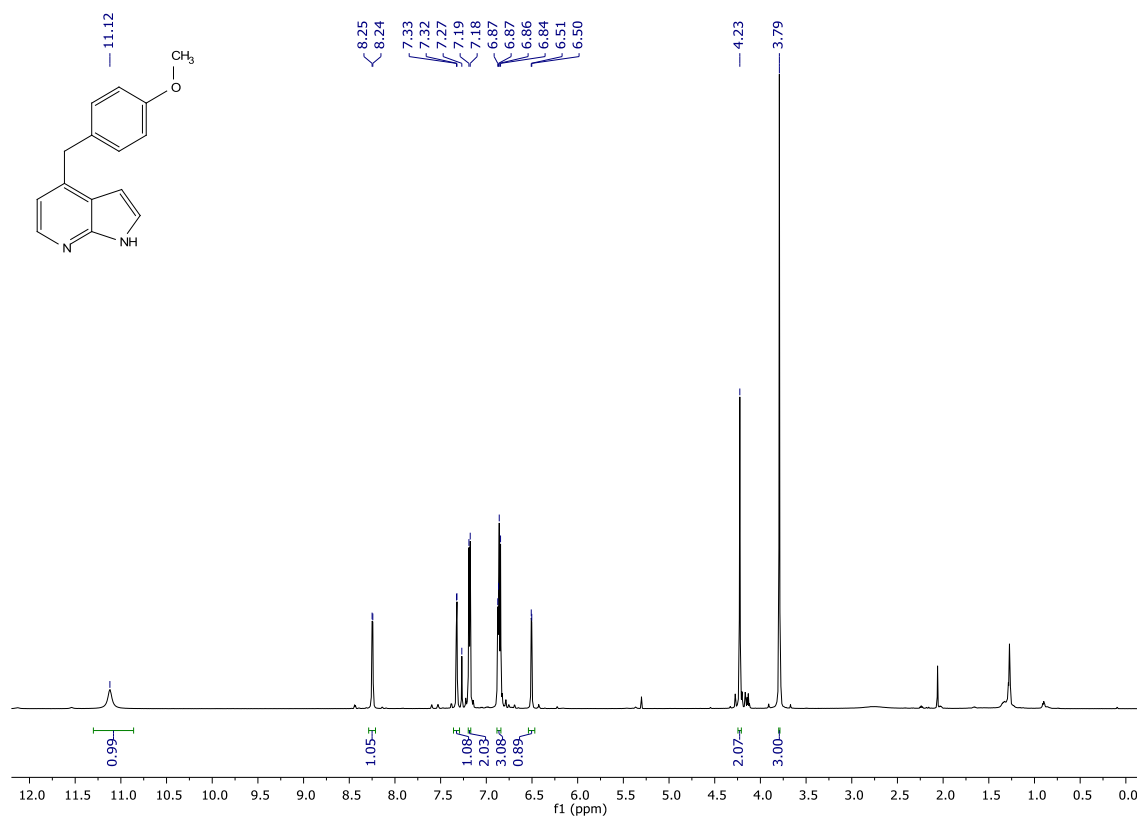
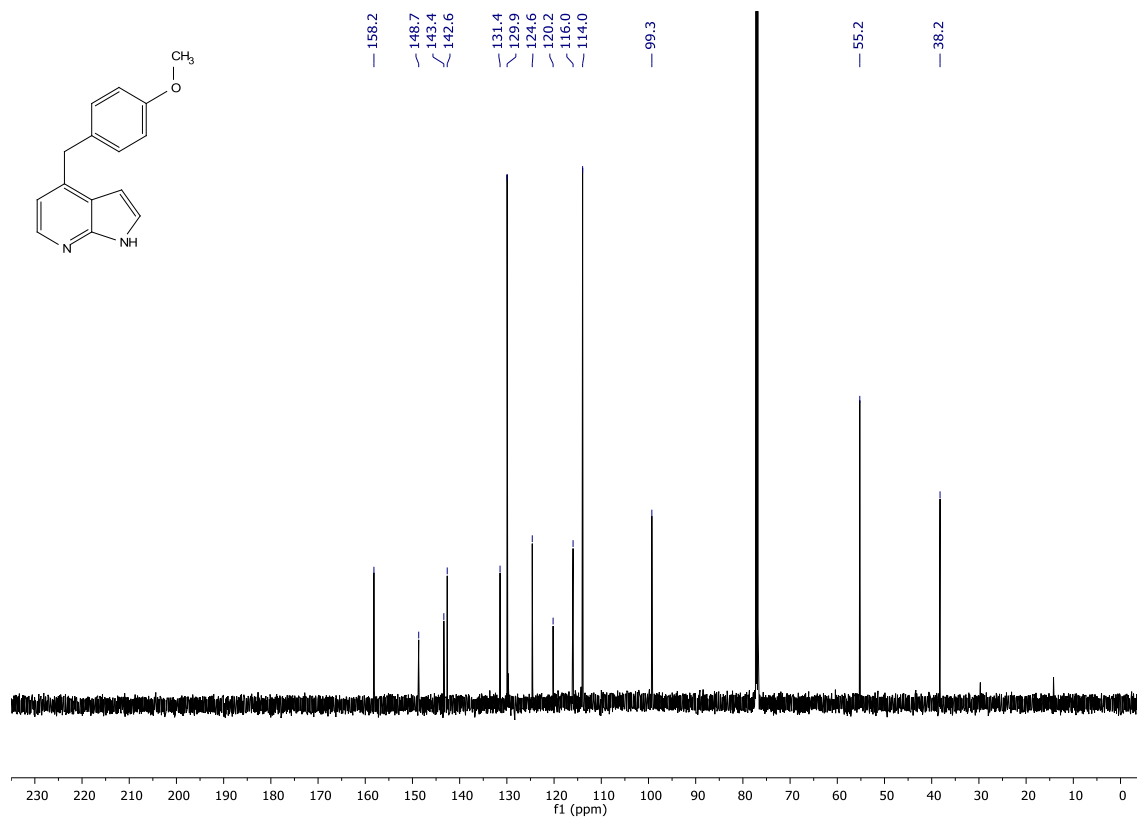


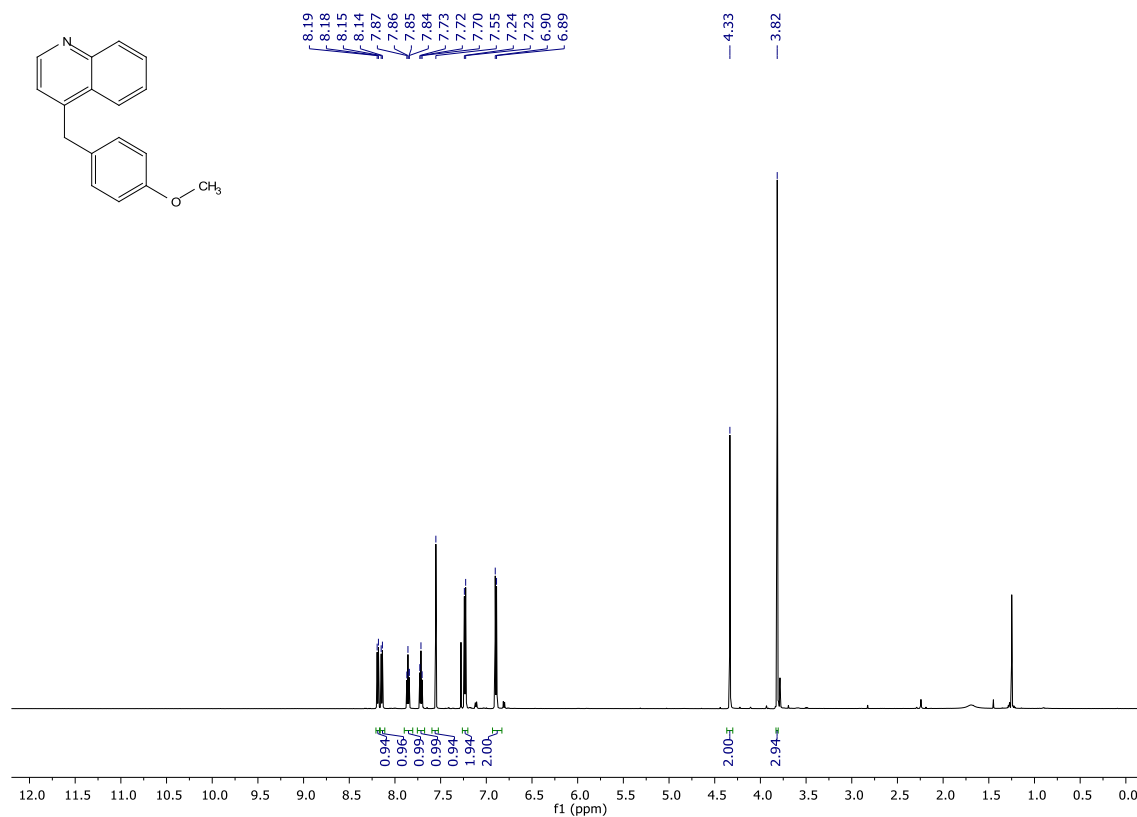
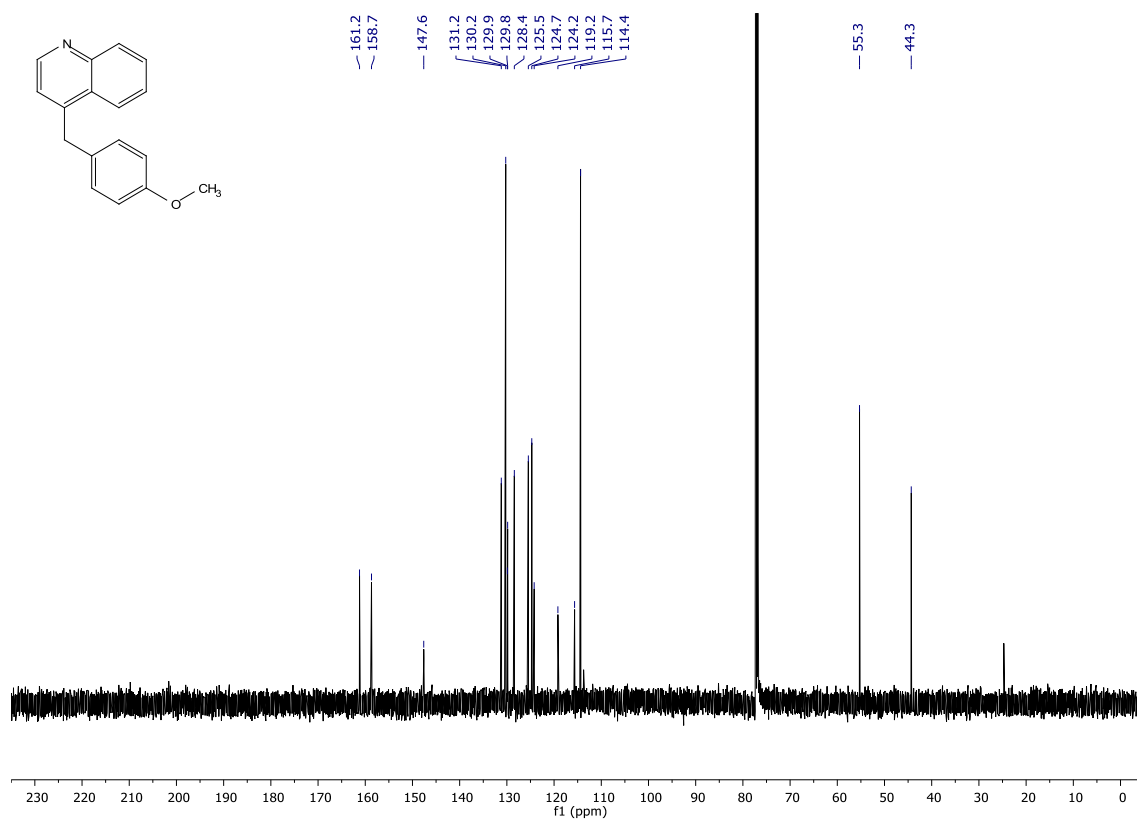
¹³C-NMR (151 MHz, CDCl₃)

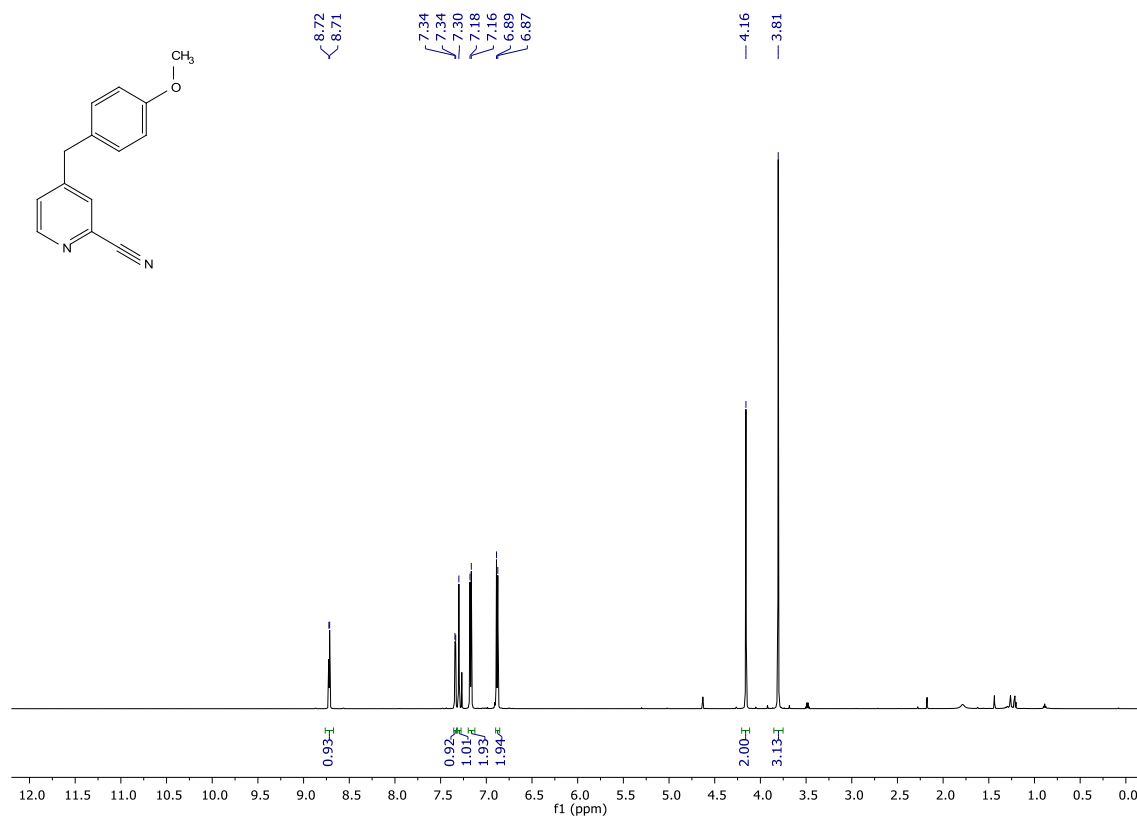
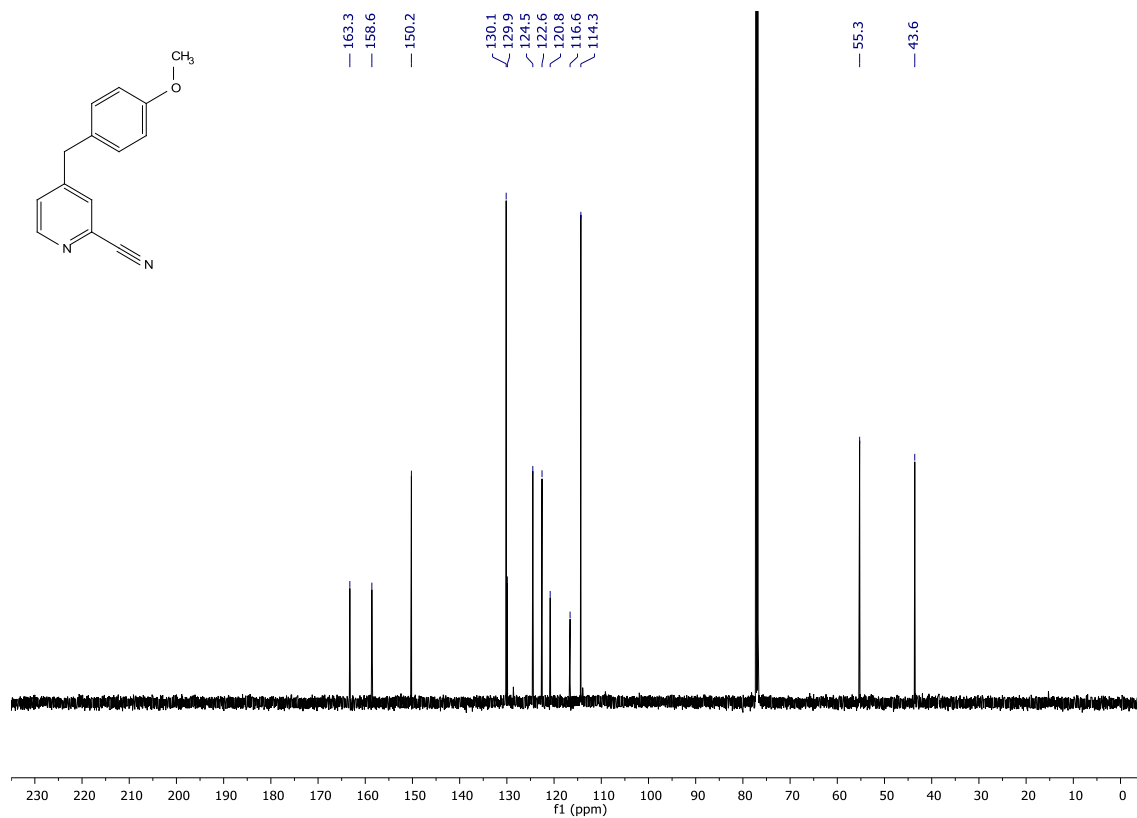


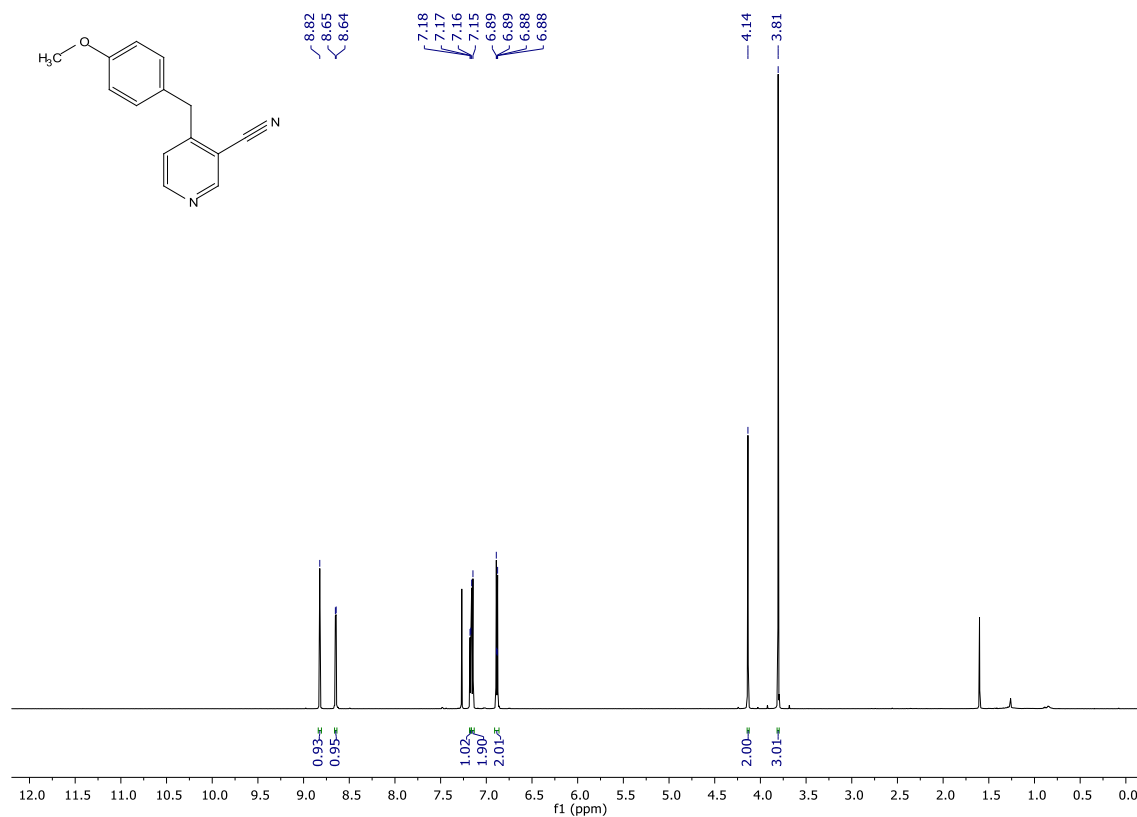
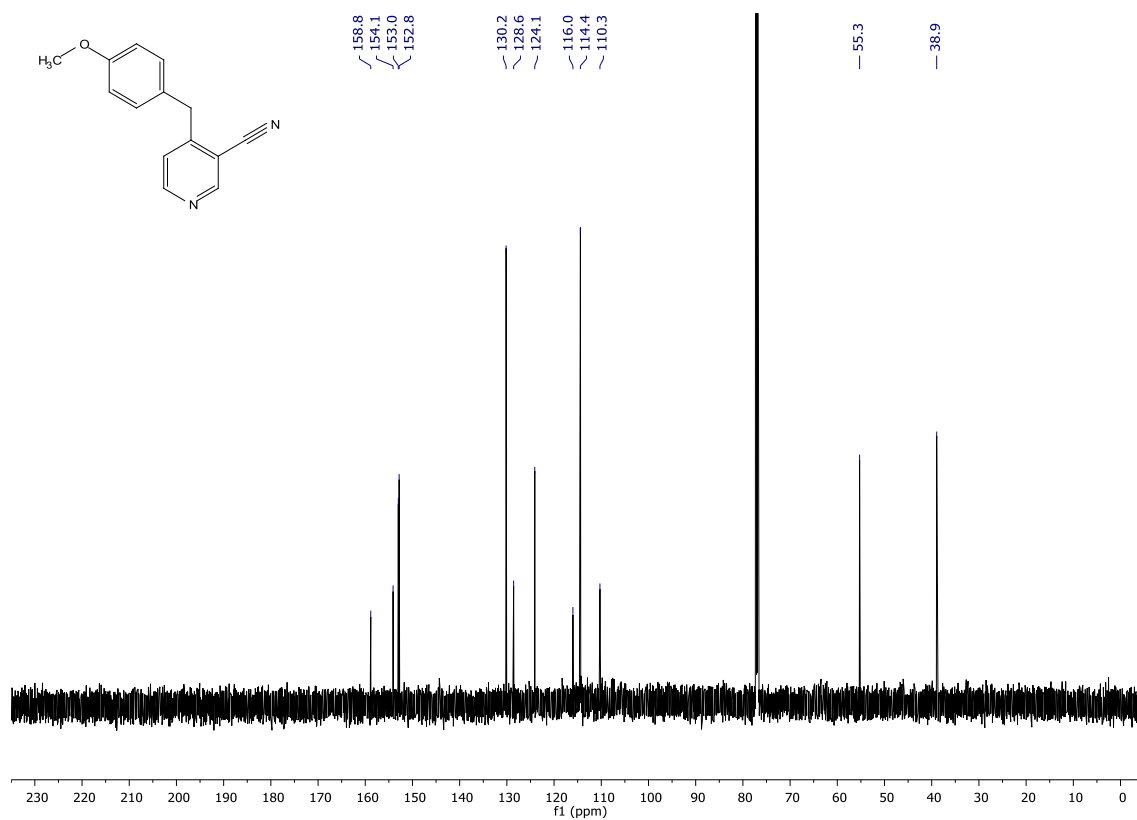
^{19}F -NMR (376 MHz, CDCl_3)

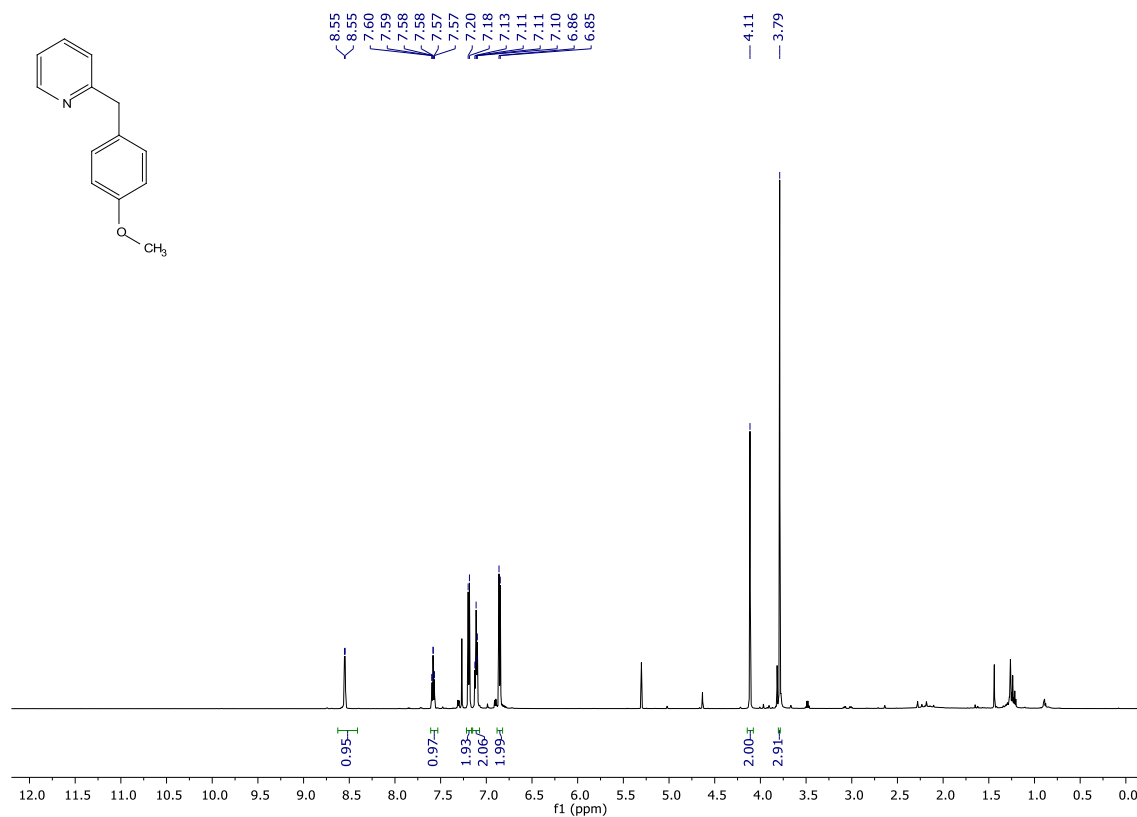
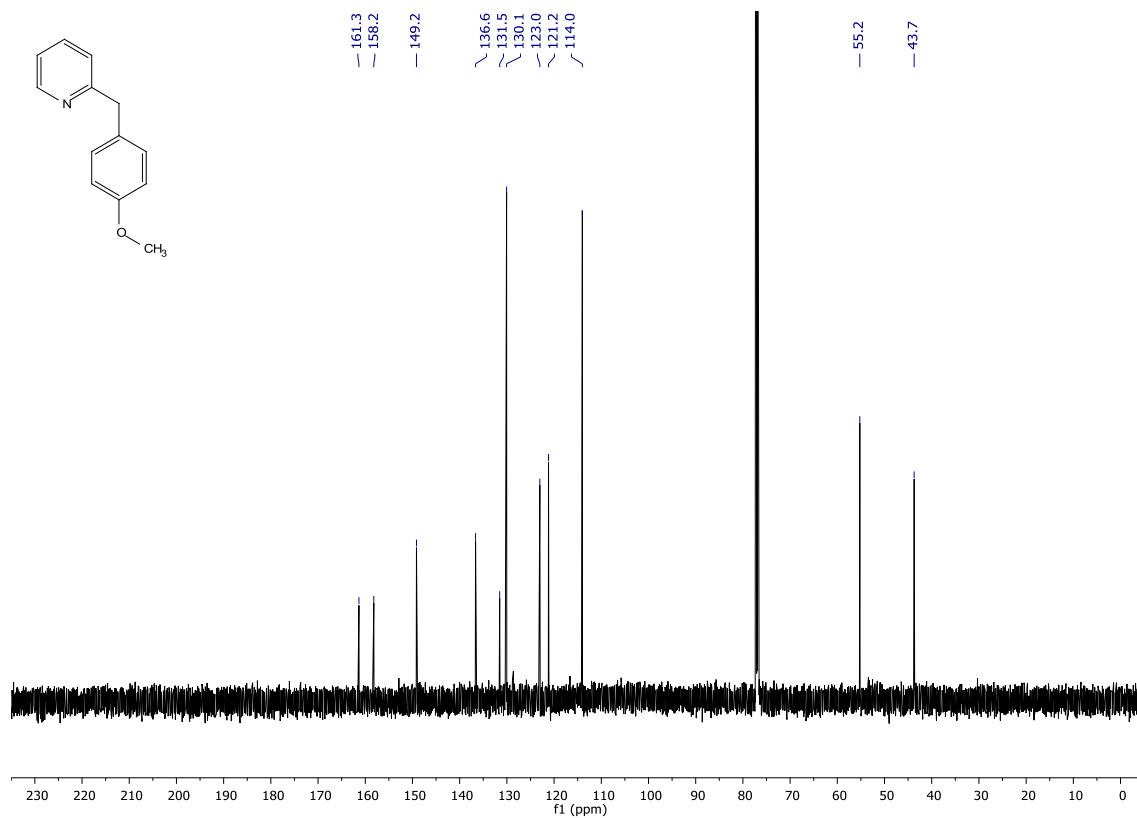
1-(3,5-dimethoxybenzyl)isoquinoline (199)**¹H-NMR (600 MHz, CDCl₃)****¹³C-NMR (151 MHz, CDCl₃)**

4-(4-methoxybenzyl)-1H-pyrrolo[2,3-b]pyridine (183) **$^1\text{H-NMR}$ (600 MHz, CDCl_3)** **$^{13}\text{C-NMR}$ (151 MHz, CDCl_3)**

4-(4-methoxybenzyl)quinoline (184) **$^1\text{H-NMR}$ (600 MHz, CDCl_3)** **$^{13}\text{C-NMR}$ (151 MHz, CDCl_3)**

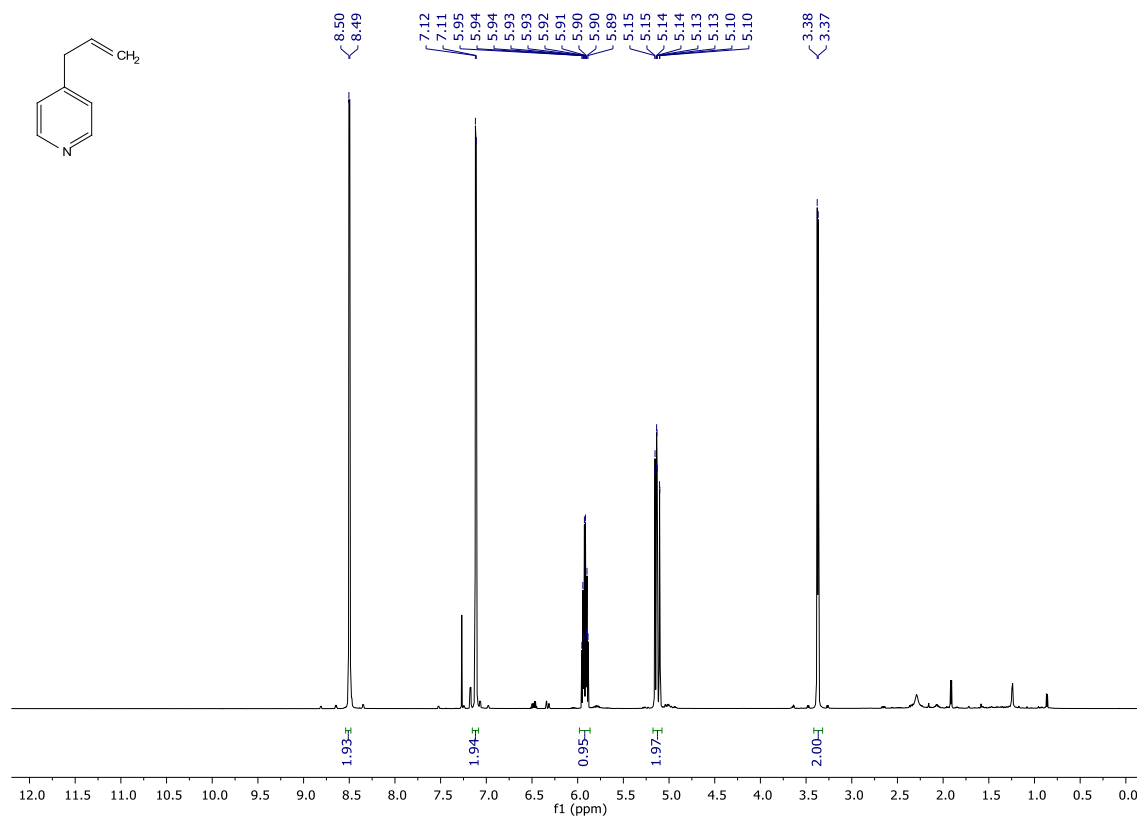
4-(4-methoxybenzyl)picolinonitrile (181)**¹H-NMR (600 MHz, CDCl₃)****¹³C-NMR (151 MHz, CDCl₃)**

4-(4-methoxybenzyl)nicotinonitrile (182)**¹H-NMR (600 MHz, CDCl₃)****¹³C-NMR (151 MHz, CDCl₃)**

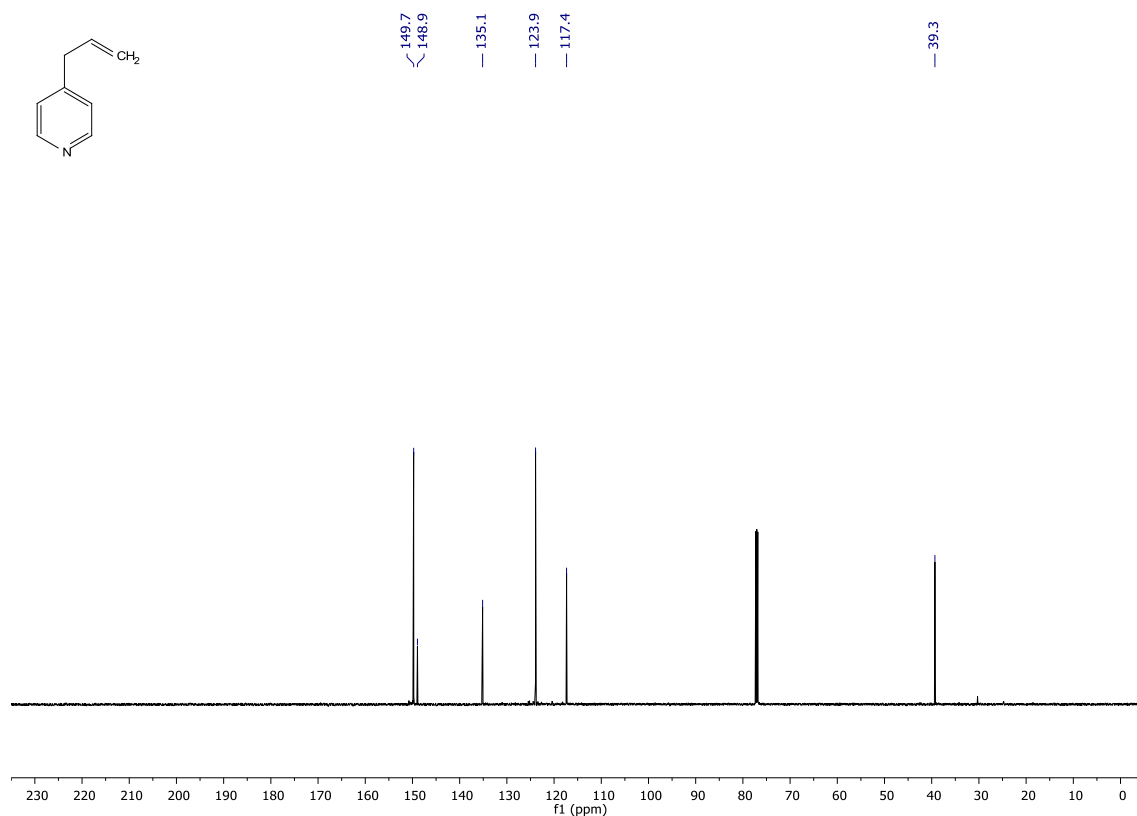
2-(4-methoxybenzyl)pyridine (170)**¹H-NMR (600 MHz, CDCl₃)****¹³C-NMR (151 MHz, CDCl₃)**

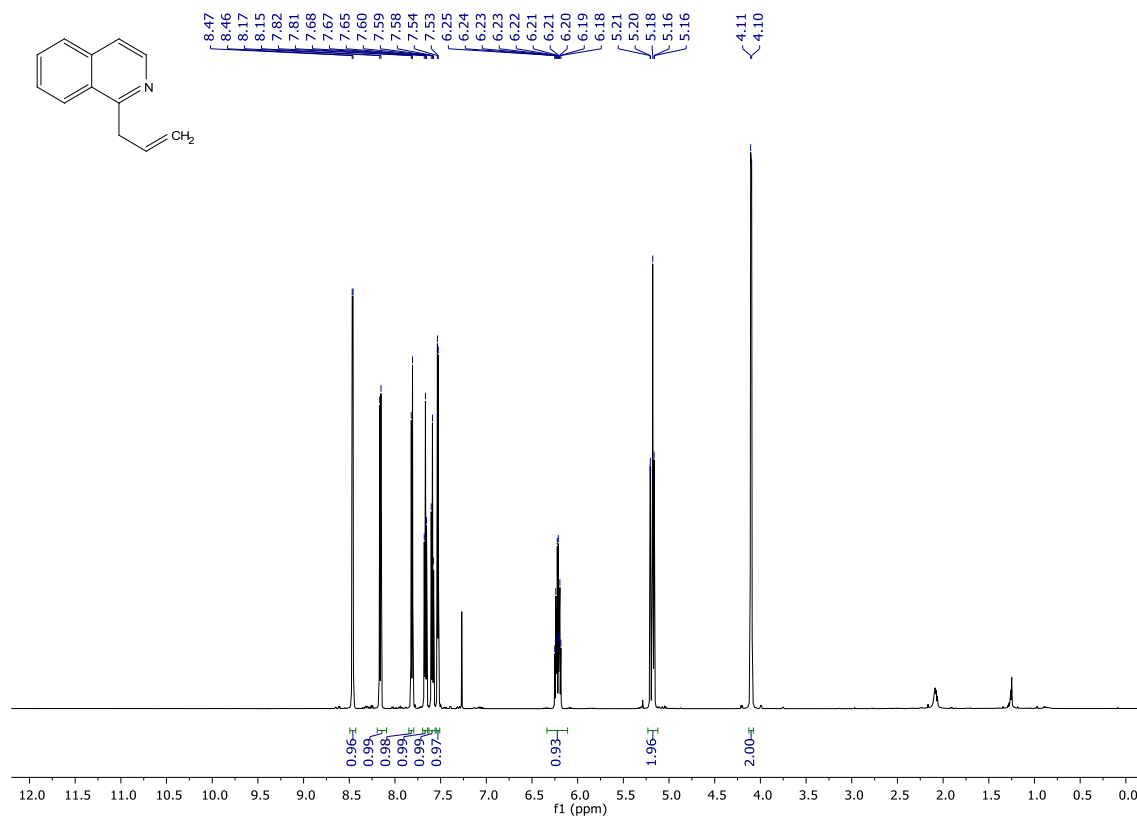
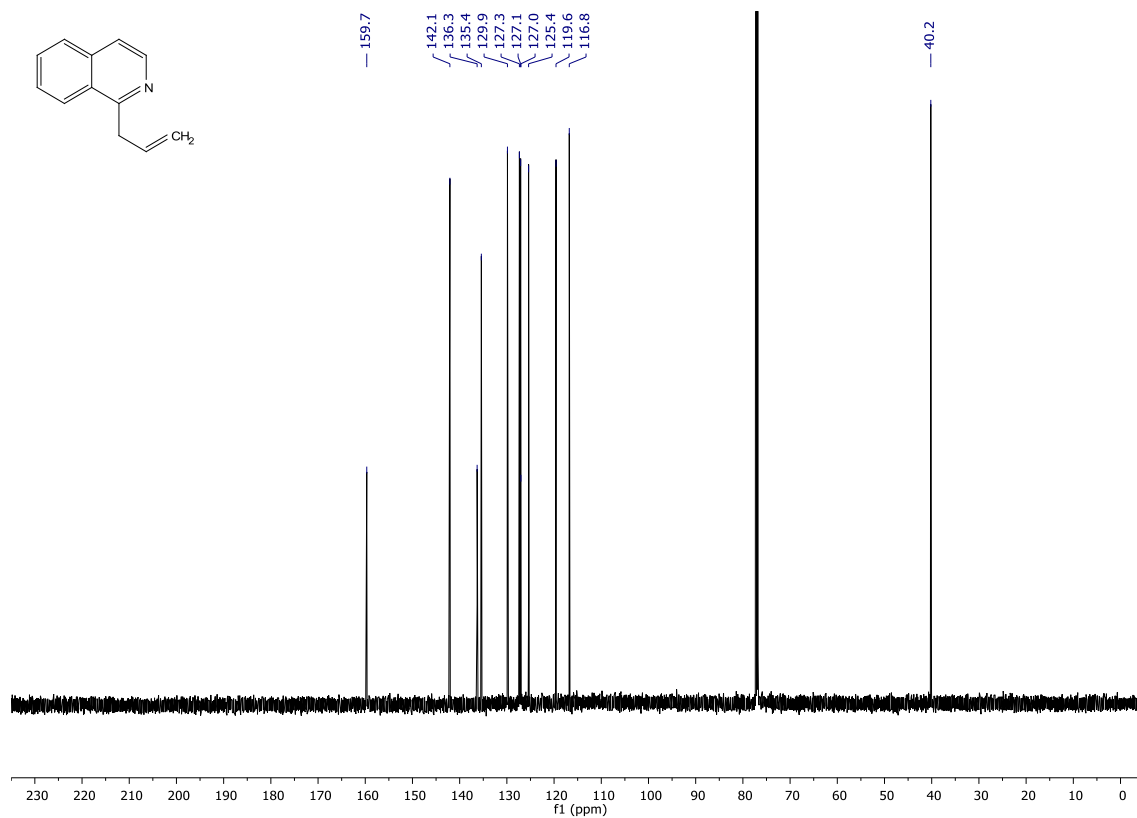
4-allylpyridine (165)

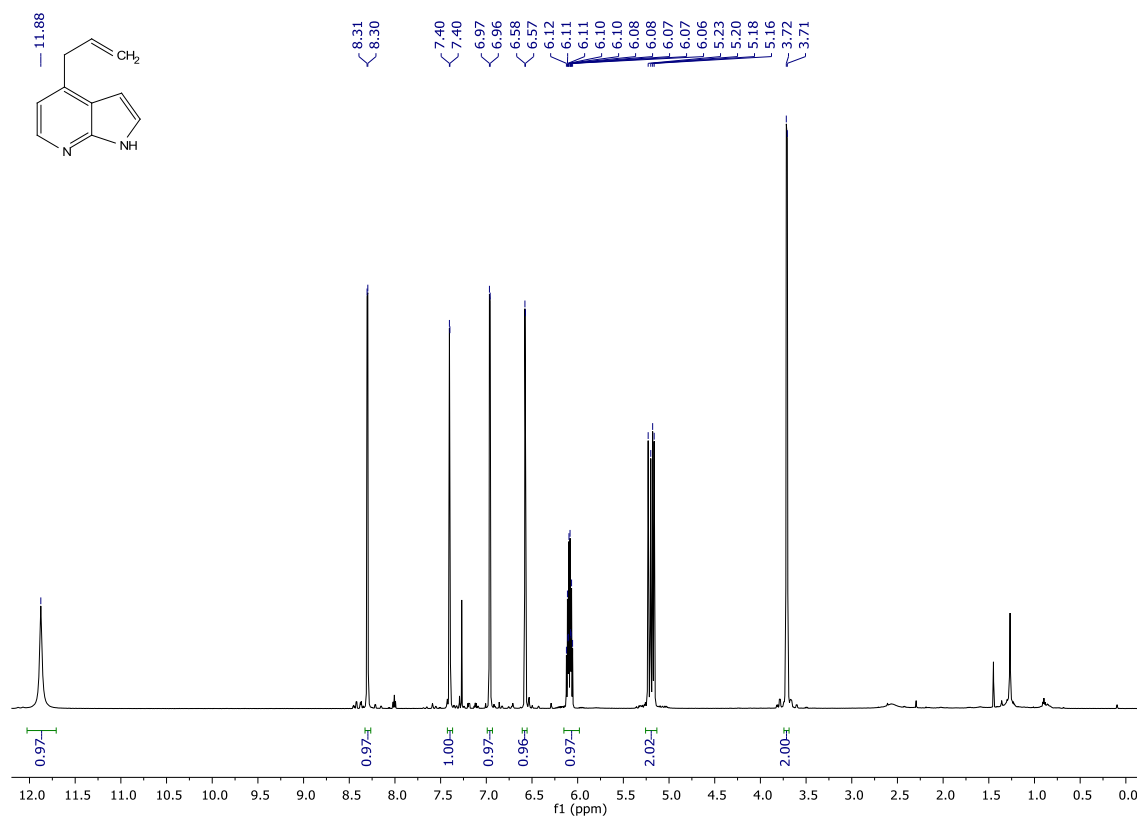
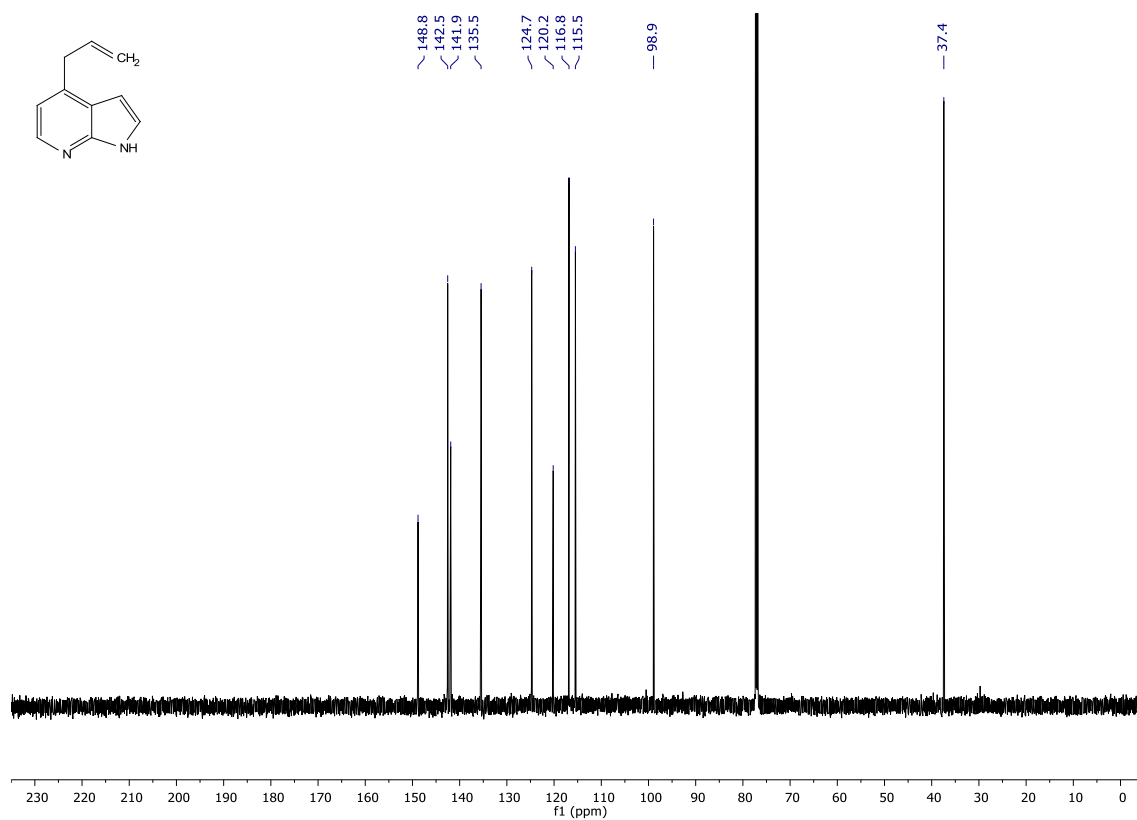
¹H-NMR (600 MHz, CDCl₃)

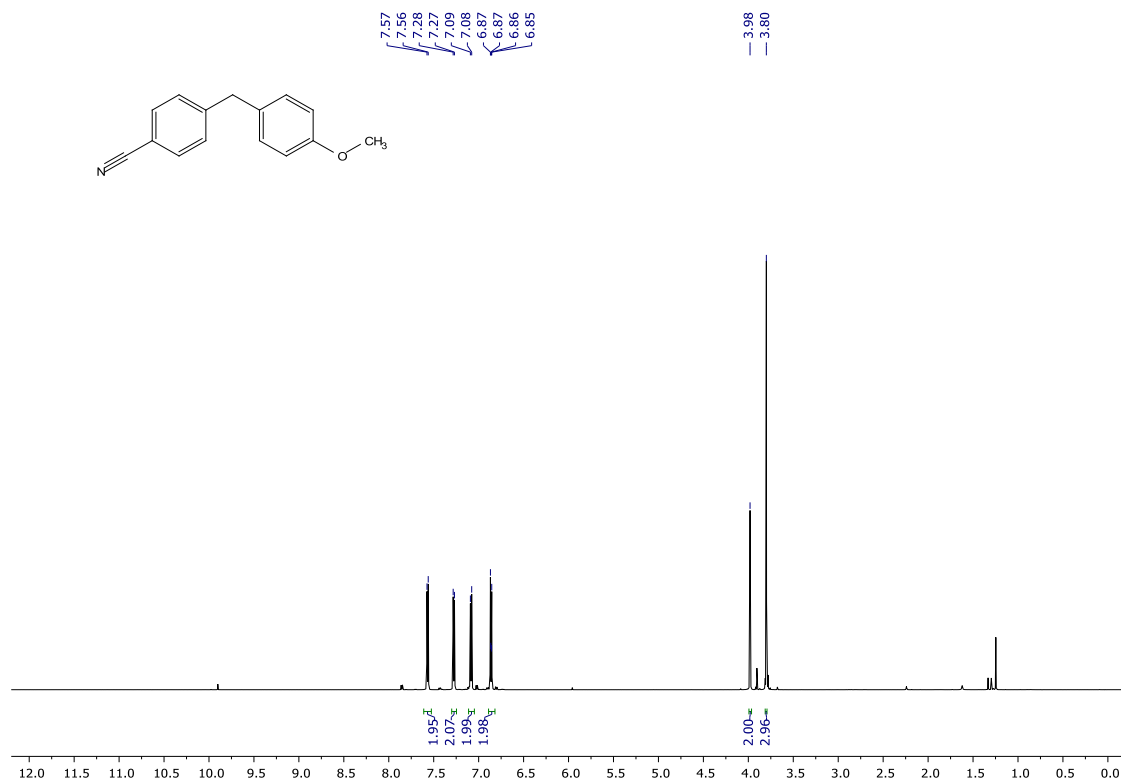
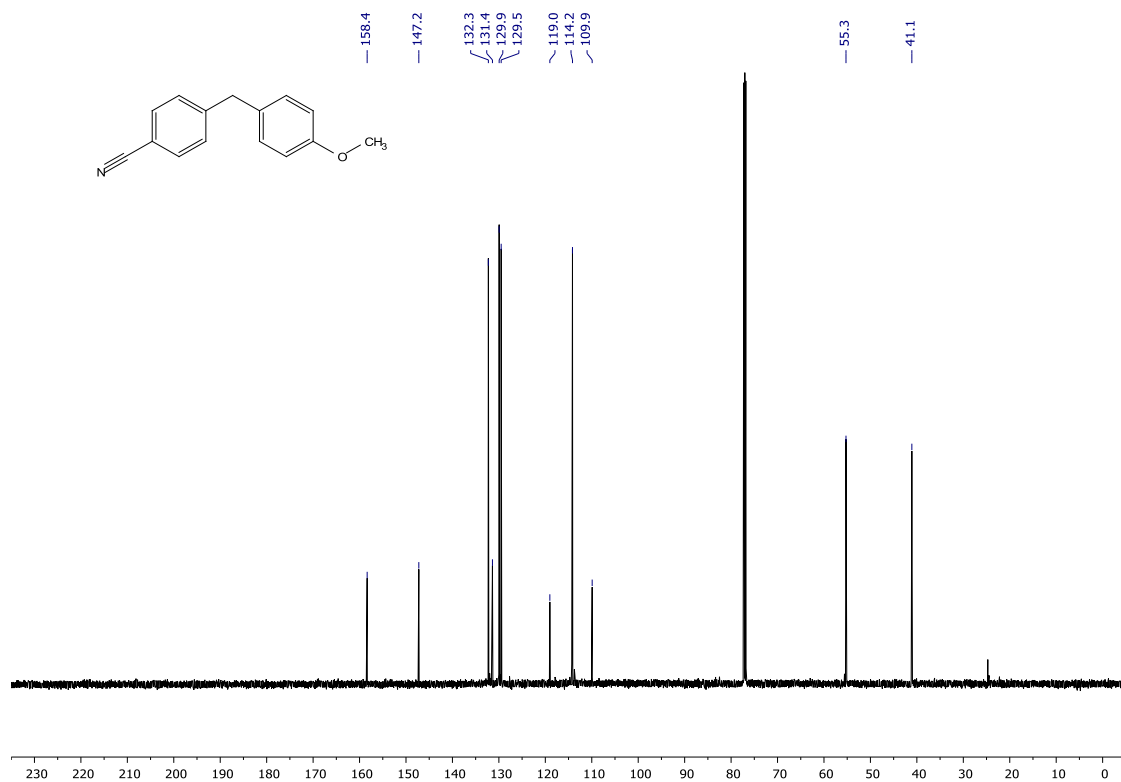


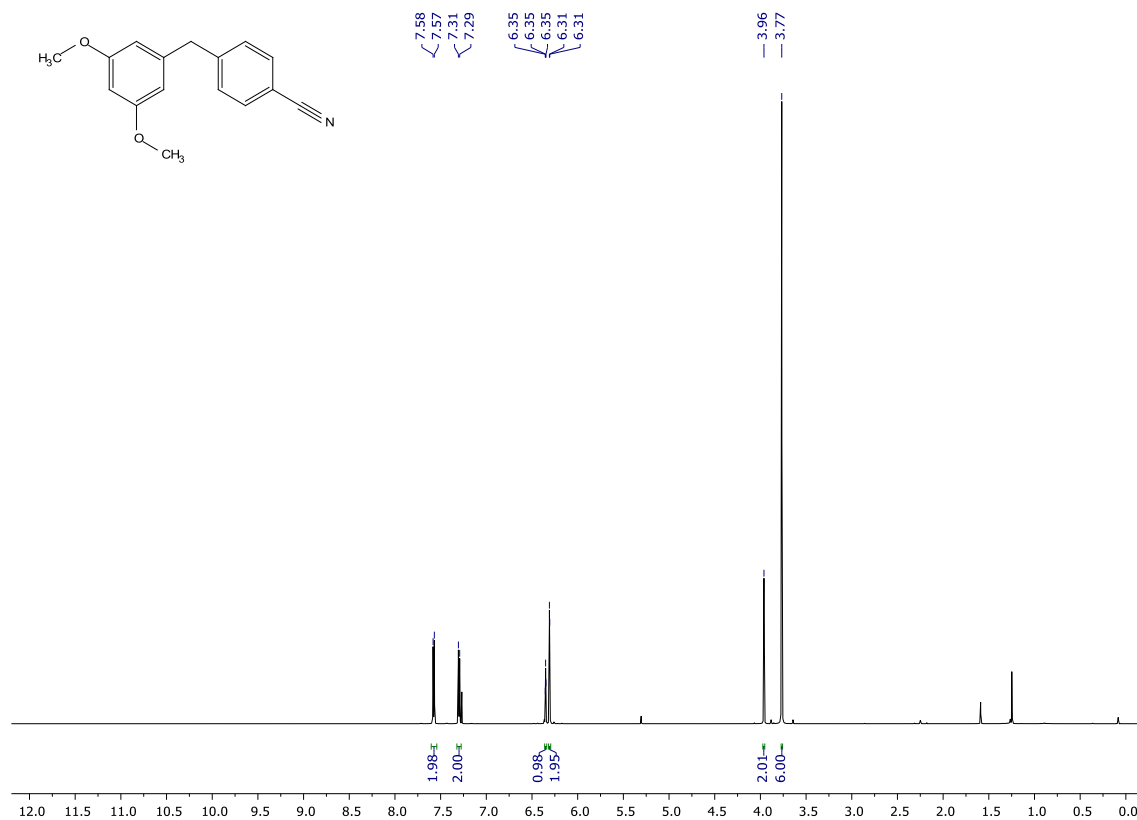
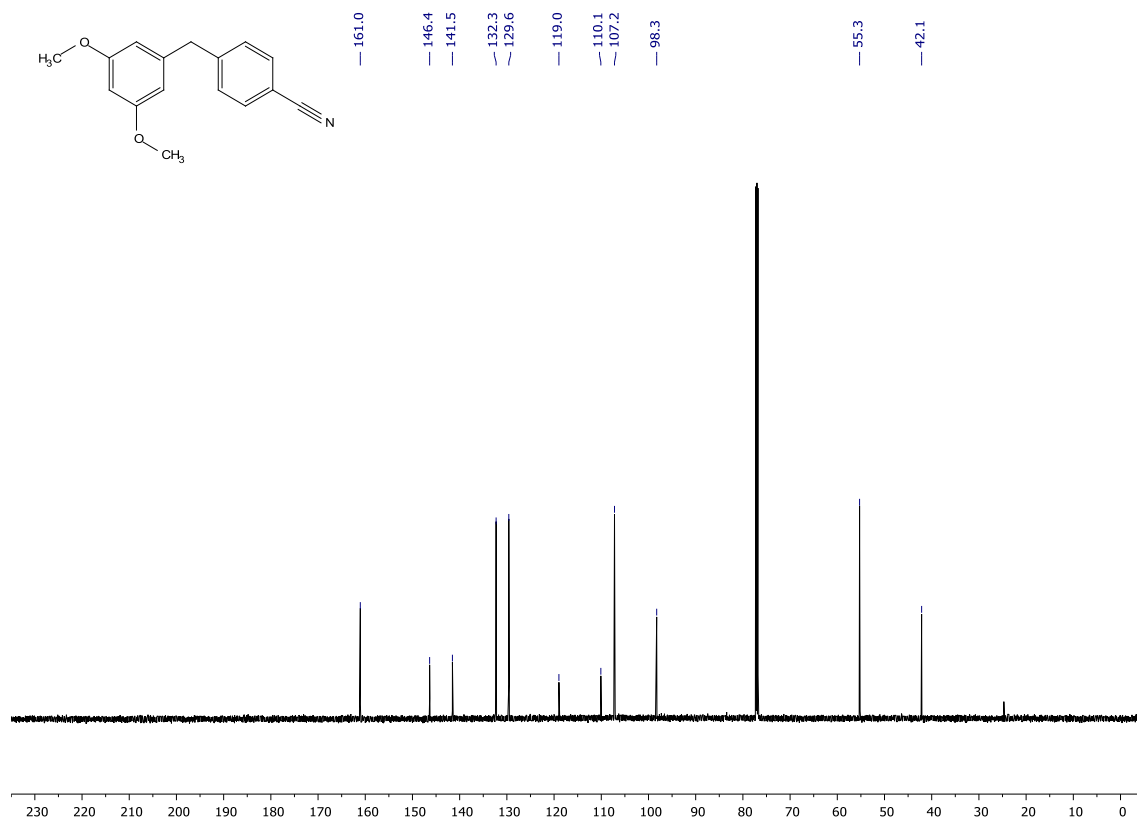
¹³C-NMR (151 MHz, CDCl₃)



1-allylisoquinoline (201) **$^1\text{H-NMR}$ (600 MHz, CDCl_3)** **$^{13}\text{C-NMR}$ (151 MHz, CDCl_3)**

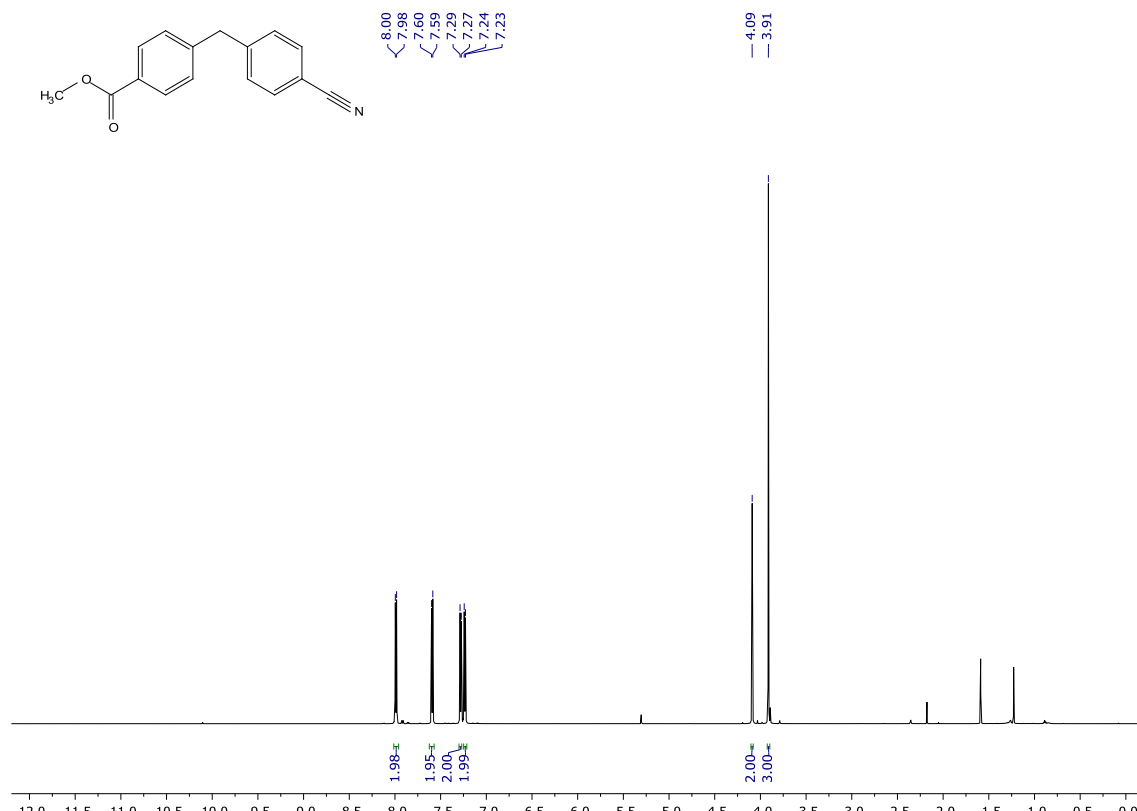
4-allyl-1H-pyrrolo[2,3-b]pyridine (202) **$^1\text{H-NMR}$ (600 MHz, CDCl_3)** **$^{13}\text{C-NMR}$ (151 MHz, CDCl_3)**

4-(4-methoxybenzyl)benzonitrile (173)**¹H-NMR (600 MHz, CDCl₃)****¹³C-NMR (151 MHz, CDCl₃)**

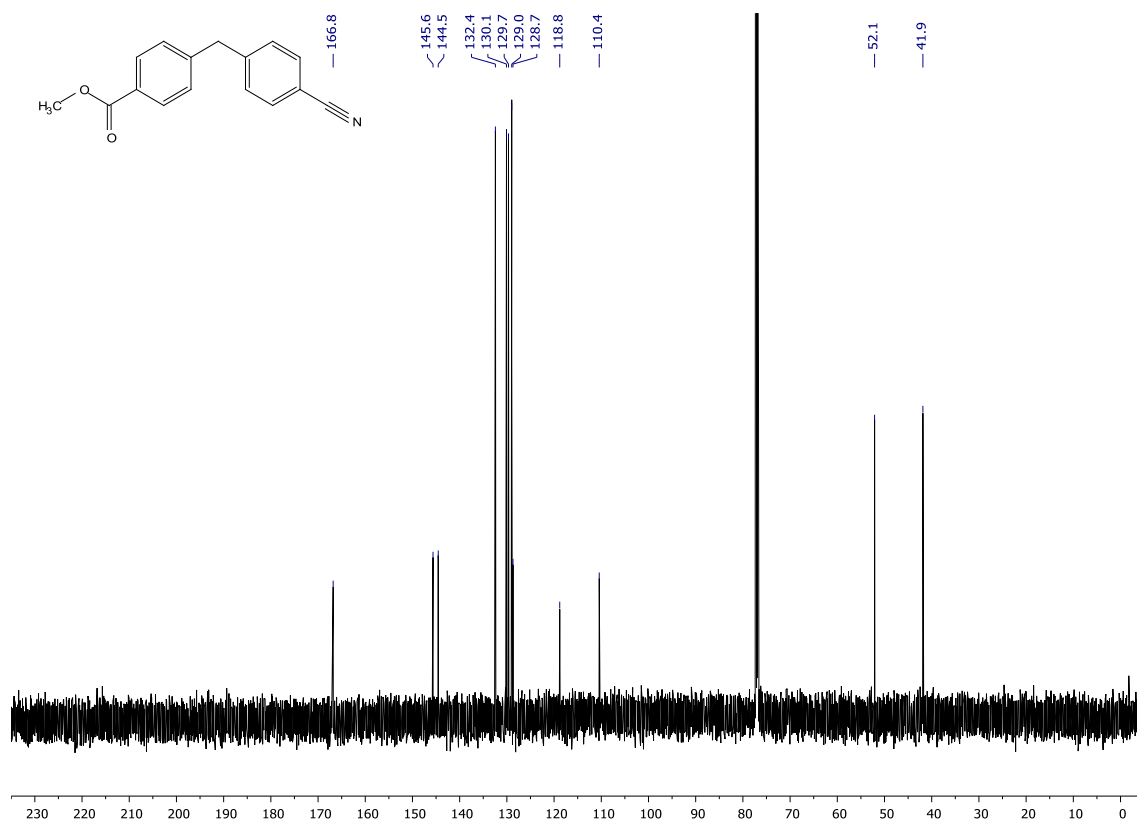
4-(3,5-dimethoxybenzyl)benzonitrile (247)**¹H-NMR (600 MHz, CDCl₃)****¹³C-NMR (151 MHz, CDCl₃)**

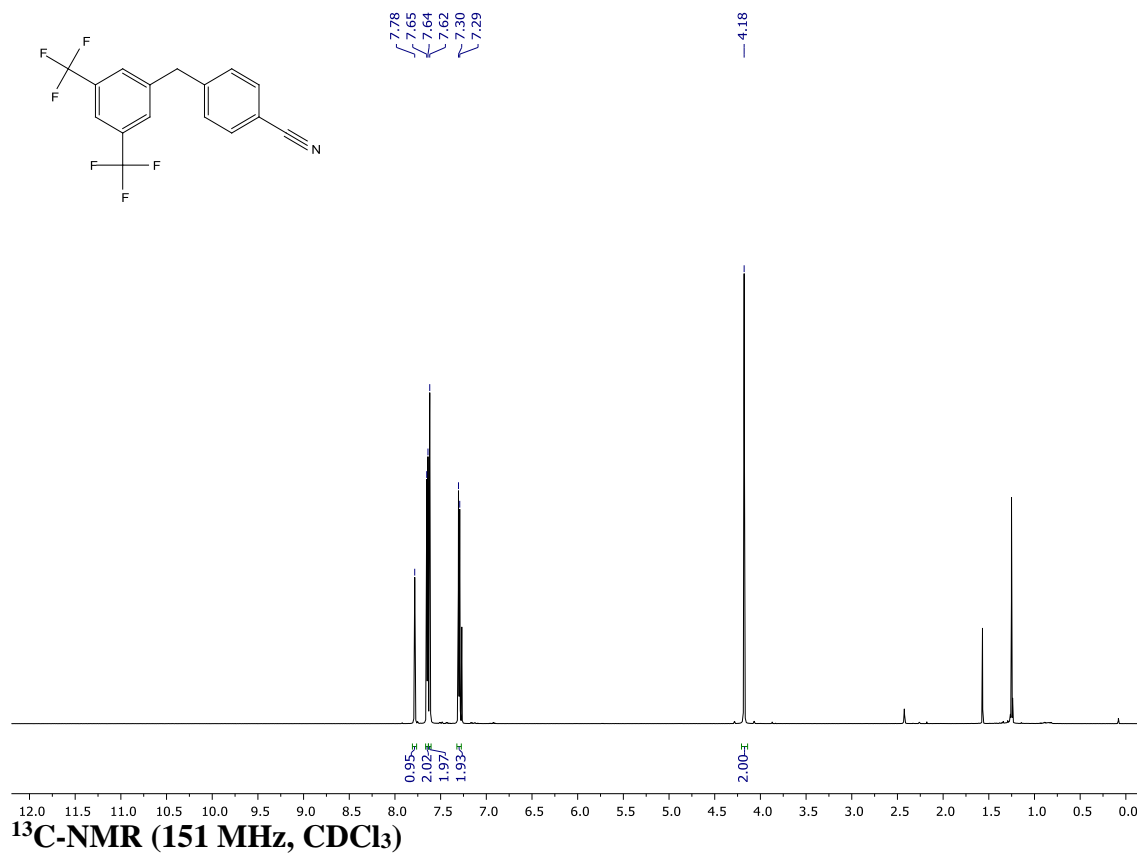
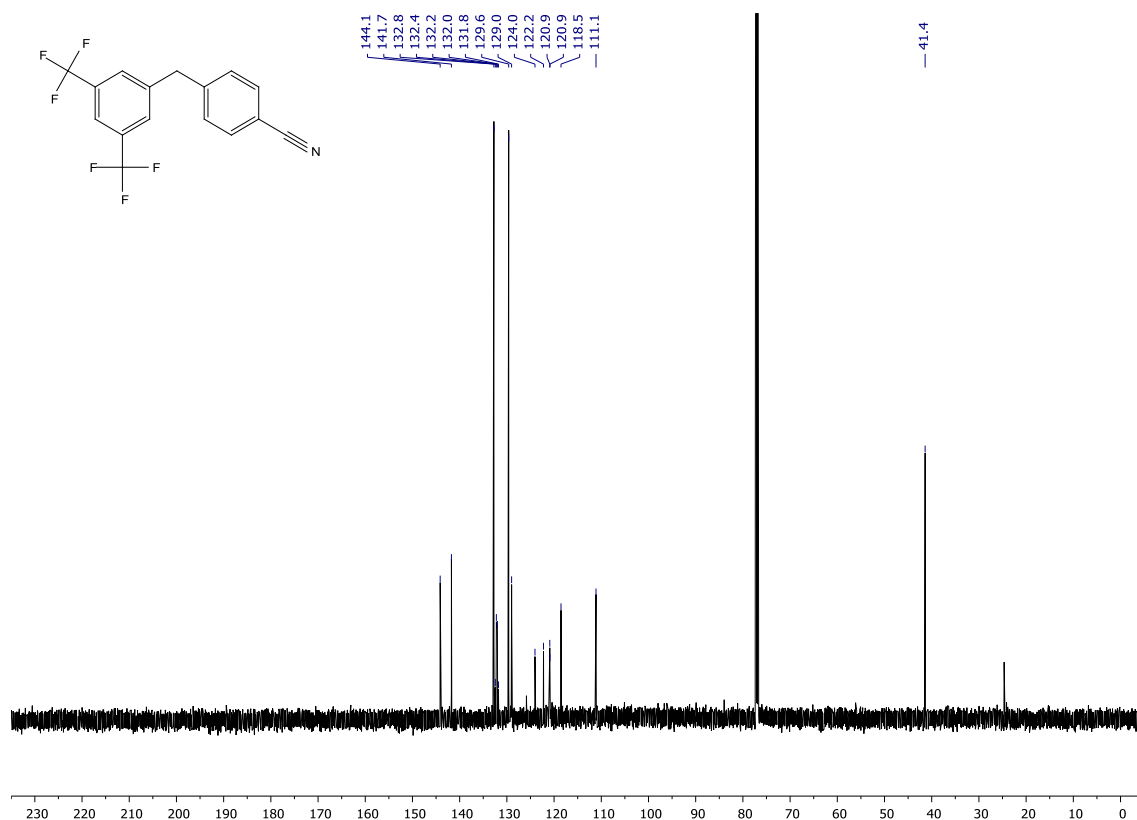
methyl 4-(4-cyanobenzyl)benzoate (248)

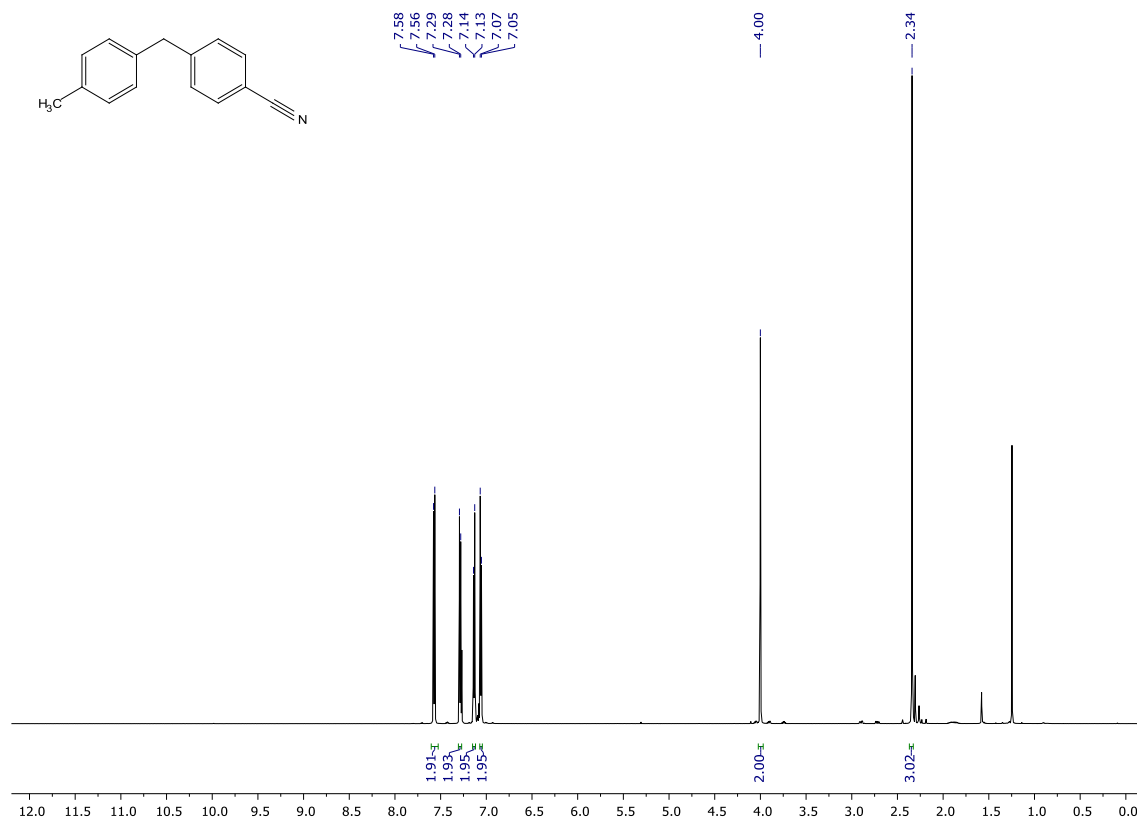
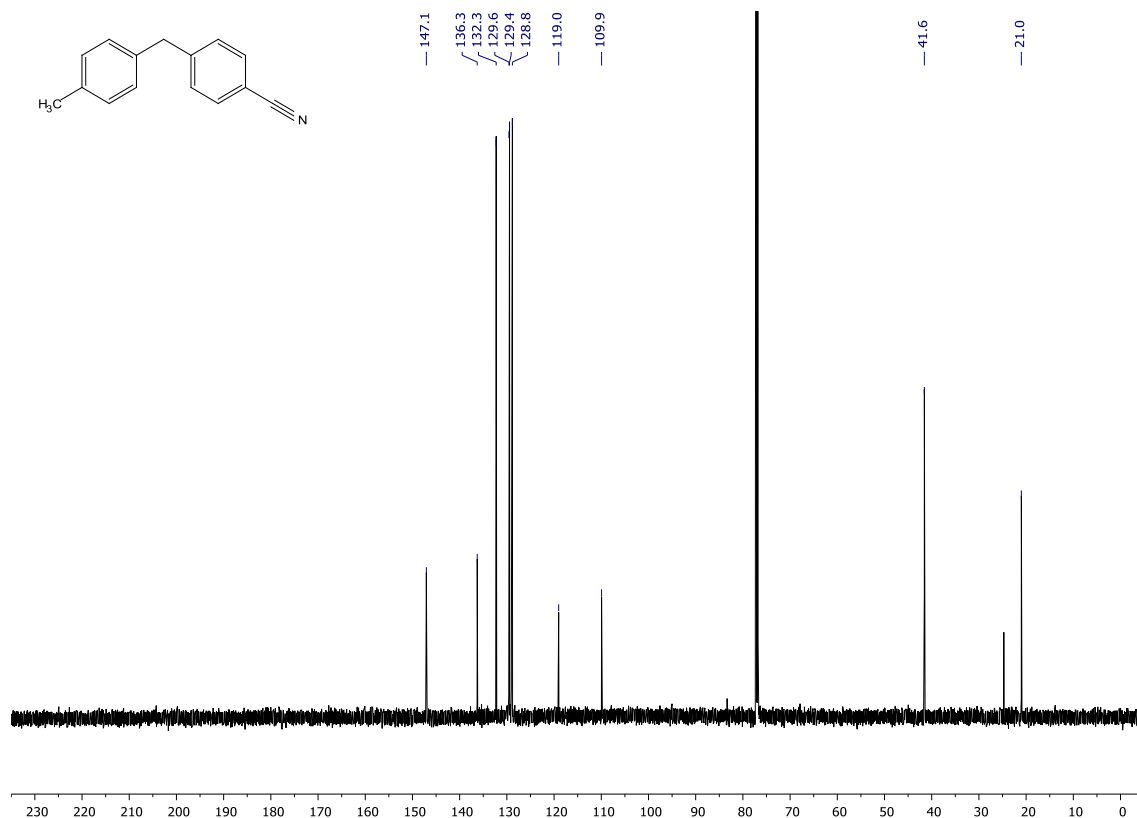
¹H-NMR (600 MHz, CDCl₃)

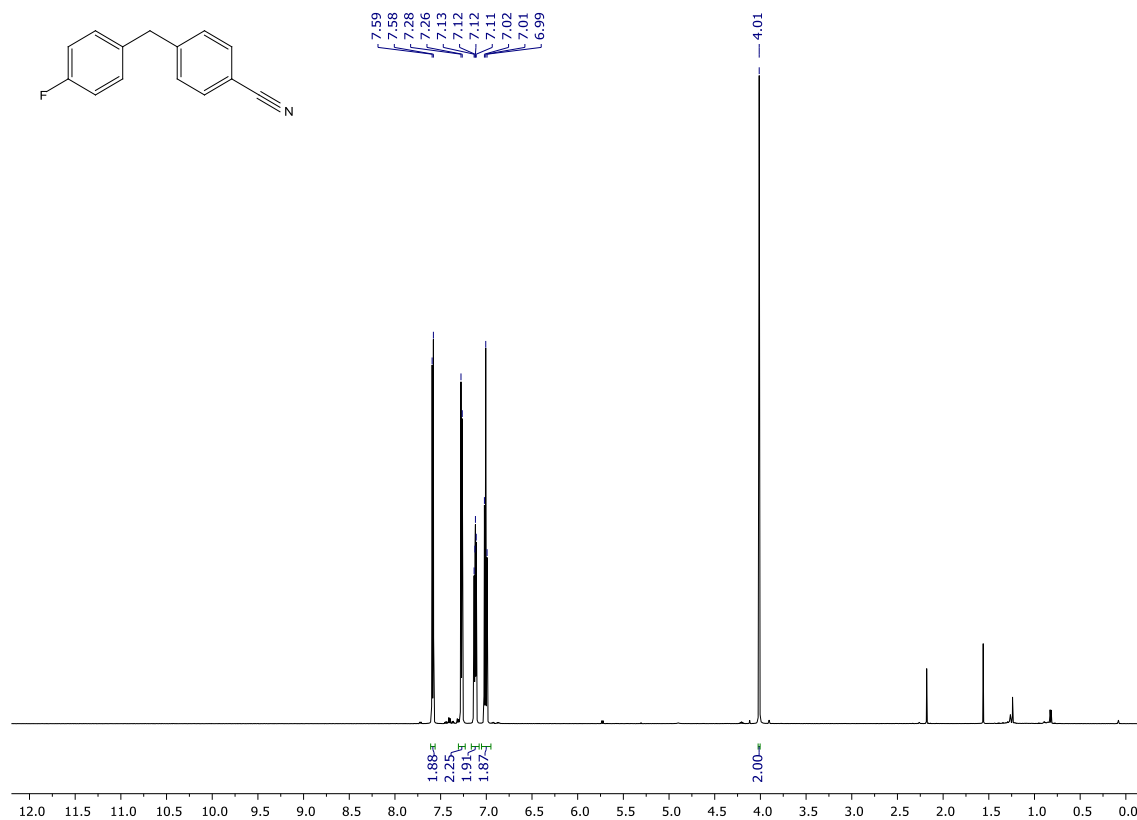
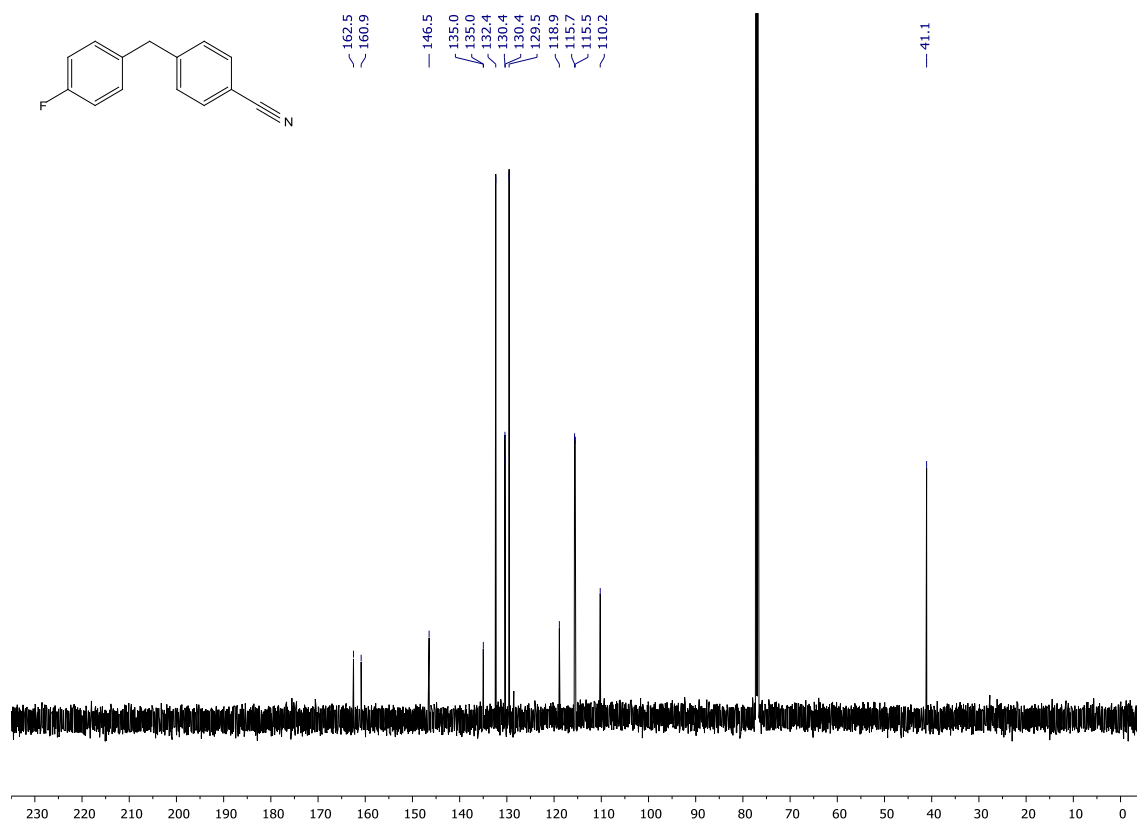


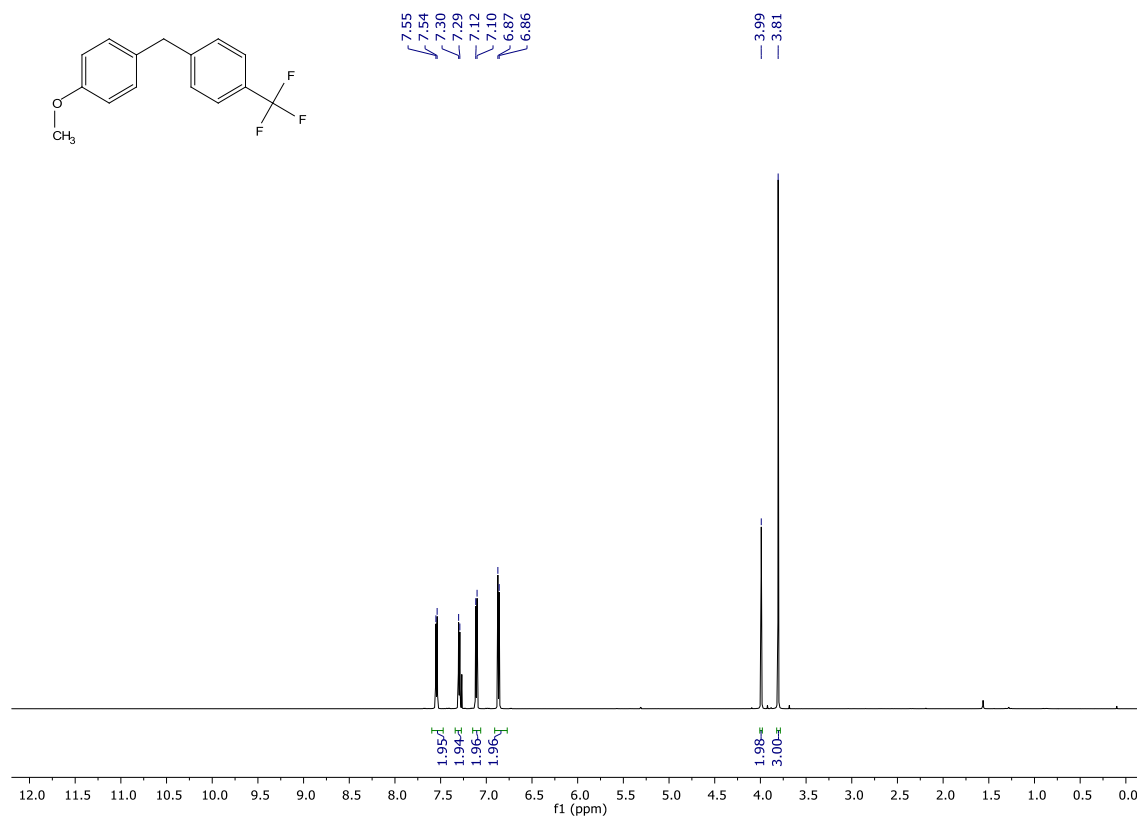
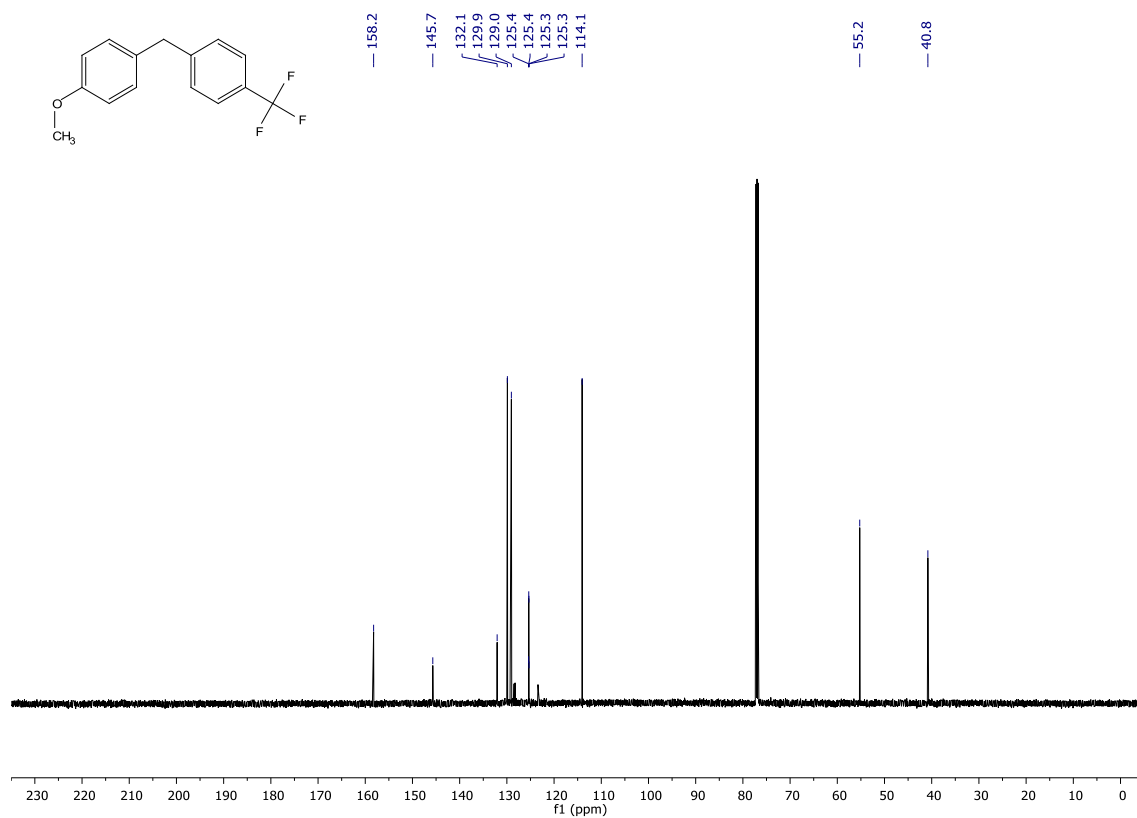
¹³C-NMR (151 MHz, CDCl₃)

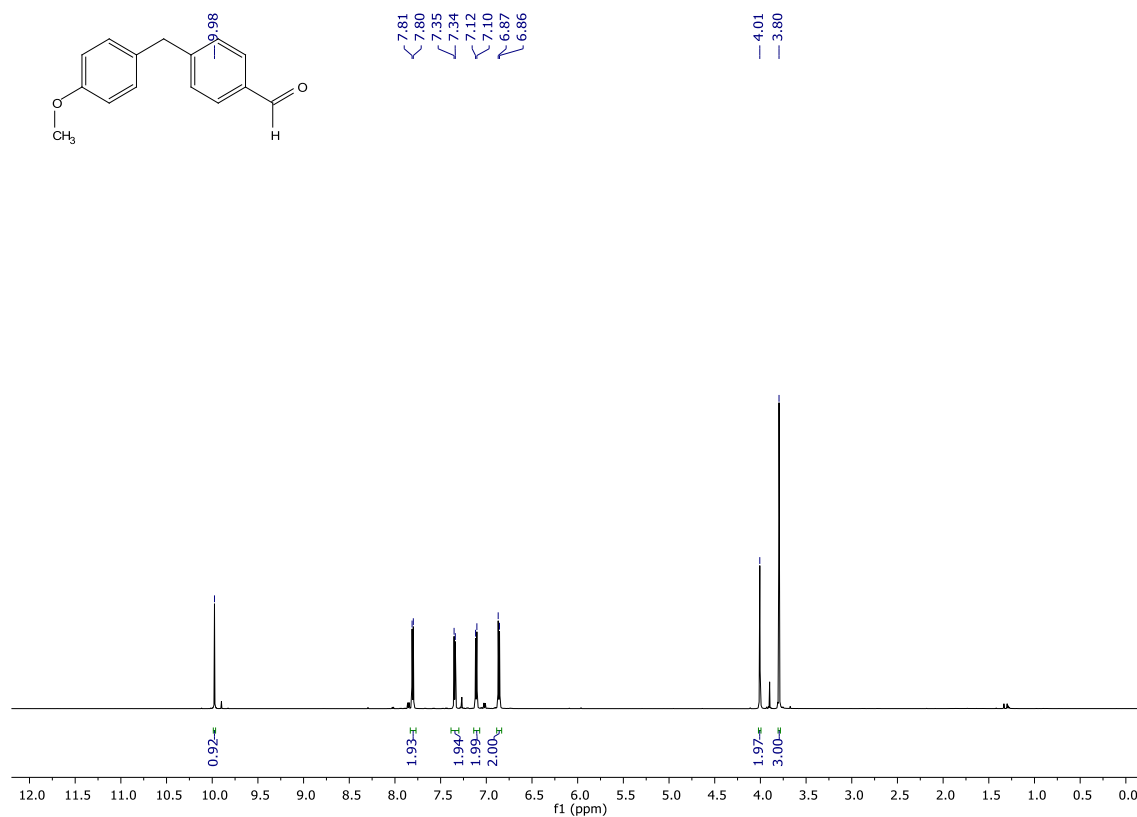
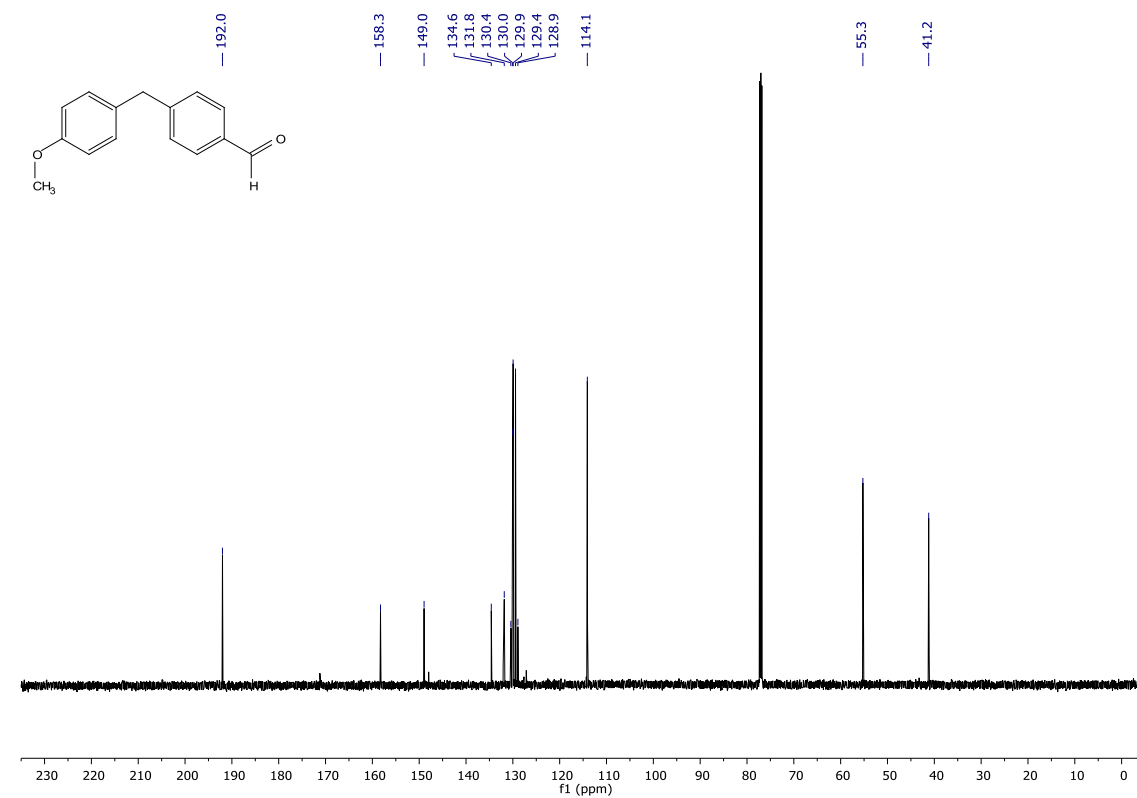


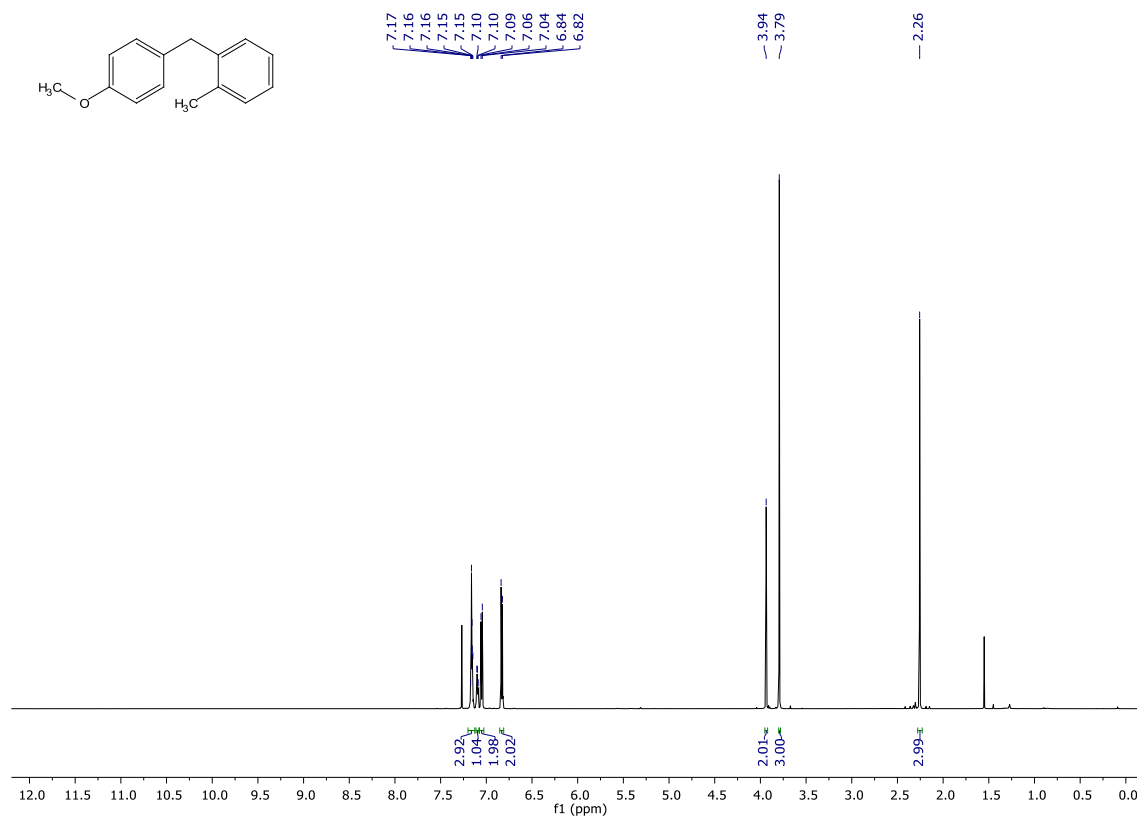
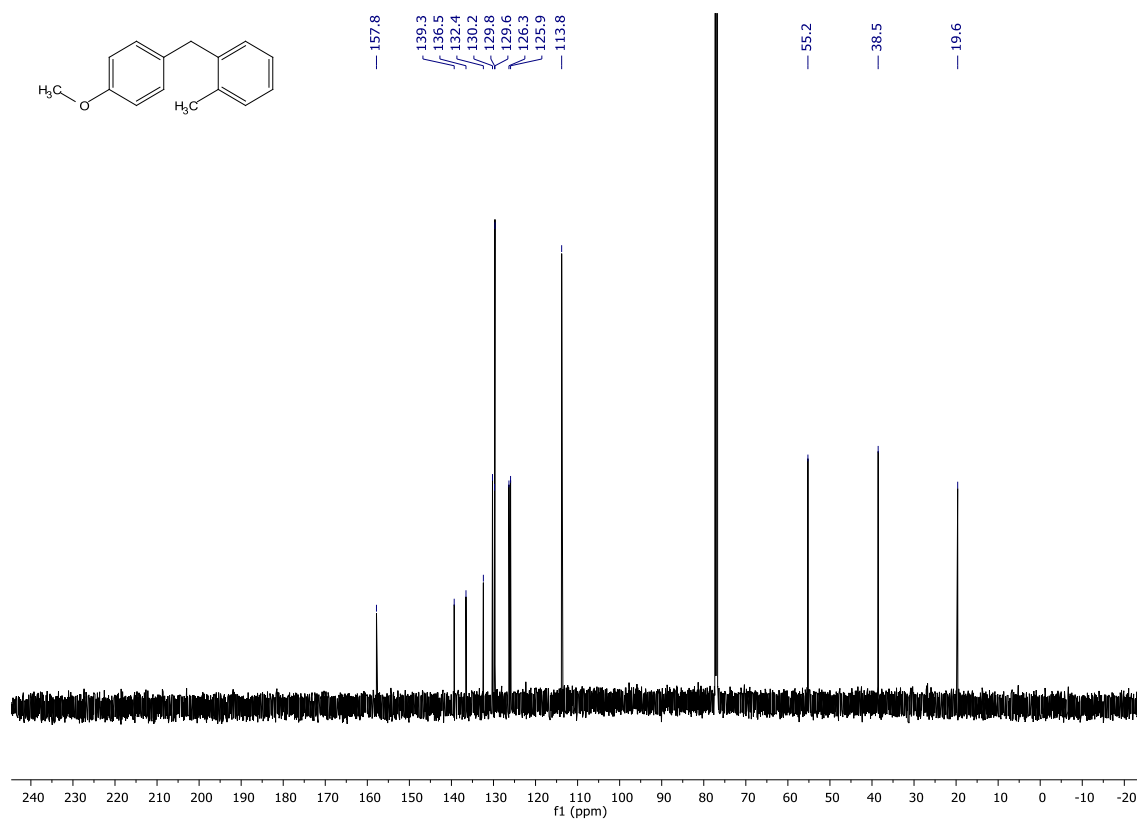
4-(3,5-bis(trifluoromethyl)benzyl)benzonitrile (249) **$^1\text{H-NMR}$ (600 MHz, CDCl_3)** **$^{13}\text{C-NMR}$ (151 MHz, CDCl_3)**

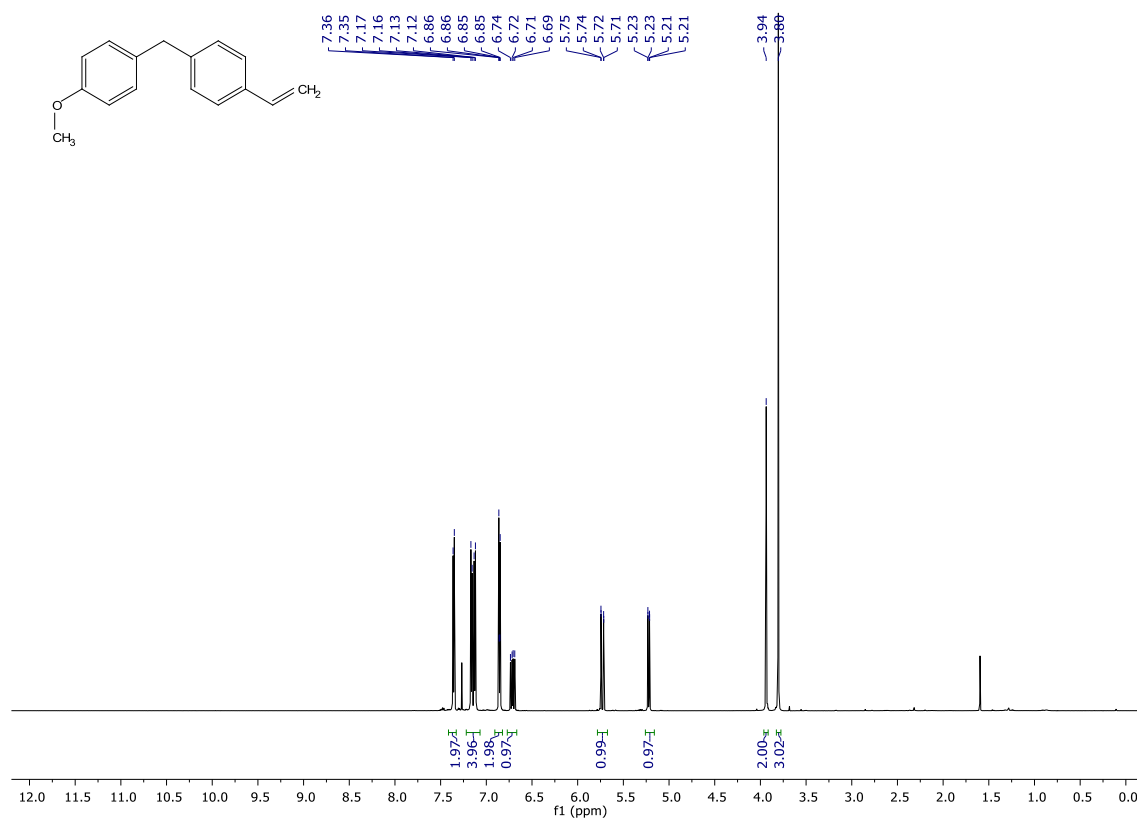
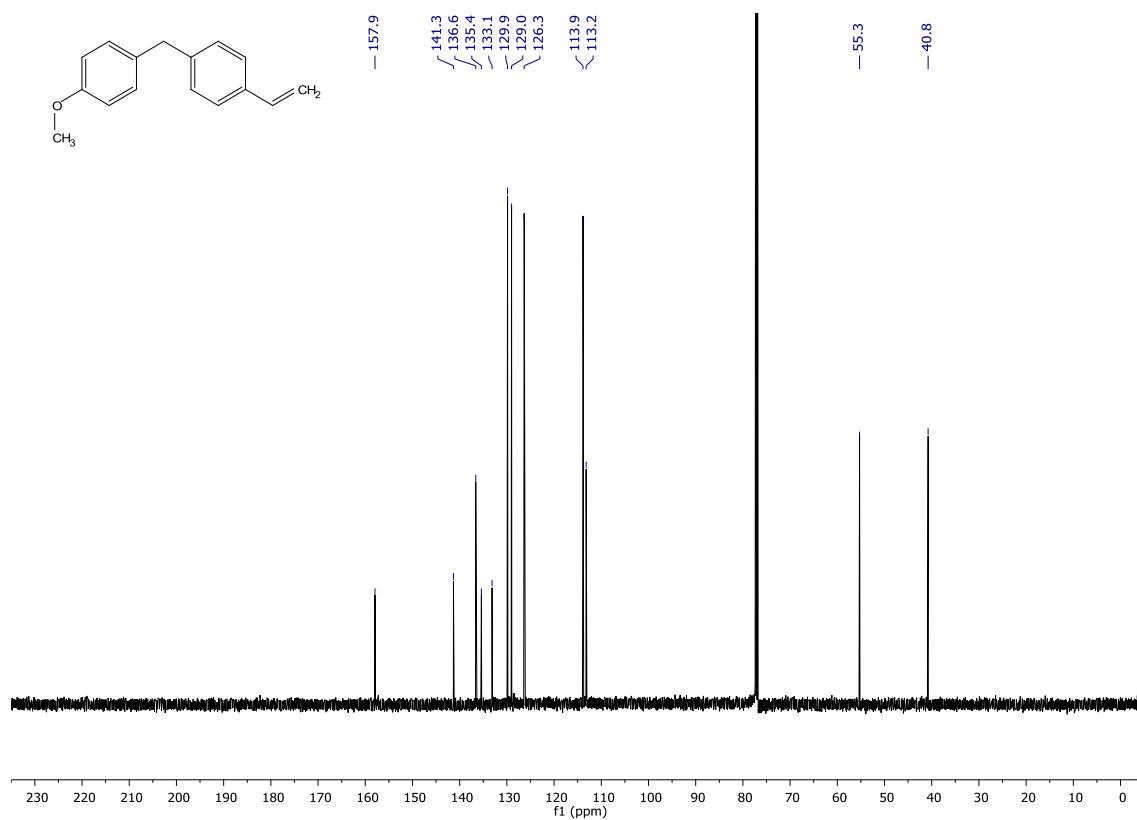
4-(4-methylbenzyl)benzonitrile (250) **$^1\text{H-NMR}$ (600 MHz, CDCl_3)** **$^{13}\text{C-NMR}$ (151 MHz, CDCl_3)**

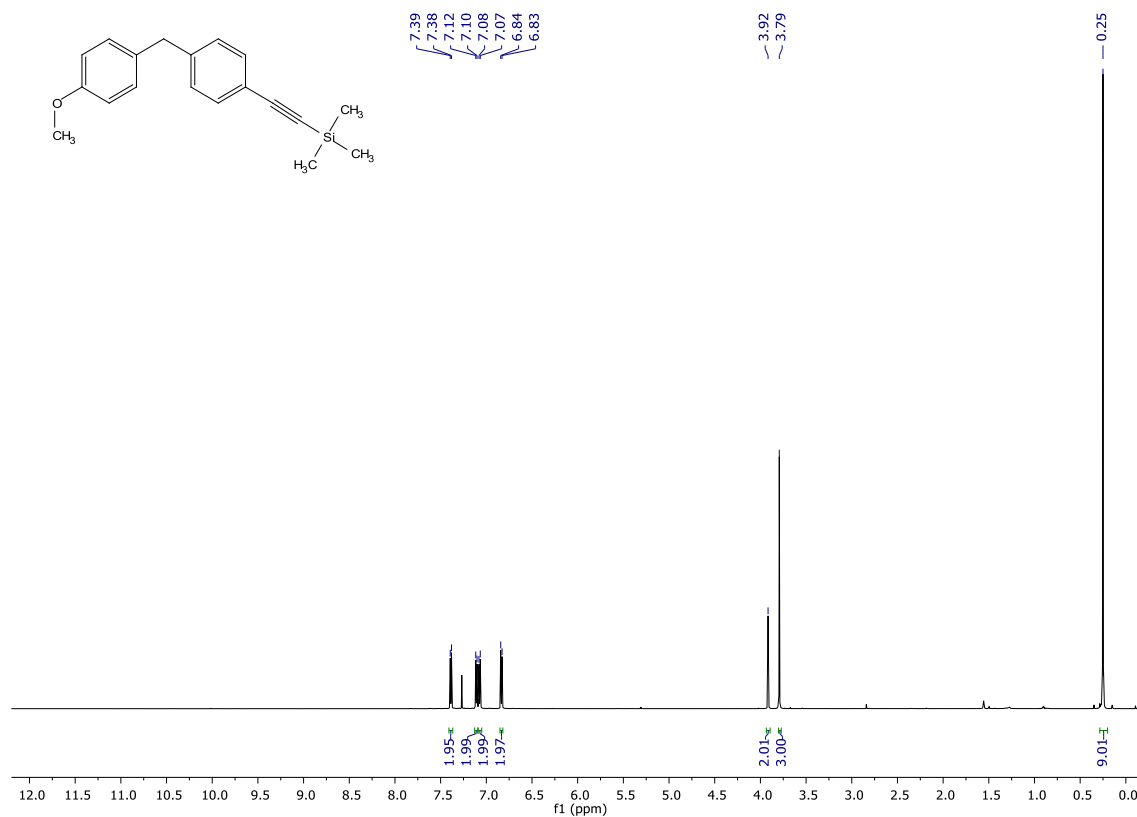
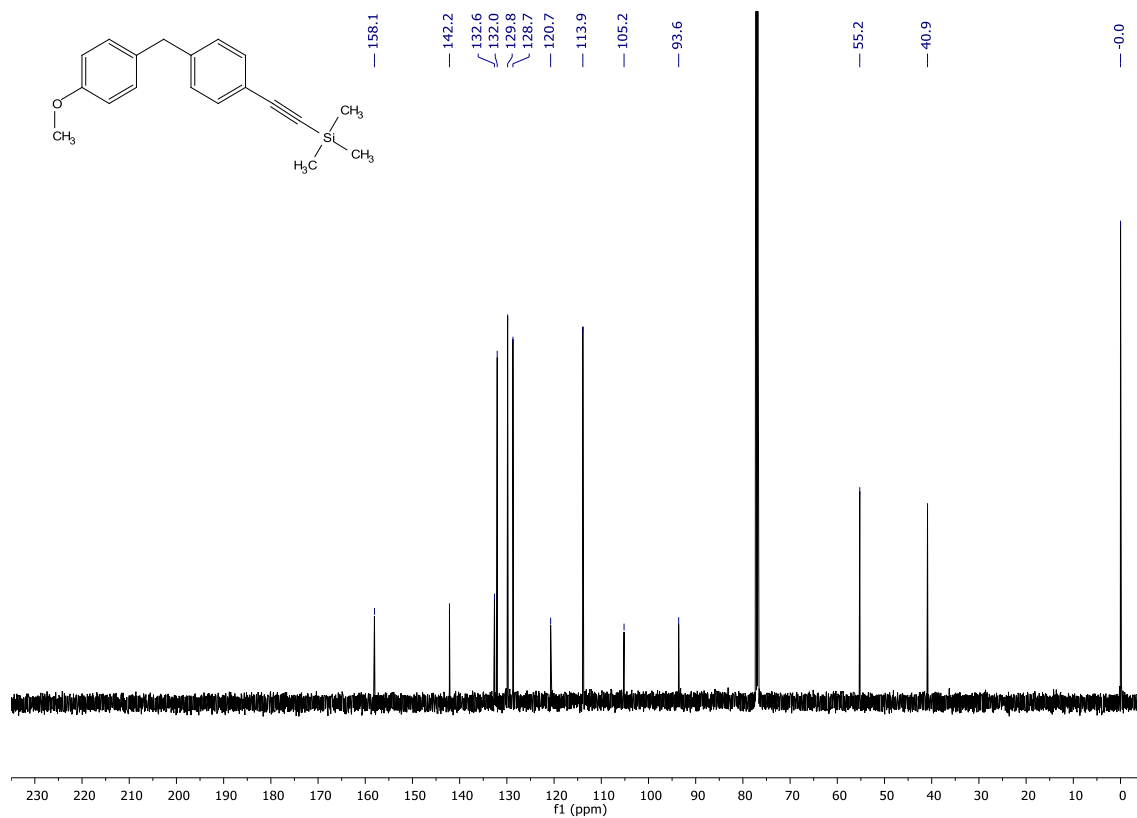
4-(4-fluorobenzyl)benzonitrile (251)**¹H-NMR (600 MHz, CDCl₃)****¹³C-NMR (151 MHz, CDCl₃)**

1-methoxy-4-(4-(trifluoromethyl)benzyl)benzene (172)**¹H-NMR (600 MHz, CDCl₃)****¹³C-NMR (151 MHz, CDCl₃)**

4-(4-methoxybenzyl)benzaldehyde (252) **$^1\text{H-NMR}$ (600 MHz, CDCl_3)** **$^{13}\text{C-NMR}$ (151 MHz, CDCl_3)**

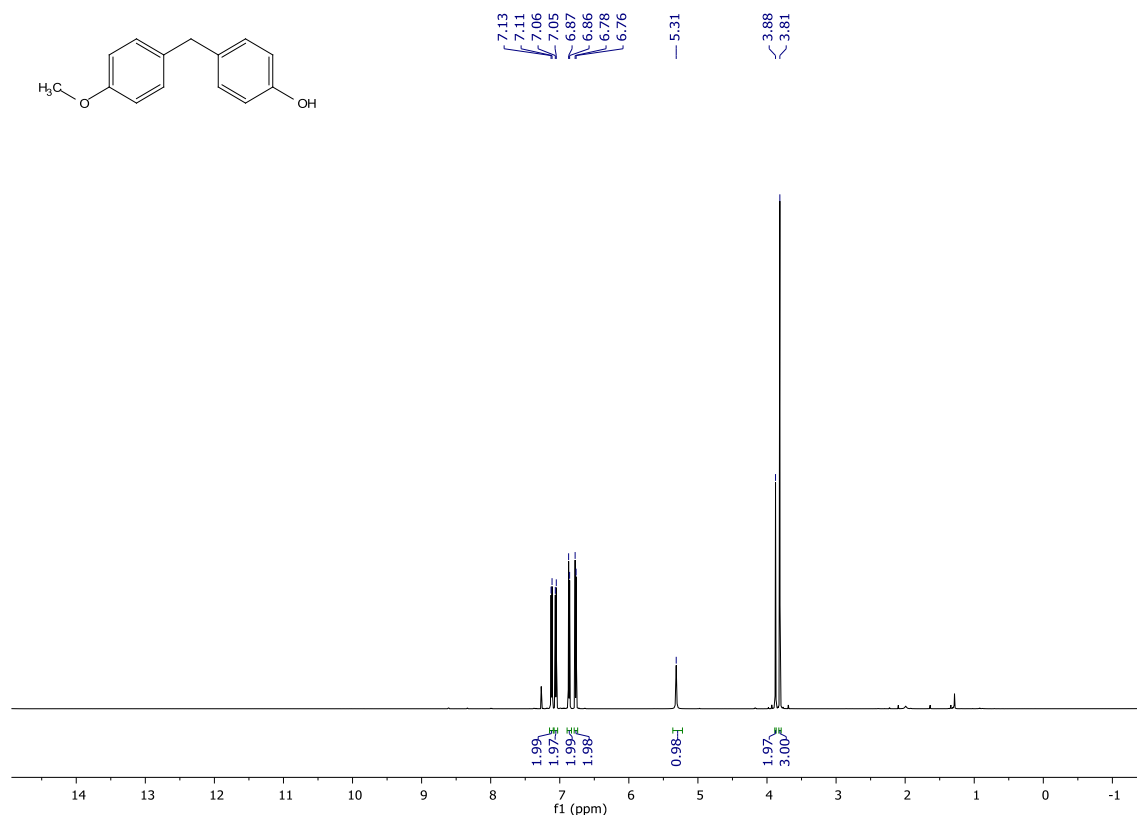
1-(4-methoxybenzyl)-2-methylbenzene (253) **$^1\text{H-NMR}$ (600 MHz, CDCl_3)** **$^{13}\text{C-NMR}$ (151 MHz, CDCl_3)**

1-methoxy-4-(4-vinylbenzyl)benzene (254) **$^1\text{H-NMR}$ (600 MHz, CDCl_3)** **$^{13}\text{C-NMR}$ (151 MHz, CDCl_3)**

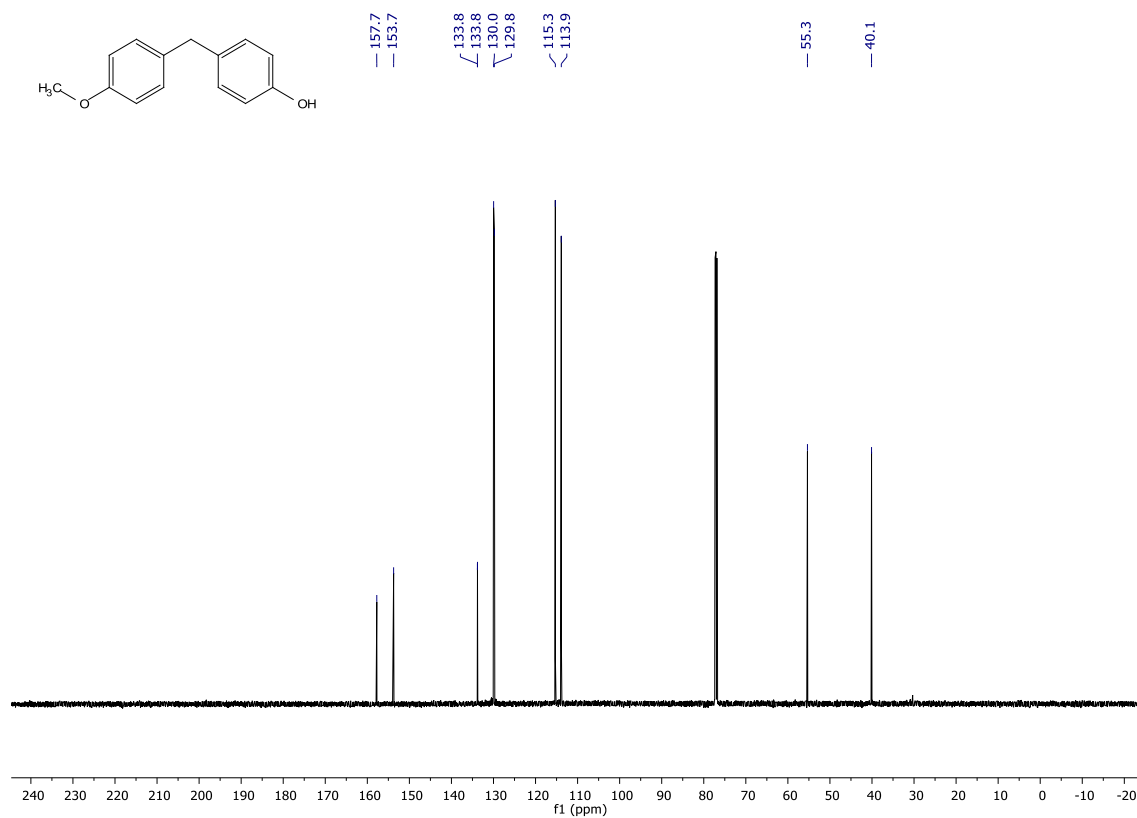
((4-(4-methoxybenzyl)phenyl)ethynyl)trimethylsilane (255)**¹H-NMR (600 MHz, CDCl₃)****¹³C-NMR (151 MHz, CDCl₃)**

4-(4-methoxybenzyl)phenol (257)

¹H-NMR (600 MHz, CDCl₃)



¹³C-NMR (151 MHz, CDCl₃)

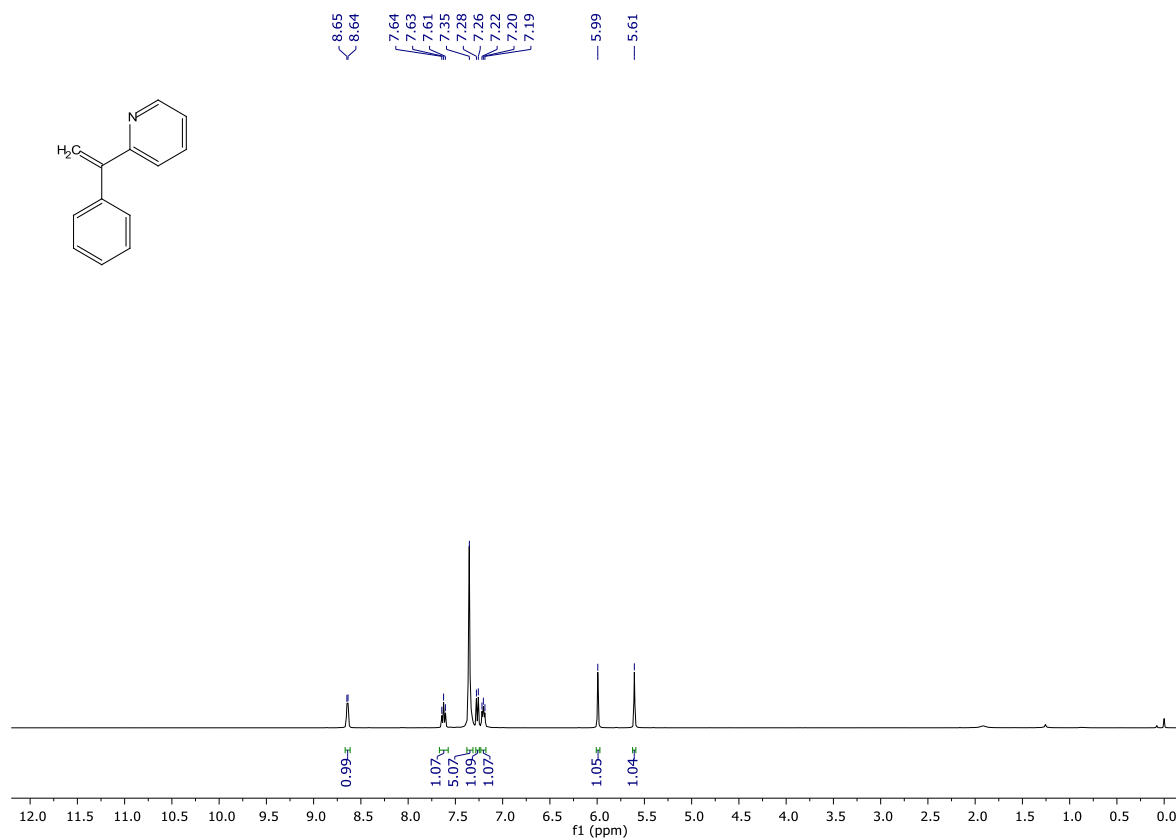


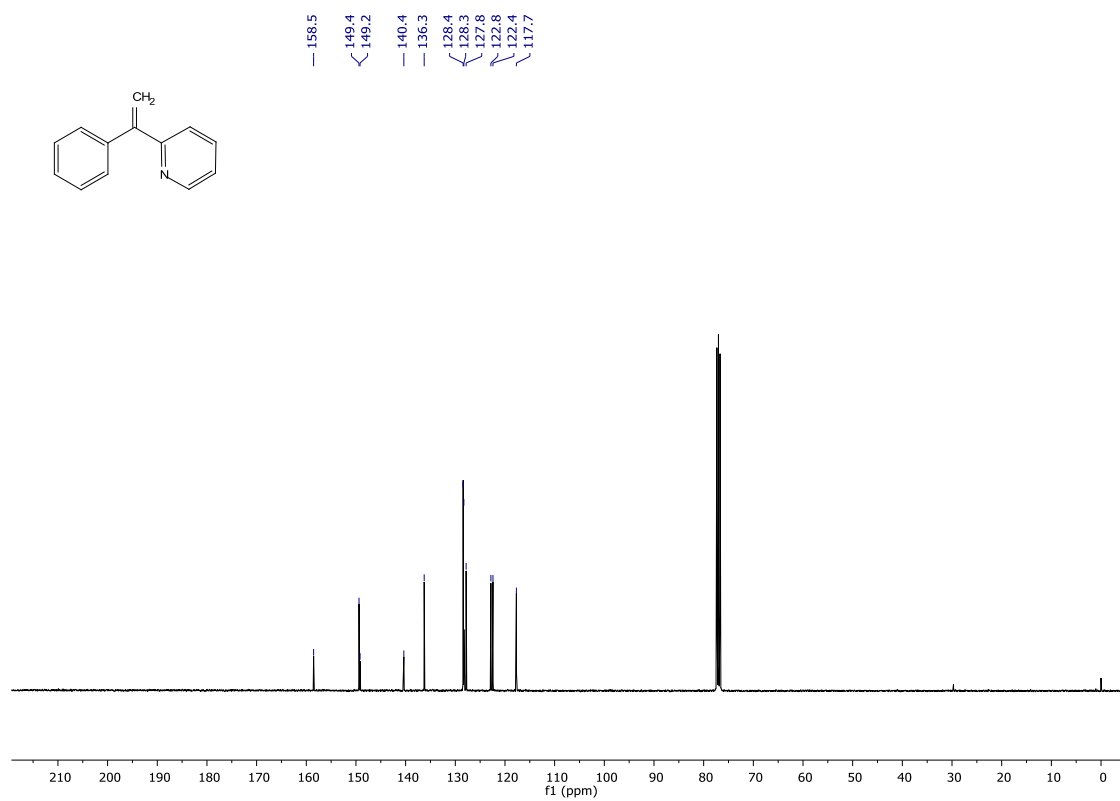
7.2 Spectra for Chapter 3

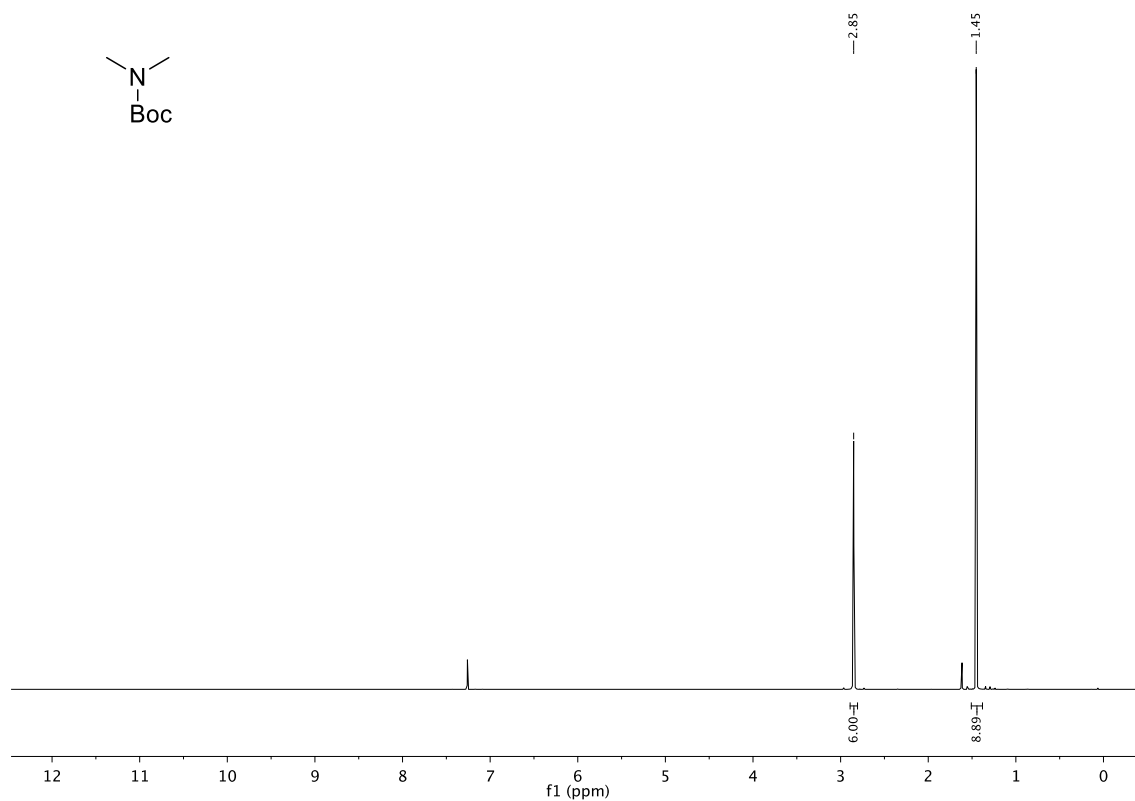
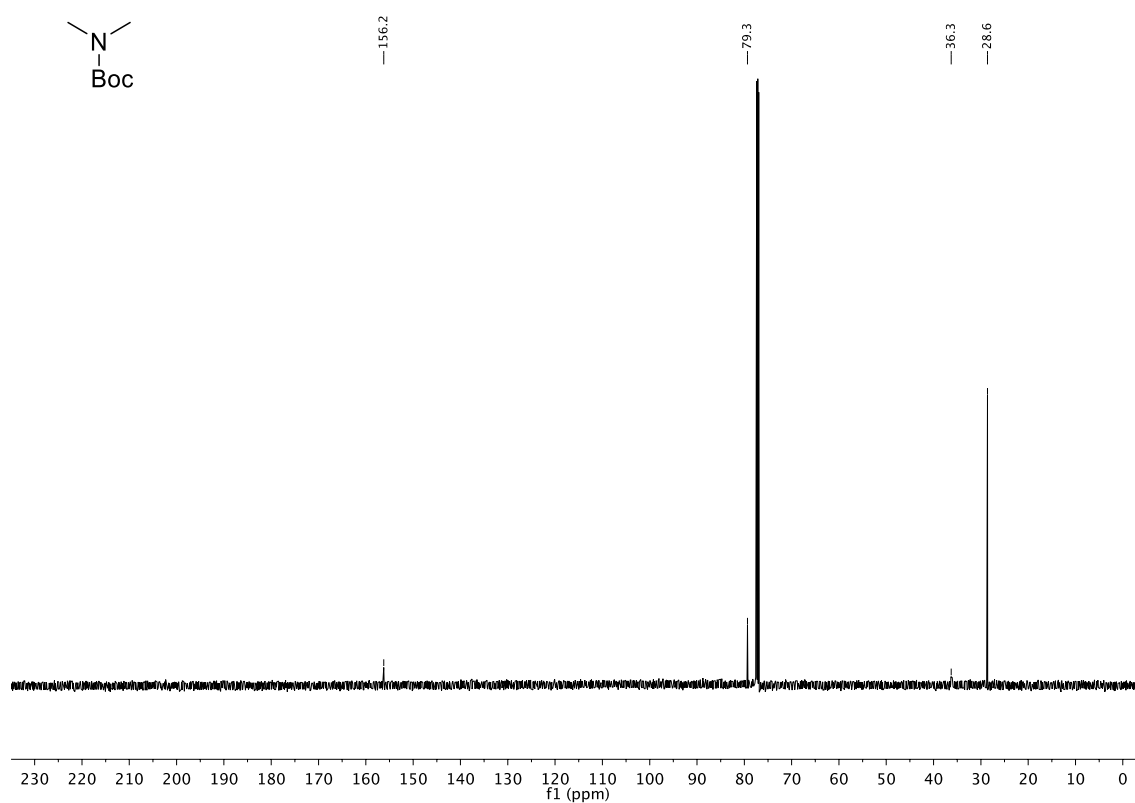
7.2.1 Starting materials spectra

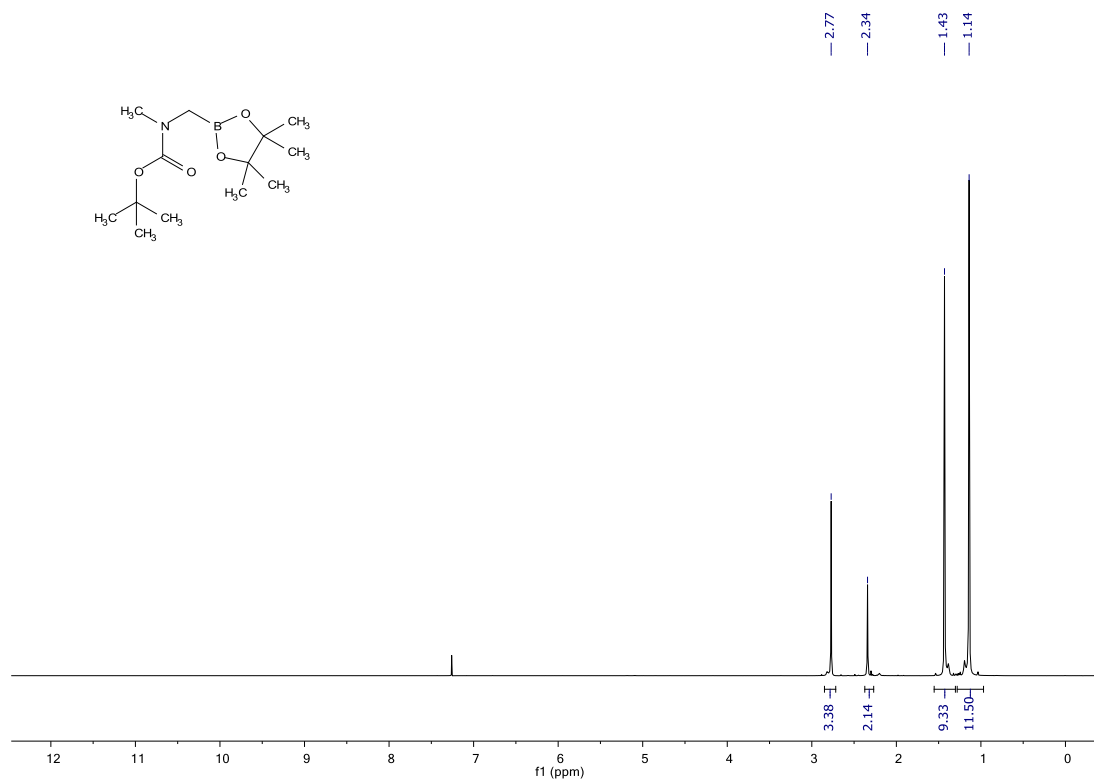
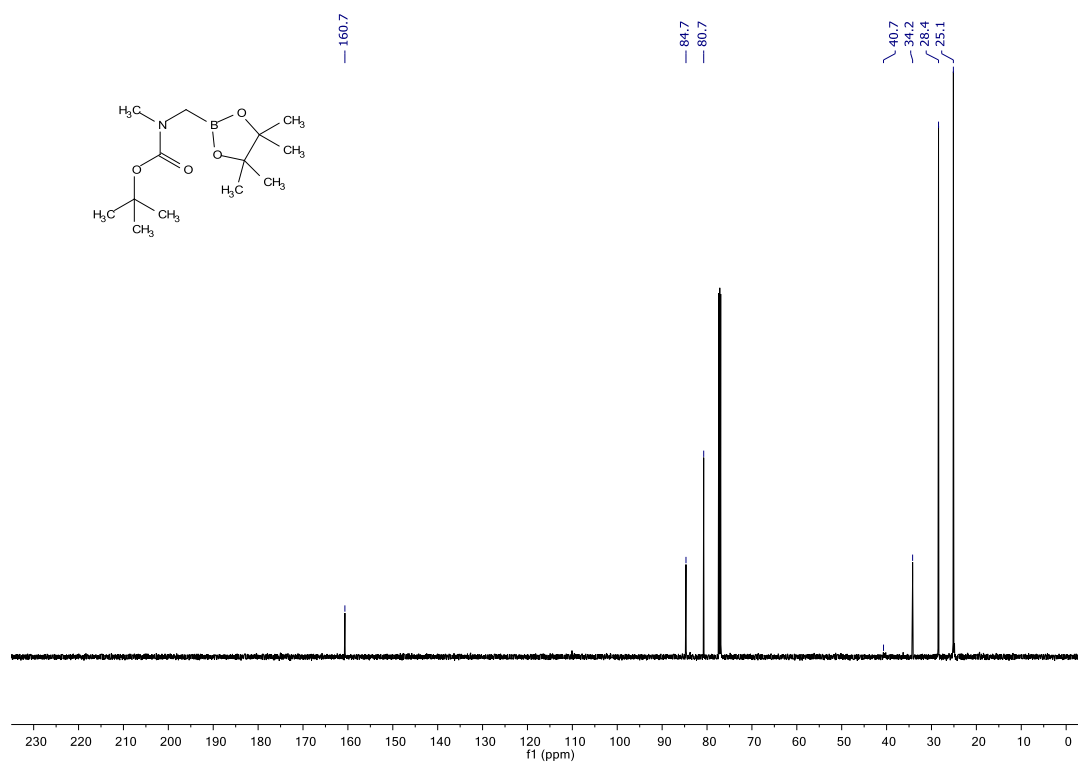
2-(1-phenylvinyl) pyridine

$^1\text{H-NMR}$ (400 MHz, CDCl_3)



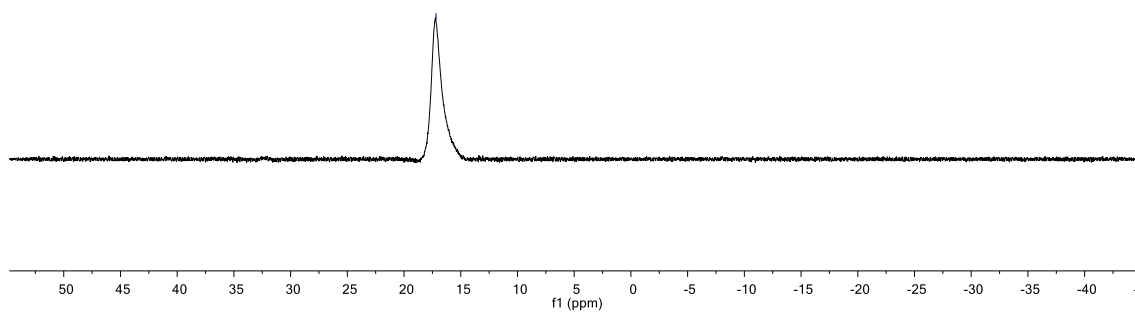
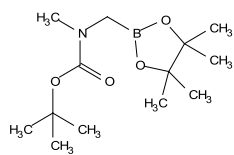
^{13}C -NMR (151 MHz, CDCl_3)

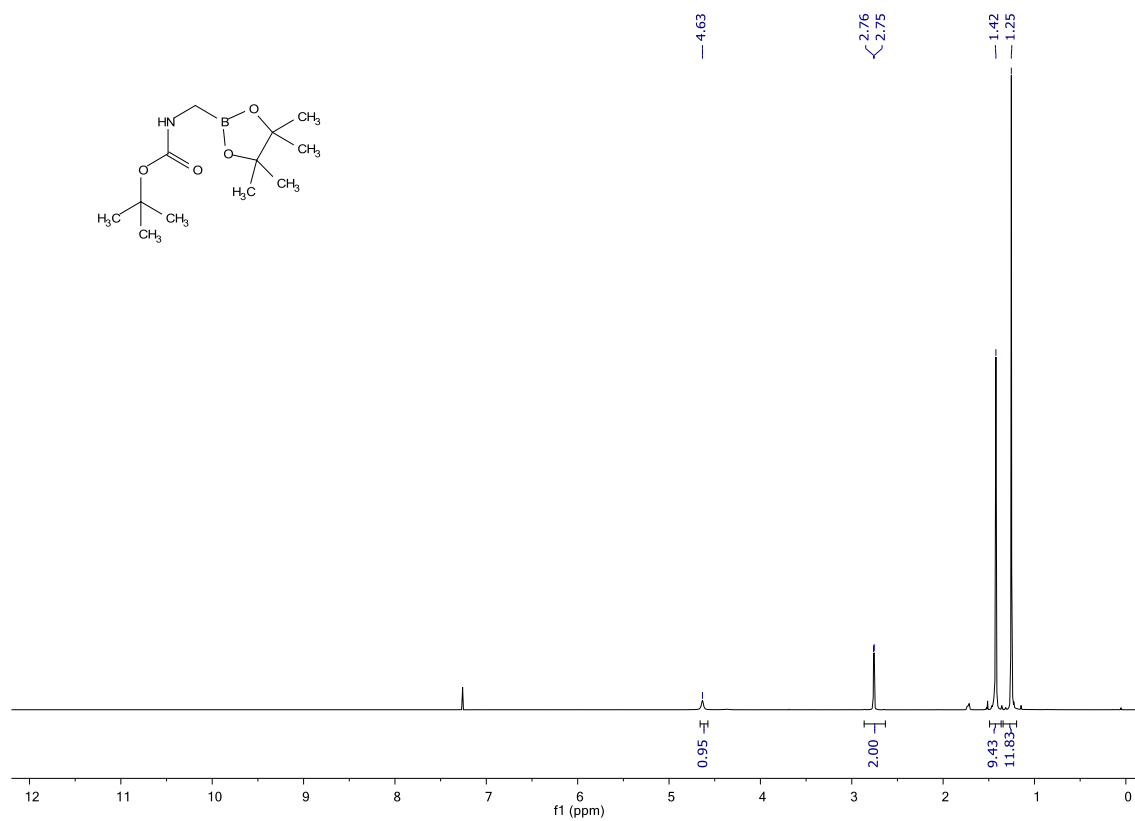
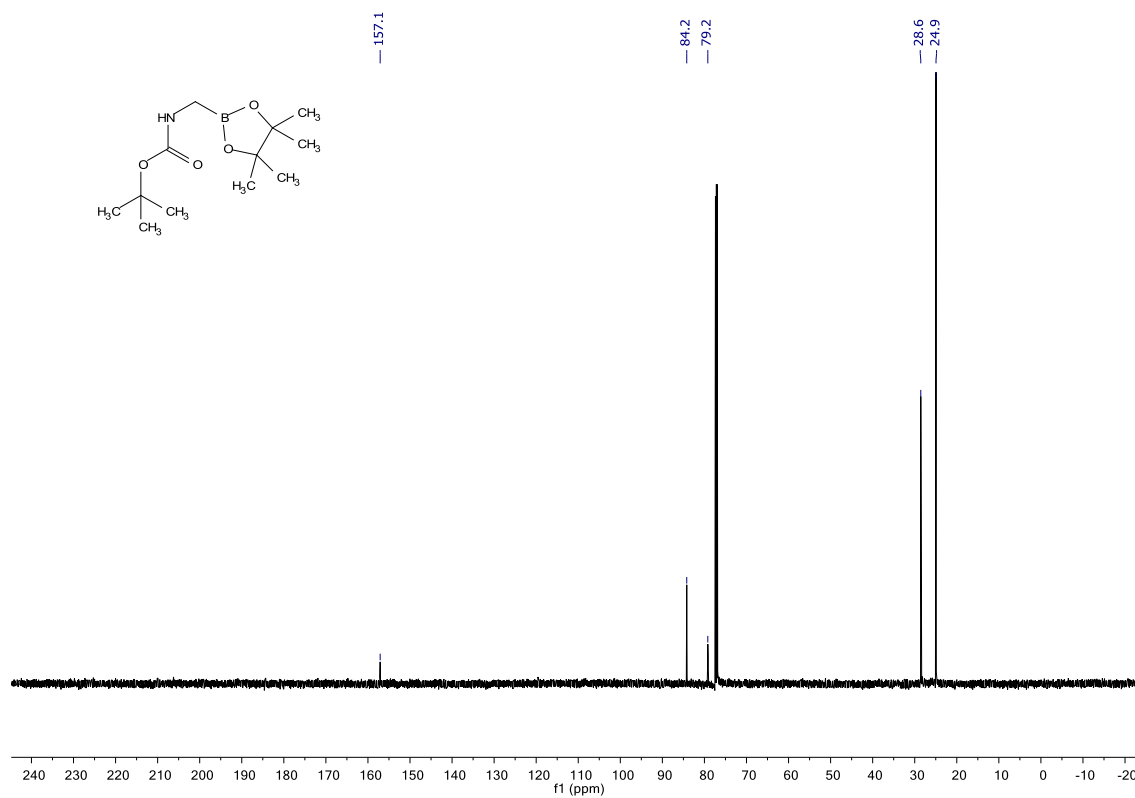
***tert*-butyl dimethylcarbamate** **$^1\text{H-NMR}$ (600 MHz, CDCl_3)** **$^{13}\text{C-NMR}$ (151 MHz, CDCl_3)**

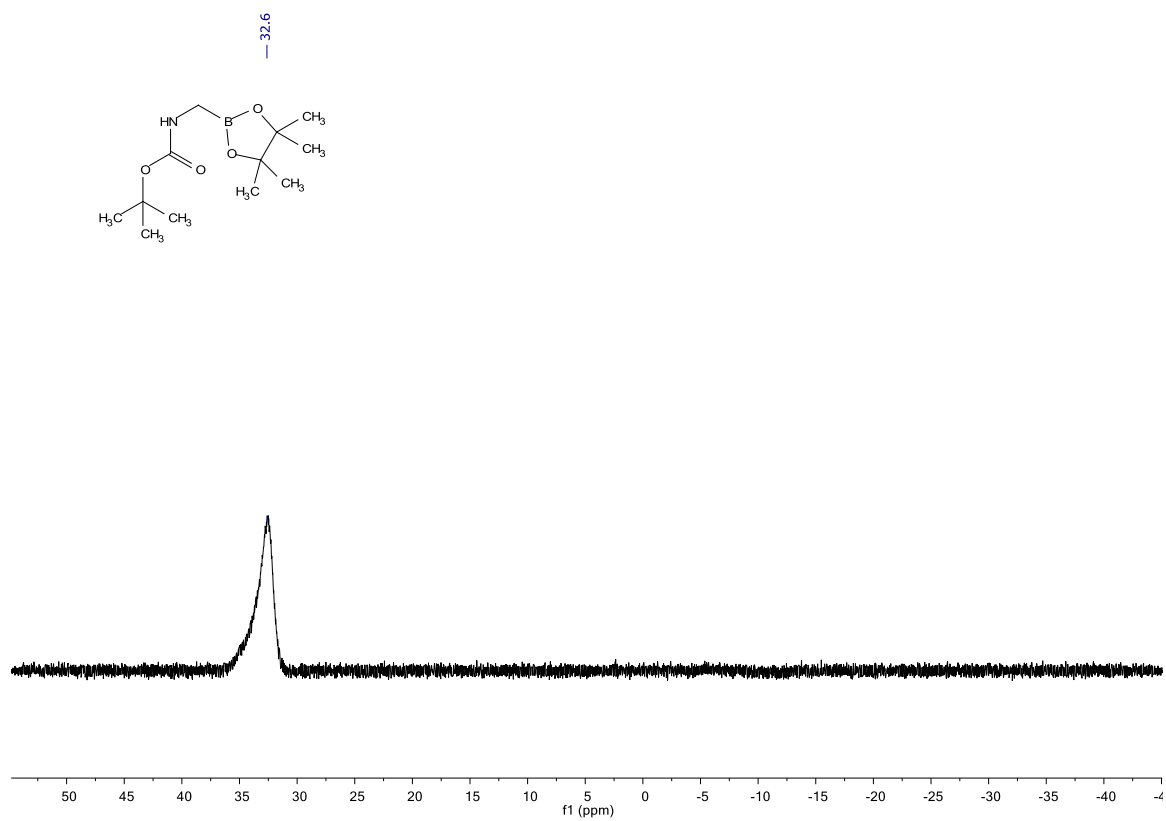
tert*-butyl methyl((4,4,5,5-tetramethyl-1,3,2-dioxaborolan-2-yl)methyl)carbamate*¹H-NMR (600 MHz, CDCl₃)****¹³C-NMR (151 MHz, CDCl₃)**

^{11}B -NMR (193 MHz, CDCl_3)

- 17.2



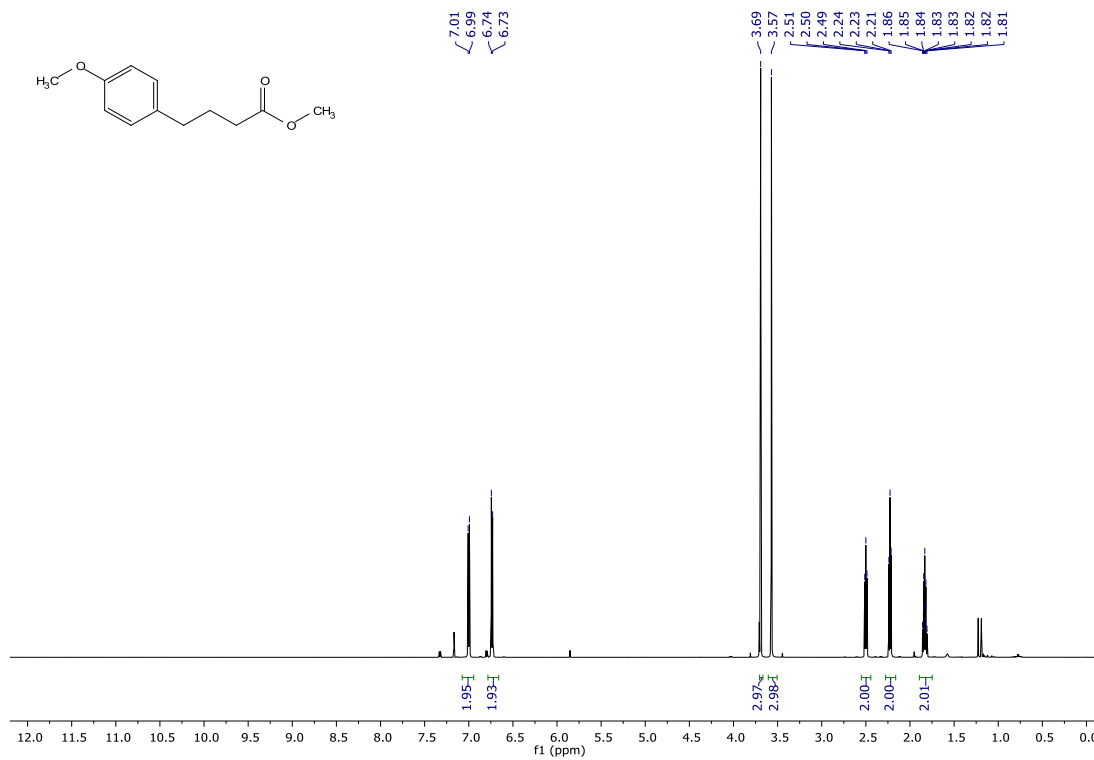
tert*-butyl ((4,4,5,5-tetramethyl-1,3,2-dioxaborolan-2-yl)methyl)carbamate*¹H-NMR (600 MHz, CDCl₃)****¹³C-NMR (151 MHz, CDCl₃)**

^{11}B -NMR (193 MHz, CDCl_3)

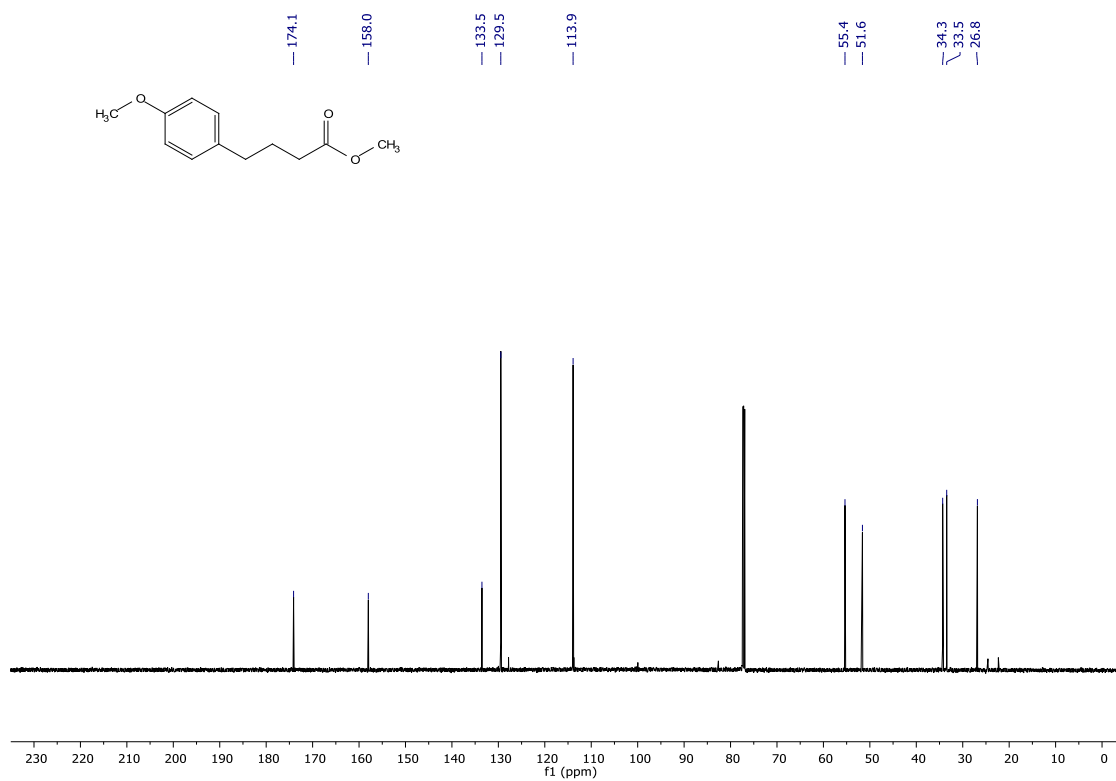
7.2.2 Coupling products spectra

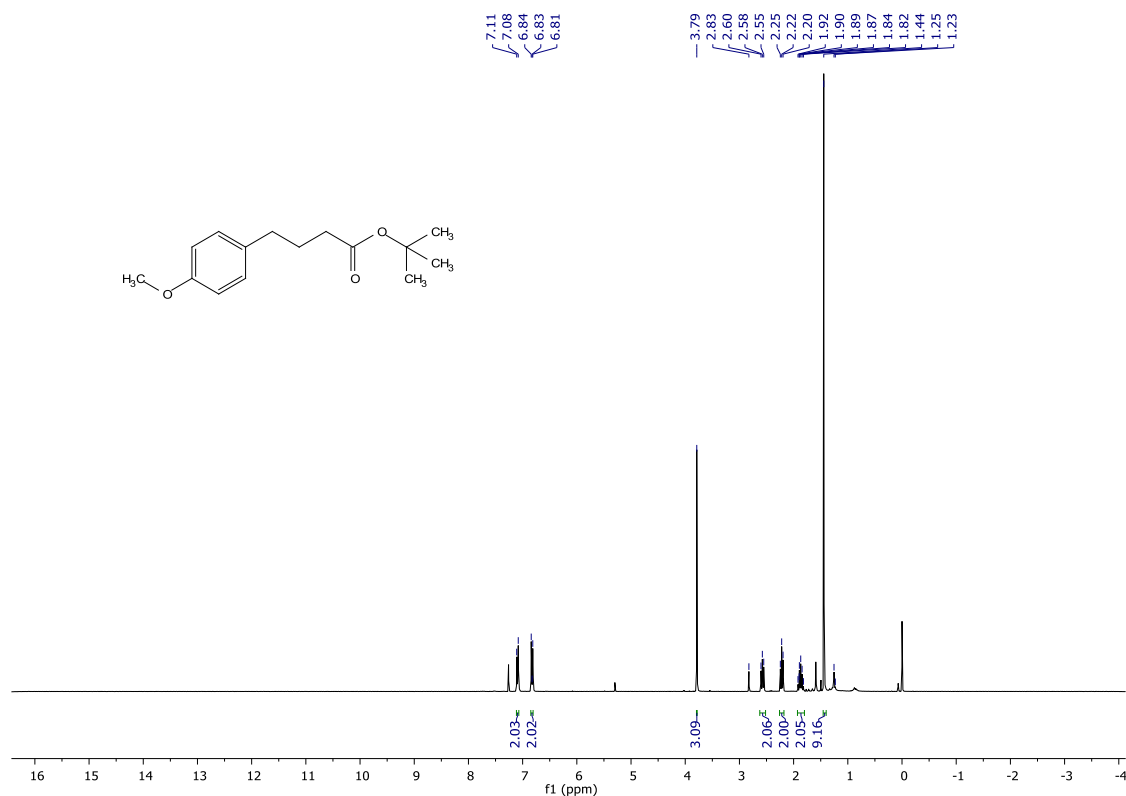
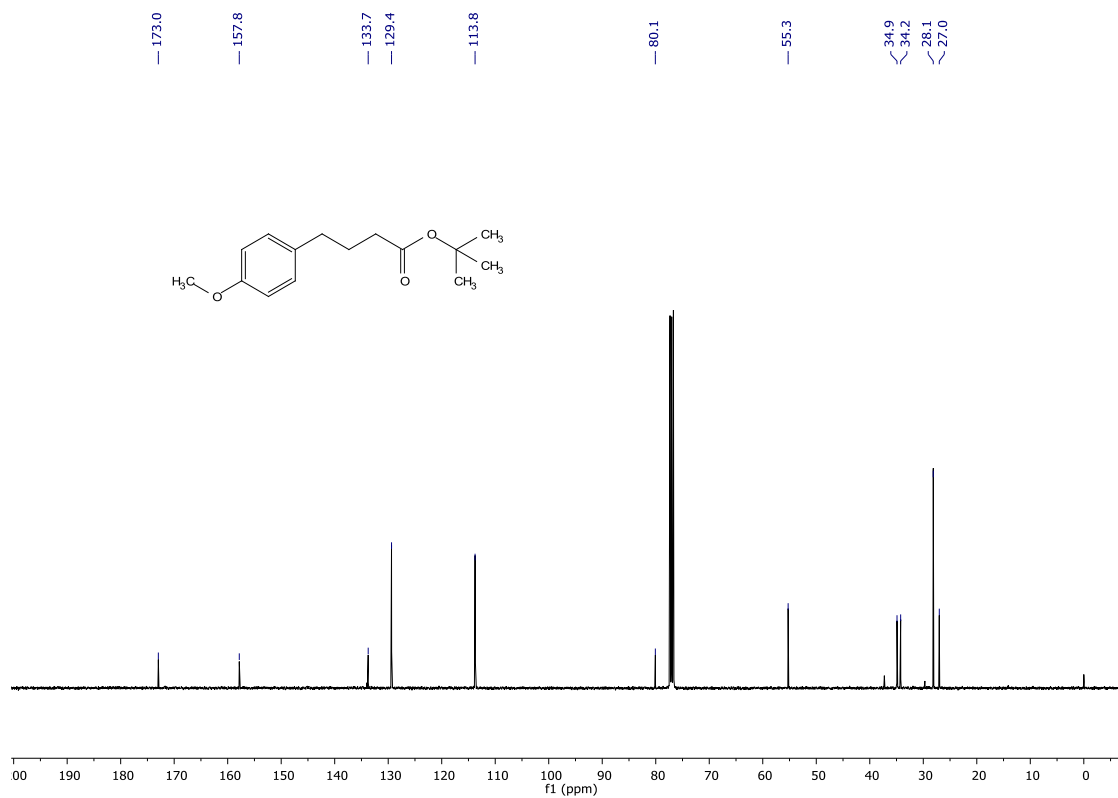
methyl 4-(4-methoxyphenyl)butanoate (263)

$^1\text{H-NMR}$ (600 MHz, CDCl_3)



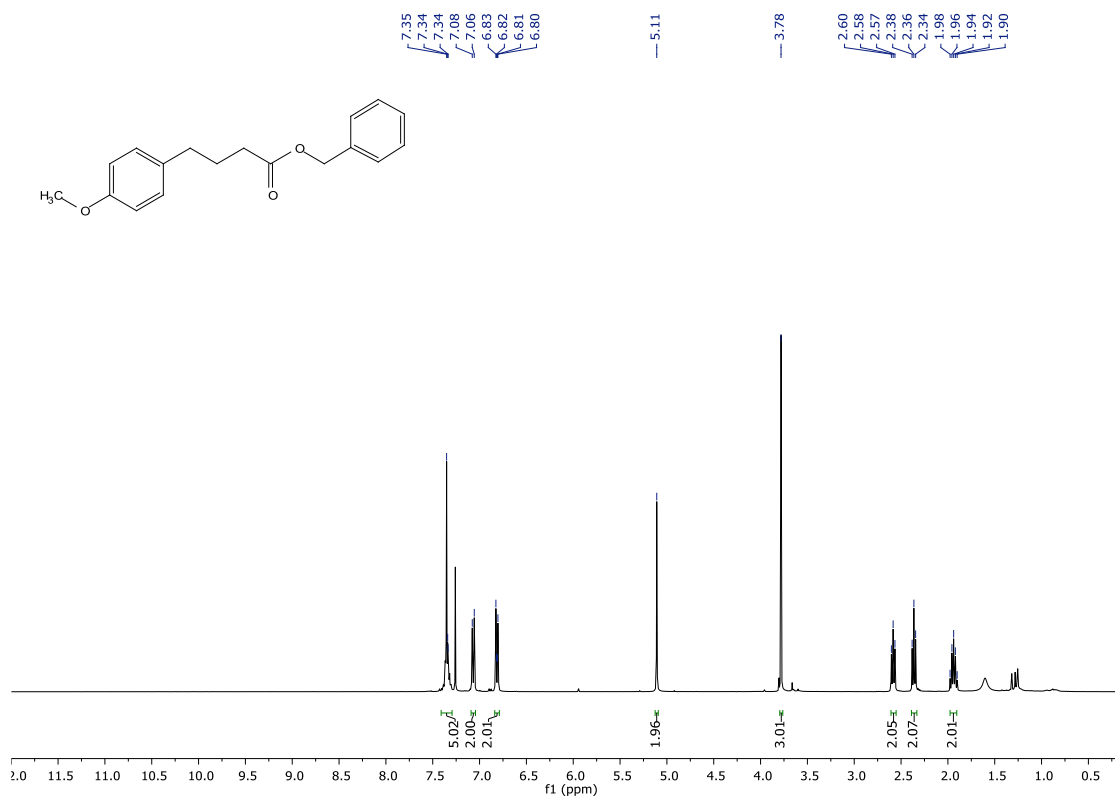
$^{13}\text{C-NMR}$ (151 MHz, CDCl_3)



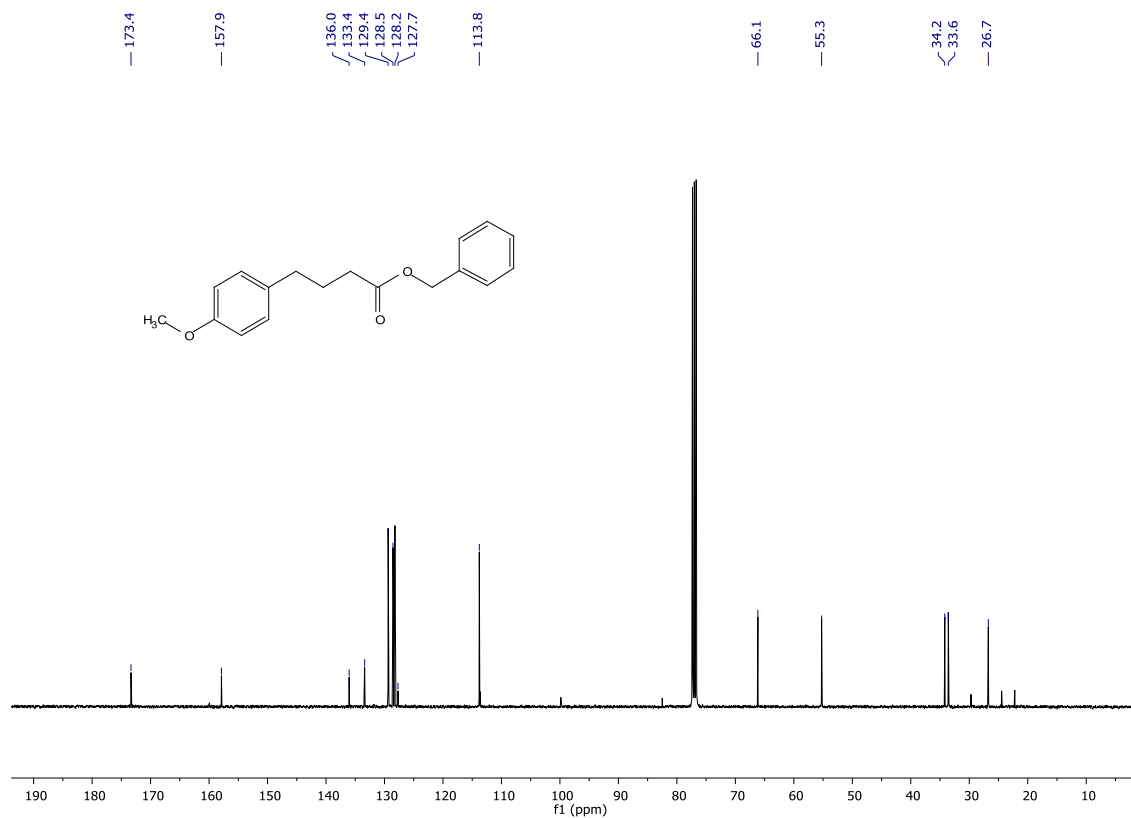
tert*-butyl 4-(4-methoxyphenyl)butanoate (264)*¹H-NMR (400 MHz, CDCl₃)****¹³C-NMR (101 MHz, CDCl₃)**

benzyl 4-(4-methoxyphenyl)butanoate (265)

¹H-NMR (400 MHz, CDCl₃)

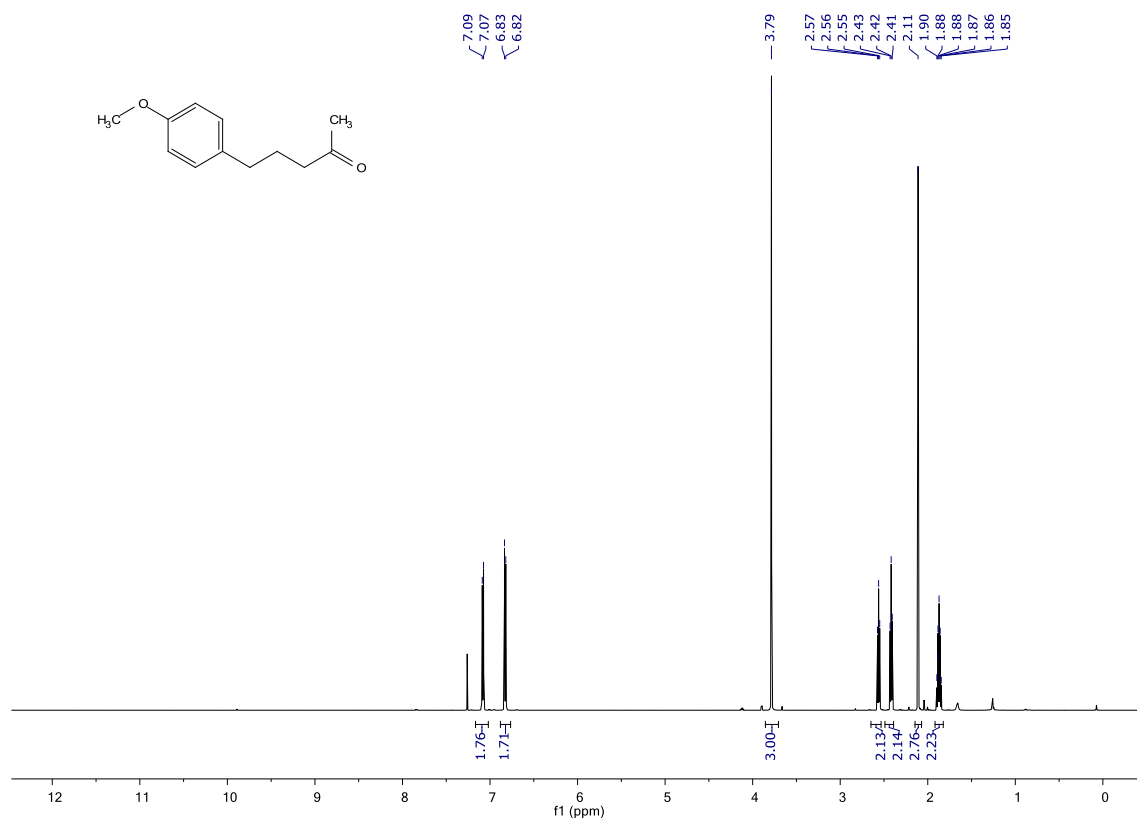


¹³C-NMR (101 MHz, CDCl₃)

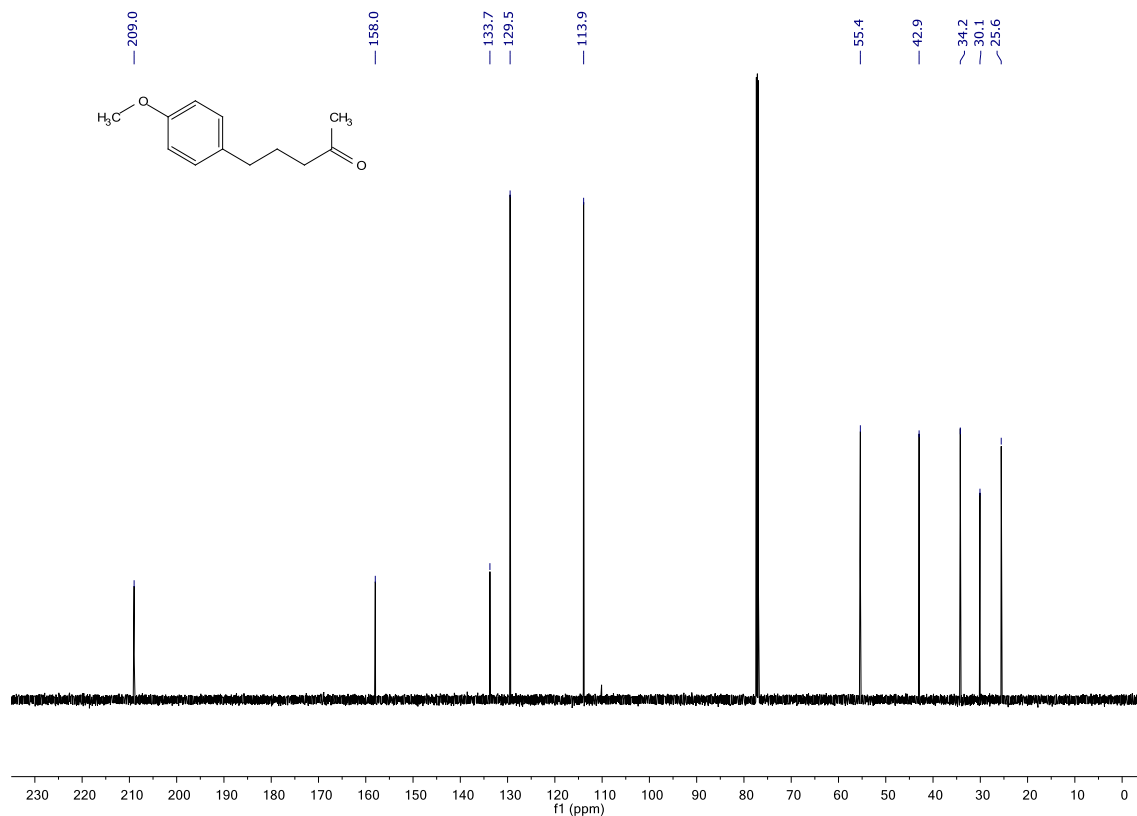


5-(4-methoxyphenyl)pentan-2-one (266)

¹H-NMR (600 MHz, CDCl₃)

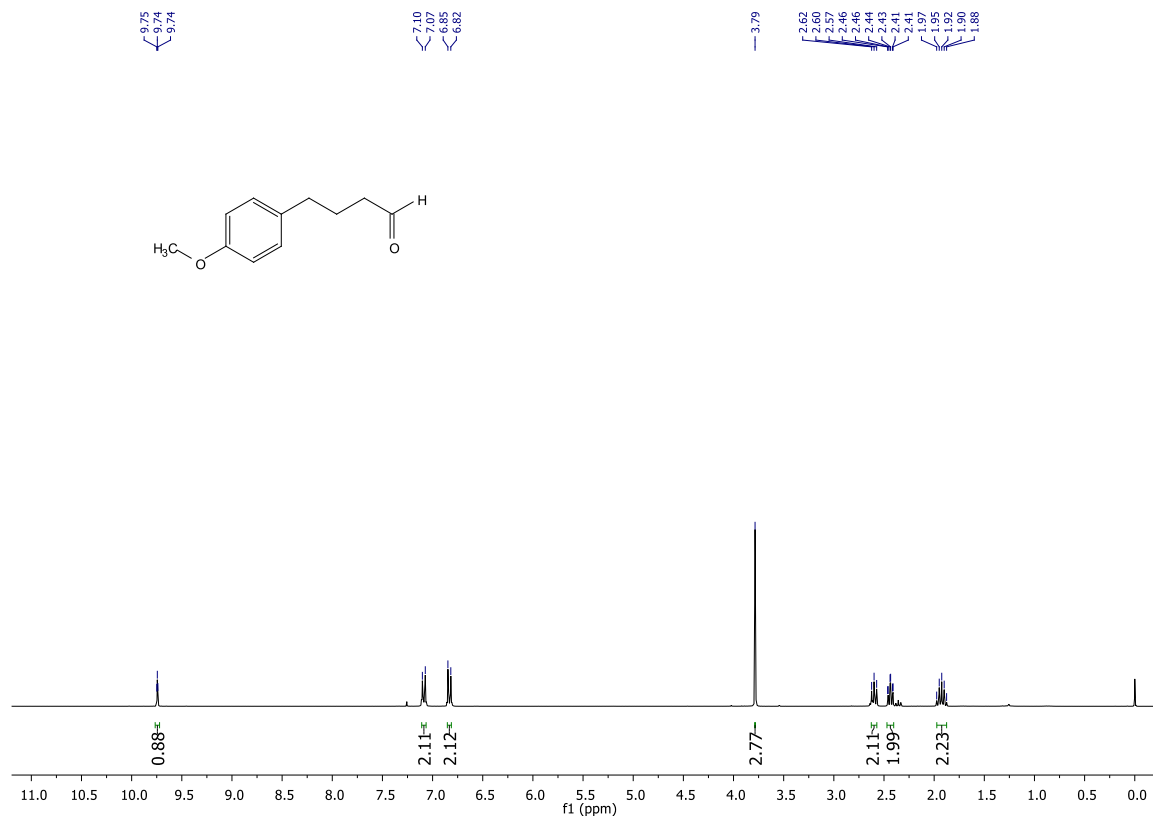


¹³C-NMR (151 MHz, CDCl₃)

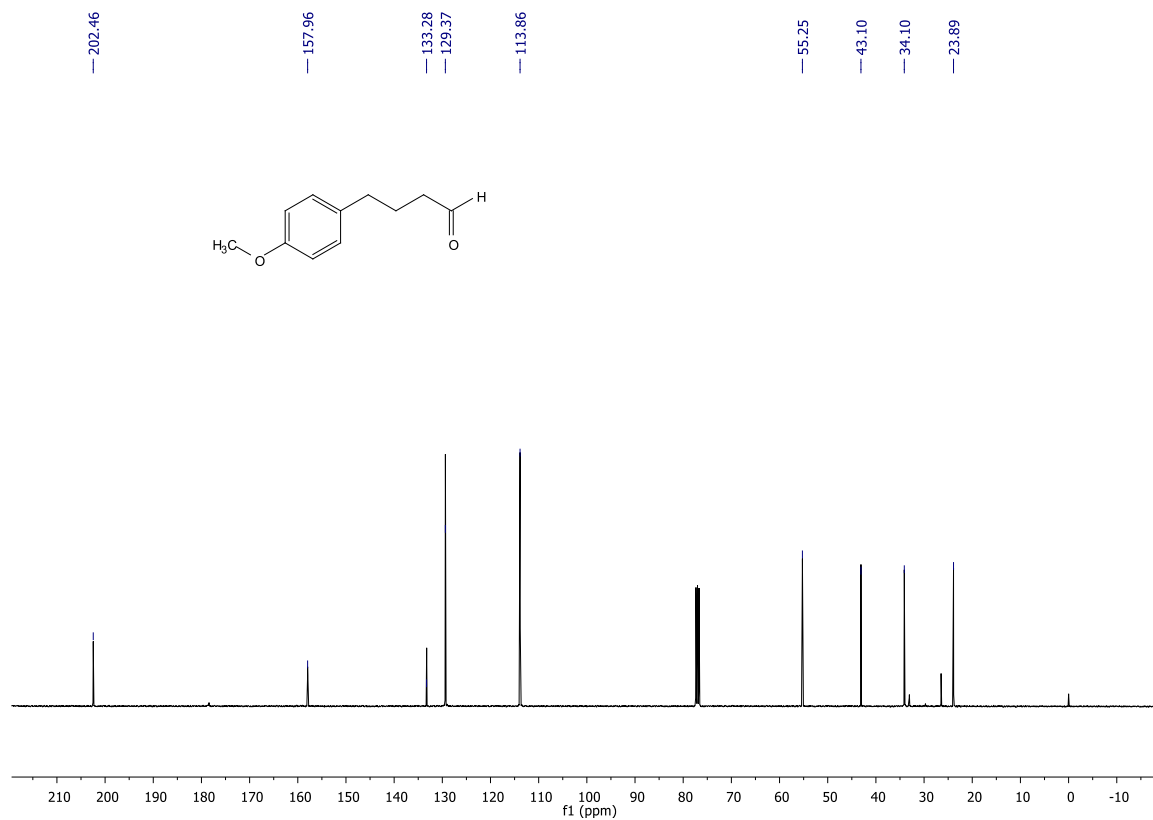


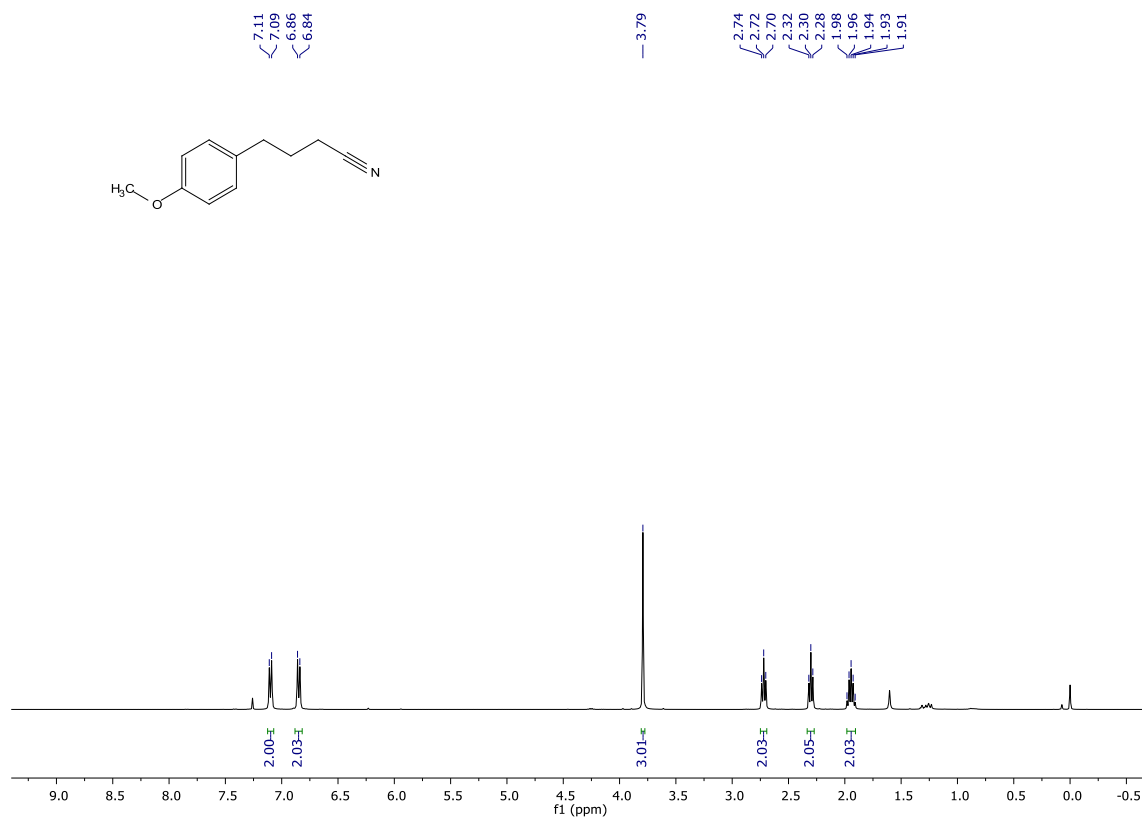
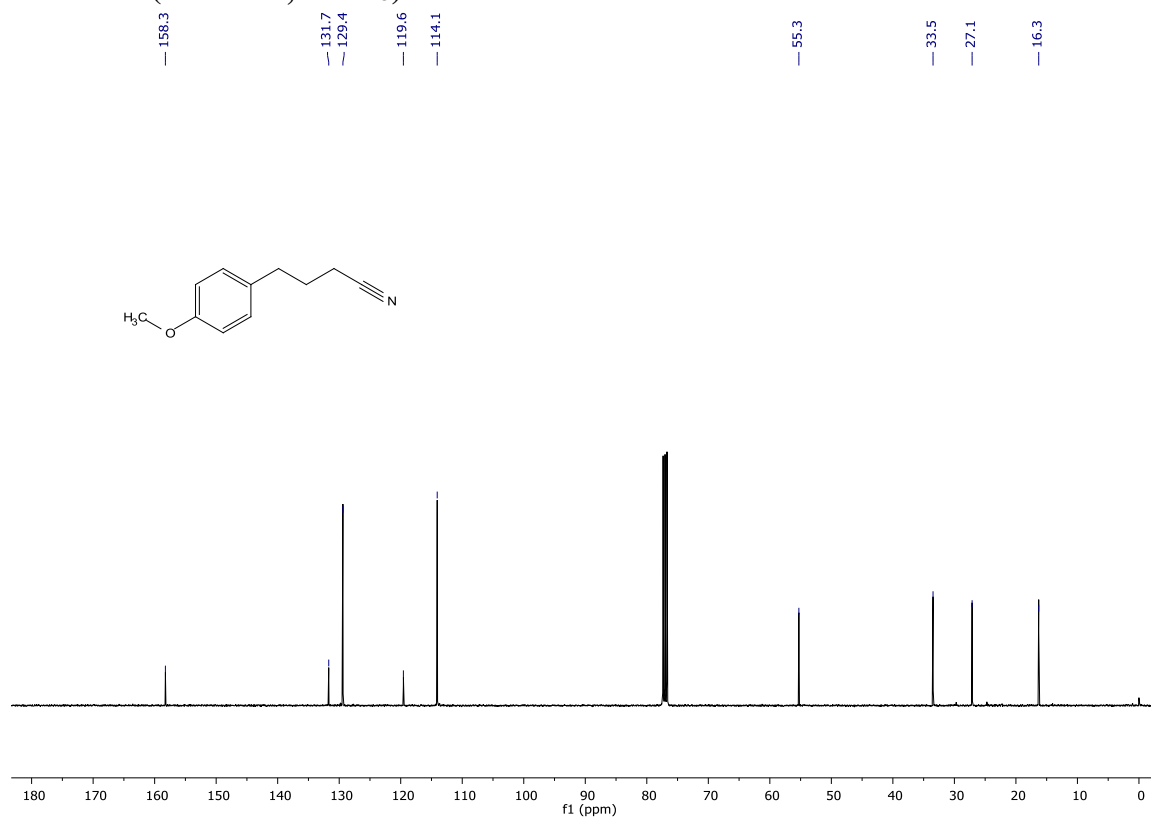
4-(4-methoxyphenyl)butanal (267)

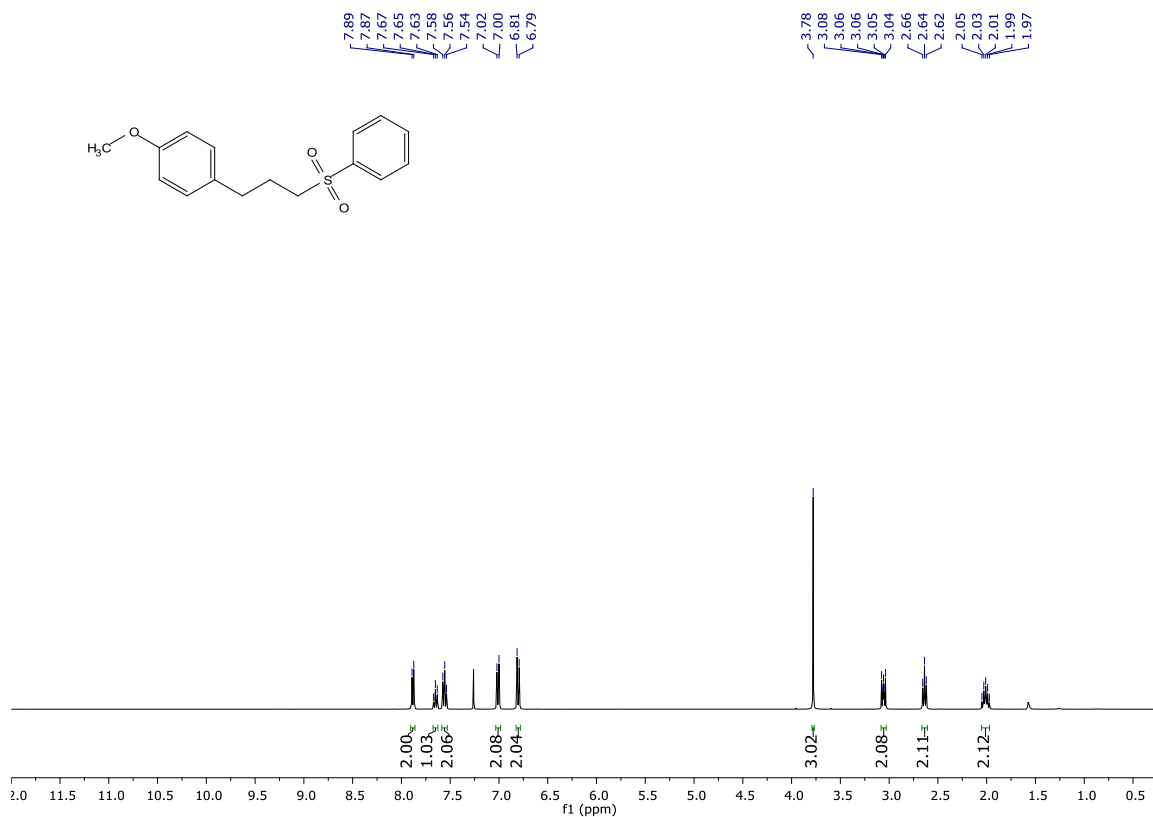
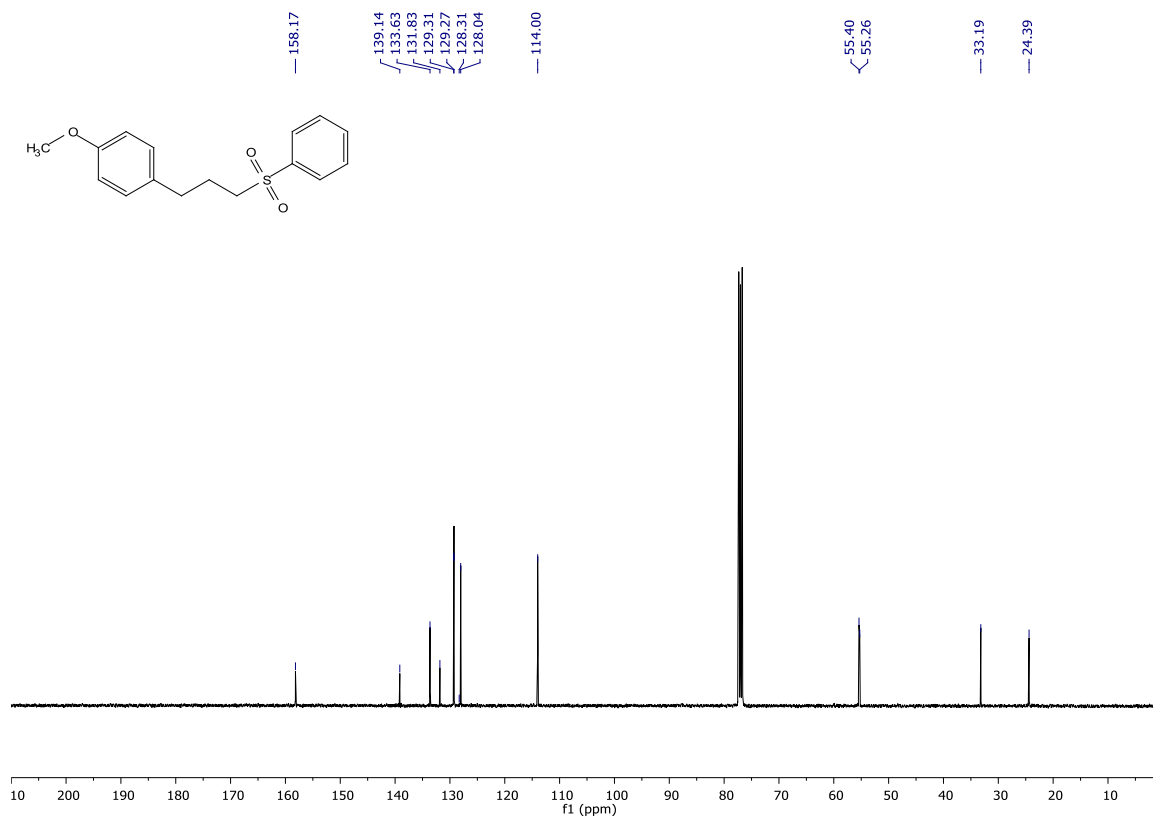
¹H-NMR (400 MHz, CDCl₃)



¹³C-NMR (101 MHz, CDCl₃)

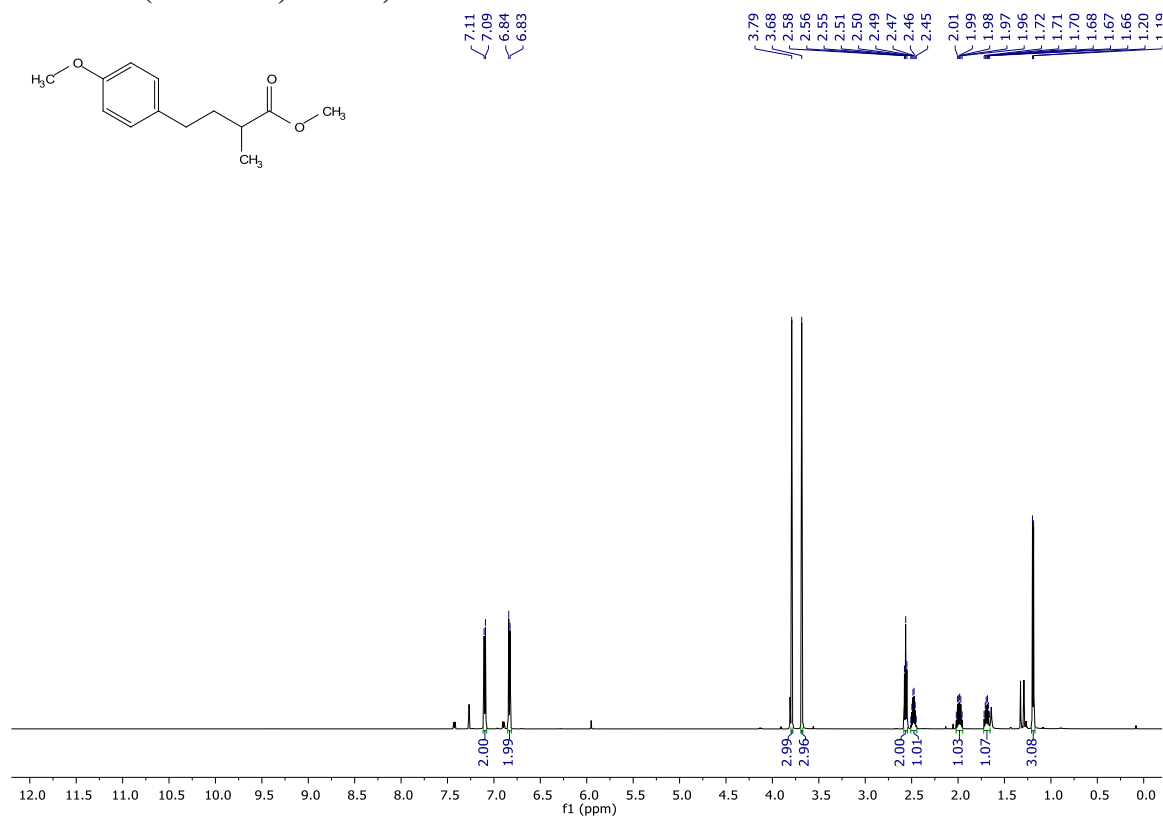


4-(4-methoxyphenyl)butanenitrile (268) **$^1\text{H-NMR}$ (400 MHz, CDCl_3)** **$^{13}\text{C-NMR}$ (101 MHz, CDCl_3)**

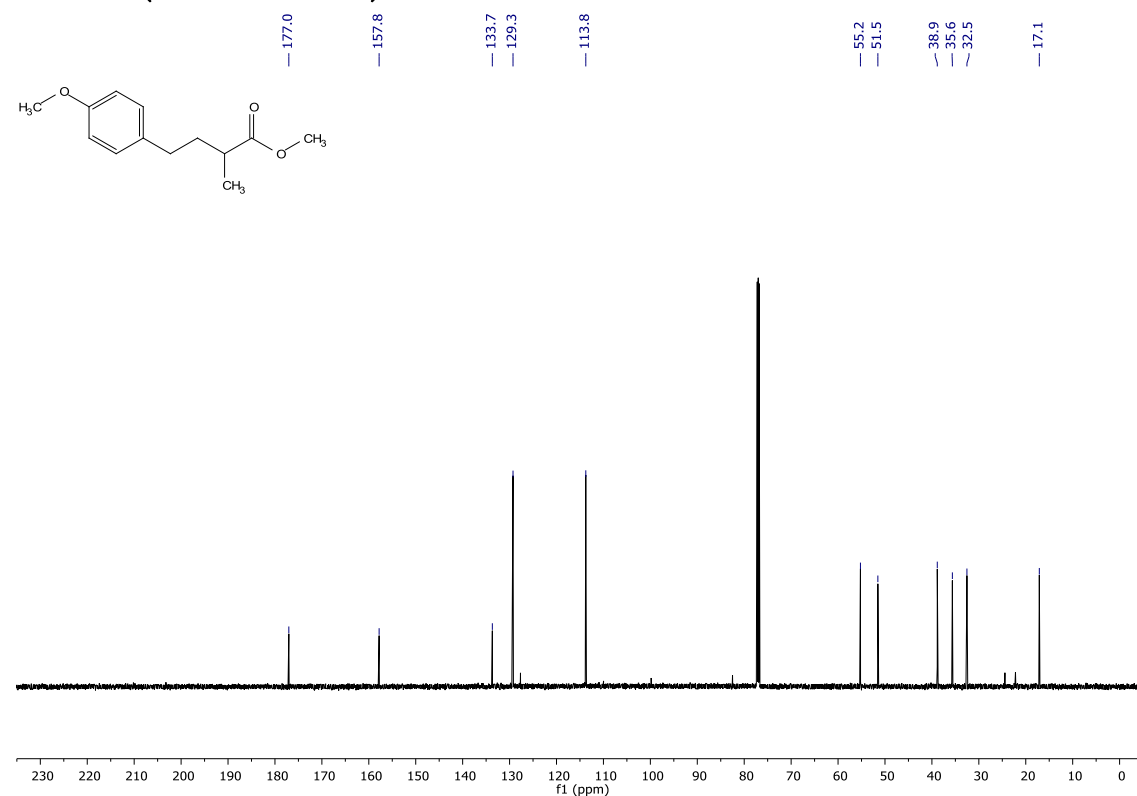
1-methoxy-4-(3-(phenylsulfonyl)propyl)benzene (269) **$^1\text{H-NMR}$ (400 MHz, CDCl_3)** **$^{13}\text{C-NMR}$ (101 MHz, CDCl_3)**

methyl 4-(4-methoxyphenyl)-2-methylbutanoate (270)

¹H-NMR (400 MHz, CDCl₃)

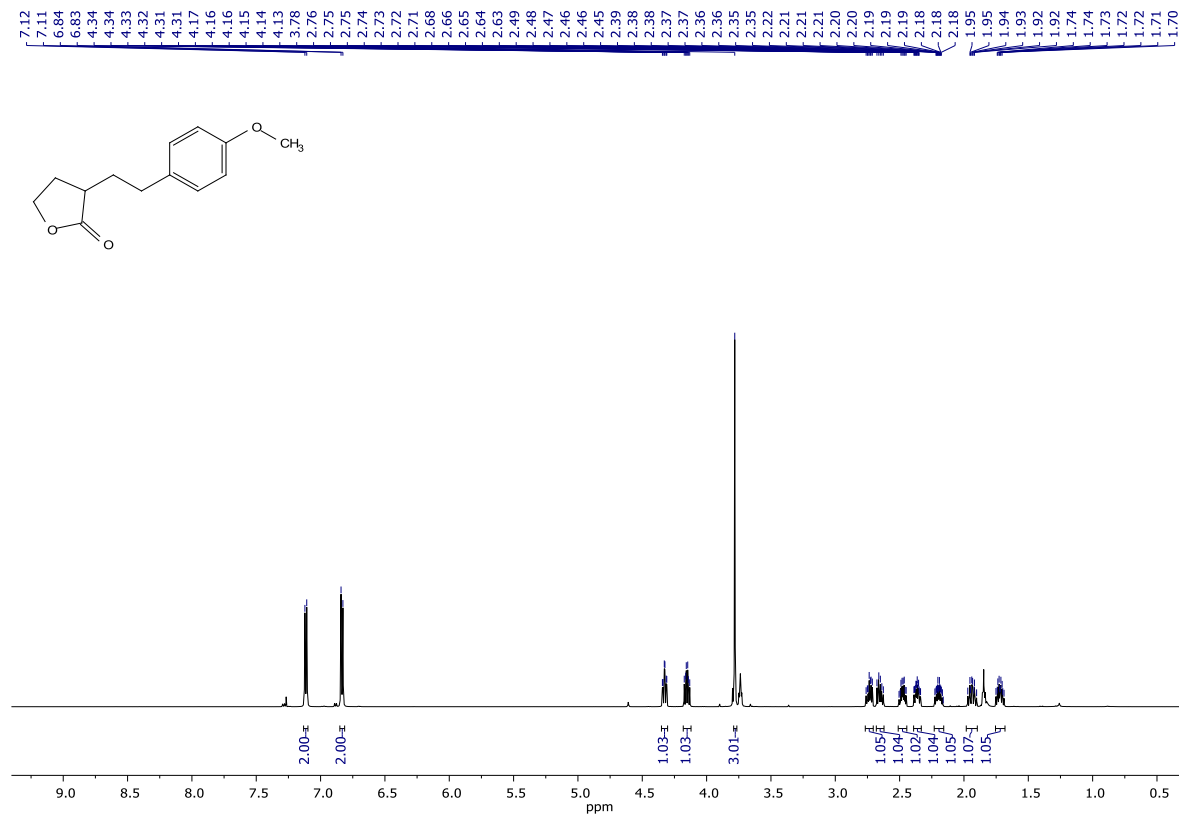


¹³C-NMR (101 MHz, CDCl₃)

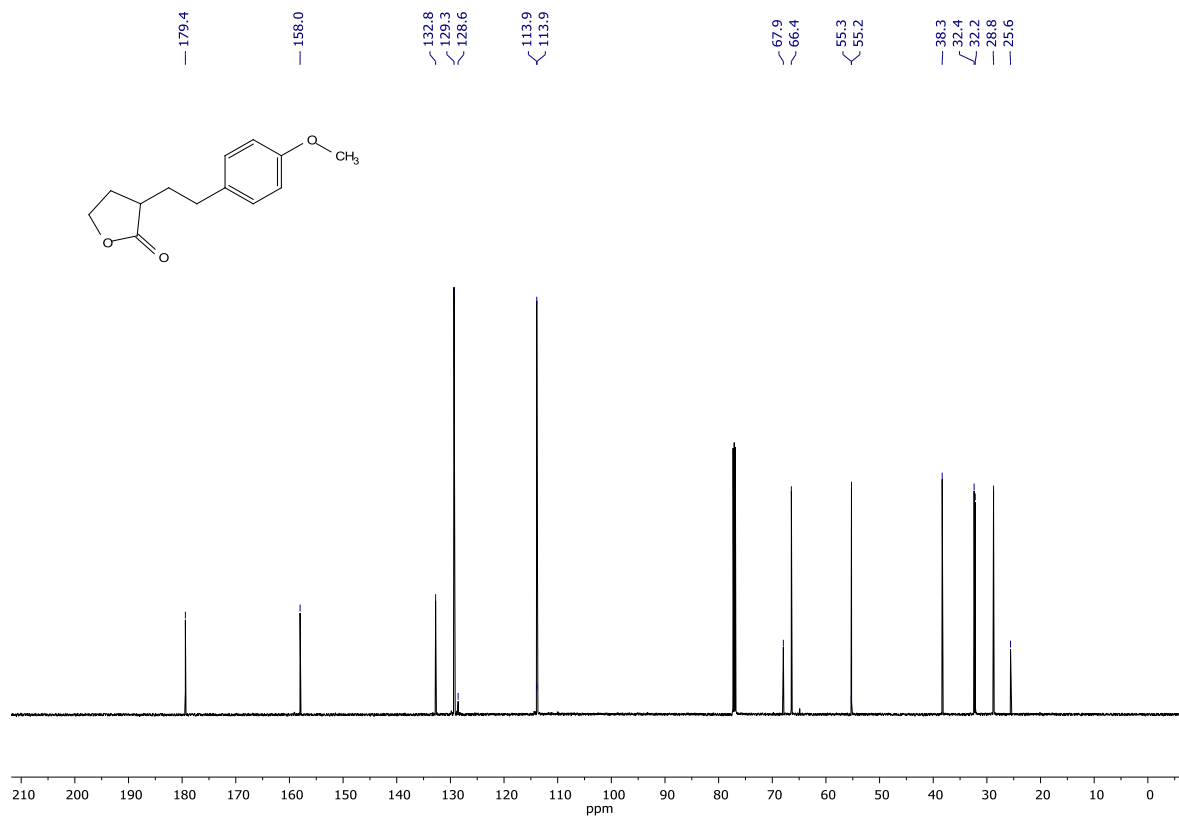


3-(4-methoxyphenethyl) dihydrofuran-2(3H)-one (271)

¹H-NMR (600 MHz, CDCl₃)

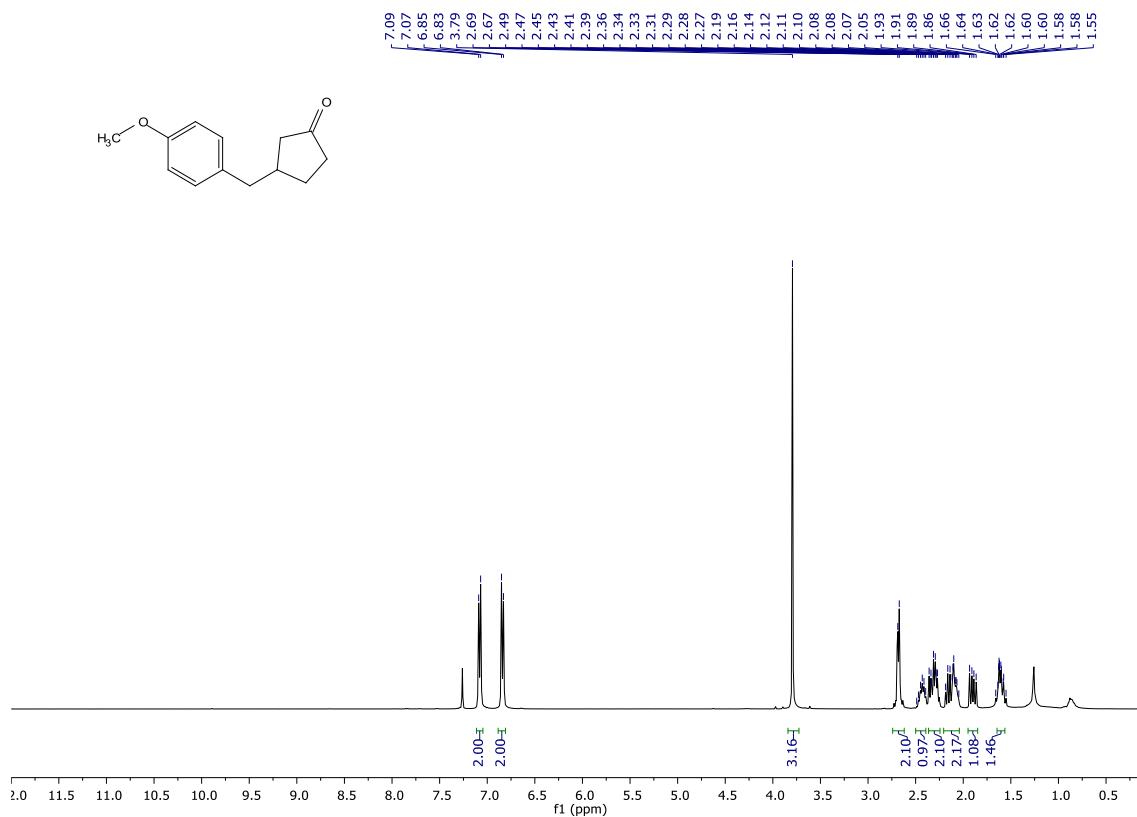


¹³C-NMR (151 MHz, CDCl₃)

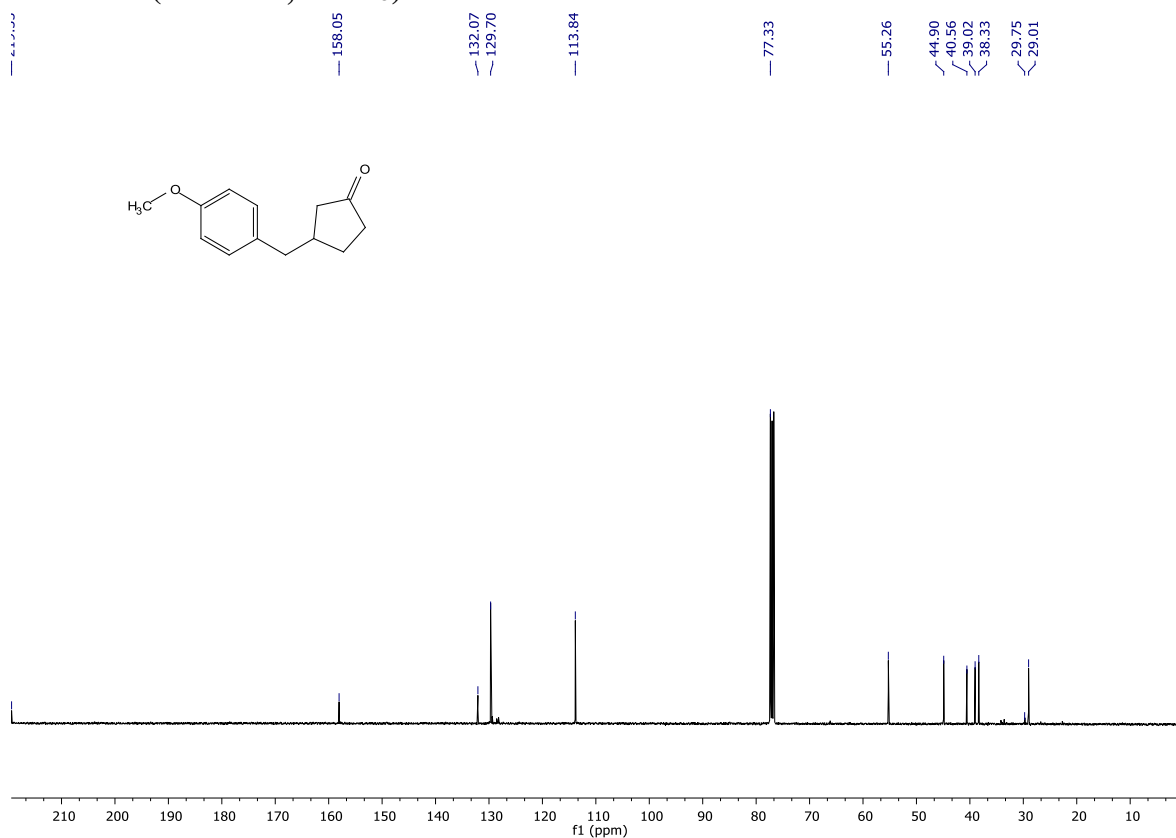


2-(4-methoxybenzyl)cyclopentanone (272)

¹H-NMR (400 MHz, CDCl₃)

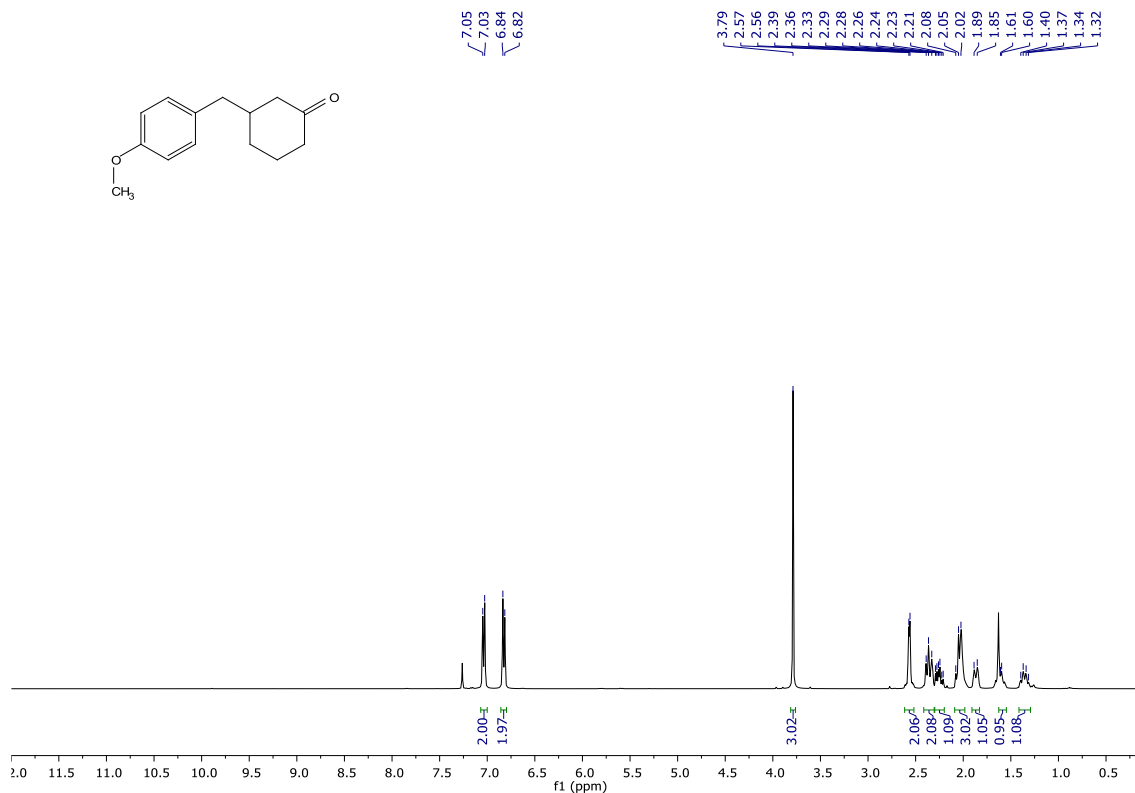


¹³C-NMR (101 MHz, CDCl₃)

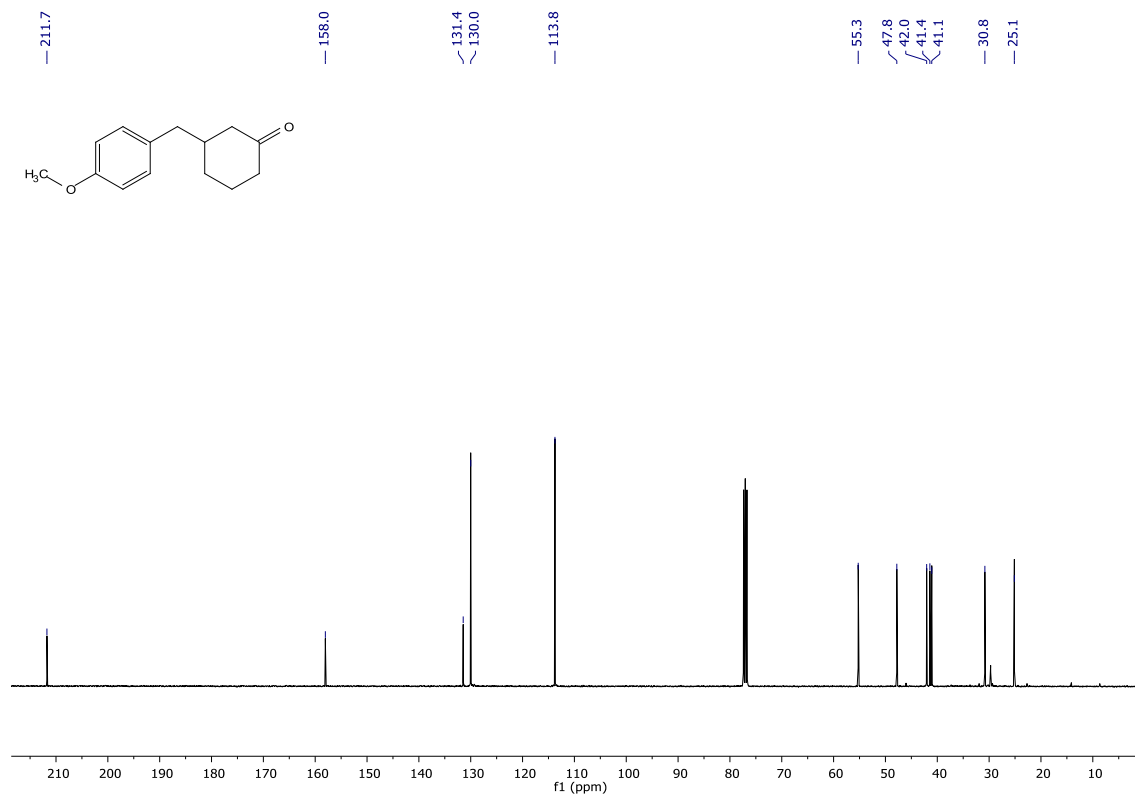


3-(4-methoxybenzyl)cyclohexanone (273)

¹H-NMR (400 MHz, CDCl₃)

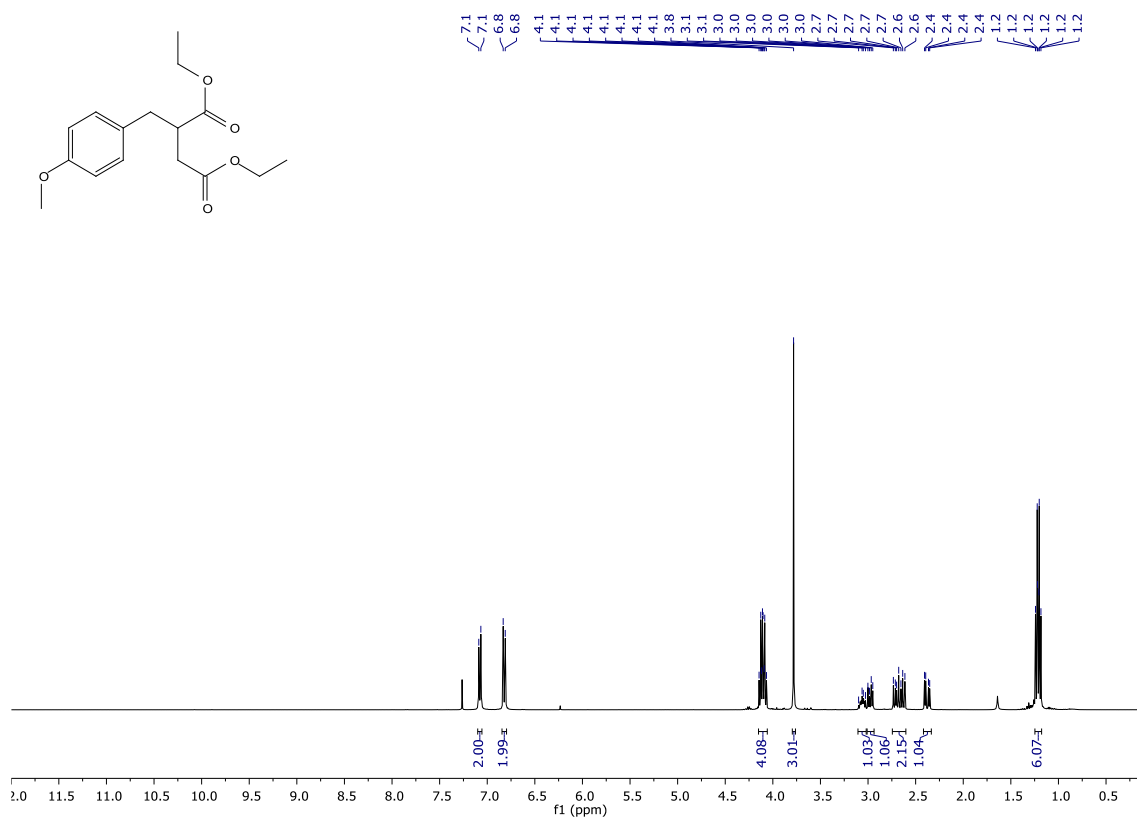


¹³C-NMR (101 MHz, CDCl₃)



Diethyl 2-(4-methoxybenzyl)succinate (274)

¹H-NMR (400 MHz, CDCl₃)

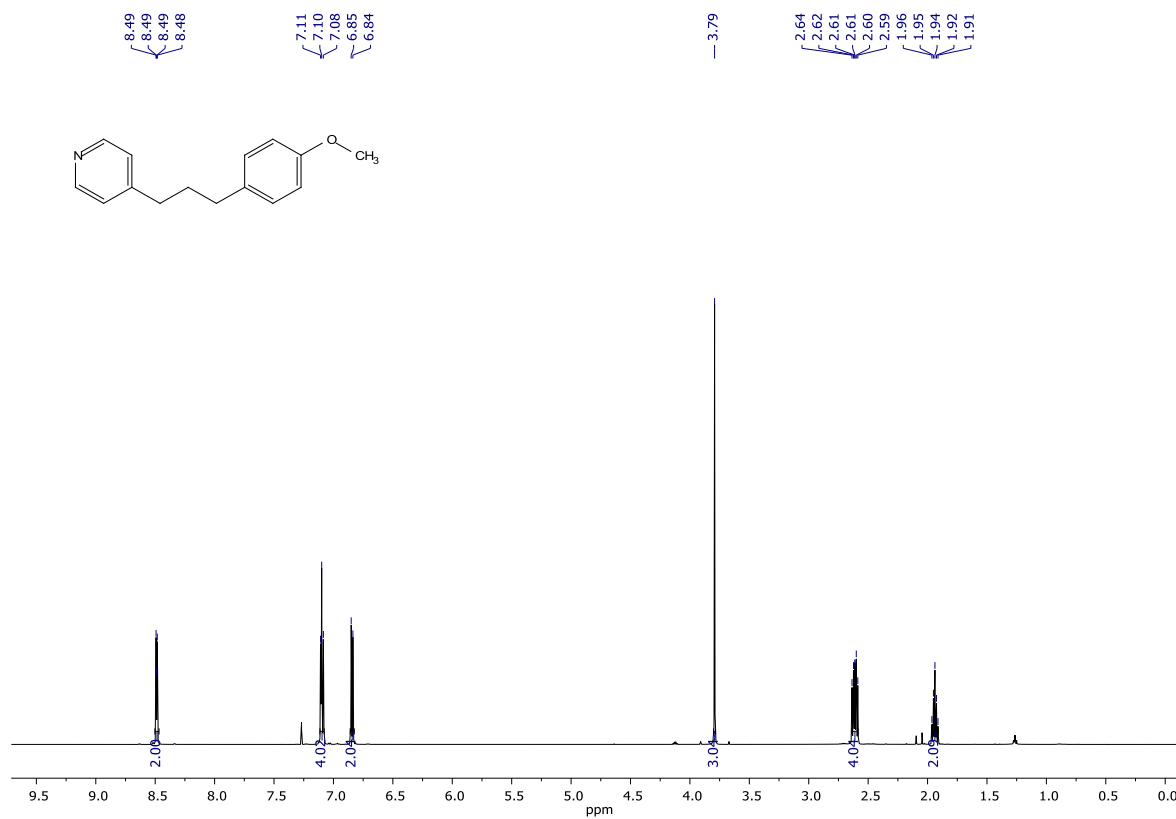


¹³C-NMR (101 MHz, CDCl₃)

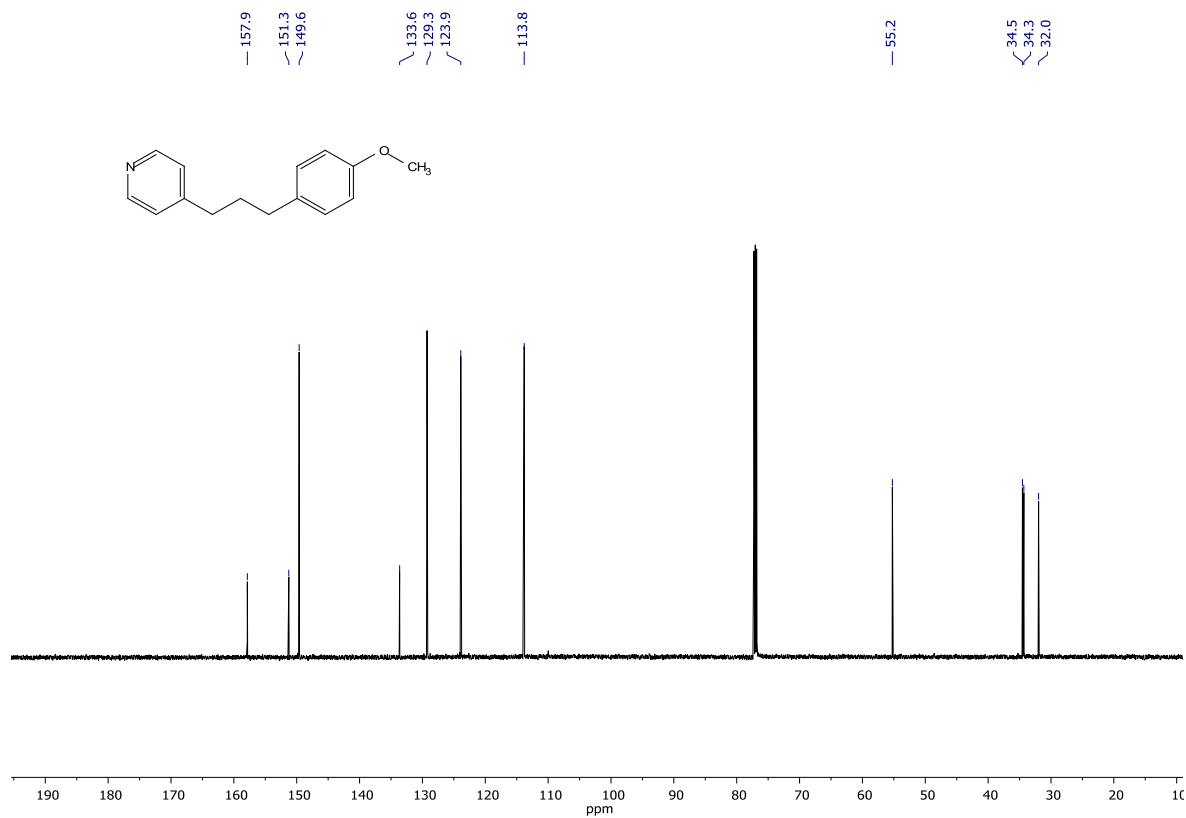


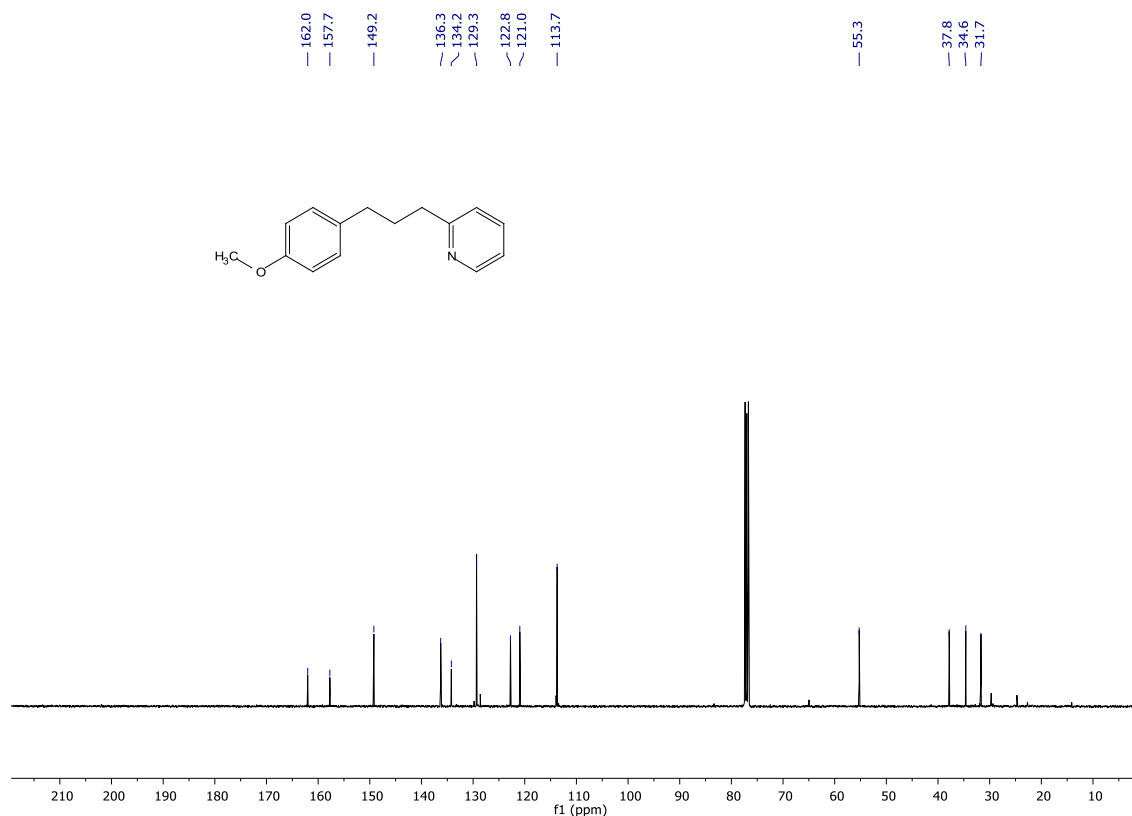
4-(3-(4-methoxyphenyl)propyl)pyridine (275)

¹H-NMR (600 MHz, CDCl₃)



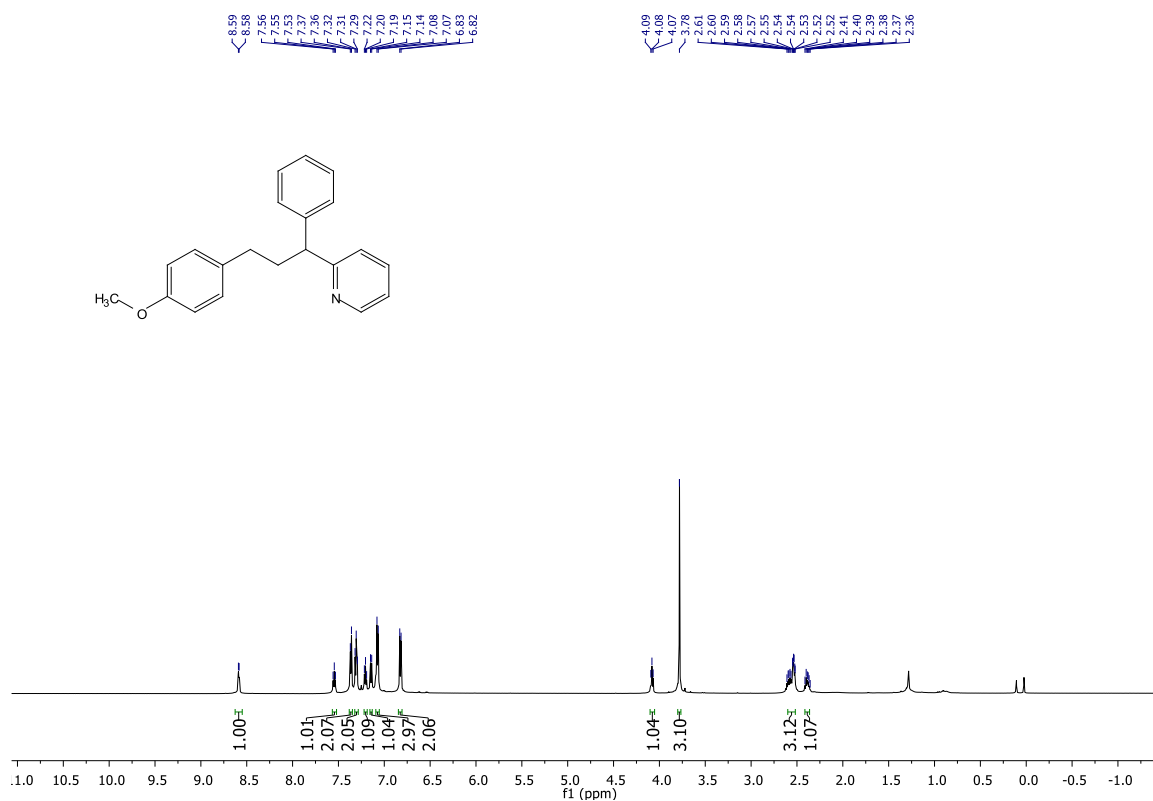
¹³C-NMR (151 MHz, CDCl₃)



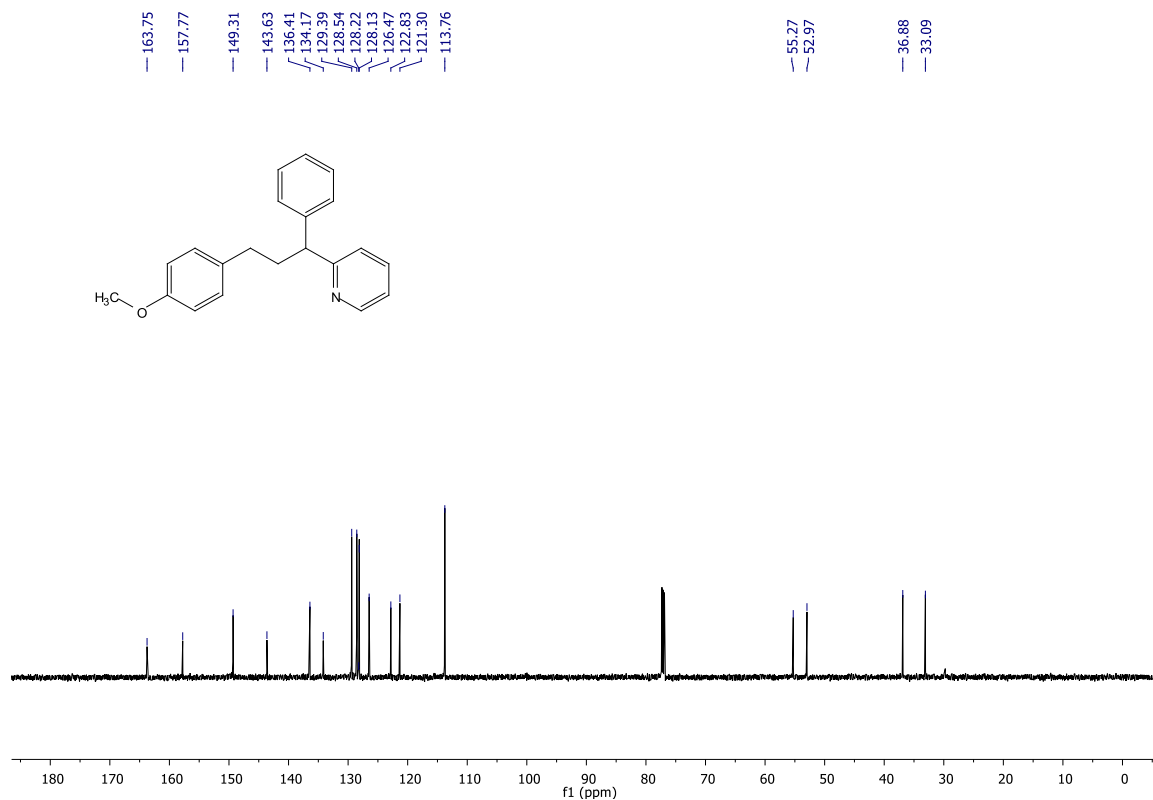
2-(3-(4-methoxyphenyl)propyl)pyridine (276) **$^1\text{H-NMR}$ (400 MHz, CDCl_3)** **$^{13}\text{C-NMR}$ (101 MHz, CDCl_3)**

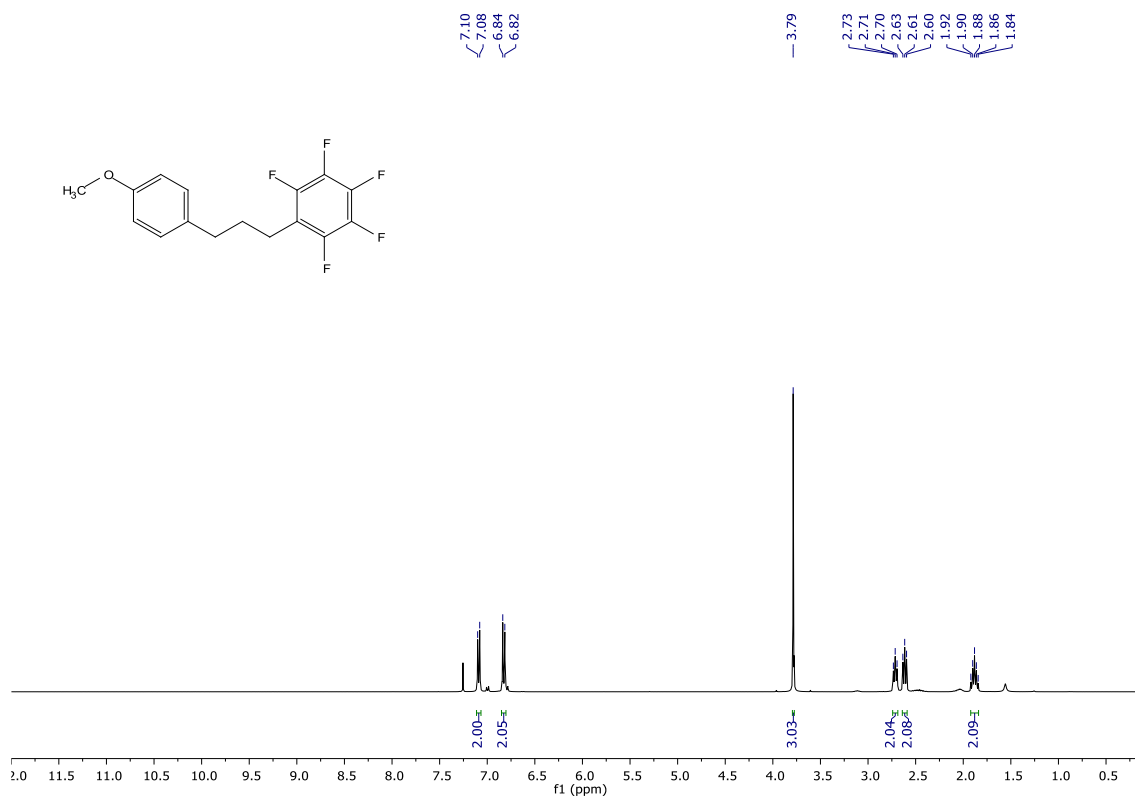
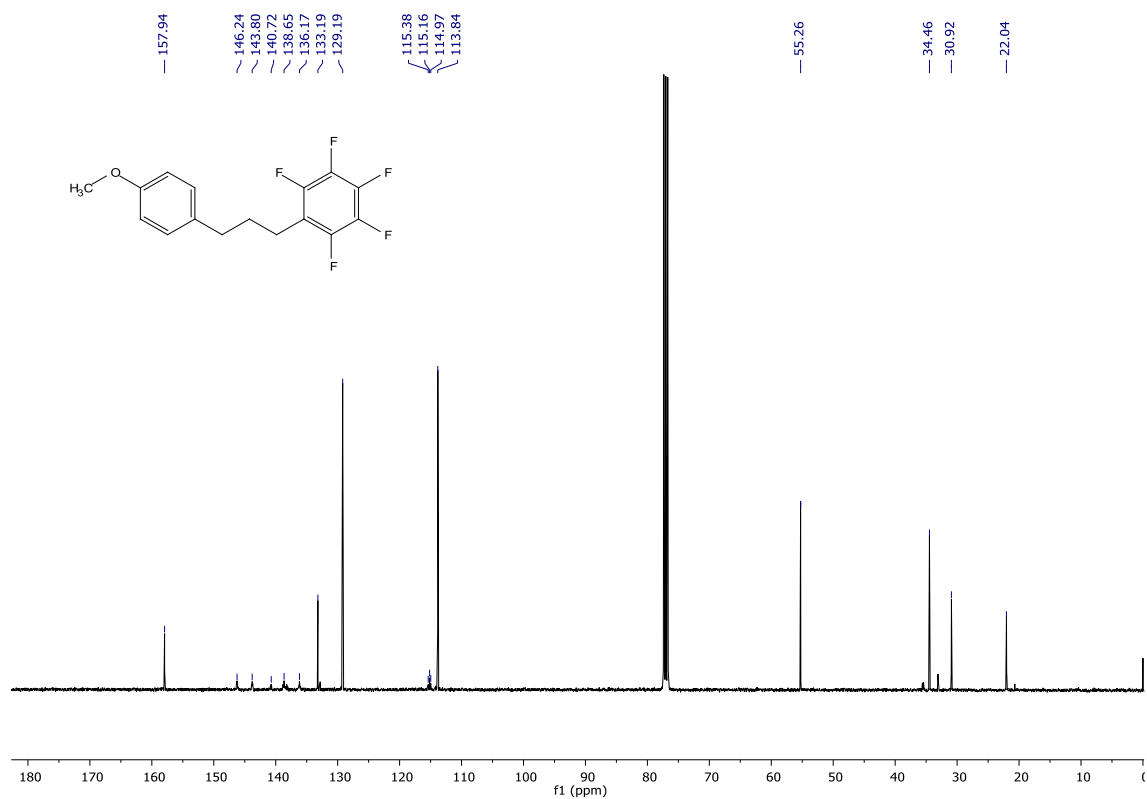
2-(3-(4-methoxyphenyl)-1-phenylpropyl)pyridine (277)

¹H-NMR (400 MHz, CDCl₃)



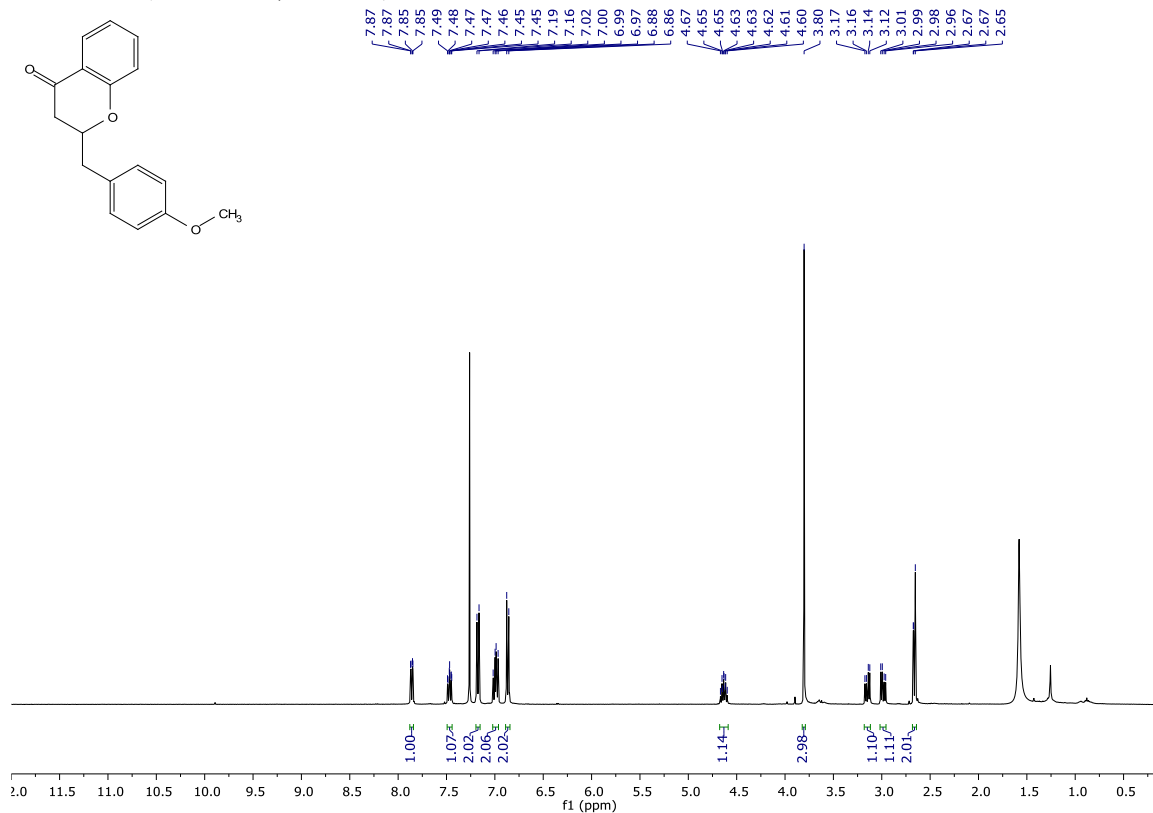
¹³C-NMR (101 MHz, CDCl₃)



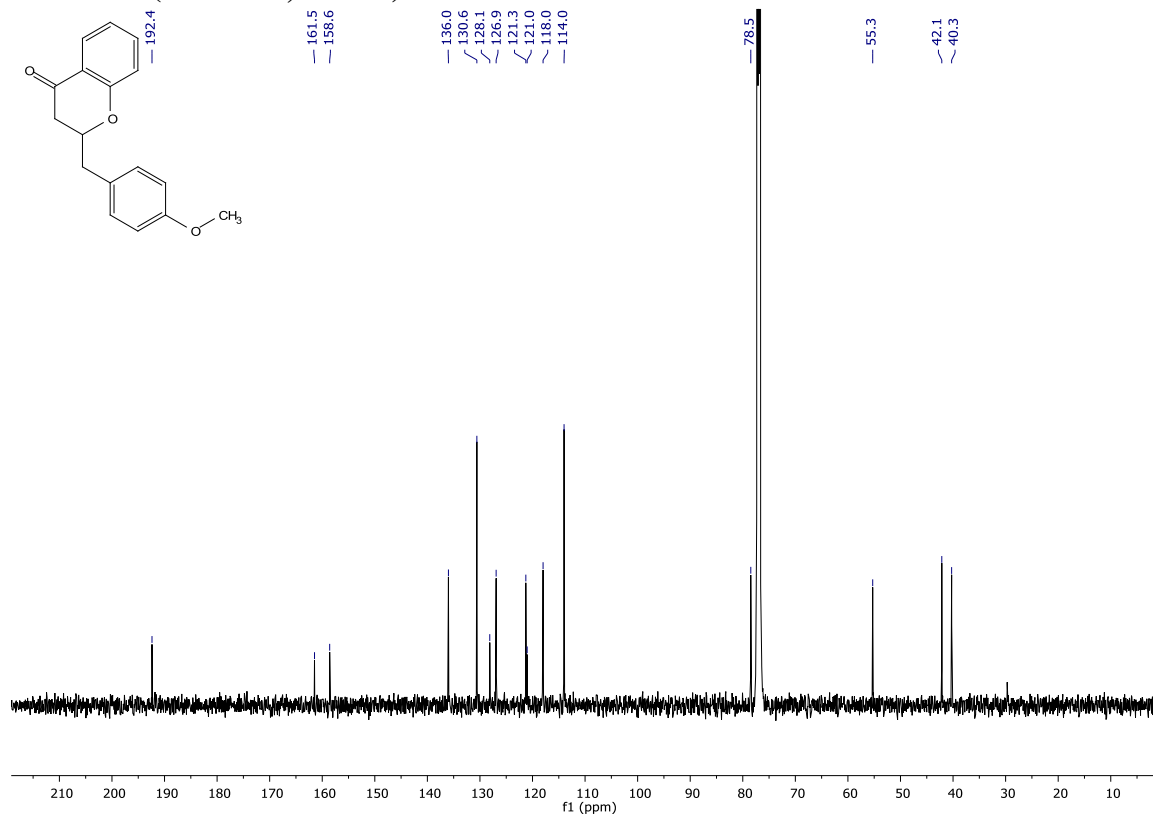
1,2,3,4,5-pentafluoro-6-(3-(4-methoxyphenyl)propyl)benzene (278) **$^1\text{H-NMR}$ (400 MHz, CDCl_3)** **$^{13}\text{C-NMR}$ (101 MHz, CDCl_3)**

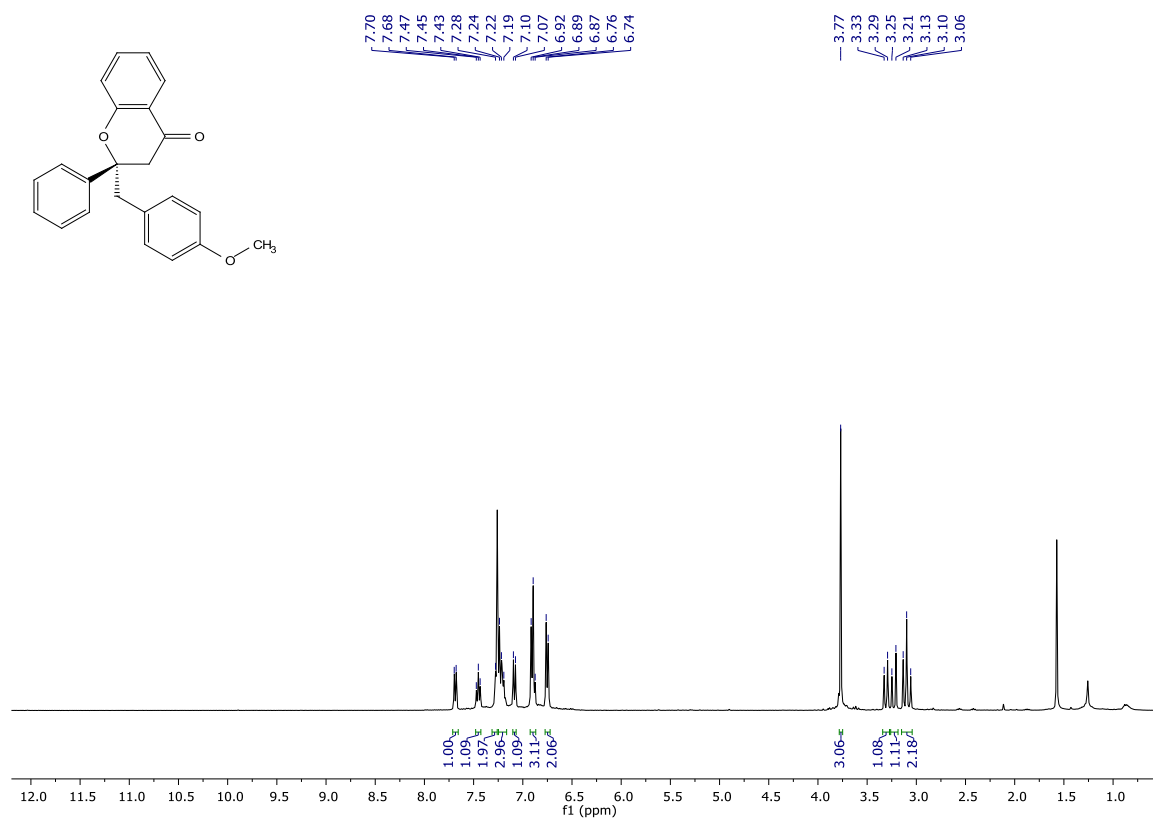
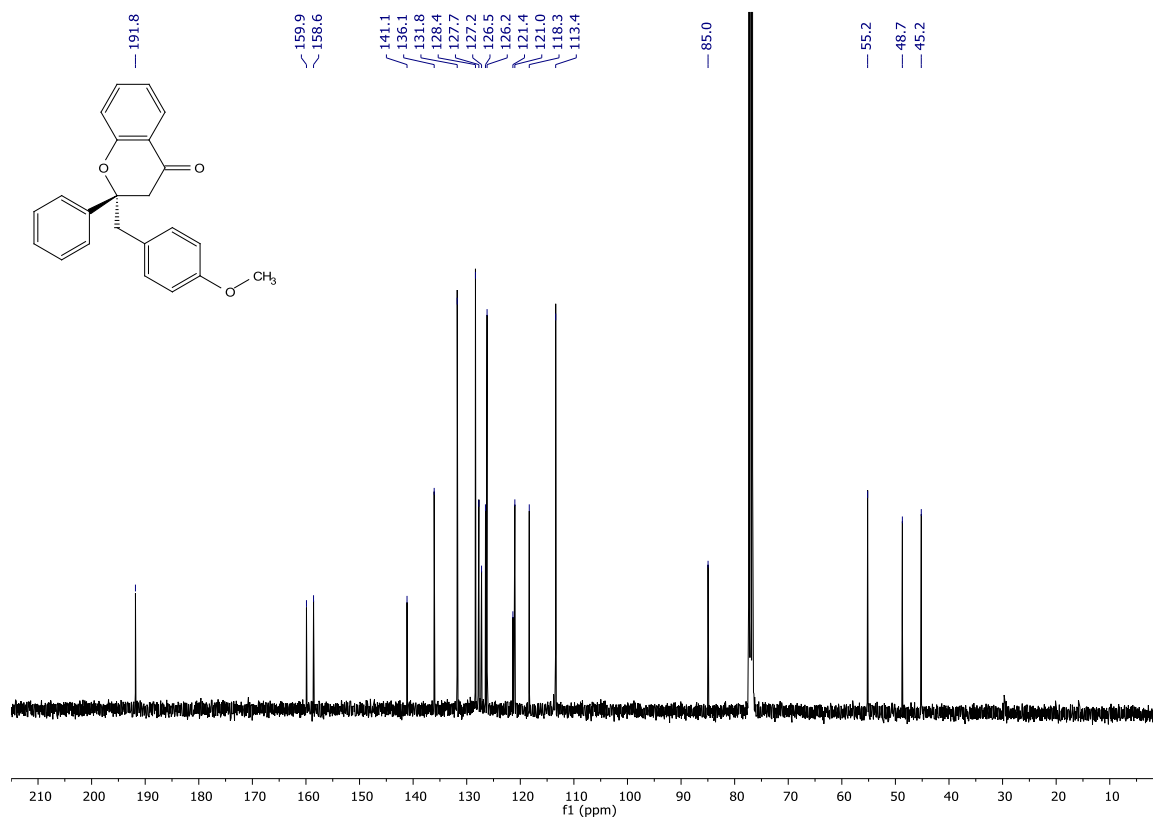
3-(4-methoxybenzyl) chroman-4-one (279)

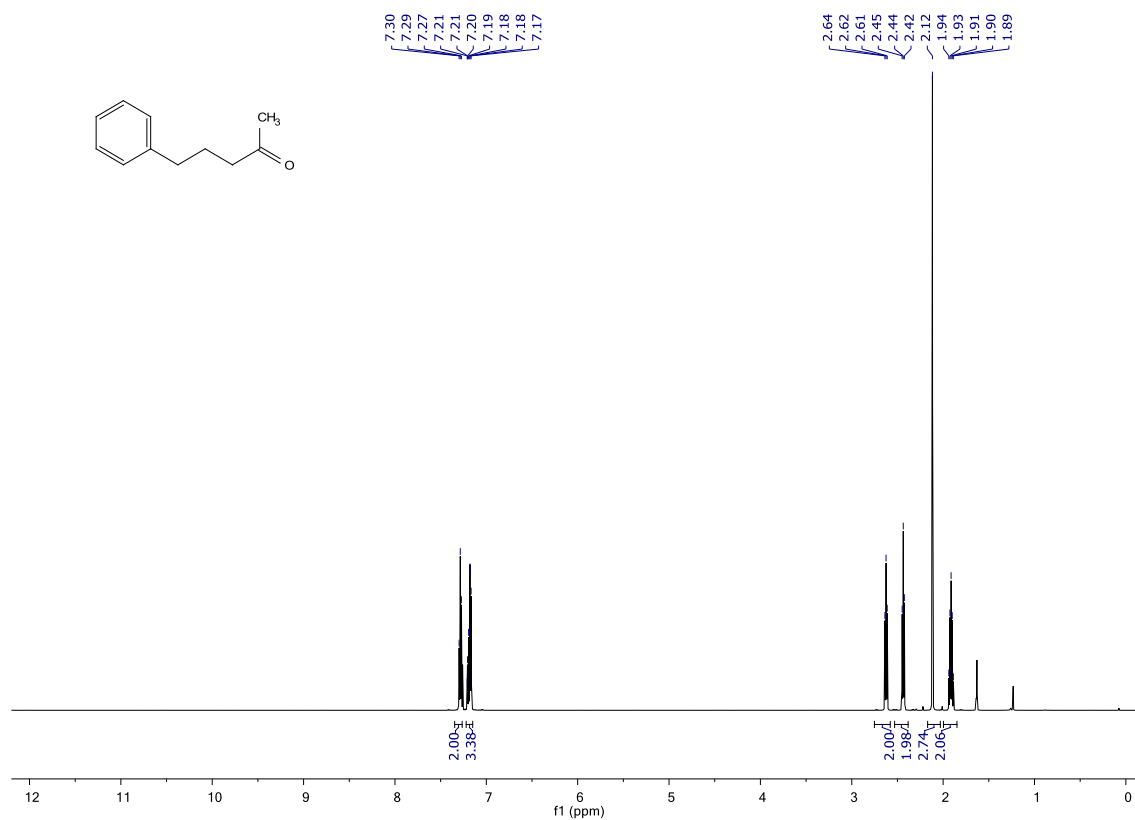
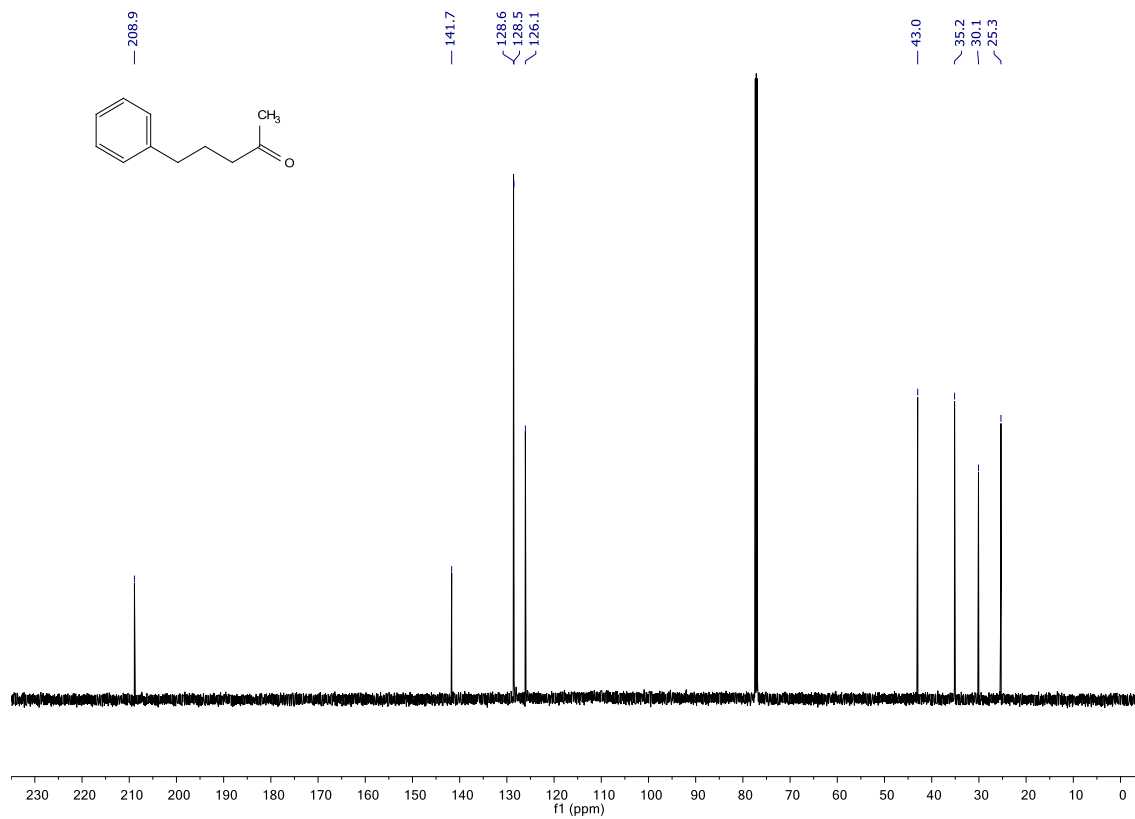
¹H-NMR (400 MHz, CDCl₃)



¹³C-NMR (101 MHz, CDCl₃)

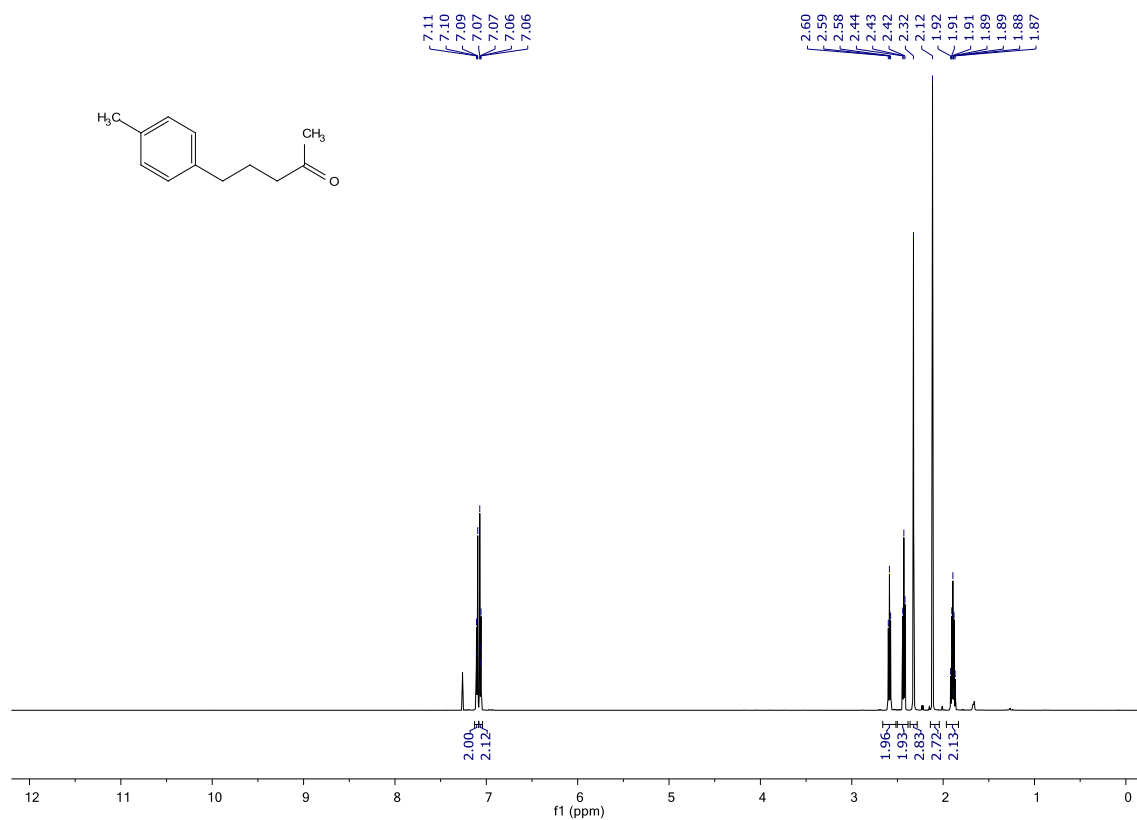


3-(4-methoxybenzyl)-2-phenylchroman-4-one (280)**¹H-NMR (400 MHz, CDCl₃)****¹³C-NMR (101 MHz, CDCl₃)**

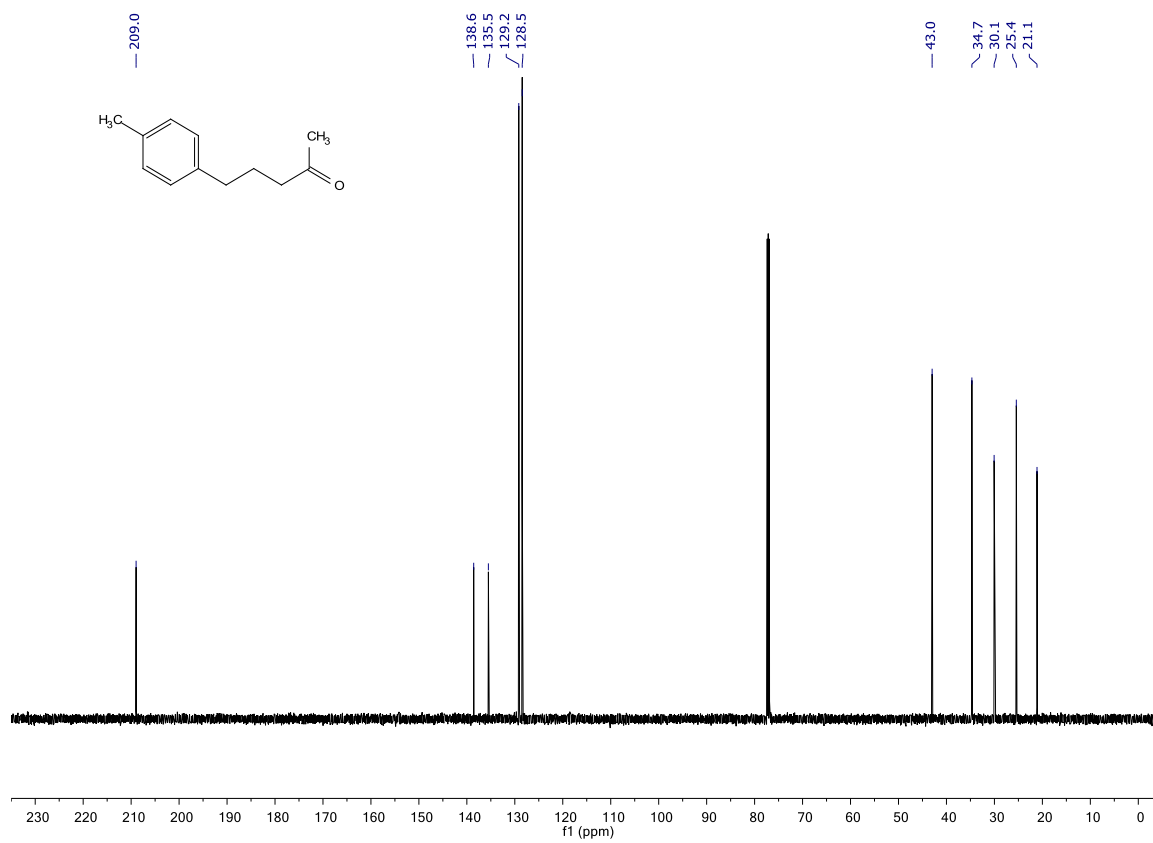
5-phenylpentan-2-one (285) **$^1\text{H-NMR}$ (600 MHz, CDCl_3)** **$^{13}\text{C-NMR}$ (151 MHz, CDCl_3)**

5-(*p*-tolyl)pentan-2-one (286)

¹H-NMR (600 MHz, CDCl₃)

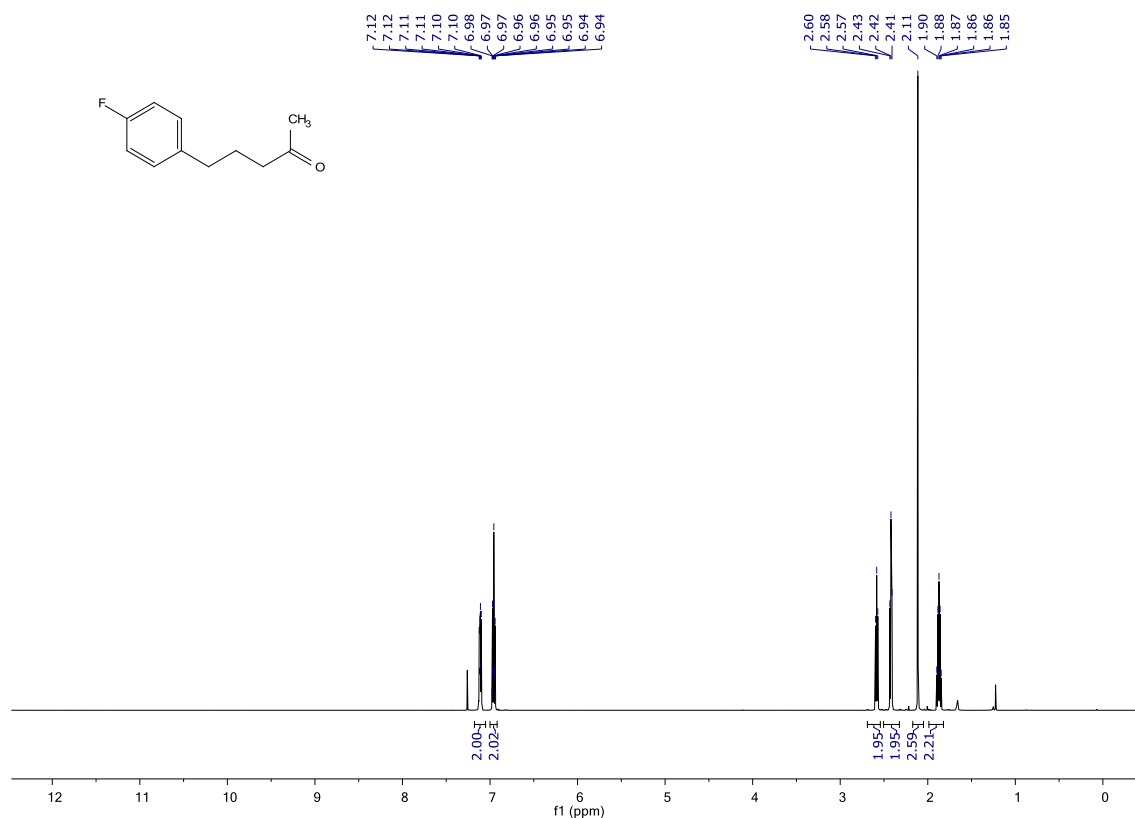


¹³C-NMR (151 MHz, CDCl₃)

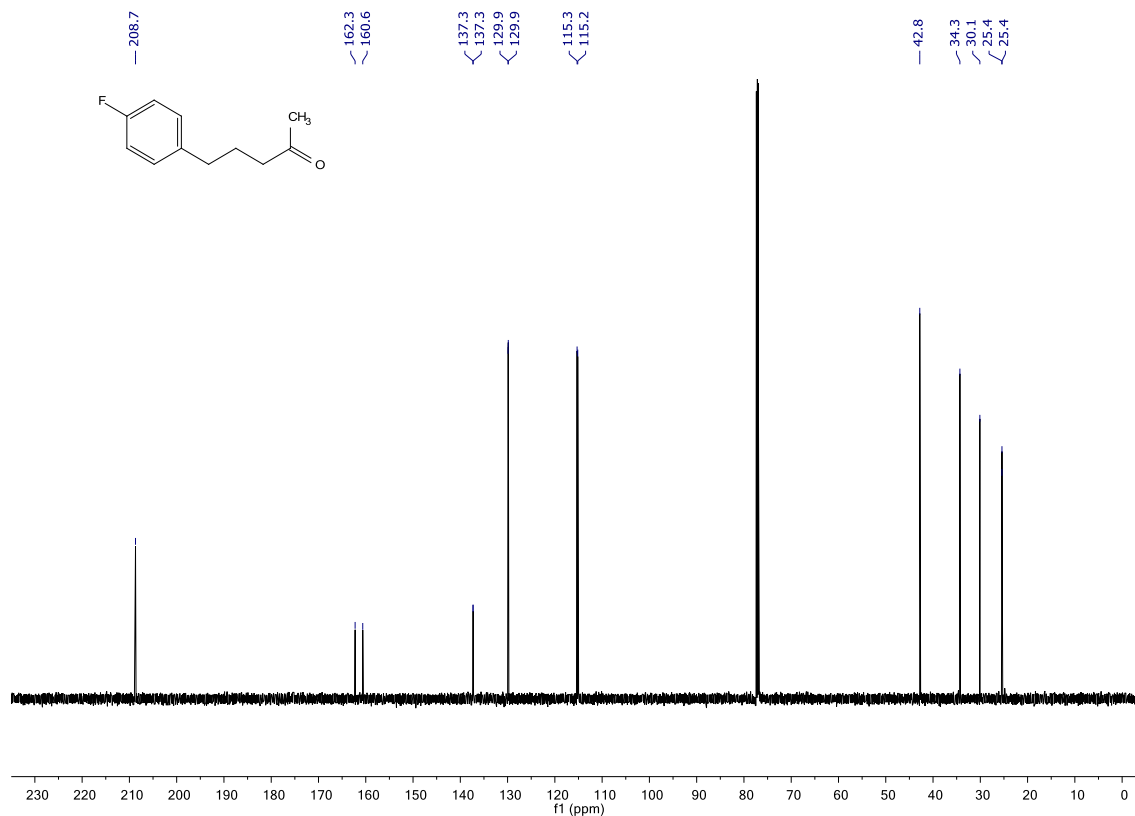


5-(4-fluorophenyl)pentan-2-one (287)

¹H-NMR (600 MHz, CDCl₃)

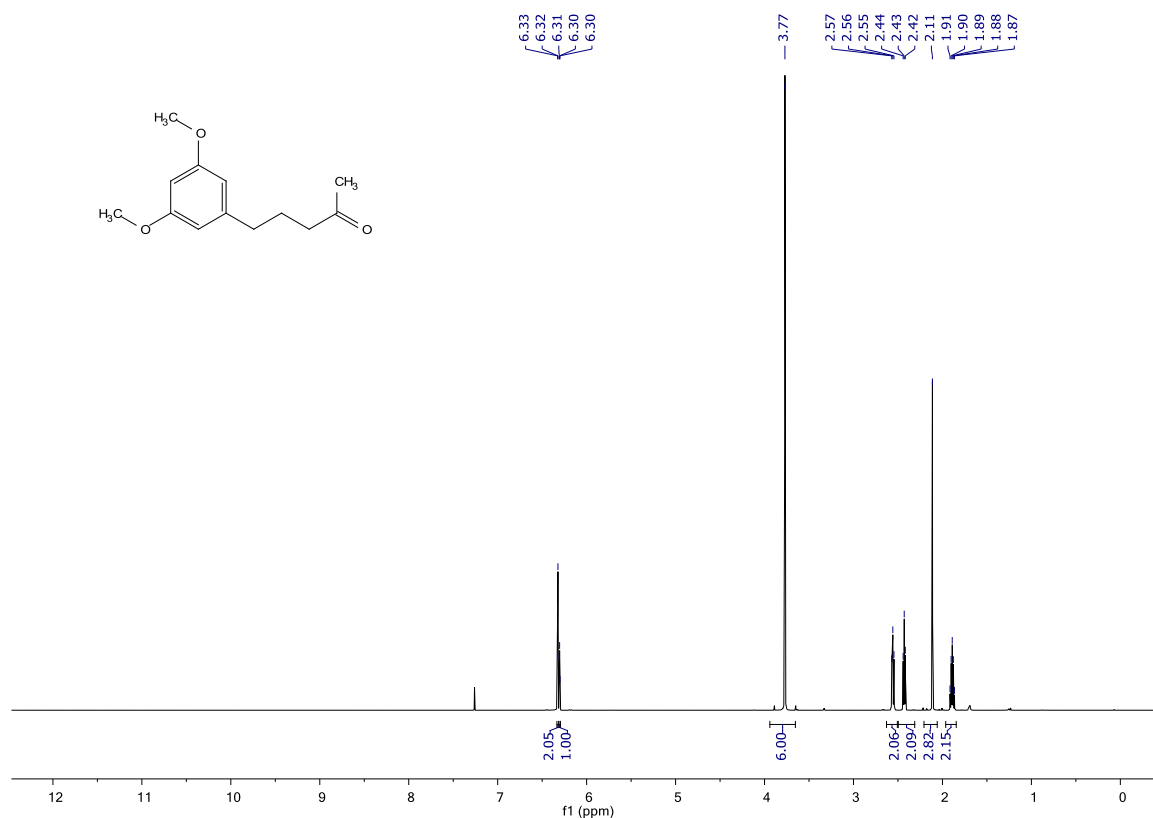


¹³C-NMR (151 MHz, CDCl₃)

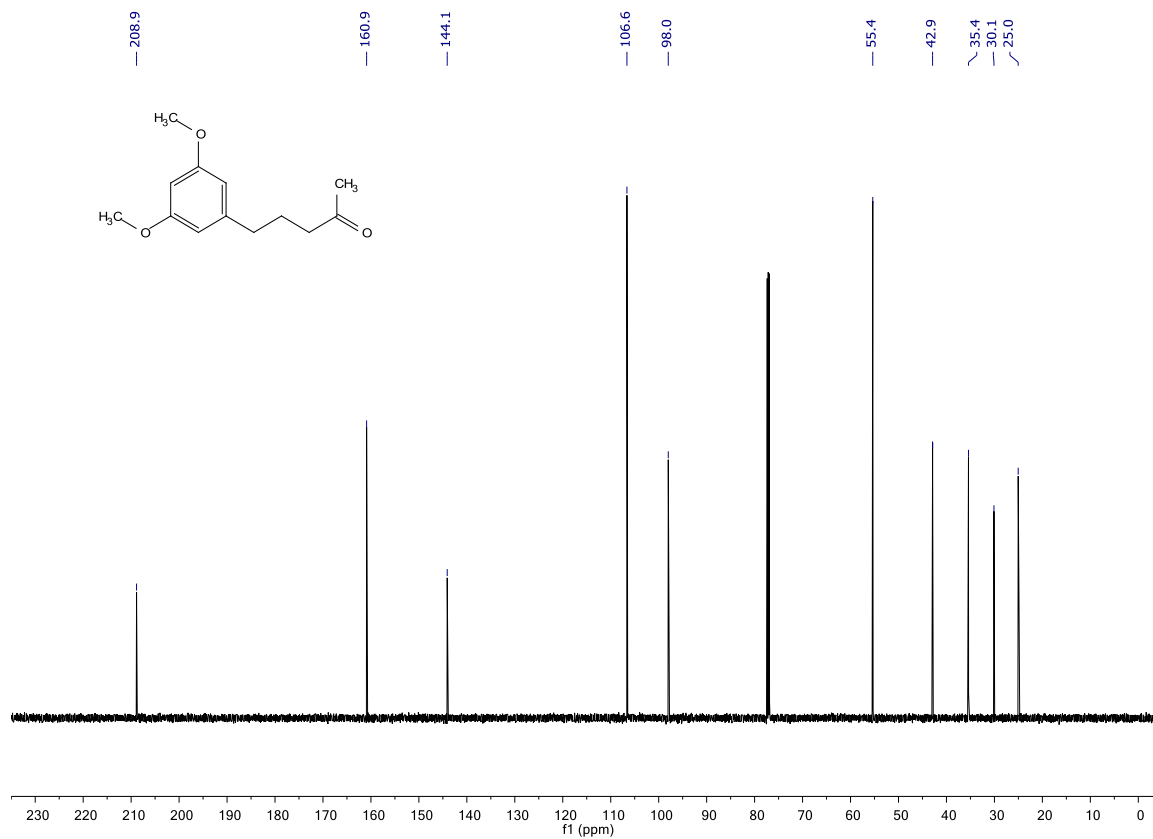


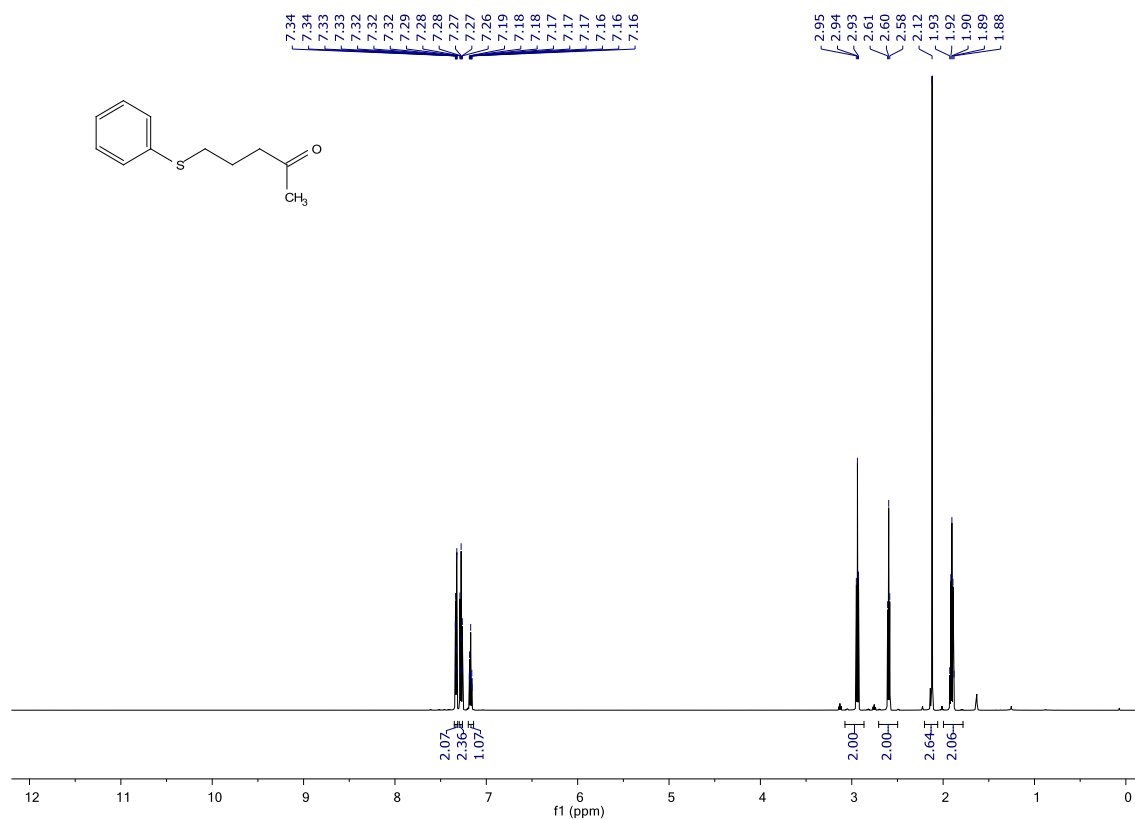
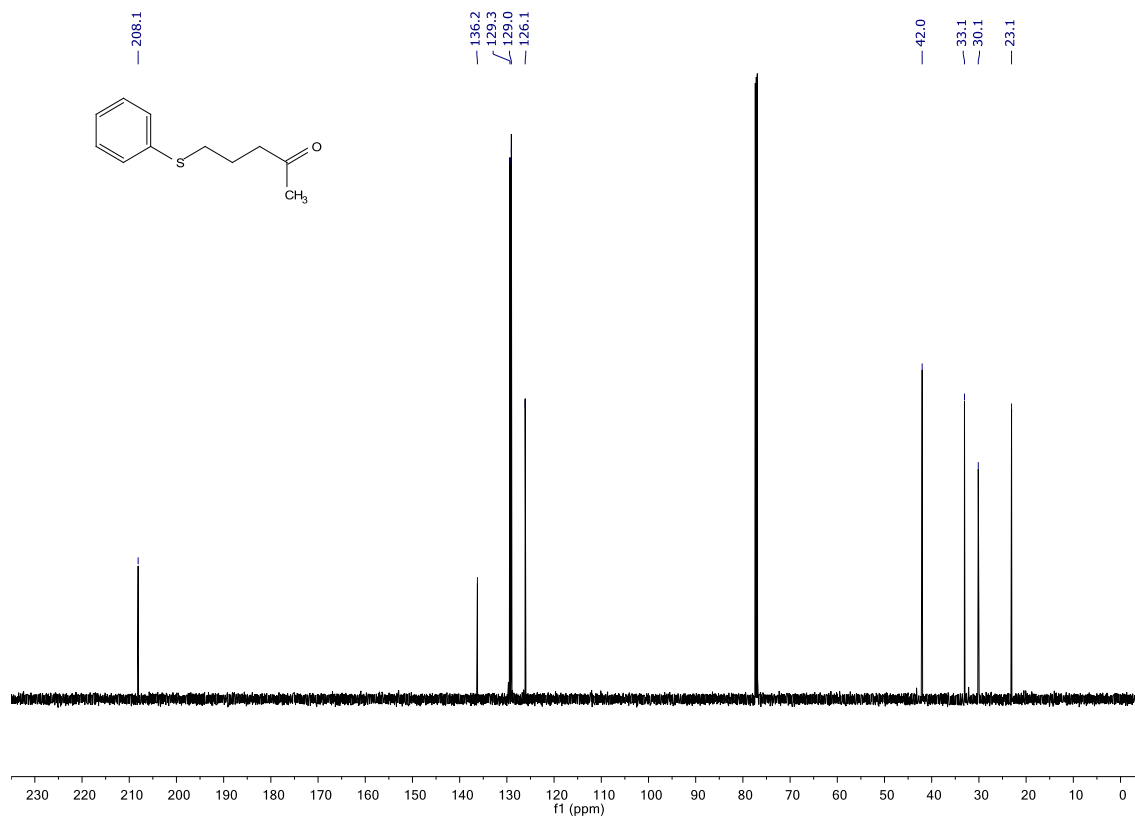
5-(3,5-dimethoxyphenyl)pentan-2-one (288)

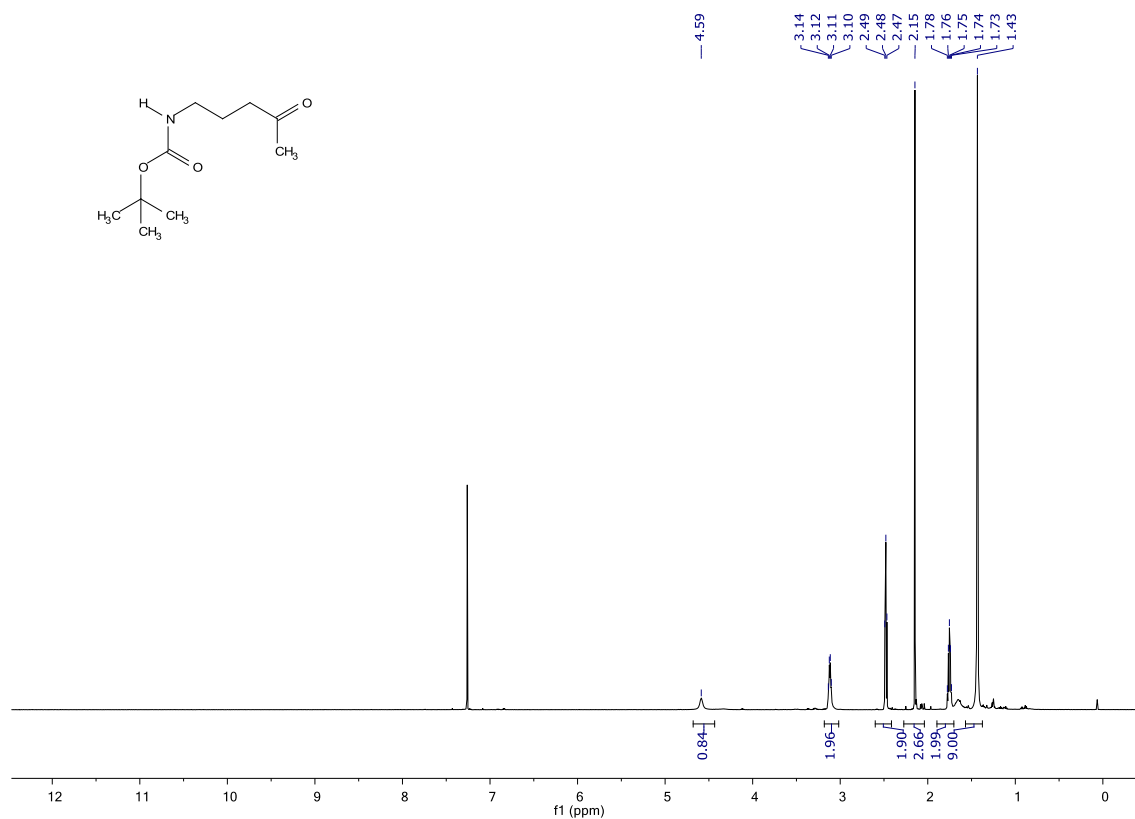
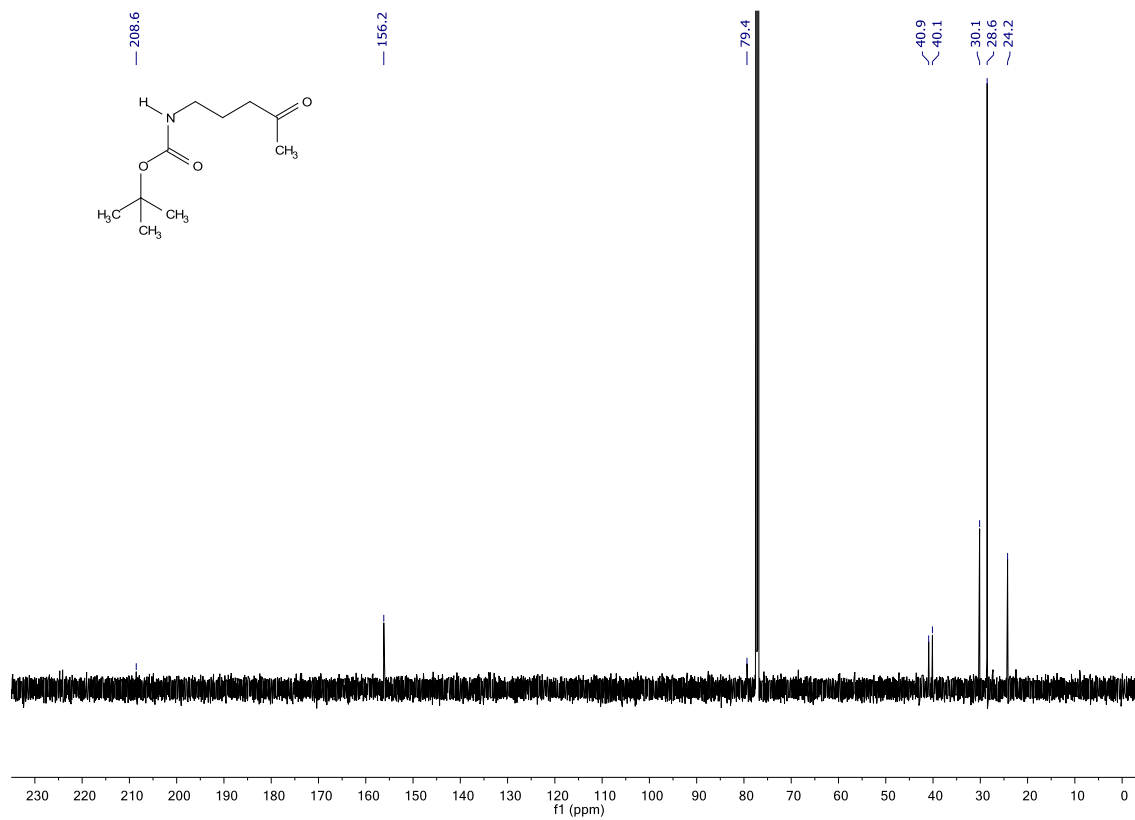
¹H-NMR (600 MHz, CDCl₃)



¹³C-NMR (151 MHz, CDCl₃)

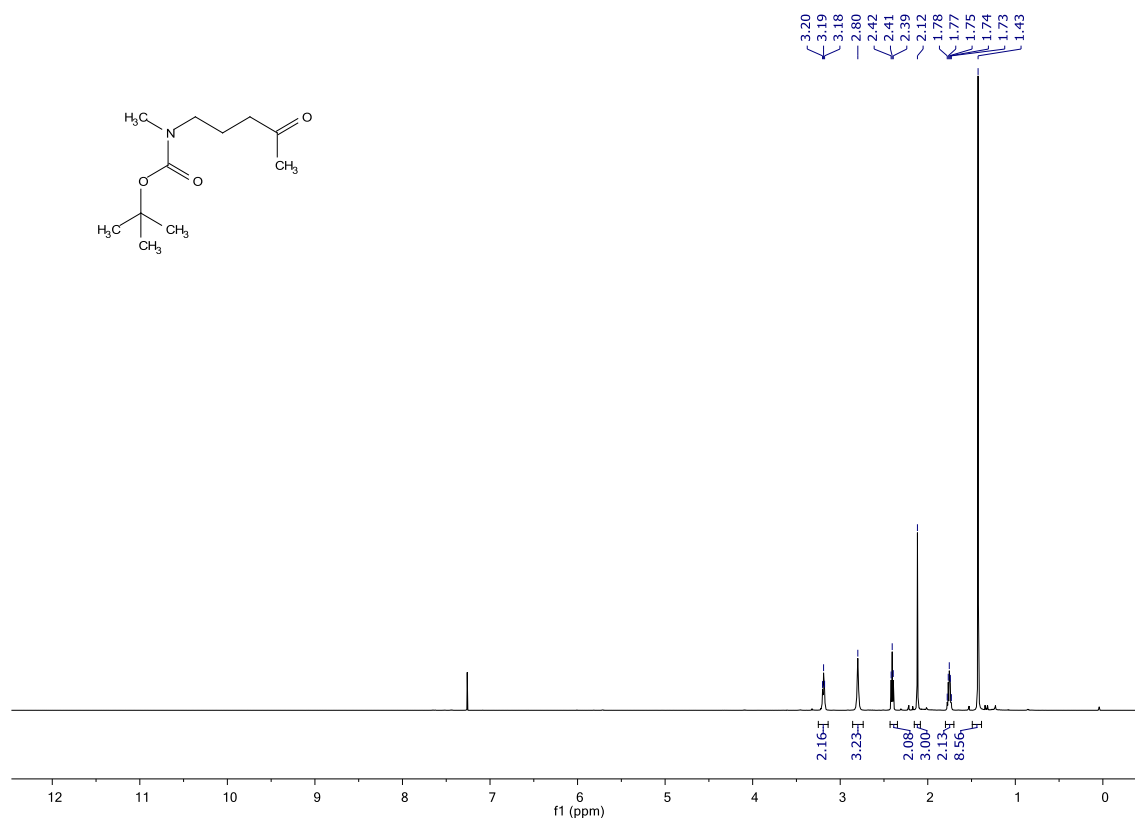


5-(phenylthio)pentan-2-one (289) **$^1\text{H-NMR}$ (600 MHz, CDCl_3)** **$^{13}\text{C-NMR}$ (151 MHz, CDCl_3)**

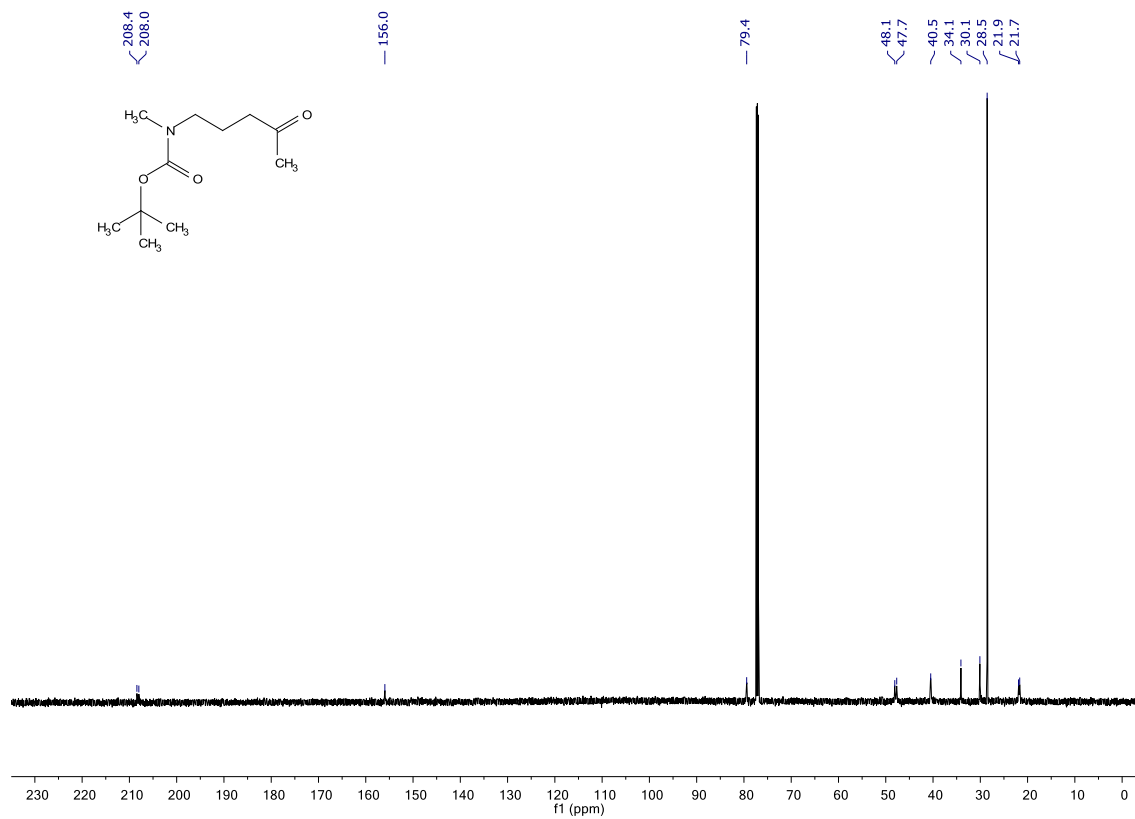
***tert*-butyl (4-oxopentyl)carbamate (290)** **$^1\text{H-NMR}$ (600 MHz, CDCl_3)** **$^{13}\text{C-NMR}$ (151 MHz, CDCl_3)**

***tert*-butyl methyl(4-oxopentyl)carbamate (291)**

¹H-NMR (600 MHz, CDCl₃)

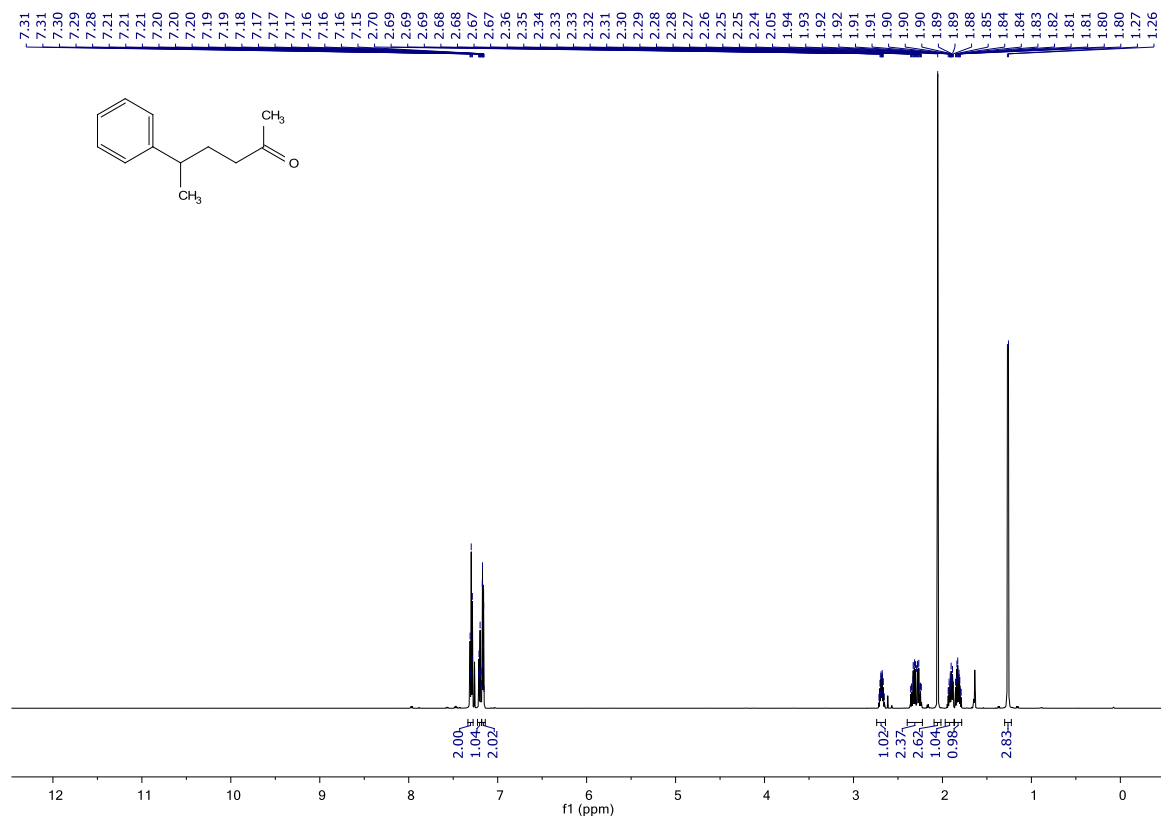


¹³C-NMR (151 MHz, CDCl₃)

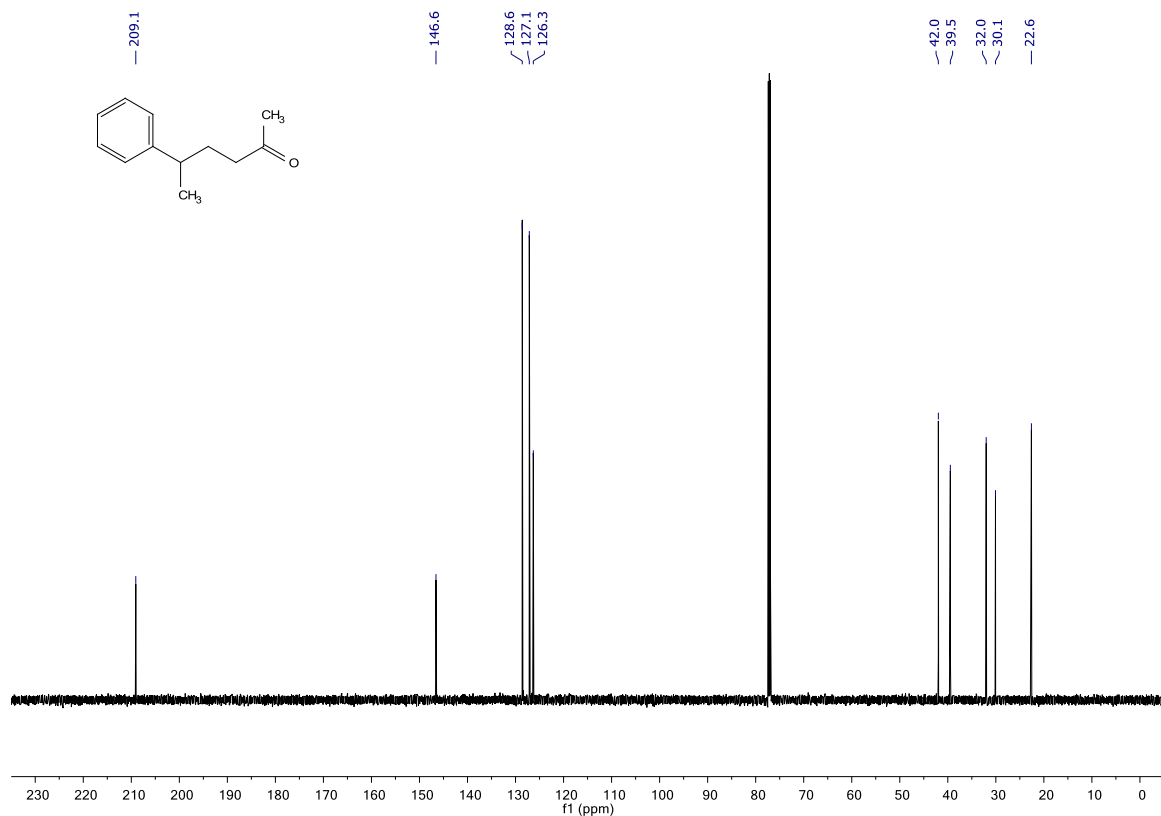


5-phenylhexan-2-one (292)

¹H-NMR (600 MHz, CDCl₃)

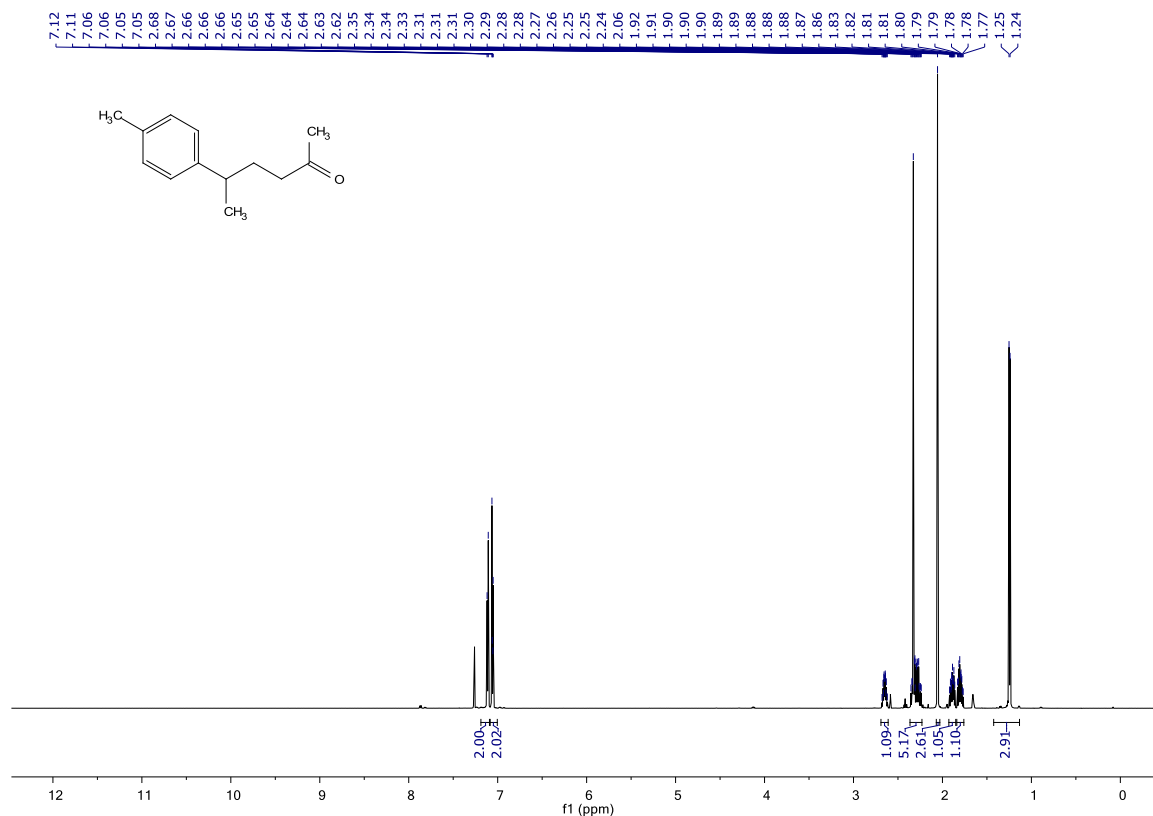


¹³C-NMR (151 MHz, CDCl₃)

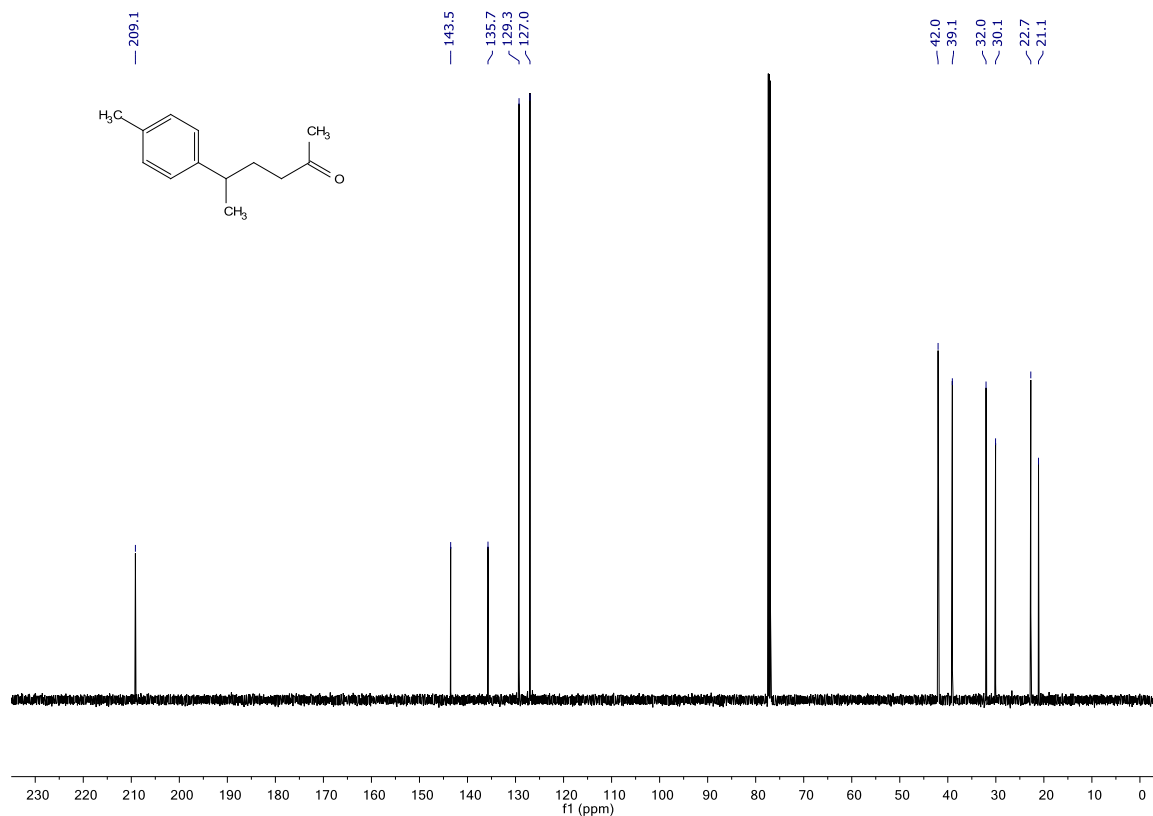


5-(*p*-tolyl)hexan-2-one (293)

¹H-NMR (600 MHz, CDCl₃)

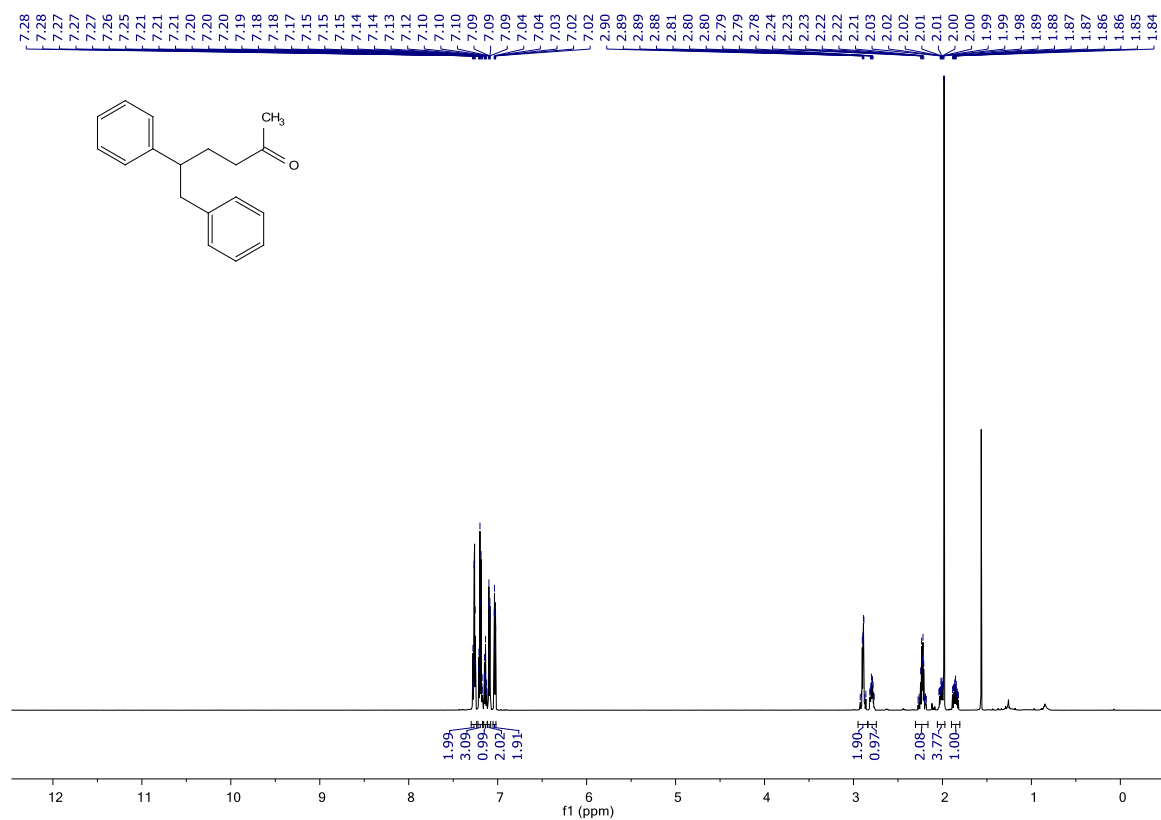


¹³C-NMR (151 MHz, CDCl₃)

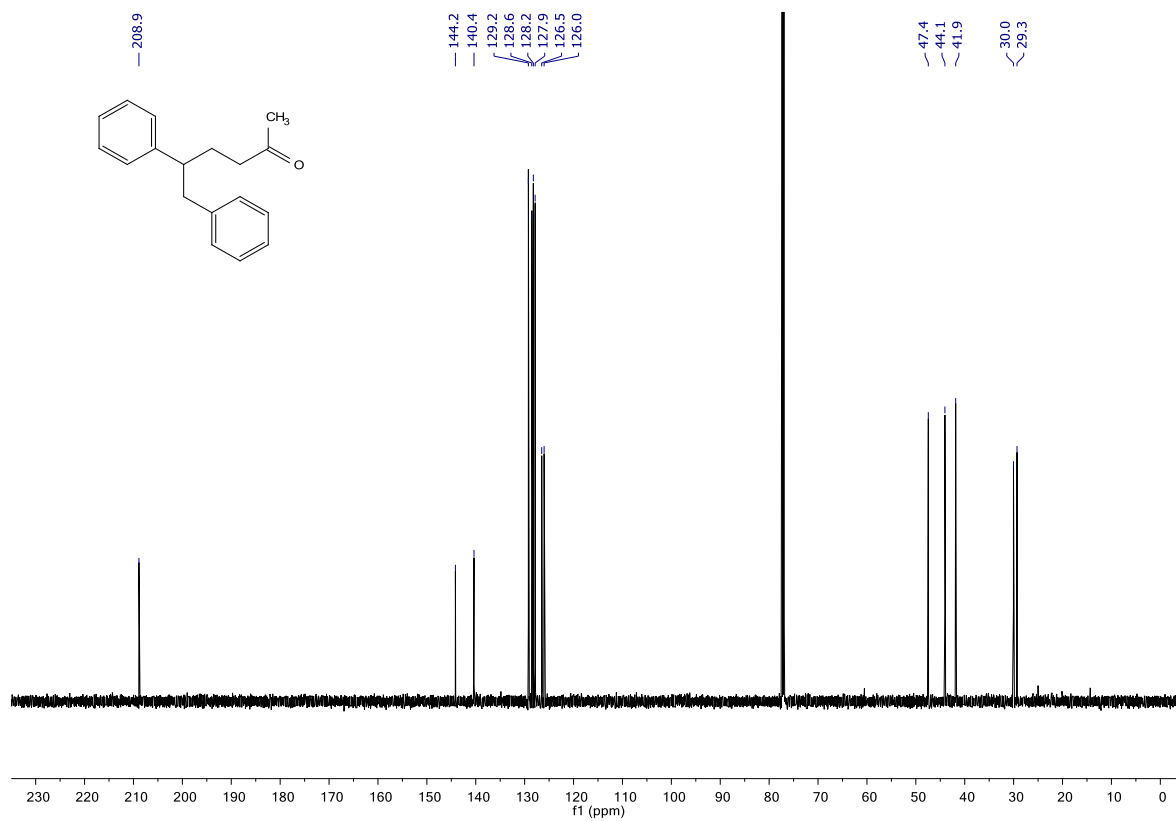


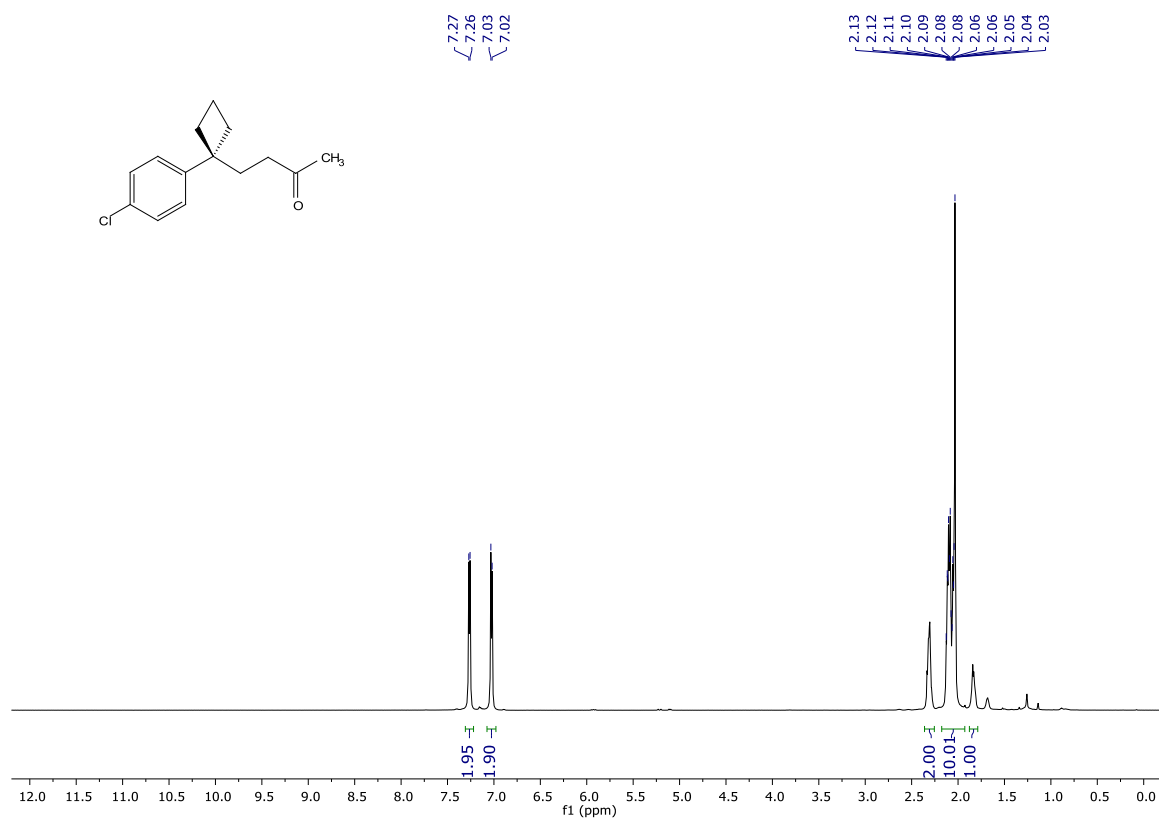
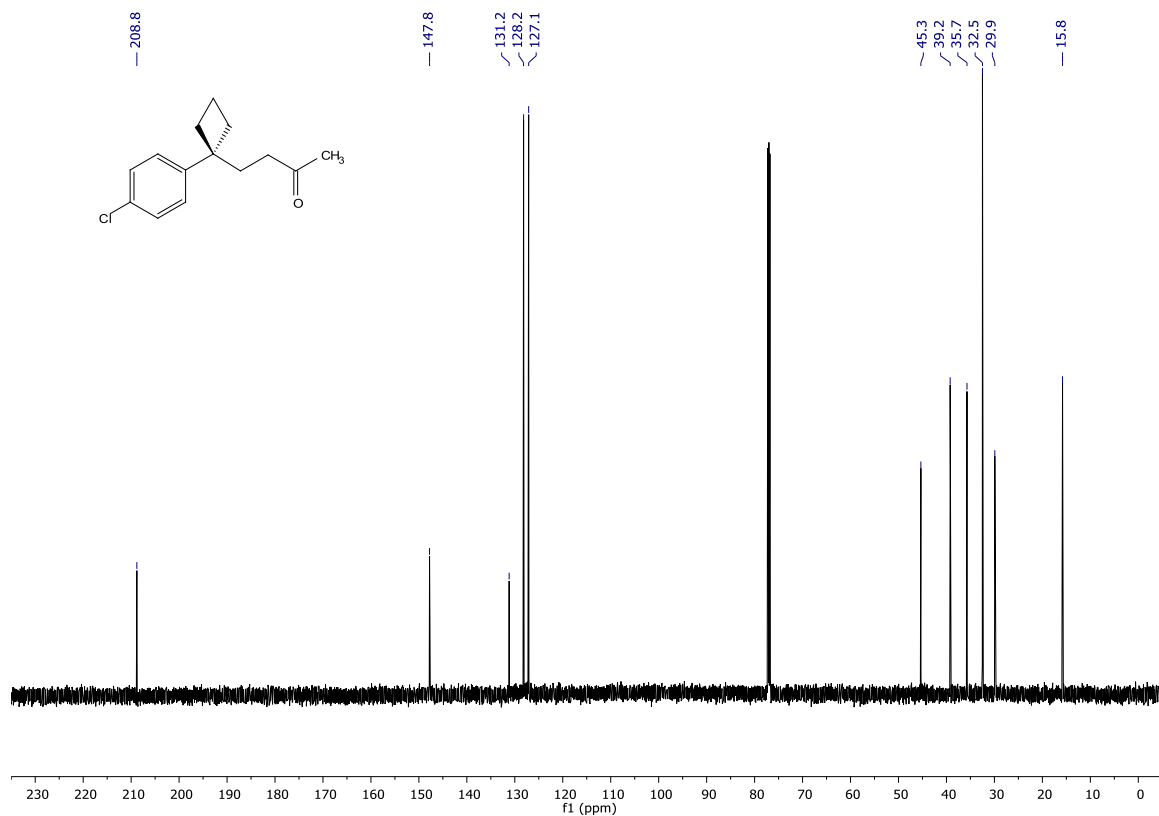
5,6-diphenylhexan-2-one (294)

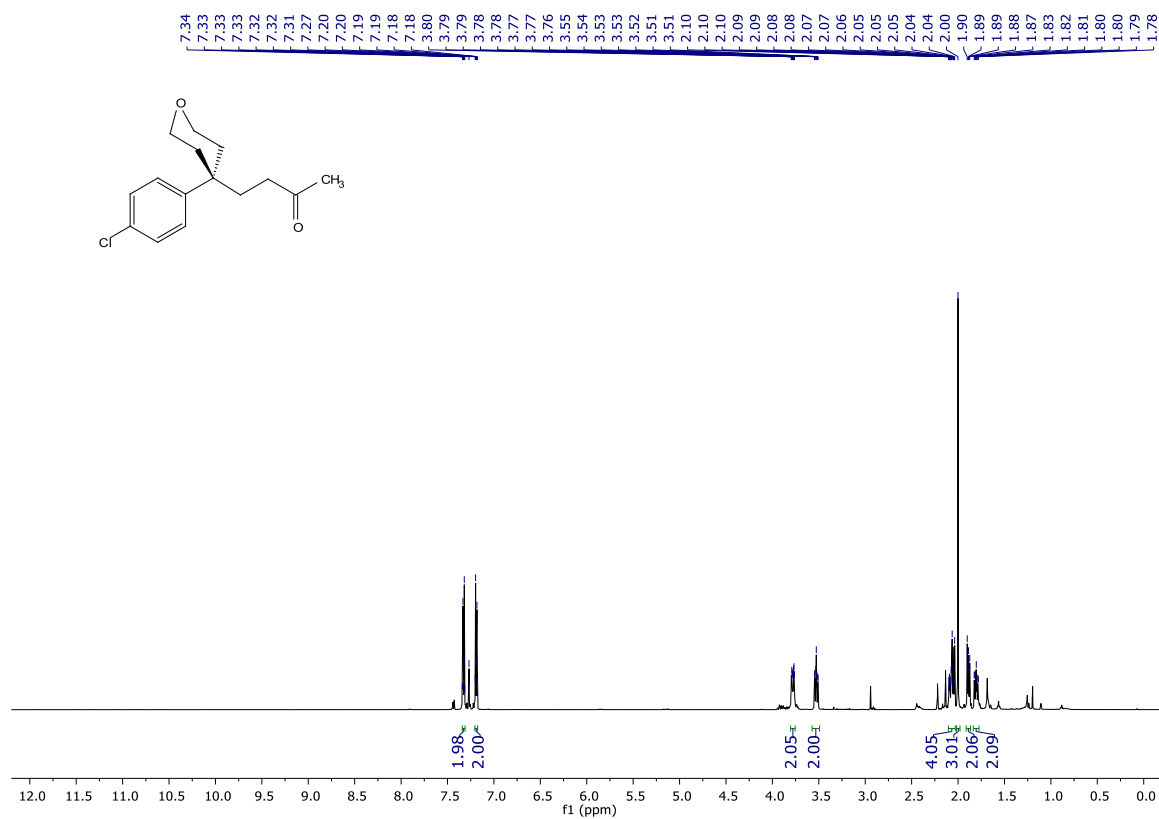
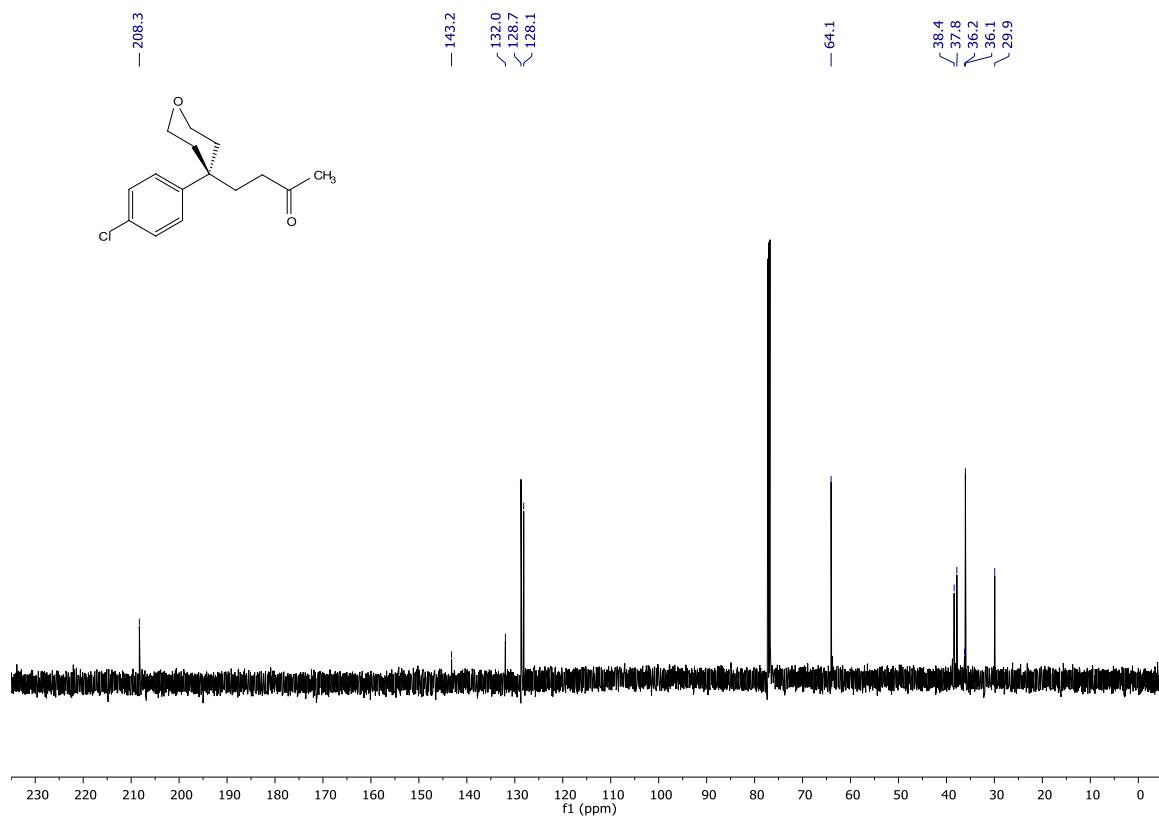
¹H-NMR (600 MHz, CDCl₃)

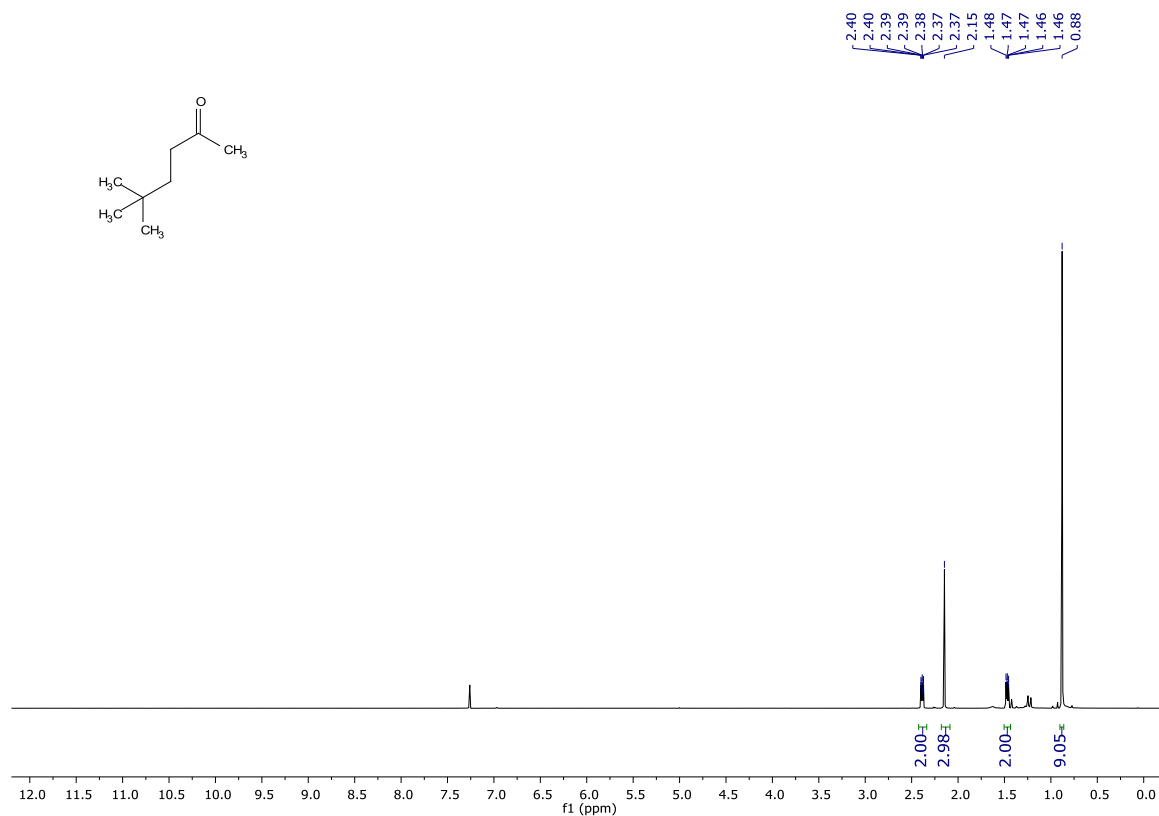
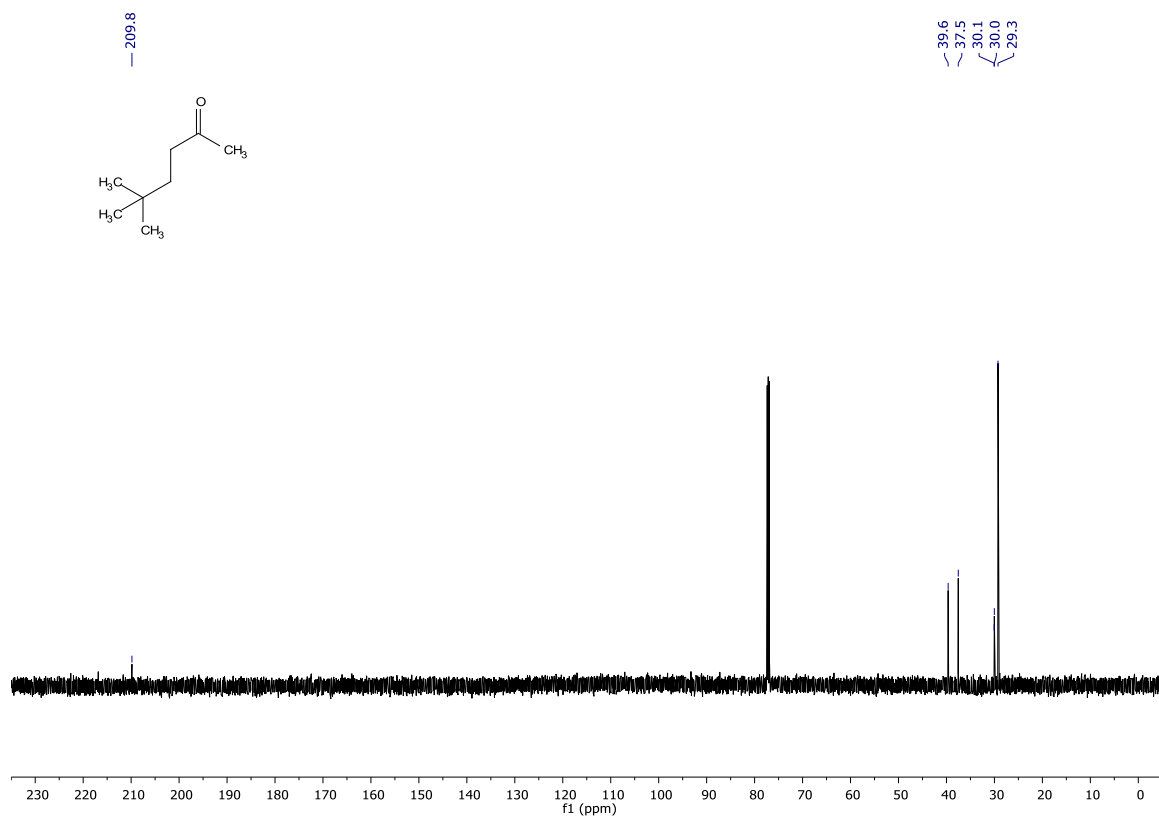


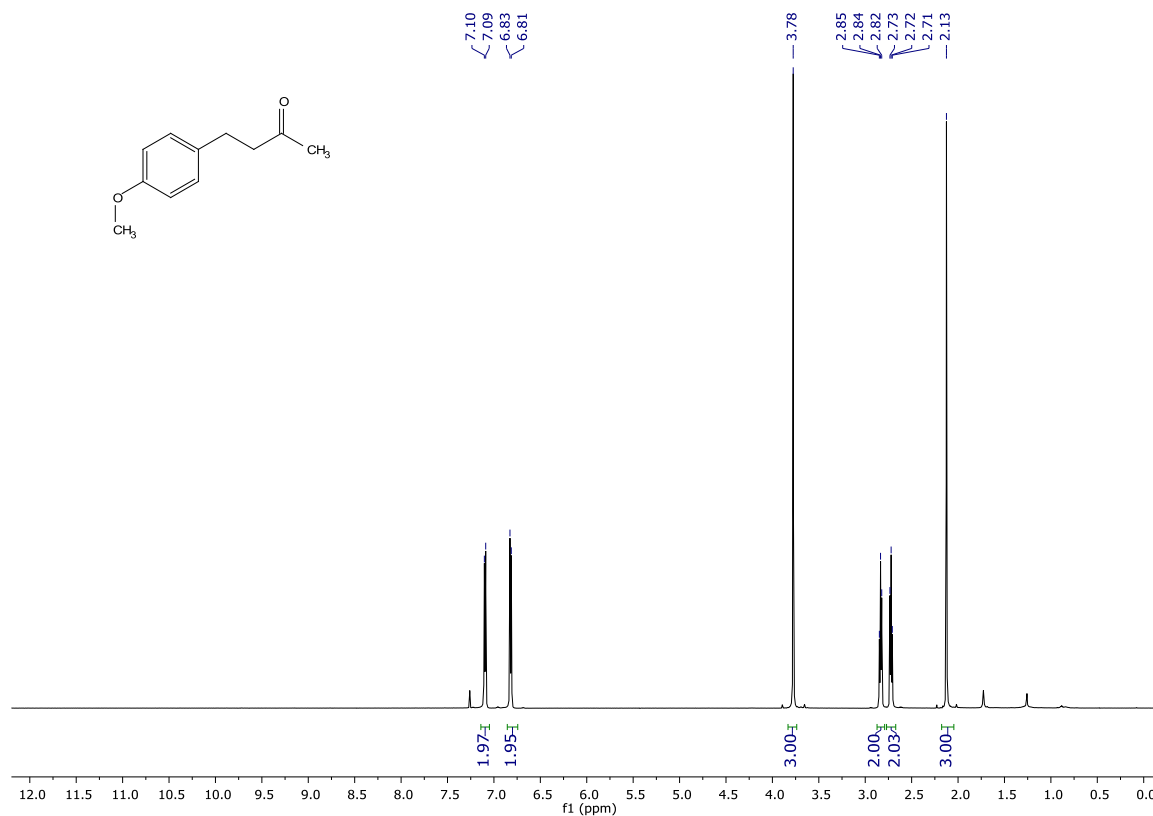
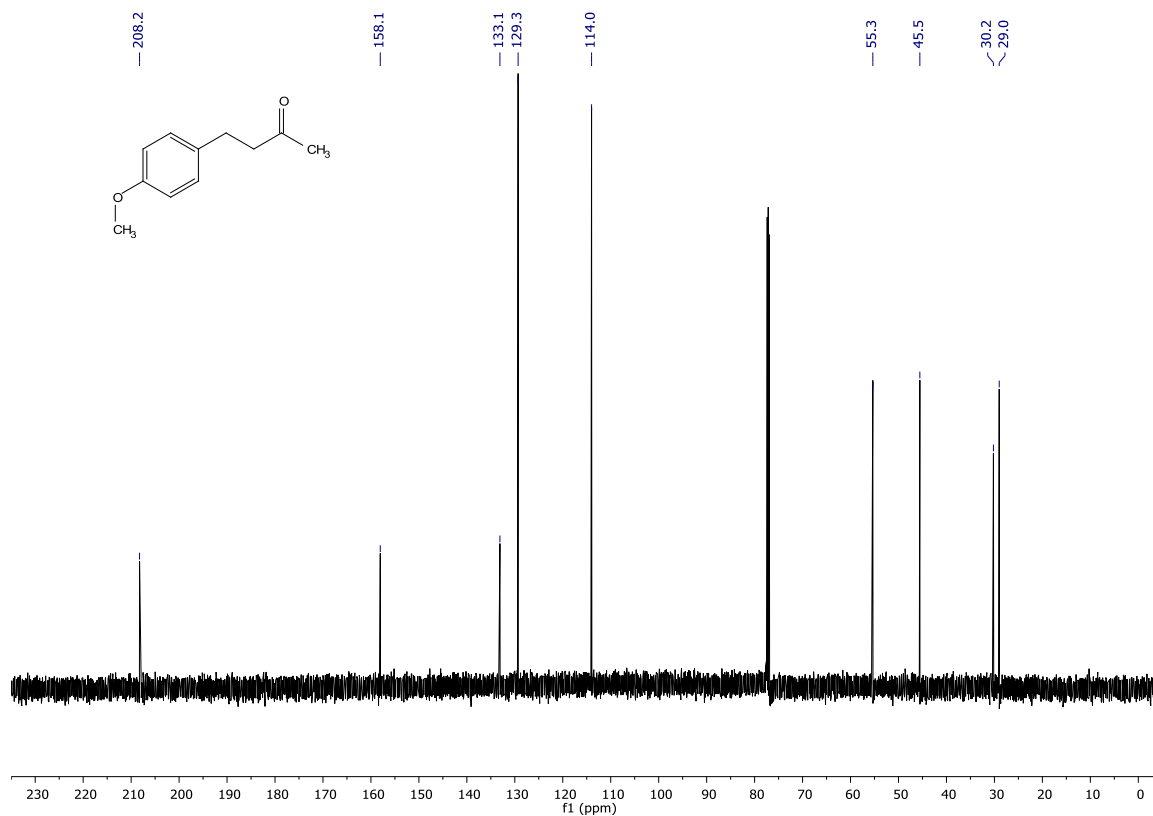
¹³C-NMR (151 MHz, CDCl₃)

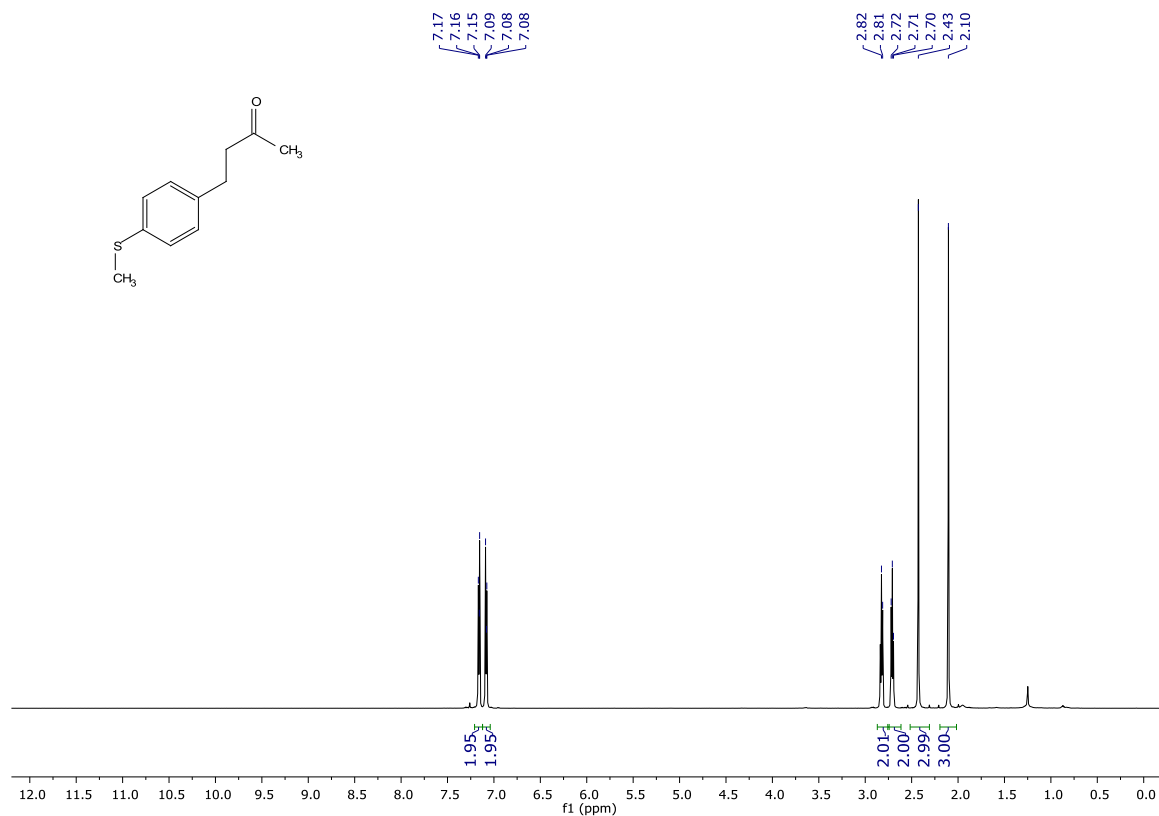
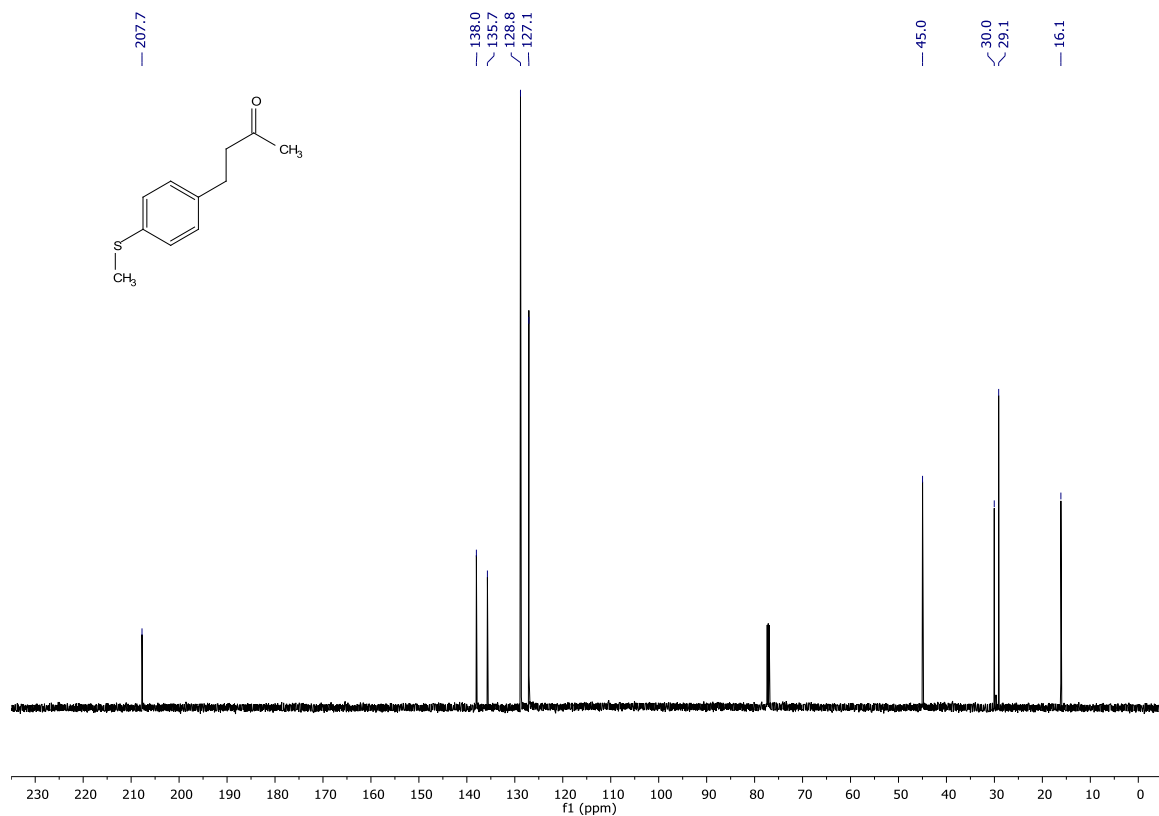


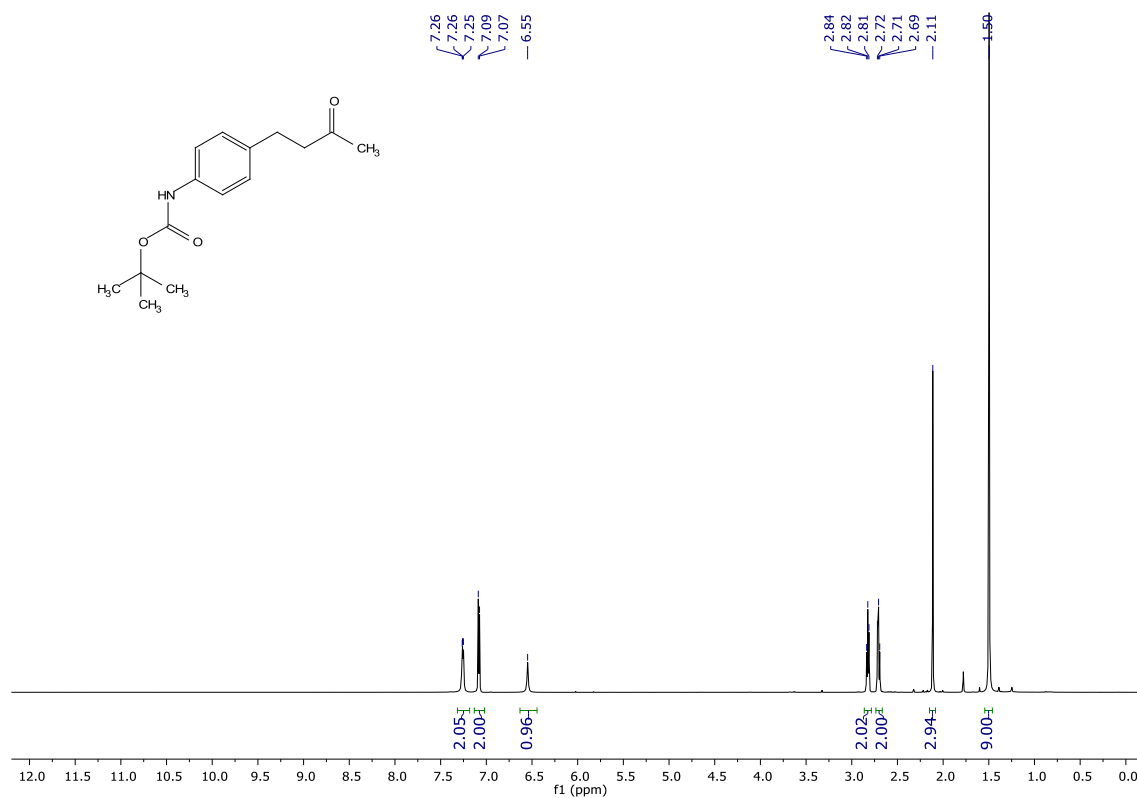
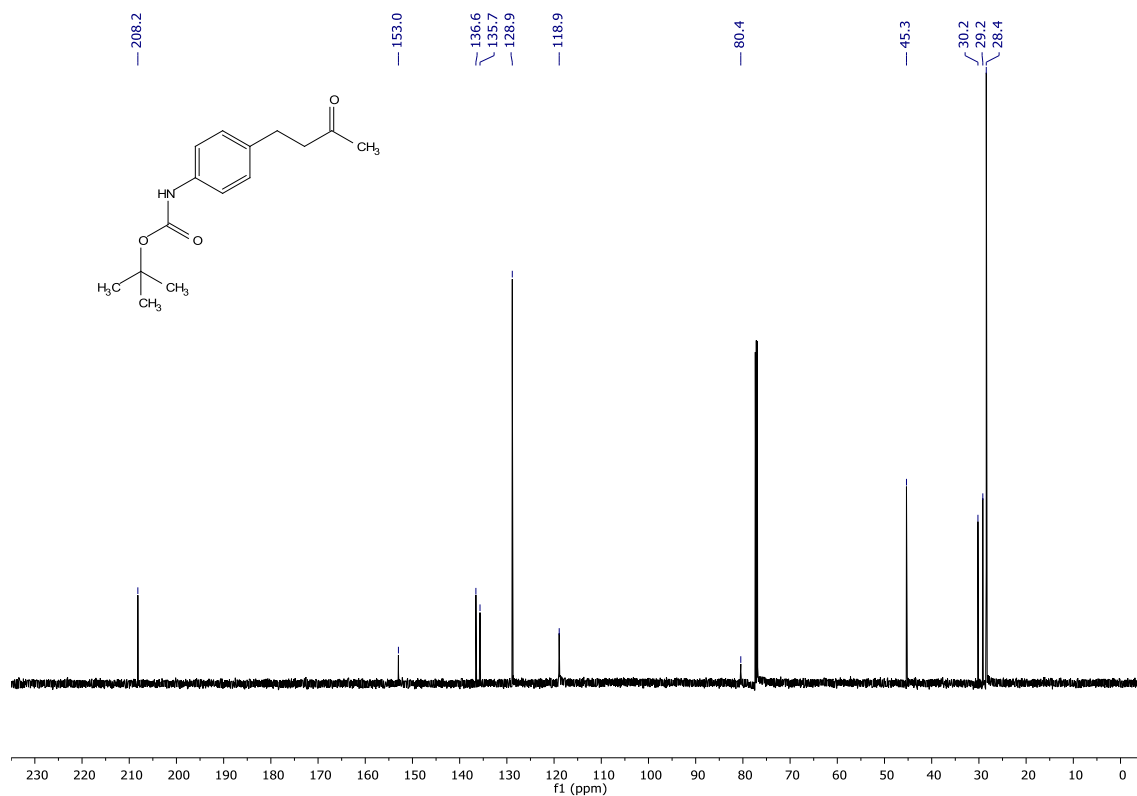
4-(1-(4-chlorophenyl)cyclobutyl)butan-2-one (297) **$^1\text{H-NMR}$ (600 MHz, CDCl_3)** **$^{13}\text{C-NMR}$ (151 MHz, CDCl_3)**

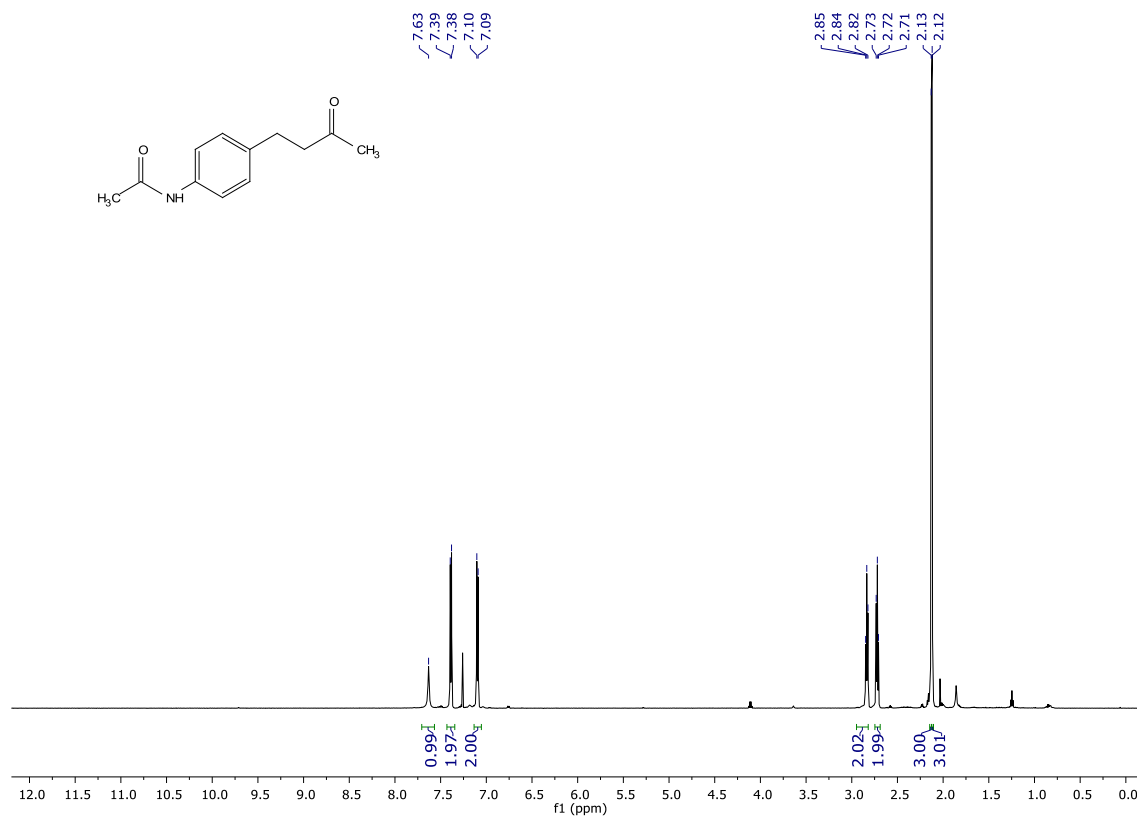
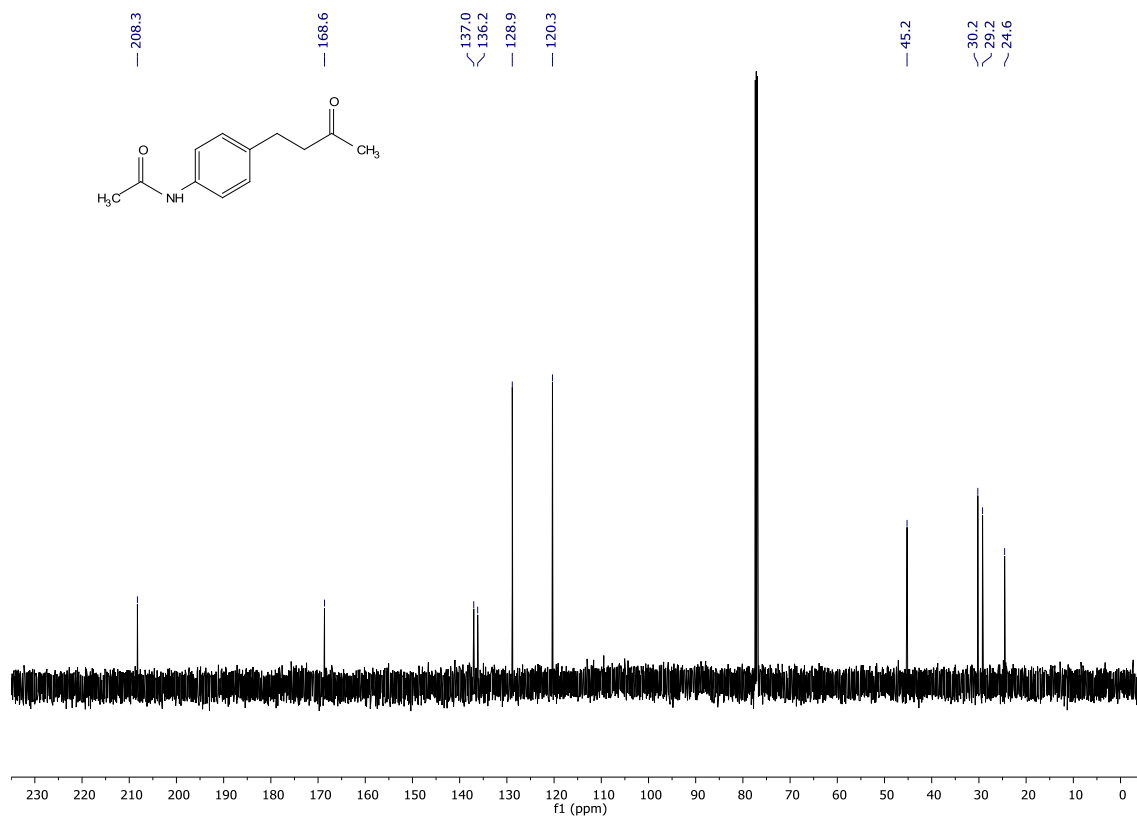
4-(4-(4-chlorophenyl)tetrahydro-2H-pyran-4-yl)butan-2-one (298) **$^1\text{H-NMR}$ (600 MHz, CDCl_3)** **$^{13}\text{C-NMR}$ (151 MHz, CDCl_3)**

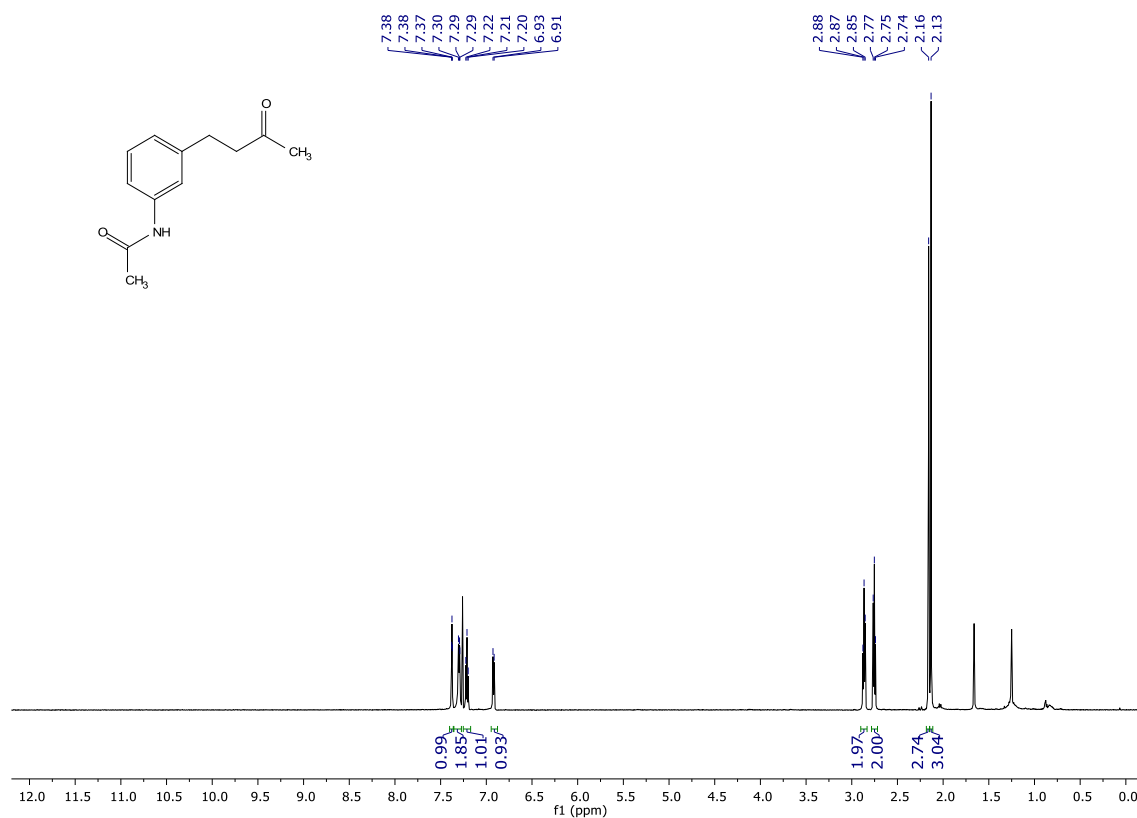
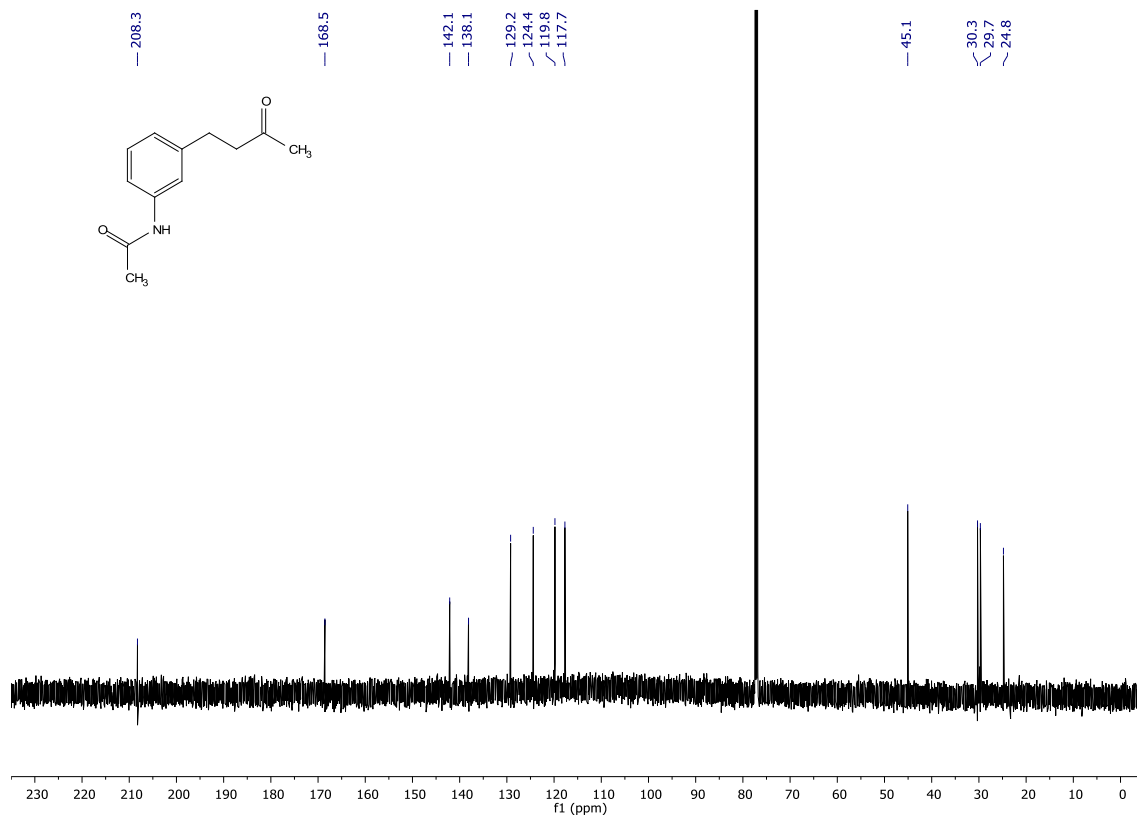
5,5-dimethylhexan-2-one (299) **$^1\text{H-NMR}$ (600 MHz, CDCl_3)** **$^{13}\text{C-NMR}$ (151 MHz, CDCl_3)**

4-(4-methoxyphenyl)butan-2-one (308) **$^1\text{H-NMR}$ (600 MHz, CDCl_3)** **$^{13}\text{C-NMR}$ (151 MHz, CDCl_3)**

4-(4-(methylthio)phenyl)butan-2-one (309) **$^1\text{H-NMR}$ (600 MHz, CDCl_3)** **$^{13}\text{C-NMR}$ (151 MHz, CDCl_3)**

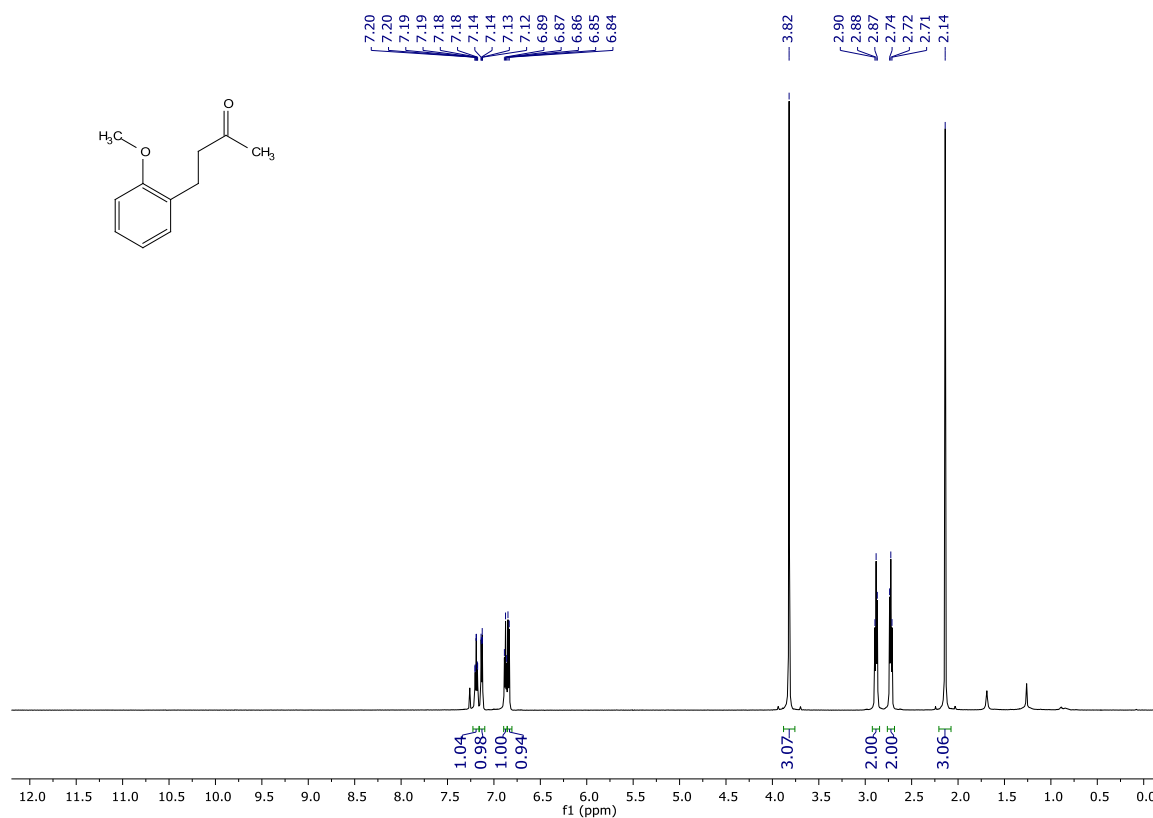
***tert*-butyl (4-(3-oxobutyl)phenyl)carbamate (310)** **$^1\text{H-NMR}$ (600 MHz, CDCl_3)** **$^{13}\text{C-NMR}$ (151 MHz, CDCl_3)**

N-(4-(3-oxobutyl)phenyl)acetamide (311) **$^1\text{H-NMR}$ (600 MHz, CDCl_3)** **$^{13}\text{C-NMR}$ (151 MHz, CDCl_3)**

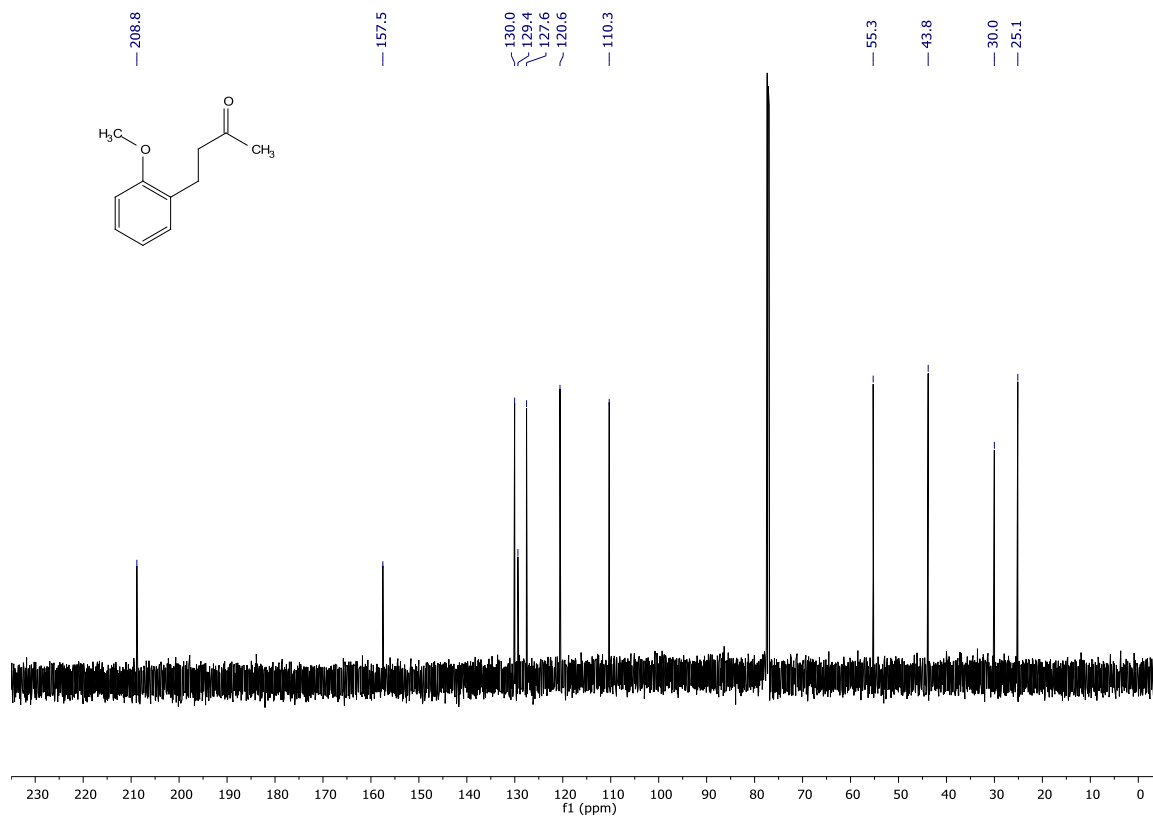
N-(3-(3-oxobutyl)phenyl)acetamide (312) **$^1\text{H-NMR}$ (600 MHz, CDCl_3)** **$^{13}\text{C-NMR}$ (151 MHz, CDCl_3)**

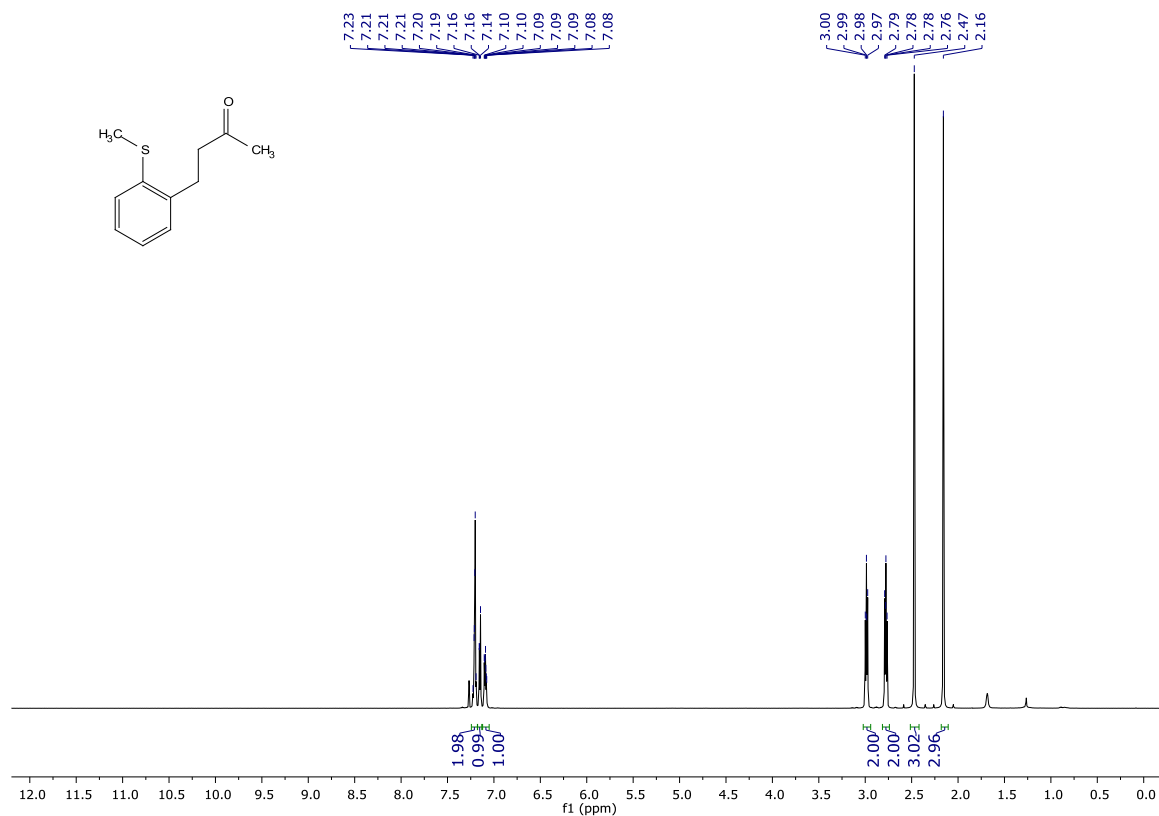
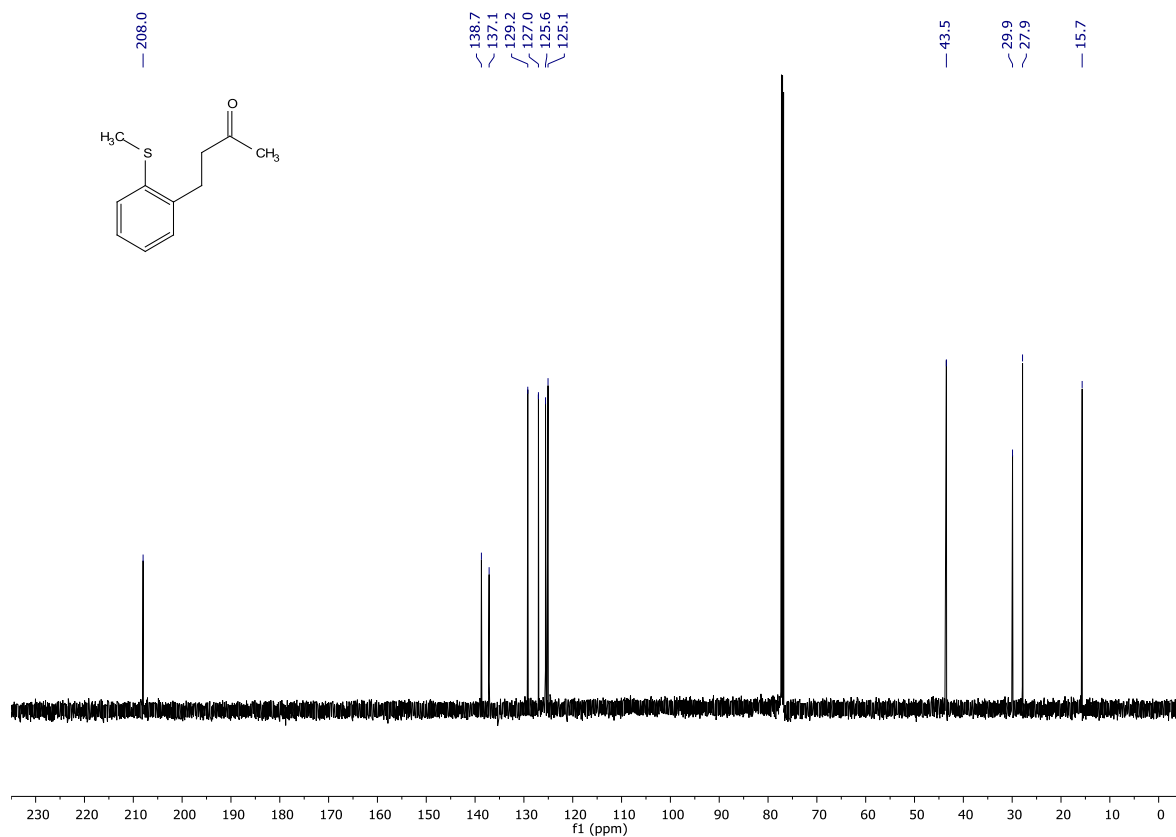
4-(2-methoxyphenyl)butan-2-one (313)

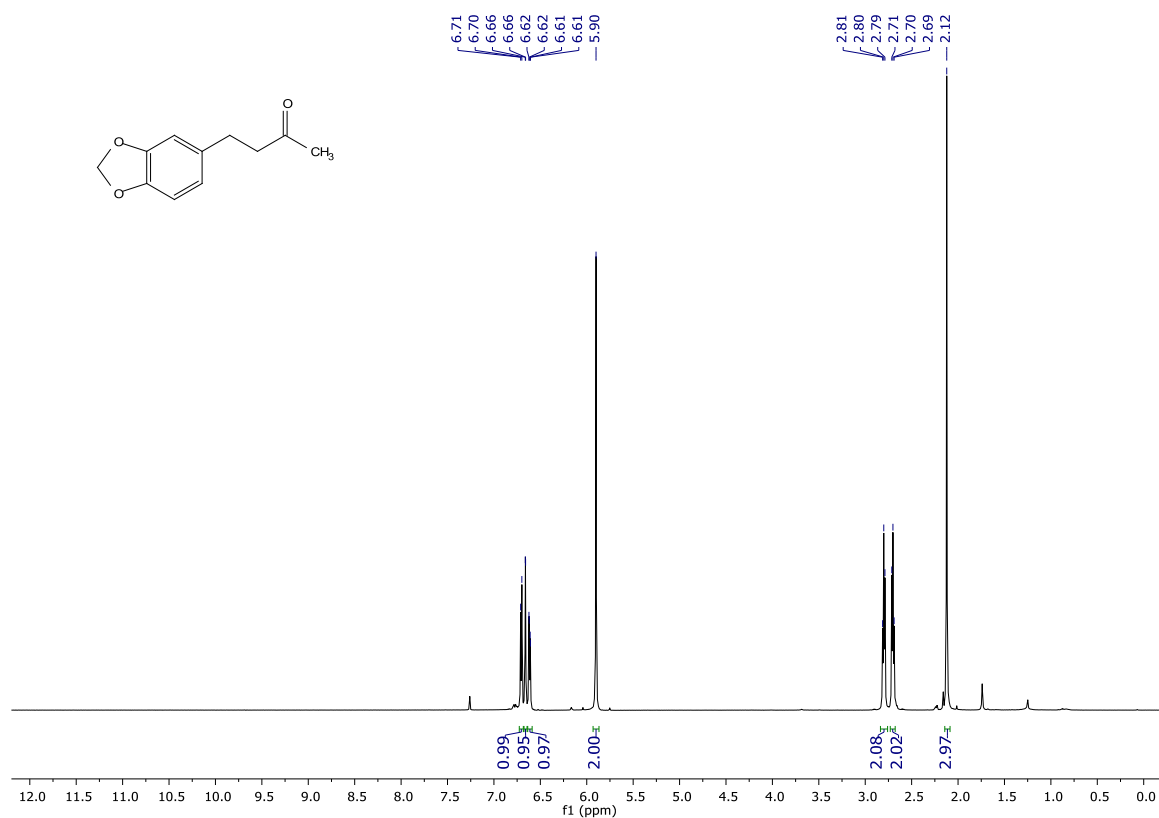
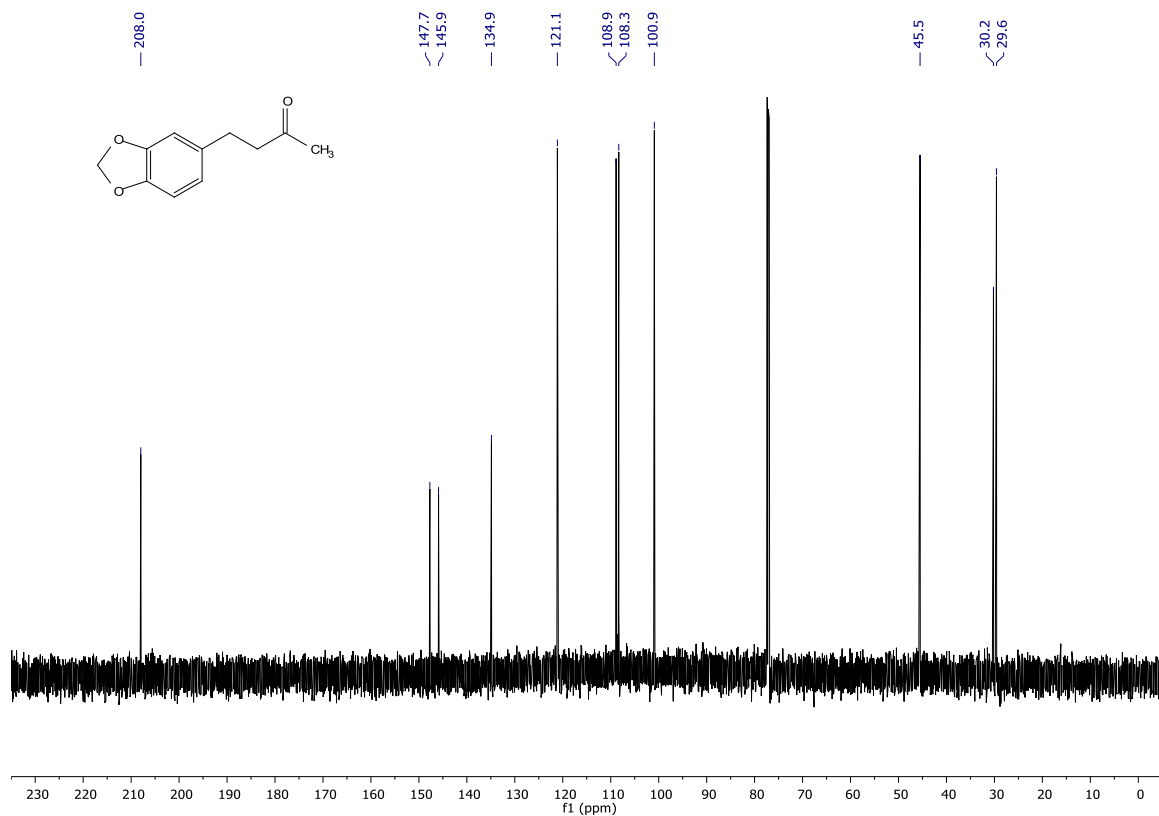
¹H-NMR (600 MHz, CDCl₃)



¹³C-NMR (151 MHz, CDCl₃)

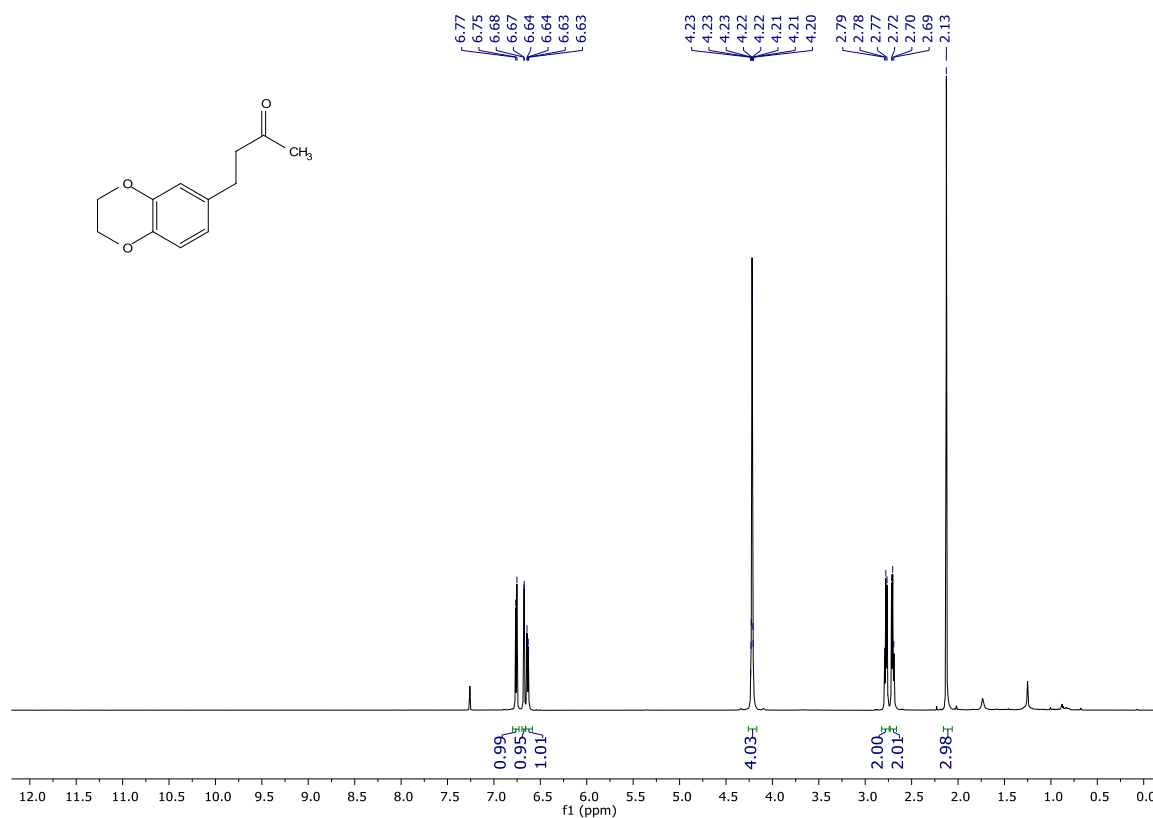


4-(2-(methylthio)phenyl)butan-2-one (314) **$^1\text{H-NMR}$ (600 MHz, CDCl_3)** **$^{13}\text{C-NMR}$ (151 MHz, CDCl_3)**

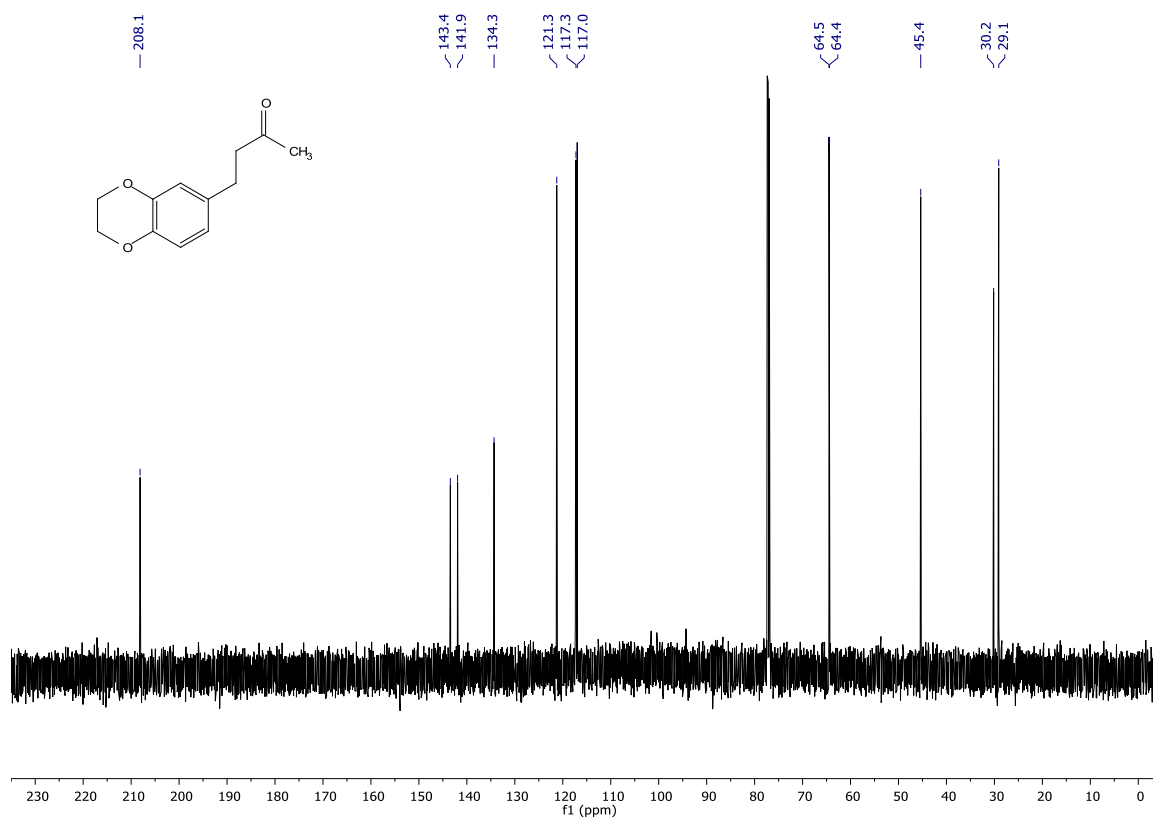
4-(benzo[d][1,3]dioxol-5-yl)butan-2-one (315) **$^1\text{H-NMR}$ (600 MHz, CDCl_3)** **$^{13}\text{C-NMR}$ (151 MHz, CDCl_3)**

4-(2,3-dihydrobenzo[b][1,4]dioxin-6-yl)butan-2-one (316)

¹H-NMR (600 MHz, CDCl₃)

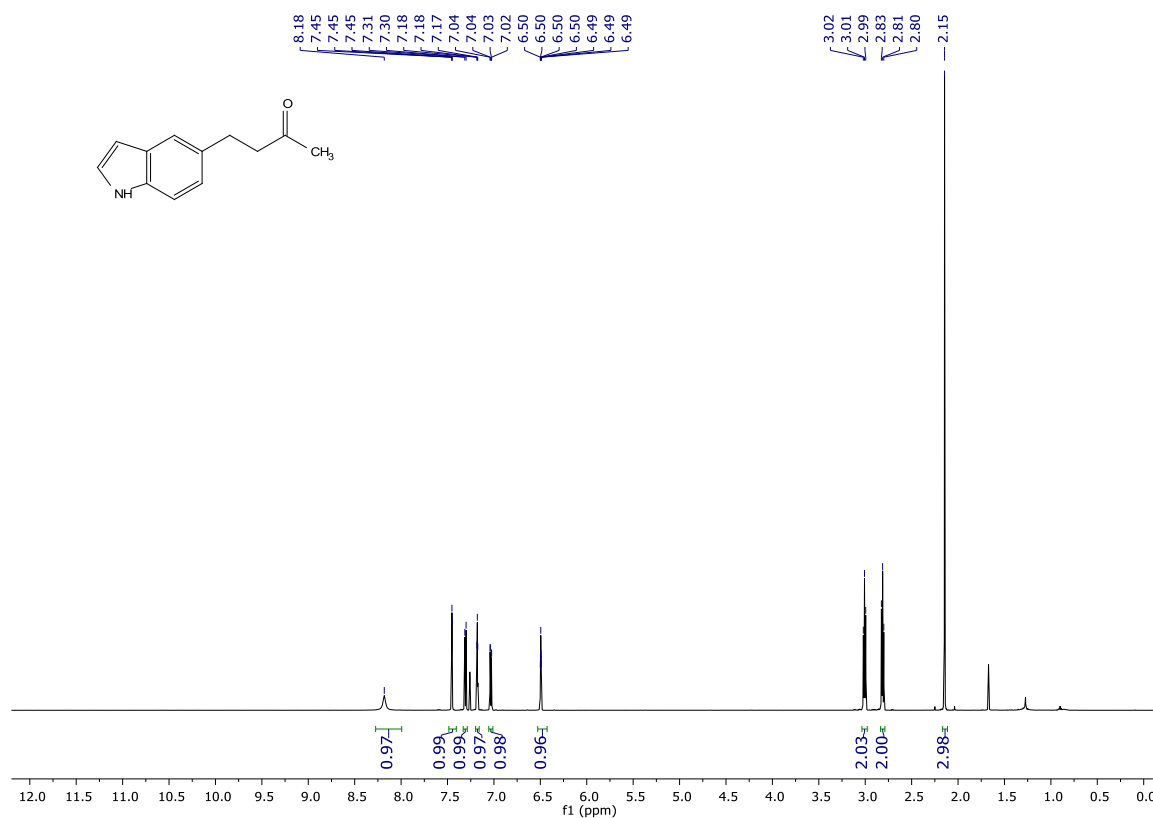


¹³C-NMR (151 MHz, CDCl₃)

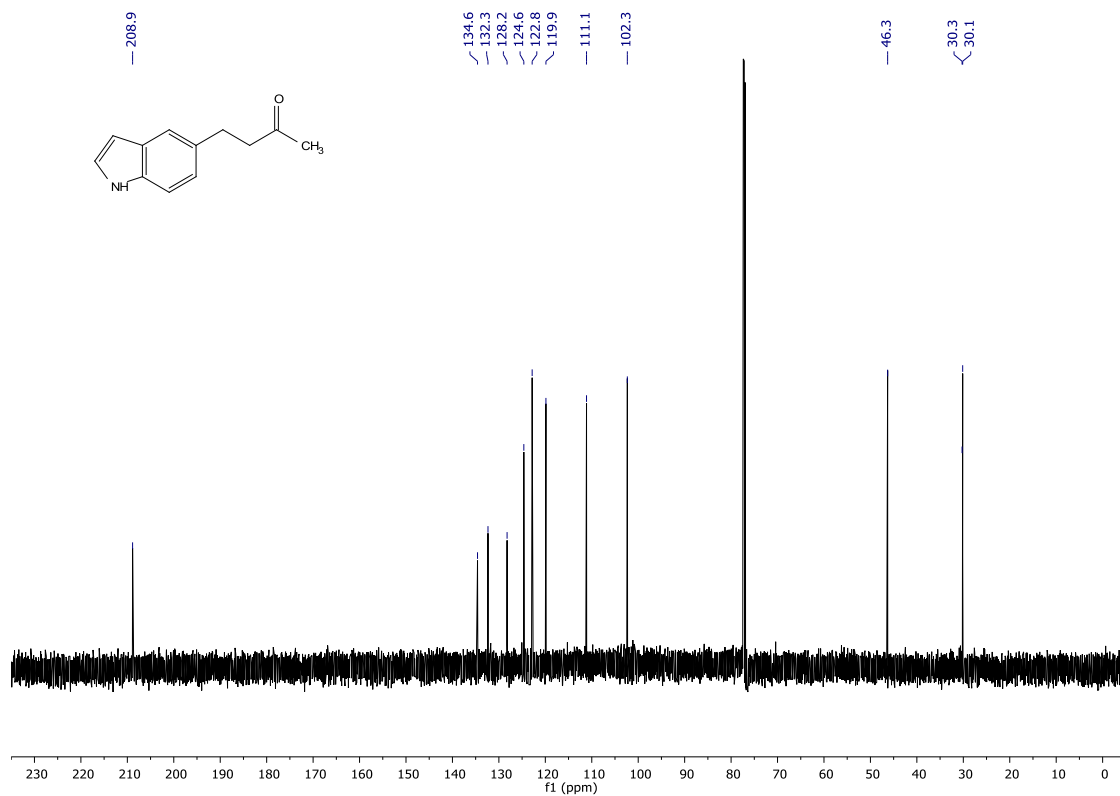


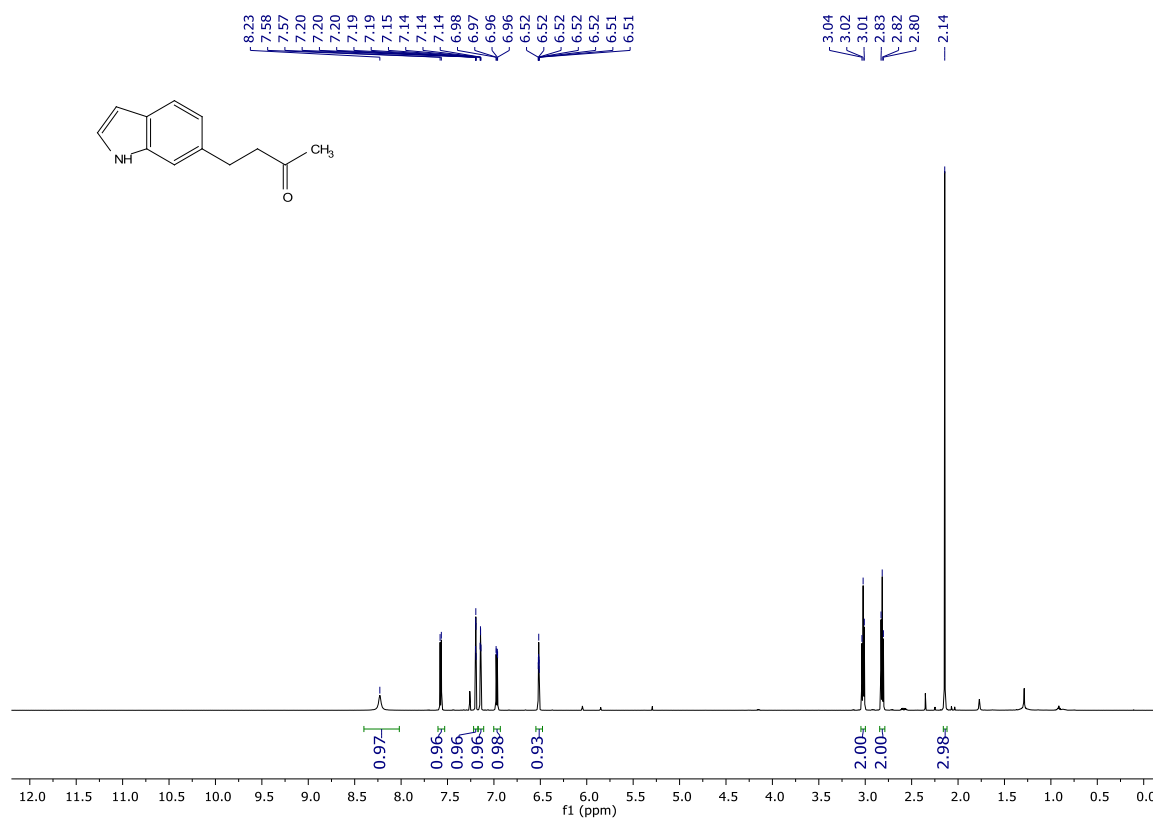
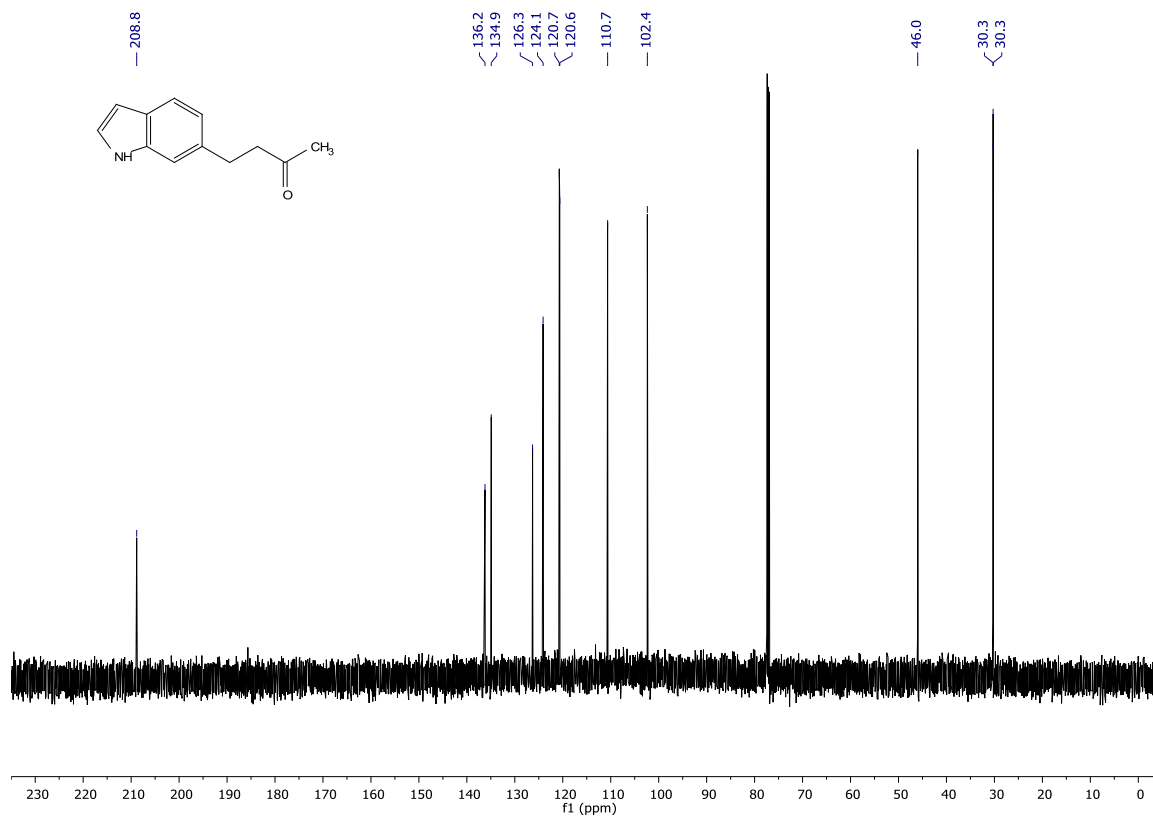
4-(1H-indol-5-yl)butan-2-one (317)

¹H-NMR (600 MHz, CDCl₃)



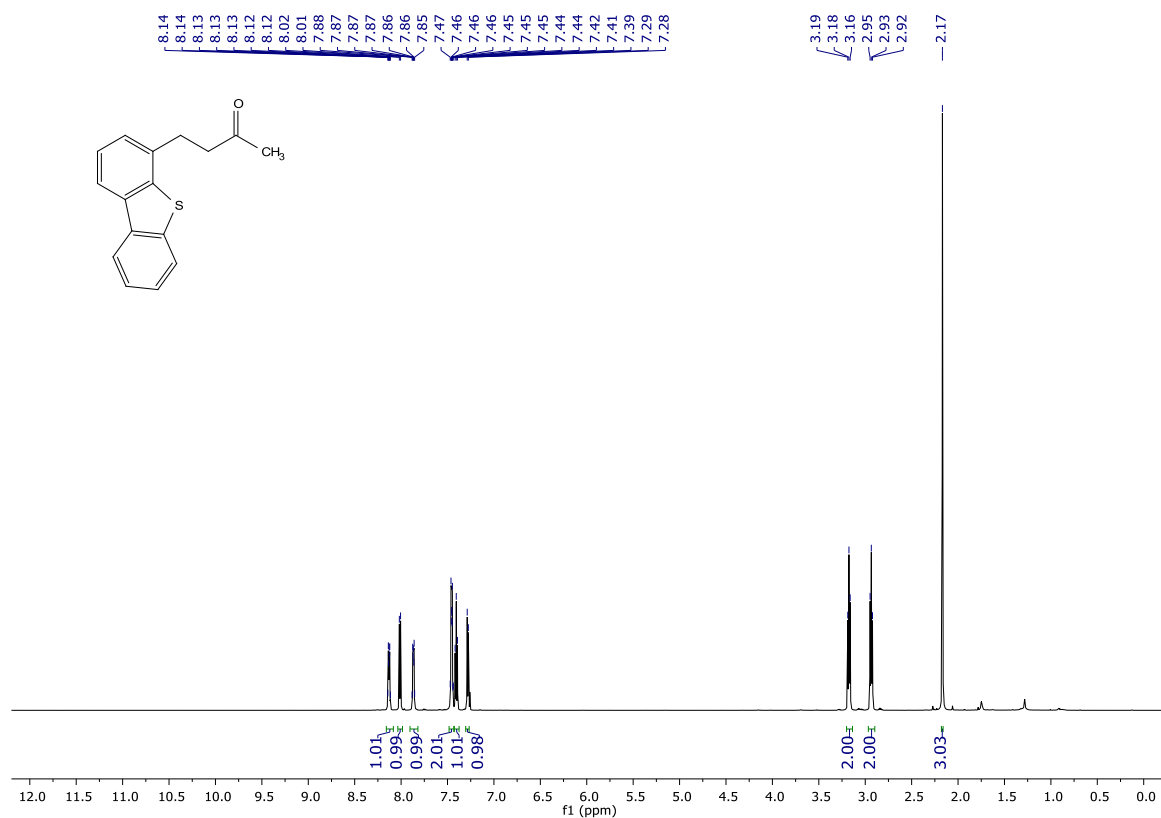
¹³C-NMR (151 MHz, CDCl₃)



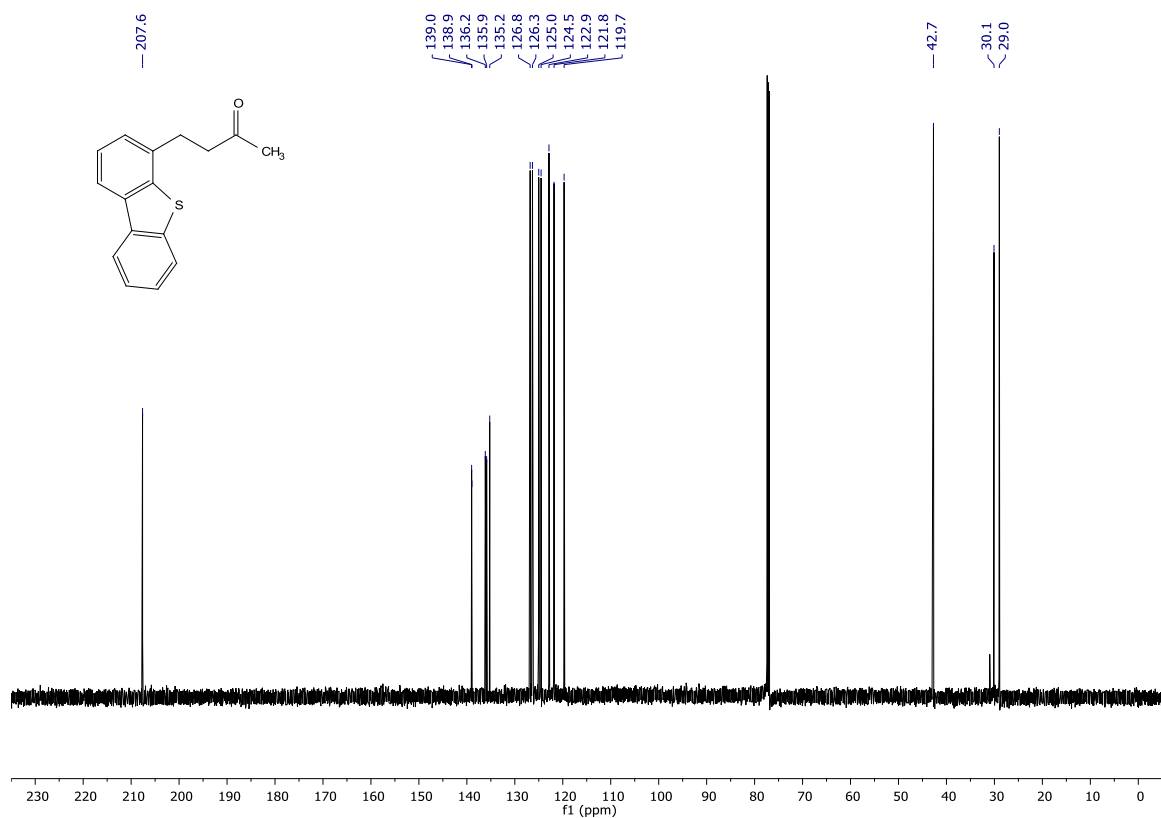
4-(1H-indol-6-yl)butan-2-one (318)**¹H-NMR (600 MHz, CDCl₃)****¹³C-NMR (151 MHz, CDCl₃)**

4-(dibenzo[b,d]thiophen-4-yl)butan-2-one (319)

¹H-NMR (600 MHz, CDCl₃)

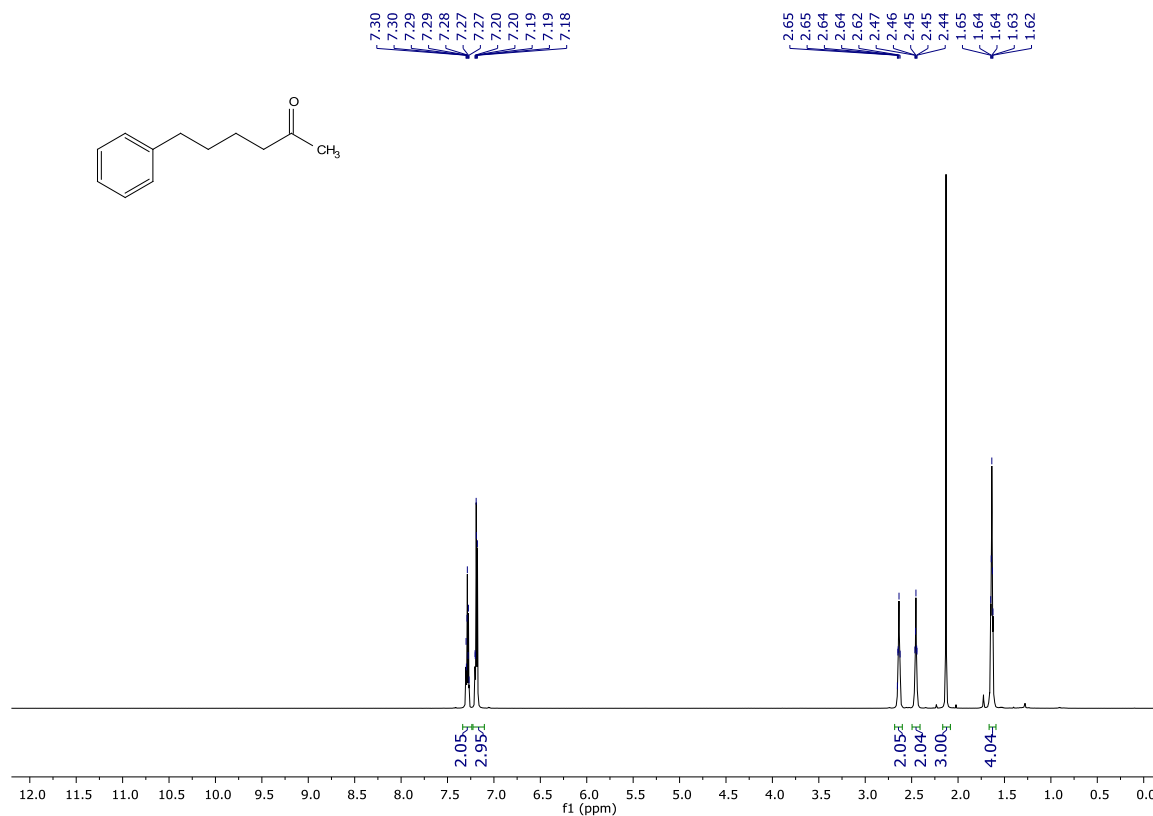


¹³C-NMR (151 MHz, CDCl₃)

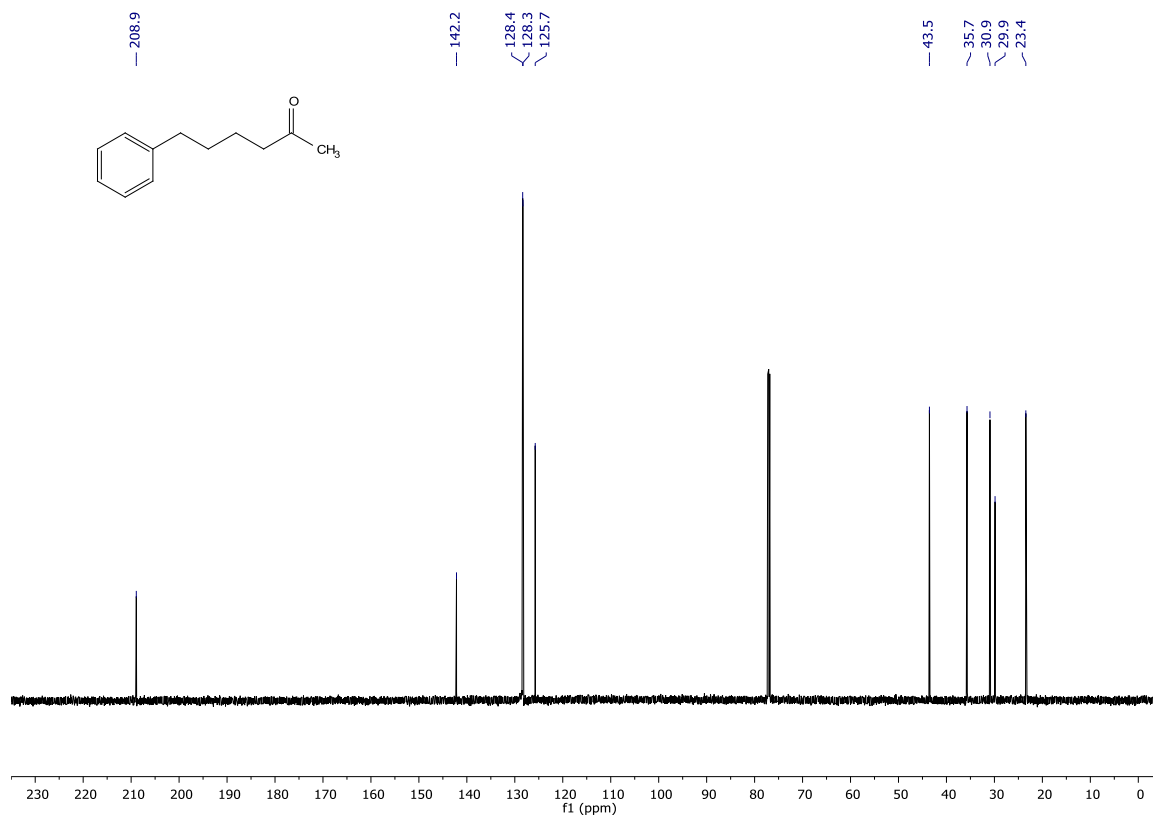


6-phenylhexan-2-one (324)

¹H-NMR (600 MHz, CDCl₃)

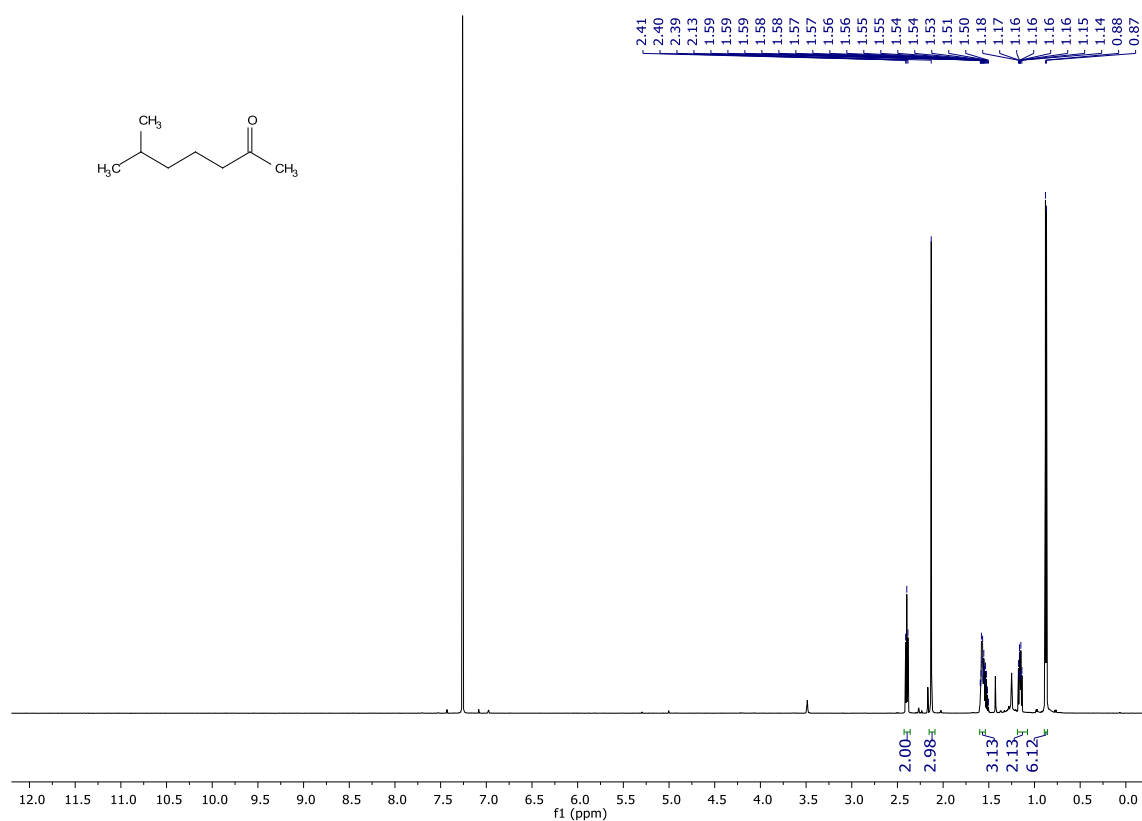


¹³C-NMR (151 MHz, CDCl₃)

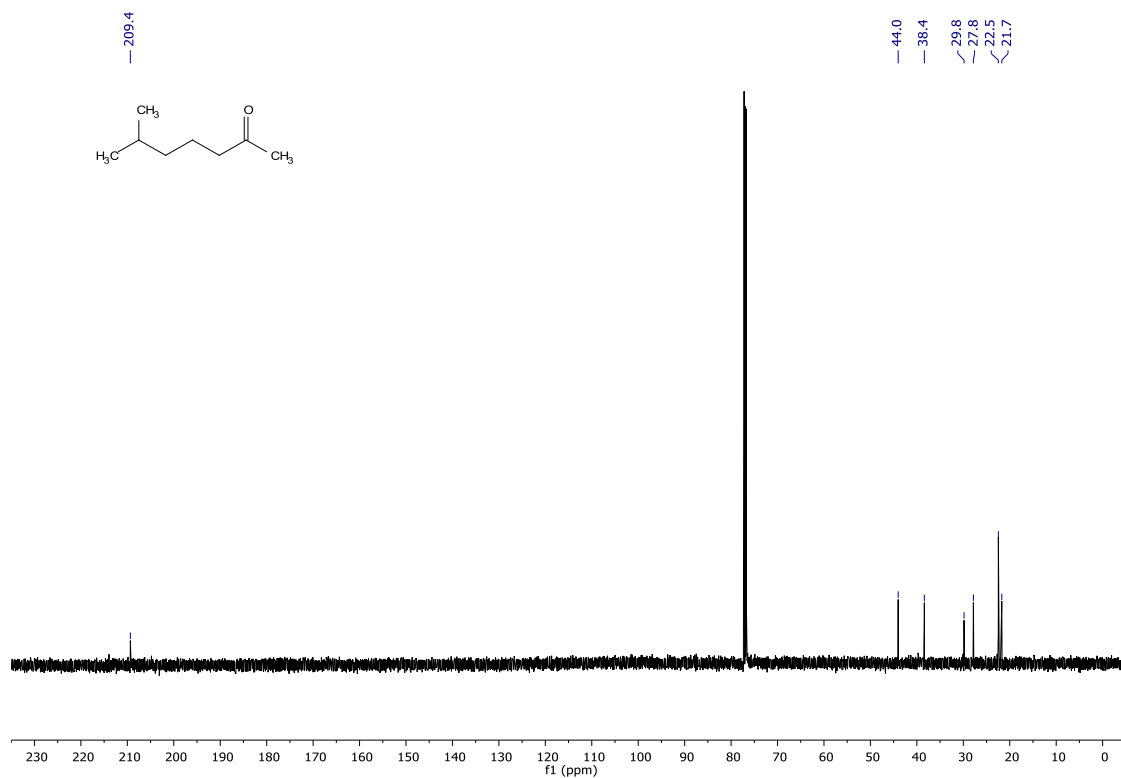


6-methylheptan-2-one (325)

¹H-NMR (600 MHz, CDCl₃)

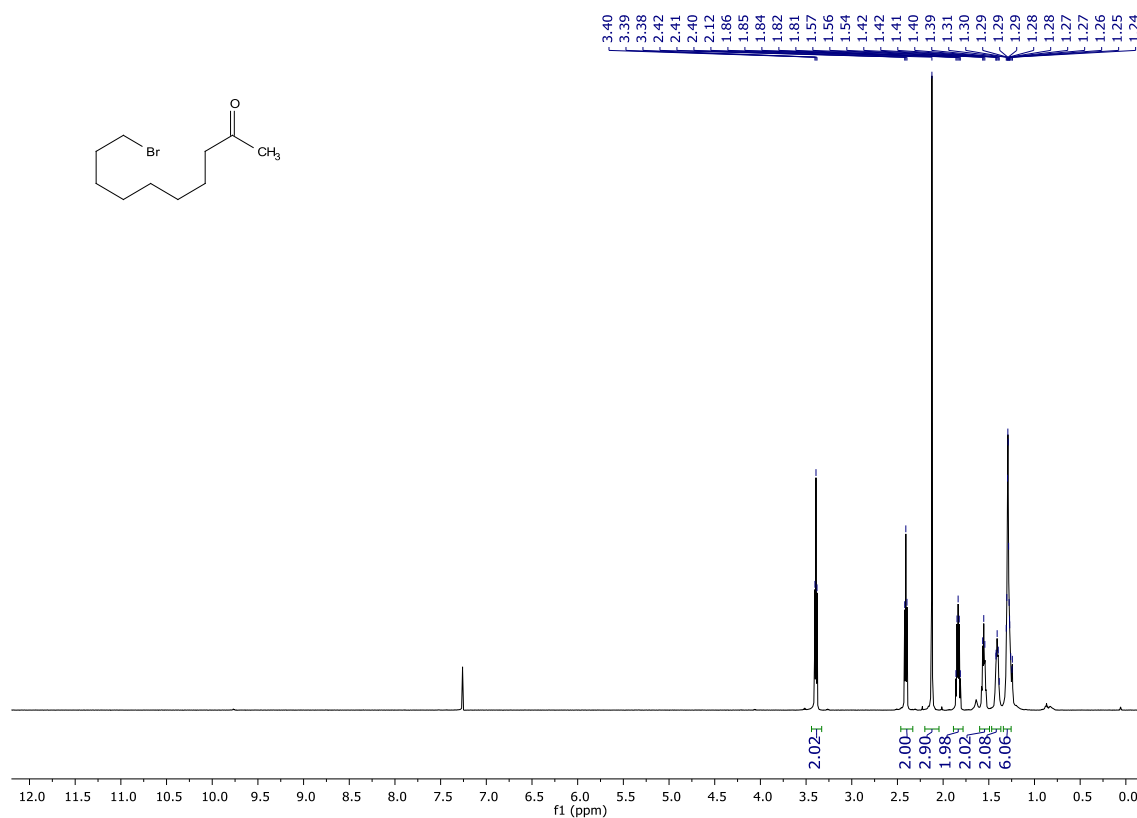


¹³C-NMR (151 MHz, CDCl₃)

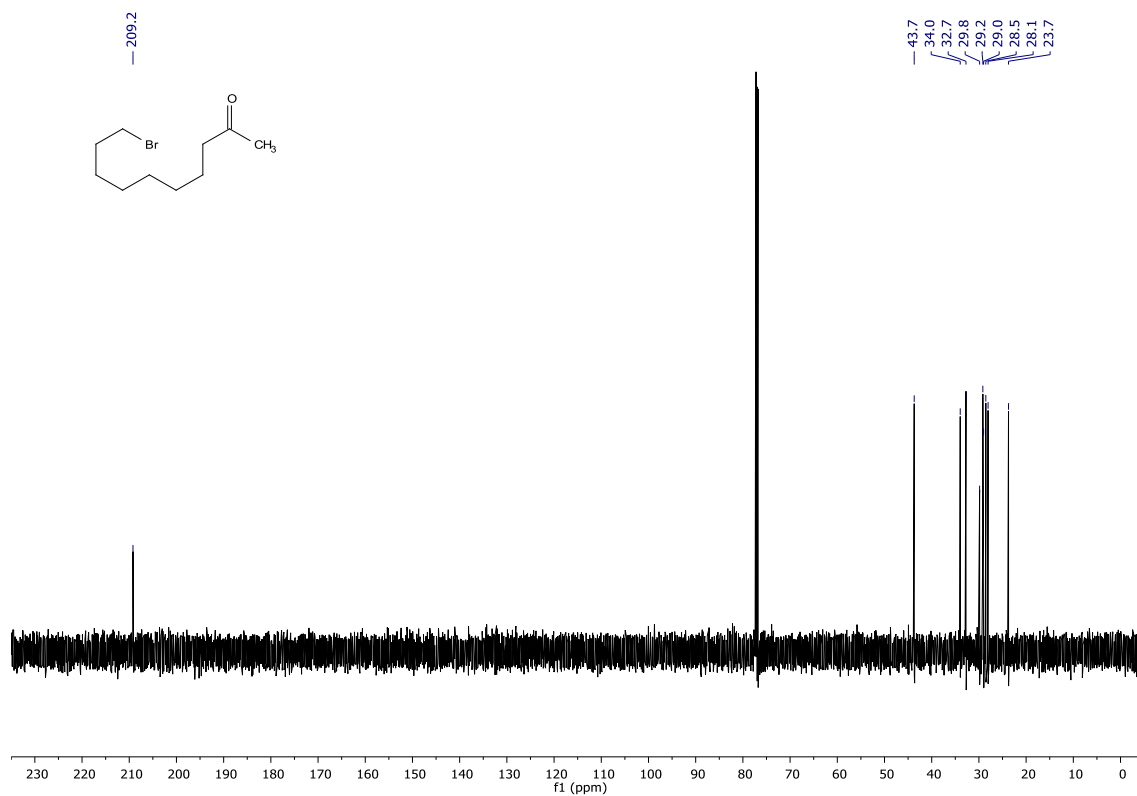


10-bromodecan-2-one (326)

¹H-NMR (600 MHz, CDCl₃)

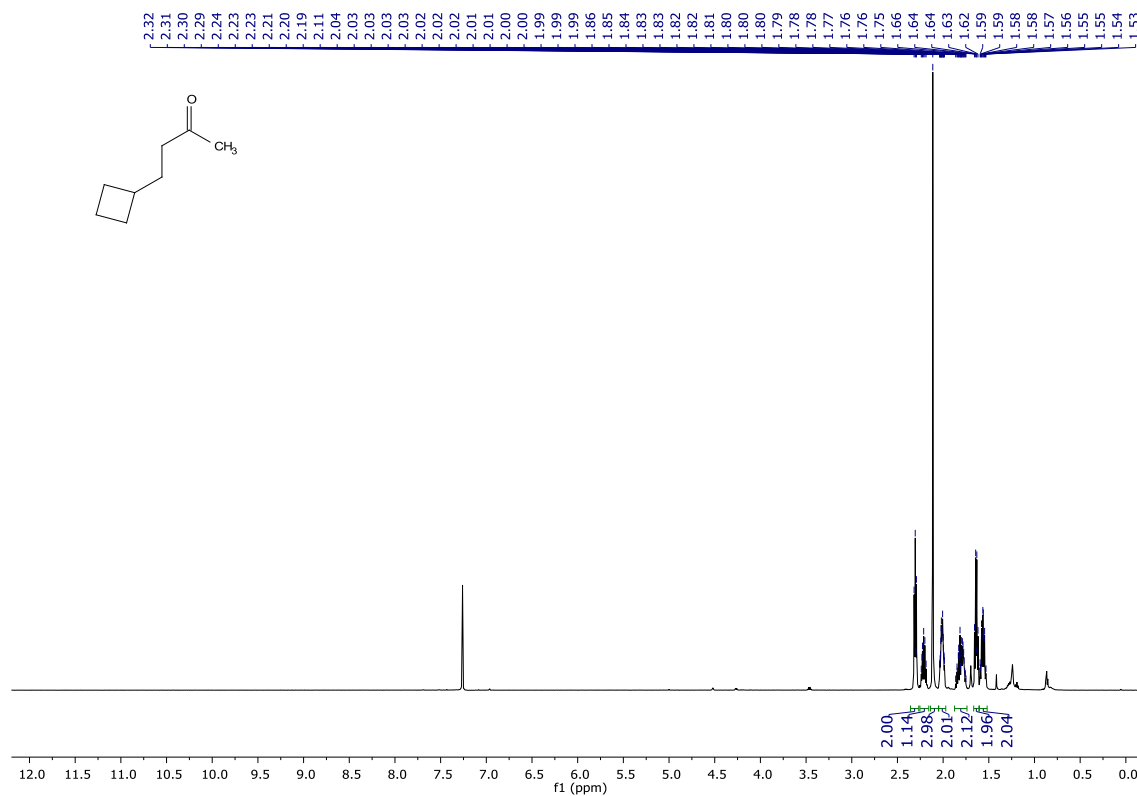


¹³C-NMR (151 MHz, CDCl₃)

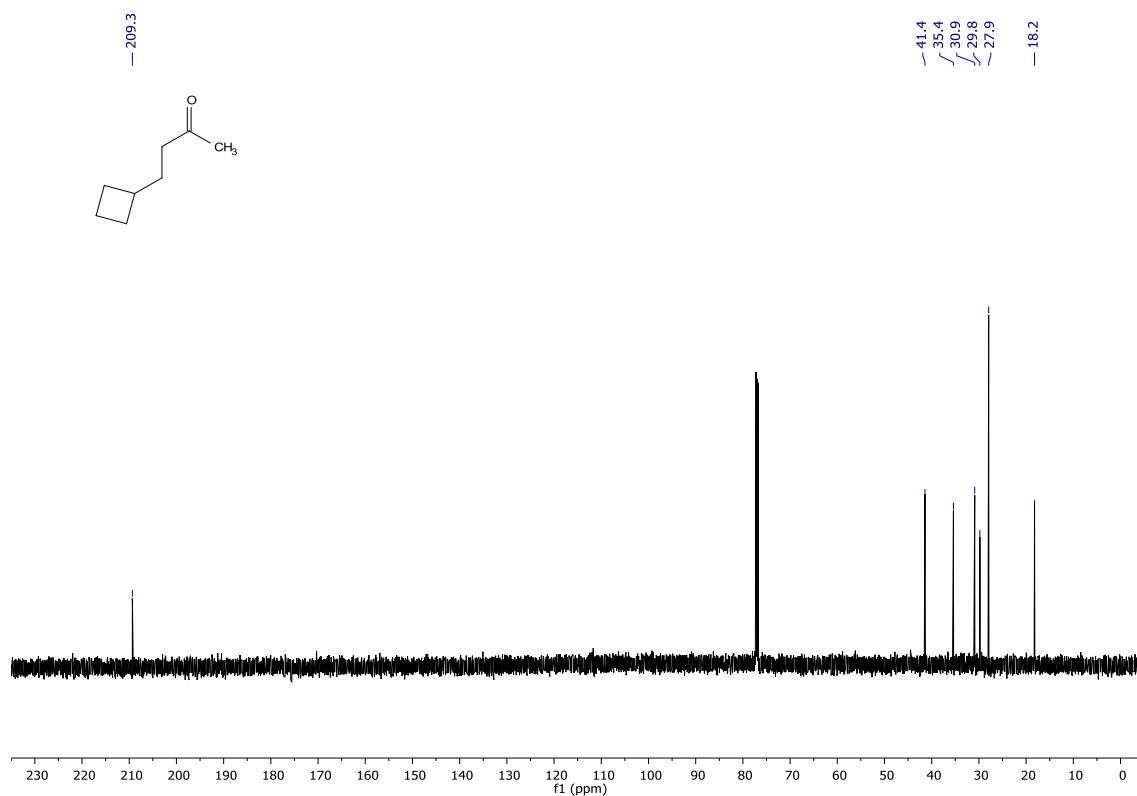


4-cyclobutylbutan-2-one (327)

¹H-NMR (600 MHz, CDCl₃)

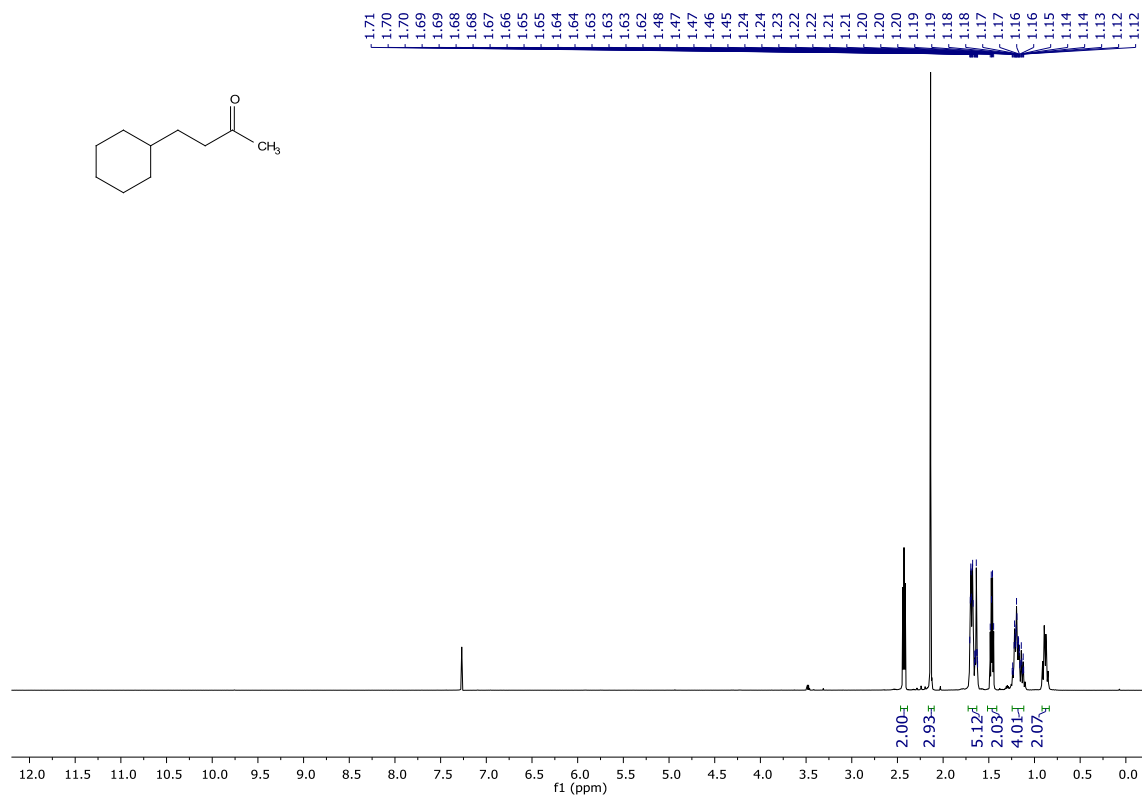


¹³C-NMR (151 MHz, CDCl₃)

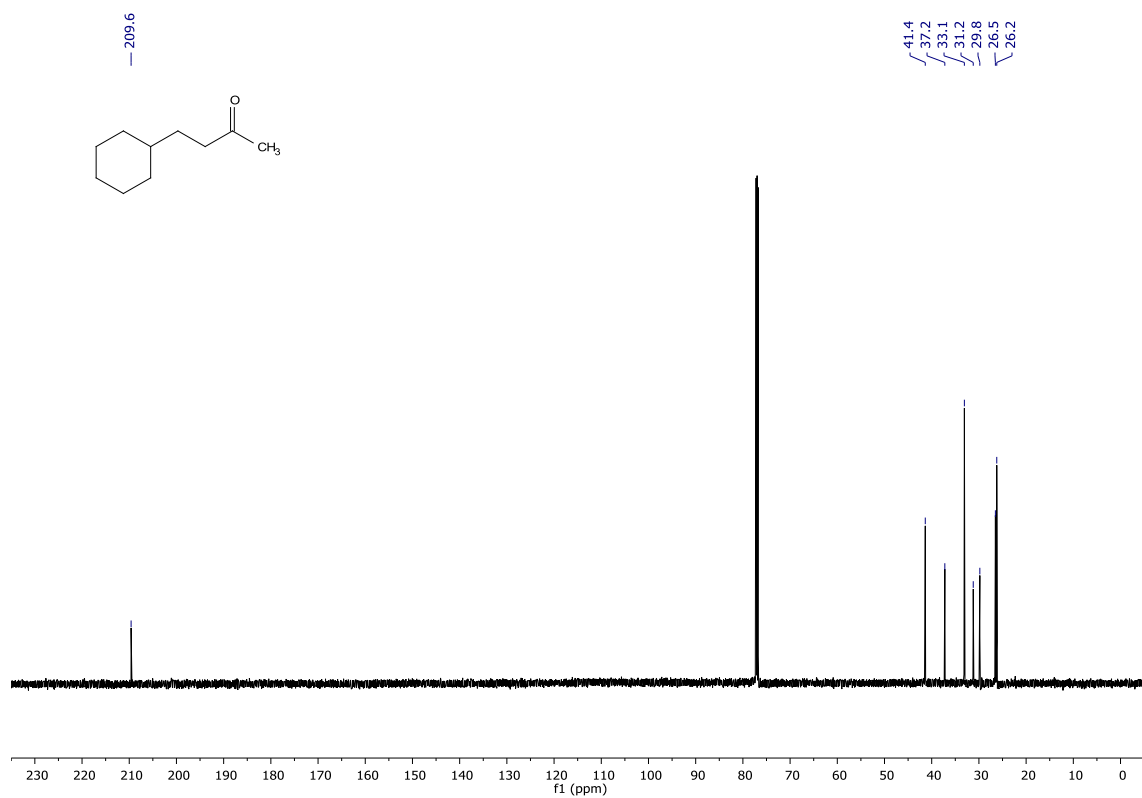


4-cyclohexylbutan-2-one (328)

¹H-NMR (600 MHz, CDCl₃)

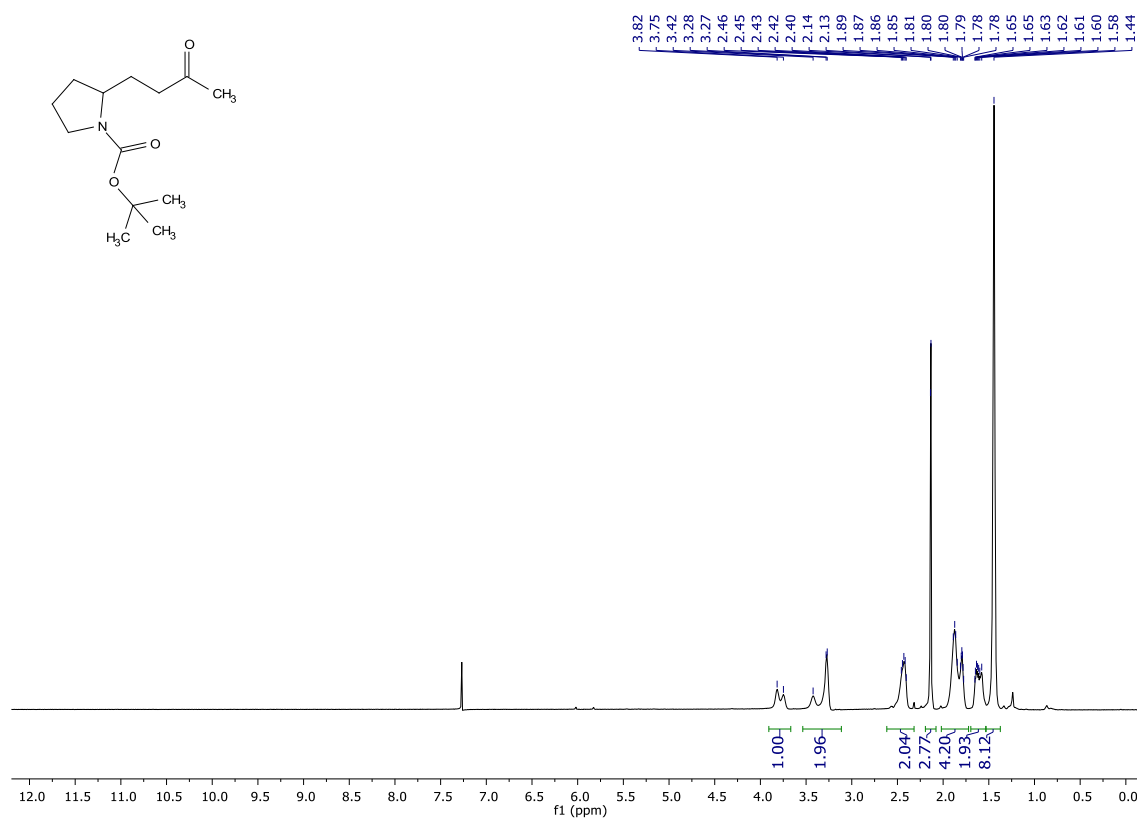


¹³C-NMR (151 MHz, CDCl₃)

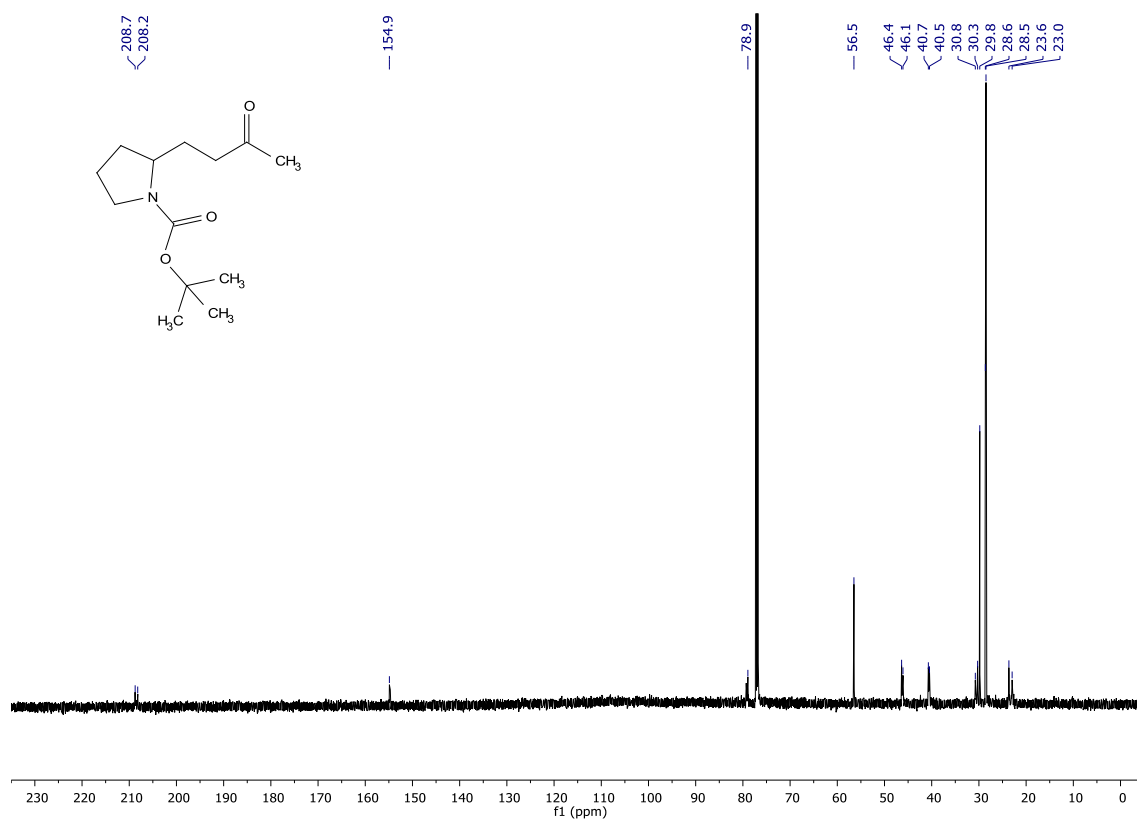


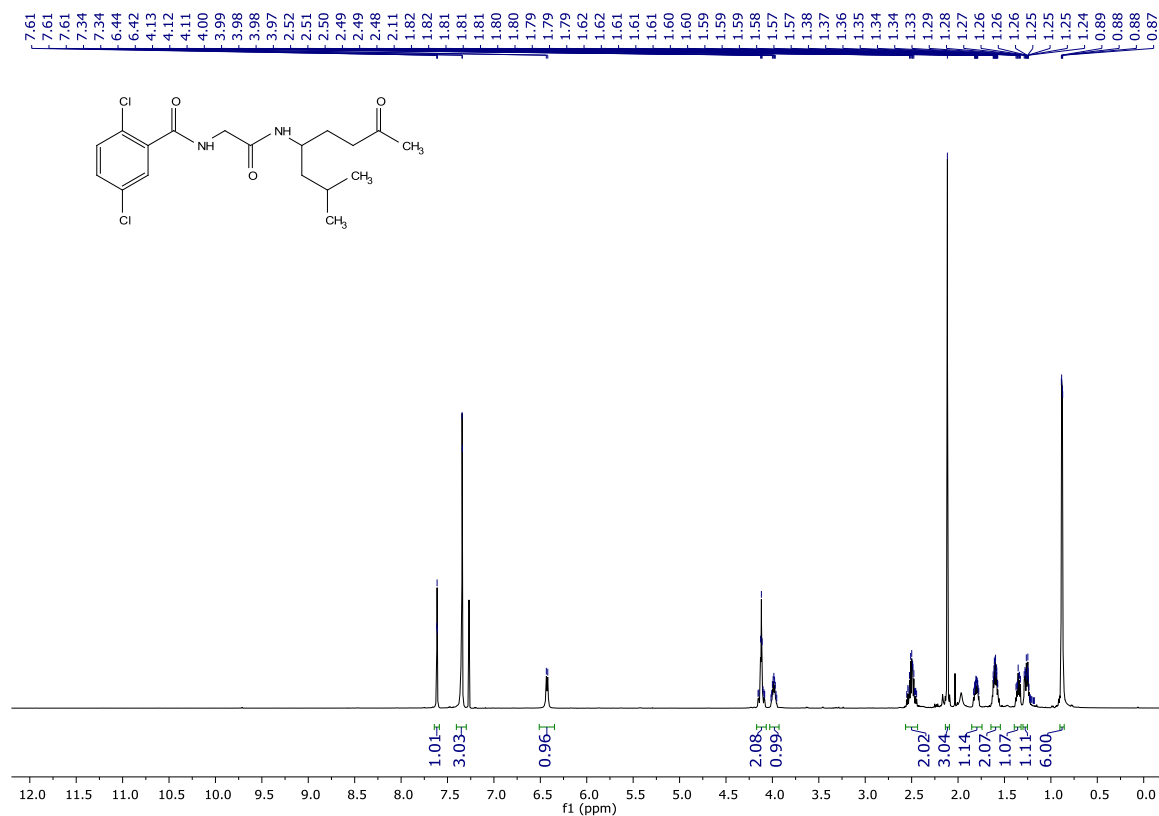
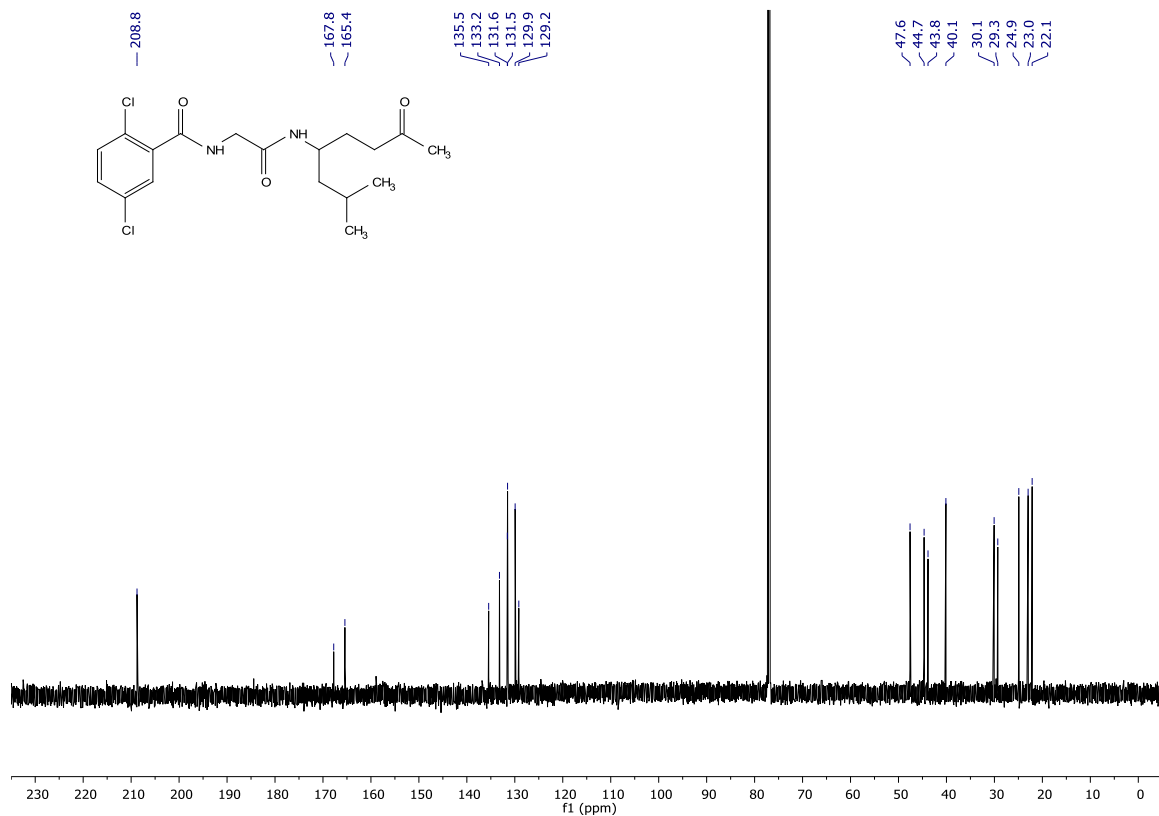
***tert*-butyl 2-(3-oxobutyl)pyrrolidine-1-carboxylate (329)**

¹H-NMR (600 MHz, CDCl₃)



¹³C-NMR (151 MHz, CDCl₃)



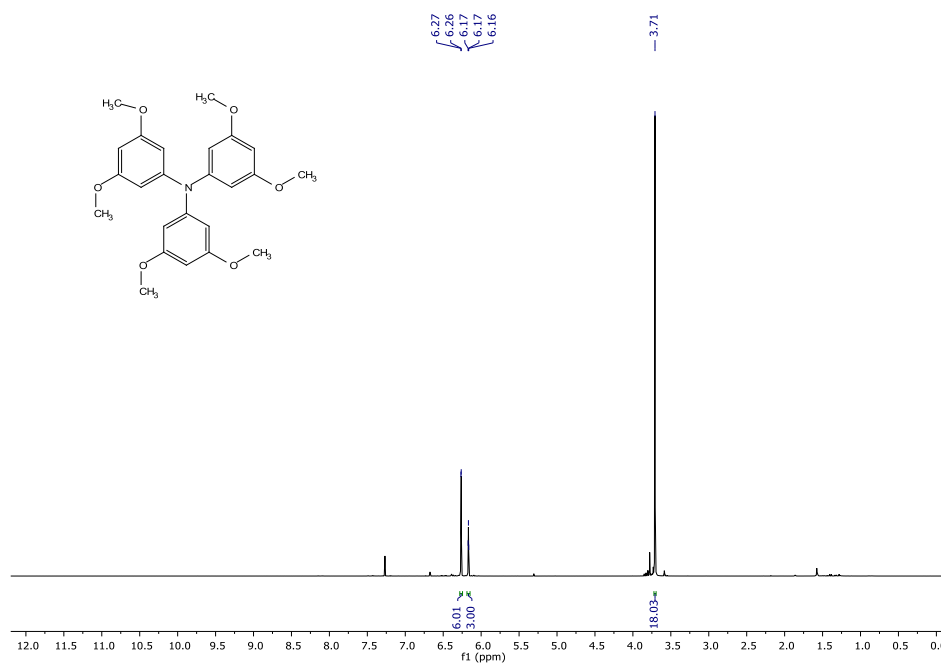
2,5-dichloro-N-(2-((2-methyl-7-oxooctan-4-yl)amino)-2-oxoethyl)benzamide (330) **$^1\text{H-NMR}$ (600 MHz, CDCl_3)** **$^{13}\text{C-NMR}$ (151 MHz, CDCl_3)**

7.3 Spectra for Chapter 4

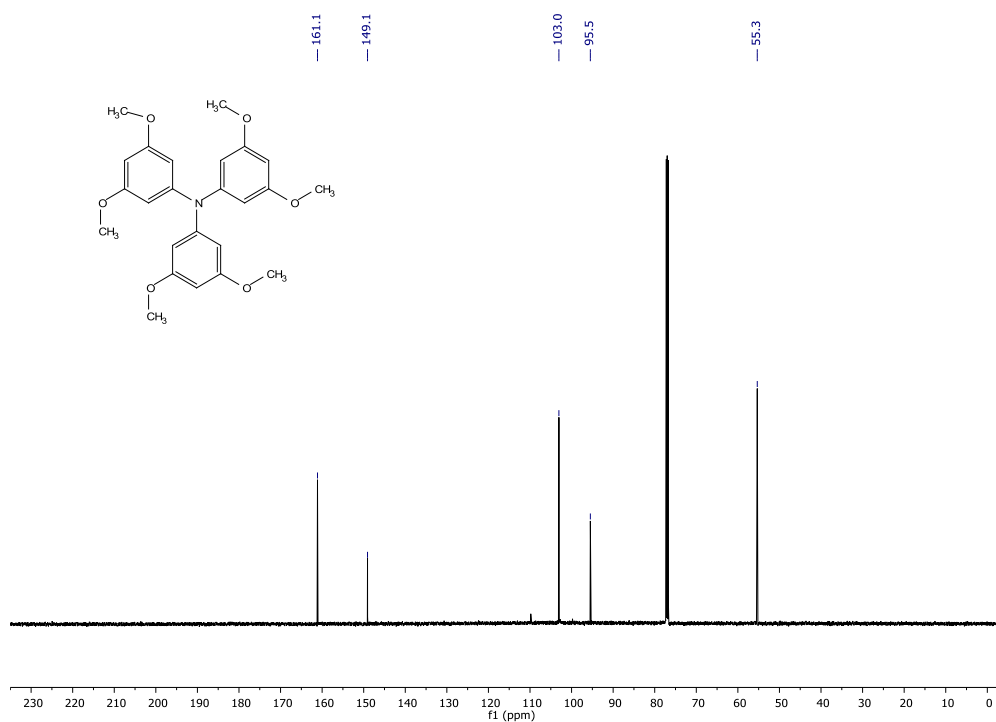
7.3.1 Organic dyes spectra

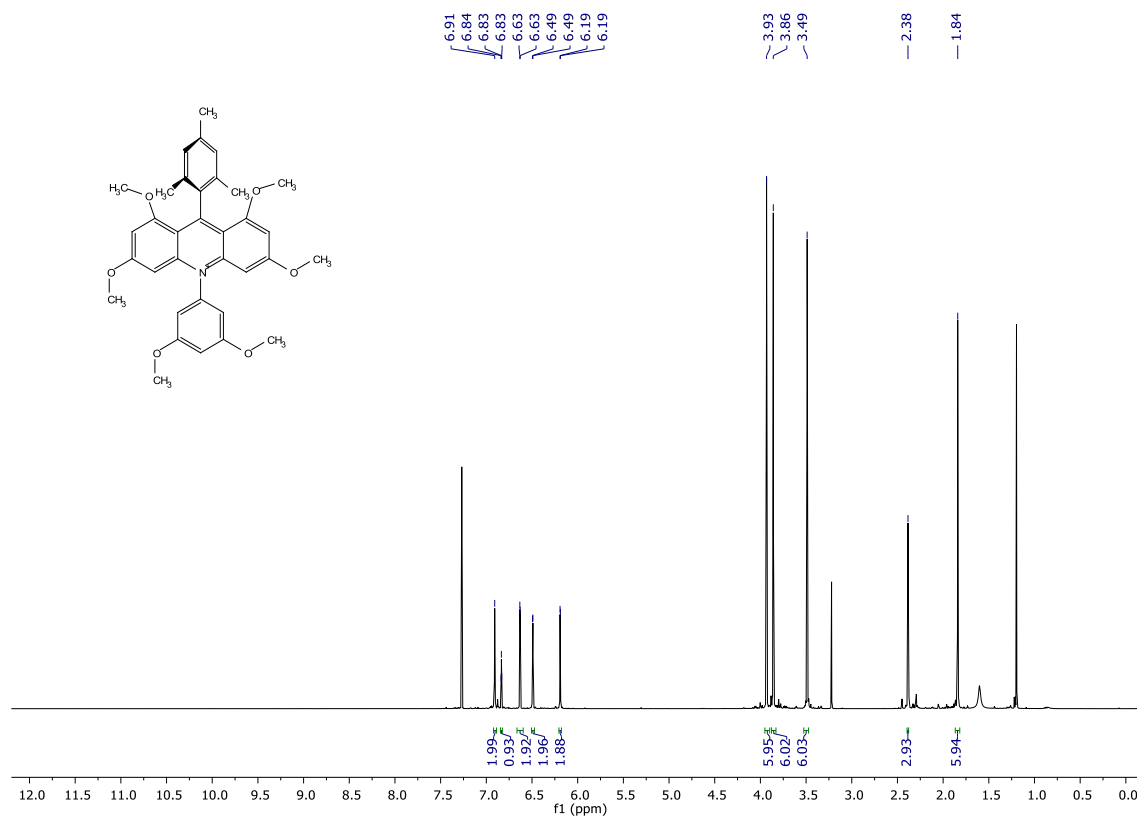
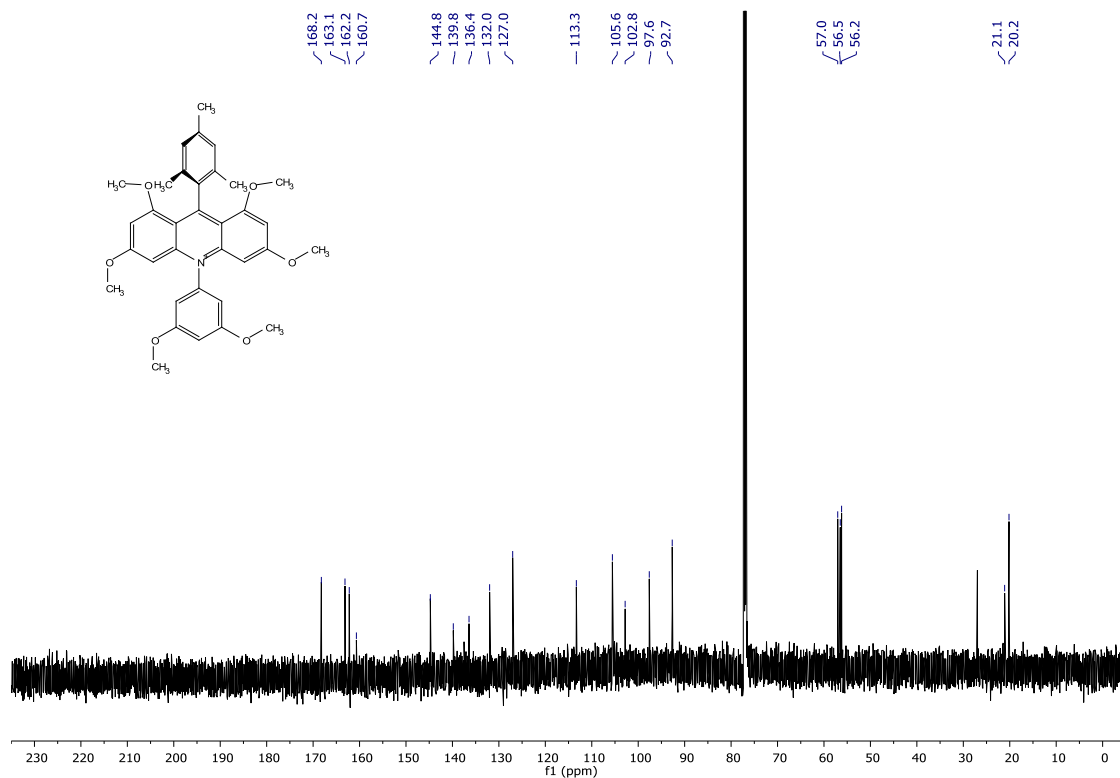
tris(3,5-dimethoxyphenyl)amine

$^1\text{H-NMR}$ (600 MHz, CDCl_3)



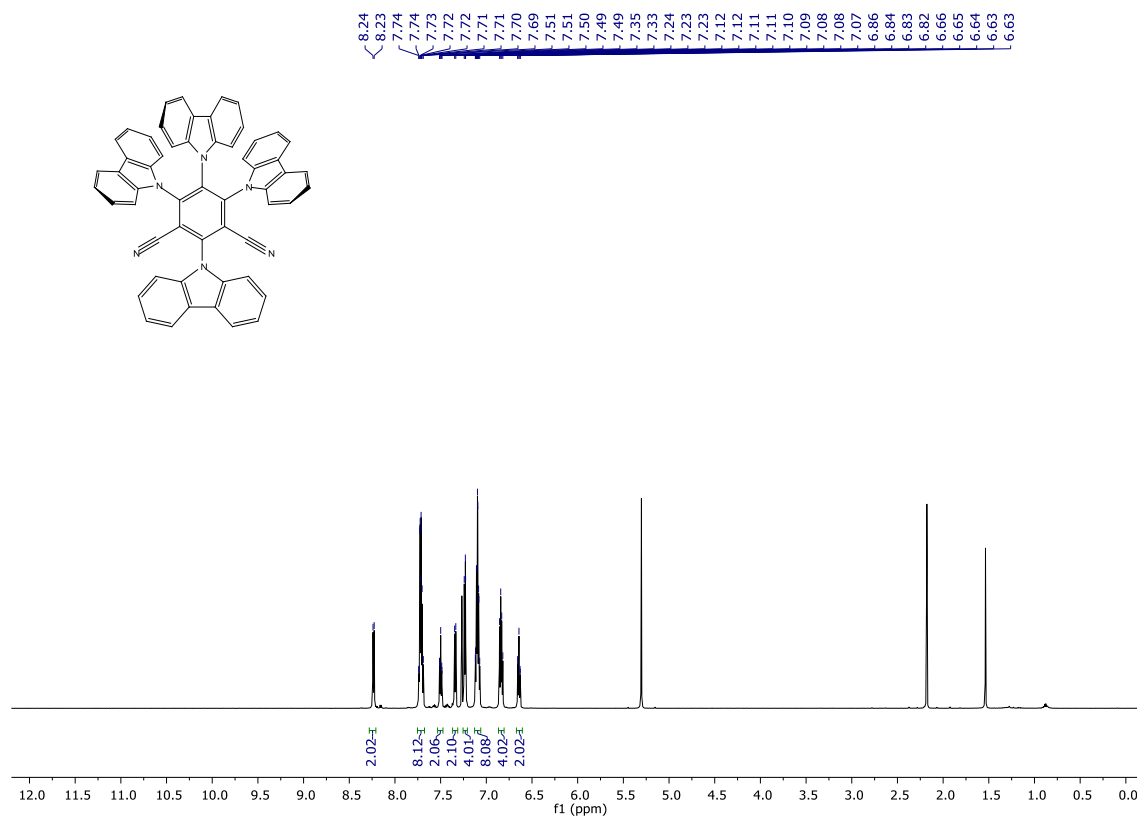
$^{13}\text{C-NMR}$ (151 MHz, CDCl_3)



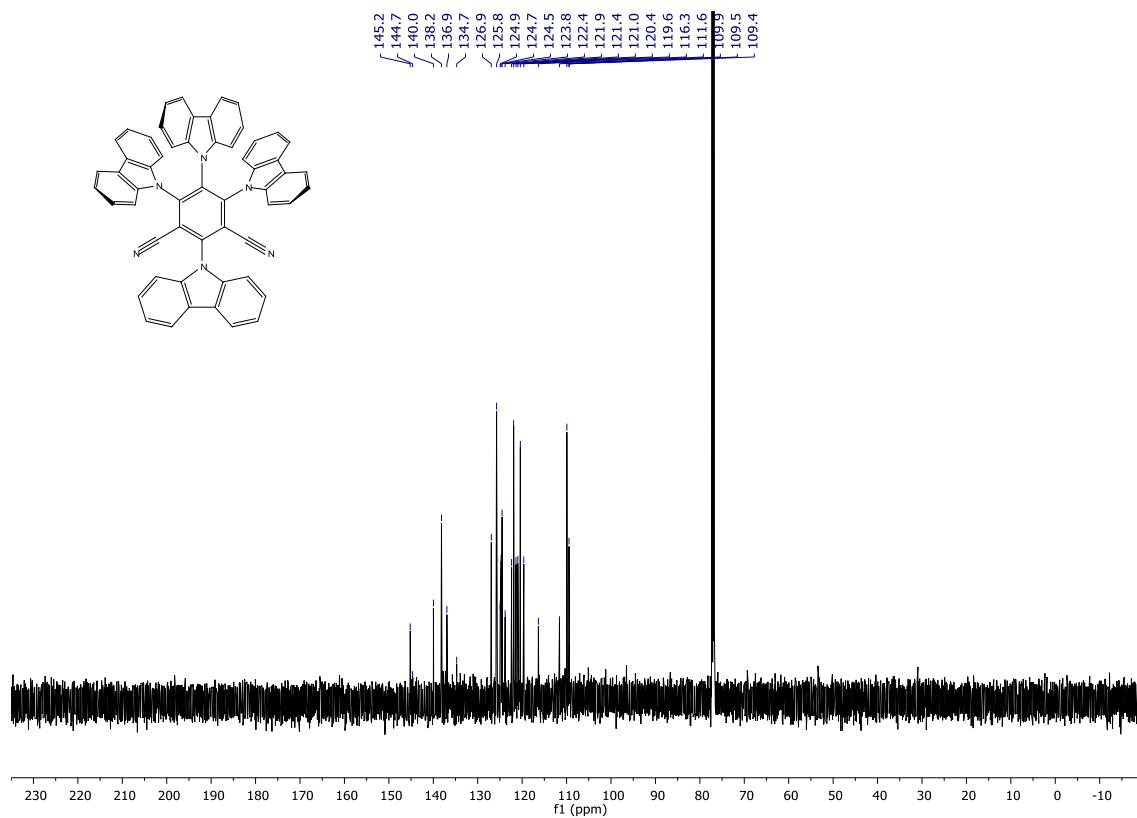
**10-(3,5-dimethoxyphenyl)-9-mesityl-1,3,6,8-tetramethoxyacridin-10-ium
tetrafluoroborate (Mes-Acr-4)** **$^1\text{H-NMR}$ (600 MHz, CDCl_3)** **$^{13}\text{C-NMR}$ (151 MHz, CDCl_3)**

2,4,5,6-tetra(9*H*-carbazol-9-yl)isophthalonitrile (4CzIPN)

¹H-NMR (600 MHz, CDCl₃)



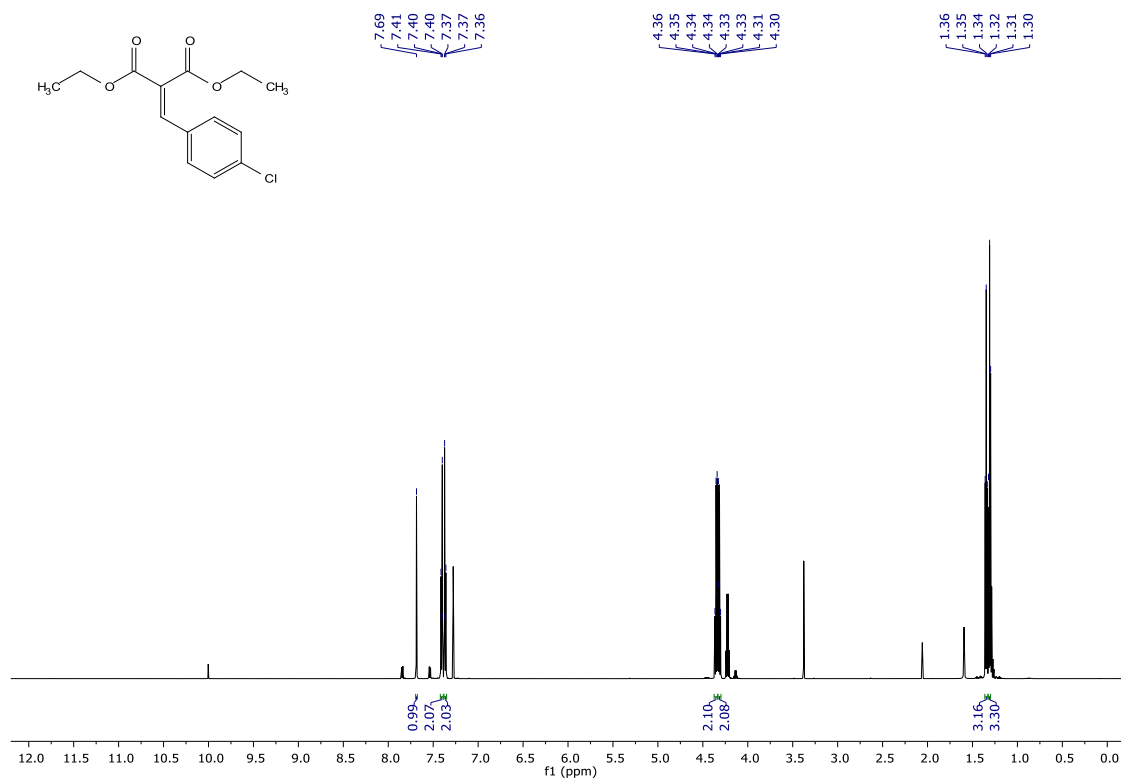
¹³C-NMR (151 MHz, CDCl₃)



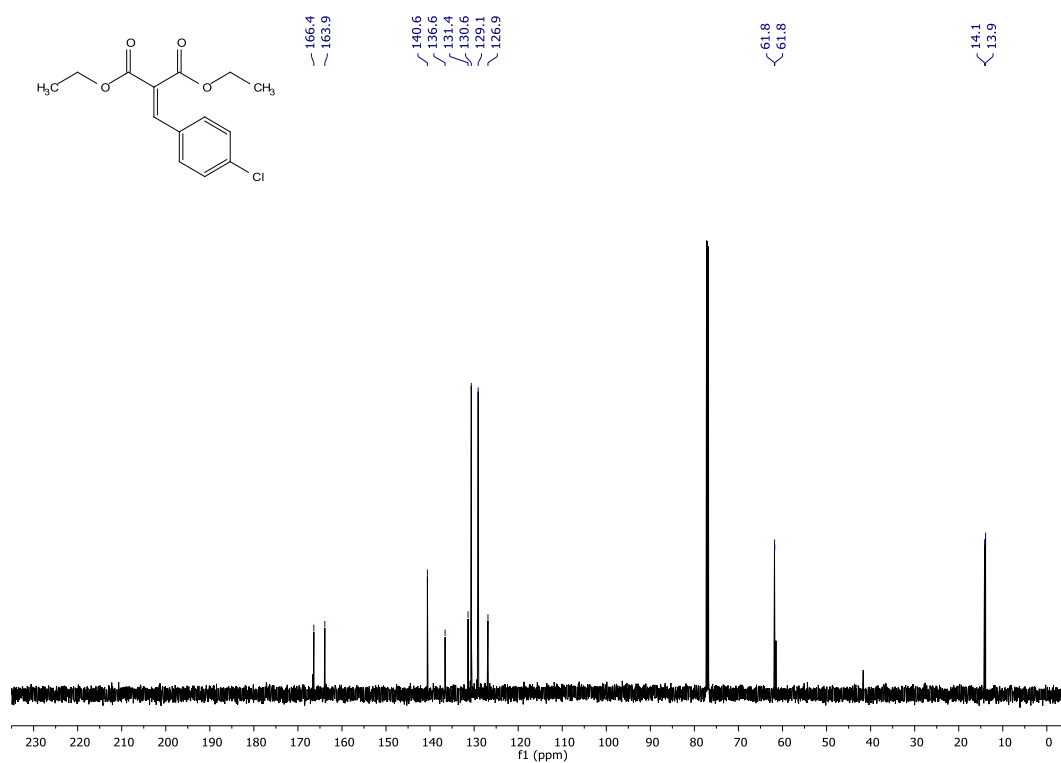
7.3.2 Starting materials spectra

diethyl 2-(4-chlorobenzylidene)malonate (357)

$^1\text{H-NMR}$ (600 MHz, CDCl_3)

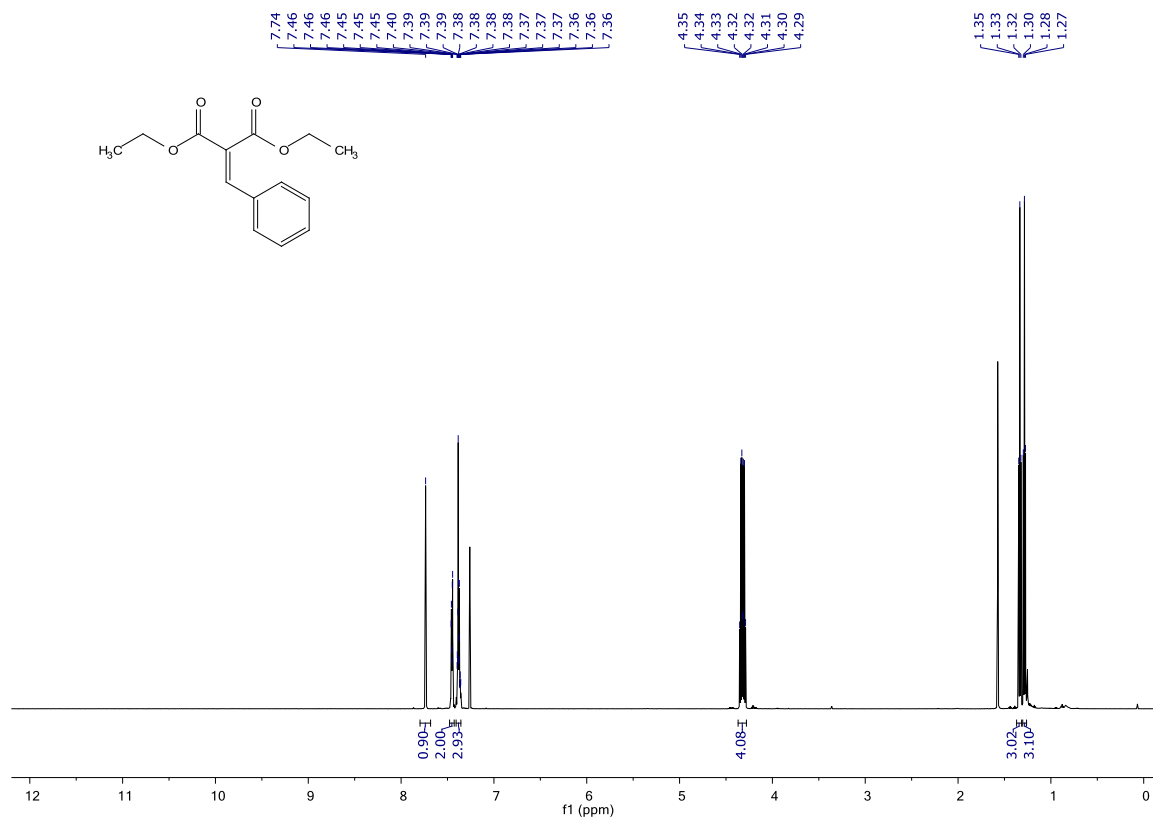


$^{13}\text{C-NMR}$ (151 MHz, CDCl_3)

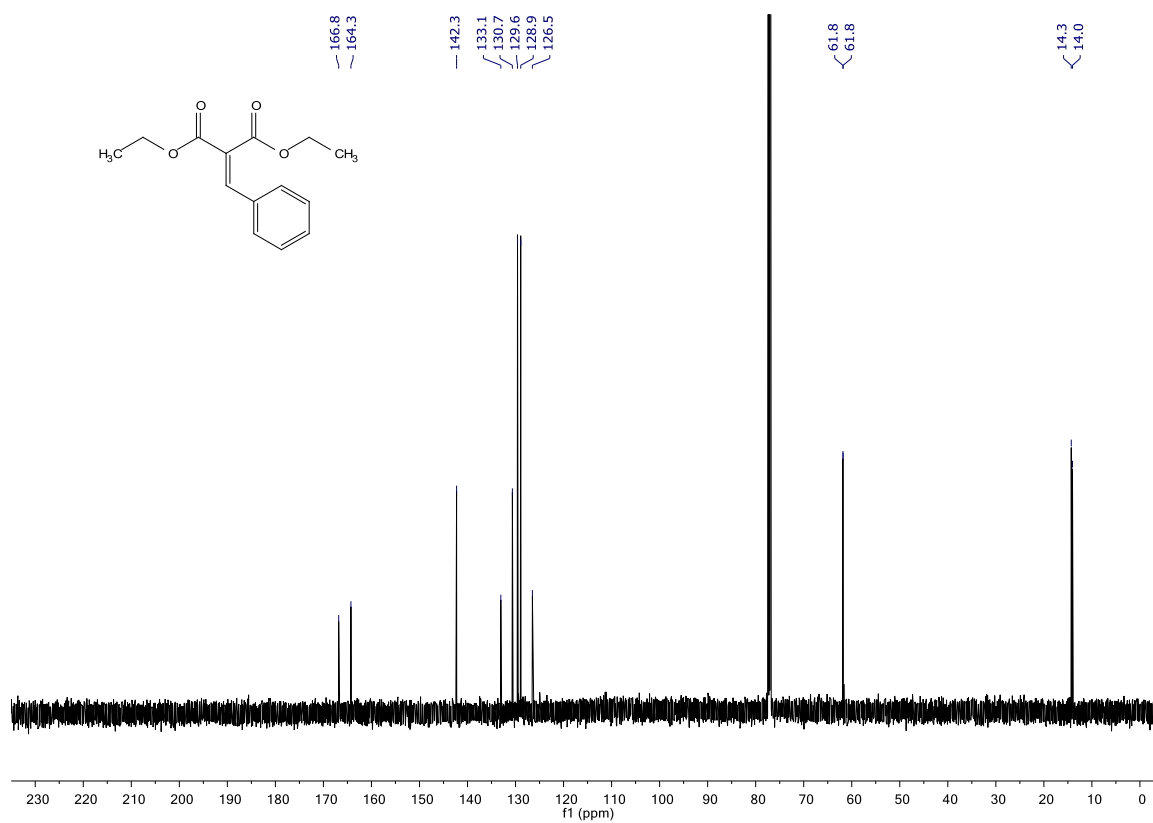


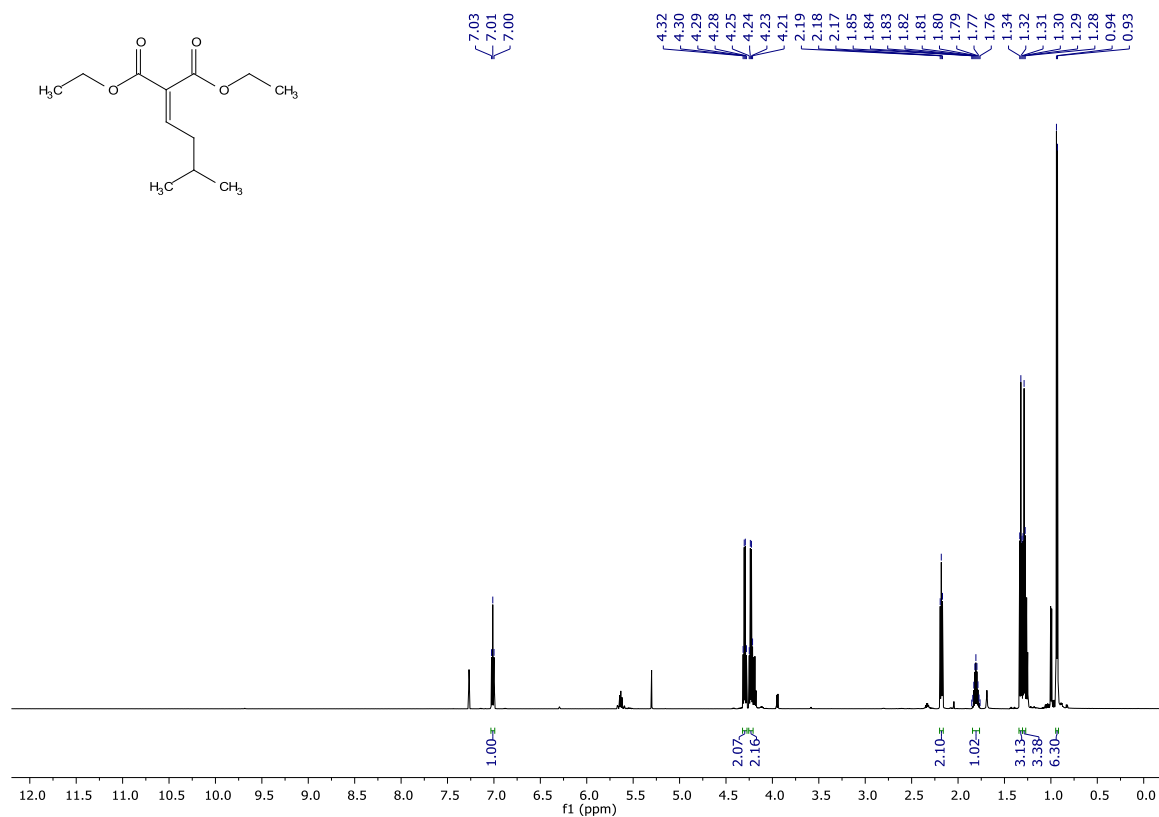
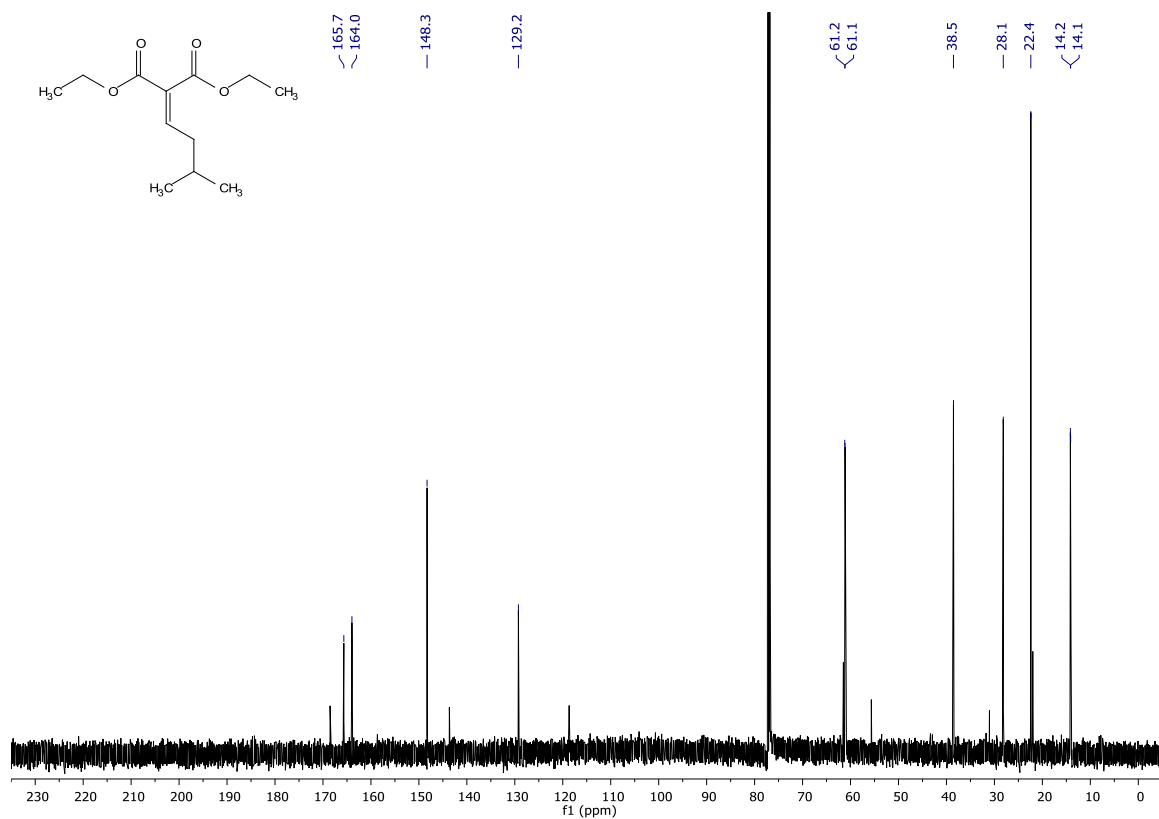
diethyl 2-benzylidenemalonate (358)

¹H-NMR (600 MHz, CDCl₃)



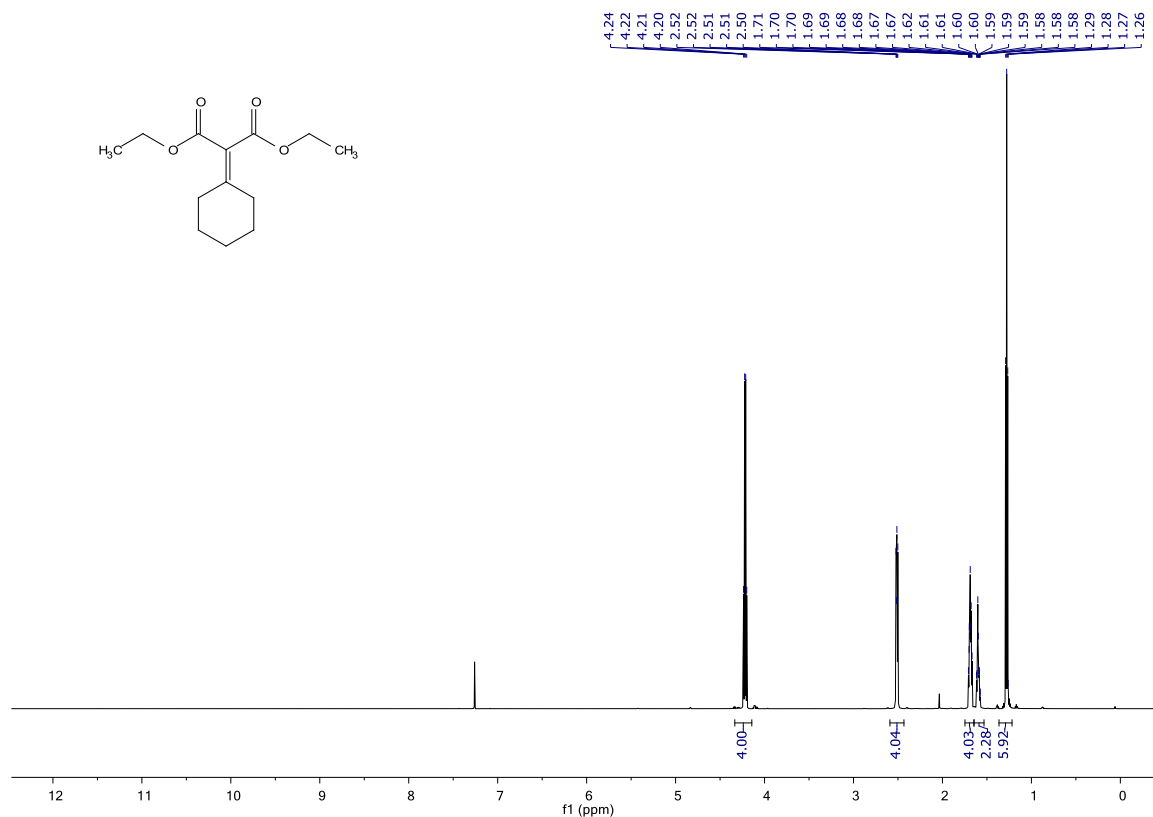
¹³C-NMR (151 MHz, CDCl₃)



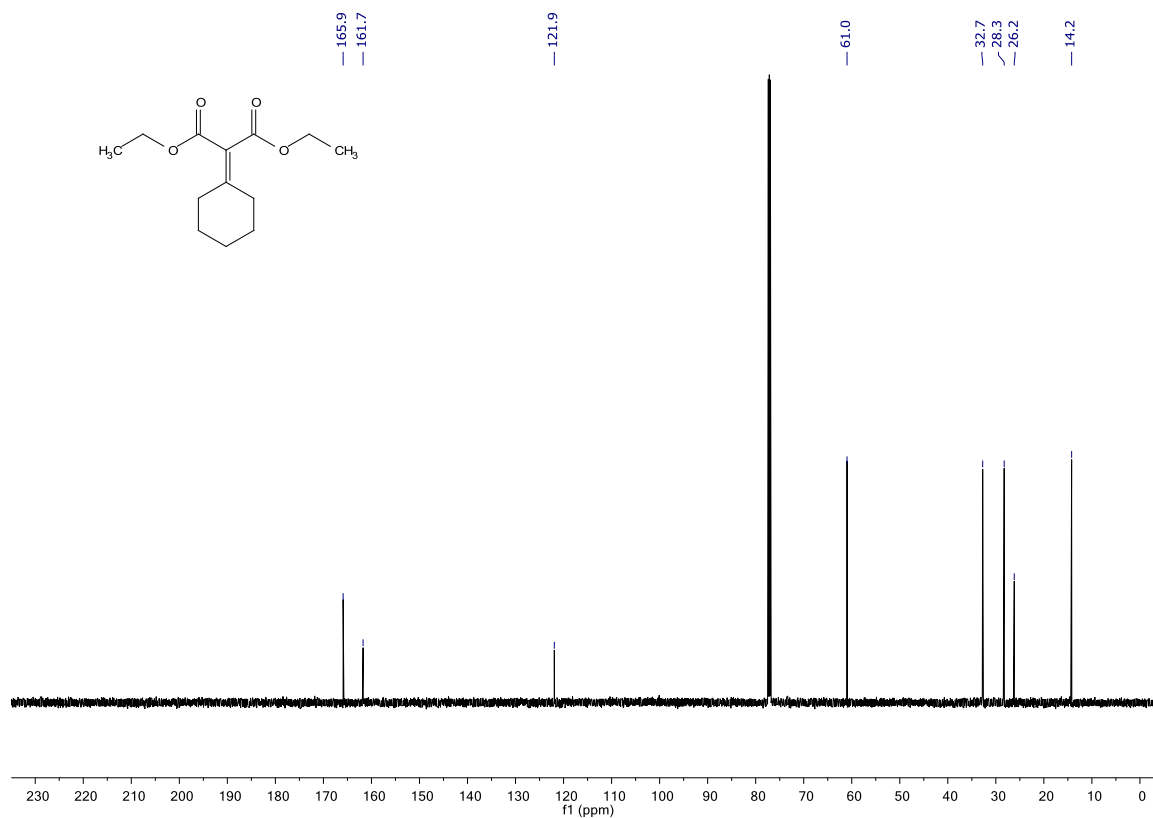
1,3-diethyl 2-(3-methylbutylidene)propanedioate (359)**¹H-NMR (600 MHz, CDCl₃)****¹³C-NMR (151 MHz, CDCl₃)**

diethyl 2-cyclohexylidenemalonate (360)

¹H-NMR (600 MHz, CDCl₃)



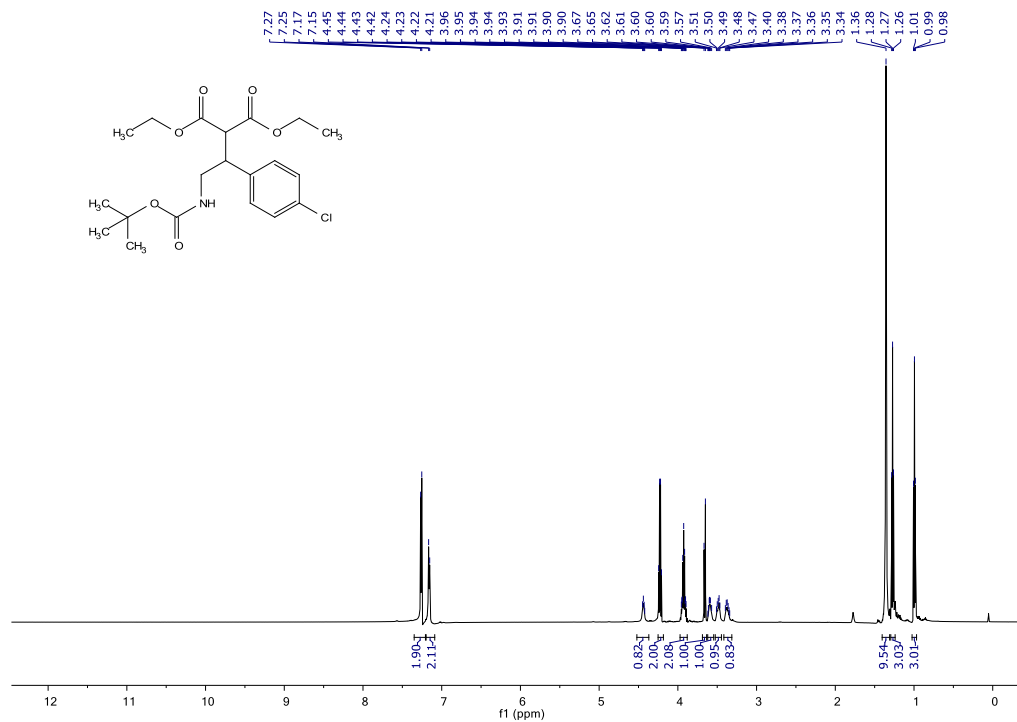
¹³C-NMR (151 MHz, CDCl₃)



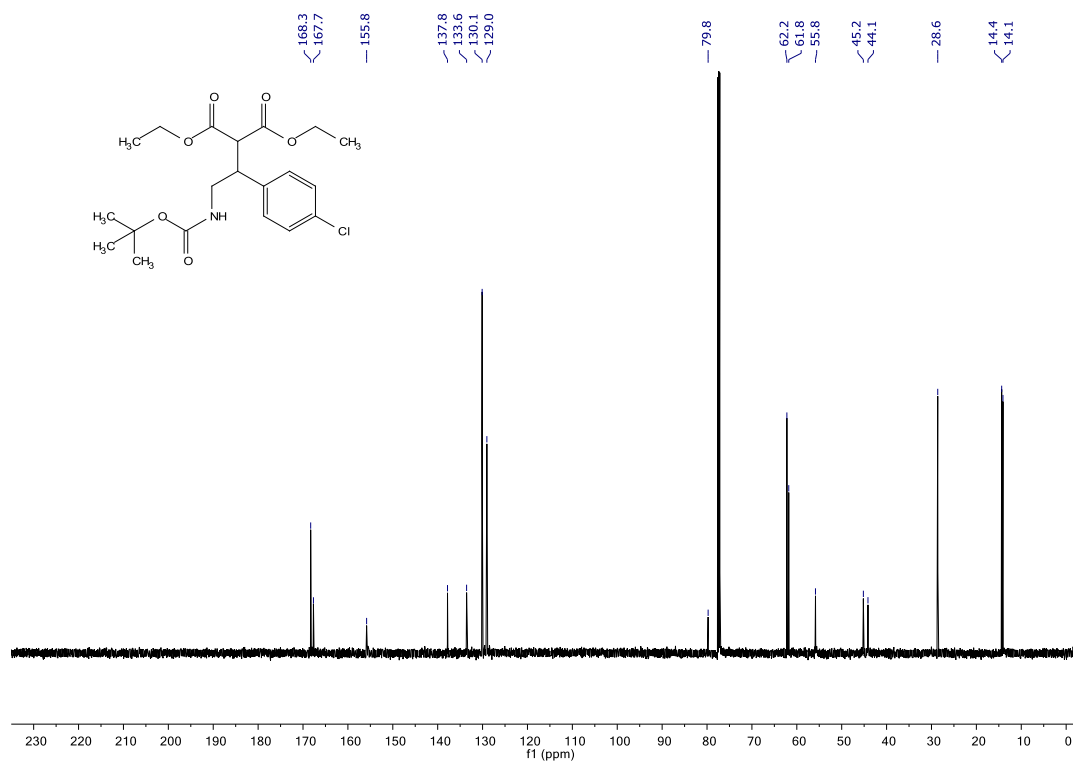
7.3.3 Coupling products and final APIs spectra

Diethyl 2-(2-((tert-butoxycarbonyl)amino)-1-(4-chlorophenyl)ethyl)malonate (361)

$^1\text{H-NMR}$ (600 MHz, CDCl_3)

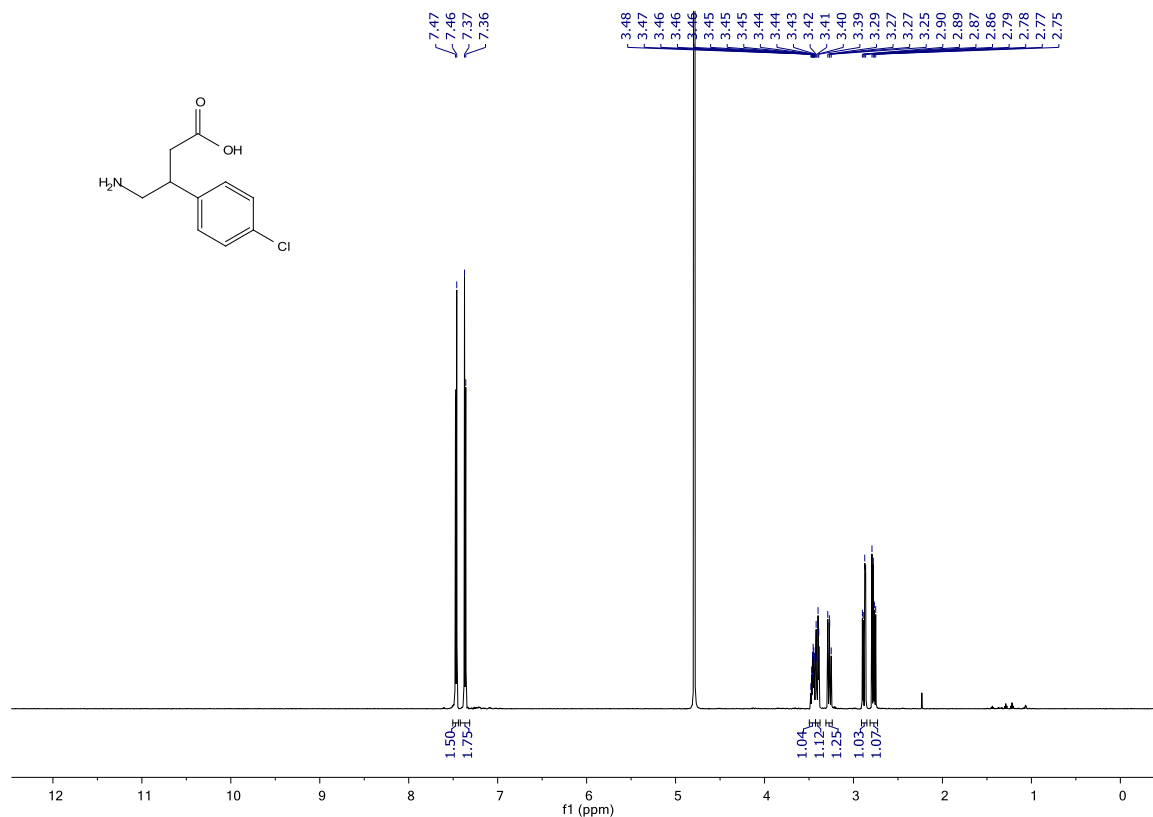


$^{13}\text{C-NMR}$ (151 MHz, CDCl_3)

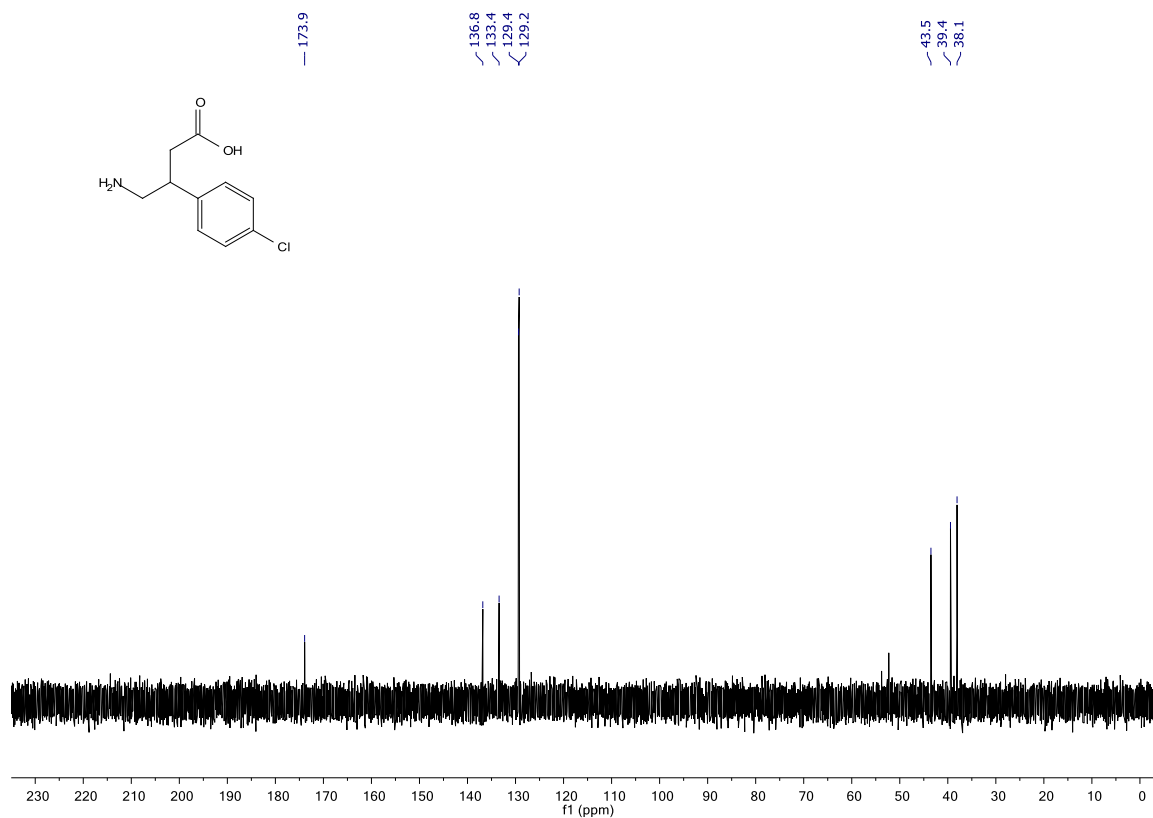


baclofen·HCl (365)

¹H-NMR (600 MHz, D₂O)

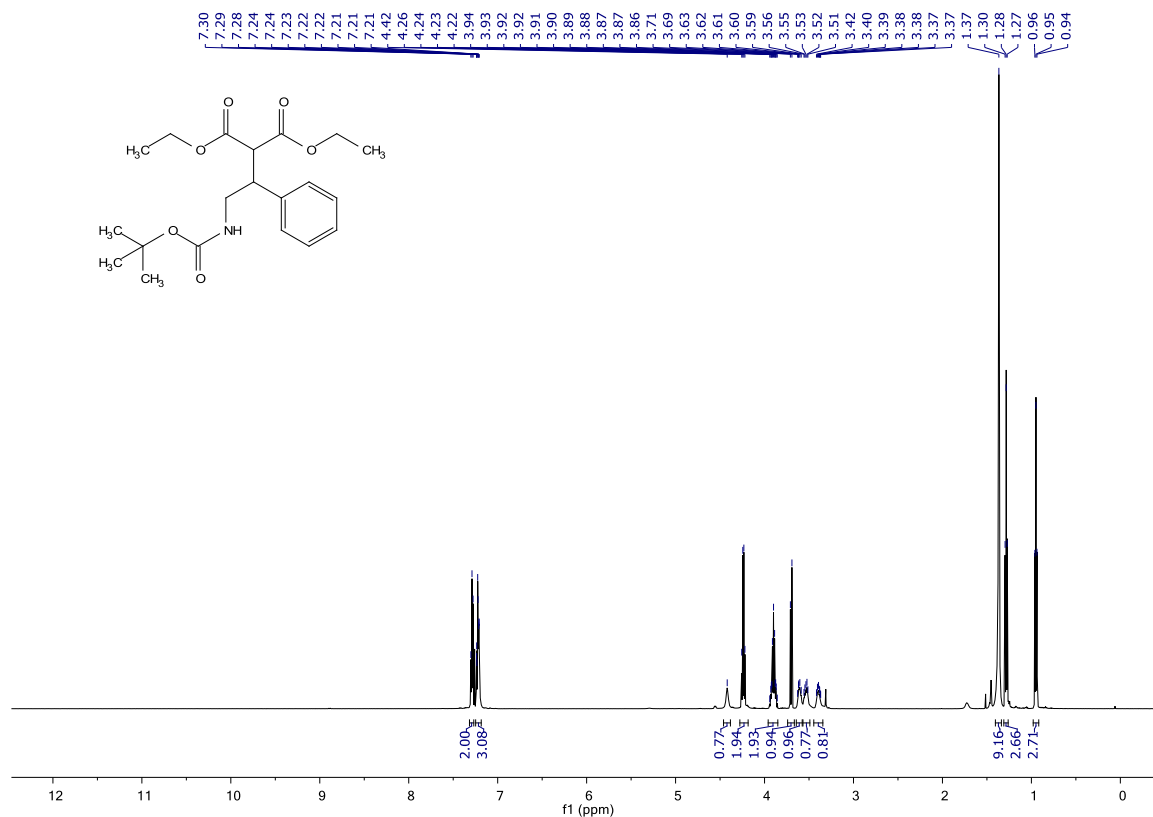


¹³C-NMR (151 MHz, D₂O)

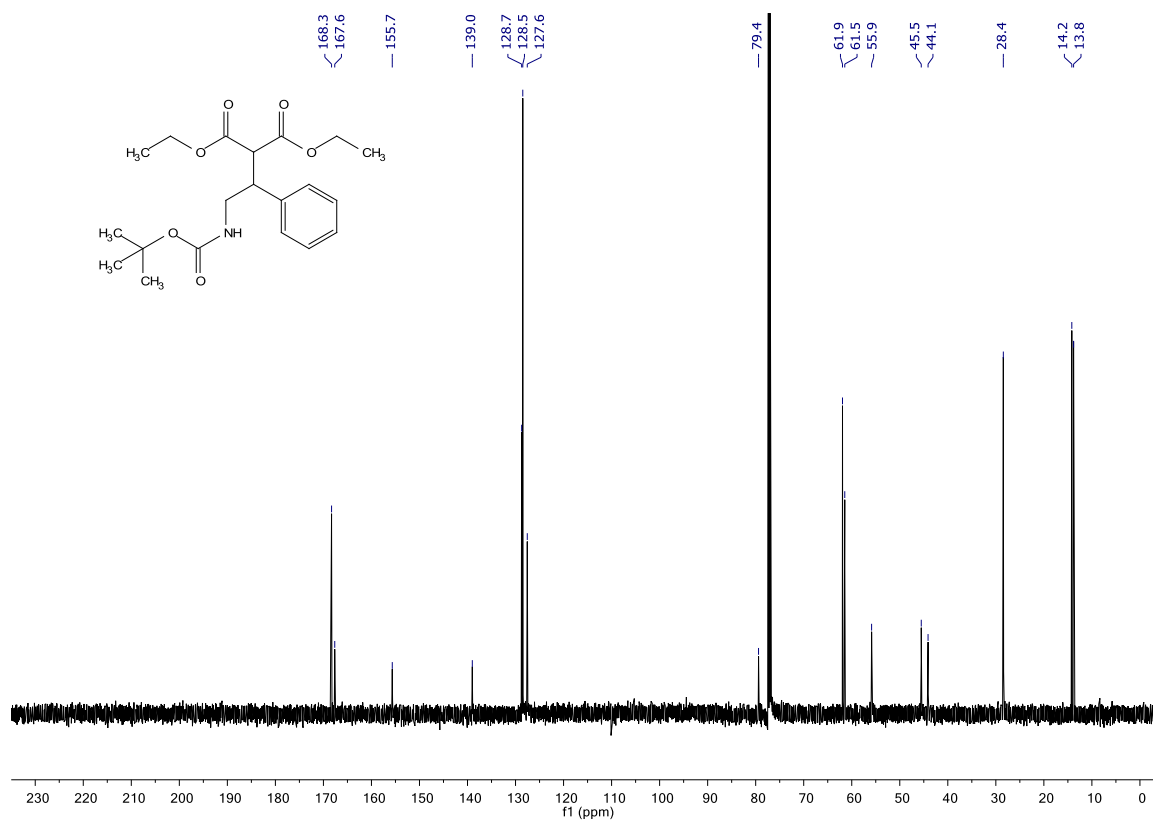


diethyl 2-(2-((tert-butoxycarbonyl)amino)-1-phenylethyl)malonate (362)

¹H-NMR (600 MHz, CDCl₃)

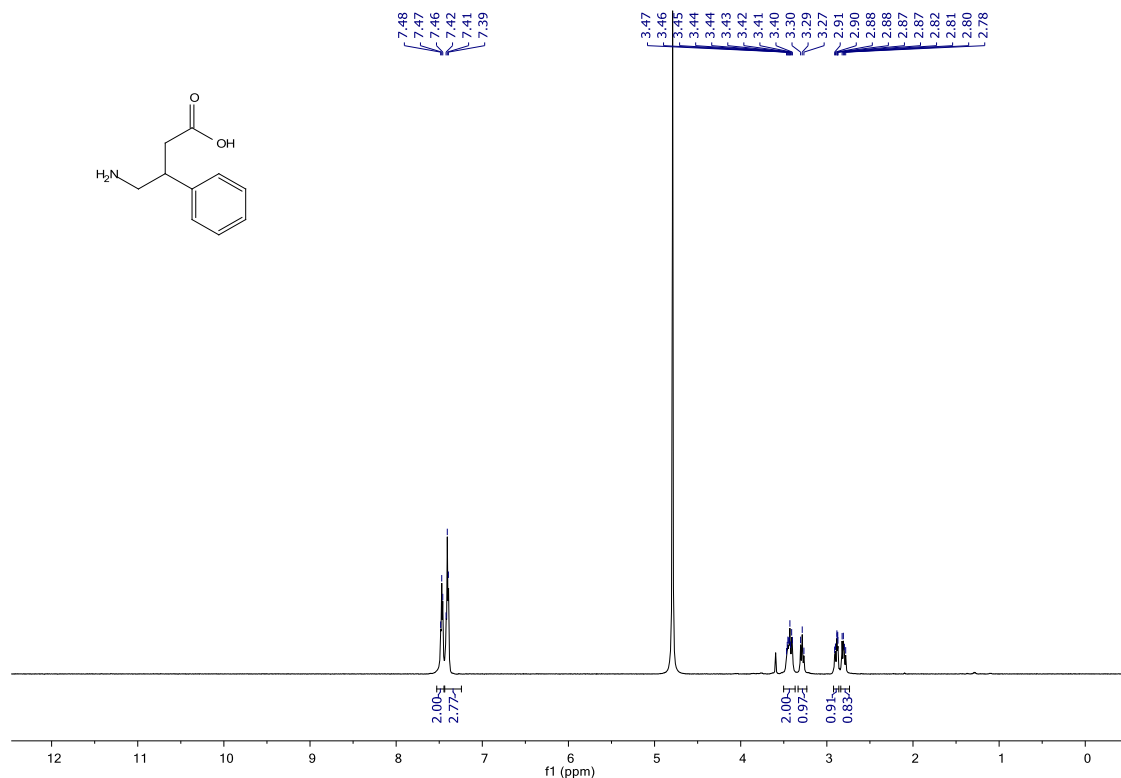


¹³C-NMR (151 MHz, CDCl₃)

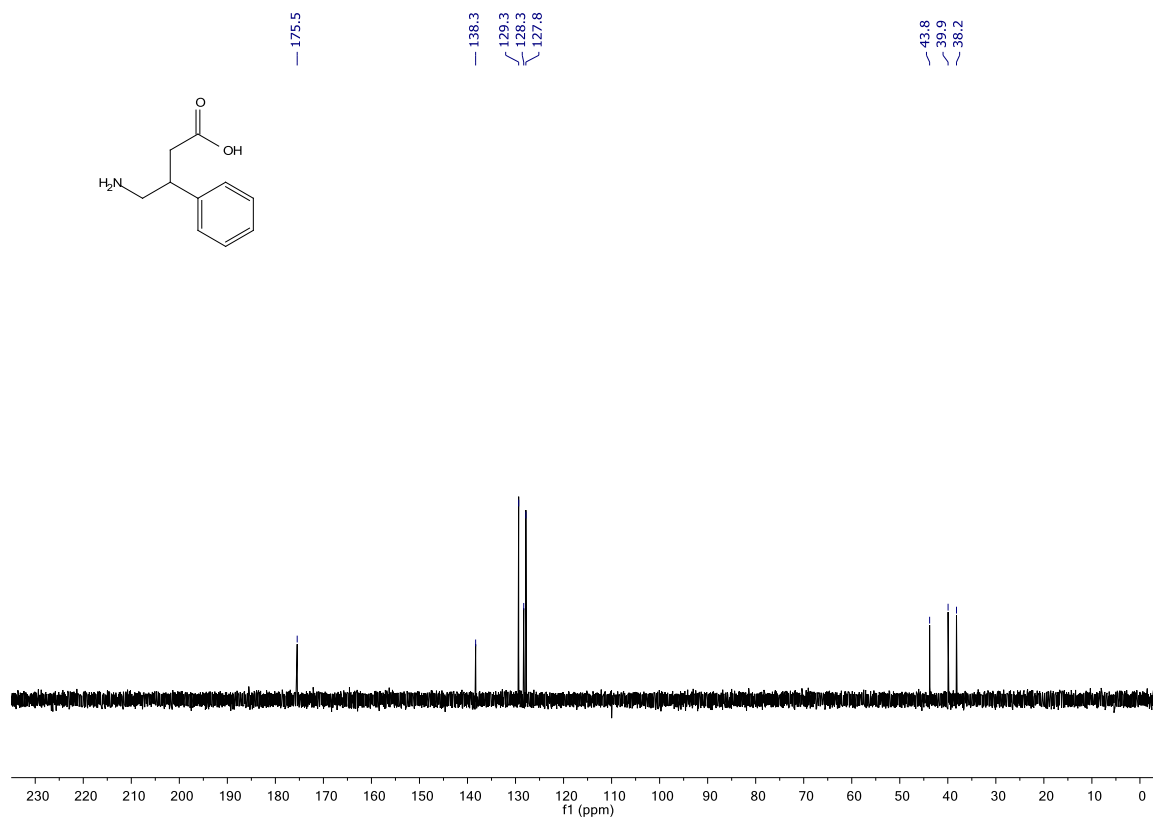


phenibut·HCl (366)

¹H-NMR (600 MHz, D₂O)

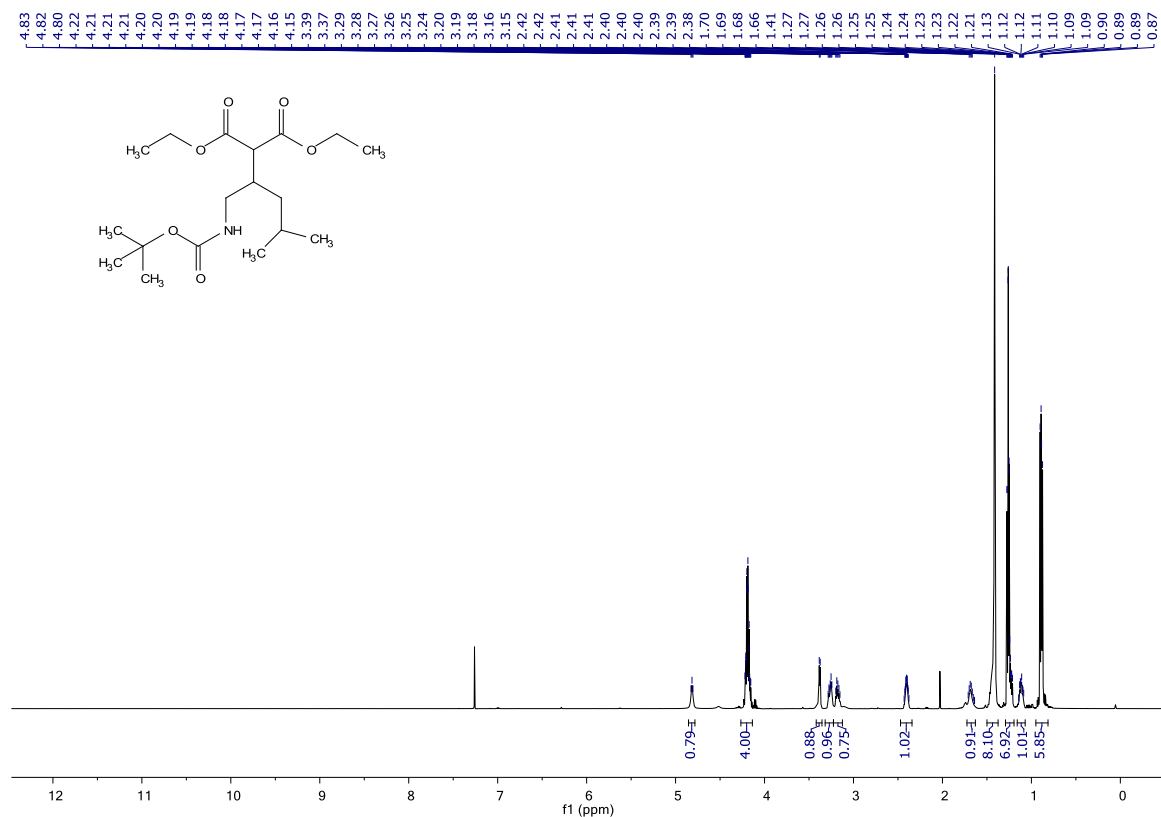


¹³C-NMR (151 MHz, D₂O)

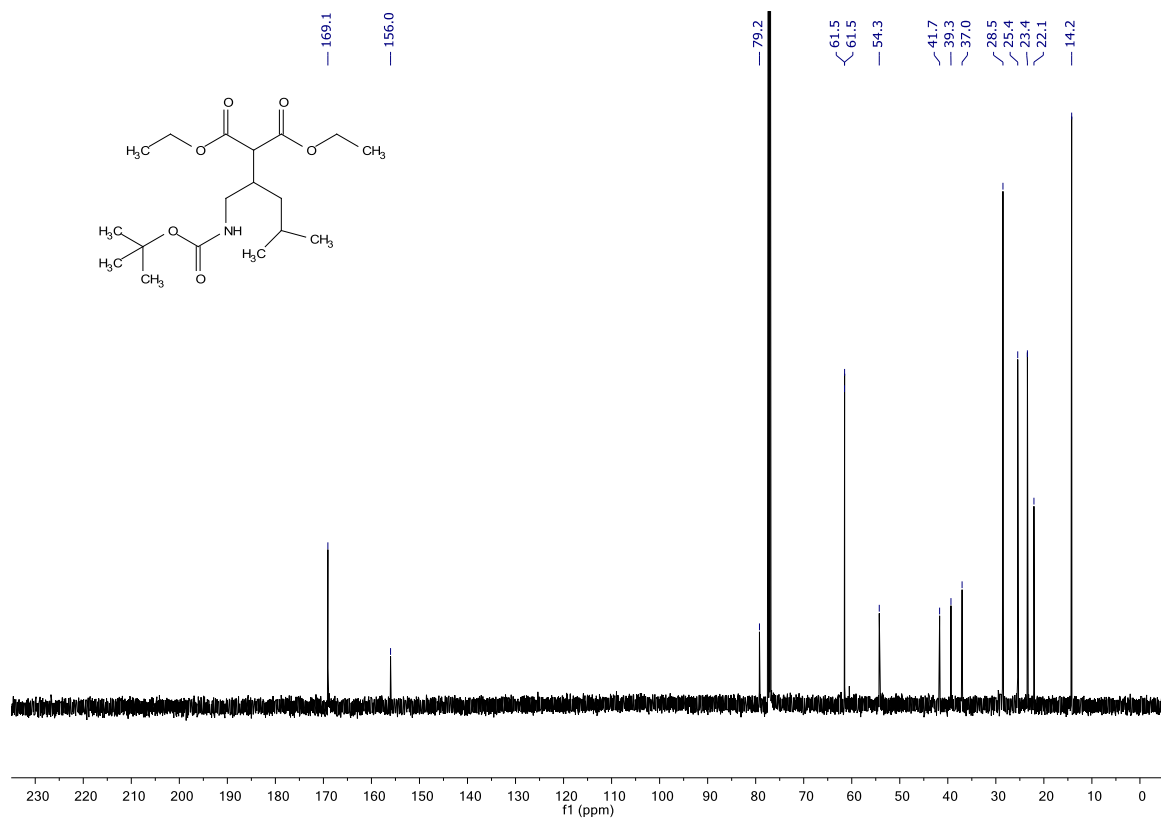


diethyl 2-(1-((tert-butoxycarbonyl)amino)-4-methylpentan-2-yl)malonate (363)

¹H-NMR (600 MHz, CDCl₃)

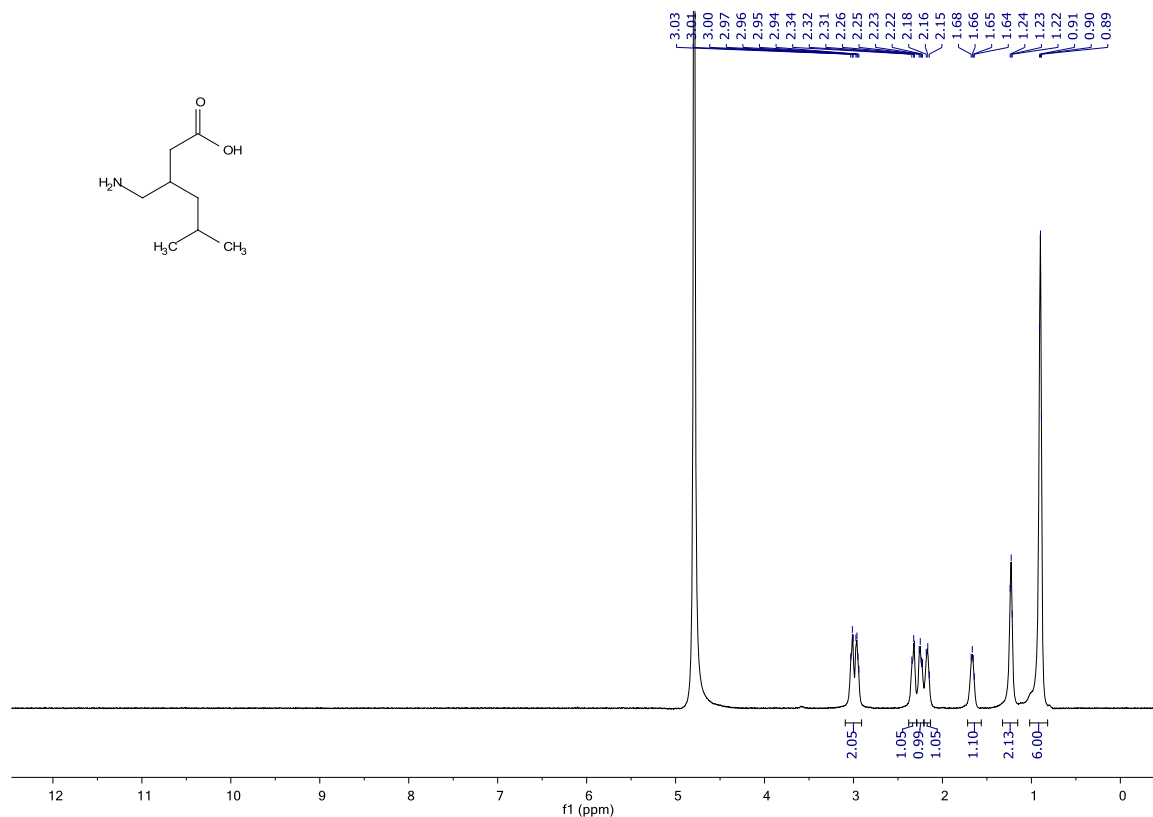


¹³C-NMR (151 MHz, CDCl₃)

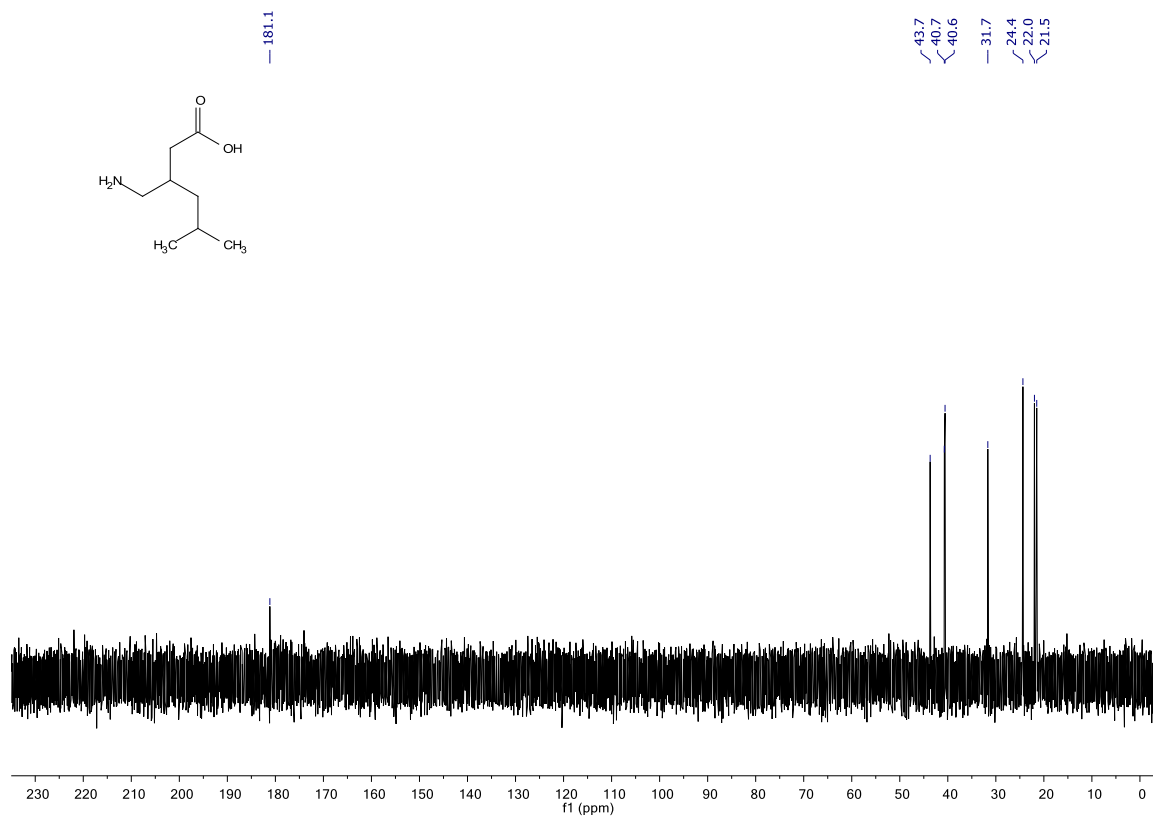


pregabalin (342)

¹H-NMR (600 MHz, D₂O)

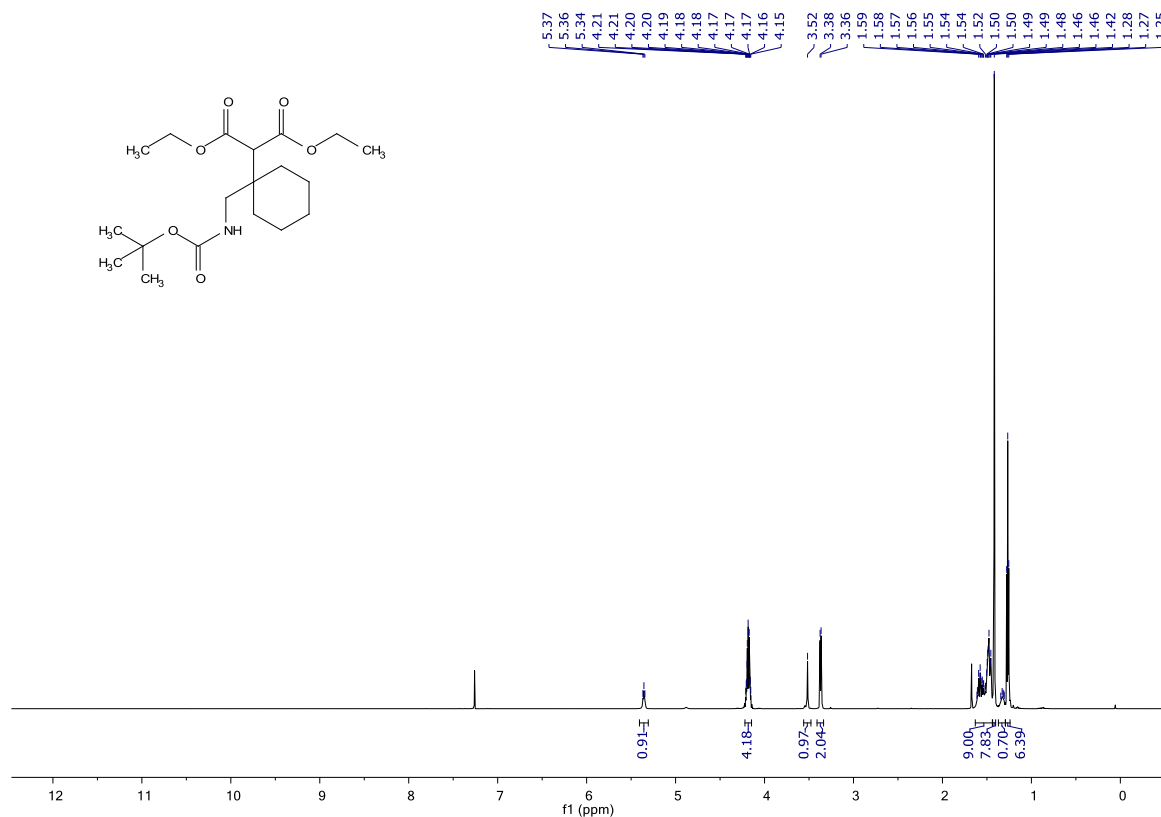


¹³C-NMR (151 MHz, D₂O)

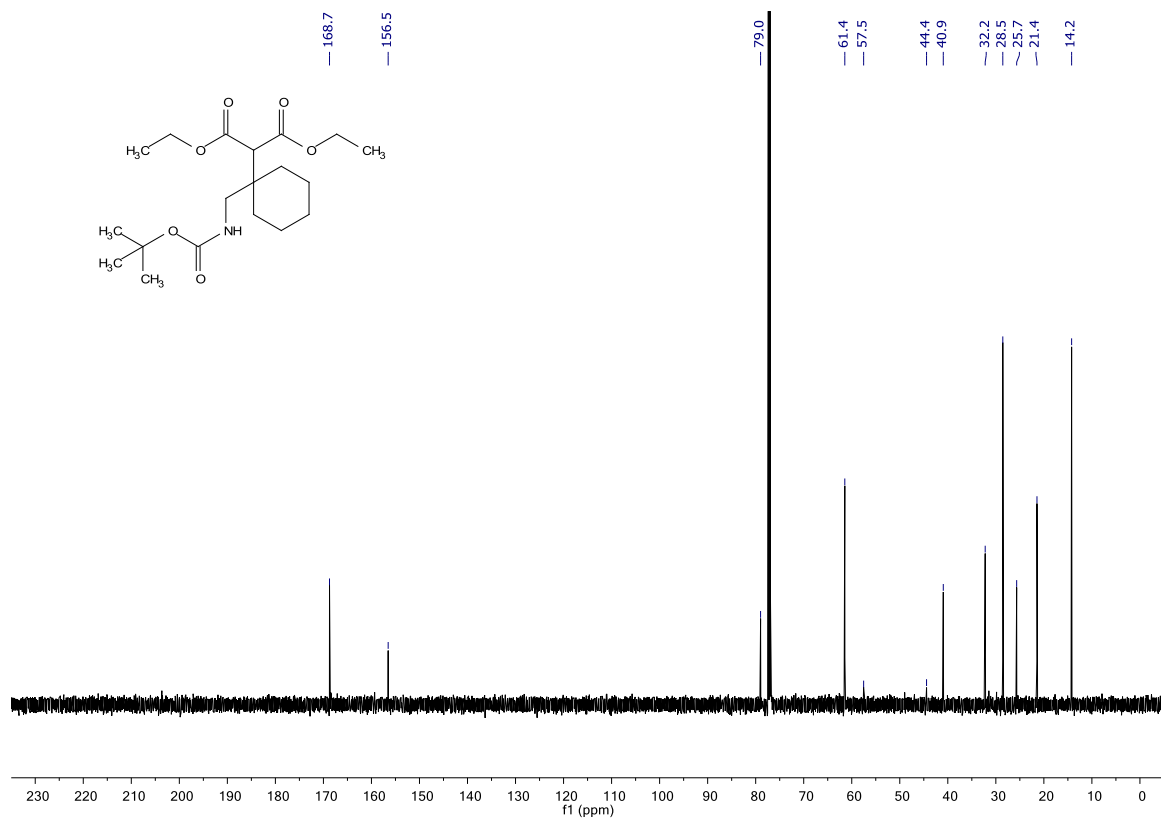


diethyl 2-(1-((tert-butoxycarbonyl)amino)cyclohexyl)malonate (364)

¹H-NMR (600 MHz, CDCl₃)

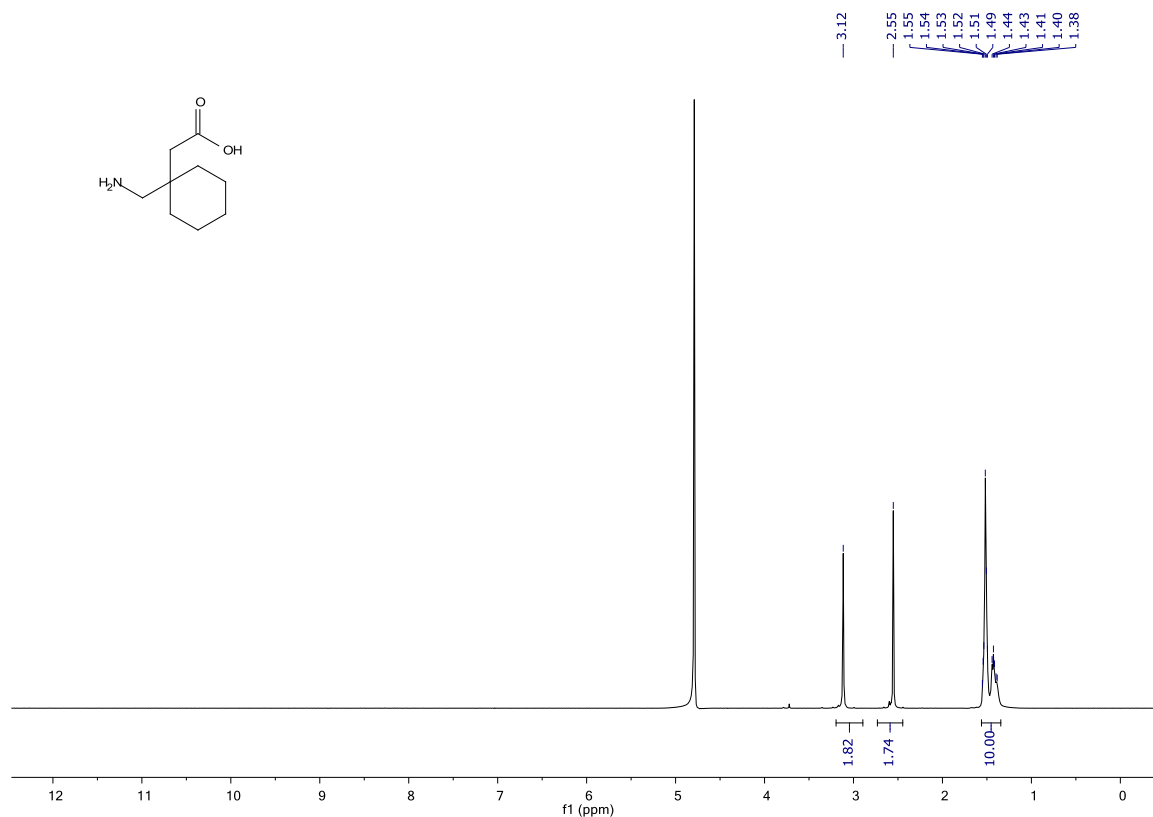


¹³C-NMR (151 MHz, CDCl₃)



gabapentin·HCl (368)

¹H-NMR (600 MHz, D₂O)



¹³C-NMR (151 MHz, D₂O)

